Wide-band channel sounding in the bands above 2GHz

Feeney, Stuart M.

Wide-band channel sounding in the bands above 2GHz

by

Stuart M Feeney BSc (Hons)

A thesis submitted to the

University of Durham

for the degree of Doctor of Philosophy

2007

Abstract

Modern telecommunication services require increasing data rates for both mobile and fixed applications. At frequencies in the range 2.5 GHz to 6 GHz physical constraints on the size of equipment result in antenna with moderate directivity typically with an antenna beam width of 20 degrees or greater. Thus building and ground clutter is present within the first Fresnel zones of the antenna system which gives rise to multi-path propagation.

This multi-path propagation (average delay and RMS delay spread) has been investigated using a wideband FMCW channel sounder that is capable of operation at a number of frequencies. The channel sounder has been based upon a parallel architecture sounder operating within the 2 GHz band with a number of frequency conversion modules to translate operation to the new frequency bands under study.

Two primary configurations have been explored. In the first of these, propagation has been measured simultaneously within the 2.5 GHz, 3.4 GHz and 5.7 GHz bands. This is believed to be novel and original. In the second configuration four parallel channels operating within the 5.7 GHz band may be operated simultaneously. This configuration supports multiple antennas at the receiver.

To support the work in the bands from 2.5 GHz to 6 GHz wideband discone antenna have been designed and fabricated. A system to provide relative gain and phase calibration for up to four antennas has been developed and demonstrated. This is also believed to represent a novel method of performing antenna and array calibration.

Finally, the frequency converters have been used in conjunction with additional components to provide an FMCW sounder operating within the 60 GHz Oxygen absorption band. This work is novel in that up to 1 GHz of spectrum can be swept.

To support this work a significant number of microwave components have been designed and developed. In particular a novel wide band balanced X3 multiplier and a novel impedance-matched amplitude-equaliser (to provide amplifier gain-slope equalisation) has been developed.

Channel soundings have been performed at three frequencies simultaneously using band specific and common antenna. The average delay and RMS delay spread have been demonstrated to be essentially frequency independent for the environments evaluated.

Declaration

No part of the work described in this thesis has been submitted in support of an application for another degree or qualification to this or any other university or institute of learning.

Acknowledgements

I would like to express my gratitude to Professor Sana Salous for her guidance and encouragement particularly during the preparation of the thesis.

I would also like to acknowledgement the help and assistance received from my colleagues Dr. Roger Lewnez, Zhe Wang and Nima Razavi-Ghods during the measurement campaigns.

Thanks are also directed to Peter Chaisty for his advice on numerous related topics.

Dedication

This thesis is dedicated to Jack and Frank for their many years of encouragement to learn and "do" and to Susan my long suffering spouse.

Chapter 4: Description of the new experimental hardware

List of figures and tables

1.1 Introduction

Modern communication networks are migrating to a packet based rather than circuit based transport since this is advantageous in supporting multiple users and different types of service efficiently whilst exploiting statistical multiplexing. In simplistic terms the service to a single user is delivered via a packet of data delivered at high transmission speed with significant spacing between packets to that user. In this time however the network resources can be made available to other users to support their interconnection.

A consequence of this is that the access network is required to support increasingly higher connection rates. In some media (for example optical fibre), the intrinsic bandwidth is such that the transport of high data rates can be provided using simple forms of modulation and coding. In other media (for example twisted pair {ADSL} or coax {cable modems}), the high signal to noise ratio and the stable time variant behaviour of the infrastructure allows high order modulation schemes to be utilised to deliver high bit rates with moderate transmission bandwidth. One disadvantage of all the above is that some form of physical infrastructure is required to facilitate the physical transmission path to the end user. In some locations the tele-density may be too low to make this viable, or the geographical terrain may make this impossible.

In these circumstances the provision of the interconnection without using wires represents the only solution. Two solutions are considered to be viable at this time, free space optics and fixed wireless access.

Here, topics pertinent to fixed wireless access have been explored. In particular the work presented here is based upon the extension of the FMCW channel sounding technique into the frequency bands above UMTS using both linear (heterodyne and amplify) and non-linear (multiplier based) up-conversion.

The work has been segmented into the bands between 2 and 6 GHz and the 60 GHz band since each are able to support differing aspects of the interconnection problem using non-licensed or lightly licensed spectrum.

It is anticipated that the bands below 6 GHz represent useful candidates to provide high bit rate services (up to 20 Mbit/sec per channel) without having to utilise MIMO techniques [1.1]. One of the characteristics of these bands is that the system gain that can be provided economically within the equipment is sufficient to support non line of sight and near line of sight over practical distances. In addition, the general development order (GDO) [1.2] imposes limits on the size of terminal equipment that can be installed without seeking planning permission. This places a size restriction on the antenna that can be used *{the maximum permitted linear dimension is 50 cm with a maximum projected surface area of 1591 cm²}*. This provides a minimum 3dB beam width in the region of 10 to 20 degrees in azimuth and elevation. A consequence of this is that many links will have clutter within the first Fresnel zones of the path and thus even apparently line of sight links will exhibit non line of sight (NLOS) frequency selective behaviour.

To increase the availability of a link, a number of strategies can be employed. Firstly a "brute force" approach can be used to raise the available signal to noise ratio on the link by increasing the transmitter power. This strategy is counter productive in that raising the level for this link impacts other links in adjacent territories due to interference. In any case regulatory limits on the transmitter effective isotropic radiated power (EIRP) have been imposed by legislation [1.3], [1.4]. *In the UK power limits of 100 mW EIRP are stipulated in the 2.4 GHz band rising to 1 W EIRP in the 5470 to 5725 MHz bands.* Some forms of space-time diversity may be included [1.5].

Additionally here, it has been postulated that using two frequencies in significantly different frequency bands may allow the link availability to be enhanced whilst using low transmitter power. This form of spectral diversity may be a very practical technique for operation in the un-licensed or lightly licensed bands since the cost of spectrum is small and generally low power limits have been imposed on the bands by regulation. Additionally this form of "super-diversity" may also provide local interference mitigation. Investigation of the simultaneous behaviour of representative wideband channels across the 2.5 GHz, 3.5 GHz and 5.8 GHz has been facilitated using the "three band sounder" configuration, designed and implemented during the course of this thesis.

A variety of channel sounding techniques could have been utilised to provide information about the frequency selective nature of the channel [1.6]. In this case, the choice of methodology was somewhat moot since the base "UMIST parallel architecture" sounder has been used to provide the FMCW source for the transmitter and correlating receiver along with the multi-channel signal conditioning and data acquisition system. The FMCW technique provides a number of advantages that have been exploited and extended within the work. The spectrum spreading has been used to provide enhanced system gain in conjunction with resistance to interference from signals within and adjacent to the channel under study. The non-linear (constant envelope) modulation used at the transmitter has been exploited in maximising the available power from the transmitter devices. This is particularly appropriate for the 60 GHz sounder which also exploits the constant envelope FMCW modulation within multiplier structures to increase both the frequency of operation and the sweep width.

A parallel four channel down converter has been produced to enable simultaneous operation in the 2.3 GHz and 5.7 GHz bands for SIMO and MIMO measurements [1.7]. This work was supported by hardware design and assembly.

In contrast to the sub 6 GHz bands, the bands above 60 GHz represent an excellent choice for very high bit rate radio links. Further, these links can utilise highly power efficient modulation since the available bandwidth is sufficient to allow spectral efficiencies of ~ 1bit/sec/Hz to be used. Spectrum is however still used efficiently since the links use directional antennas which provide spatial isolation between the links. At 60 GHz in particular oxygen absorption restricts the maximum link distance to ~1.6 km with on-antenna-beam re-use possible within twice this distance. To facilitate longer links that retain the high bandwidth additional spectrum above the oxygen absorption has been made available at 70 GHz paired with 80 GHz. At this frequency links up to ~ 5 km are feasible. At the millimetric frequencies the channel sounder has been developed to investigate channel behaviour for very high bandwidths (up to ~ 1 GHz) in addition to providing operation in the high frequency bands.

A general approach to FMCW millimetric channel sounders has been explored using non-linear multiplication. A specific sounder operating in the 60 GHz oxygen absorption band has been assembled using a X4 multiplier. Spectrum has been allocated in the 60 GHz band [1.8] to provide short range links that benefit from the additional attenuation so that spectrum can be re-used at short distances. Additional spectrum has been allocated in the 70/80 GHz bands [1.9] to allow longer links. Both of these allocations are significant and different to those at other bands in that contiguous channels of 1250 MHz (and up) have been made. This is sufficient to support very high bit-rates with simple forms of modulation and coding. These bands are now being commercialised [1.10] with systems providing radio based Gigabit Ethernet connectivity that otherwise could only be supplied using fibre optic cables or free-space optics. This sounder can be extended into additional frequency bands by changing the multiplication ratio, for example into the 32 GHz band using X2 or the 110 GHz band using X6 multipliers. Satisfactory phase noise performance has been demonstrated to support this work.

1.2 Organisation of the thesis

Chapter 2 includes a review of the propagation of radio signals in a scattering environment. The use of the power delay profile is explored as are the basic parameters to be measured and presented.

Chapter 3 reviews the options for wideband channel sounding. The swept correlation-impulse sounder and network analyser techniques are presented and contrasted prior to a more thorough presentation of the FMCW chirp technique.

Chapter 4 presents the configuration of the new sounder configurations; simultaneous three-band, 5.7 GHz parallel down-converter and 60 GHz. This chapter also provides a detailed review of the new hardware that has been designed and fabricated to support this work. This chapter also documents the concepts that were modified or abandoned during development and enhancements made to the base sounder. The antenna calibration phase-tracking down-converter and the survey vehicle are also described.

Chapter 5 presents the work that has been performed to characterise and validate the various sounder configurations. This includes the determination of the noise figure for the converters and the effective noise sensitivity limit for the complete sounders. The intrinsic resolution due to phase noise has been explored. The polar response of the four antenna assembly used for parallel measurements in the 5.7 GHz band is also presented.

Chapter 6 presents the results derived from the measurements performed using the different sounder configurations. Specific examples of the measurements are included to demonstrate Doppler for the multi-frequency configuration and the different delay responses observed for the multi-channel sounder at 5.7 GHz.

Chapter 7 included the conclusions and suggestions for additional work that have arisen from the work performed to date.

Annex 1 includes the circuit schematics of the new assemblies.

Annex 2 includes papers that have been authored or co-authored during the research.

1.3 References

[1.1] "802.16-2004 IEEE Standard for Local and metropolitan area networks Part 16: Air Interface for Fixed Broadband Wireless Access Systems", ISBN: 0-7381-4069-4

[1.2] "The Town and Country Planning (General Permitted Development) (Amendment) (England) Order 2001", published by The Stationery Office Limited, ISBN 0 11 029796 2, available at: http://www.opsi.gov.uk/SI/si2001/20012718.htm

[1.3] "IR 2005 UK Interface Requirement 2005 Wideband Transmission Systems Operating in the 2.4 GHz ISM Band and Using Spread Spectrum Modulation Techniques", available from: http://www.ofcom.org.uk/radiocomms/ifi/tech/interface_req/mso9140.pdf

[1.4] "IR 2006 UK Interface Requirement 2006 Short Range, Broadband, Data Services (HIPERLAN) operating in the frequency range 5-6 GHz", from: http://www.ofcom.org.uk/radiocomms/ifi/tech/interface_req/mso12E75.pdf

[1.5] Alamouti S.M.: "A simple transmit diversity technique for wireless communications"; IEEE Journal on Selected Areas in Communications 16 (8): 1451–1458

[1.6] Parsons J.D., Demery D.A., Turkmani A.M.D.; "Sounding Techniques for Wide-band Mobile Radio Channels: A Review"; IEE Proceedings-I Vol 138, No 5, October 1991

[1.7] Salous S., Feeney S., Razavi-Ghods N., Lewenz R.; "Measurements in the 2-6 GHz Band"; presented at the URSI general assembly in New Delhi October 23rd to 29th 2005

[1.8] FCC part 15 available at: http://www.fcc.gov/oet/info/rules/

[1.9] FCC notice FCC 05-45 available at: http://hraunfoss.fcc.gov/edocs_public/attachmatch/FCC-05-45A1.pdf

[1.10] Data sheets for example 60 GHz and "E-band" products available at: http://www.bridgewave.com

2.1 Introduction

The signal available at the receiver antenna is a function of the signal introduced to the channel by the transmitter, modified by the actual transmission channel that is present between the transmitter and the receiver antennas.

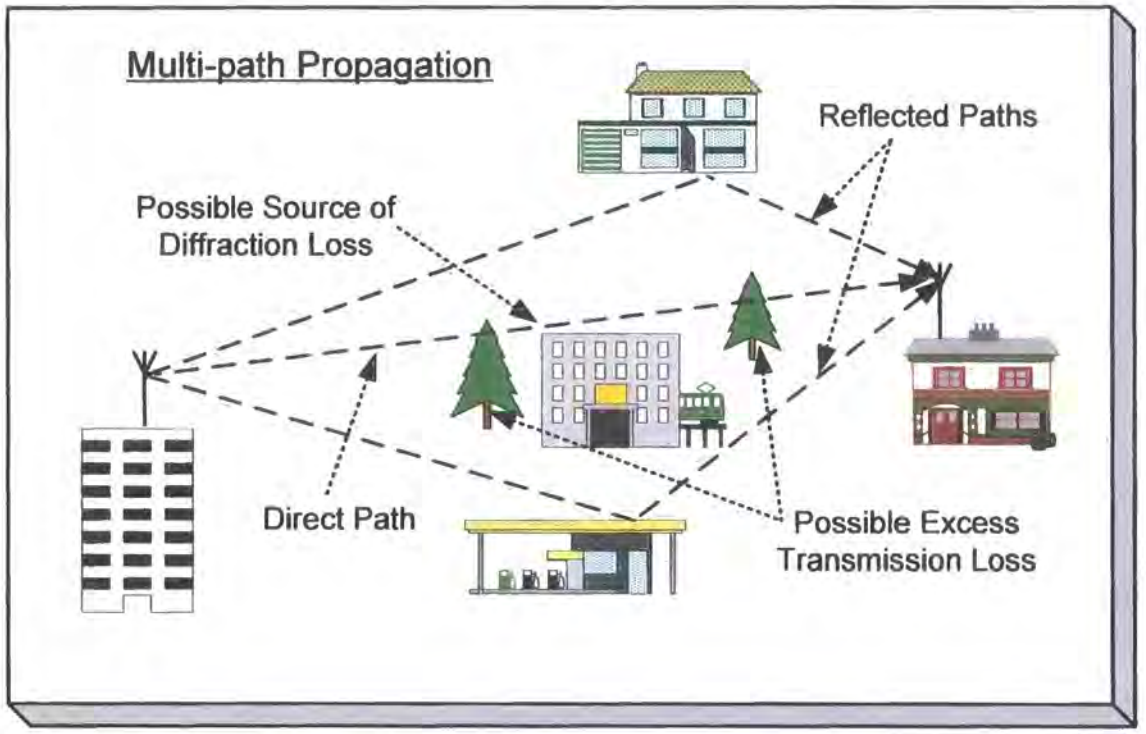

Figure 2.1 Propagation in the built environment

Within most environments this signal will be formed from a number of individual signal components that arrive at the receiver via different routes (refer to figure 2.1). The different path components may have interacted with obstacles within the environment which cause reflection and diffraction of the radio frequency signals. Under some circumstances components may have suffered refraction due to atmospheric anomalies.

These individual path components may (usually will) have different path lengths. The transmission delay and thus the phase of the signal components will therefore be different. These components will sum on a vector basis to provide the resultant signal at the receiver antenna. The resultant signal will therefore vary as the relative amplitude and phase of the components vary.

The general level of the signal available at the receiver is also reduced as a function of distance. This follows a log-normal distribution due to the free space transmission loss and additional losses introduced by obstacles and reflections in the propagation environment. This general reduction in signal level with increasing transmitter to receiver separation is termed "large scale" fading.

When the received signal includes a number of signal components the relative phase of the individual components may vary rapidly with small changes in distance (on the order of one wavelength). The signal level may vary significantly over the small change in distance particularly where signal components null due to destructive cancellation. This is termed "small scale" fading.

The resultant signal at the receiver may either have a dominant component due to a strong line of sight or coherent specular reflected component or, may be formed without a single dominant component. Where no dominant component is present the signal exhibits Rayleigh statistics. When a dominant component is present the signal exhibits Ricean statistics [2.1].

At a specific location, the phase of the signal components arriving at the antenna will vary as the wavelength changes. Therefore the net signal amplitude varies as a function of frequency. Thus the channel also exhibits frequency selective behaviour.

2.2 Propagation mechanisms in the cluttered environment

The measurements in the 2.5 GHz to 5.7 GHz bands have been limited to transmission distances of less than 5 km. For these conditions the effects of absorption due to atmospheric gases and rain attenuation are negligible. At 60 GHz the measurements have been limited to transmission distances of ~100 m under dry conditions. The additional path attenuation due to Oxygen absorption is limited to 2 dB maximum.

The channel sounder can be used to provide signal level information to allow the large scale fading to be observed and quantified. Numerous models have been developed to

fit the observed data. However, this aspect of propagation has not been pursued within this research project which has concentrated on the time-dispersion of the signals due to multi-path propagation.

The primary propagation mechanisms considered here are:

- The "line-of-sight" transmission loss of direct components
- Reflection from the surface of obstacles
- Diffraction around obstacles
- Transmission through obstacles
- Refraction in the atmosphere

2.3 Line-of-sight transmission

The signal level tends to reduce as the distance of the receiver from the transmitter is increased. This is due to the energy per unit area available to the receiver being reduced as the distance from the source increases. In a free space environment this reduction in signal level would exhibit an inverse square law. This form of free space propagation can only occur when there is only a single direct transmission path. Point to point microwave links with highly directional antenna and satellite links exhibit this type of propagation. This is described by Friis's equation [2.2]:

$$\frac{P_R}{P_T} = G_T G_R \left(\frac{c}{4\pi f d}\right)^2 \quad (2.1)$$

Where: P_R is the power available at the receiver
P_T is the power delivered from the transmitter
G_T is the transmit antenna gain
G_R is the receiver antenna gain
d is the separation, f is transmission frequency

From this it is noted that:

- the transmission loss is proportional to the frequency squared
- the transmission loss is proportional to distance squared
- the transmission loss is reduced by the gain (directivity) of the antennas

Where the propagation path includes both a direct path and a strong component that is reflected from the ground Parsons [2.2] demonstrates that Friis's equation can be modified to become the "plane earth propagation equation":

$$\frac{P_R}{P_T} = G_T G_R \left(\frac{h_t h_r}{d^2} \right)^2 \qquad \text{(subject to } d >> h_T, h_R \text{)} \qquad (2.2)$$

Where: h_t and h_r are the antenna heights at the transmitter and receiver

From this, it is noted that:

- the path loss is predicted to be independent of frequency
- the transmission loss is proportional to the fourth power of distance
- the transmission loss is reduced by the antenna height squared
- the transmission loss is reduced by the gain (directivity) of the antennas

2.4 Reflection from obstacles

When the radio signal is incident upon an obstacle in the environment the signal will be both reflected from and refracted into the surface of the obstacle. The proportions of the signal that are reflected and refracted depend upon the angle of incidence of the incoming signal and the refractive index. When the surface irregularities are small relative to a wavelength, specular reflection occurs. For surfaces that exhibit irregularity that is comparable or greater than a wavelength the reflection becomes diffuse.

Buildings, foliage, vehicles and the topology of the land are typical examples of obstacles that occur within the propagation environment.

When the electric field of the reflecting signal is parallel to or orthogonal to the reflecting surface, the phase of the signal is inverted however the plane of polarisation of the signal is preserved. The phase inversion is a particular problem for digitally modulated systems since the phase inversion causes the sense of the modulation to be inverted. If "non-minimum phase" multi-path is possible, where the reflected signal could be larger than the direct path, then it is necessary to use differential signal coding.

When the plane of the reflecting surface is not normal to the incoming signal then conversion between planes of polarisation will occur. (This aspect of multi-path propagation has been exploited in cellular networks where polarisation diversity is used for base station antennas. Also, when strong reflections are anticipated for example in news gathering links, circular polarisation is used since the reflected signal now has opposite polarisation and is discriminated by the antenna.)

2.5 Diffraction around obstacles

The radio signal can also propagate behind obstacles in the environment due to diffraction at the boundaries of the obstacle.

The description of this mode of propagation is generally developed using the Huygen's construction which states; "Each point on a primary wave-front serves as the source of spherical secondary wavelets that advance with a speed and frequency equal to those of the primary wave. The primary wave-front at some time later is the envelope of these wavelets" [2.3]

The Huygen's construction was originally developed in the 18^{th} century to account for optical reflection and refraction. Fresnel subsequently modified the construction so that the new wave-front was calculated including the relative amplitude and phases of the wavelets. This modification allows the construction to describe optical diffraction in addition to reflection and refraction.

Whilst this approach provides an explanation of the phenomena Schwarz [2.4] has noted that: "*Huygens' principle tells us to consider each point on a wave-front as a new source of radiation and add the "radiation" from all of the new "sources" together. Physically this makes no sense at all. Light does not emit light; only accelerating charges emit light. Thus we will begin by throwing out Huygens' principle completely; later we will see that it actually does give the right answer for the wrong reasons.*"

The Huygen's-Fresnel construction was later demonstrated to be in accordance with the wave equation by Kirchoff. [2.5] This provides a correct mathematical basis for the diffraction problem.

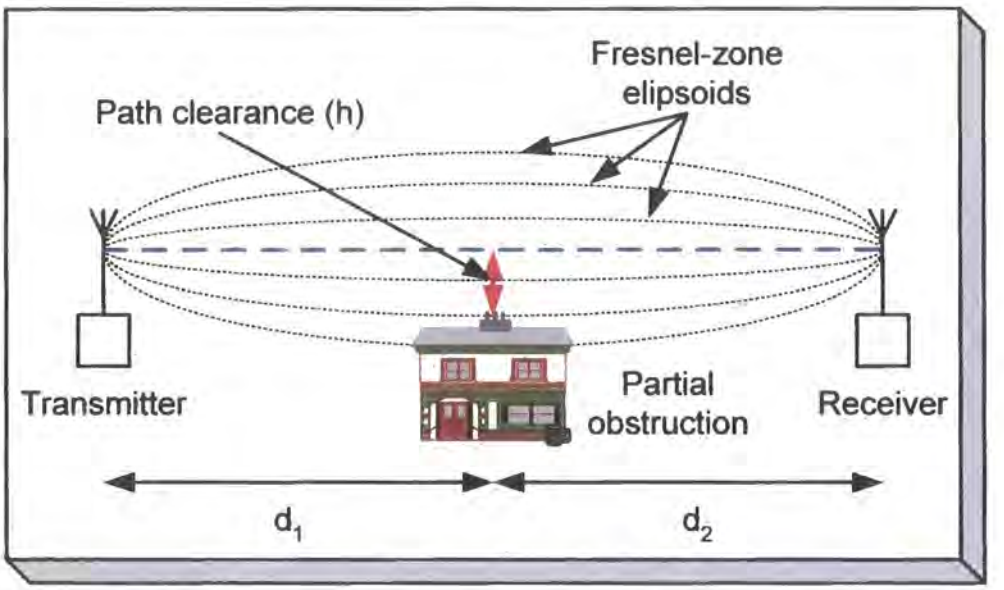

Figure 2.2 Fresnel zones and path clearance

In addition to propagation behind an obstruction within the path it is also necessary to consider propagation where the path is partially obstructed.

The Fresnel-Kirchoff diffraction parameter (v) is described by:

$$\upsilon = h\sqrt{\frac{2(d_1+d_2)}{\lambda d_1 d_2}} \qquad (2.3)$$

Where h, d_1 and d_2 are as defined in figure 2.3 above and λ is the wavelength of the signal.

The path clearance parameter "h" is the separation of the obstacle from the centre of the path between the antennas.

The diffraction loss can be evaluated using the complex Fresnel integral. This has been approximated by Lee [2.6] for path clearance parameters of "h" = -0.8 and above. Negative values of "h" represent clearance from the blockage to the centre of the path between the antennas. When the obstacle extends to the centre of the path, this represents "grazing" incidence, for which the excess path loss is 6 dB. At values below "h" = -0.8 the solution to the Fresnel integral is oscillatory with an amplitude of ~1 dB and is considered to be not relevant here. The excess path loss due to diffraction is presented in figure 2.4 based on Lee's approximation:

$$L_{(\upsilon)} = -20\log(0.5-0.62\upsilon) \qquad \text{for } -0.8 < \upsilon < 0 \qquad (2.4)$$

$$L_{(\upsilon)} = -20\log[0.5\exp(-0.95\upsilon)] \qquad \text{for } 0 < \upsilon < 1 \qquad (2.5)$$

$$L_{(\upsilon)} = -20\log[0.4-\sqrt{(0.1184-\{0.38-0.1\upsilon\}^2)}] \qquad \text{for } 1 < \upsilon < 2.4 \qquad (2.6)$$

$$L_{(\upsilon)} = -20\log(0.225/\upsilon) \qquad \text{for } \upsilon > 2.4 \qquad (2.7)$$

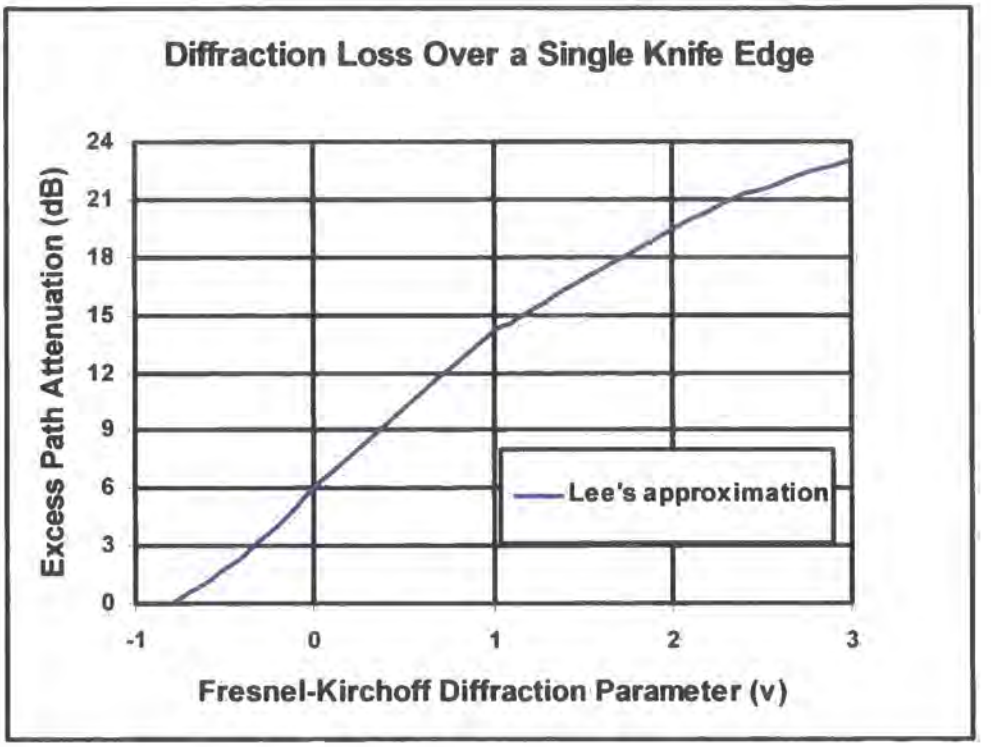

Figure 2.3 Excess path loss due to diffraction

2.6 Transmission through obstacles

The cluttered environment will typically include foliage and building which will introduce loss to both the wanted and multi-path components.

Rogers et al [2.7] observed that attenuation through foliage tended to increase with the amount of tree canopy present and the propagating frequency. The observed excess attenuation was high even for moderate levels of tree canopy within the path (see table 2.4). *This has been observed in the 5.7 GHz measurements at Durham where multi-path measurements through tree cover adjacent to the university were abandoned due to insufficient signal to noise ratio due to the high level of attenuation.*

Foliage Details	2 GHz Attenuation	6 GHz Attenuation	
Sycamore, 4m, in leaf	45	65	dB
Sycamore, 42m, in leaf	55	75	dB
Sycamore, 4m, no leaf	45	45	dB

Sycamore, 42m, no leaf	55	80	dB
Maple, 5m, in leaf	20	35	dB
Maple, 41m, in leaf	35	60	dB
London Plane, 5m, in leaf	20	40	dB
London Plane, 42m, in leaf	35	60	dB

Table 2.4 Summary of attenuation due to trees

Rappaport [2.8] has reported measured losses for common building materials at 1,300 MHz. He reports losses of 13 to 20 dB for a concrete block wall, loss between two floors in the range 20 to 30 dB and losses of 40 to 50 dB for transmission between a wall and two floors.

2.7 Atmospheric refraction

Under some circumstances the signal propagation can be modified by refraction. This is due to the change in refractive index of the atmosphere close to the ground. In particular when a temperature inversion occurs, the refractive index varies with height such that the signal is "guided" and does not diverge with vertical distance. This can provide a short term "up-fade" to the signal. Where the direct signal interacts with any ground reflection this can also cause signal cancellation resulting in a reduction in signal strength at the antenna. This is a particular problem for high availability microwave links over water and can only be mitigated using antenna / path diversity techniques.

It would be useful to consider this type of anomalous propagation where interference between co-frequency networks could occur. (This problem does occur for terrestrial television between continental Europe and the south east of the UK).

2.8 The Doppler shift

Any movement of either, the transmitter, receiver or the elements responsible for multi-path in the environment will introduce Doppler shift to the signal and / or its components. Where the movement is shortening the path, the Doppler shift will be

positive and the frequency of the components will rise. Where the movement is lengthening the path, the Doppler shift will be negative and the frequency of the components will fall. In a cluttered environment both conditions may apply simultaneously if the transmitter and receiver are moving relative to each other.

2.9 Signal time dispersion due to multi-path propagation

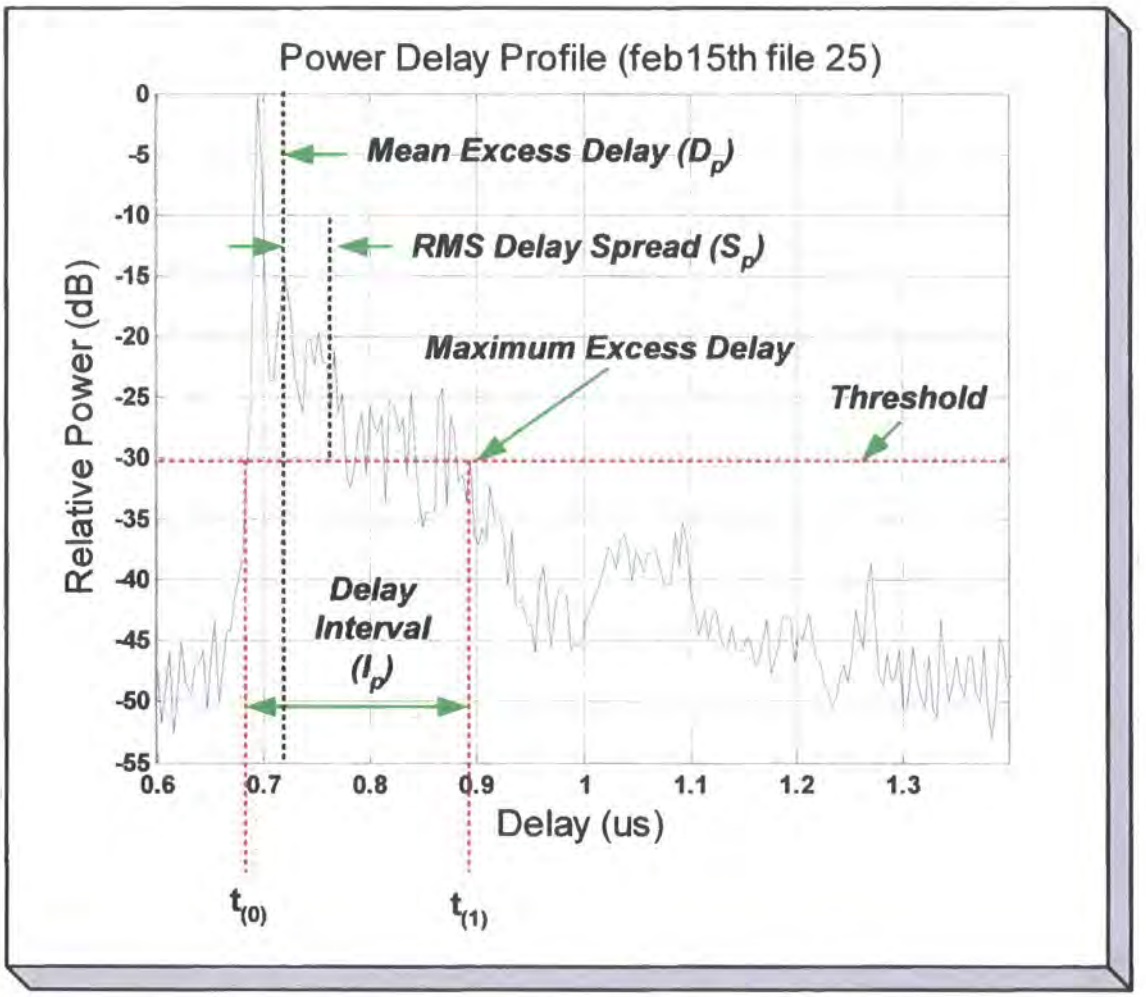

Figure 2.4 The Power Delay Profile

The power delay profile (figure 2.4) is produced from the average of a series of individual channel impulse responses. The profile describes the amplitude of the impulse response as a function of delay time. This corresponds to the relative amplitude and time of arrival of the power contained within the multi-path components.

The power delay profile can be used to determine the degree of time dispersion present in the channel for the measurement location. For the duration of the measurement it is necessary to restrict any shift in position such that only "small scale" fading effects are being observed. Rappaport [2.8] suggests distances of < 2 m for indoor and < 6 m for outdoor measurements in the 450 MHz to 6 GHz frequency range.

The power delay profile can be used to derive parameters which describe the time dispersion characteristics of the channel and that can be used to make informed system design choices. Useful channel descriptors include; the average excess delay, the RMS delay spread and the delay interval. These descriptors are related to a specific range of signal components which are referenced to the peak of the power delay response. The descriptors change as the threshold is reduced (to include more signal components).

The excess delay is defined as the delay present in the signal that is above the propagation delay for the direct signal component. The point at which the power delay profile crosses the threshold is used to define the propagation delay $\{t_{(0)}\}$ for the direct signal component, since this arrives first it represents the component that has the shortest possible path at that power threshold value. The average (mean) calculation is performed up to the point at which the power delay profile finally falls below the threshold value $\{t_{(1)}\}$.

$$D_p = \frac{\int_{t_{(0)}}^{t_{(1)}} tP_{(t)}dt}{\int_{t_{(0)}}^{t_{(1)}} P_{(t)}dt} \qquad (2.8)$$

The RMS delay spread (S_p) is calculated for the excess delay components relative to the mean value.

$$S_p = \sqrt{\frac{\int_{t_{(0)}}^{t_{(1)}} (t-D)^2 P_{(t)}dt}{\int_{t_{(0)}}^{t_{(1)}} P_{(t)}dt}} \qquad (2.9)$$

The delay interval (I_p) represents the time interval from when the power delay profile makes the first transition up through the threshold until it makes the final transition down through the threshold.

$$I_p = (t_{(1)} - t_{(0)}) \qquad (2.10)$$

2.10 References

[2.1] Pattan B.; "Robust Modulation Methods and Smart Antennas in Wireless Communications"; Prentice-Hall 2000; ISBN 0-13-022029-9

[2.2] Parsons J.D.; "The Mobile Radio Propagation Channel"; 2nd Edition; Wiley 2000, ISBN: 0-471-98857-X

[2.3] Tipler A. P., Mosca G.; "Physics for Scientists and Engineers"; 5th Edition, W. H. Freeman and Company 2004; ISBN: 0-7167-4389-2

[2.4] Schwartz M.; "Principles of electrodynamics"; Dover Publications 1987; ISBN: 0486654931

[2.5] Gu M.; "Advanced Optical Imaging Theory"; Springer 2000; ISBN 3540662626

[2.6] Lee W.C.Y. (1983); "Mobile Communications Engineering"; 2nd Edition; McGraw Hill, New York; ISBN: 0-07-037103-2

[2.7] Rogers N.C., Seville A., Richter J., Ndzi D., Savage N., Caldeirinha R.F.S., Shukla A.K., Al-Nuaimi M.O., Craig K., Vilar E., and Austin J.; "A Generic Model of 1-60 GHz Radio Propagation through Vegetation - Final Report"; available from: http://www.ofcom.org.uk/static/archive/ra/topics/research/topics/propagation/vegetation/vegetation-finalreportv1_0.pdf

[2.8] Rappaport T.S.; "Wireless Communications, Principles and Practice"; 2nd Edition, Prentice Hall 2002; ISBN 0-13-042232-0

3.1 Introduction

The characteristics of the radio channel can be explored by sounding the channel. This can provide data from which descriptive parameters such as path loss, multi-path delay and frequency selectivity as a function of location and time may be derived. The data used to characterise the channel can be derived from measurements performed in either the time domain or the frequency domain.

The impulse response of the channel can be directly observed in the time domain using a pulse that has a width which is narrow relative to the delayed echoes within the channel. The frequency transfer characteristic of the channel can be computed from the impulse response using the inverse Fourier transform. Alternatively the frequency transfer characteristic of the channel can be measured in the frequency domain. The impulse response may then be derived from this data using the Fourier transform.

Several approaches to performing frequency domain measurements are presented in this chapter in conjunction with a discussion of several impulse sounding techniques.

The FMCW technique that has been utilised to support this research project is presented in more detail along with the primary functional parameters of the sounder configurations used.

Frequency domain methods

3.1 Stepped Narrow Band CW Measurements

The channel frequency transfer function may be approximated by performing a series of consecutive narrowband CW measurements spaced across the channel.

Matthews and Molkdar [3.1] implemented this approach by stepping across the channel under study in 50 kHz and 200 kHz steps. At the time that this work was performed it was time consuming to step the signal sources and impractical to co-ordinate the

switching at both the transmitter and the receiver. This precluded mobile measurements. Thus no Doppler shift information was recovered and hence no angle of arrival information was derived. Therefore no identification of significant single scatterers was possible.

Subsequently, Purwaha et al [3.2] used a spectrum analyser with an associated down-converter as the receiver to perform swept frequency domain measurements at 59.9 GHz with a sweep width of 100 MHz. In this implementation the generator and the spectrum analyser was incremented in 100 KHz steps and the data from the spectrum analyser was recorded on a laptop via a GPIB link.

3.2 Swept channel measurement using a spectrum analyser as receiver

The real component of the channel frequency transfer characteristic can be obtained directly by exciting the channel and recording the signal available at the receiver using a spectrum analyser with "max-hold" facility.

The channel can be excited with either a PRBS source or from a swept CW source for example from a microwave sweep oscillator. The source is required to have an amplitude that is constant as a function of frequency across the channel. Otherwise some form of "normalisation" is required. The PRBS signal generation method produced a spectrum that exhibits a (sinx)/x envelope which must be equalised to provide a "flat" amplitude characteristic over the channel.

A major disadvantage of this technique is that the measurement time is significant in the range of 10s to 1000s of seconds. Thus the time variant behaviour of the channel cannot usefully be observed. This also precludes mobile measurements. This approach also only provides magnitude information. No phase information is recovered from this type of measurement.

An additional problem is that the measurement records the peak amplitude due to all signals present in the channel. This restricts the use of this technique to channels that do not include interfering signals within the observation bandwidth.

However this technique does not require any synchronisation between the sounder components and can be made to operate over wide channel band-widths.

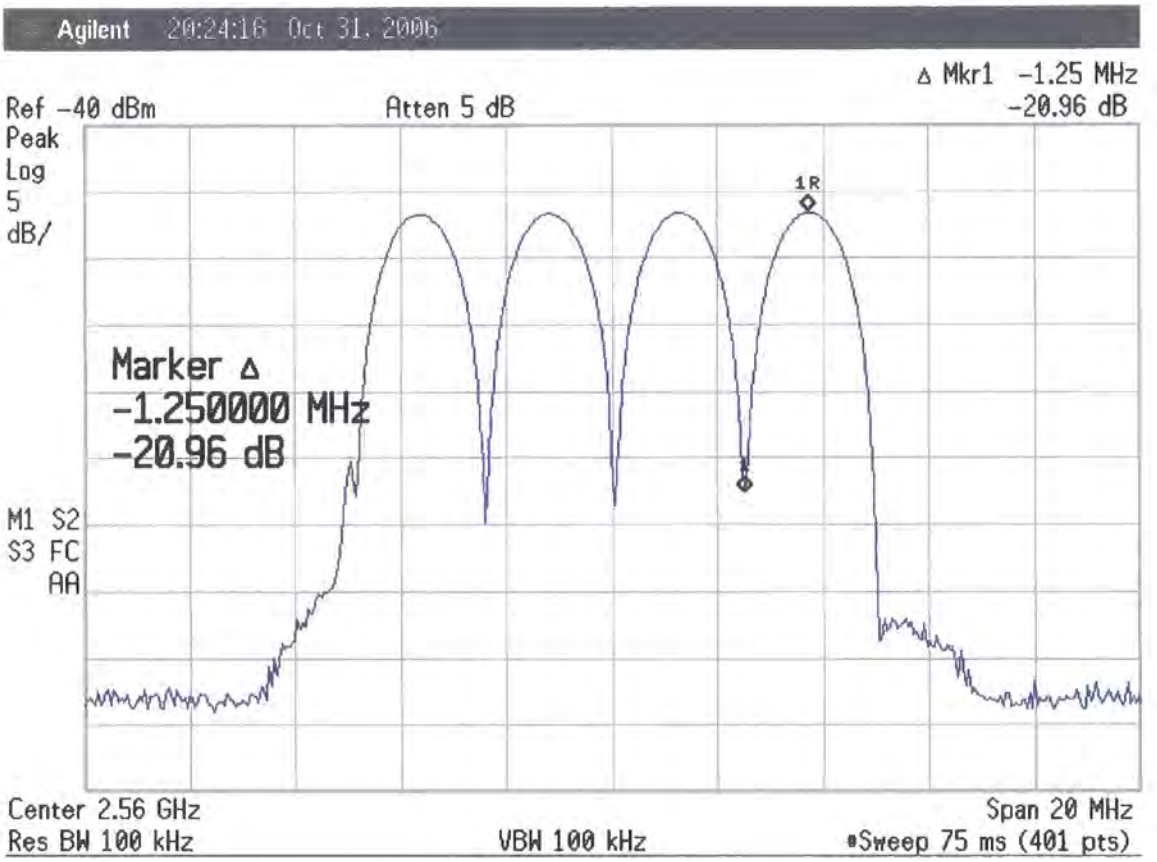

Figure 3.1 Channel transfer function recorded using a spectrum analyser

Figure 3.1 provides an example of a channel transfer function measurement performed with a spectrum analyser. In this case the channel was a two-delay path in coax. Although each individual sweep only takes 75 ms the total time to build up the above display above using the "max hold" function was approximately 60 seconds.

3. 3 Swept channel measurement using a network analyser

The channel frequency transfer characteristic can also be obtained directly using a network analyser. This is not entirely surprising since providing the frequency transfer characteristic of a network is exactly what the network analyser is intended to do!

Two forms of network analysers are in general use, the scalar analyser and the vector analyser. For both types of system, the recording display and the frequency of the source need to be synchronised. This technique is therefore most applicable to moderate distances between the transmitter and the receiver since interconnection between the transmitter and the receiver is necessary.

The scalar network analyser uses a swept source to excite the network (channel) in conjunction with a broadband power detector as the sensing element (receiver). This type of system can provide sampling at up to ~ 20 sweeps per second and is capable of operating over a very wide range of frequencies (limited only to the frequency range of the available sources and detectors). Since the detector does not have frequency selectivity (to reduce the detection bandwidth) and has a limited peak signal capacity the dynamic range for directly utilising the scalar analyser is limited to approximately 80 dB (-60 to +20 dBm). As the detector operates on the envelope of the signal receiver this type of network analyser does not provide phase information and is not therefore able to provide Doppler information. The scalar analyser detector does not provide any discrimination against interference. It can only be used therefore in scenarios where the only signals present within the detection band have been generated to facilitate the measurement. The primary advantage of the scalar network analyser is that only one signal is required to be passed between the transmitter and the receiver. This is the sweep input to the transmitter from the scalar processing display. This is a low bandwidth, low frequency signal and can be transferred over significant distances using coax. (In principle this signal could be derived using two rubidium stabilised references as has been used in the FMCW chirp sounder). This type of equipment is frequently used to investigate the frequency selective and spatial behaviour of antennas.

The vector analyser makes use of coherent sampling of the signal at the receiver. This sampling system facilitates a reduction in processing bandwidth as well as recovery of the phase relationship between the transmitted and received signals. A dynamic range of up to 110 dB can be achieved for narrow IF bandwidths. While it is possible to recover the phase relationship between the transmitter and the receiver, the Doppler that may be observed is restricted to ½ of the sweep repetition rate which is typically less than 10 sweeps / second. The main limitation in using the vector analyser to perform channel sounding is that a sample of the transmit signal is required at the network analyser processor to provide the reference for phase and frequency tracking. This signal is at the operating frequency and thus it becomes difficult to extend the separation between the transmitter and the receiver.

The network analyser approach does however represent a practical method of sounding an ultra wideband channel for a static environment where some form of interconnection is practical between the transmitter and the receiver.

Nobels et al [3.3] used a vector network analyser to make indoor measurements at 2 GHz, 5 GHz and 17 GHz with a bandwidth of 500 MHz. The measurement distance was limited to 25 m due to the transmitter to receiver interconnection cable. The impulse response was computed by performing an inverse Fourier transform on the frequency domain data. The results claimed a time domain resolution of 1 ns based on the use of a 1024 point FFT. Thus appears erroneous since the sweep bandwidth was only 500 MHz. The results and analysis presented show a decrease in the RMS delay spread as a function of frequency.

Yang et al [3.4] used a vector network analyser to perform indoor measurements at 57 GHz to 61 GHz. Transmission measurements (S21) were made and the impulse response was then derived by performing the inverse Fourier transform of the frequency domain data.

Time domain based channel sounding

3.4 Periodic pulse sounding measurements

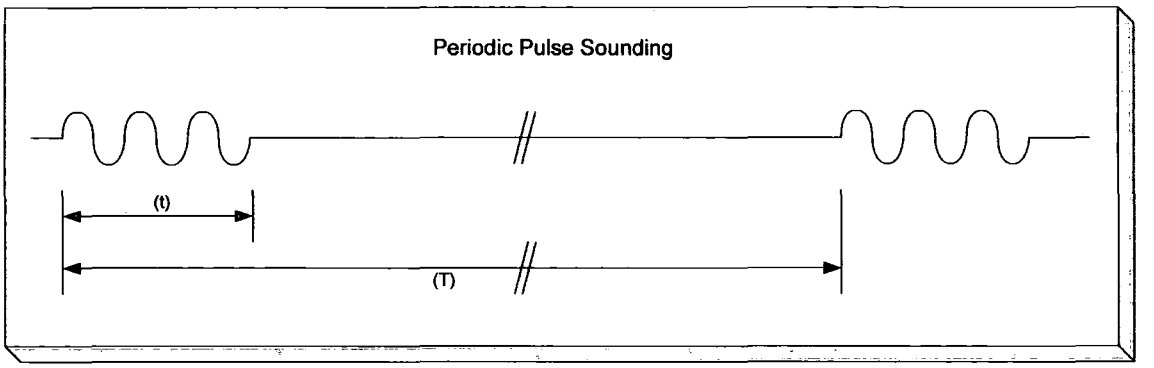

Figure 3.2 Periodic Pulse Sounding

In the periodic pulse sounding technique, the channel is excited using a short duration RF pulse (an approximation to the Dirac delta function). The pulse is repeated on a regular basis with a pulse separation that is sufficient to allow all the echo components to be recorded before the next channel excitation pulse. However the pulse repetition rate needs to be sufficiently high to allow the time variant behaviour of the channel to be observed. The bandwidth requirements of the receiver and any data acquisition are inversely proportional to the duration of the pulse.

Refer to figure 3.2. The pulse duration (t) determines the range resolution. The pulse repetition interval (T) determines the range of delays which can be unambiguously resolved. The PRF = 1/T. The observable Doppler shift is limited to ½ of the channel sampling rate. This is the PRF / 2.

This approach was employed by Young and Lacy [3.5] at 450 MHz with a spatial resolution of 150m. This utilised a 0.5 us duration pulse. Other studies have been performed with shorter pulses (down to 50ns) [3.6] and at higher frequencies (up to 2920 MHz) [3.7].

To provide useful spatial discrimination and moderate delay range, the duty cycle of the transmitter is low (the ratio of t/T). The receiver and data acquisition systems need sufficient bandwidth (> 1/t) to accommodate the narrow pulse (t). This requires a wide bandwidth which reduces the available signal to noise ratio at the receiver. To compensate for the low duty cycle, a high peak power is required to couple sufficient energy into the channel to maintain usable signal to noise ratio. This has implications for the generation of the RF power at the transmitter and control of interference to other users of the radio channel resource.

Pulse compression

The peak power problem can be mitigated using pulse compression techniques at the transmitter. Here we consider spreading the transmitter power across a range of frequencies as a function of time. This can either be implemented by modulating the carrier with a pseudo-noise sequence (PRBS) or by explicitly sweeping the transmitter across a band of frequencies (FMCW). In both approaches the average power transmitted is constant.

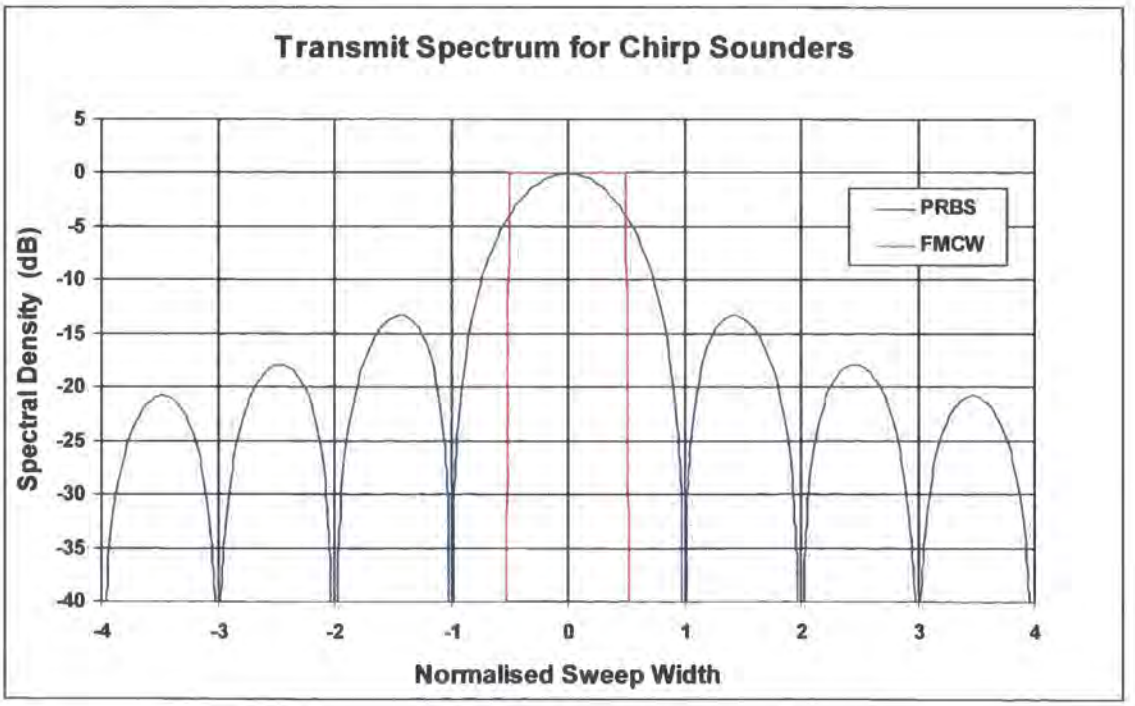

Figure 3.3 Unfiltered RF Spectrum of Pulse Compression Transmitters

The unfiltered RF spectrum for the PRBS and FMCW transmitters are shown in figure 3.3. If it is necessary to restrict the out-of band transmission of the PRBS sounder the signal can be filtered since the output spectrum will have a (sinx)/x distribution. Practically, the spectrum filtering may be implemented using a low-pass structure prior to the modulator or as a band-pass filter at the carrier frequency. However, introducing band limiting requires that the operating power level of the transmitter is reduced to prevent spectrum re-growth. As the excess bandwidth is reduced, the peak to average ratio of the transmit signal increases. For a defined amplifier peak output, the average power of the transmitter needs to be reduced to prevent "clipping".

In comparison, the FMCW spectrum does not require further spectrum shaping to provide band-limiting. The transmit amplitude is constant and therefore the output of the transmitter can be hard limited without introducing additional close-to-band spectral components. The FMCW transmitter can therefore be used with non-linear elements, for example heavily compressed amplifiers and frequency multipliers.

The spatial resolution of the PRBS sounder is defined by the "chip" rate, which is the clock rate for the PRBS sequence. The repeat length of the PRBS sequence defines the maximum unambiguous range that can be resolved.

The spatial resolution of the FMCW sounder is defined by the sweep width. It is however also necessary to include a window function to reduce the level of side-lobes which occur in the FFT process due to "spectral leakage". Spectral leakage is due to the output of the FMCW correlator being discontinuous relative to the sample period. Typically a Hamming window is utilised which expands the width of the main lobe to 1.8 bins at -6dB. The side-lobes in the output frequency (delay) domain are reduced to -43 dB. Other window functions can be used, however this introduces different trade-offs between the side-lobe level and main-lobe width expansion. This is discussed in detail by Harris [3.8]

3.5 Pulse compression transmitter based on the PRBS generator

The PRBS based transmitter uses a "noise like" sequence which modulates a carrier to produce a double-sideband suppressed carrier output. This technique was used by Cox [3.9] to provide wideband (10 MHz) channel stimulus at 910 MHz.

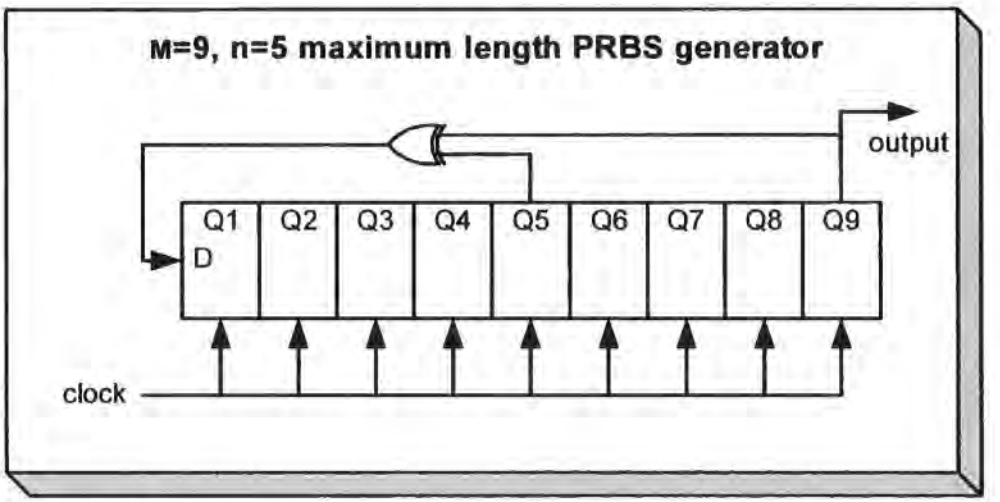

Figure 3.4 Example shift register implementation of a PRBS generator

The "noise like" sequence can be generated using a shift register with feedback from the intermediate register stages to produce a pseudo-random sequence of transitions. The minimum interval between transitions is determined by the shift register clock rate. The maximum length of the sequence is determined by the number of shift register stages and the feedback tap position. For a "maximal length" sequence, the repeat length for a feedback shift-register with "m" stages is 2^m-1. Figure 3.4 depicts a PRBS generator with a repeat length of 511 clock cycles. (Note additional logic to initiate the sequence and to prevent lock-up for the all-zeros state have not been included here for clarity).

3.6 The PRBS receiver

At the receiver it is necessary to recover the signal. This requires de-spreading of the signal.

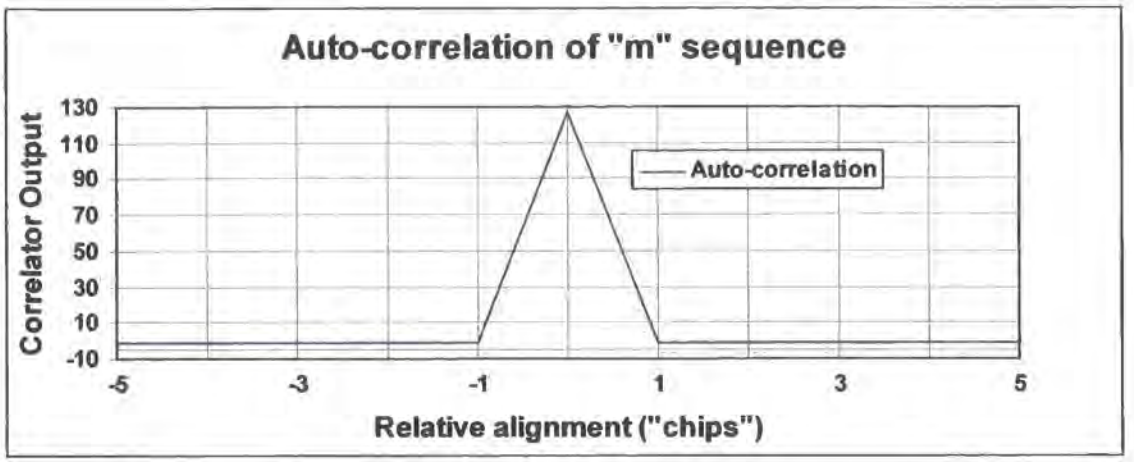

Figure 3.4 Example cross-correlation from two 127 state "m" sequences

The de-spreading is based on the cross-correlation between the transmitted signal and a delayed replica of the transmit sequence. When the two sequences are aligned a signal maximum occurs. For all other alignment a minimum signal is produced from the correlator. (refer to figure 3.4). The "chip" time is the clock period of the PRBS sequence.

The amplitude of the echoes in the channel at a particular delay time can be evaluated by adjusting the relative time position of the receiver correlation signal.

The correlation may be implemented in software or hardware. For a software implementation it is necessary to record the output of the channel before de-spreading. This approach has been used in the "Propsound" equipment available from Electrobit [3.10]. This has the advantage that all the channel information is available for subsequent off-line processing. However, the data acquisition and storage system needs to operate at the Nyquist sampling rate of the channel, > twice the channel width.

A parallel correlator can also be implemented using large-scale digital integration. In this approach the multiple individual correlators are operated with each separated by individual clock intervals along the "m" sequence. This approach is used to speed up sequence acquisition in direct sequence spread spectrum systems in particular GPS. However no channel sounder example has been found in the literature.

Most researchers appear instead to have implemented a "swept time-delay" cross-correlation (STDC) technique. This uses a single correlator at the receiver which then needs to be shifted in time This approach was pioneered by Cox [3.9]. In this implementation the transmitter and receiver PRBS "m" sequences were clocked at a slightly different rate. Cox used clocks of 10 MHz and 9.998 MHz to clock 511 state sequences in his equipment. This causes the two sequences to drift past each other at a pre-determined rate which allows all possible time-alignments between the two sequences to be explored. The time scaling reduces the bandwidth of the output signal which simplifies the data acquisition and storage requirements. For this example, the maximum signal bandwidth is now 2 kHz which requires a minimum sample rate of 4 ksamples / sec. However, the time to probe the channel is also increased. This imposes a restriction on the channel sampling rate and therefore the maximum observable Doppler frequency. Cox restricted the range of observable delays to 15 us instead of 51.1 us by resetting the receiver correlator every 75 us. This improved the channel sample rate to 13.3 Hz. This provided an observable Doppler frequency range of +/- 6 Hz.

To recover the complex impulse response of the channel phase information is derived by performing quadrature sampling. This requires two channels of measurement "I" and "Q" from which both the magnitude and phase information can be derived:

$$\text{Amplitude, } A = \sqrt{I^2 + Q^2} \qquad (3.1)$$

$$\text{Phase, } \Phi = \tan^{-1}\left(\frac{Q}{I}\right) \qquad (3.2)$$

The PRBS transmitter and STDC technique has been used at a variety of frequencies.

Nche et al [3.11] used this technique to perform soundings with a 30 MHz bandwidth at 1.8GHz. Smithson [3.12] and Glover [3.13] produced a sounder for operation at 2 and 5 GHz. This sounder was reported to have a time resolution of 10 ns with a measurement time of 5 ms. Mohamed et al [3.14] have reported this technique at 62.5 GHz. This system operated with a PRBS clock rate of 1.2 GHz to provide a theoretical resolution

of 25 cm. The sequence length was 127 giving a maximum delay range of 105.8 ns (31.75 m). However the results presented demonstrated only 20 dB of signal to noise ratio.

Finally, the matched filter can be implemented using a series of delayed versions of the received signal that are then combined with appropriate weighting. This can by implemented using a SAW filter. This technique was used by Bajwa and Parsons [3.15] to evaluate multi-path behaviour at 436 MHz. However the practical manufacturing limits for the SAW filter introduce limits to the degree of correlation that can be achieved. These correlation impairments provide a limit to the instantaneous dynamic range and also introduce side lobes which appear on the correlated signal at the output.

3.7 The FMCW channel sounding technique

The FMCW sounder is based on a frequency "chirp" which is used to probe the channel. The chirp is a linear change in frequency over a bandwidth of B Hz in time T sec. The sense of the frequency sweep can be positive (frequency increasing with time) or negative (frequency decreasing with time). In practice both senses are used within this project due to frequency inversion which occurs in the frequency converters. The base channel sounder has a negative sense. This is inverted by the up-converter so that the transmitted signal has a positive sweep. This is then converted back to a negative sense sweep by the down-converter.

The chirp has been produced using a direct digital frequency synthesiser (DDFS) and up-converter as shown in figure 3.5. This uses a clock rate of 1.6 GHz and is capable of providing a maximum output frequency of 390 MHz. The output from the DDFS is up-converted to the 2 GHz band using a heterodyne mixer. The local oscillator is derived from a synthesiser. A band-pass filter at the output is used to select the lower sideband and to provide rejection of the local oscillator leakage signal. The filter rejection characteristic requires that the minimum input frequency to the base sounder IF up-converter is 130 MHz. Thus the practical maximum chirp bandwidth is 260 MHz.

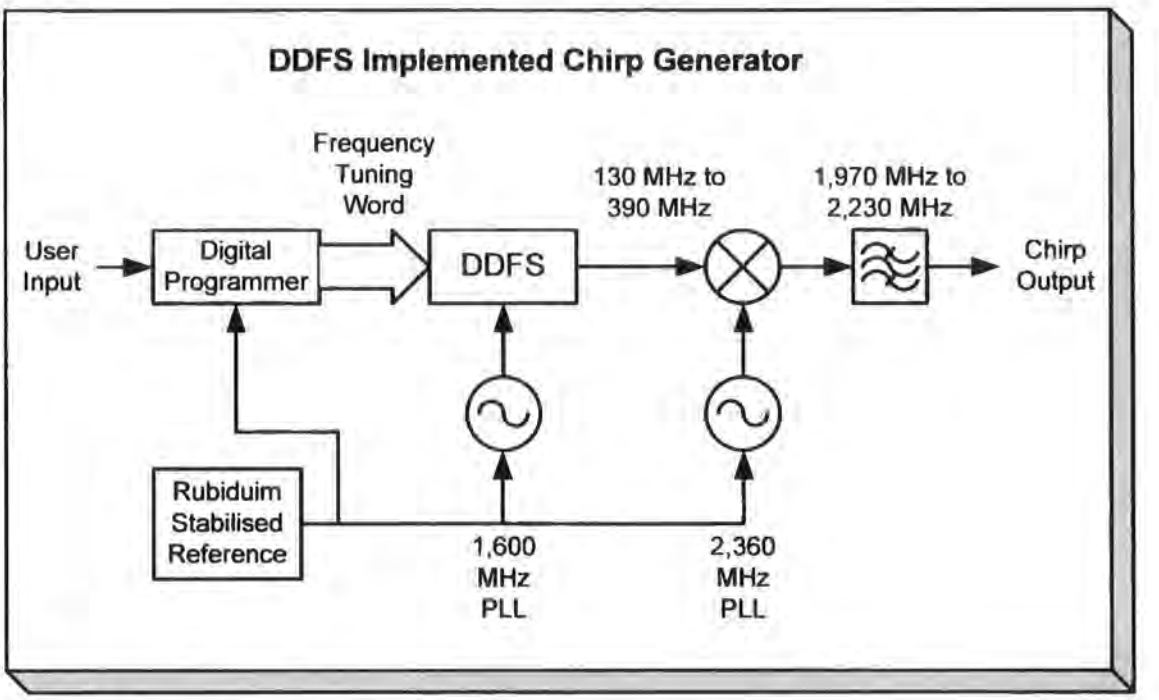

Figure 3.5 Chirp source and heterodyne up-converter

The chirp waveform is produced by incrementing the DDFS in equal steps across the frequency band. The frequency tuning input to the DDFS is provided using a frequency accumulator. Salous and Green [3.16] have demonstrated that the update rate of the frequency accumulator can be much lower than the clock rate of the DDFS.

Salous and Green [3.16] demonstrate that the staircase approximation to the sweep introduces side-bands that are spaced either side of the instantaneous sweep signal which are separated by +/- 1/(increment rate). These sidebands are due to the phase offset between the steps relative to a contiguous linear sweep. This provides frequency modulation with a low modulation index. The relative amplitude of the sidebands is a function of the phase error. The phase error is proportional to the frequency increment and duration between increments.

The DDFS used in the sounder has demonstrated a maximum frequency tuning update rate of 1.25 MHz. Thus any spurious sidebands produced therefore occur at +/- 1.25 MHz. This is outside the bandwidth of the signal conditioning and data acquisition system (30 kHz to 250 kHz).

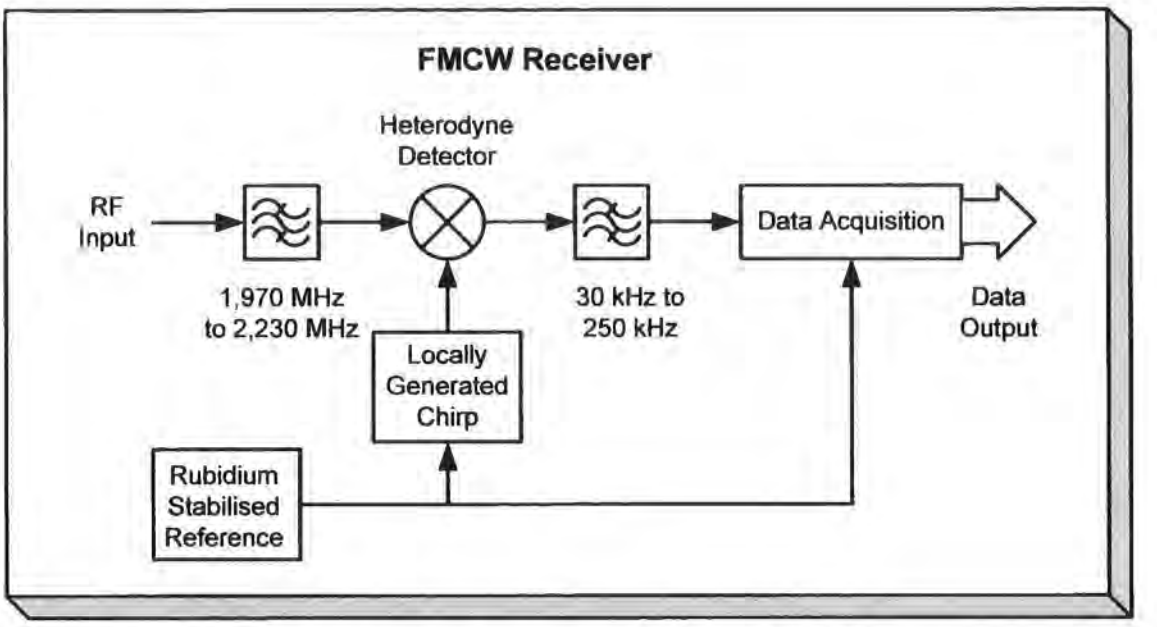

Figure 3.6 FMCW Receiver implemented with a heterodyne detector

The FMCW receiver (refer to figure 3.6) is implemented using a heterodyne detector which is used to provide compression of the bandwidth of the receive signal. The heterodyne detector correlates the received signal with a locally generated chirp signal that has the same characteristics as the transmitted chirp signal. The output from the heterodyne detector is the difference in frequency between the locally generated sweep and the receive signal. The receive signal is constructed from all the possible components from the transmitted signal with their individual propagation delays. The lower usable frequency limit of the output from the heterodyne detector is limited by the requirement to introduce an explicit high pass function to attenuate the sweep repetition waveform. The upper usable frequency limit for the output of the heterodyne detector is imposed by the need to provide attenuation of frequencies which would be aliased due to the sampling processes in the data acquisition system. The usable range of signals here are 30 kHz to 250 kHz. This supports a sweep repetition rate of up to 250 sweeps per second and a sample rate of 1 Msample per second. This also provides a minimum of four samples per period at the maximum beat frequency. This allows amplitude and phase information to be extracted from a single sampled channel (no quadrature detection requirement).

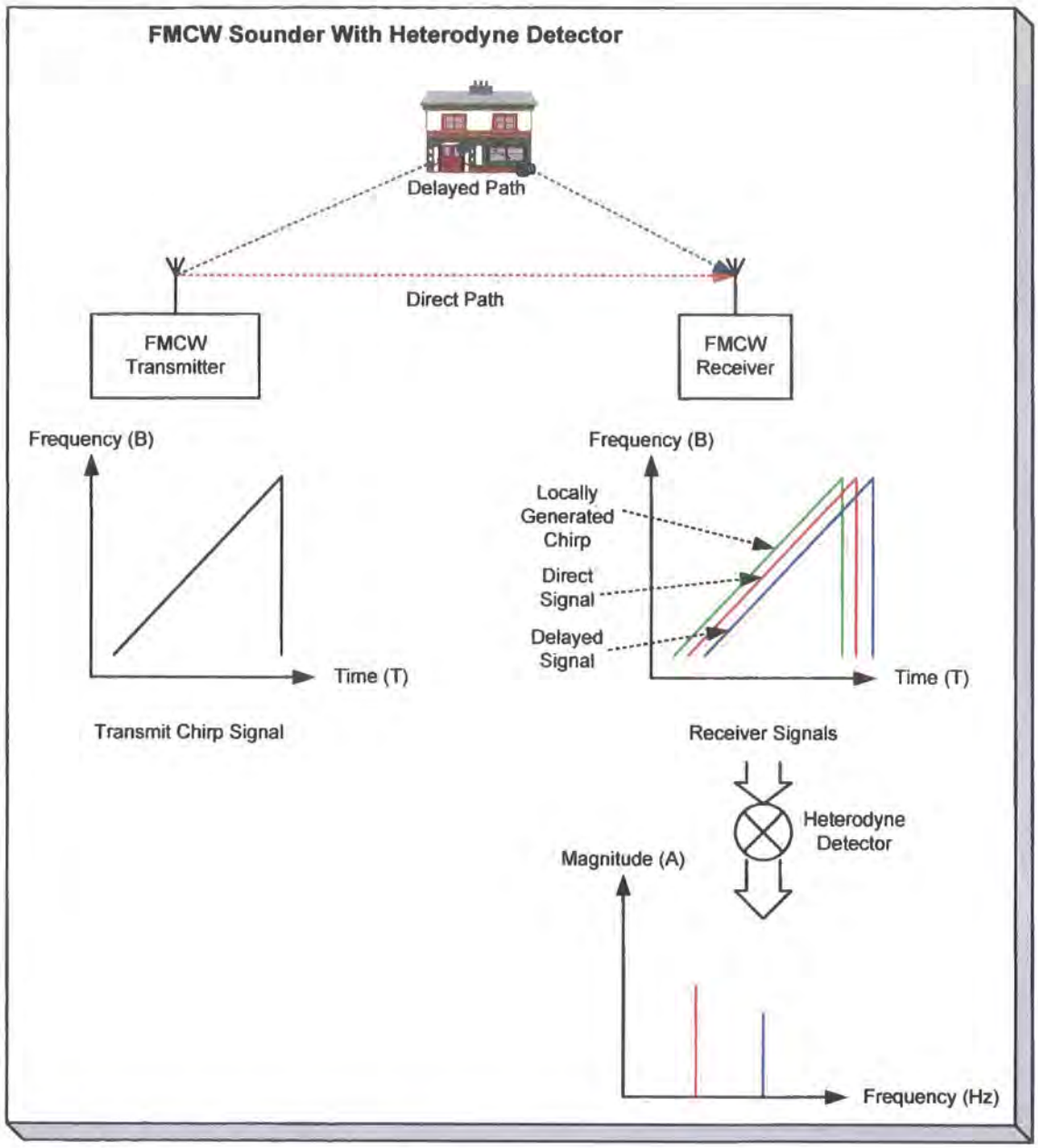

Figure 3.7 FMCW sounder principle

With the receive sweep aligned to the transmit sweep, the output frequency (as shown in figure 3.7) of the heterodyne detector is proportional to the propagation delay time (τ) of the individual multi-path components and the sweep rate (B Hz in T seconds).

Beat frequency $$f_b = \tau\left(\frac{B}{T}\right) \quad (3.3)$$

The amplitude of the beat is directly proportional to the amplitude of the multi-path component at that propagation delay.

For a fixed range of beat frequencies it can be seen that the range of delays that can be instantaneously observed is inversely proportional to the sweep rate. This provides limits to the range of propagation distances that can be observed within the power delay window. For the output range of 30 kHz to 250 kHz from the heterodyne detector, this is summarised in table 3.1 below.

SRF (Hz)	ΔF (MHz)	Sweep Rate (GHz/sec)	τ_{min}	τ_{max}	Δτ	Δ (m)
250	10	2.5	12 us	100 us	88 us	2640
250	150	37.5	0.8 us	6.67 us	5.87 us	1760
250	260	65	0.46 us	3.85 us	3.39 us	1015
250	1040	260	115 ns	962 ns	846 ns	253

Table 3.1 Instantaneous observable delay range and corresponding path lengths

The Doppler frequency range is determined by the rate at which the channel is sampled. For the FMCW sounder the channel is sampled at the sweep repetition frequency (SRF). With an SRF of 250 Hz the unambiguous Doppler frequency range is +/- 125 Hz.

The velocity (v) that produces a Doppler shift (F) at carrier frequency (f) is:

$$\upsilon = c\frac{F}{f} \text{ (m/s)} \qquad (3.4)$$

The frequency specific parameters of the channel sounders developed to support this research program are depicted in table 3.2. Note that as the processing bandwidth is constant for all versions of the sounders, variations in the noise floor are determined by the down-converter noise figure.

Parameter	2.5 GHz	3.5 GHz	5.7 GHz	61 GHz
Transmit power	+20 dBm	+20 dBm	+20 dBm	+7 dBm
Noise Floor	-141 dBm	-143 dBm	-143 dBm	-133 dBm
System Gain	161 dB	163 dB	163 dB	140 dB
Dynamic Range at -90 dBm	>40 dB	>40 dB	>40 dB	>30 dB (1)
Sweep Repetition Frequency	250 Hz	250 Hz	250 Hz	250 Hz
Doppler range	+/- 125 Hz	+/- 125 Hz	+/- 125 Hz	+/-125 Hz
Velocity	15 m/s	11.2 m/s	6.7 m/s	0.6 m/s
Velocity	54 km/hr	40 km/hr	24 km/hr	2.1 km/hr

Table 3.2 Frequency Dependent Sounder Parameters

(1) The value reported here is based on the homodyne calibration measurements reported in chapter 5. The data set used in chapter 6 used an alternative configuration which exhibits close-in spurious which restricts the dynamic range to approximately 20 dB.

3.8 References

[3.1] Matthews, P.A. and Molkdar D; "Wideband Measurements of the UHF Mobile Radio Channels"; IEE conference publication 274, 1987, part 2, pp 73 to 76

[3.2] J. Purwaha, A. Mank, D. Matic, K. Witrisal, and R. Prasad; "Wide-band Channel Measurements at 60 GHz in Indoor Environments"; in Proc. IEEE Benelux 6th Symposium on Vehicular Technology and Communications, Brussels, Belgium, Oct. 1998

[3.3] P. Nobles, D. Ashworth, and F. Halsall; "Indoor Radiowave Propagation Measurements at Frequencies up to 20 GHz"; In Proceedings 44th IEEE Vehicular Technology Conference, June 1994.

[3.4] H. Yang, M.H.A.J. Herben and P.F.M. Smulders; "Channel Measurement and Analysis for the 60 GHz Radio in a Reflective Environment"; Proc. WPMC 2005, Vol. 1, pp. 475-478, Sept. 2005.

[3.5] Young W R and Lacy L Y; (1950); " Echos in Transmission at 450 MHz from Land-to-Car Radio Units"; Proceedings of the IRE, No 38, pages 255 to 258

[3.6] Turin G.L., Clapp F.D., Johnston T L, Fine S B and Lavery D A; (1972); "Statistical Model of Urban Multipath Propagation"; in IEEE Trans, VT21(1), pages 1 to 9

[3.7] Van Rees J.; (1986); "Measurements of the Wideband Radio Channel Characterisation for Rural, Residential and Suburban Areas"; IEEE Trans, VT36(1), pages 2 to 6

[3.8] F. J. Harris; "On the Use of Windows for Harmonic Analysis with the Discrete Fourier Transform"; Proceedings of the IEEE, vol 66, No 1, January 1978.

[3.9] Cox D.C.; (1972); "Delay Doppler Characterisation of Multipath Propagation at 910 MHz in a Suburban Mobile Radio Environment"; IEEE Transactions, AP-20, No5, pages 625 to 635

[3.10] Electrobit "Propsim CS"; information available at: http://www.propsim.com

[3.11] Nche C, Turkmani A.M.D, Arowojolu A.A; "Channel Sounder for PCN Networks"; in "High Bit Rate UHF / SHF Channel Sounders – Technology and Measurement"; 3rd December 1993, IEE Digest No: 1993/233.

[3.12] Smithson A G; "Wide Area Radio Channel Modelling Across The Indoor / Outdoor Interface"; PhD Thesis, The University of Bath, October 2005

[3.13] Smithson A G and Glover I A; "High Performance Digital Radio Channel Sounder for use at 2 and 5 GHz"; 12th International Conference on Antennas and Propagation (ICAP 2003), (CP491), p. 805 -808, Exeter, UK, 31st March to 3rd April 2003 , ISBN: 0 85296 752 7

[3.14] Mohamed S.A, McKeown J.H.A, DaCosta F, Coote F.D.G; "Indoor Channel Sounding Measurements at Millimetre Wave Frequencies"; in "High Bit Rate UHF / SHF Channel Sounders – Technology and Measurement" 3rd December 1993, IEE Digest No: 1993/233.

[3.15] Bajwa A.S. and Parsons J.D.; (1982); "Small-area Characterisation of UHF Urban and Suburban Mobile Radio Propagation"; Proceedings of the IEE Part F, 129(2), pages 102 to 109

[3.16] Salous S. and Green P.R.; "A Novel Chirp Generator Using a Dual Clock Field Programmable Gate Array Architecture"; IEE "HF Radio Systems and Techniques", July 4th to 7th 1994, Conference publication No 392.

Chapter 4

Description of the new experimental hardware

4.0 Introduction

Three configurations of channel sounder have been explored within this research project.

- Configuration 1 provides simultaneous operation at three frequencies within the bands 2.3 GHz to 2.7 GHz, 3.3 GHz to 4.5 GHz and 4.5 GHz to 6.0 GHz.
- Configuration 2 provides simultaneous operation of four parallel receiver channels within the band 4.5 GHz to 6.0 GHz.
- Configuration 3 provides a single channel sounder that operates within the 60 GHz oxygen absorption band with up to 1 GHz of channel width.

The sounder used in the present study has been designed and implemented to operate in the 2 GHz band with parallel receive channels and transmits an FMCW chirp within the band 1.8 GHz to 2.2 GHz. In this study the original sounder transmitter has provided the IF for the up-converter to move to the higher frequency bands. Similarly the parallel architecture receiver and associated data acquisition system [4.1] are used as the IF for the down-converters for operation at 2.5 GHz, 3.4 GHz and 5.7 GHz. The 60 GHz system further builds on the 5.7 GHz frequency converters. By using frequency multipliers operating from an IF in the 15 GHz band, the sweep bandwidth and carrier frequency are multiplied by four to generate up to ~1 GHz of sweep in the 60 GHz band.

An overview of the equipment arrangement for the three configurations is described in figure 4.1 below.

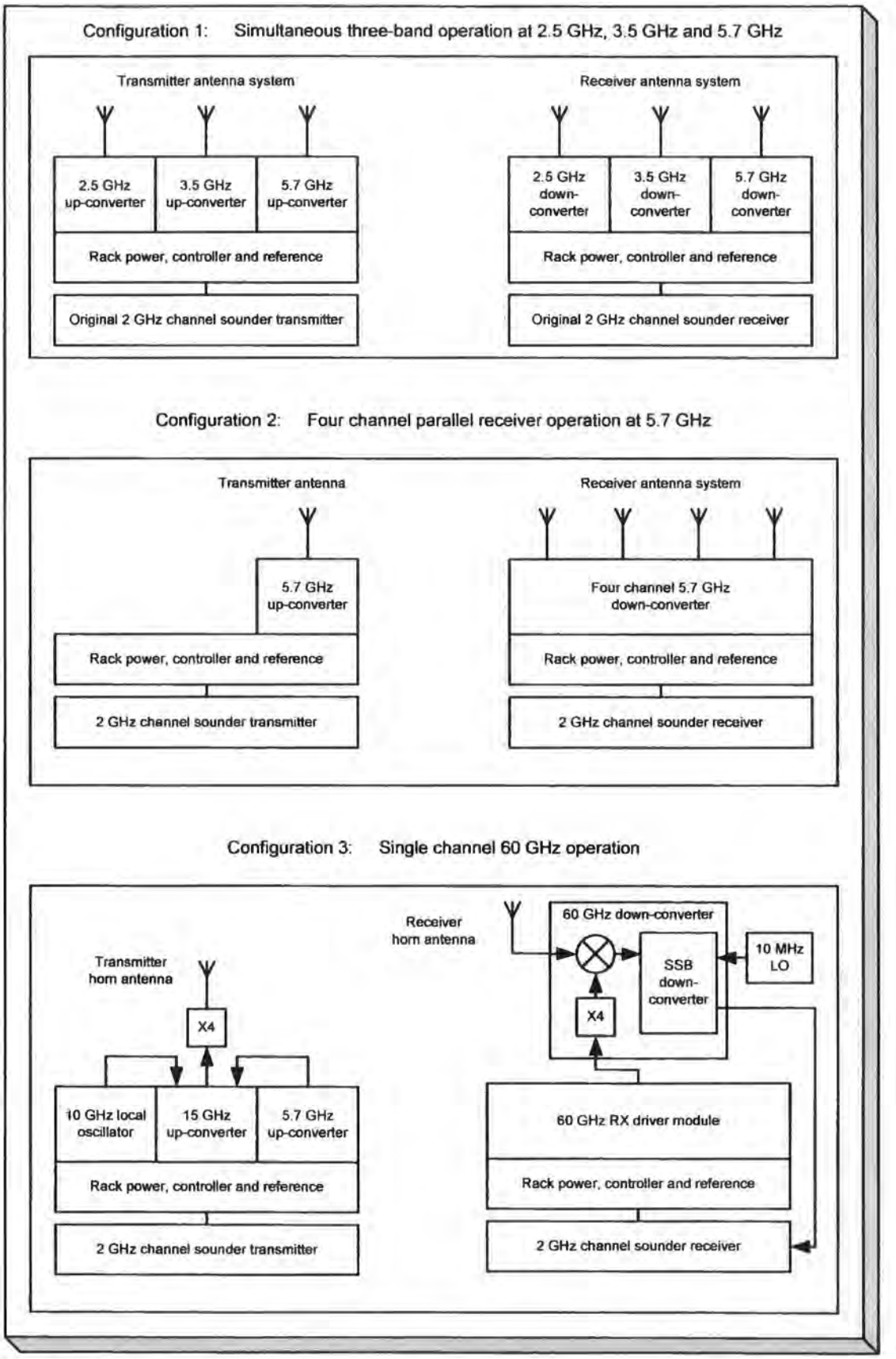

Figure 4.1 Equipment arrangements for different measurement configurations

For all configurations the frequency conversion modules are housed in 3U * 19" rack frames, one for the transmitter and one for the receiver. The final 60 GHz up-converter is housed within a small die-cast enclosure that can be fitted directly to the 60 GHz transmit antenna to minimise transmission losses. The 60 GHz down-converter is similarly housed within a die-cast box to facilitate direct connection to the 60 GHz receive antenna to minimise transmission losses.

Both racks include a module that provides the power supply, 10 MHz reference distribution and programming of the PLL sources. The rack also includes a low phase noise OCXO based 10 MHz reference which can be utilised to provide independent operation. An auxiliary synthesiser output is also included to provide a low phase noise source to the base channel sounder to translate the DDFS signal into the 2 GHz band.

The frequency conversion racks in conjunction with the internal reference have been used for antenna measurements. This mode has also been used to perform simultaneous CW path loss measurements in the 2.5 GHz, 3.4 GHz and 5.7 GHz bands using a spectrum analyser as the receiver IF at 2 GHz.

The auxiliary sources can also be utilised to provide an additional offset between the sweep signals. This can be utilised in the 60 GHz system which uses an IF of approximately 12.5 MHz to minimise the contribution of 1/f noise from the GaAs devices in the 60 GHz receive mixer.

The 5.7 GHz four channel down-converter was used to perform MIMO related research [4.2]. This program also included a configuration providing four receive channels at 2.2 GHz to 2.3 GHz as well as four channels at 5.75 GHz to 5.85 GHz. The base sounder receiver was modified to provide four sweep channels at 2.2 GHz to 2.3 GHz and four channels operating at 2.04 GHz to 2.14 GHz using both the upper and lower sidebands from the DDFS to 2 GHz band conversion. Additional filters for signal generation and processing within the 2.2 GHz to 2.3 GHz and 2.04 GHz to 2.14 GHz bands were also produced. Discone antennas within the band 2.2 GHz to 6.0 GHz were also designed and fabricated to support this work.

In addition to the frequency converter assemblies that have been used to perform channel sounding in the new frequency bands, the following additional work has been completed.

1. Equipment that has been designed and developed specifically to perform the calibration for amplitude and relative phase of an antenna array of up to four elements.

2. A long wheel base landrover has been modified and configured to support mobile measurements. This includes an on-board power supply, equipment racking and pneumatic telescopic mast.

This chapter presents the new equipment and systems in the following sequence:

1. The first section describes the modules that have been designed and assembled to produce the three complete sounder measurement configurations outlined above. This includes the individual converters that are housed in 3U 19" rack modules and the front-end 60 GHz RF assemblies which are mounted with the 60 GHz antennas to minimise signal losses.
2. Section two describes the overall configuration of the sounders for the new bands described above including the new hardware and the base sounder.
3. The individual converters have been fabricated from a range of components and integrated "super-components" that have been specifically designed and implemented. These super-components were produced by identifying the individual circuit elements that were required. These circuit elements were then designed and confirmed individually. An integrated design was then produced from the individual circuit elements. During this phase of the project only one circuit element did not work as initially designed. This was the two stage amplifier (used in the 3.5 / 5.7 GHz up-converters and down-converters) which exhibited a gain peak at the lower end of the band due to excess ground

inductance. This was corrected for use in the integrated design. Section three describes the principal attributes and considerations for these hardware items.

4. During the course of the project some hardware revisions were made due to specific performance issues. Section four reviews and records these aspects of the programme.
5. The development of the 60 GHz system raised the visibility of performance limitations due to the phase noise performance of the base sounder. It was observed that the synthesisers used to perform up-conversion from the output of the DDFS to the 2 GHz band were actually the dominant phase noise source in the 60 GHz system. Section five summarises the system improvement made by changing to the new synthesiser design.
6. Section six documents the new equipment that has been designed to provide the capability to perform antenna array calibration (in conjunction with the frequency converter assemblies) in the new bands (2.5 GHz, 3.5 GHz and 5.7 GHz). The antenna array calibration system is based on a four-channel down-converter based on quadrature mixers to extract both amplitude and phase information. The base measurement system operates at 10 MHz and includes a phase-tracking reference channel to attenuate the phase noise of the microwave sources. This has demonstrated the capability to measure an array of four antennas at 5.7 GHz. This approach has demonstrated an amplitude accuracy of better than 1 dB and a phase accuracy of +/- 1° over a 55 dB dynamic range when used in the 2 GHz band.
7. Section seven describes the survey vehicle. This is based on a long wheelbase Landrover that has been modified and configured to support mobile measurements. This includes equipment racks and power to support the base channel sounder receiver and the receiver frequency extender rack. An 8m telescopic mast is also mounted on the rear of the vehicle.
8. The chapter specific references are included in section eight.

4.1 Frequency converters, racks and other complete modules

The transmit signal up-converters and receiver down-converters are housed in 3 U high rack modules mounted in a 19" rack frame. The 60 GHz radio frequency modules are mounted in die-cast enclosure to allow direct connection to the 60 GHz antennas. A common module provides synthesiser programming, 10 MHz reference distribution and power supply functions is fitted to both racks. These units are identical and can be used to support either the transmitter or receiver converter modules.

4.1.1 Controller / PSU / reference distribution

The racks include a common module shown in figure 4.2. This contains the micro-controller (for programming the PLLs), the main PSU (for +5V, +12 V and +24V), the auxiliary power supply (for -12V) and the 10 MHz reference signal distribution module. This module supports up to three RF modules and an auxiliary synthesiser. There are two unused PLL programming ports which could be used to support other synthesisers if required, for example to replace the 1.6 GHz DDFS clock in the base channel sounder. The module includes a connector to provide access for the flash programmer without disassembling the equipment. This allows code development and up-dating in-situ. A connector has also been included to provide an RS-232 connection to the microcontroller. This feature has been disabled at this time as the on-board RS-232 interface device includes local negative power supply generation using a switched capacitor converter. This was observed to cause a large increase in power supply noise levels which was observed as phase and amplitude disturbances on the RF signals.

The power supply has been assembled from commercial integrated switched-mode converters. The switching frequency of these units is ~350 kHz. Any residual noise due to the switching power supply therefore appears beyond the range of the spectrum used to perform measurements. This power supply was designed to adequately support the sounder work in the sub 6 GHz bands before the 60 GHz version of the sounder was developed.

The 60 GHz sounder introduced several new power supply issues. Firstly a negative supply was required to support the SSB down-converter. It was then decided to use the negative supply for a very low noise op-amp in the synthesiser loop filter. In addition the 60 GHz multiplier modules and the microwave amplifiers used in the multiplier drivers introduced additional current load. This problem was addressed by providing local regulation of the input 24V supply for the external 60 GHz assemblies and for the microwave amplifiers used in the second RF up-converters (5 GHz to 15 GHz).

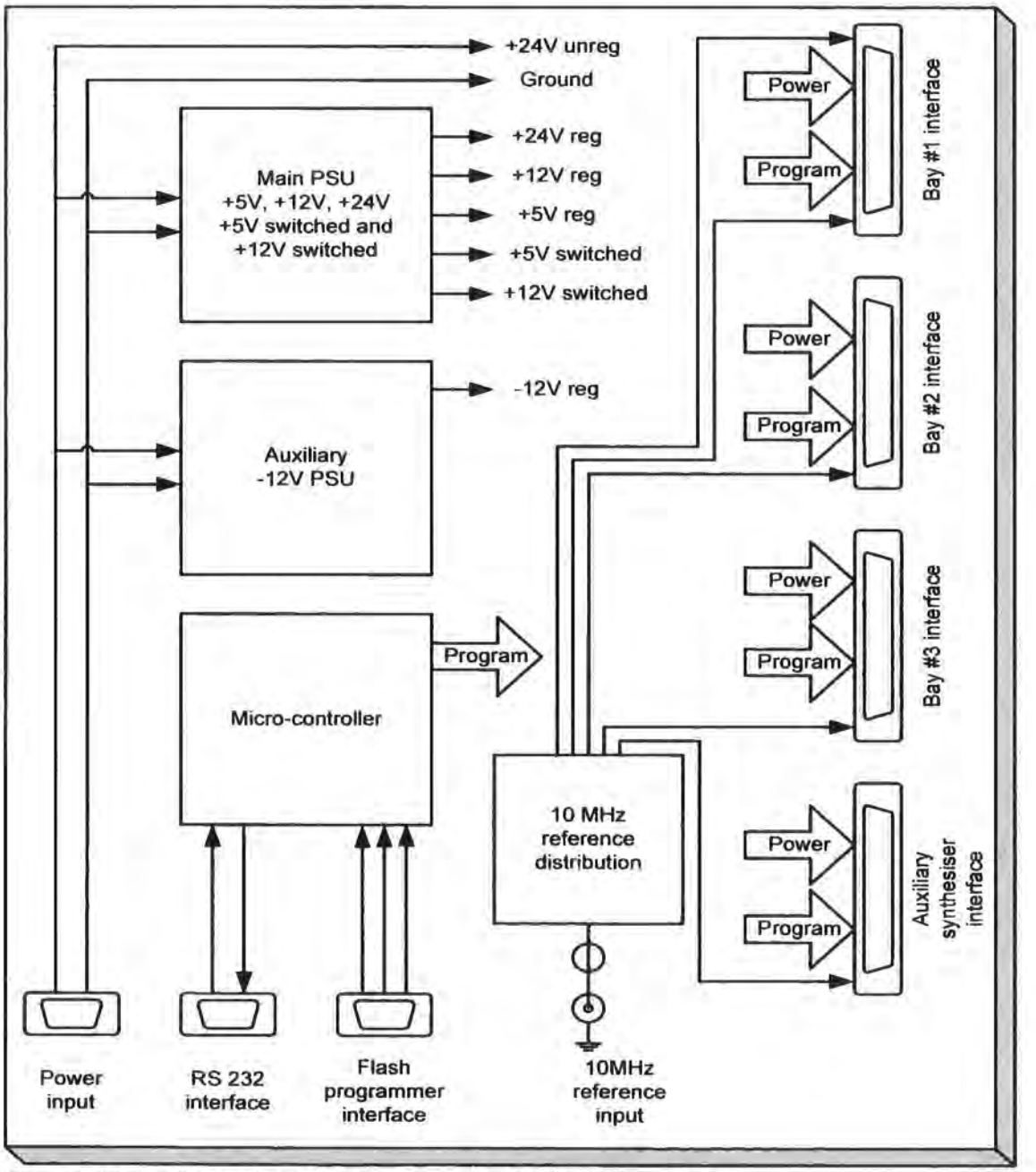

Figure 4.2 Control, PSU and reference distribution module

All three bays use an identical connection assembly (refer to figure 4.3). This eliminates the possibility of damage should any of the cable assemblies be incorrectly configured.

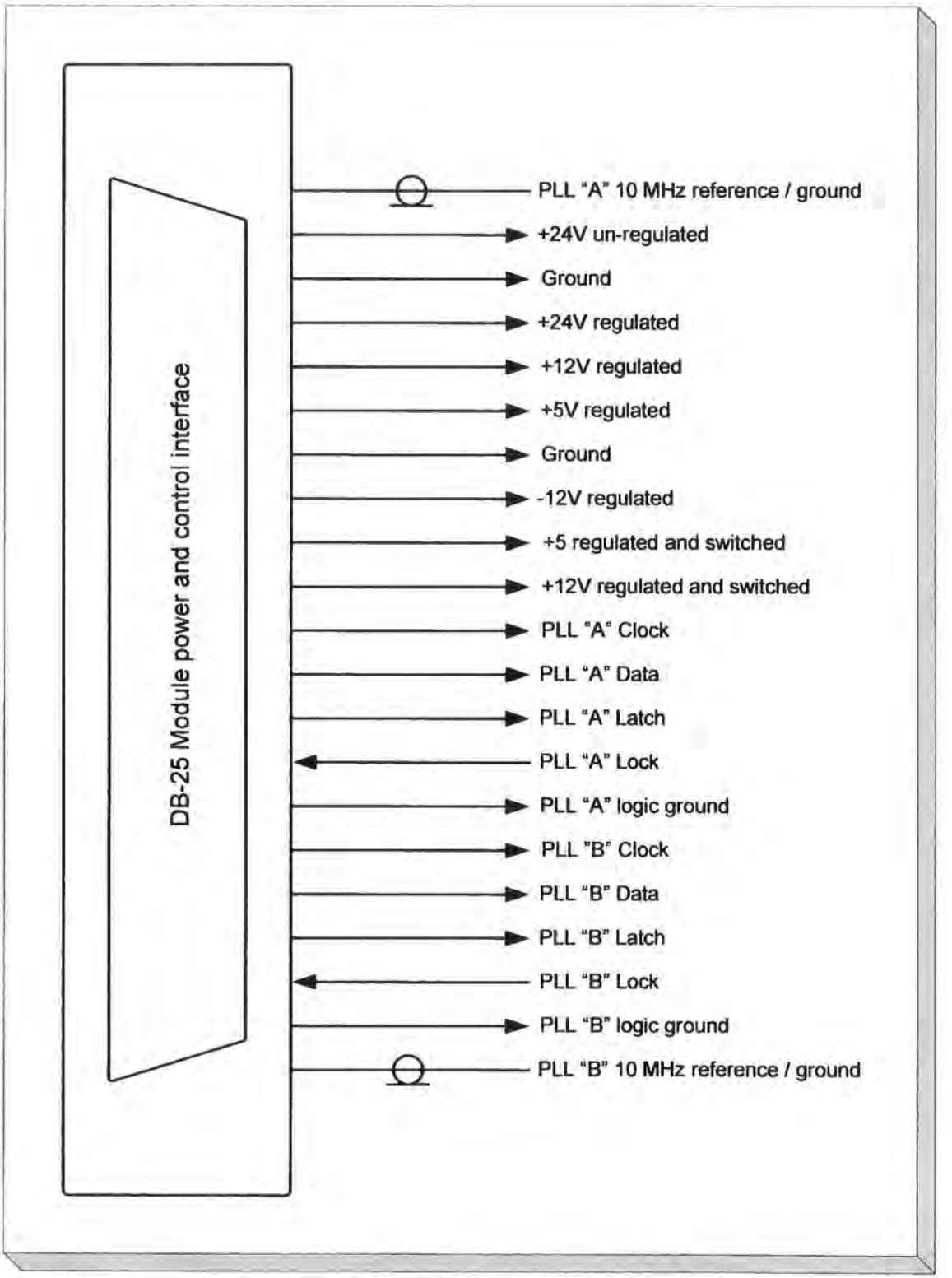

Figure 4.3 Module interconnection assignment

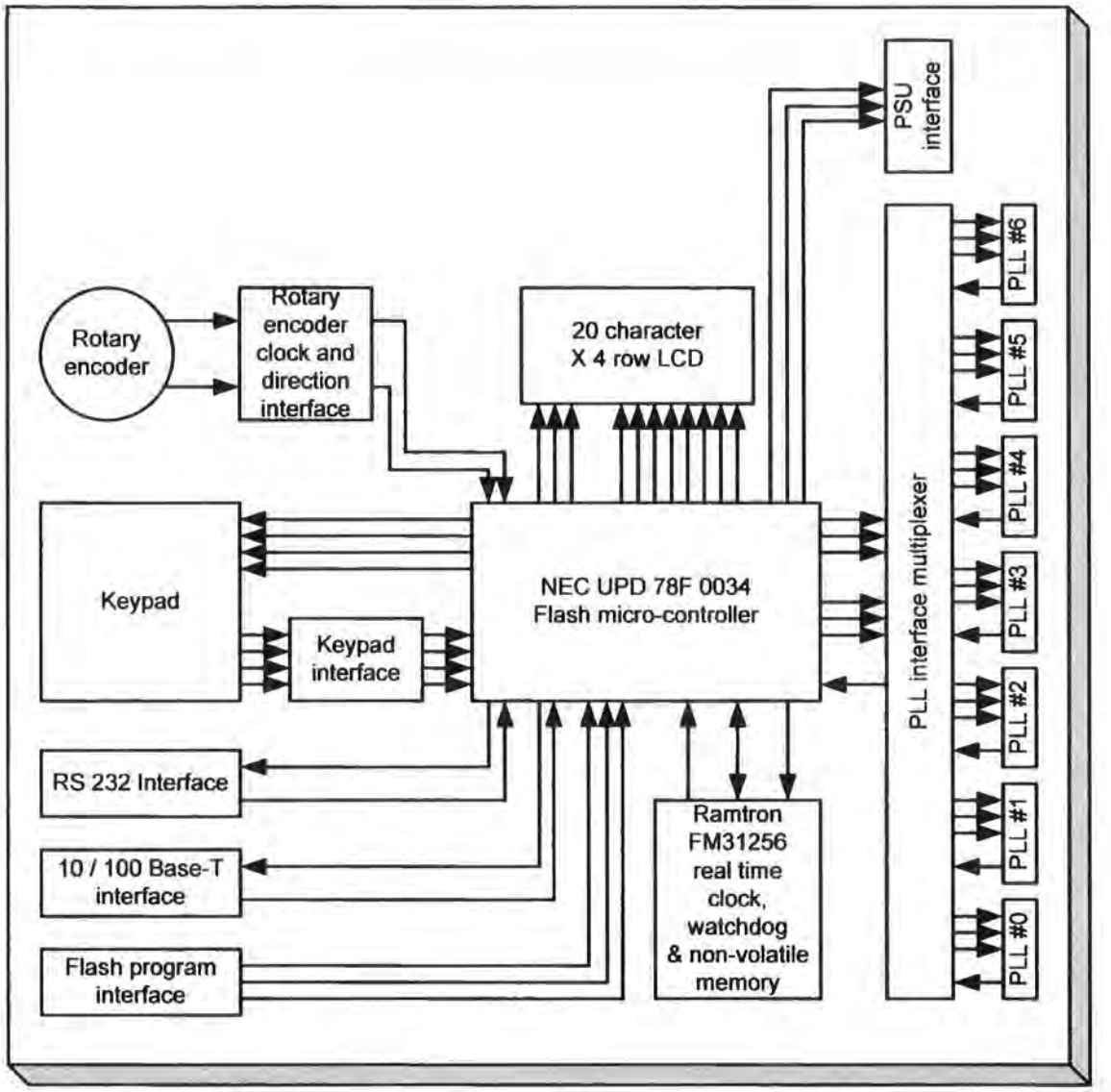

Figure 4.4 Micro-controller

The micro-controller system (depicted in figure 4.4) provides the programming of up to seven PLLs. Each PLL also includes a lock-state indicator to provide feedback to confirm correct operation of the synthesisers. The micro-controller includes an interface to an LCD to provide feedback to the operator. This is used to provide text confirming the basic frequency converter operational parameters at this time. A keypad and rotary encoder are also used as operator input devices. Both of these input devices have been confirmed to operate at the hardware level but have not been accommodated within the software at this time. The micro-controller also provides three logic level signals which are used to switch +5V and +12V supplies to the RF bays. This allows the transmitters to be "muted" until the synthesisers are locked.

4.1.2 2.5 GHz up-converter assembly

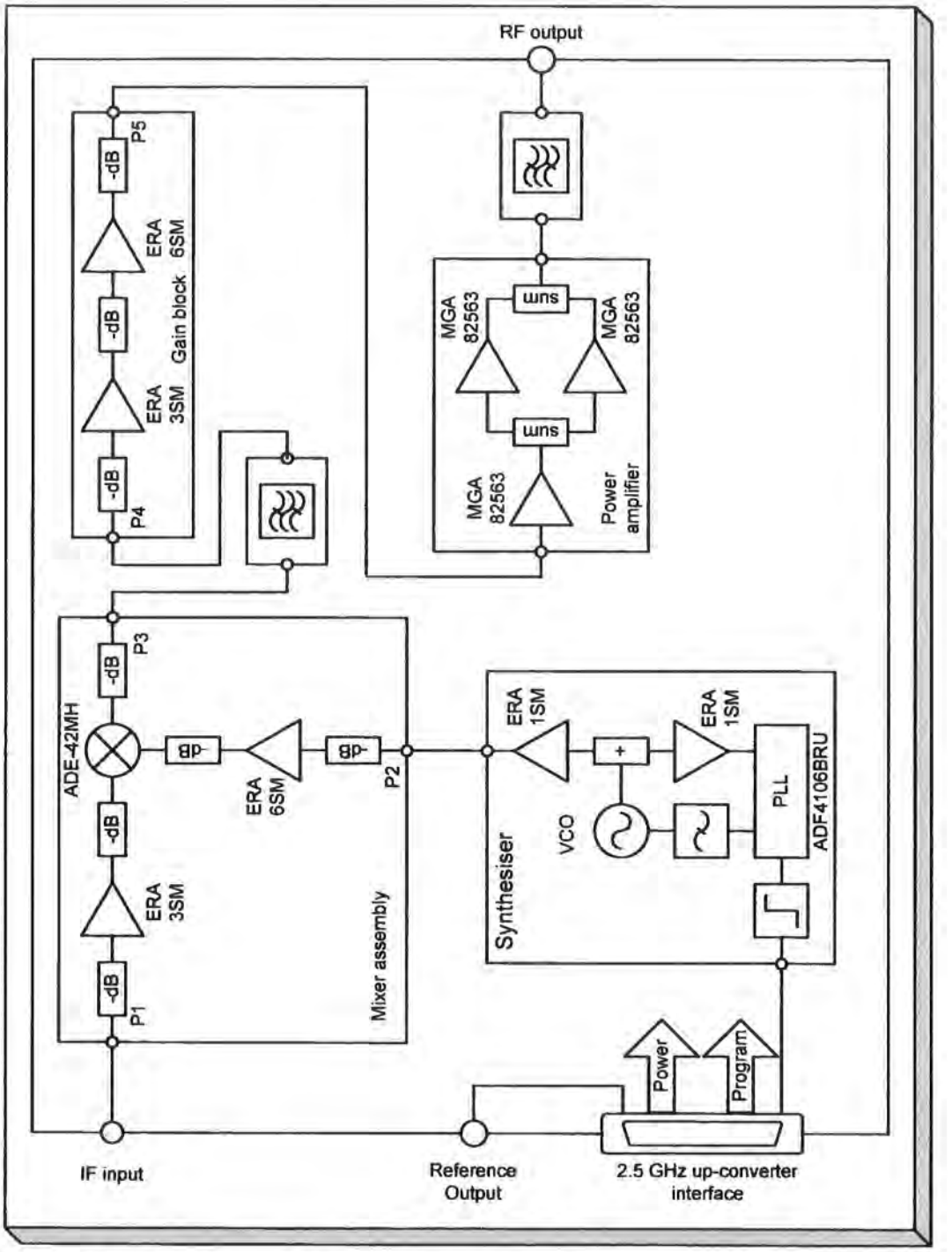

Figure 4.5 Up-converter assembly for 2.5 GHz

The 2.5 GHz up-converter assembly (figure 4.5) is housed in a 3U high, 220mm deep, 14 HP wide enclosure. The input and output connections are made via SMA coax and

DB-25 multi-way connectors mounted at the rear of the module. Two status indicator LEDs are on the front panel. One indicates that power is present at the module and the second indicates the "mute status" of the module.

The 2.5 GHz up-converter module includes a synthesiser that provides the local oscillator signal. This can be programmed in the frequency range 4.4 GHz to 4.6 GHz. The step size of the synthesiser is 10 MHz. Since there is no multiplication of the local oscillator in the converter assembly, the output frequency can also be adjusted in 10 MHz steps. The local oscillator provides a high side injection signal to perform up-conversion from the 2 GHz IF band up to 2.5 GHz. The output signal is defined as:

$$F(out) = F(LO) - F(IF)$$

The output from the mixer in the converter block is filtered using a five section inter-digital filter. This has a bandwidth of 400 MHz centred at 2.5 GHz. This filter provides attenuation of the local oscillator signal and the mixer sum product in the 6.5 GHz band. The filter also provides moderate attenuation to signals in the IF band at 1.8 GHz to 2.2 GHz.

The output of the filter is amplified with the two stage amplifier in the converter block. This signal is then further amplified by the two stage power amplifier. The output of the amplifier is then filtered using a second five-section inter-digital filter. This provides additional attenuation to any IF signals in the 1.8 GHz to 2.2 GHz band and provides significant attenuation to the second harmonic which falls in the 5 GHz band.

The group delay at the edges of the filter pass-band limit the useable frequency range at the output of the converter to 2.35 GHz to 2.65 GHz.

The 2.5 GHz up-converter is assigned to bay 1 of the rack. This bay is provided with two 10 MHz reference signals. One is used internally by the synthesiser. The second is presented on an SMA coax connector at the rear of the module.

4.1.3 3.4 GHz up-converter assembly

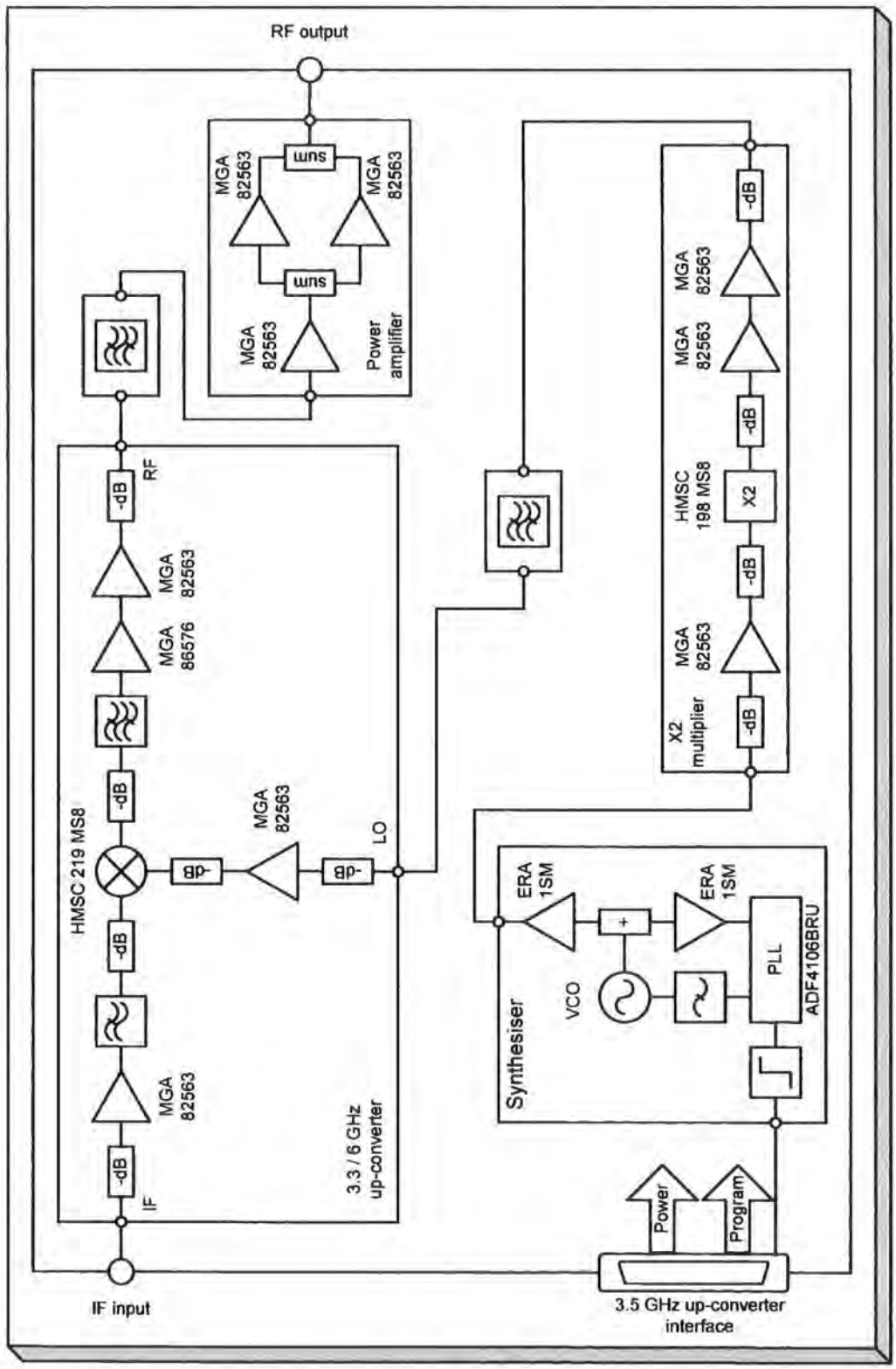

Figure 4.6 Up-converter assembly for 3.4 GHz

The 3.4 GHz up-converter assembly (figure 4.6) is housed in a 3U high, 220mm deep, 14 HP wide enclosure. The input and output connections are made via SMA coax and DB-25 multi-way connectors mounted at the rear of the module. Two status indicator LEDs are on the front panel. One indicates power to the module and the second indicates the "mute status" of the module. The 3.4 GHz converter is assigned to bay 2 of the rack.

The 3.4 GHz up-converter module includes a synthesiser that provides the local oscillator signal. This can be programmed in the frequency range 2.65 GHz to 3.25 GHz. The step size of the synthesiser is 10 MHz. The synthesiser output is multiplied by two within the X2 multiplier module to provide an effective local oscillator signal at 5.3 GHz to 6.5 GHz. The output frequency can therefore only be adjusted in 20 MHz steps.

The local oscillator provides a high side injection signal to perform up-conversion from the 2 GHz IF band up to 3.4 GHz. The output signal is defined as:

$$F(out) = F(LO) - F(IF)$$

The 3.3 GHz to 6 GHz up-converter module includes internal filtering and amplification. The internal filtering is only sufficient to ensure that the internal amplifier is operated within its linear region.

An additional inter-digital filter is used to filter the output of the up-converter module prior to final amplification in the power amplifier. This filter is required to attenuate the local oscillator, IF and image frequencies at the output of the up-converter module. The present build of the 3.4 GHz up-converter assembly uses a five-section filter. This provides an output frequency range of 3.3 GHz to 3.9 GHz. A seven section filter would allow operation from 3.3 GHz to 4.5 GHz.

The output power amplifier raises the output power level to +20 dBm.

4.1.4 5.7 GHz up-converter assembly

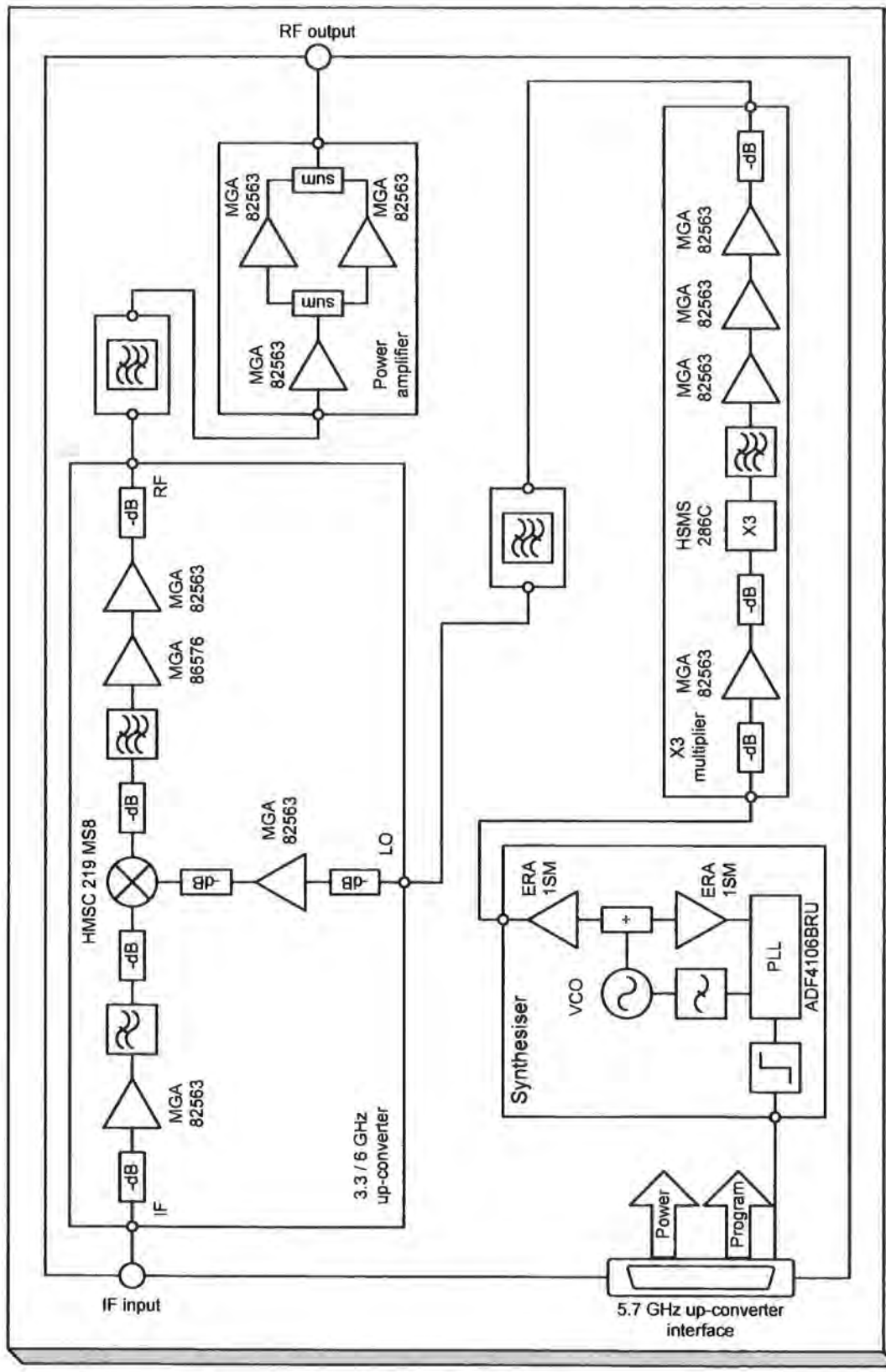

Figure 4.7 Up-converter assembly for 5.7 GHz

The 5.7 GHz up-converter assembly (figure 4.7) is housed in a 3U high, 220mm deep, 14 HP wide enclosure. The input and output connections are made via SMA coax and DB-25 multi-way connectors mounted at the rear of the module. Two status indicator LEDs are on the front panel. One indicates power to the module and the second indicates the "mute status" of the module. The 5.7 GHz up-converter is assigned to bay 3 of the rack.

The 5.7 GHz up-converter module includes a synthesiser that provides the local oscillator signal. This can be programmed in the frequency range 2.23 GHz to 2.67 GHz. The step size of the synthesiser is 10 MHz. The synthesiser output is multiplied by three within the X3 multiplier module to provide an effective local oscillator signal at 6.5 GHz to 8.0 GHz. The output frequency can therefore only be adjusted in 30 MHz steps.

The local oscillator provides a high side injection signal to perform up-conversion from the 2 GHz IF band up to 5.7 GHz. The output signal is defined as:

$$F(out) = F(LO) - F(IF)$$

The 3.3 GHz to 6 GHz up-converter module includes internal filtering and amplification. The internal filtering is only sufficient to ensure that the internal amplifier is operated within its linear region.

An additional inter-digital filter is used to filter the output of the up-converter module prior to final amplification in the power amplifier. This filter is required to attenuate the local oscillator, IF and image frequencies at the output of the up-converter module. The present build of the 5.7 GHz up-converter assembly uses a five-section filter. This provides an output frequency range of 5.0 GHz to 6.0 GHz. A seven section filter would support operation from 4.5 GHz to 6.0 GHz.

The output power amplifier raises the output power level to +20 dBm.

4.1.5 2.5 GHz down-converter assembly

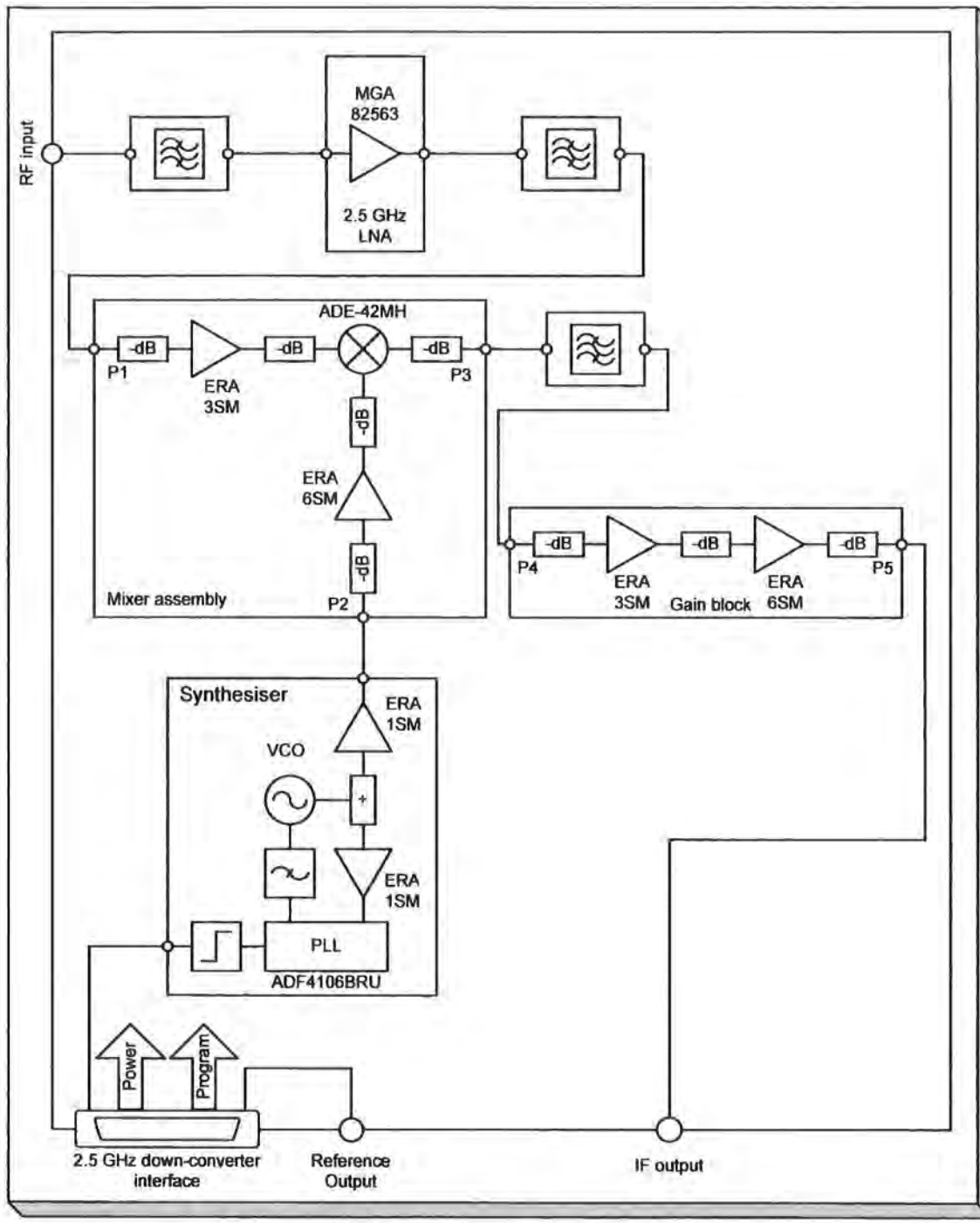

Figure 4.8 Down-converter assembly for 2.5 GHz

The 2.5 GHz down-converter assembly (figure 4.8) is housed in a 3U high, 220mm deep, 14 HP wide enclosure. The input and output connections are made via SMA coax and DB-25 multi-way connectors mounted at the rear of the module. Two status

indicator LEDs are on the front panel. One indicates power to the module and the second indicates the synthesiser lock status of the module.

The input signal is filtered using a five-section inter-digital filter. This provides significant attenuation of signals in the UMTS and GSM-1800 MHz bands. The filter output is routed to a single stage low noise amplifier. The output of the LNA is filtered using a second five-section inter-digital filter to provide further attenuation of the UMTS and GSM-1800 MHz signals in addition to the image-band noise. The output of this filter is presented to the input of the 2.5 GHz converter module.

The 2.5 GHz down-converter assembly includes a synthesiser that provides the local oscillator signal. This can be programmed in the frequency range 4.4 GHz to 4.6 GHz. The step size of the synthesiser is 10 MHz. Since there is no multiplication of the local oscillator in the converter assembly, the output frequency can also be adjusted in 10 MHz steps. The local oscillator provides a high side injection signal to perform down-conversion from the 2.5 GHz RF band down to the 2 GHz IF band. The output signal is defined as:

$$F(IF) = F(LO) - F(RF)$$

The output from the mixer in the converter block is filtered using a five section inter-digital filter. This has a bandwidth of 400 MHz centred at 2.0 GHz. This filter provides attenuation of the local oscillator signal and the mixer sum product in the 6.5 GHz band.

The output of the filter is amplified by the two stage amplifier in the converter block.

The group delay at the edges of the filter pass-band limit the useable frequency range at the input of the converter to 2.35 GHz to 2.65 GHz.

The 2.5 GHz down-converter is assigned to bay 1 of the rack. This bay is provided with two 10 MHz reference signals. One is used internally by the synthesiser. The second is presented on an SMA coax connector at the rear of the module.

4.1.6 3.4 GHz down-converter assembly

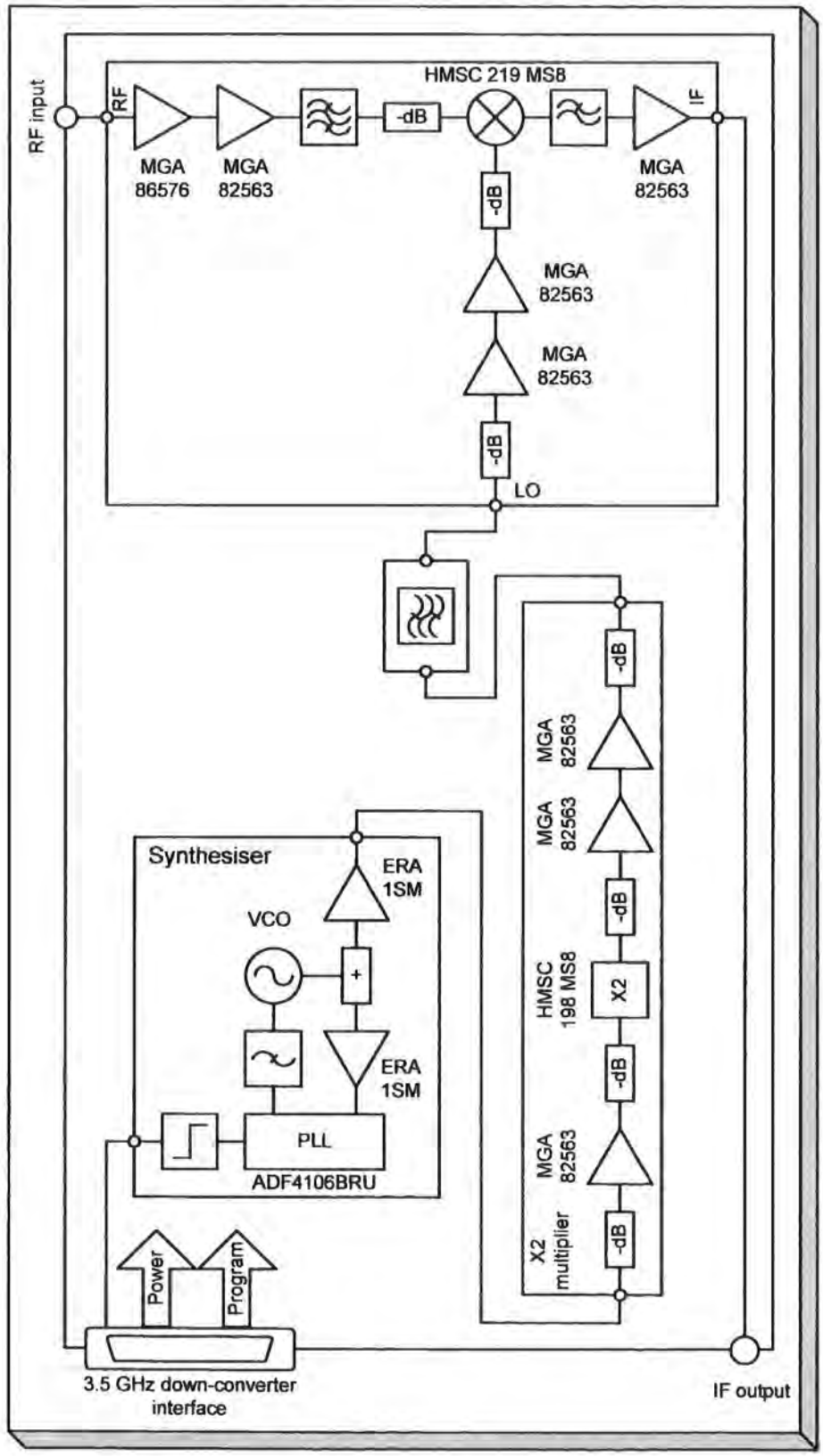

Figure 4.9 Down-converter assembly for 3.4 GHz

The 3.4 GHz down-converter assembly (figure 4.9) is housed in a 3U high, 220mm deep, 14 HP wide enclosure. The input and output connections are made via SMA coax and DB-25 multi-way connectors mounted at the rear of the module. Two status indicator LEDs are on the front panel. One indicates power to the module and the second indicates the synthesiser lock status of the module.

The 3.4 GHz down-converter module includes a synthesiser that provides the local oscillator signal. This can be programmed in the frequency range 2.65 GHz to 3.25 GHz. The step size of the synthesiser is 10 MHz.

The synthesiser output is multiplied by two within the X2 multiplier module to provide an effective local oscillator signal at 5.3 GHz to 6.5 GHz. The output frequency can therefore only be adjusted in 20 MHz steps. The local oscillator provides a high side injection signal to perform down-conversion from the 3.4 GHz RF band to the 2 GHz IF band. The output signal is defined as:

$$F(out) = F(LO) - F(IF)$$

The 3.3 GHz to 6 GHz down-converter module includes internal filtering and amplification.

The 3.4 GHz down-converter assembly supports operation from 3.3 GHz to 4.5 GHz by changing the operating frequency of the local-oscillator only.

The internal filtering present in the integrated down-converter has been found to be sufficient to support measurements in the signal environment to date. This work has been performed using either low gain wide-band discone or higher gain band specific antennas.

The 3.4 GHz down-converter assembly is assigned to bay two of the rack.

4.1.7 5.7 GHz down-converter assembly

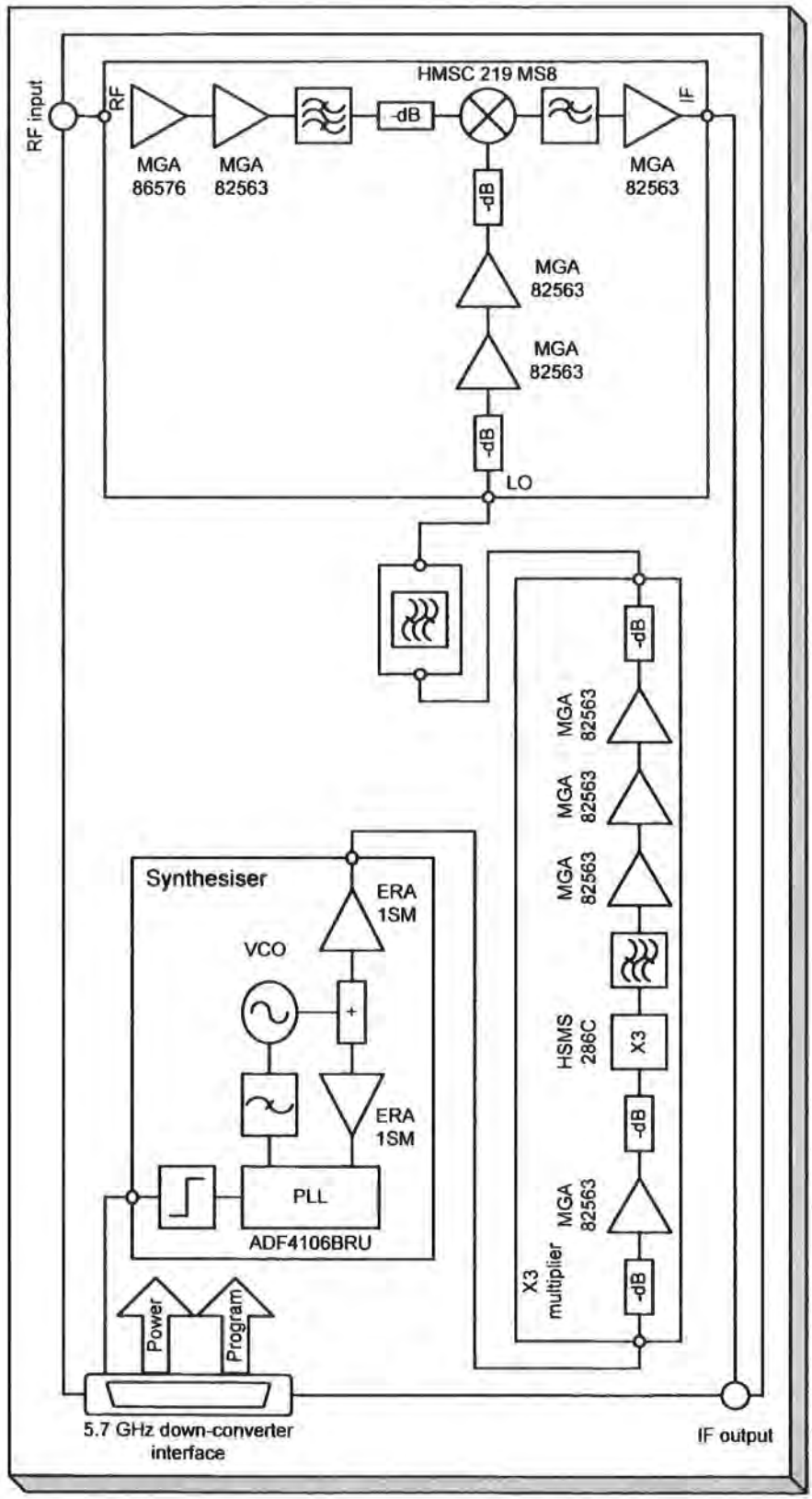

Figure 4.10 Down-converter assembly for 5.7 GHz

The 5.7 GHz down-converter assembly (figure 4.10) is housed in a 3U high, 220mm deep, 14 HP wide enclosure. The input and output connections are made via SMA coax and DB-25 multi-way connectors mounted at the rear of the module. Two status indicator LEDs are on the front panel. One indicates power to the module and the second indicates the synthesiser lock status of the module.

The 5.7 GHz down-converter module includes a synthesiser that provides the local oscillator signal. This can be programmed in the frequency range 2.23 GHz to 2.67 GHz. The step size of the synthesiser is 10 MHz.

The synthesiser output is multiplied by three within the X3 multiplier module to provide an effective local oscillator signal at 6.5 GHz to 8.0 GHz. The output frequency can therefore only be adjusted in 30 MHz steps. The local oscillator provides a high side injection signal to perform down-conversion from the 5.7 GHz RF band to the 2 GHz IF band. The output signal is defined as:

$$F(out) = F(LO) - F(IF)$$

The 3.3 GHz to 6 GHz down-converter module includes internal filtering and amplification.

The 5.7 GHz down-converter assembly supports operation from 4.5 GHz to 6.0 GHz by changing the operating frequency of the local-oscillator only.

The internal filtering present in the integrated down-converter has been found to be sufficient to support measurements in the signal environment to date. This work has been performed using either low gain wide-band discone or higher gain band specific antennas.

The 5.7 GHz down-converter assembly is assigned to bay three of the rack.

4.1.8 Four channel 5.7 GHz down-converter assembly

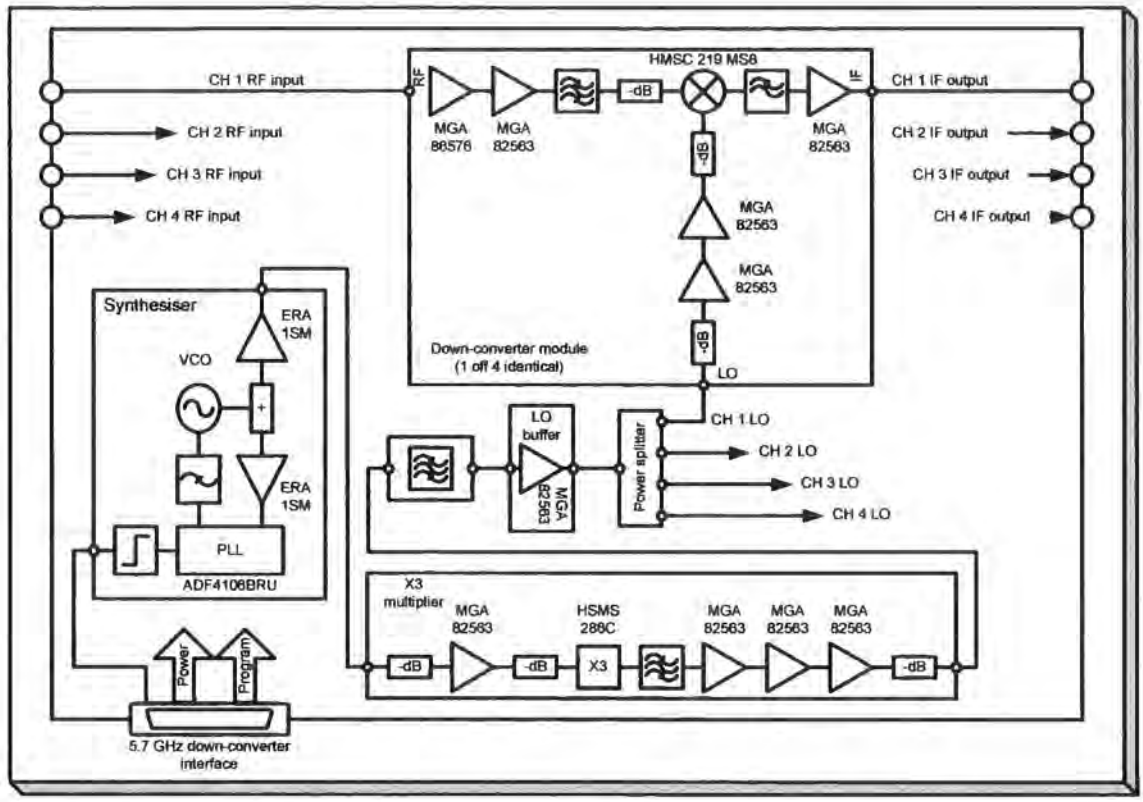

Figure 4.11 Four channel down-converter assembly

The four channel down-converter module (refer to figure 4.11) is housed in a 3 U * 42 HP rack module. It is assigned to the interconnect harness for bay three. The rear panel provides four input and four output SMA coax connectors for the input RF and output IF signals. The power, control and 10 MHz reference is provided via a DB-25 connector. The front panel includes two LED indicators. One provides power to module indication and the other reports the phase lock status of the synthesisers.

The assembly contains four identical 3.3 GHz to 6.0 GHz down-converter modules.

The local oscillator generation is identical to that used in the 5.7 GHz up-converter and down-converter with the addition of an additional amplifier and power splitter. The additional LO amplifier provides ~ 6 dB gain with an output of ~ +16 dBm. This is fitted after the LO filter prior to the four-way power splitter. The amplifier offsets the

loss due to the splitter. The four outputs from the power splitter are used to provide an LO signal of nominally +10 dBm to each of the down-converter modules.

4.1.9 Second local oscillator for 60 GHz transmitter

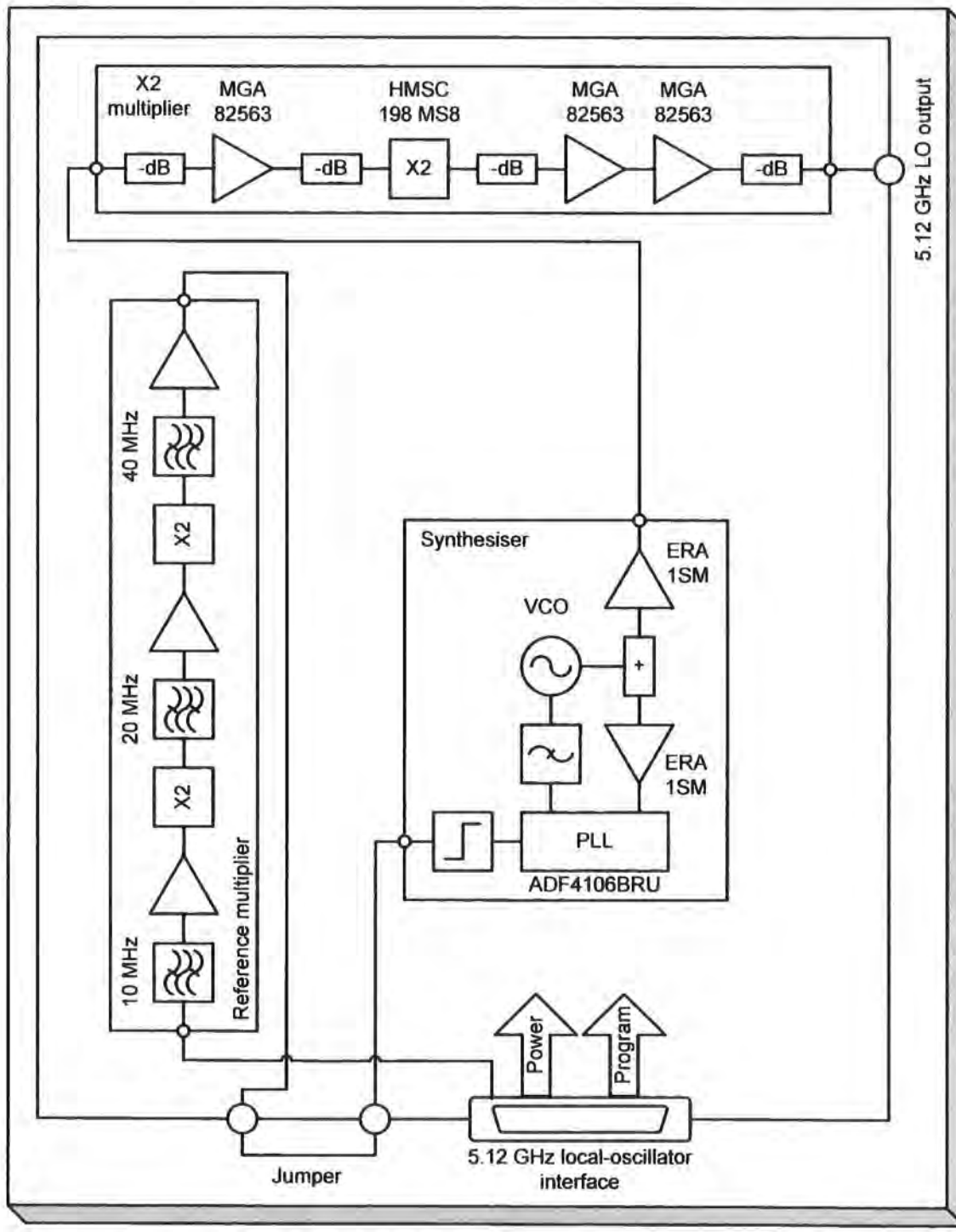

Figure 4.12 Low-noise 5.12 GHz local oscillator

The 60 GHz sounder transmitter uses a separate low phase noise local oscillator assembly (figure 4.12) to provide the local oscillator that is used to provide the up-conversion from the 5 GHz band to the 15 GHz band. This module is housed in a 3U by 14 HP rack case and is assigned to bay one of the rack.

This module includes a synthesiser operating at 2.56 GHz followed by a frequency doubler to provide an output at 5.12 GHz. The doubler is the same design as used in the 3.4 GHz up and down-converters.

The synthesiser uses a reference frequency of 40 MHz. The 40 MHz reference is obtained by multiplying the 10 MHz system reference using two doublers. This function is provided by the reference multiplier module.

This approach provides possible output frequencies of 5.12 GHz, 5.2 GHz, 5.28 GHz, 5.36 GHz and 5.44 GHz due to limitations in the range of valid synthesiser divide values.

4.1.10 Second up-converter for 60 GHz transmitter

The 5 GHz to 15 GHz up-converter (figure 4.13) is used to perform up-conversion from the 5 GHz band to the 15 GHz band to provide the drive signal for the 60 GHz transmitter. This module is housed in a 3 U * 14 HP rack case and is assigned to bay two of the rack.

This module has been assembled using commercially sourced microwave components.

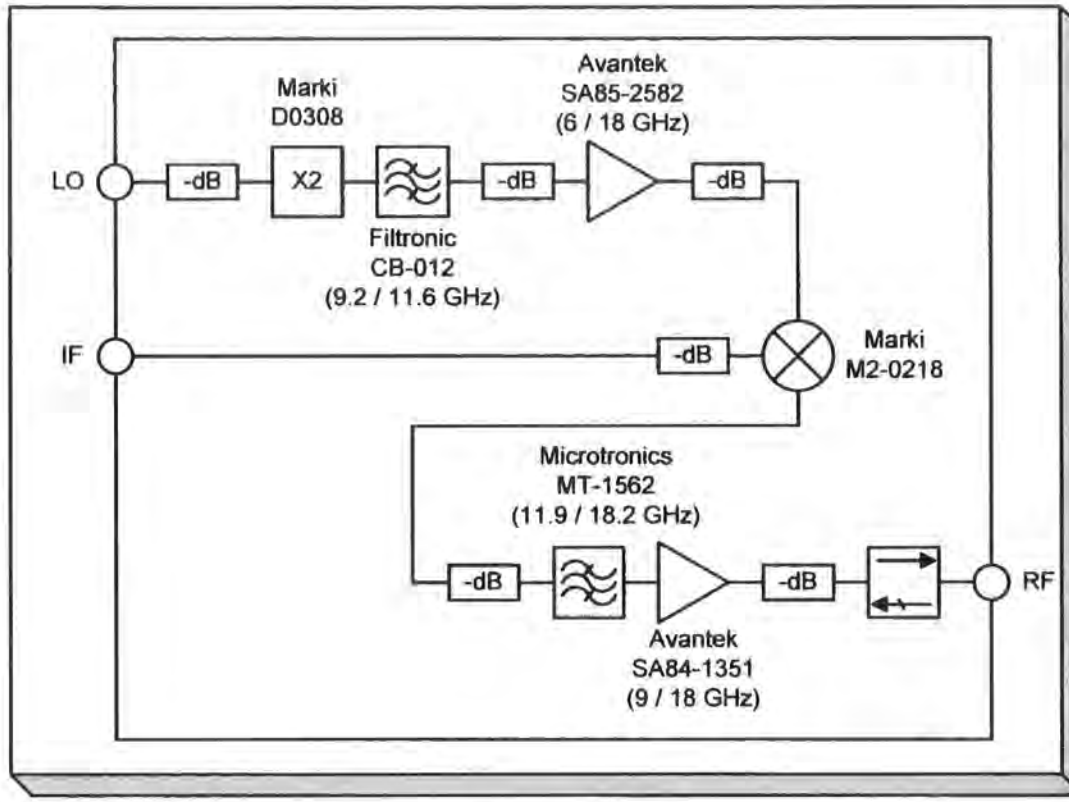

Figure 4.13 Second up-converter for 60 GHz TX

The local oscillator signal at 5.12 GHz is multiplied by two using a Marki-Microwave double-balanced diode doubler to provide an effective local oscillator signal of 10.24 GHz. The output of the doubler is filtered using a Filtronics CB102 band pass filter. This filter supports a pass band from 9.2 GHz to 11.6 GHz and provides > 80 dB of attenuation for the unwanted outputs of the doubler which occur at 7.68 GHz and 12.8 GHz (due to no filter between the doubler from 2.56 GHz to 5.12 GHz). The output of the filter is attenuated to a level of nominally -10 dBm which is then amplified to produce a signal level of nominally +20 dBm at the output of the amplifier.

The local oscillator signal is attenuated to nominally +15 dBm with an attenuator mounted at the mixer LO input. The IF signal is presented via a 20 dB attenuator (the input signal is from the output of the 5.7 GHz up-converter at +20 dBm) that is mounted on the mixer IF input. The output port is fitted with a 10 dB attenuator, again on the output port of the mixer. This arrangement provides both the appropriate signal levels

for the mixer and the following amplifier. The attenuators also provide a broad band 50 Ω operating environment for the mixer.

The attenuated output of the mixer is band limited using a Microtronics MT-1562 band-pass filter. This provides >70 dB of attenuation of the local oscillator signal (at 10.24 GHz) and the IF and image signals (in the 5 GHz band). The output of the filter is amplified to provide an output level of +22 dBm (compressed). An attenuator and isolator are included on the output of the amplifier to provide a module output level of +16 dBm.

The output signal is provided via an SMA connector on the front panel of the module in addition to a multi-way connector to provide dc power to the 60 GHz transmit module.

4.1.11 60 GHz transmitter module

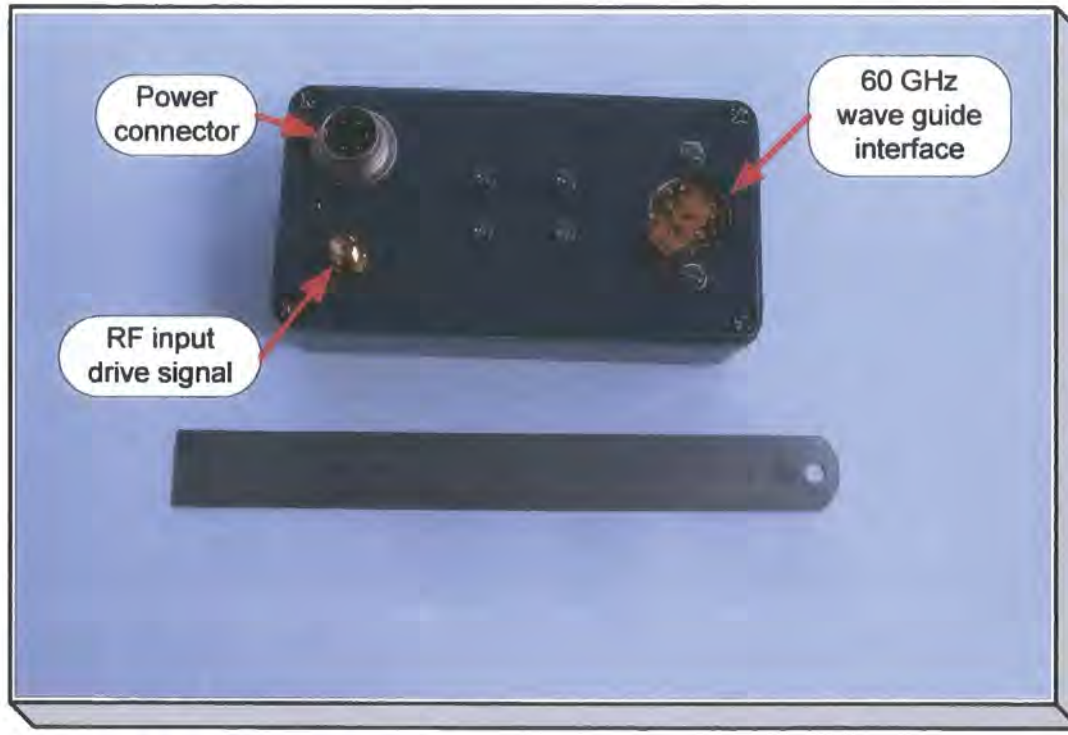

Figure 4.14 Transmitter module for 60 GHz

The 60 GHz transmitter module (figure 4.14) has been assembled using a Spacek-labs commercial X4 multiplier / amplifier assembly and a transition form coax to waveguide.

This module is mounted in the lid of a die-cast box to provide a heat sink to support the 3.3 W dissipation of the module. A further 6.7 W is dissipated in a linear regulator which provides +8 V from the + 24 V supply. The module has subsequently had an additional heat sink fitted to the box to improve the thermal transfer which reduces the operating temperature of the unit.

This module requires dc supply via the multi-way connector and an RF drive of nominally +12 dBm at the SMA coax connector. (With +16 dBm available from the transmit driver, a cable loss of up to 4 dB can be accommodated. This allows a flexible cable of ~2 m to be used between the driver and the transmitter module).

The RF output is provided at the waveguide flange. This flange conforms to UG-385/U and supports waveguide type WR-15 / WG 25 operating in the 50 GHz to 75 GHz range.

For all the 60 GHz sounding measurements made to date a small 20 dB conical horn has been fitted directly to the output flange. (Some limited calibration data was also taken using a waveguide connection to this port).

4.1.12 Driver for 60 GHz receiver

The 60 GHz receiver driver is mounted in a 3 U * 42 HP rack case. (Refer to figure 4.15 and 4.16). This module is assigned to bay one of the rack as two 10 MHz reference signals are required.

This assembly includes an up-converter to translate from the 2 GHz sounder IF band to the 5.7 GHz band. This portion of the equipment is identical to that used in the 5.7 GHz transmit up-converter but without the output power amplifier which is not necessary.

This module also includes a 5.12 GHz low phase noise local oscillator and 5 GHz to 15 GHz up-converter that are identical to those used for the 60 GHz transmitter. The mixer

input IF port attenuator has been reduced to 6 dB in accordance with the reduction in power level associated with the removal of the 5.7 GHz power amplifier.

The output signal is provided via an SMA connector on the front panel of the module in addition to a multi-way connector to provide dc power to the 60 GHz down-converter module.

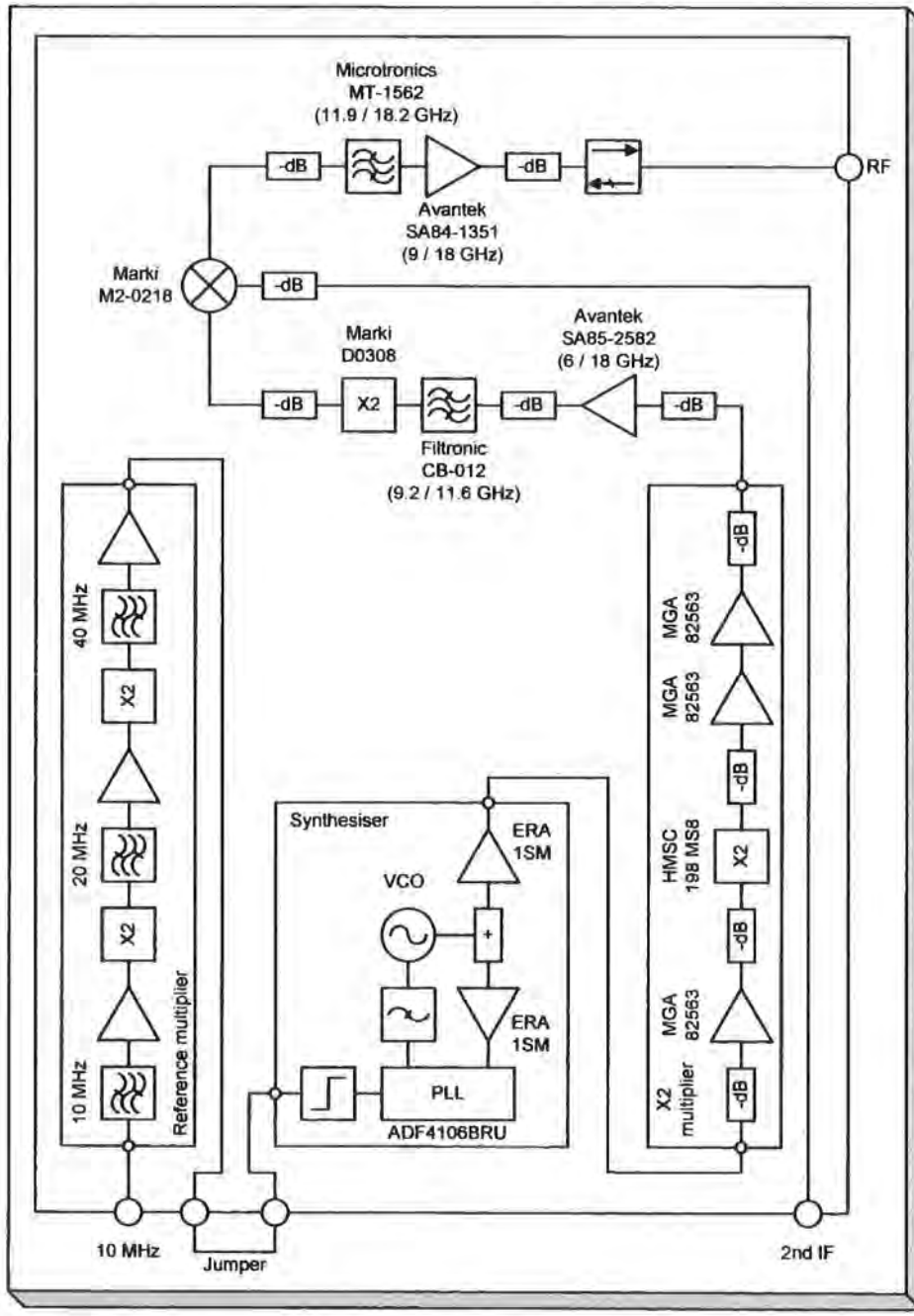

Figure 4.15 Receiver 60 GHz driver (part 1)

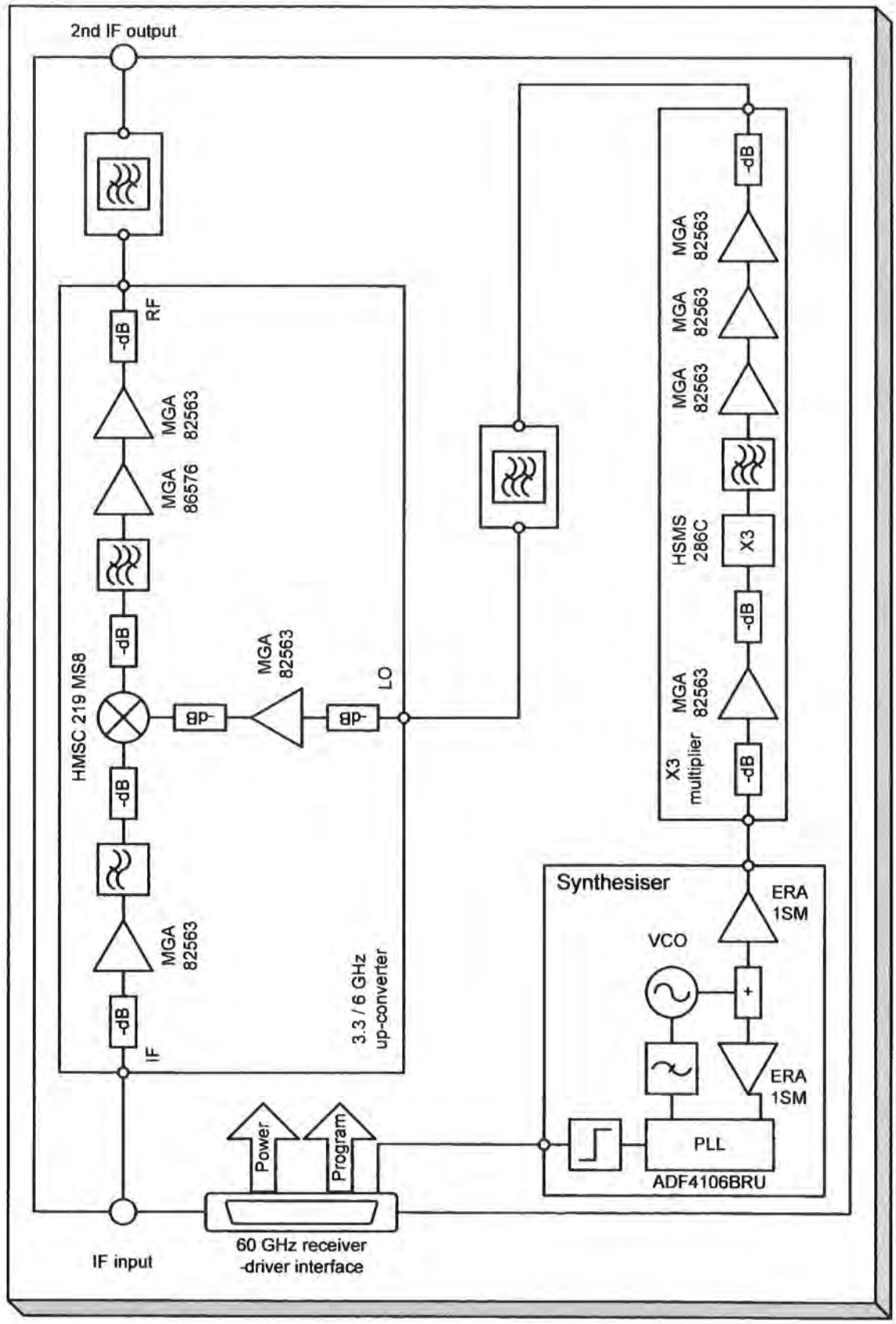

Figure 4.16 Receiver 60 GHz driver (part 2)

4.1.13 60 GHz receiver down converter

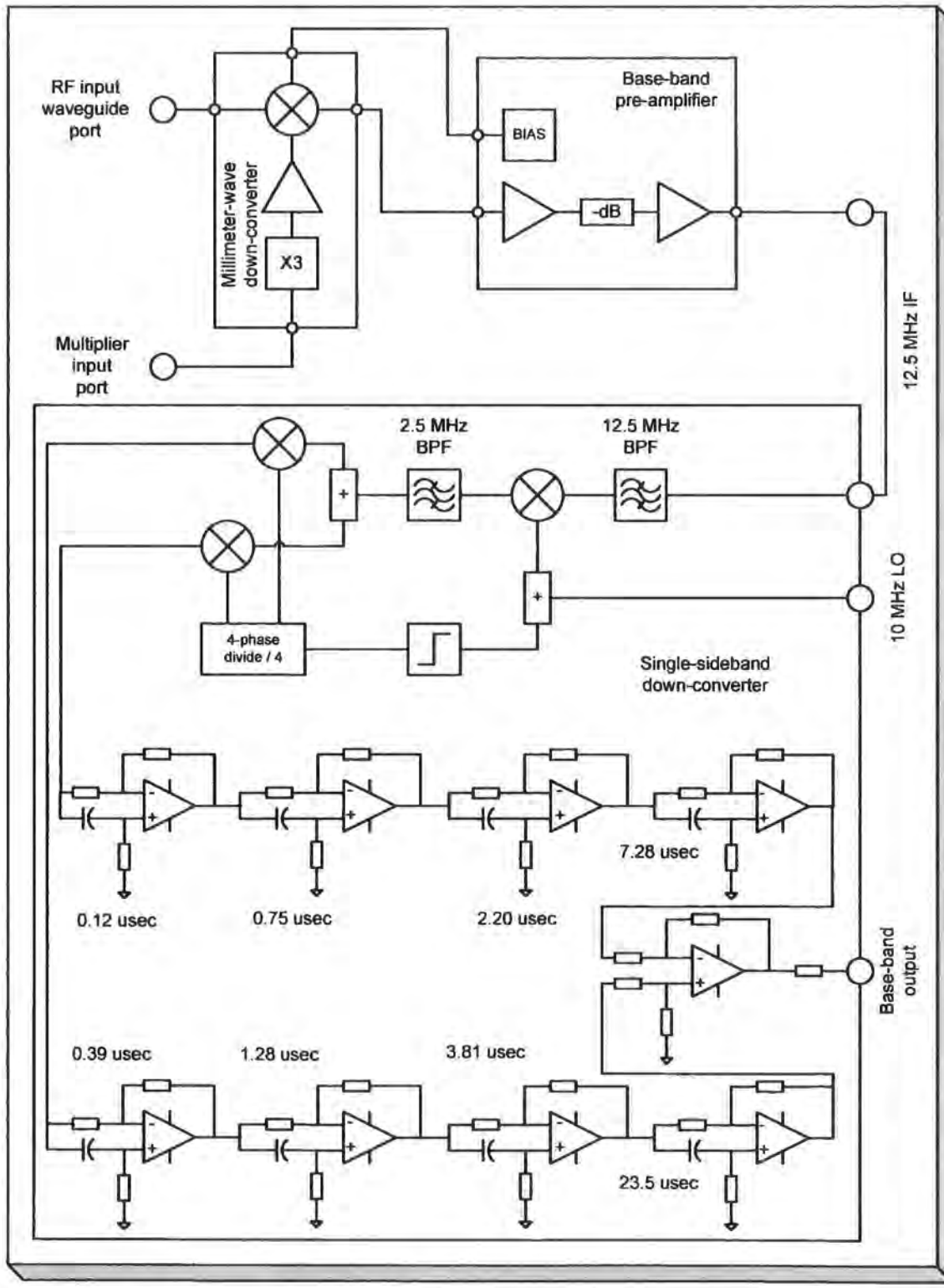

Figure 4.17 Block schematic of the 60 GHz receive down-converter assembly

The 60 GHz down-converter module is mounted within a die-case enclosure (Refer to figures 4.17 for the block schematic). This houses the mm-wave multiplier and mixer on the front cover. The base-band pre-amplifier and the SSB down-converter are mounted in the bottom of the box.

Local regulators have been included to provide +12 V at 500 mA for the SSB down-converter and base-band pre amplifier and +8 V at 400 mA for the mm-wave multiplier. Both of these regulators are supplied from the +24 V unregulated supply to the converter racks.

The down-converter assembly requires dc supply via the multi-way connector and an RF drive of nominally +12 dBm at the SMA coax connector. (With +16 dBm available from the 60 GHz receiver driver assembly, a cable loss of up to 4 dB can be accommodated. This allows a flexible cable of ~2 m to be used between the driver and the down-converter module).

The mixer is mounted directly to the output of the multiplier. The mm-wave components are heat-sunk to the box cover. The output of the mixer is routed directly to the input of the base-band pre-amplifier using a short length of coax. Since this is only transferring signals in the region of 12.5 MHz the loss is negligible. The output of the base-band pre amplifier is routed to an SMA connector on the side of the box. This allows the beat signal to be "ranged" using a spectrum analyser as the useful bandwidth of the pre amplifier extends to ~ 200 MHz. For normal operation this connection is fitted with a short jumper-cable to transfer the signal to the input of the SSB down-converter. The output of the SSB down-converter and the LO input for the SSB down-converter are provided by SMA connectors mounted through the side wall of the box.

In the present configuration all five bits of the step attenuator are wired together and are operated via a toggle switch mounted on the enclosure. This provides a low gain and a high gain mode with 31 dB of relative gain adjustment.

The RF input is provided to the waveguide flange. This flange conforms to UG-385/U and supports waveguide type WR-15 / WG 25 operating in the 50 GHz to 75 GHz range.

For all the 60 GHz sounding measurements made to date a small 20 dB conical horn has been fitted directly to the output flange. (Some limited calibration data has also been taken using a waveguide connection to this port).

4.2.1 Configuration 1: Multi-band 2.5 GHz, 3.5 GHz and 5.7 GHz

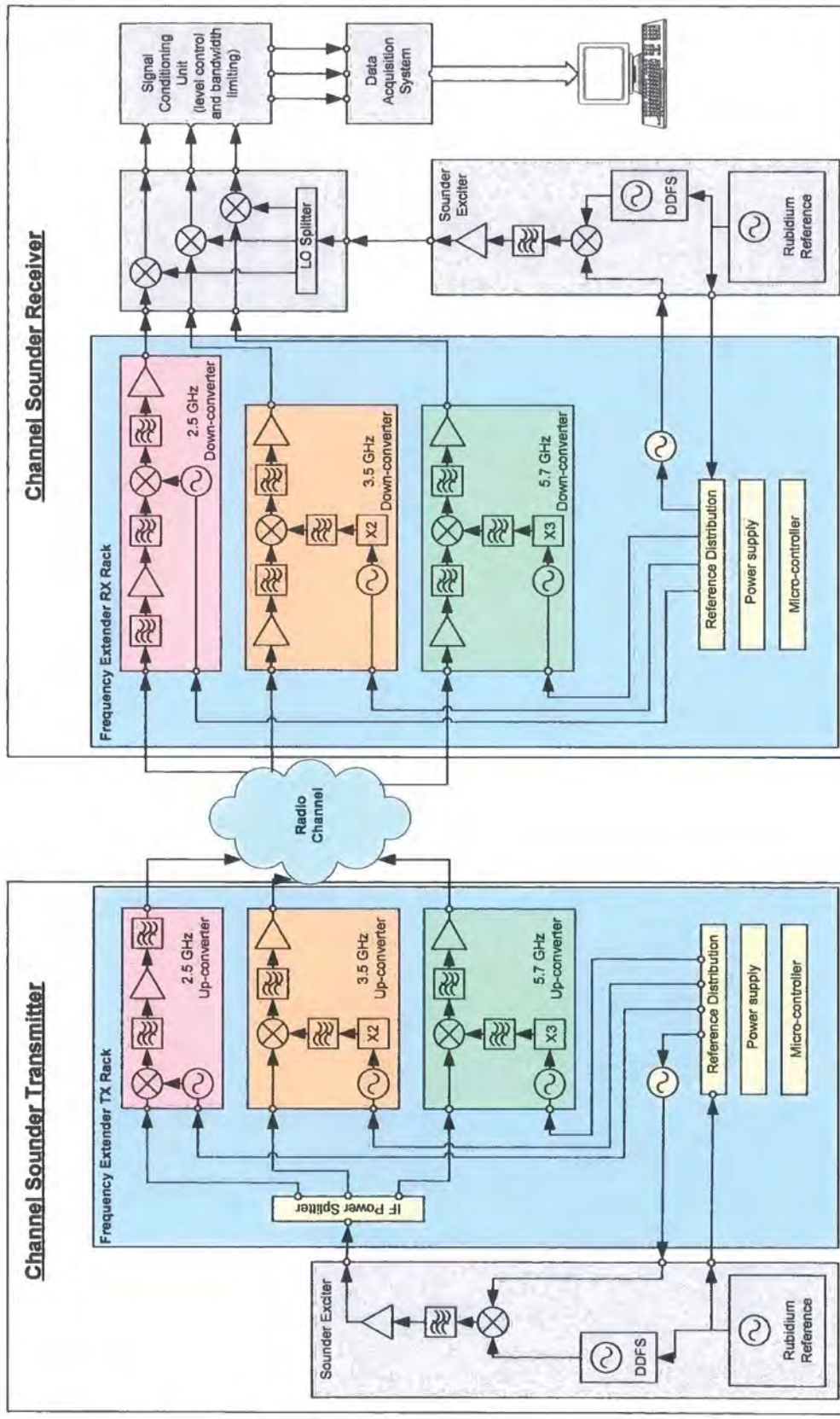

Figure 4.18 Multi-band channel sounder

The multi-band sounder (shown in figure 4.18) uses the UMTS sounder to provide a sweep signal within the 1.8 GHz to 2.2 GHz band. This signal is split using a three way power divider. This provides three identical signals that are used as the input to the three up-converters.

The UMTS sounder includes two low phase noise rubidium stabilised reference sources that provide the 10 MHz system reference for the transmitter and the receiver. These references also provide the reference signals to the synthesisers in each of the up-converters.

The up-converter rack (figure 4.19) also includes a synthesised source that can be programmed from 1.6 GHz to 2.5 GHz. This is used to provide the source to up-convert from the output of the DDFS (which is restricted to 400 MHz maximum) to the 2 GHz band. For this application the local signal is placed on the high side of the output at nominally 2.36 GHz. This source has a step size of 10 MHz.

The output power of each up-converter is nominally + 20 dBm (100 mW). These signals are made available to the transmit antennas (optionally with antenna mounted output amplifiers to raise the power level to +30 dBm (1 W)) or combined and transmitted through a single wideband discone antenna.

At the receiver, the channel sounder receiver is operated in the IF band (1.8 GHz to 2.2 GHz). The down-converters (2.5, 3.5 and 5.8 GHz) are used to translate the incoming RF signals down to the 2 GHz IF range. The converters operate with noise figures below 5 dB and nominally 30 dB of associated gain. The multi-band down-converter rack is shown in figure 4.20.

The rubidium stabilised reference at the receiver is used to synchronise the synthesised signal sources in the down-converters. The down-converter rack also includes a synthesised source that is used to provide the sweep translation signal for the receiver DDFS into the IF band. This source can be configured to provide signals in the range

1.6 GHz to 2.5 GHz with a step size of 3.333' MHz. For the multi-band down converter this is set to 2.36 GHz.

The sounder receiver is operated in a homo-dyne mode in which the IF signal is heterodyned with the locally generated sweep signal to produce a base-band signal within the range 30 kHz to 300 kHz for each of the down-converted bands. These signals are amplified and filtered using the signal conditioning module to provide signals that have the optimum peak signal level and alias band attenuation prior to sampling.

The data acquisition is performed by a card mounted inside the PC. The data acquisition has eight bits and is operated at 1 M sample / sec. Up to eight channels can be sampled simultaneously. For this application three channels only are utilised.

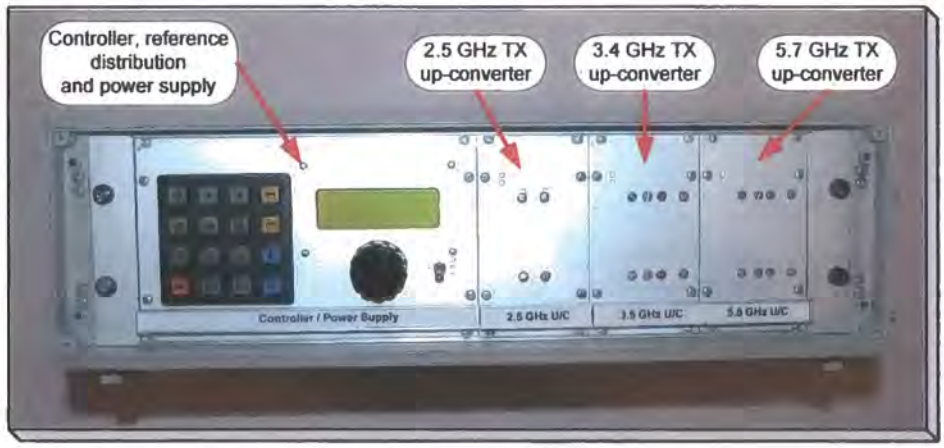

Figure 4.19 Multi-band transmitter up-conversion rack

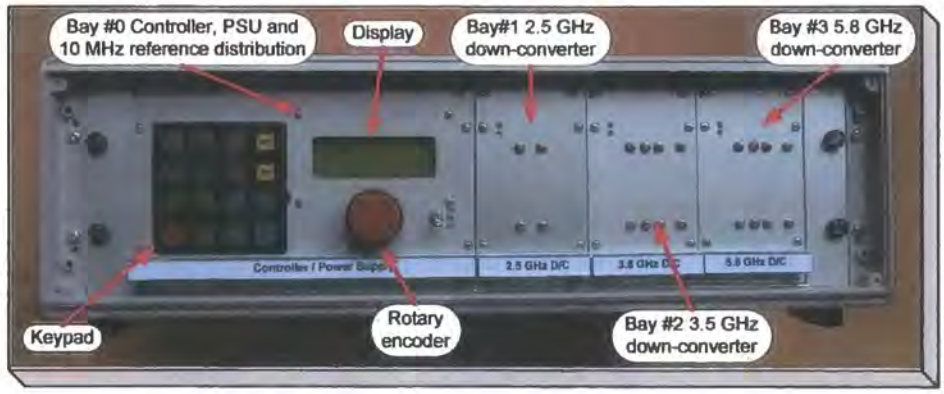

Figure 4.20 Multi-band receiver down-conversion rack

4.2.2 Configuration 2: Four parallel channels at 5.7 GHz

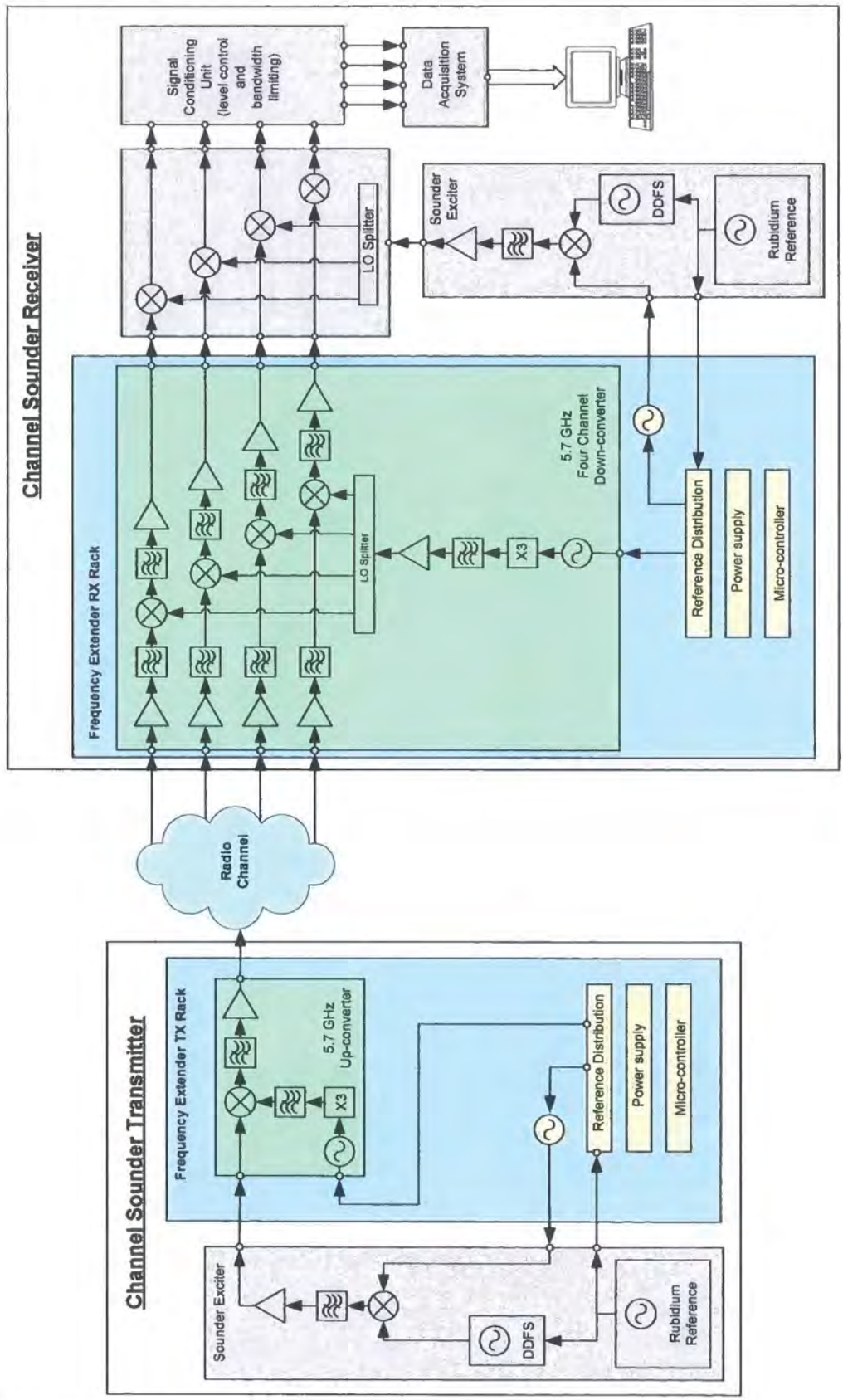

Figure 4.21 Four channel parallel receiver sounder

The four parallel channel configuration (fig 4.21) uses the 5.7 GHz up-converter at the transmitter. As in the previous configuration the UMTS sounder transmitter provides the 10 MHz system reference and the frequency extension hardware provides the 2.36 GHz signal to up-convert the DDFS into the 2 GHz band.

At the receiver signals are converted from the 5.7 GHz band to the 2 GHz IF band using a four parallel channel down-converter (figure 4.22). This module has been implemented using four down-converters that share a common local oscillator. The local oscillator is derived from a synthesiser followed by a X3 multiplier. The output of the multiplier is filtered and then amplified to compensate for the loss of the four-way LO splitter.

As in the previous configuration the UMTS sounder receiver provides the 10 MHz system reference and the frequency extension hardware provides the 2.36 GHz signal to up-convert the DDFS into the 2 GHz band.

Figure 4.22 Four channel 5.8 GHz down-conversion rack

4.2.3 Configuration 3: Single channel 60 GHz

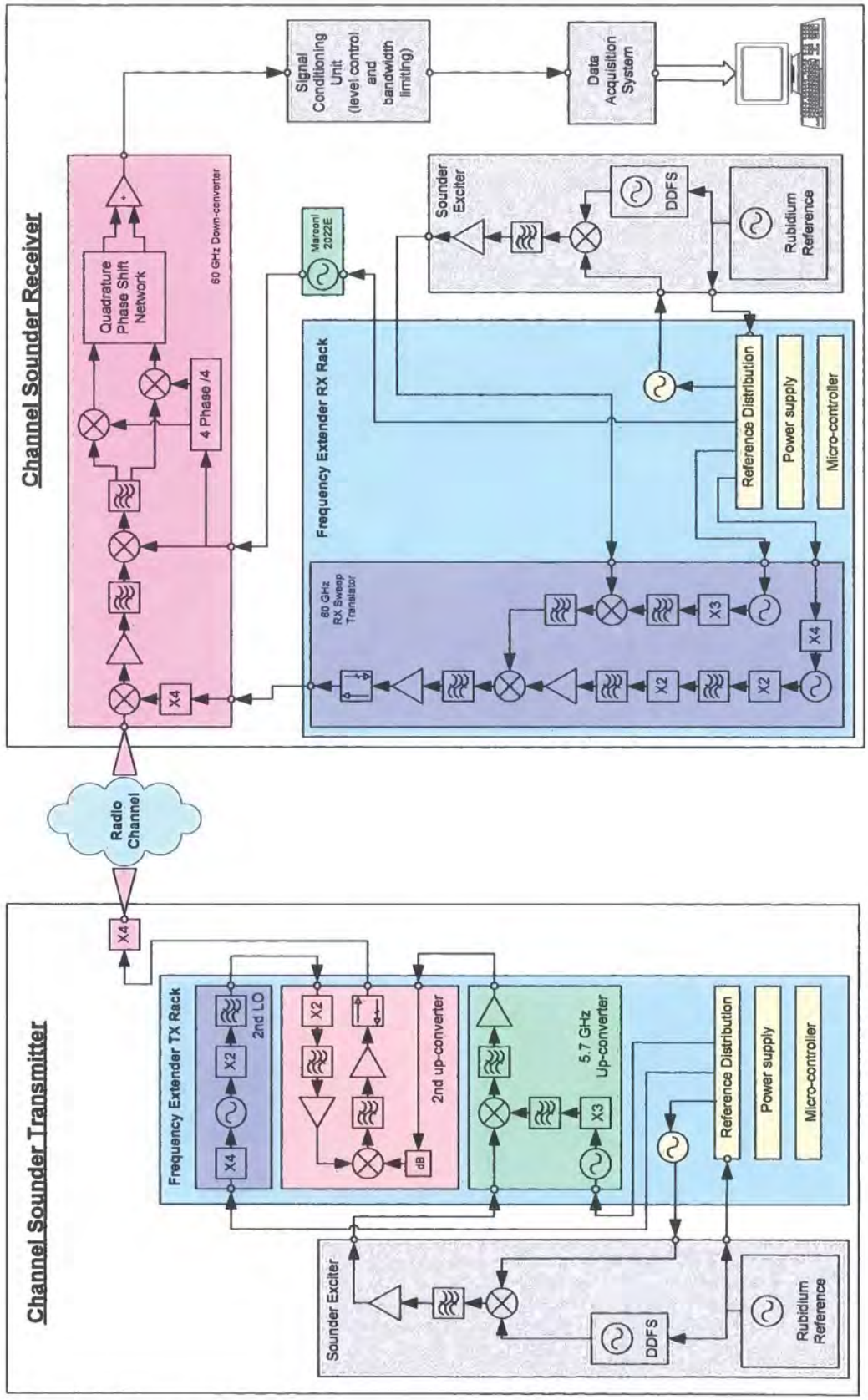

Figure 4.23 The 60 GHz channel sounder

The 60 GHz system (fig 4.23) uses several stages of up-conversion to produce an RF signal in the 60 GHz band. The same frequency generation scheme is used for both transmit and receive sweep generation.

The FMCW sweep is first up-converted to the 5 GHz band. This is then up-converted again to the 15 GHz band using a local oscillator at 10.24 GHz. The 10.24 GHz source is derived from a fundamental oscillator operating at 2.56 GHz followed by two doublers. The 15 GHz signals are routed from the TX (figure 4.24) and RX rack (figure 4.25) to the mm-wave multipliers via a 2 m coax cable. X4 mm-wave multipliers are then used to derive the RF signal in the 60 GHz band.

At the transmitter the swept signal is coupled to the channel using a small horn antenna. The transmitter output power is nominally + 7 dBm (5 mW).

At the receiver the sweep signal is used to provide the local oscillator to a balanced diode mixer. This 60 GHz receive mixer uses GaAs diodes which exhibit high levels of 1/ f noise. This reduces the sensitivity at low IF frequencies due to the degradation of the mixer IF noise floor.

While homodyne performance is possible (and has been demonstrated) an IF of ~ 12.5 MHz has been selected. Additional advantages of this configuration are that the mixer can be provided with dc bias to reduce and stabilise the conversion loss. This approach allows the large steps (200 kHz) due to the "delay increment" of the DDFS programmer to be accommodated in the subsequent down-conversion to baseband.

The receiver front end is contained in a die-cast box (figure 4.26). This includes the mm-wave local oscillator multiplier, balanced mixer, 12.5 MHz IF amplifier and SSB down-converter. The net gain of the receiver front end is nominally 50 dB. This is equivalent to the 2 GHz sounder front end gain. The operational noise figure is anticipated to be in the region of 10 dB.

The transmitter and receiver sweeps are offset to produce a beat signal in the range 12.5 MHz to 12.8 MHz. This offset can be achieved by setting the receiver IF local oscillator 3.333 MHz below the transmitter IF local oscillator and then using the "sweep delay" function to provide further adjustment. Alternatively the sweeps can be offset using the "sweep delay" function only. Since the step size of the fundamental DDFS is ~ 50 kHz for a sweep width of 250 MHz this results in a step size of ~200 kHz at 60 GHz after multiplication. Final adjustment of the beat frequency is achieved by adjusting the frequency of the local oscillator used in the SSB down-converter.

All signal sources at the transmitter are locked to the transmitter rubidium stabilised reference. Similarly all sources at the receiver (including the external synthesised signal generator used to provide the LO signal for the SSB down-converter) are locked to the receiver rubidium stabilised source.

The mm-wave components were purchased as complete modules from Spacek Labs in the US. All components operating at up to 8 GHz were designed and manufactured specifically for the project. The components operating in the 8 GHz through 16 GHz band were purchased.

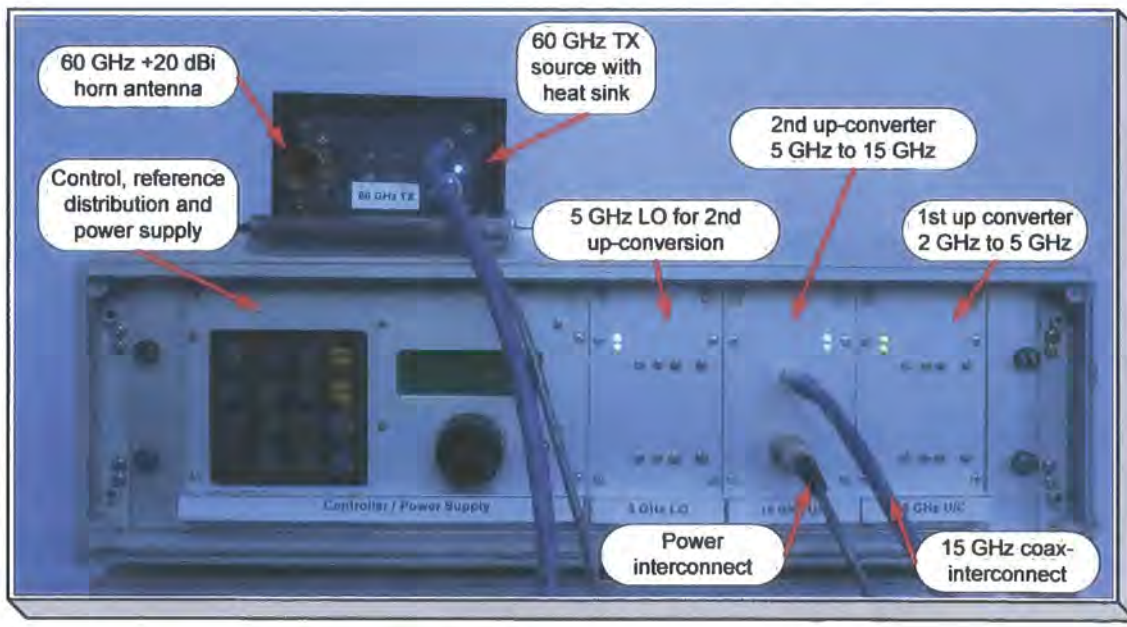

Figure 4.24 60 GHz transmitter driver rack and output multiplier

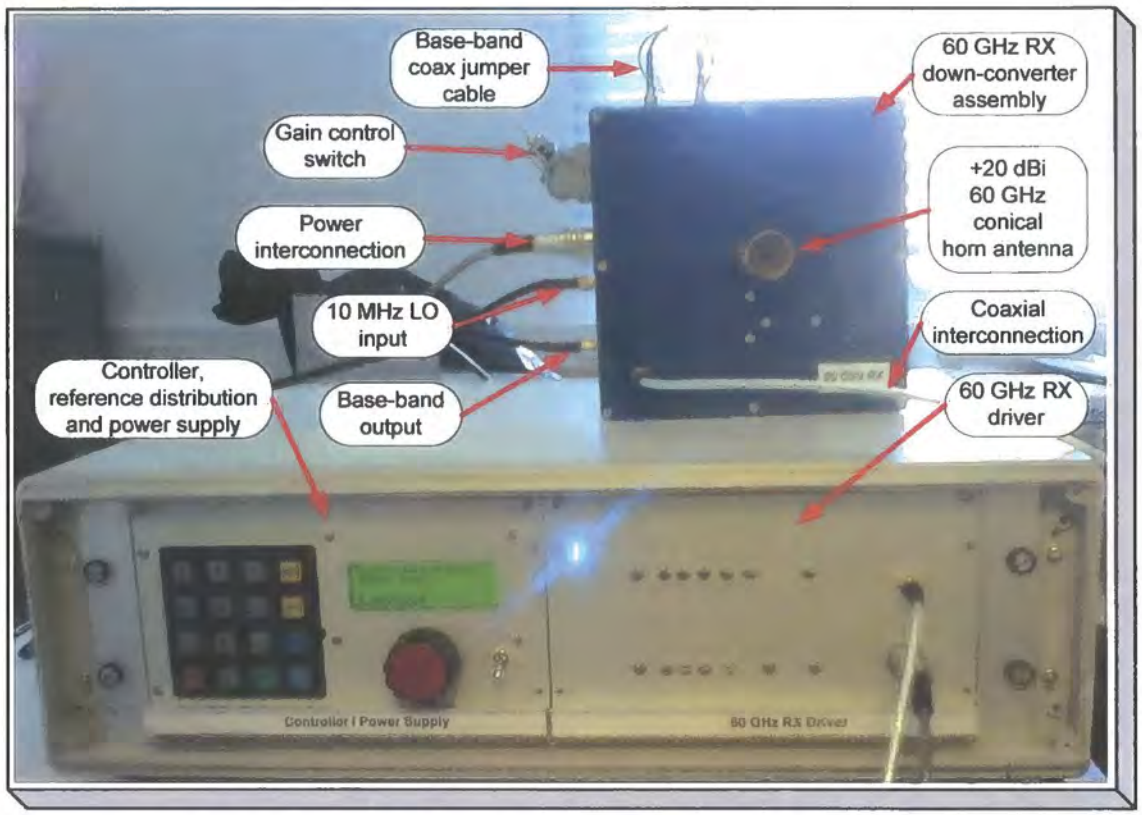

Figure 4.25 60 GHz receiver driver rack and down converter

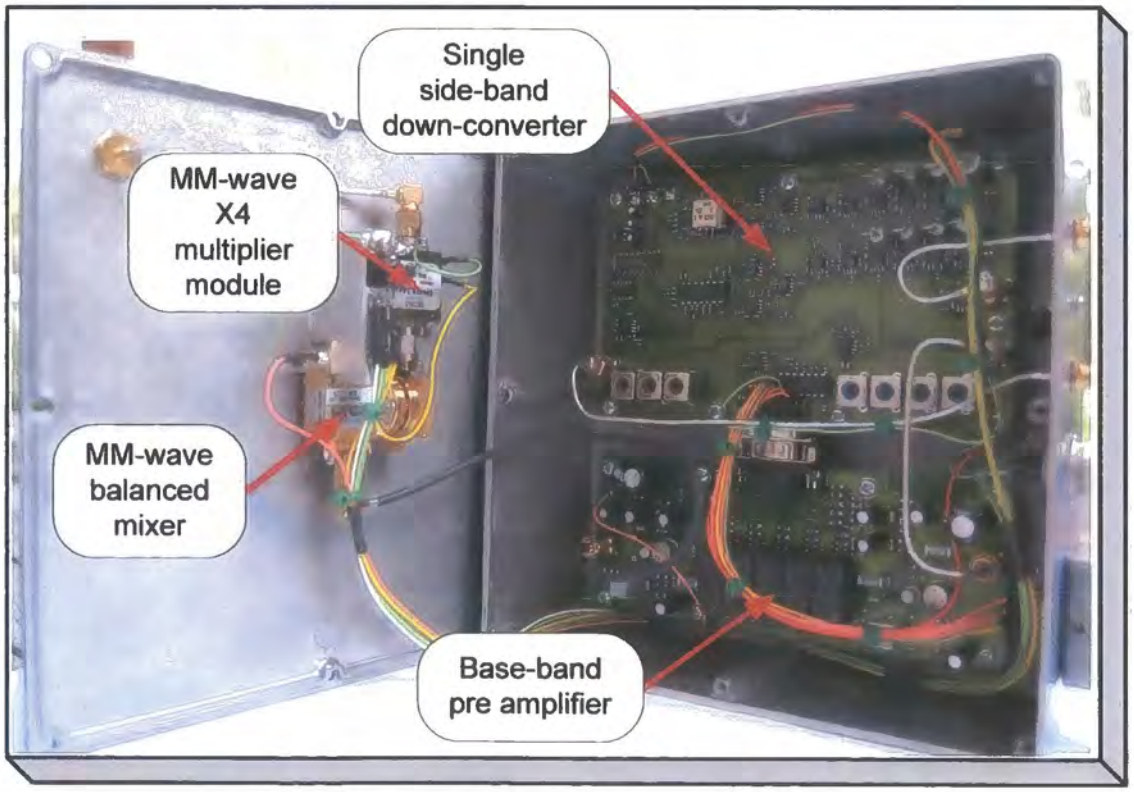

Figure 4.26 60 GHz receiver down-converter assembly

4.3 Description of the converters / key module performance

The frequency converters have been produced using a number of application specific components that have been designed for this research project. The application of the individual modules is indicated in table 4.1.

	Transmit rack	Receive Rack	2.5 GHz up-converter	3.5 GHz up-converter	5.7 GHz up-converter	2.5 GHz down-converter	3.5 GHz down-converter	5.7 GHz down converter	5.7 GHz 4 Ch down-converter	60 GHz TX 2nd LO	60 GHz RX driver	60 GHz RX assembly	Dual band MIMO equipment	Total modules
Reference source	1	1												2
Reference distribution	1	1												2
Main power supply	1	1												2
Auxiliary power supply	1	1												2
Micro-controller	1	1												2
10 / 40 MHz multiplier										1	1			2
1.6 / 2.5 GHz PLL	1	1												2
2.1 / 2.7 GHz PLL					1			1	1		1			4
2.4 / 3.0 GHz PLL										1	1			2
2.6 / 3.2 GHz PLL				1			1							2
4.4 / 4.6 GHz PLL			1			1								2
X2 RF multiplier				1			1			1	1			4
X3 RF multiplier					1			1	1		1			4
2.5 GHz converter			1			1								2
3.3 / 6.0 GHz up-converter				1	1						1			3
3.3 / 6.0 GHz down-converter							1	1	4					6
Power amplifier			1	1	1									3
2.5 GHz LNA						1								1
LO buffer amplifier									1					1
1.8 / 2.2 GHz 5 pole filter						1								1
2.04 / 2.14 GHz 9 pole filter													2	2
2.20 / 2.30 GHz 9 pole filter													2	2
2.20 / 2.30 GHz 7 pole filter													4	4
2.3 / 2.7 GHz 5 pole filter			2			2								4
3.3 / 4.5 GHz 7 pole filter				1										1
4.5 / 6.0 GHz 7 pole filter					1						1			2
5.3 / 6.5 GHz 7 pole filter				1			1			1	1			4
6.5 / 8.0 GHz 7 pole filter					1			1			1			3
Baseband pre-amplifier												1		1
SSB down-converter												1		1
Module per assembly	6	6	5	6	6	6	4	4	7	4	9	2	8	73

Table 4.1 summary of new hardware

The integrated converters, RF multipliers and amplifiers have been fabricated from Rogers 0.8mm thickness double sided 4003 substrate material. 0402 surface mount passive devices have been used. The base printed circuits were fabricated by the prototype facility at UMIST (now Manchester University) using the Gerber RS274X file output from the CAD tool.

The other circuits assemblies have been fabricated from 1.6mm thick, double sided epoxy-glass FR4 material with 0603, 0805 and 1206 surface mount passive devices. The base printed circuits were fabricated by "PCB Pool". Data were provided as a ".GWK" file format as the output from "GC-Prevue" that was used to provide post processing of the Gerber file format. This additional step allows the design layout checks to be fully completed before despatching the design file.

All the circuits were manually assembled with the assistance of a low power (20X) stereo microscope.

All the radio frequency sensitive circuits have been housed in machined aluminium housings. This provides an RF screened enclosure which also provides mechanical and thermal stability. The mechanical filters and discone antenna have been machined from aluminium and brass with PTFE insulation. The 60 GHz horn antennas were machined from brass. The metal housings and mechanical filters were fabricated using a "Thiel 159" precision universal milling machine equipped with a Heidenhein DRO system with a resolution of 10 μm. The antennas were fabricated using an "Ajax" CNC lathe equipped with a GE "Fanuc" control system with a resolution of 1 μm.

All the circuits have been designed using Mentor Graphics "Power PCB" tools for schematic capture and layout generation. The high frequency circuits have also been simulated and optimised using AWR "Microwave Office". The specific RF layout elements have then been exported from "Microwave Office" to "Power PCB" as "PADS" format elements.

4.3.1 Reference source

The primary reference for the converter is a Stanford Research PRS-10 rubidium disciplined OCXO oscillator that is housed in the channel sounder. An OCXO based reference that provides equivalent short term stability has been included within the rack for test purposes. (Figure 4.27)

The in-rack local reference uses an Agilent (HP) 10811 oscillator (figure 4.27). This uses an overtone SC cut crystal that is enclosed with all the oscillator and temperature regulation electronics within an insulated temperature regulated enclosure. The oscillator is mounted on an FR4 epoxy-glass PCB which is mounted inside an Aluminium box with anti-vibration mountings. Local voltage regulators are provided to minimise drift and noise due to power supply disturbances. A monitor circuit is included to provide indication that the oscillator oven is under temperature control. An electrical tune input is available that provides +/- 0.5 ppm of adjustment range.

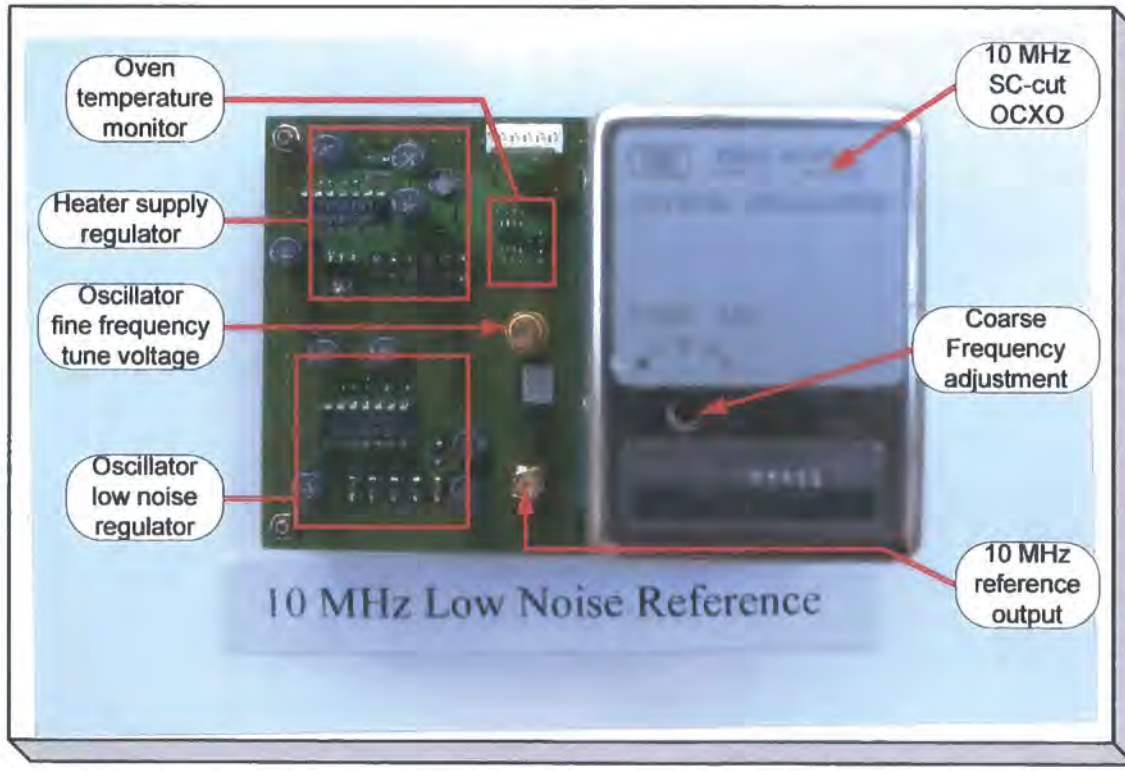

Figure 4.27 Low phase-noise reference frequency source

4.3.2 Reference distribution

Contingent upon the measurement configuration up to five common reference signals are required. A 50 Ω coax environment has been selected for the physical distribution of the reference signal between modules. The nominal signal level is 5 mW (+7 dBm). A sine wave has been utilised with "double termination" of the cables with source and load matched to the 50 Ω characteristic impedance of the cable.

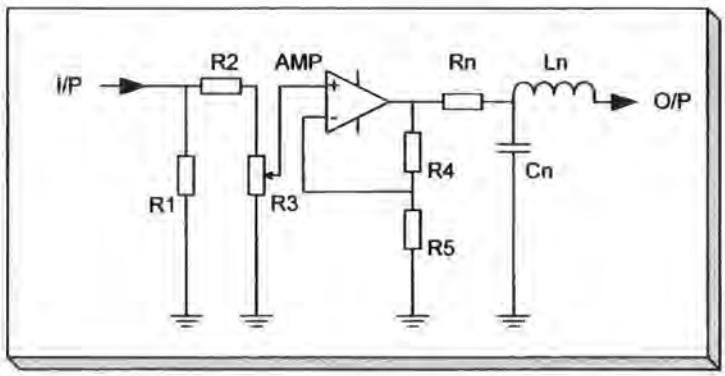

Figure 4.28 Reference distribution concept

The reference distribution module uses a series input / shunt output voltage feedback amplifier that is realised using a PNP / NPN transistor pair. This configuration results in a high input impedance and a low output impedance [4.3]. An input network including an adjustable attenuator (R1, R2 and R3) is used to provide an input matched to 50 Ω, (figure 4.28). At the output of the amplifier a series output termination impedance (Rn) of nominally 250 Ω is provided for each reference channel. This impedance is then transformed down to nominally 50 Ω using a shunt capacitor / series inductance "L" matching network that is resonant at 10 MHz (Cn / Ln). Five channels of this network are connected to the output of the amplifier to provide five individual outputs each of which present an impedance of 50 Ω. The five parallel channels individually provide a load impedance of 500 Ω. Thus the total load presented to the amplifier is 100 Ω. The termination network reduces the amplitude by a factor of two due to the double termination and then by a further 2.24 times due to the transformation from 250 Ω to 50 Ω impedance. To provide the required output of 0.5 V rms the output swing for the amplifier is required to be 6.3 V peak to peak into 100 Ω. The measured isolation of the

complete assembly (figure 4.29) between reference output channels was measured to be 37 dB. The reverse isolation from output to input has been measured to be greater than 80 dB. The amplifier is used to maintain the input / output levels at +7 dBm.

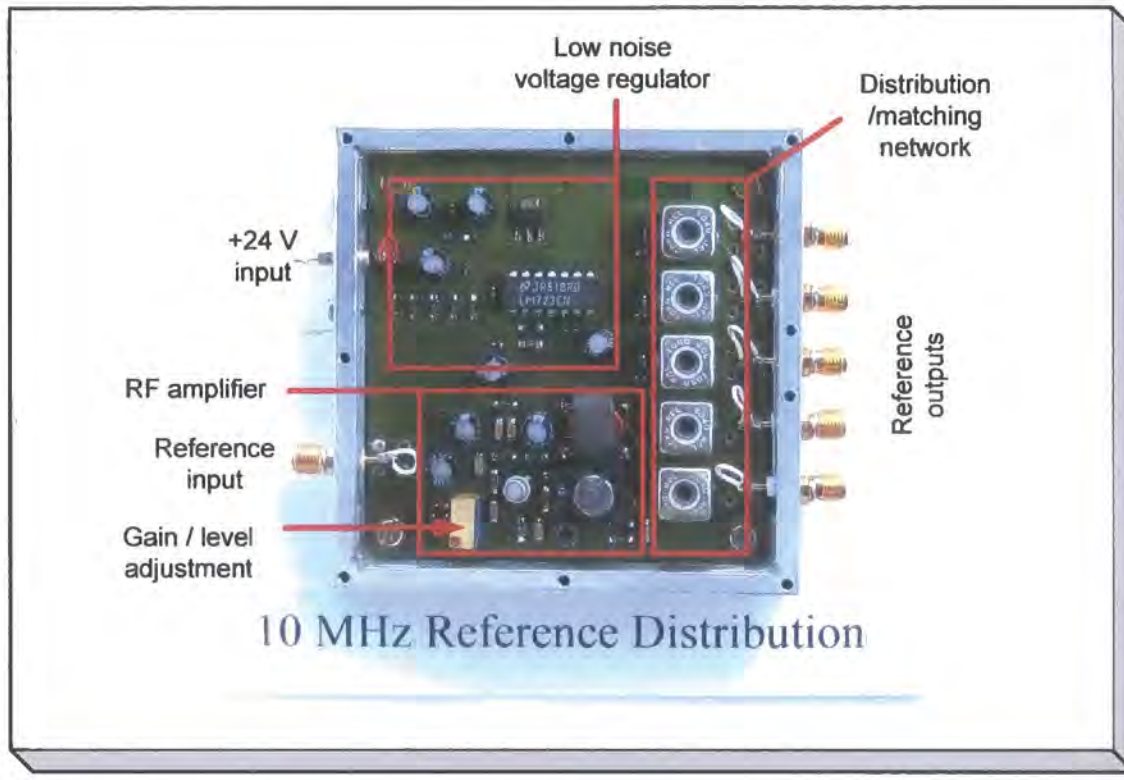

Figure 4.29 Reference distribution module

4.3.3 Main power supply

The input power to the equipment racks is nominally 24 V from either batteries or from an external mains power supply. The primary power supply (refer to figure 4.30) is + 5 V for all circuit modules built on Rogers 4003. This supply is also used by the micro-controller. A maximum of 5 A is available from the + 5 V supply. The other modules use + 12 V and + 24 V (synthesisers). These voltages are derived from two isolated 12 V converters stacked to provide + 12 V and +24 V. The maximum current available is 1.3 A distributed between the two supplies. The main supply includes three sets of switched outputs at + 5V and +12 V. These are controlled using logic level signals from the micro-controller to provide an RF "mute" function. All the power supply voltages

are derived using commercial switched mode converters with additional noise filtering provided to the input and outputs to reduce the level of switching spikes.

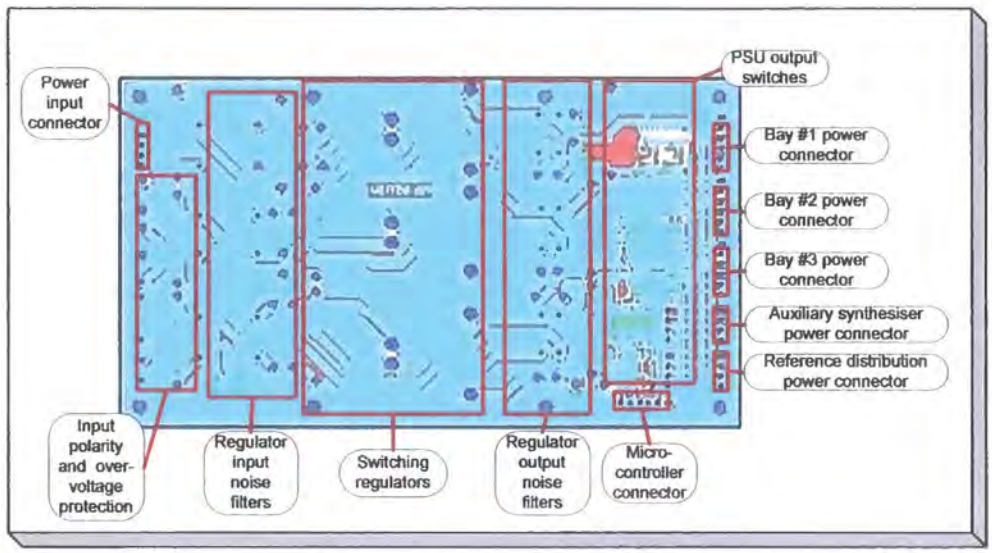

Figure 4.30 Main power supply

The commercial microwave amplifiers used in the 60 GHz sweep converters use + 15 V. This is derived directly from the input + 24 V using three terminal regulators since the current requirements exceed that available from the switching power supply.

4.3.4 Auxiliary power supply

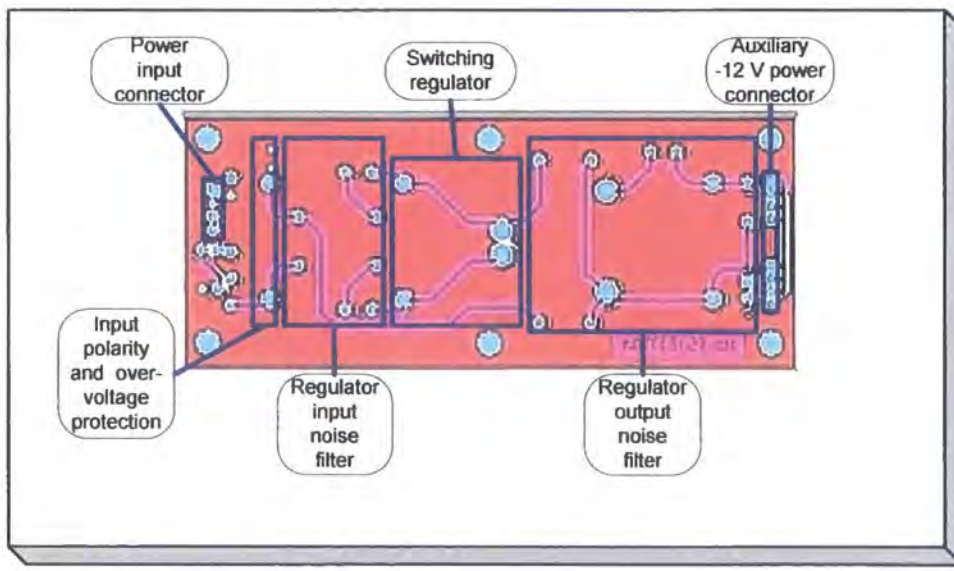

Figure 4.31 Auxiliary -12 V power supply

An additional auxiliary power supply provides – 12 V which is used by the synthesisers and the single sideband IF down-converter in the 60 GHz receiver (refer to figure 4.31). This uses an isolated 12 V switching converter with additional filtering provided. A maximum of 1.3 A is available from this supply.

4.3.5 Micro-controller

The micro-controller is assembled on a single PCB. (Refer to figure 4.32). This unit is primarily used to support the programming of the synthesisers used in the up-converter and down-converter rack.

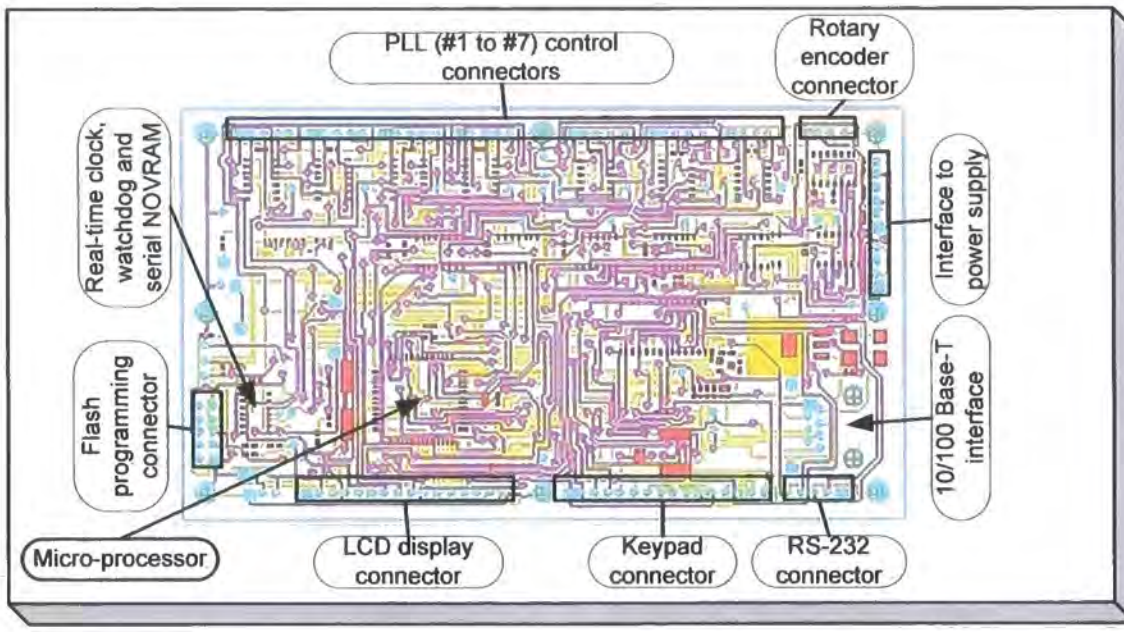

Figure 4.32 Micro-controller PCB

In addition the capability to support an LCD display, keypad / rotary encoder for data entry and an RS232 / Ethernet interface for connectivity have been provided. The LCD uses a parallel interface. The keypad uses a Maxim MAX6818 device. This provides keypad de-bouncing and an interrupt generation to indicate that a key has been operated. The rotary encoder provides a two-phase signal that has a 90° relative phase shift. Discrete logic has been used to extract the direction sense of the encoder. This information can be used with a counter (on the micro-processor) to complete the hardware interface. The RS-232 interface is provided using a Maxim MAX3110 device.

This includes on-chip negative voltage generation. The Ethernet interface uses a Lantronix "XPORT" module. This provides a serial interface to the micro-processor with all the physical layer, MAC and TCP-IP handshaking performed within the module itself.

A watch dog timer is included. This device (Ramtron FM31256) also provides a battery backed real time clock and 32 K bytes of non-volatile storage that is accessed via serial communication with the host microprocessor.

The microcontroller supports the programming and monitoring of up to seven individually addressed synthesisers. The program interface consists of serial clock, serial data and device latch signals to the synthesisers. A lock status signal is returned from the synthesiser. Three logic level outputs are also available which are used to enable / disable the output of the transmit converters / receive down-converters by switching the supply power to these circuits.

The micro-controller is flash programmed with device specific code compiled from a program written in "C". For the purpose of this project, however, the programming has been performed with hard-coded values for the synthesiser and LCD display with no software support for other functions at this time. The RS-232 and Ethernet functions have been removed from the PCB at this time to eliminate unnecessary sources of electrical noise from the +5 V power supply.

4.3.6 Reference 10 MHz to 40 MHz multiplier

The 10 MHz to 40 MHz reference multiplier is used to minimise the in-band phase noise for the 2.56 GHz sources that are used in the 60 GHz second up-conversion process. This module uses a cascade of two balanced Schottky diode doublers with intermediate amplifiers and filters.

(Refer to figure 4.33). The doubler uses a transmission line transformer T1 to provide two outputs that are in anti-phase. Each of these signals is used to switch the diodes D1

and D2. The outputs from the two diodes are then combined in phase using a second transmission line transformer T2. This approach provides attenuation of the fundamental and odd harmonic components due to the destructive combination of the anti-phase signals in the output transformer. The transmission line transformers are fabricated using twisted coupled wires wound through a twin-hole ferrite core. The conversion loss of the doublers has been measured to be nominally 10 dB.

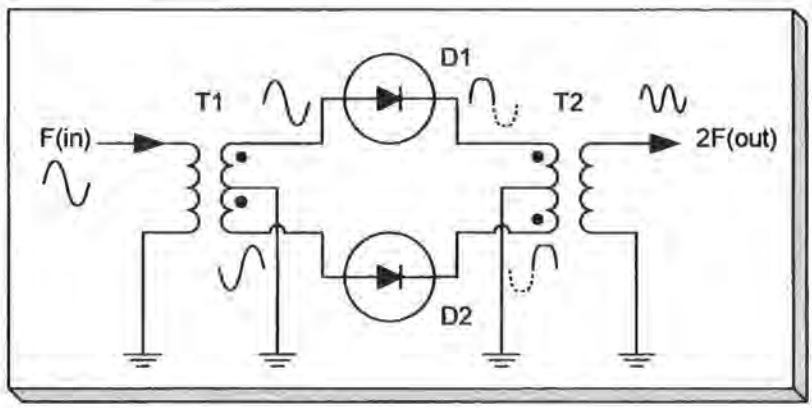

Figure 4.33 Reference doubler concept

The diode doublers are intrinsically broad band, limited in this design by the useable frequency range of operation of the transmission line transformers. (In fact the same design is used for both the 10 MHz to 20 MHz and the 20 MHz to 40 MHz doublers).

The actual bandwidth of the complete module (figure 4.34) is deliberately dictated by the bandwidth of the lumped element inter-stage filters. For this application a bandwidth of 10% has been provided. The inter-stage filters are designed as capacitive coupled resonators using three resonators in each filter. The filters are designed with 50 Ω terminating impedances to allow the filters to be aligned prior to the assembly of the rest of the multiplier circuit assembly.

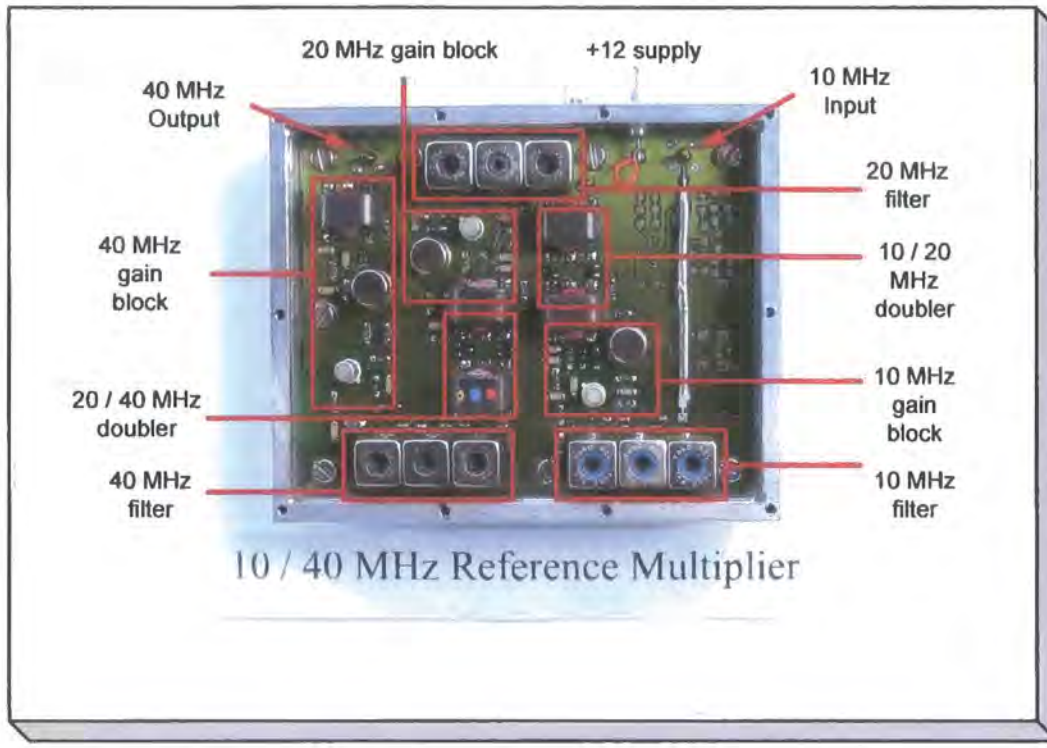

Figure 4.34 Reference multipler module

4.3.7 Signal sources

The converter system requires a range of short term stable radio frequency sources providing signals at up to 10.24 GHz. To provide these signals commercial VCO components operating within the range 1.6 GHz to 4.6 GHz have been used in conjunction with other commercially available devices to produce a source that is phase locked to the reference signal. The RF output from the PLL modules is then utilised directly or, where required is further multiplied to the required frequency.

The ADF4106 device was selected to provide the feedback divider and charge pump phase detector. The OP27 device was selected as the loop amplifier. Since the sources are only required to provide a fixed frequency it has been possible to include an AC voltage divider that operates well inside the closed loop bandwidth of the phase locked loop. This allows the effective gain coefficient for the VCO to be reduced from up to 120 MHz / volt to nominally 5 MHz / volt without compromising closed loop stability. The loops have been configured with a wide tracking bandwidth of typically 100 kHz

with a phase margin of nominally 70 degrees. This provides a closed loop response that provides an optimally flat noise floor (minimal noise peaking) within the loop band width. This approach also provides a closed loop response that is very tolerant to changes of open loop gain (The closed loop bandwidth reduces with falling loop gain, however, the phase margin remains fairly constant). For example, the sources within the 3.5 GHz and 5.7 GHz converters are required to provide operation over a range of frequencies. Operation over a range of frequencies tends to introduce gain changes within the phase locked loop due to change in feedback divider ratio and the typical reduction of VCO tuning sensitivity at the higher tuning voltages required for operation at the upper frequency range of the VCO.

The phase locked loops have been designed to provide a third order response. This allows the effect of the RF decoupling that is required on the VCO tune line (to reduce noise pick-up and provide an RF bypass) to be factored into the design.

The ADPLL design tool [4.4] provided by Analog Devices has been used to perform the design of the loops and to evaluate sensitivity to gain variations.

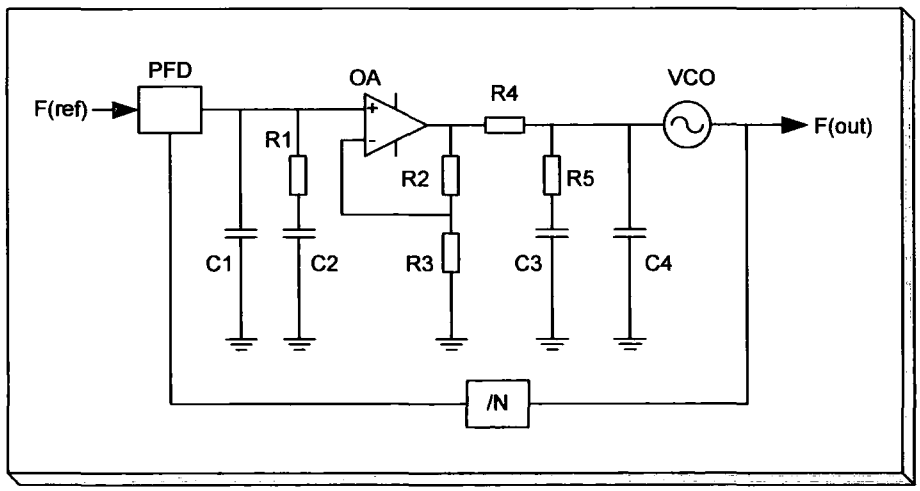

Figure 4.35 Phase locked loop overview

(Refer to figure 4.35). The PFD and the /N functions are contained within the ADF4106 device. The output of the PFD is presented as a current switched charge pump. This charge current is integrated by the capacitors C1 and C2. The resistor R1 provides the

phase lead around the 0 dB closed loop gain region necessary to ensure closed loop stability. The choice of R1, C1 and C2 are primarily responsible for defining the loop gain and phase margin. The output of the PFD is restricted to 0 to 5 V. The operational amplifier OA is used to provide voltage gain and to isolate the charge pump from the additional filter elements. The resistors R4 and R5 provide a voltage attenuator which is effective for frequencies where the reactance of C3 is << than R5. This provides an attenuation of the high frequency noise from the loop amplifier. The frequency at which this occurs is chosen to be << than the closed loop bandwidth of the loop. This has been configured at typically 30 Hz, for the PLL sources used here. Resistor R4 in conjunction with C4 provides an additional integration term which has values chosen to become significant at approximately ten times the closed loop bandwidth of the PLL. This pole provides additional an attenuation of residual reference signals.

Figure 4.36 shows the predicted phase noise response for the 4.5 GHz source used in the 2.5 GHz converters. This figure illustrates that the total phase noise is determined by the noise performance of the reference at frequencies below 1 kHz and by the noise floor of the PLL device for frequencies above 1 kHz.

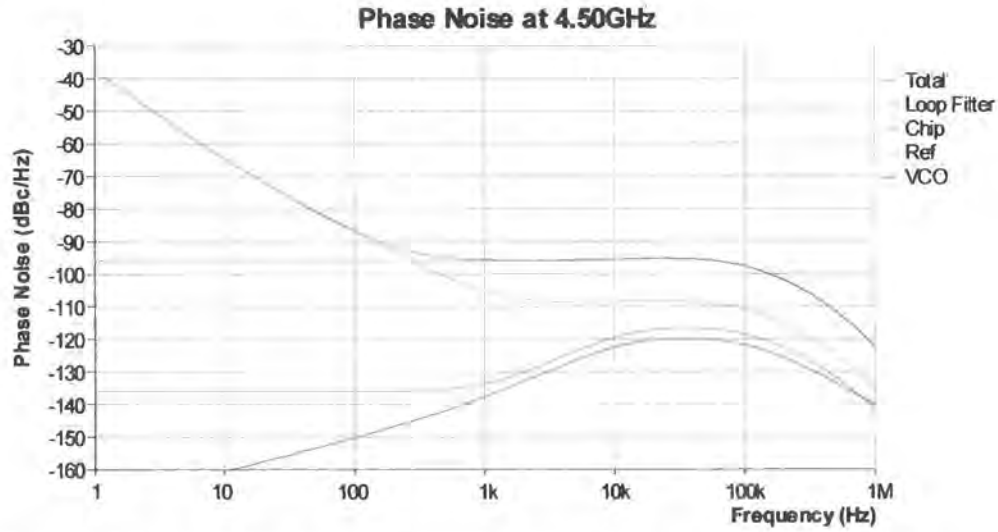

Figure 4.36 PLL noise prediction for 4.5 GHz

The PLL module includes local voltage regulation to reduce feed-through of power supply noise. The voltage regulators use a band-gap reference to provide low noise, low drift and tight tolerance. The logic control lines are filtered into and out of the module.

The output of the VCO is divided equally using a resistive splitter that provides wide bandwidth with a match close to 50 Ω. The feedback signal is buffered using resistive attenuators and a silicon MMIC gain block. The other output signal from the power divider is amplified using an additional silicon MMIC gain block. The specific MMIC devices have been selected on a case by case basis to provide an output signal of nominally 5 to 10 mW (+7 to +10 dBm) without the amplifier being driven into saturation. This is important to avoid signals on the amplifier bias supply from being heterodyned onto the local oscillator output [4.5].

The closed loop phase noise performance of the source is defined by the multiplied noise of the reference at low offset frequencies (typically <= 1 kHz). Above this, the noise floor is due to the noise floor of the phase / frequency detector multiplied up to the output frequency. For the ADF4106 device selected here, the phase detector noise floor exhibits a response that is proportional to the phase comparison frequency. Since the multiplication provides a degradation that is proportional to frequency squared, the optimum noise performance implies operation with as high a reference frequency as practical. For the majority of the sources used within the project a reference frequency of 10 MHz has been used. (A reference frequency of 3.333 MHz is used for the receiver auxiliary signal source to provide a nominal ramp offset of 13.333 MHz (after multiplication by four) for the 60 GHz system. The 2.56 GHz sources that are used within the 60 GHz second up-converters use a 40 MHz reference).

Using a high reference frequency was initially problematic. The first revision of the source design included a very high speed comparator to provide a square wave signal to the reference input of the ADF4106 from the sine wave reference. This approach resulted in the in-band noise floor of the source being ~ 10 dB worse than predicted. Under "normal" configurations the reference would be divided to typically 1 MHz which would make this degradation not apparent since the reference phase noise would be attenuated by 20 dB.

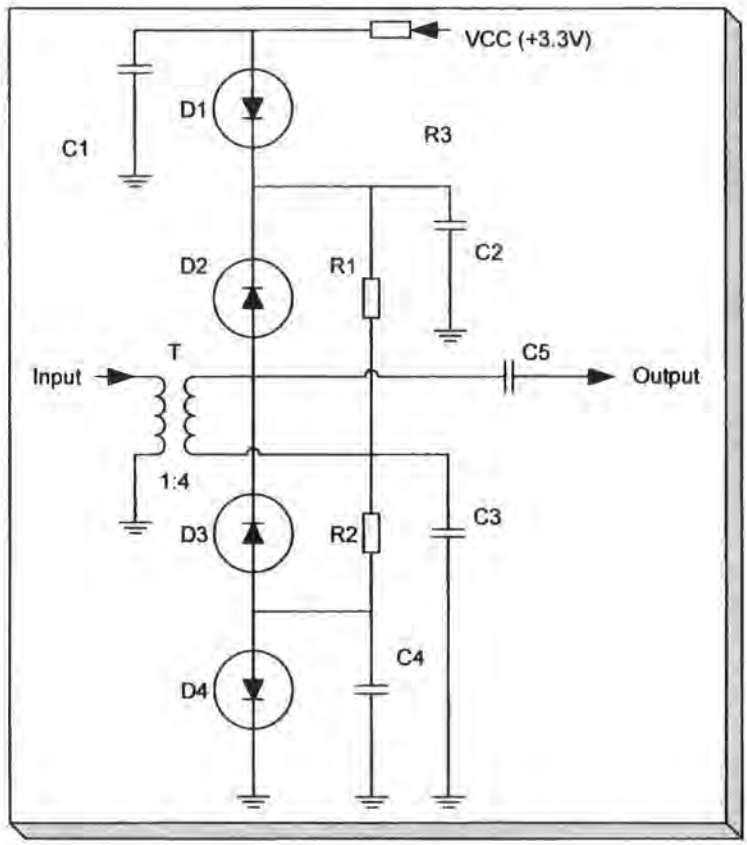

Figure 4.37 Reference interface concept

Rather than attempt to produce a very high speed differential limiter [4.5] an alternative circuit to "square" the reference circuit was adopted (refer to figure 4.37). The input signal level of ~0.5 V rms is increased to ~2 V rms using a Minicircuits T16-1 RF transformer with a ratio of 1:4. The output of this is clamped between the PLL digital supply rail and ground using fast switching Schottky clamp diodes. This approach has been demonstrated to operate successfully for reference frequencies of 10 MHz and 40 MHz.

A source operating at 2.56 GHz is used to provide the 10.24 GHz local oscillator signal for the second up-conversion function within the 60 GHz converters. This source uses a reference of 40 MHz for the phase / frequency detector. The 40 MHz reference is derived from the 10 MHz reference using a cascade of two X2 multipliers. This provides a net improvement in phase noise of this source of approximately 6 dB relative to operation with the 10 MHz reference directly.

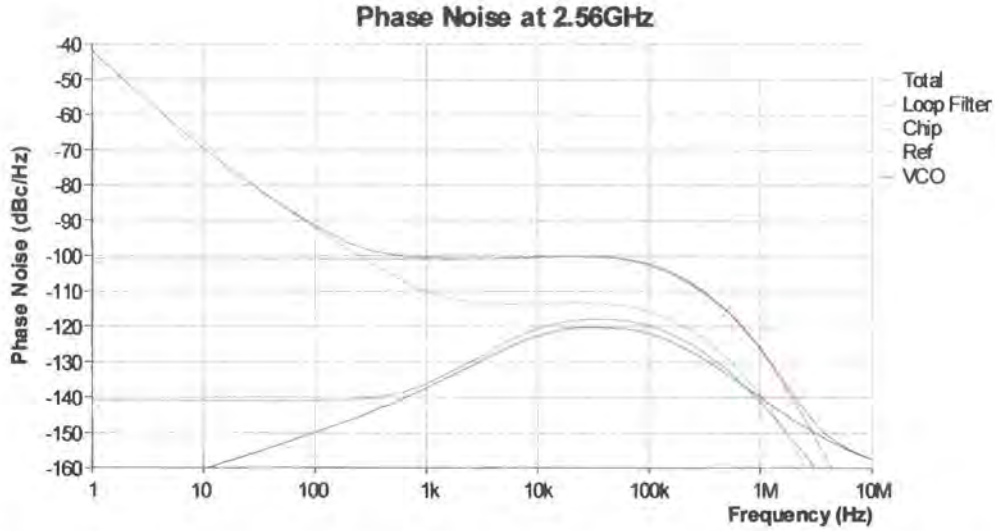

Figure 4.38 PLL phase noise prediction using a 10 MHz comparison frequency

Figure 4.38 shows the predicted phase noise for the 2.56 GHz source using a 10 MHz reference. This demonstrates that the closed loop phase noise of the source from 1 kHz to 100 kHz is defined almost entirely by the noise floor of the phase detector since this is ~ 14 dB above the effective noise floor of the 10 MHz reference multiplied up to 2.56 GHz.

Figure 4.39 shows the predicted phase noise for the 2.56 GHz using a 40 MHz reference that has been realised by direct multiplication of the 10 MHz reference using a cascade of two diode doublers. This approach provides a reduction in the closed loop phase noise of ~ 6dB. In principle this technique could be extended further using a reference frequency of 80 MHz. This would provide an additional noise reduction of ~ 2 dB. This has not been pursued since the system phase noise floor is already dominated by the noise in the first up-conversion from 2 GHz to 5.5 GHz.

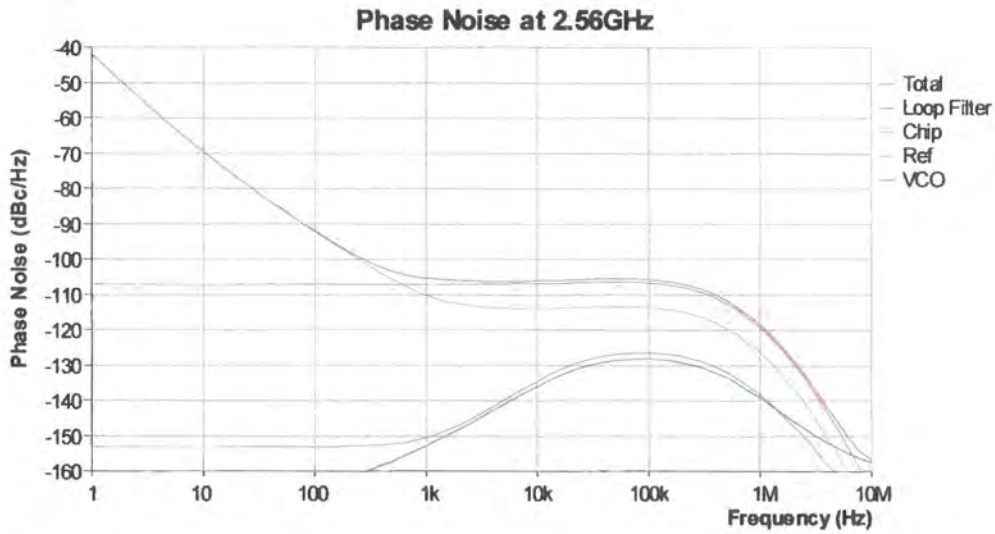

Figure 4.39 PLL phase noise prediction using a 40 MHz comparison frequency

The complete synthesiser module is shown in figure 4.40.

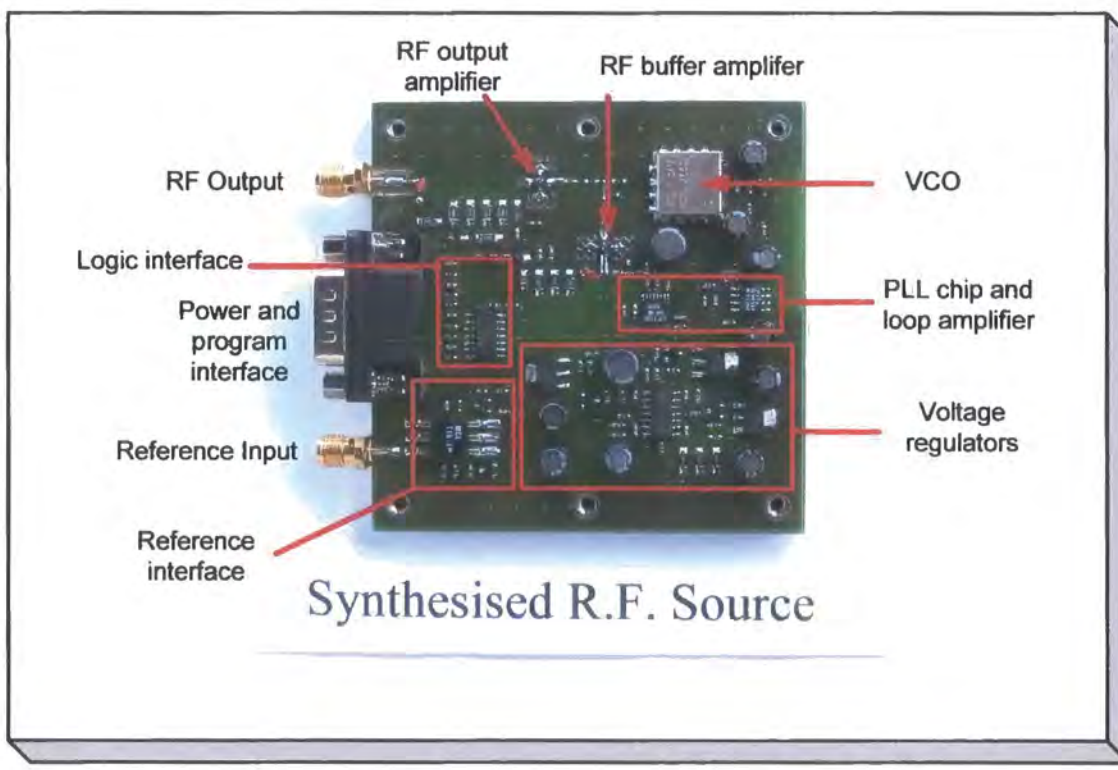

Figure 4.40 Synthesised RF source

4.3.8 Radio frequency X2 multiplier

The 3.5 GHz converter requires an effective local oscillator of 5.5 GHz to 6.3 GHz. This is produced by multiplying a fundamental source operating at 2.75 GHz to 3.15 GHz.

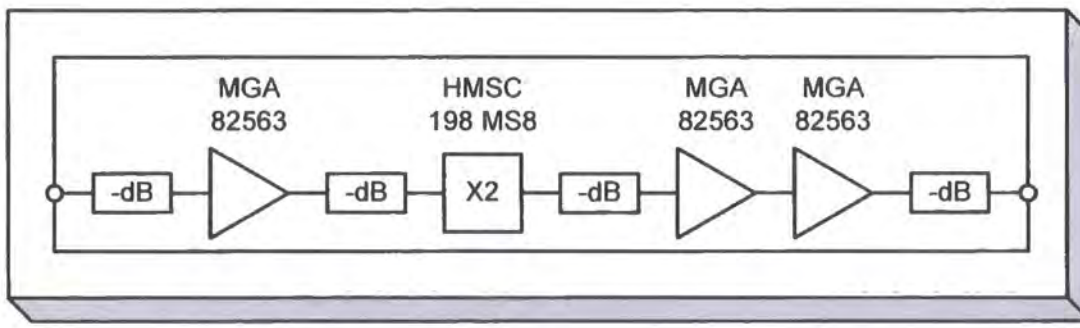

Figure 4.41 X2 multiplier block schematic

This module (refer to figures 4.41 and 4.42) uses an input amplifier to drive a GaAs MMIC doubler device (HMC189MS8) supplied by Hittite. This has a nominal conversion loss of 13 dB with relative suppression of the fundamental and third harmonic of > 20 dB. A two stage amplifier and level setting attenuators provide a nominal module output level of + 10 dBm.

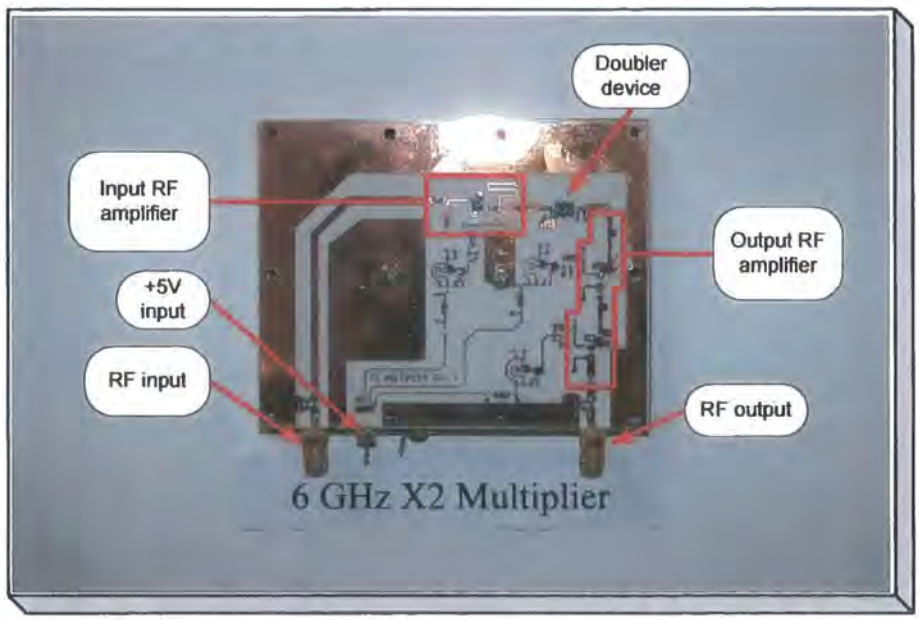

Figure 4.42 X2 multiplier module

4.3.9 Radio frequency X3 multiplier

The 5.7 GHz converters require a local oscillator within the range 6.7 GHz to 8.0 GHz. This is achieved by multiplying the output of a fundamental source operating from 2.23 GHz to 2.67 GHz by a factor of three times.

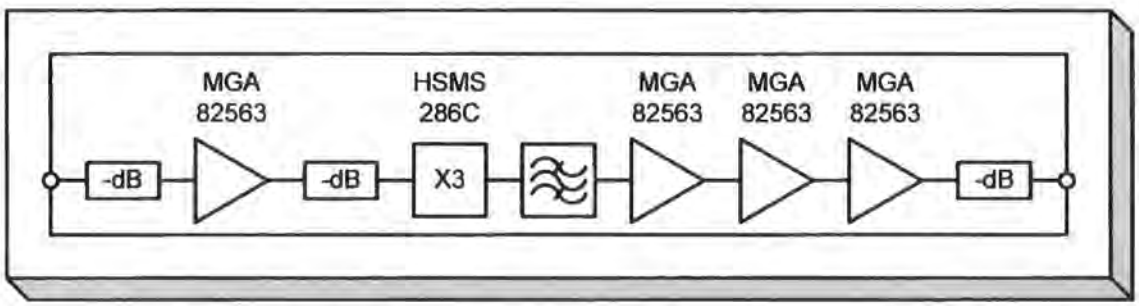

Figure 4.43 X3 multiplier block schematic

This module (refer to figures 4.43 and 4.44) uses a novel balanced anti-parallel diode multiplier fabricated using a series dual diode "T" structure. The multiplier uses a high impedance input line ($\lambda/4$ at the output frequency) which is resonated at the input frequency with a series capacitor. This ensures that the input matching structure is isolated from the multiplier at the output frequency. The real component of the input impedance of the multiplier was estimated to be 20 Ω using the non-linear simulation tool set within the AWR package [4.6]. This is matched to 50 Ω using a conventional $\lambda/4$ matching transformer. The third harmonic component is extracted from the output of the diode multiplier through a five section branch-line filter. This uses parallel shunt lines at the input and output sections of the filter to provide practical impedances and therefore line widths. The filter at the output is coupled to the multiplier diodes using a high impedance line (which is $\lambda/2$ at the output frequency). This decouples the filter from the diode structure at the input frequency since the filter would otherwise provide a short circuit to ground at the input frequency. A three stage amplifier and level adjustment attenuators provide a nominal output level of +10 dBm.

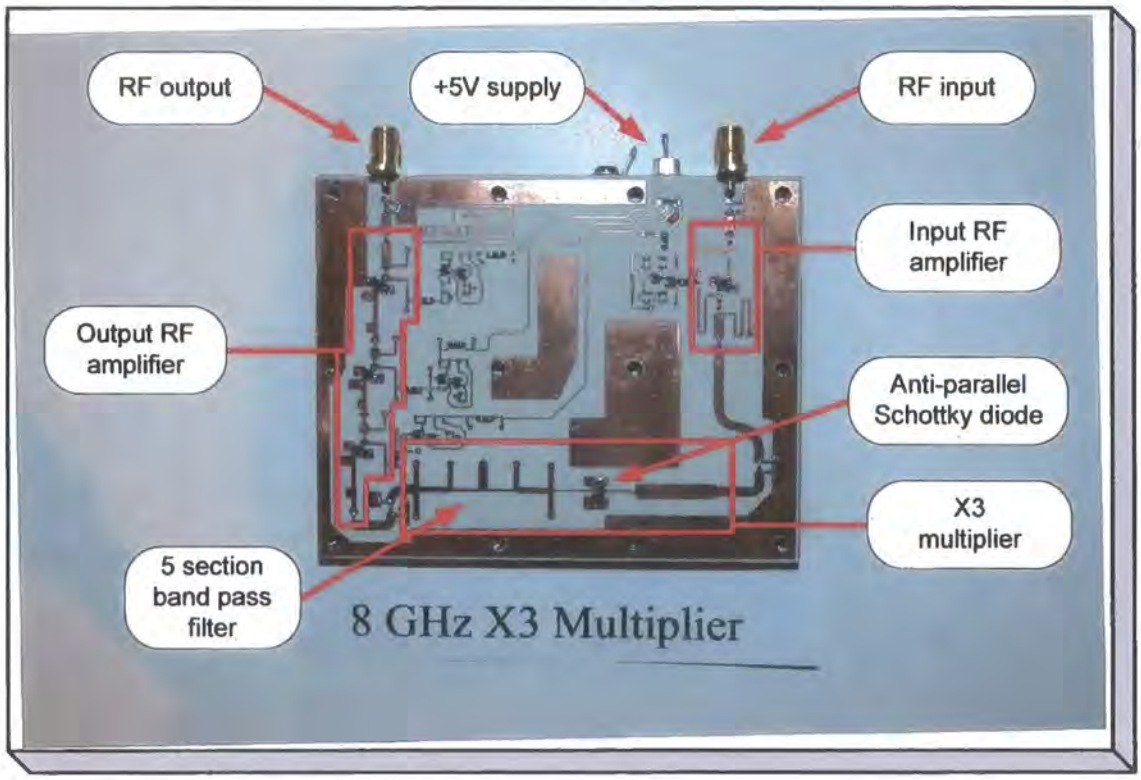

Figure 4.44 X3 multiplier module

4.3.10 2.5 GHz converters

This converter design support conversion between the 2 GHz and 2.5 GHz bands. This uses a high side local oscillator signal of nominally 4.5 GHz. The converter is used both as an up-converter and as a down-converter with minor component changes. (These component changes are used to adjust the distribution of gain and attenuation levels within the module to optimise the noise figure for the receive converter and output power for the transmit converter). The module includes a mixer stage that includes buffer amplifiers for the LO and input signals. A separate amplifier section is included that is separated from the mixer so that inter-stage filtering can be included.

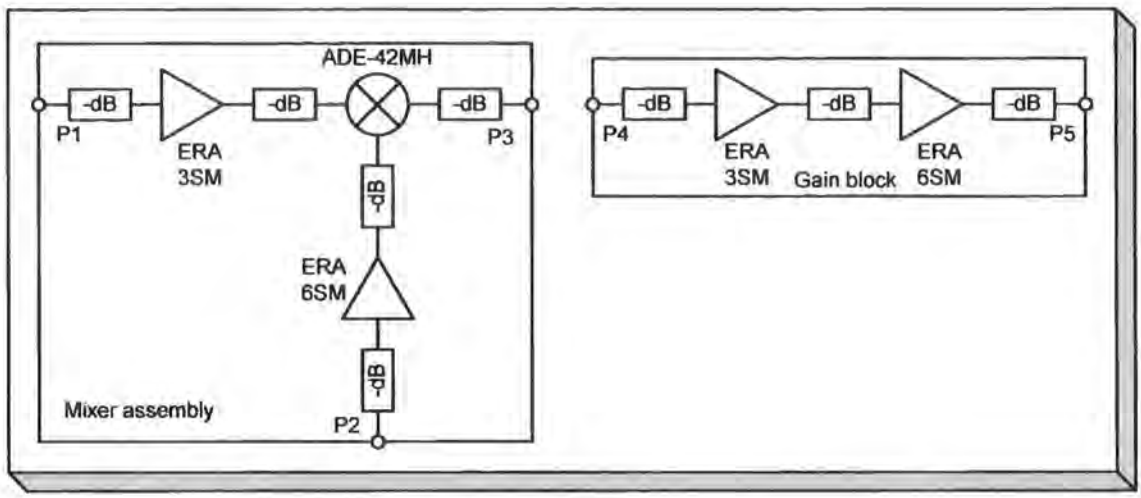

Figure 4.45 2.5 GHz converter block diagram

(Refer to figure 4.45). The input signal is presented to P1. This is the RF input (after the LNA and image filters) for the down-converter and the IF input when used as an up-converter. The local oscillator is presented to P2. The LO is provided on the high side of the signals being converted such that F(LO) = F(IF) + F(RF). The output from the frequency conversion mixer is available on port P3. An ERA-3SM gain block is used to provide additional signal amplification for the RF / IF input. The output power from the synthesiser is nominally +7 dBm. The ERA-6SM provides additional amplification to provide a mixer LO drive power of +13 dBm. The mixer is provided with 3 dB attenuators on all three ports. This provides broadband operational impedance close to 50 Ω on all ports, and the necessary termination of all mixer products. This is necessary to maintain a "flat" conversion loss and to minimise amplitude distortion due to the mixing process and to facilitate operation at higher signal levels. Additional attenuators are provided at the RF / IF input and LO input to enable the signal levels to be adjusted to the correct levels.

The separate gain block is assembled from two MMIC amplifiers (ERA-3SM and ERA-6SM) with input, output and inter-stage attenuators. The attenuators allow the optimum signal levels to be maintained through the amplifiers and provides input and output terminations that are close to 50 Ω. This is particularly important for port P4 (gain block input) when used as an up-converter (or down-converter) as this port is terminated with

a band-pass filter which provides nearly complete reflection of the signal outside the filter pass-band.

The attenuator values are adjusted to optimise the signal levels for operation as either an up-converter or a down-converter.

Figure 4.46 shows the physical layout of the 2.5 GHz converters. This assembly is fabricated using 1.6 mm thick epoxy-glass FR4 material with a copper ground plane with RF tracks on the top surface. To compensate for the loss in the material at these high frequencies additional gain is provided.

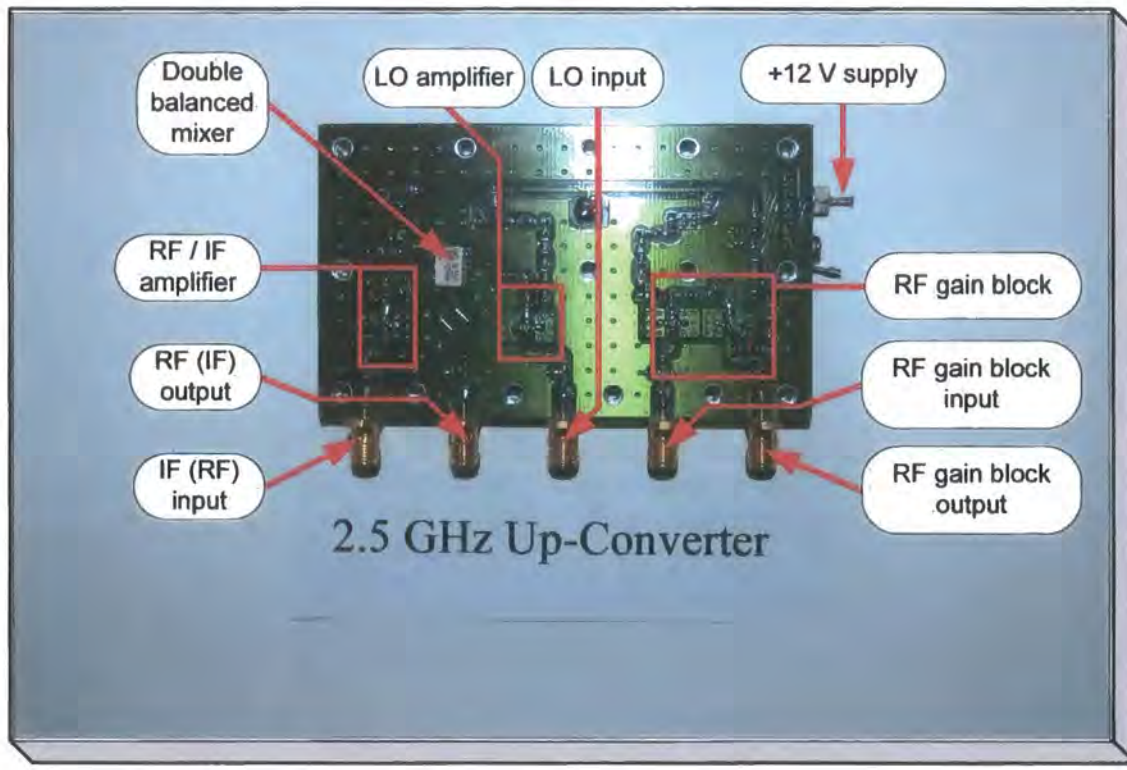

Figure 4.46 Photograph of the 2.5 GHz converter PCB

4.3.11 3.3 GHz to 6.0 GHz up-converter

This design is used to support operation at both 3.5 GHz and 5.7 GHz bands without any component changes.

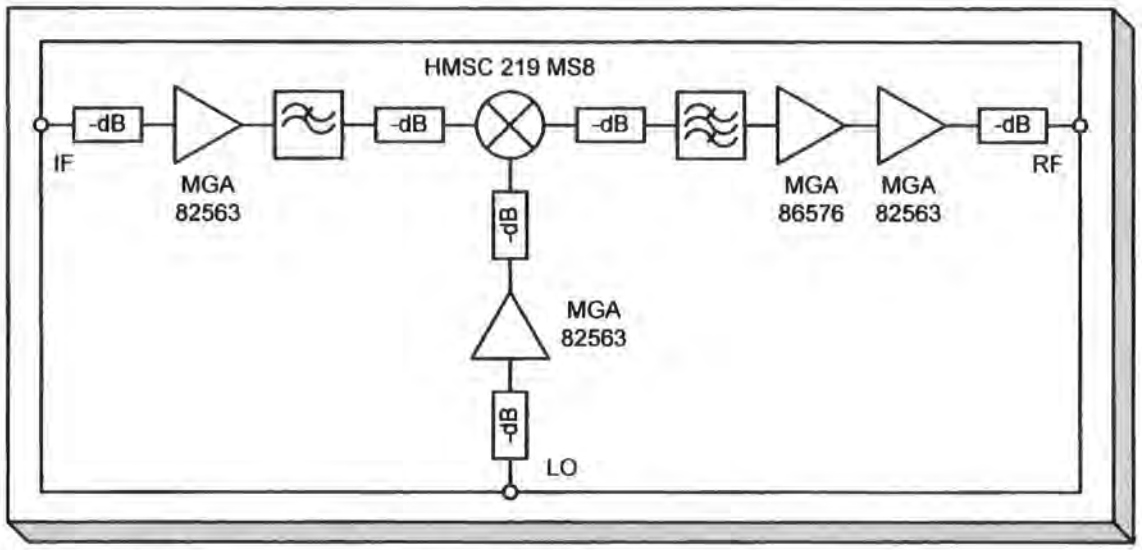

Figure 4.47 Up-converter module block schematic

This module (see figures 4.47 and 4.48) includes amplifiers for the local oscillator, IF input and RF output signals in addition to an RF image filter and mixer. A Hittite GaAs MMIC mixer (HMC219MS8) has been utilised. The RF amplifier is required to provide approximately constant gain from 3.3 GHz to 6.0 GHz. This has been achieved using a two stage design with the active devices (GaAs MMIC) matched to 50 Ω for both input and output. An MGA 86576 has been used for the first stage followed by an MGA 82563 device. This provides a matched amplifier that exhibits a significant gain slope across the band. A novel slope attenuator has been developed that provides a frequency selective attenuation function to provide an overall level response. This structure uses two resistor loads that are coupled to the through transmission line using a nominal quarter wavelength line at the top of the band. Thus at the high frequency little or no energy is coupled from the main through line to the shunt resistors. At the lower end of the band the lines are approximately $1/8^{th}$ of a wavelength and the through line has a complex load presented in shunt. By separating two of these structures at approximately 1/4 of a wavelength at the lower frequency the reactive component can be cancelled.

The behaviour of this candidate structure was investigated using AWR Microwave Office and was confirmed to represent a practical solution to this problem. Two stages of equalisation have been included in the up-converter, one after the first device which provides nominally 20 dB of gain and the second after the output device which provides nominally 10 dB of gain. This equaliser structure is believed to be novel as no similar approach has been identified to date.

A seven section branch-line band pass filter is included between the mixer and the output amplifier to provide attenuation of the upper sideband (image) signal. This filter has been realised using a distributed branch line structure.

A nine section low pass filter is used to reject IF signals above 2.3 GHz. This filter has been realised using a distributed structure of cascaded low and high impedance lines.

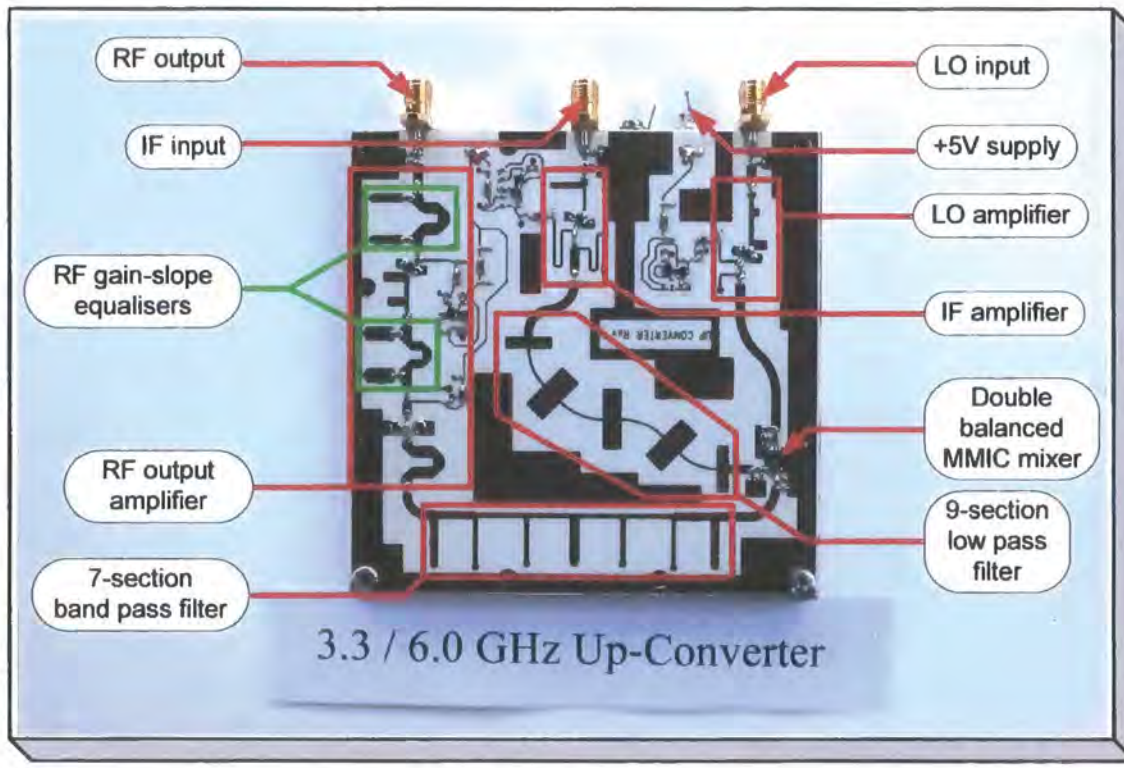

Figure 4.48 Photograph of 3.3 GHz to 6.0GHz up-converter

4.3.12 3.3 GHz to 6.0 GHz down-converter

This design is used to support operation at both 3.5 GHz and 5.7 GHz. This module includes amplifiers for the local oscillator, IF input and RF output signals in addition to an RF image filter and mixer. This design utilises the same functional circuit "building blocks" that have been used in the 3.5 GHz / 5.7 GHz up-converters.

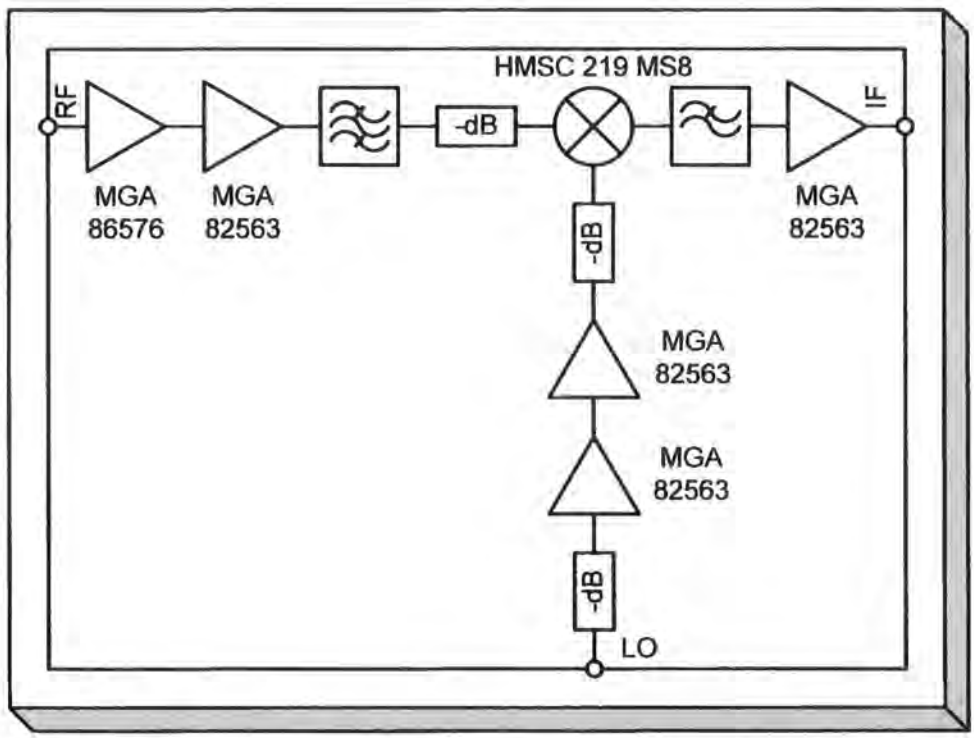

Figure 4.49 Integrated down-converter for 3.3 GHz to 6.0 GHz

(Refer to figures 4.49 and 4.50). In this configuration, the input signal is amplified using a two stage gain block. The output of this gain block is filtered using a seven section band pass filter. This filter provides attenuation of signal in the IF band and at the image frequencies. The output of the filter provides the input signal to the down conversion mixer. Note that broadband resistive attenuators have been provided to the RF (signal) and LO ports to flatten the conversion loss and to provide optimum distortion behaviour for the mixer. The IF output signal is band limited using a nine section low pass filter. This filter is followed by an IF amplifier. The local oscillator path includes two stages of amplification.

This module can be used for down-conversion from 3.3 GHz to 6.0 GHz by changing the local oscillator signal. The down-converter has been measured to provide a conversion gain of nominally 27 dB with an associated noise figure of 3 dB.

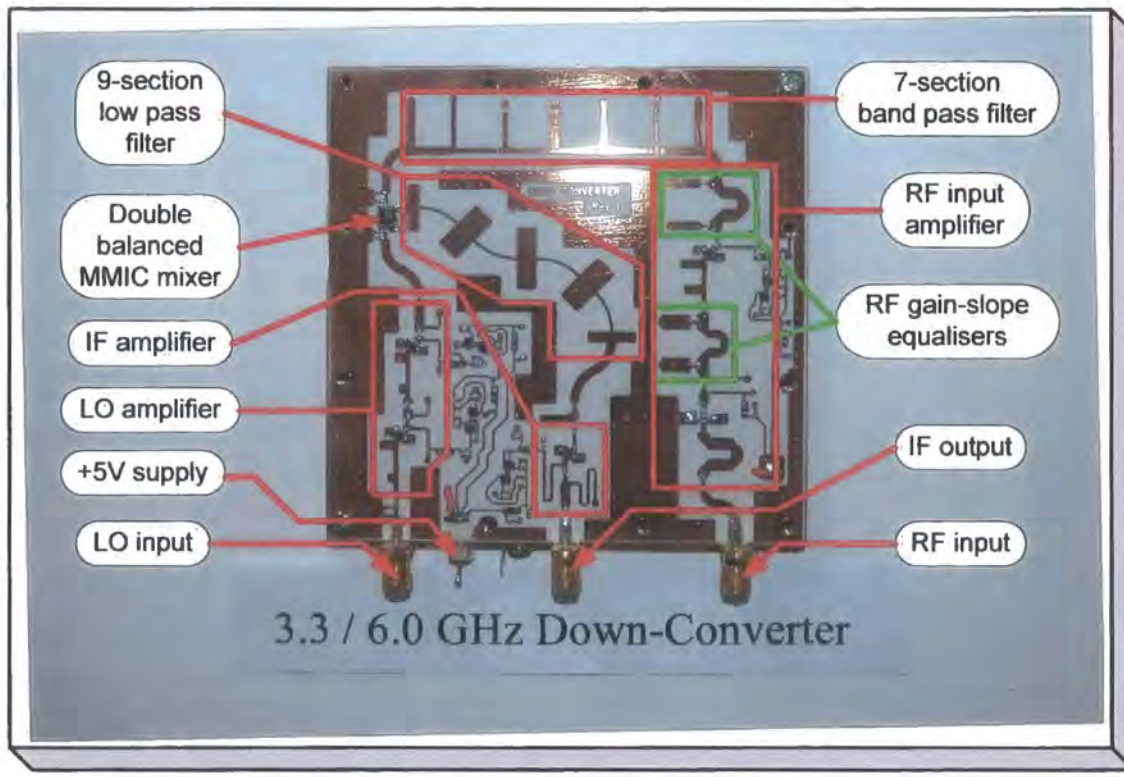

Figure 4.50 Photograph of 3.3 GHz to 6.0 GHz down-converter

4.3.13 Power amplifiers

All three up-converter assemblies include a medium power amplifier (+20 dBm at P(-1 dB) / +23 dBm P(sat). This amplifier (figure 4.51) uses a single stage driver with two parallel output stages that are driven and combined using Wilkinson couplers. Gain equalisation has been incorporated on the input of the amplifier devices. Agilent GaAs MMIC devices (MGA 82563) have been used. The overall gain is ~ +16 dB with a tolerance of +/1 dB over the range 2.3 GHz to 6.0 GHz.

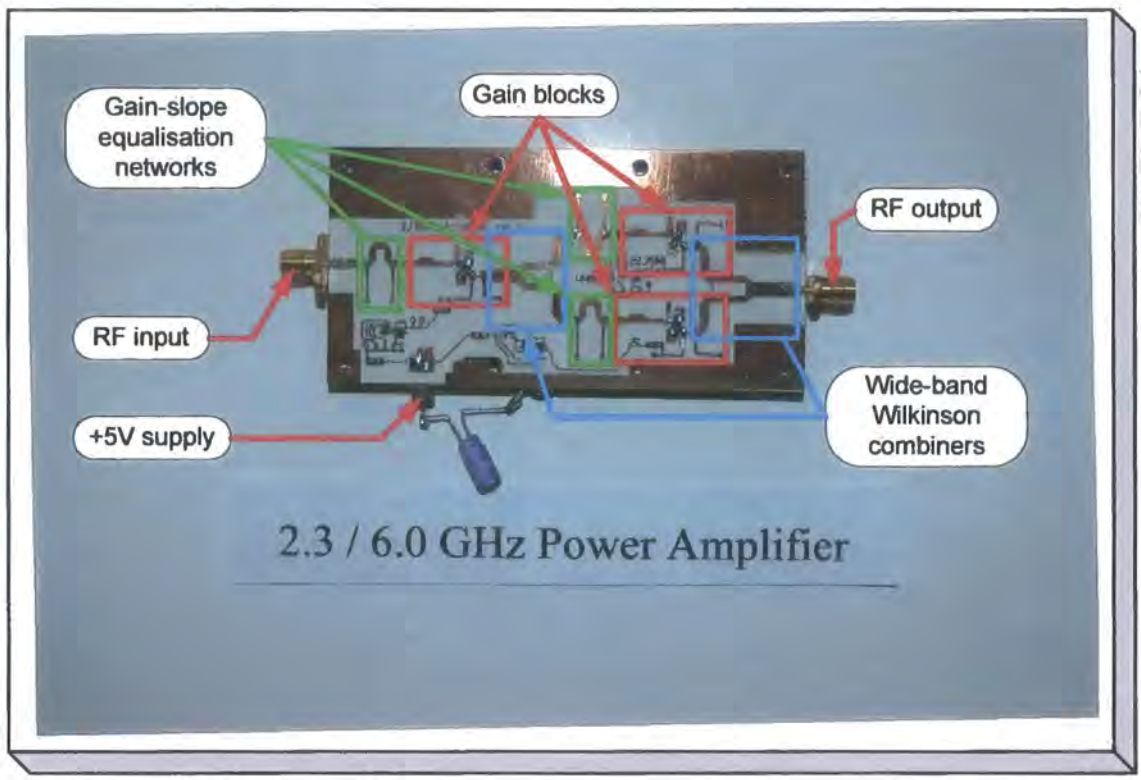

Figure 4.51 Power amplifier

4.3.14 2.5 GHz low noise amplifier

The 2.5 GHz down-converter uses a single stage low noise amplifier. This is the design that has also been used as the local oscillator input amplifier used in the frequency multipliers and as the IF amplifier used in the up and down-converters. This design provides a gain of + 13 dB with an associated noise figure of ~ 2.5 dB. The output 1 dB compression is ~ +17 dBm.

The amplifier (figure 4.52) uses a single Agilent MGA 82563 GaAs MMIC amplifier. Reactive matching has been included on the input to the device to improve the return loss to > 15 dB. The output network uses a "PI" network to introduce the amplifier bias and to block the RF output from the amplifier dc bias. This network also provides a high pass function. This attenuates the amplifier gain response below ~ 500 MHz.

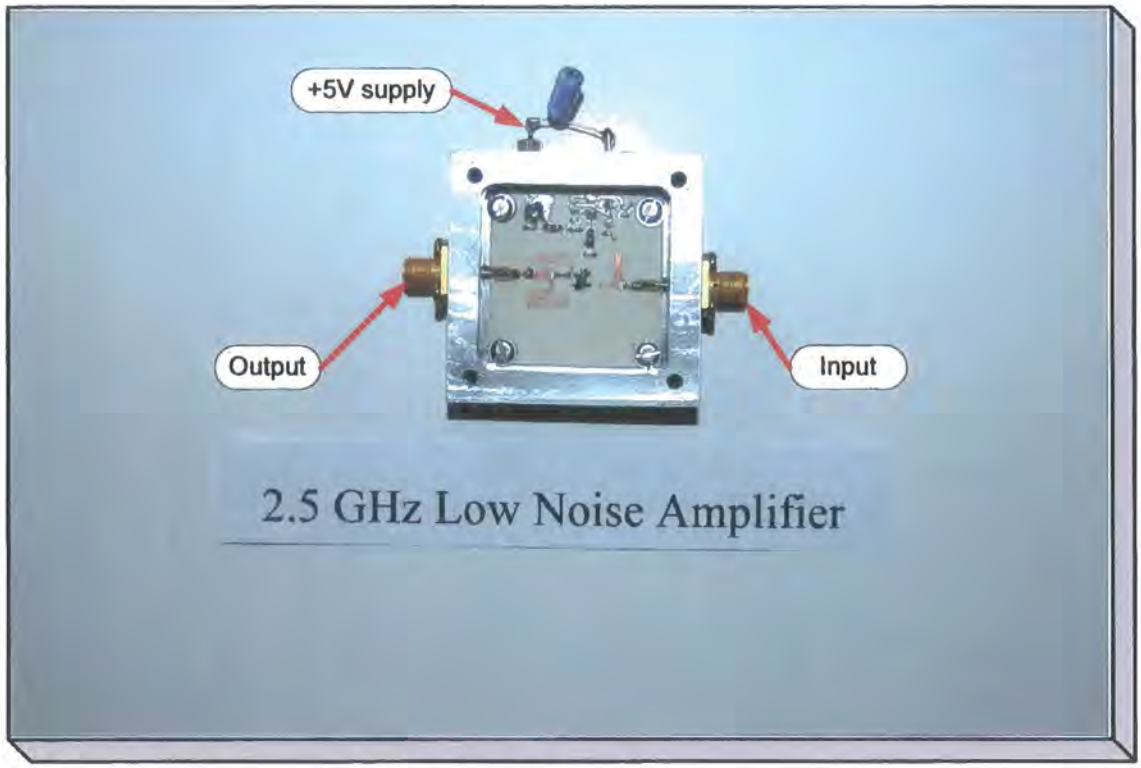

Figure 4.52 Low noise amplifier for 2.5 GHz

4.3.15 Local oscillator buffer amplifier

A single stage buffer amplifier has been included in the four channel down-converter to compensate for the additional loss due to the four way power divider that has been used to derive the local oscillator signals. This amplifier is a single stage of the design used within the medium power amplifier and includes a gain-slope equalisation network on the input to the device. This provides an amplifier that has a substantially flat frequency response across the LO frequency band.

4.3.16 Mechanical Filters

A number of mechanical filters have been designed and fabricated to provide harmonic selection at the output of the frequency multipliers, local oscillator / image suppression within the up-converter assemblies and to provide band-limiting and harmonic suppression within the 2.5 GHz converters.

The design approach used is broadly that outlined by Mattei et al [4.7]. However, in this original work the filter was wholly optimised for loss by selecting geometry to provide maximum resonator "Q" factor. This approach tends to produce a design in which the first resonator within the filter has a poor mechanical aspect ratio (is thin). Since the designs here are relatively broad band the effect of losses within the filters is not a significant problem. Thus the filter design has been iterated to provide filter resonators that have an approximately "square" aspect ratio. This is achieved by varying the internal admittance factor "h" and repeating the calculation to determine the bar width and spacing until an acceptable aspect ratio is realised. A spread sheet has been produced to ease this process. The filter is then coupled to 50 Ω using the input / output coupling bars. The potential downside to this design methodology is that since the filter internal impedance is now lower the gap between the input and output coupling sections is smaller. This issue has been circumvented by making the input and output coupling bars as separate components. In principle it would be highly desirable to make the separation of the input coupling bars adjustable to allow the matching of the filter to be adjusted. This has not been attempted here and as a consequence the return loss available from the filters is nominally 13 dB. (The designs are for 0.1 dB ripple which should provide a return loss of 16 dB). It is however noted that the rejection characteristics of the filter are in accordance with a 0.1 dB ripple design. Actual filter return loss has been observed to vary between 9 dB and 16 dB.

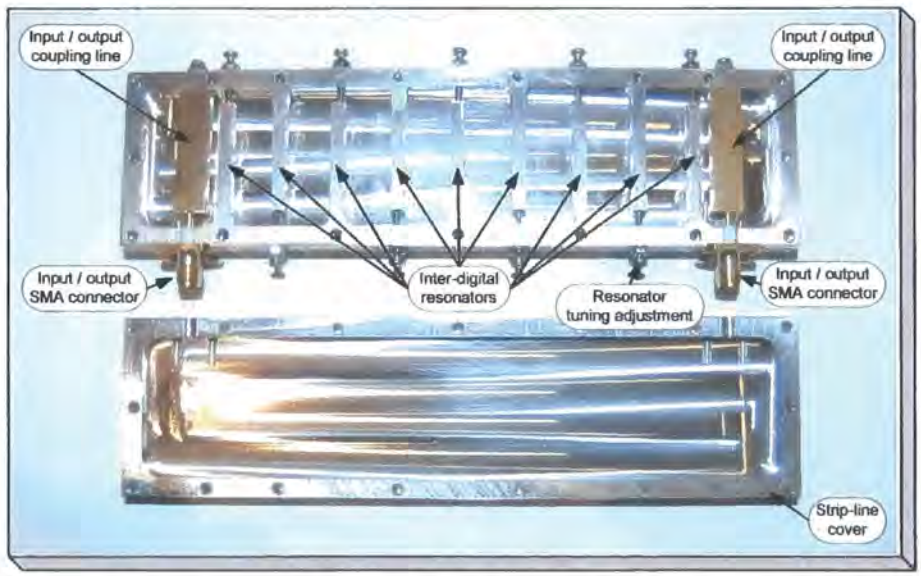

Figure 4.53 Internal view of 2.09 GHz nine section inter-digital filter

Five pole designs have been produced for 2 GHz, 2.5 GHz, 3.5 GHz, 6 GHz and 7.5 GHz, seven pole designs for 2.25 GHz, 3.9 GHz, 5.3 GHz, 5.9 GHz and 7.3 GHz, and nine section designs (figure 4.53) for 2.09 GHz and 2.25 GHz.

4.3.17 Base-band Pre-Amplifier

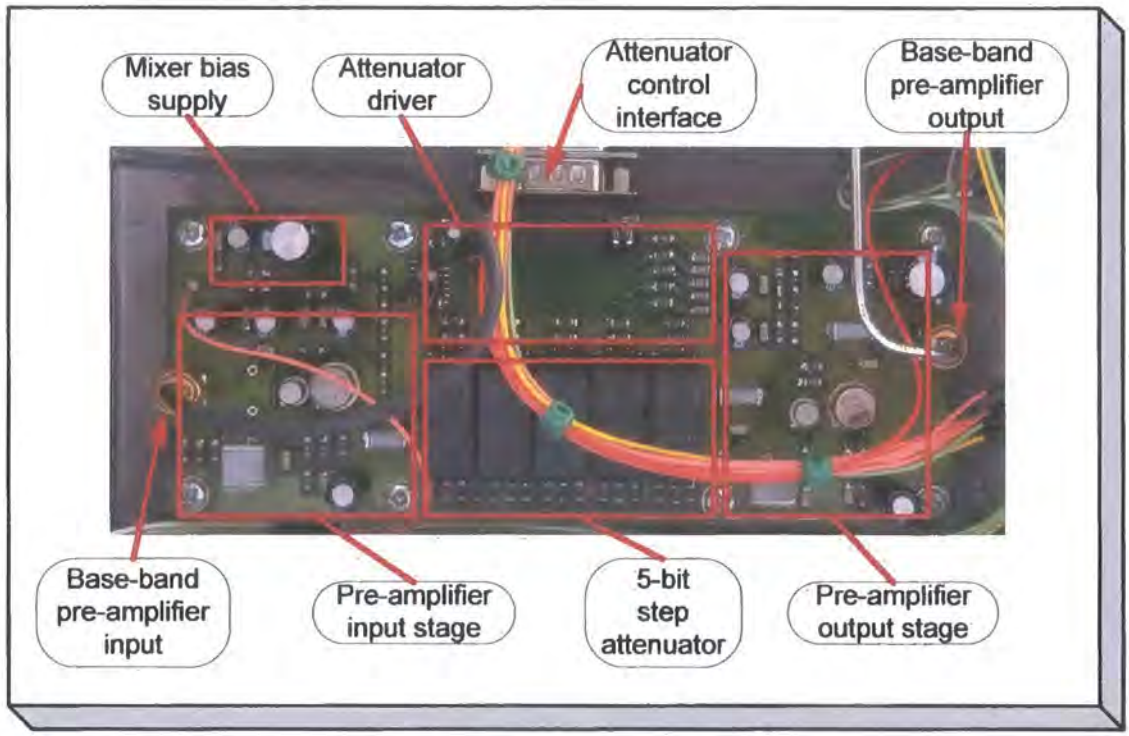

Figure 4.54 Photograph of the base-band pre-amplifier

The base-band pre-amplifier (figure 4.54) is used in the 60 GHz receiver. The input frequency is nominally 12.5 MHz to 13 MHz. This module uses two stages of amplification with an intermediate five bit step attenuator.

This attenuator provides 0 dB to 31 dB of attenuation in 1 dB steps. The attenuator uses individual "Π" and "T" section matched attenuators of 1, 2, 4, 8 and 16 dB. The attenuation sections are then switched into or bypassed on the interconnection between the output of the first stage amplifier and the input of the second stage amplifier. Since the attenuators are only used to perform manual level adjustment to avoid overloading

for high input signals the attenuators are switched using individual relays. A logic level interface is provided for the five step attenuators.

Each amplifier stage is fabricated using a two transistor cascade with local feedback. This overall two stage pre amplifier provides high gain (49 dB), wide band-width (30 MHz at -3 dB) with low distortion and a measured noise figure of 3 dB. The amplifier output 1 dB compression level is +12 dBm.

The 60 GHz mixer requires a low current, low noise supply to provide forward bias for the Schottky mixer diodes. This function is also supported on this card.

4.3.18 Single Sideband Down-Converter

The single sideband down-converter is used to convert the 12.5 MHz IF signal (used in the 60 GHz receiver) to the baseband input range of the channel sounder signal conditioning / data acquisition system. The sideband cancellation is performed at base-band using the phasing technique [4.8].

The down converter (shown in fig 4.55) includes an input band pass filter to provide image rejection for a down-conversion from nominally 12.5 MHz to 2.5 MHz. This mixing process uses a local oscillator signal at nominally 10 MHz. This 10 MHz local oscillator signal is divided to 2.5 MHz using a four-phase divider to provide two pairs of quadrature signals. This provides two pairs of signals that have a 90 degree phase shift between the pairs. Each pair includes differential signals to provide the local oscillator drive to the double balanced mixer. The 2.5 MHz signal from the output of the 12.5 MHz / 2.5 MHz conversion is split and mixed down to base-band using two parallel channels. The two base-band channels are phase shifted with a differential phase shift of 90 degrees. The phase shift network uses two cascaded all-pass delay sections. Williams [4.9] provides tabulated data based on the work of Bedrosian. These tables provide the time constants for each of the delay elements based upon the phase tolerance and the relative bandwidth. Here the upper to lower pass-band ratio of 11.47:1 has been chosen to support the required range of 30 kHz to 300 kHz (10:1). With a total

of eight delay elements (four in each path) the design ripple of the delay network is 0.0075°. The delay networks have been constructed using polystyrene film capacitors with a selection tolerance of +/- 1% and drift of -50 to -170 ppm / °C. The capacitors are used in conjunction with metal film resistors with a selection tolerance of +/- 0.1 % and a drift of <= 10 ppm / °C. As constructed, the sideband rejection was greater than 40 dB. An amplitude fine-adjustment trim was added to one of the I/Q mixers to provide relative gain adjustment for the "I" and "Q" networks. This allowed the sideband rejection to be improved to > 50 dB as depicted in figure 4.56. This result indicates a realised phase matching of ~0.3° between the two channels. Further improvement in performance could be achieved by making accurate measurement of the capacitors used in the assembly and then making corresponding adjustments to the associated resistors in the all-pass delay networks.

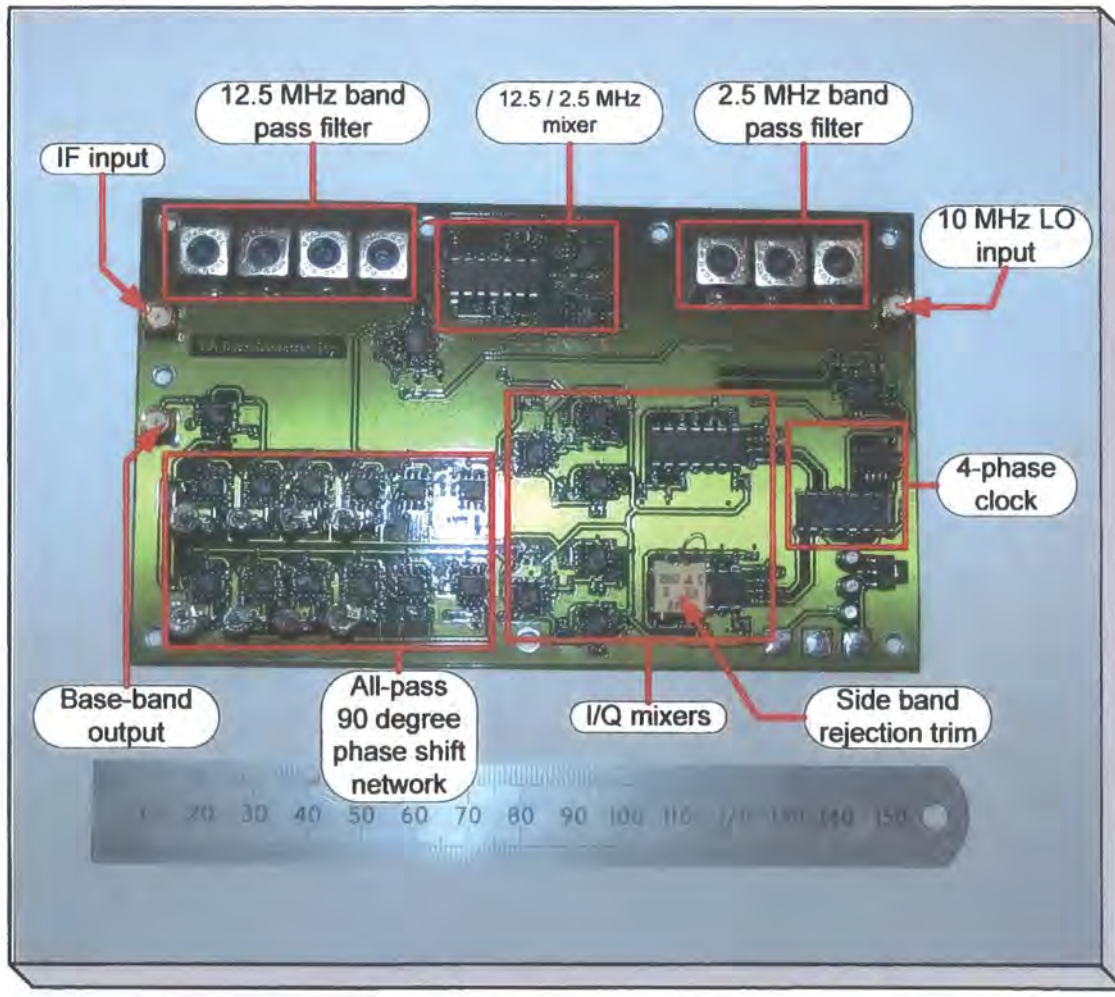

Figure 4.55 Photograph of the single sideband down-converter

When combined, the two base-band signals provide cancellation of the un-wanted sideband (since the signals from this mixing process are now in anti-phase). The wanted sideband is summed since both signals are in phase. The selection of the sideband can be made either via inversion of the phase of the local oscillator to one of the mixers, or by inverting the base-band signal prior to recombination.

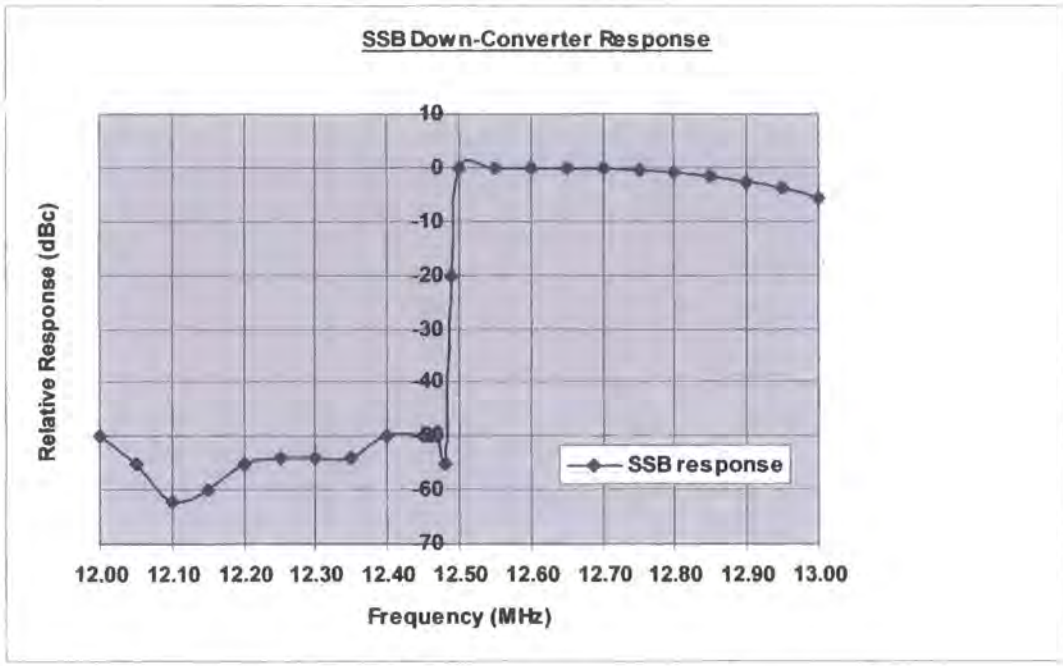

Figure 4.56 Measured response of the SSB down-converter

4.3.19 Discone antenna

A discone structure was selected as a candidate structure to provide an omni-directional response in azimuth over a wide frequency range (2.3 GHz to 6.0 GHz). The prototype was designed by scaling design data for an antenna operating in the range 100 MHz to 400 MHz [4.10]. The diameter of the top disc and the separation between the disc and the antenna cone were adjusted experimentally to provide an optimum return loss over the target operation frequency range. A return loss of > 7 dB was realised over the full band.

Eight identical antennas were prepared to allow a variety of arrays to be configured. Figure 4.57 shows a uniform circular array of four discone antenna that has been used to perform MIMO measurements [4.2].

Figure 4.57 Array of 4 discone antennas operating at 2.3 and 5.7 GHz simultaneously

4.4 System concepts which were either revised or abandoned

In addition during the course of the project three hardware ideas and approaches were pursued that either were improved or became unnecessary due to other changes made to the base sounder. All provided a useful experience base.

4.4.1 Synthesiser reference noise issue

The initial design of the synthesiser used a fast comparator to provide the interface between the reference signal (sinusoid in a 50 Ω environment) and the logic level input of the Analogue Devices PLL. This introduced jitter which was manifested as an increased noise floor present within the closed loop bandwidth of the synthesised sources. This raised the noise floor by up to 10 dB which was observable for the initial configurations of the 5.7 GHz converters. This was corrected during the course of the 60 GHz project. The solution to this problem is outlined in detail within the synthesiser discussion.

4.4.2 Self interference within 2.5 GHz dual conversion frequency converters

The initial build of the 2.5 GHz converters used a double conversion technique with an IF in the 600 MHz to 900 MHz band. This was an initially attractive solution since the upper synthesiser frequency allowed the use of commercial VCOs from Minicircuits. This configuration placed the two synthesisers above each of the converter output bands to minimise mixer M*N products. However the configuration suffered from in-band interference at very low signal levels, which appeared as "spikes" in the transfer function due to the sweep at the receiver producing an in-band output as the receiver swept through the static interference signal. The interference signals were observed to be located at multiples of the 10 MHz reference and were at a level equivalent to ~ -100 dBm at the input to the 2.5 GHz down-converter. This effect was not apparent for the 3.5 GHz and 5.7 GHz converters which led to the conclusion that the effect was due to either the low IF containing harmonics of the 10 MHz reference or signals being regenerated at multiples of 10 MHz from the two synthesisers. Both of these architectural differences were addressed by changing to the same converter configuration used for the 3.5 GHz and 5.7 GHz converters. This approach became viable as a solution with the identification of a suitable 4.5 GHz VCO from Z-Com.

4.4.3 Mitigation of close to carrier noise on the rubidium references

The initial development of the converter systems and sounder used rubidium references supplied by Tekelec and Efratom-Ball. Both of these references are based on an analogue phase lock technique which uses a phase comparison frequency in the region of 82 Hz. The sum product that occurs at the output of the phase detector due to any duty cycle differences is in the region of 164 Hz. This signal provides low level modulation of the reference unit which while immeasurable at 10 MHz becomes significant when observed at the output of the 5.7 GHz converter LO at ~ 8 GHz due to effective multiplication of X 800.

To address this problem a tracking reference was designed. This was based on a 10 MHz OCXO that was phase locked to the primary reference with a tracking bandwidth of approximately 3 Hz. With a type two third order PLL this provided ~ 50 dB of attenuation of the close to carrier spurious signals. The phase locked loop was implemented using discrete devices. A Golledge HCD-81 OCXO was used. This is based on an A-T cut quartz resonator. This successfully addressed the spurious issue. However the loop did cause deterioration of the reference at low offset frequencies.

Figure 4.58 displays the spectrum analyser monitor of the output from the complete 5.7 GHz up and down converter system with a 2 GHz test source at the input to the up-converter. The green response was the measured spectrum using the Telelec rubidium references for the up-converter and the down-converter. The red trace demonstrates the behaviour of the tracking loop. The purple trace is taken with the OCXO "free-running". This figure demonstrates successful operation of the tracking loop but with degradation of the reference at frequencies below 200 Hz offset.

This approach was not pursued further after the rubidium references in the sounder were replaced with Stanford Research PRS-10 units. The PRS-10 uses a different architecture which eliminates this spurious problem.

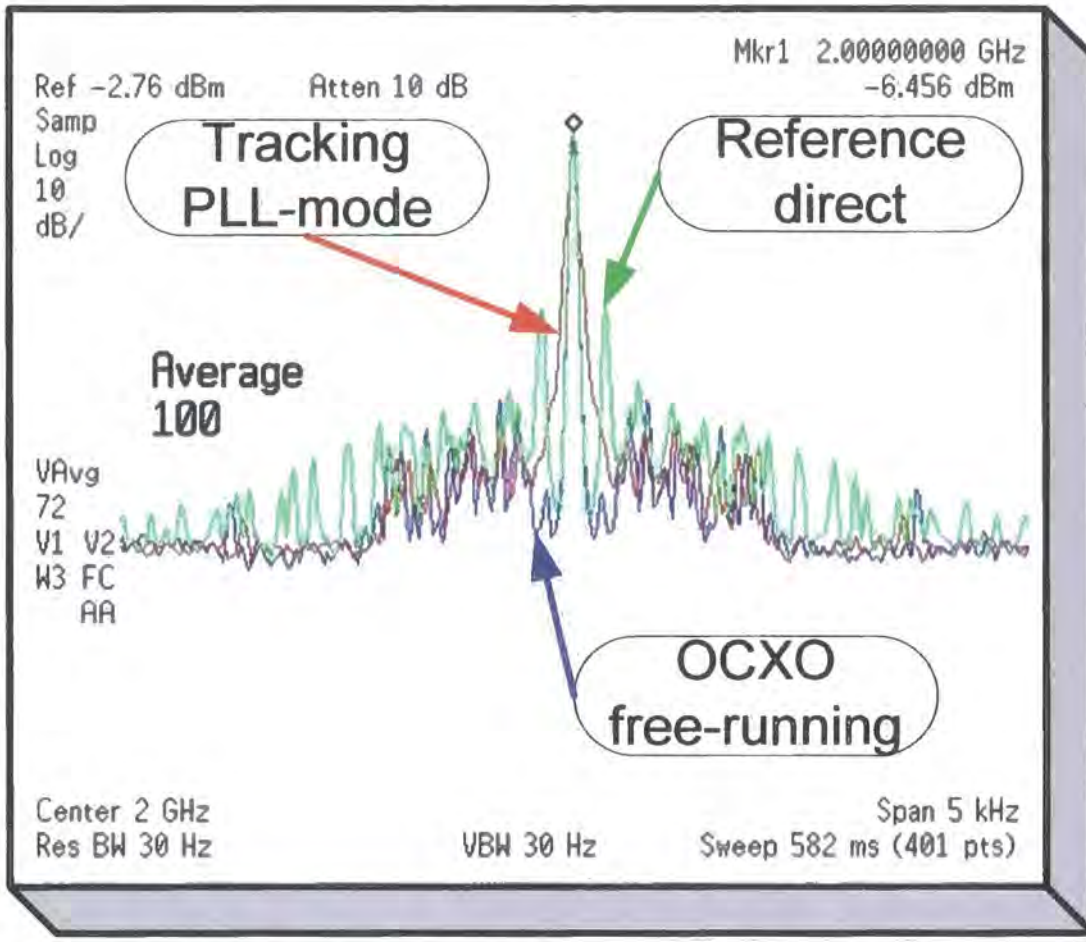

Figure 4.58 Attenuation of Tekelec Rubidium reference noise sidebands

4.5 System enhancement due to auxiliary synthesisers in the base sounder

Figure 4.59 illustrates the improvement in system phase noise that was achieved from using the auxiliary synthesisers in the up-converter and down-converter racks instead of the original synthesisers that were based on Zarlink SP8855E PLL devices. This measurement was performed at the output of the second up-converter for the 60 GHz system prior to the output multiply-X4 stage. The deterioration in the in-band noise is due to the limits of the synthesiser device. The loop peaking at ~ 30 kHz is in accordance with the loop design parameters that were used in this design (45° phase margin). The new synthesisers have closed loop bandwidths of ~100 kHz to ~250 kHz with a design phase margin of ~70°. This provides the lowest achievable close to carrier noise. This is discussed in more detail in the synthesiser description.

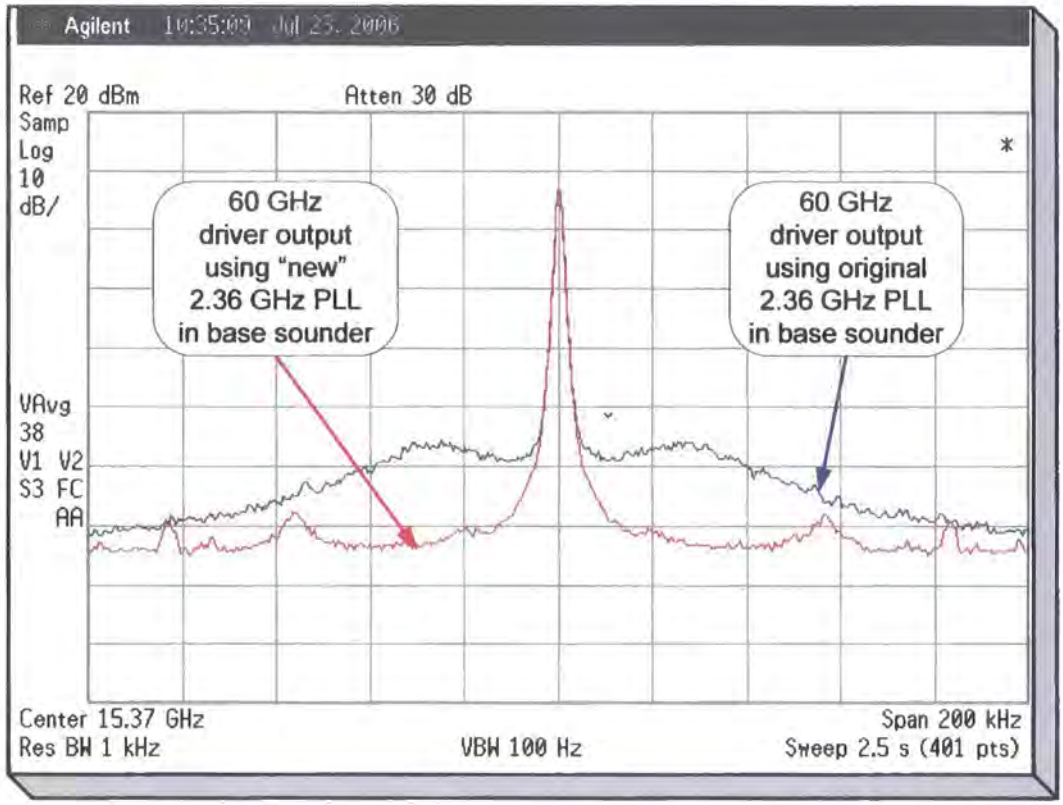

Figure 4.59 Comparison of phase noise at 15 GHz (60 GHz driver) for different PLLs

This particular issue was of minor significance for the base sounder and the 2.5 GHz, 3.5 GHz and 5.7 GHz converters. However for the 60 GHz system this was a significant source of phase noise (due to a further 12 dB degradation associated with the X4 multiplication) which limits the available measurement range. The degradation at 2 GHz is depicted in figure 4.60 and 4.61. Each range bin is separated by approximately 250 Hz.

This measurement was performed using a Fluke 6071A synthesiser and a Rhode and Schwarz SMS synthesiser operating at 260 MHz in place of the DDFS sources in the base sounder.

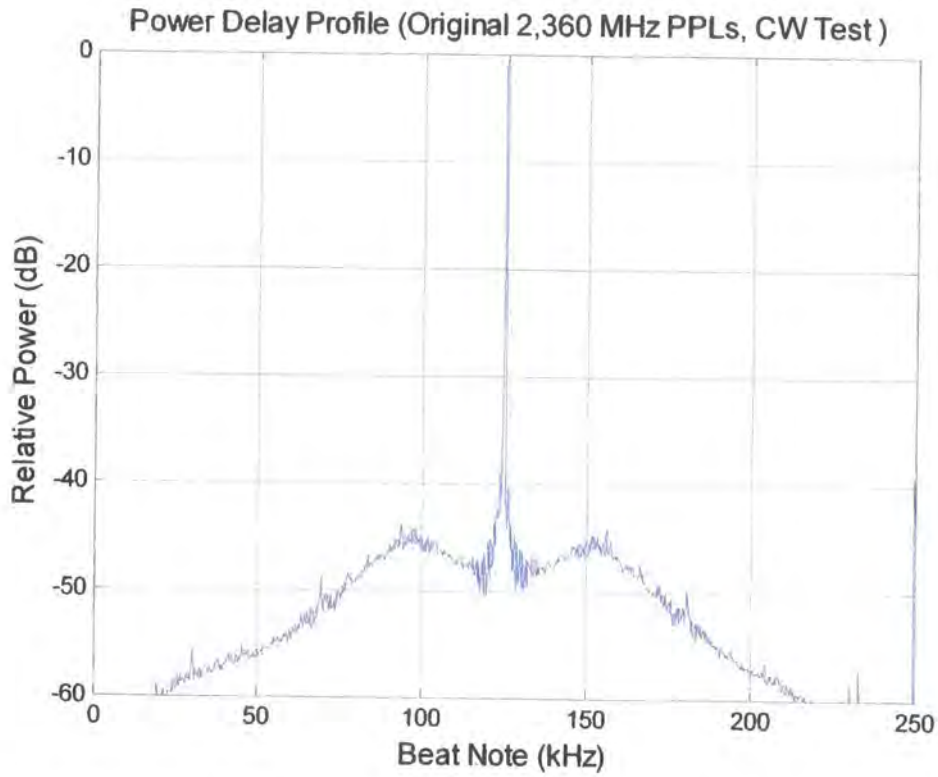

Figure 4.60 Base 2 GHz sounder using original synthesisers.

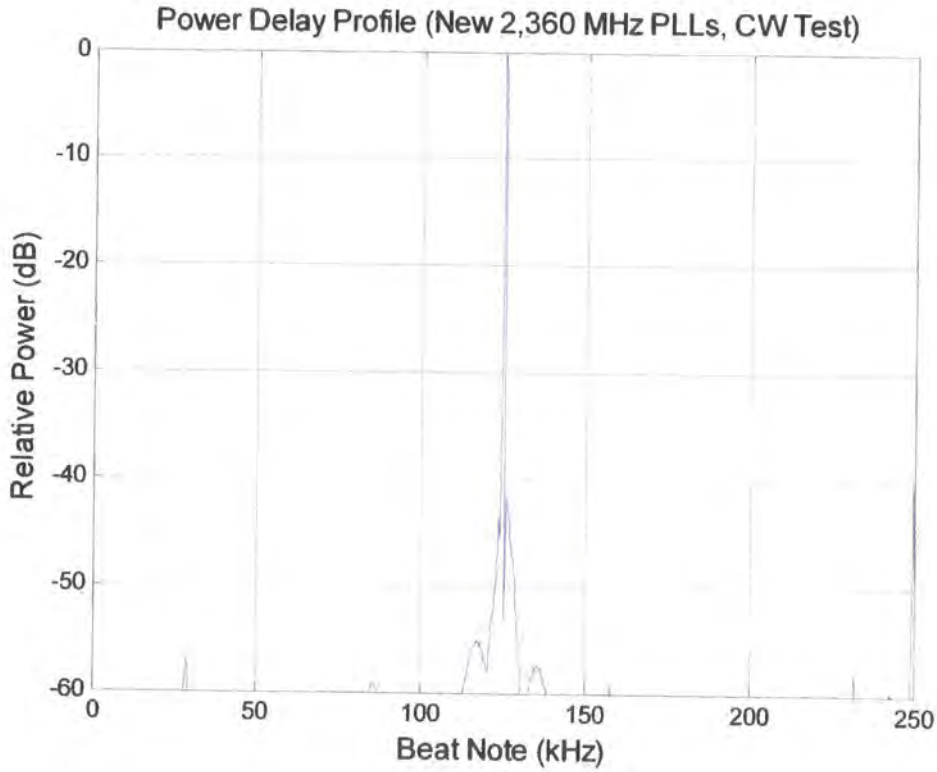

Figure 4.61 Base sounder CW response using new auxiliary synthesisers

4.6 Antenna calibration equipment

Antenna pattern data including both amplitude and relative phase information was required to enable the estimation of the direction of arrival and direction of departure of multi-path components.

It was observed that direct measurement was problematic due to the phase noise present within the transmit test source and the receiver down-conversion system.

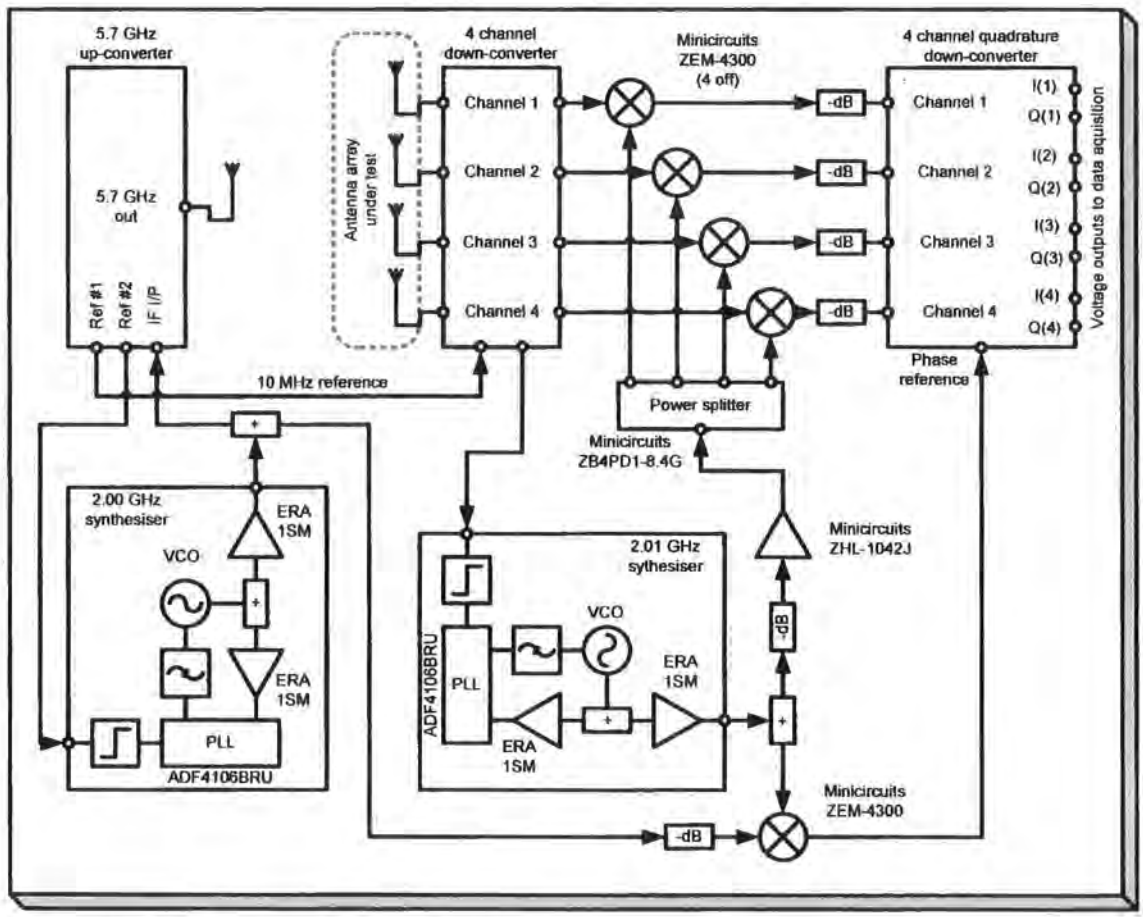

Figure 4.62 Antenna phase and amplitude response test set

The basic concept was developed to operate at 2 GHz in conjunction with antenna position and control equipment described by Lewenz et al [4.12]. This has been extended to operate at 2.5 GHz, 3.5 GHz and 5.7 GHz by incorporating the up and down-converter modules (refer to figure 4.62). All the sources within the converters are locked to a common 10 MHz reference. Since these sources all have closed loop

bandwidths of ~ 100 kHz the sources will track the reference close to carrier. The up and down-converters are programmed to the same frequency. Any close to carrier perturbations (less than the post detection bandwidth of 30 Hz) are effectively cancelled.

The 2.00 GHz and 2.01 GHz sources are provided by the auxiliary synthesisers which are also locked to the common 10 MHz reference. Since the frequencies are different, any close to carrier disturbances within the reference cannot be totally cancelled at this point in the system. The tracking phase locked loop does however address this problem.

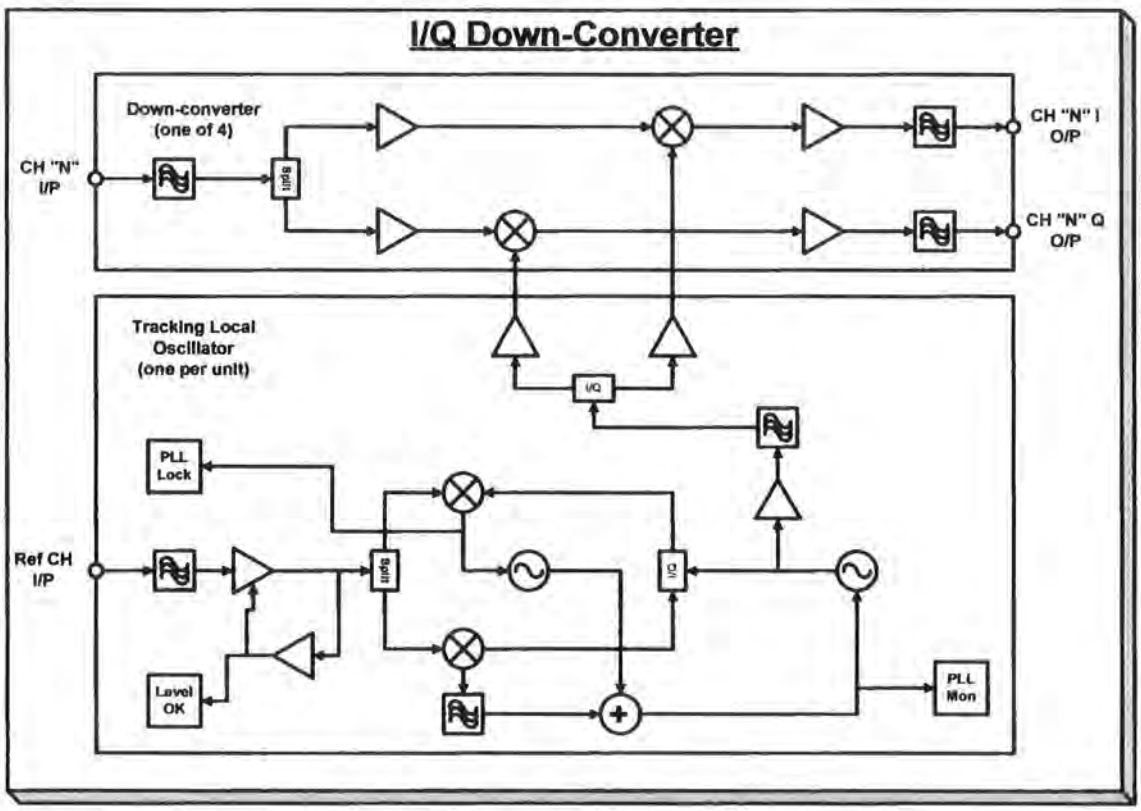

Figure 4.63 Detail of I/Q down-converter used in the antenna calibration test set

To address this, a system (figure 4.63) using phase tracking of the source and receive down-converter sources was used [4.11]. The phase tracking uses a reference channel which uses a sample from the transmit source and the receive source that are heterodyned to provide an IF signal of 10 MHz. This signal contains the sum of the phase noise that is present on both sources. A phase locked loop is used to track this

signal to provide a 10 MHz local signal that also contains the same phase noise spectrum. A local signal is regenerated by the PLL. This is then processed to provide two quadrature (90° relative phase shift) signals using an L-C-R phase shift network. These signals are used to provide the quadrature local oscillator drive for the down-conversion mixers that are operated at 10 MHz.

Four RF measurement channels have been provided (refer to figure 4.61). Each channel uses a mixer at 2 GHz using the common receiver local oscillator and mixes the signal from the antenna under test, via the down-converter to an IF of 10 MHz. This IF signal is split into two identical copies and each are then mixed down to base-band using two mixers operated with quadrature local oscillator sources.

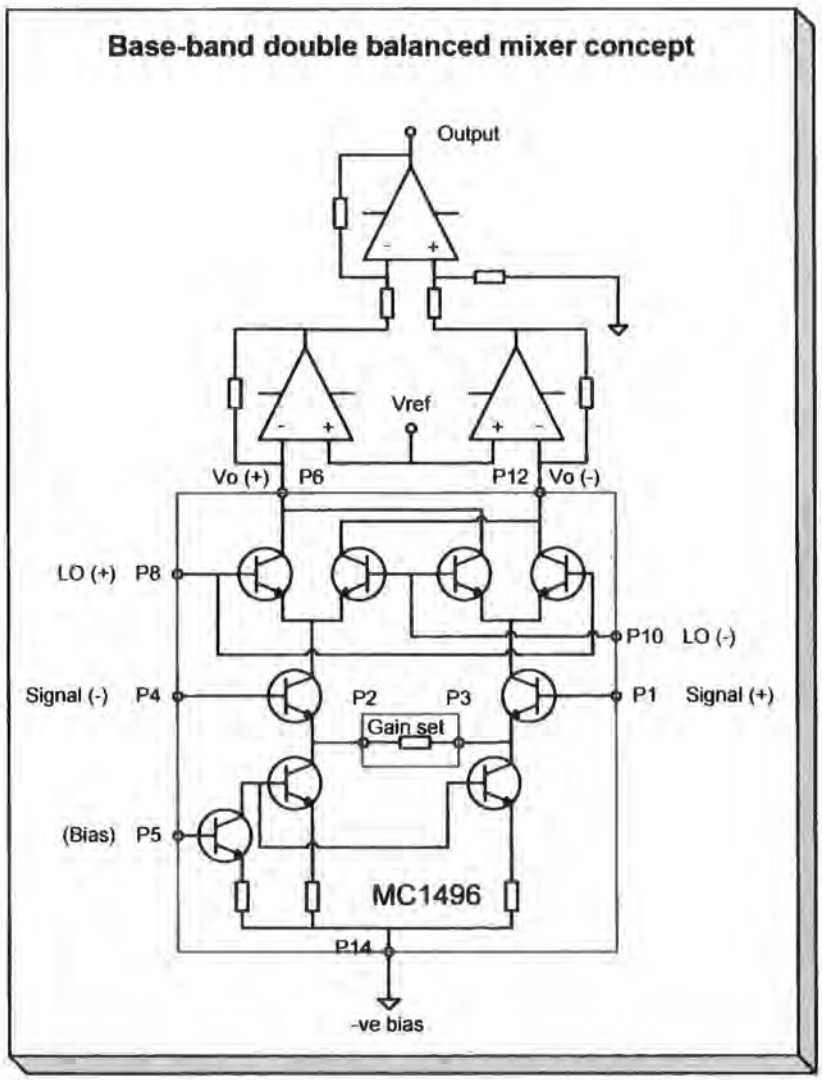

Figure 4.64 DC coupled mixer

The mixer system is dc coupled. A novel differential mixer structure (figure 4.64) was implemented that uses a commercial four quadrant multiplier integrated circuit with the output loads provided by two current to voltage converters. This provides very low distortion within the mixer structure and high output swing (up to 8 V peak). (This mixer structure has subsequently been utilised in the SSB down converter).

The mixer structure is based upon an MC1496 balanced modulator / demodulator device. This device is optimised for operation in the frequency range up to 100 MHz. The local oscillator signals are driven in anti-phase. In the quadrature down-converter this has been achieved using an NE592 differential video amplifier that has complimentary outputs. (This approach has also been used in the SSB down-converter for the first mixer that is used to perform a frequency translation from 12.5 MHz to 2.5 MHz).

The input signals are also presented in anti-phase to pins 1 and 4. In the quadrature down-converter this is also achieved using an NE 592 that also provides a fixed gain of X100 (40 dB). (In the SSB down-converter the input to the first mixer is provided from the input band-pass filter which is used to provide a filter function, single-ended to balanced conversion and impedance transformation). The signals within the SSB down-converter remain balanced until the output summing / difference amplifier that is used to select the wanted sideband. In the published applications for this device, the output is produced by terminating the output of the transistor array with a resistor in series with the +ve bias supply. To achieve moderate conversion gain these resistor values are required to be in the region of 3.9 kΩ. Thus for appreciable current swings at the output, the voltage across the output transistors of the array changes significantly with signal level which introduces signal distortion. In our application our objective was to minimise dc offset voltages since the output would be dc coupled to the data acquisition system. Based on this it was intended to use a differential amplifier to recover the output from the complimentary outputs of the multiplier. It was observed that these two structures could be combined and by incorporating a current to voltage converter the voltage swing at the output of the array would be reduced to zero since the input impedance of the current to voltage converter is close to 0 Ω. In addition to improving

the distortion behaviour which is of high importance in the quadrature down-converter, this also minimises the reduction in output bandwidth due to the capacitance present at the output of the transistor array. The "Miller integrator" effect due to capacitance between the collector and base of the output transistors is also minimised since the output voltage is fixed (principle of the cascade amplifier structure). The output bandwidth is now defined by the bandwidth of the amplifiers used to perform the current to voltage conversion and the subsequent summing amplifier. Using LF353 devices (4 MHz gain bandwidth) the output signal was observed to be reduced by only 0.9dB at 2 MHz output.

The mixer structure described above has also been used as a phase detector within the reference tracking loop used in the quadrature down-converter. The closed loop bandwidth achieved was ~800 kHz.

Since in this measurement application we are interested in the dc voltage representing the relative phase and amplitude of the IF input signal relative to the reference the output signals are band-limited with a - 3 dB corner of ~ 30 Hz. The output includes level shifting and scaling to provide + / - 4 V which corresponds to the data acquisition system. The eight channels of the antenna pattern data acquisition system allows four RF channels to be measured simultaneously with the system response computed from the "I" and "Q" channel components.

The phase noise suppression of the sources was measured to be 115 dB at 10 Hz offset. The amplitude accuracy was better than 1 dB and the phase error measured to be within +/- 1° for an input signal level (at 10 MHz IF) from – 85 dBm to – 30 dBm.

The complete four-channel 10 MHz quadrature-demodulator is shown in figure 4.65. This is constructed on a single printed circuit mounted inside an aluminium box to provide electrical screening and mechanical mounting for the coax connectors. A pair of precision voltage regulators (based on LM723 devices) was added to eliminate any offset drift due to variations in power supply voltage.

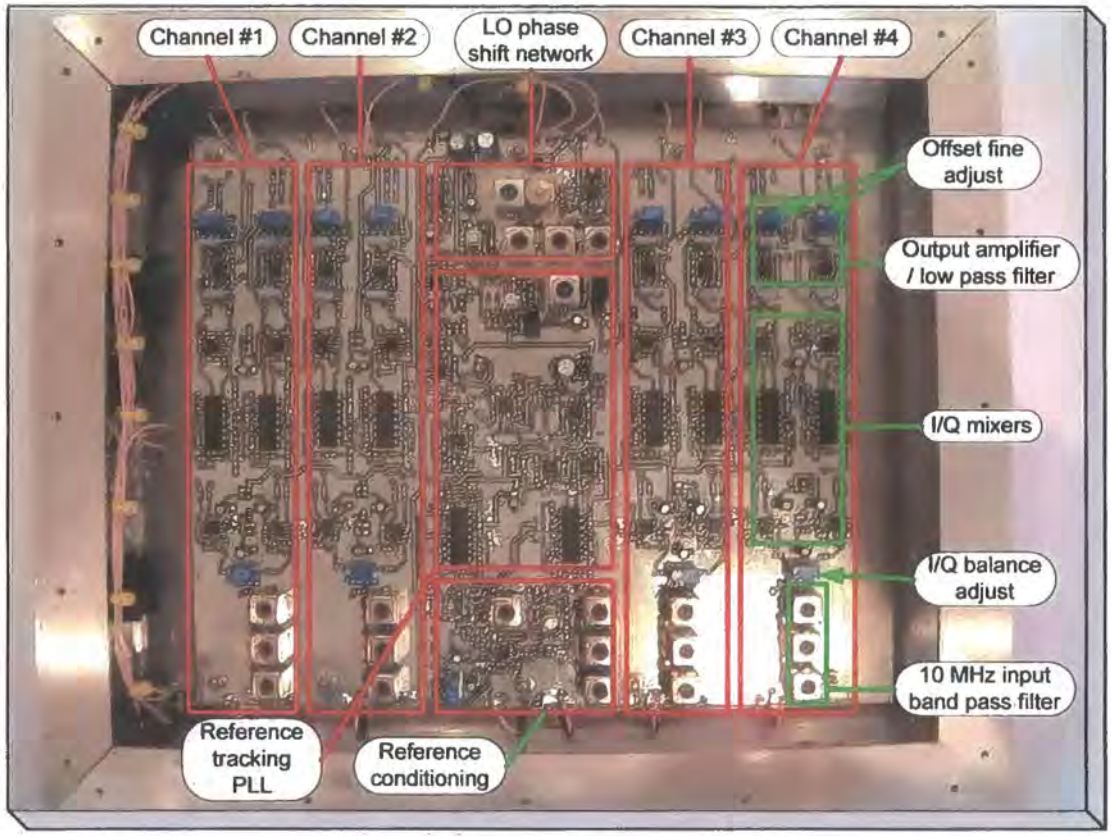

Figure 4.65 Photograph of the 10 MHz I/Q down converter assembly

4.7 Survey equipment

Measurements within the university buildings have been performed using small trolleys onto which the channel sounder equipment and back-up battery supplies have been fitted to allow temporary disconnection from the mains supply.

Collaborative measurements with British Telecom were performed using a BT supplied survey vehicle. This vehicle did not include an antenna mast or secure bays to contain the equipment. In addition the electrical supply was found to be very unreliable when used to operate the channel sounder receiver continuously. This was due to repeated failure of the low voltage input wiring when operated at a continuous current of 50 A.

Subsequently a Landrover 110" was supplied by Sinon Ltd. This has been modified to provide a mobile survey vehicle capable of supporting the channel sounder receiver for extended periods of operation. Particular attention has been paid to the safety of the

operators and the equipment under both normal and "crash" situations. The vehicle uses an auxiliary alternator to maintain the charge on a high capacity battery (330 AH at 12 V). This battery is used to provide power to a marine specification sine wave inverter that provides 230 V ac at a continuous rating of 1200 VA. Under normal operating conditions the channel sounder receiver in conjunction with the data acquisition PC and frequency extender requires a sustained supply of 500 VA. The input current to the inverter at this power output is approximately 50 A. This current can be supplied by the auxiliary alternator whilst the vehicle engine is idling. At fast idle the alternator can provide 120 A which is sufficient to maintain operation at the full 1200 VA capacity of the inverter. The battery voltage, alternator current into the battery and load current out of the battery are monitored on the inverter input. The output voltage and load current are monitored on the output of the inverter. The 230 V ac output is provided through an RCCB to protect the operator in the event of an insulation failure.

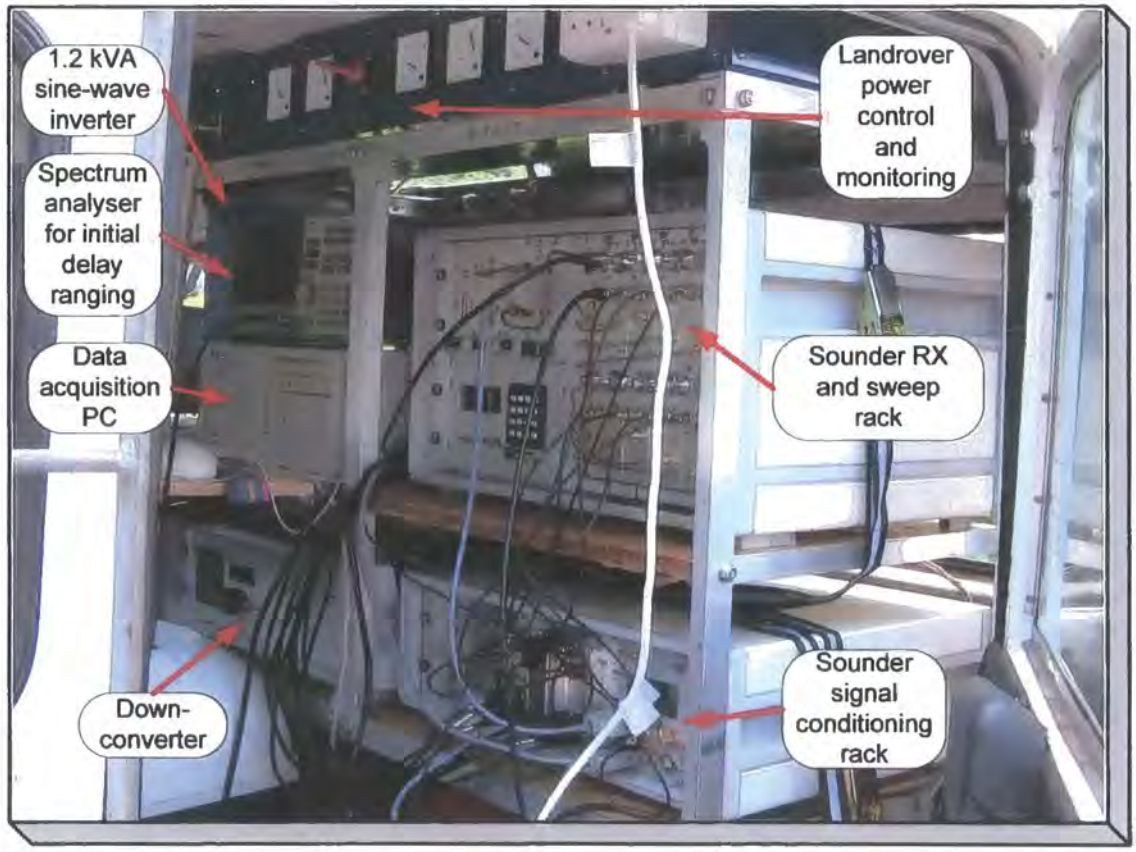

Figure 4.66 Photograph of the sounder installed in the Landrover survey vehicle

The equipment is mounted within a rack (refer to figure 4.66) that is fitted in place of one of the rear rows of seats. The battery is mounted in a vented enclosure at the bottom of the rack. The power supply monitoring and control equipment is mounted at the top of the rack. Two 19" equipment bays have been provided. Each of these bays has been subdivided to accommodate one 3U and one 6U rack unit. A foldout table has been included to support a PC keyboard, monitor and mouse.

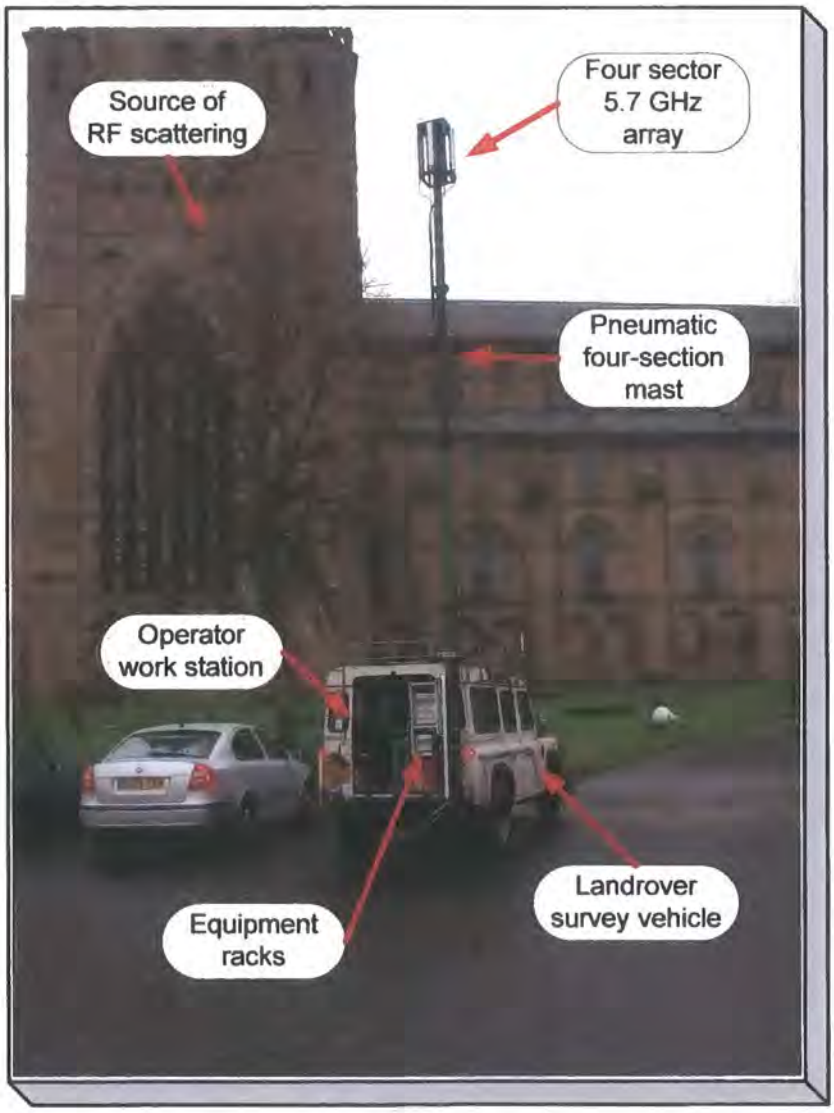

Figure 4.67 Photograph of survey vehicle pneumatic mast

At the rear of the vehicle a pneumatic mast has been fitted (refer to figure 4.67). At present a 4 section unit has been used to provide an extended mast height of 8 m. No antenna stabilisation guys are required in this configuration.

4.8 References

[4.1] Salous S., Filippidis P., and Hawkins I.; "A Multi-channel Sounder Architecture for Spatial and MIMO Characterisation of the Mobile Radio Channel"; presented at the IEE seminar on MIMO systems; IEE pub, 01/175, 12 Dec. 2001, pp 18/1-18/6.

[4.2] Salous S., Feeney S.M., Razavi-Ghods N. and Lewenz R.; "Measurements in the 2-6 GHz Band"; presented at the URSI general assembly in New Delhi, October 23rd to 29th 2005.

[4.3] Millman J.; "Microelectronics: Digital and Analogue Circuits and Systems"; McGraw Hill 1979, ISBN 007042327.

[4.4] "ADIsimPLL"; Phase Locked Loop design and simulation package available from www.Analog.com

[4.5] Rhode U.L.; "Digital PLL Frequency Synthesizers Theory and Design"; Prentice Hall 1983, ISBN 0-13-214239-2.

[4.6] "AWR Microwave Office 2002"; microwave circuit design and simulation package available from Applied Wave Research Inc.

[4.7] Matthaie G., Young L., Jones E.M.T.; "Microwave Filters Impedance-Matching Networks and Coupling Structures"; Artech House, ISBN 0-89006-099-1.

[4.8] "New Low Power Single Sideband Circuits"; AN1981 in Mullard Technical Handbook; Book 4 Integrated Circuits, Part 6 1988 Linear Products

[4.9] Williams A.B.; "Electronic Filter Design Handbook" 2nd Edition; McGraw Hill 1988, ISBN 0070704341.

[4.10] Glazier E.V.D. and Lamont H.R.L.; "The Services Textbook of Radio Volume 5 Transmission and Propagation"; Her Majesty's Stationery Office (HMSO) 1958.

[4.11] Abdalla M., Feeney S.M., and Salous S.; "Antenna Array and Quadrature Calibration for Angle of Arrival Estimation"; SCI2003, Florida, July 2003.

[4.12] Lewenz R., Fillipidis P., and Salous S. ; "Antenna Array Calibration for a Multi-channel Direction of Arrival Sounder" ; High frequency Postgraduate Conference ; Cardiff, September, 2001, pp 119-124.

5.0 Introduction

The complete sounder requires detailed verification to determine the fundamental performance limitations of the equipment when used to make measurements. These measurements have been organised in three phases:

- The up-converters have been measured to evaluate the transmitter power output and spectrum "flatness". This provides a useful, basic indication of the performance of the up-converter. These measurements and results are presented in section 5.1.
- The down-converters have been measured to evaluate the noise figure and gain. The primary consideration is that the noise figure does not adversely affect the sensitivity of the sounder. The gain measurement is useful to understand the additional losses that can be included between the down-converter and the UMTS channel sounder receiver. These measurements and results have been presented in section 5.2.
- The channel sounder in conjunction with the up and down converters has been evaluated at the system level. This is a practical approach to gaining an insight into the effect of phase noise within the signal sources and to make a measurement of the system noise floor (and therefore sensitivity limit) under operational conditions. This work is presented in section 5.3 for the following:
    - Limitations due to phase noise evaluated using CW sources
    - Receiver noise floor exploration
    - Single delay measurement
        - power delay profile
        - Doppler ambiguity
        - frequency transfer function
    - Two path delay discrimination
    - Channel matching (four channel converter)

The channel sounder swept performance has been evaluated for typical measurement scenarios. These scenarios are:

- Three band wide-area outdoor measurement (10 MHz channel width)
- Wideband indoor measurement (260 MHz {150 MHz} channel width)
- Very wideband indoor measurement (1040 MHz, 60 GHz only)

The assessment of the 60 GHz system has not included characterisation of the up-converter and down-converter at the 60 GHz interfaces since no measurement equipment supporting direct measurements in this frequency range was available.

Phase noise measurements are not presented here since the sounder CW response measurement provides a valid and representative indication of any performance limitations due to phase noise. In any case the phase noise performance of the new synthesisers developed to support the project are lower than the self noise of the available Agilent E4407B spectrum analyser for frequency offsets of <~ 10 kHz. For the FFT bin spacing of 250 Hz used in this system, +/- 10 kHz corresponds to +/- 40 bins.

During the verification program it became apparent that the original 2.36 GHz sources within the original UMTS channel sounder TX and RX were the dominant source of phase noise within the system. This issue was resolved by using the auxiliary synthesisers that are included within the frequency extender racks to replace these sources. As documented in section 4.5, this provided an improvement in the equipment noise floor of approximately 15 dB. The auxiliary synthesisers were originally assembled to support the general development of the up-converters and the 60 GHz system.

The measured pattern data for the four-sector 5.7 GHz antenna array is presented in section 5.4

5.1 Transmitter power and flatness assessment

Figure 5.1 shows the test configuration used to measure the average power from the up-converter and the amplitude versus frequency response. The up-converter was provided with a swept IF signal from the base channel sounder transmitter. This IF signal was recorded for comparison. The output of the transmitter was monitored using the "max-hold" function of the spectrum analyser to record the amplitude versus frequency spectrum.

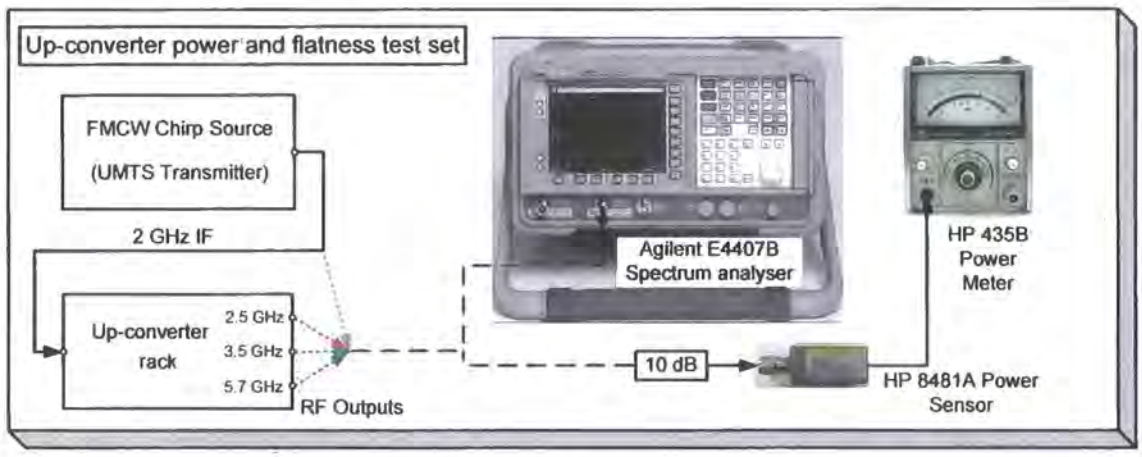

Figure 5.1 Equipment configuration for transmitter power and flatness measurement

The output power of the up-converted signal was measured using a power meter with an additional 10 dB attenuator included to provide an appropriate level (+30 dBm full scale) to the measurement head which was rated for + 20 dBm (100 mW) maximum.

These measurements were performed at the output connector of the up-converter. An interconnection cable was required for the spectrum analyser. The loss of this cable has not been included since it is not considered relevant for the spectrum flatness measurement. No additional losses were present for the power measurement since these were performed by directly attaching the attenuator and power head to the RF output connectors at the rear of the up-converter rack.

The summary results are presented in table 5.1. The amplitude versus frequency spectrum plots for the outputs of the up-converters is presented in figures 5.2 to 5.10.

Band	2 GHz (IF)	2.5 GHz (TX)	3.5 GHz (TX)	5.7 GHz (TX)
Power level	0 dBm	+ 21.3 dBm	+ 22.5 dBm	+22.5 dBm
Flatness (260 MHz)	+/- 0.8 dB	+/- 0.6 dB	+/- 0.3 dB	+/- 0.6 dB
Flatness (10 MHz)	<+/- 0.2 dB	<+/- 0.2 dB	<+/- 0.2 dB	<+/- 0.2 dB
Flatness (150 MHz)	Not Recorded	+/- 0.5 dB	Not Recorded	Not Recorded

Table 5.1 Transmitter power output and flatness results

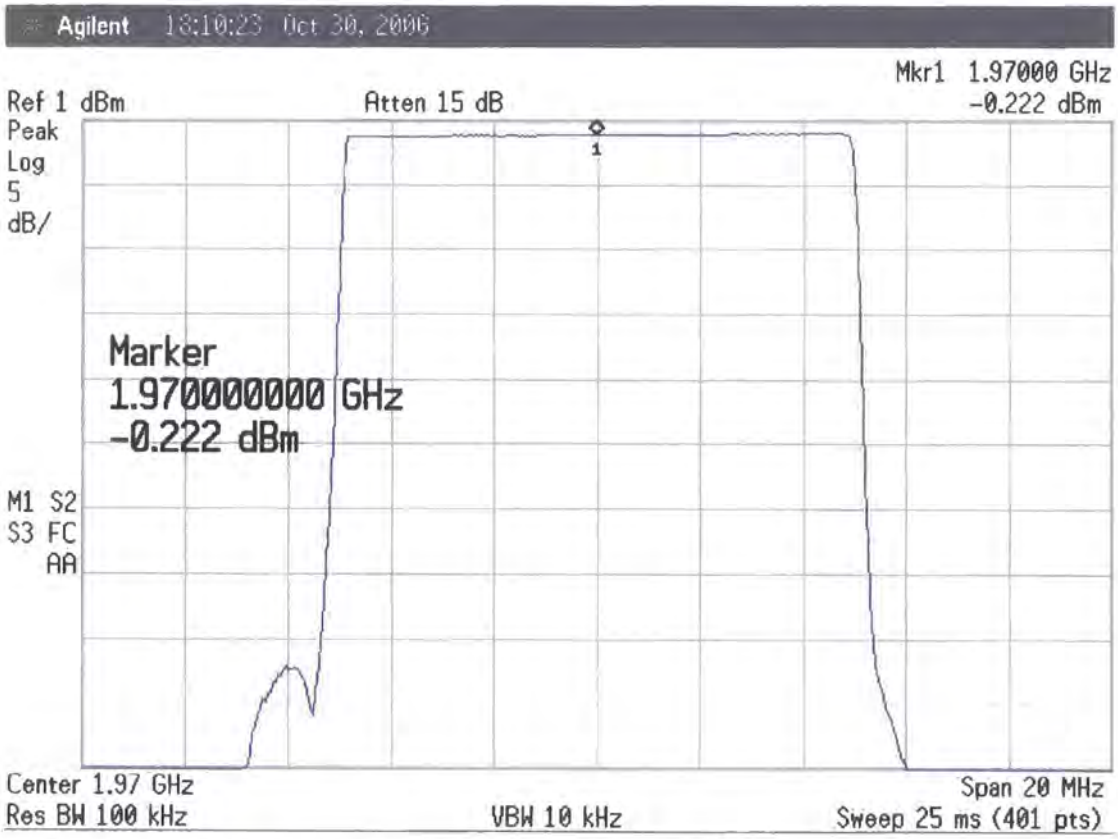

Figure 5.2 1.97 GHz IF flatness for 10 MHz sweep width

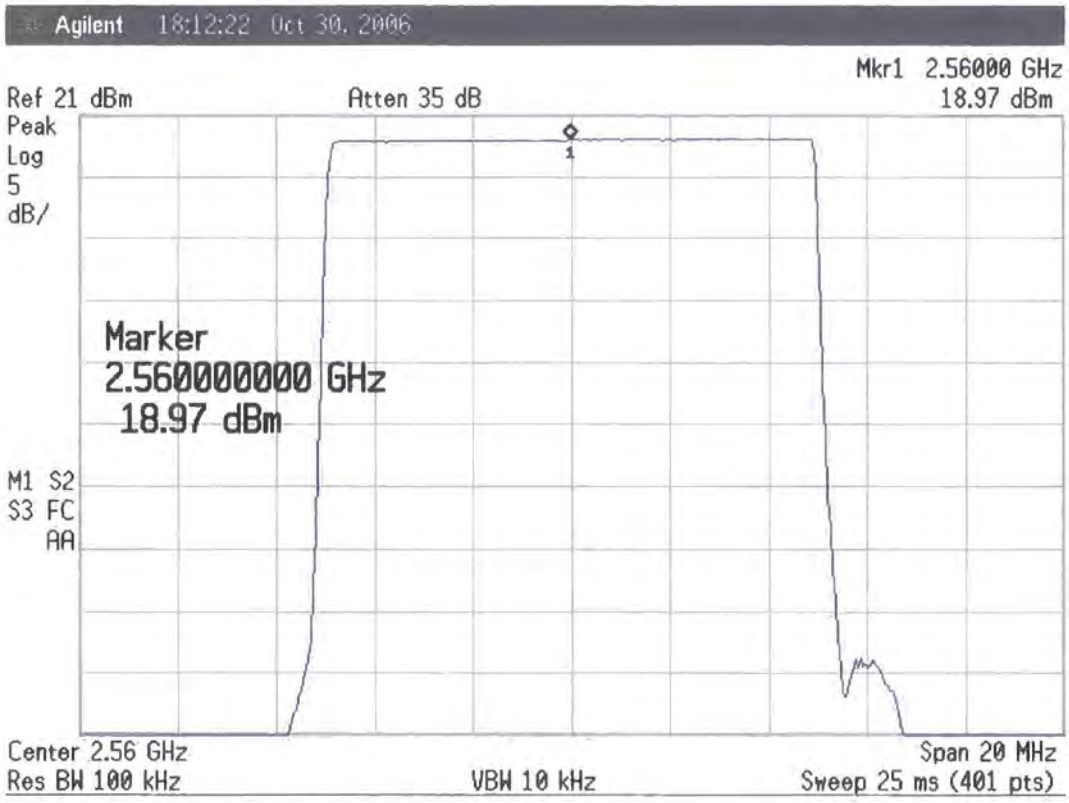

Figure 5.3 2.56 GHz TX flatness for 10 MHz sweep width

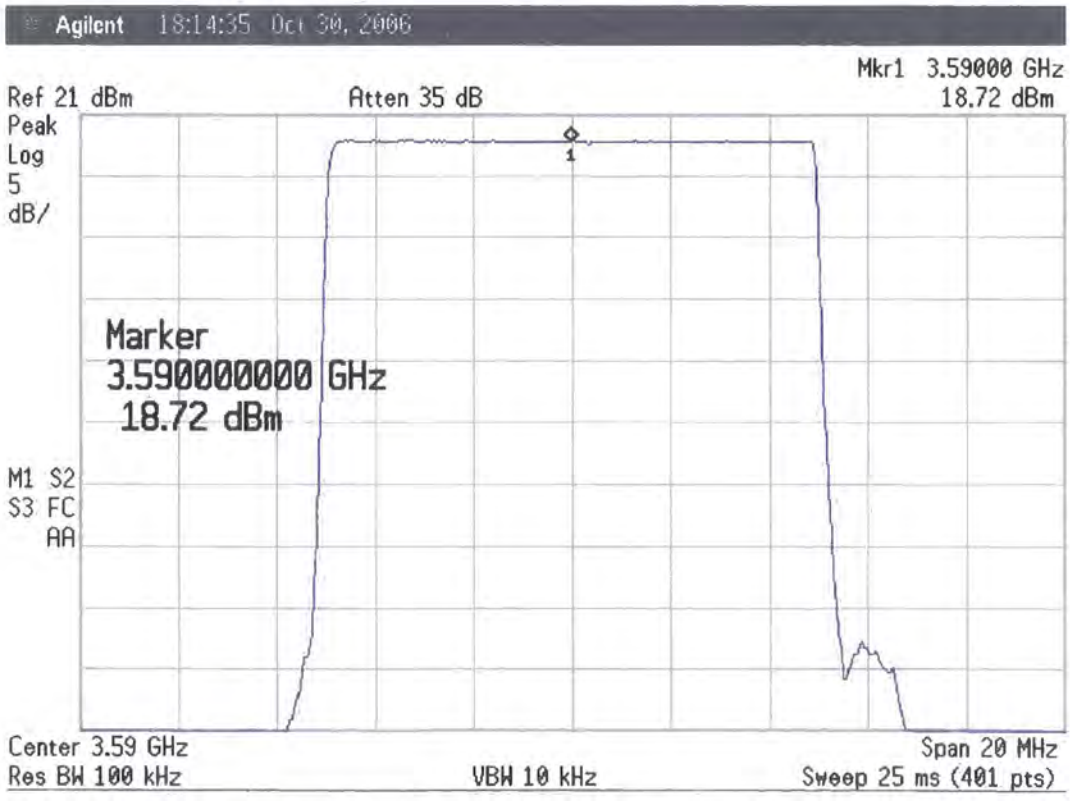

Figure 5.4 3.59 GHz TX Flatness for 10 MHz sweep width

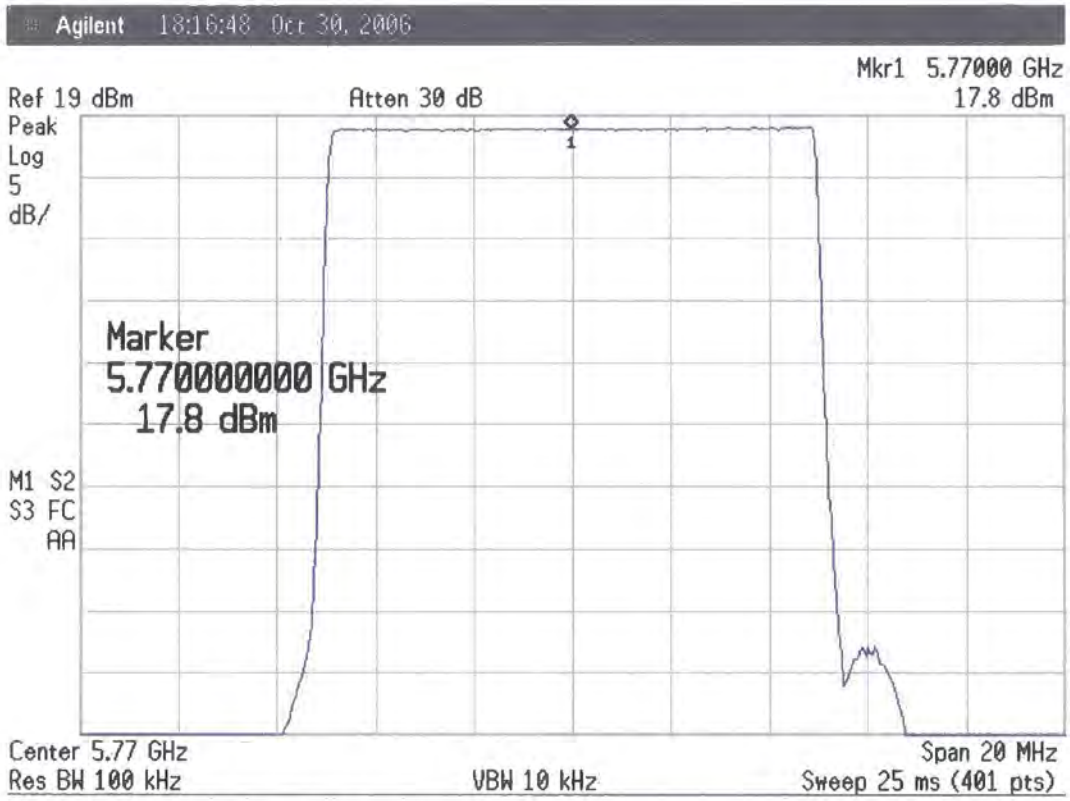

Figure 5.5 5.77 GHz TX flatness for 10 MHz sweep width

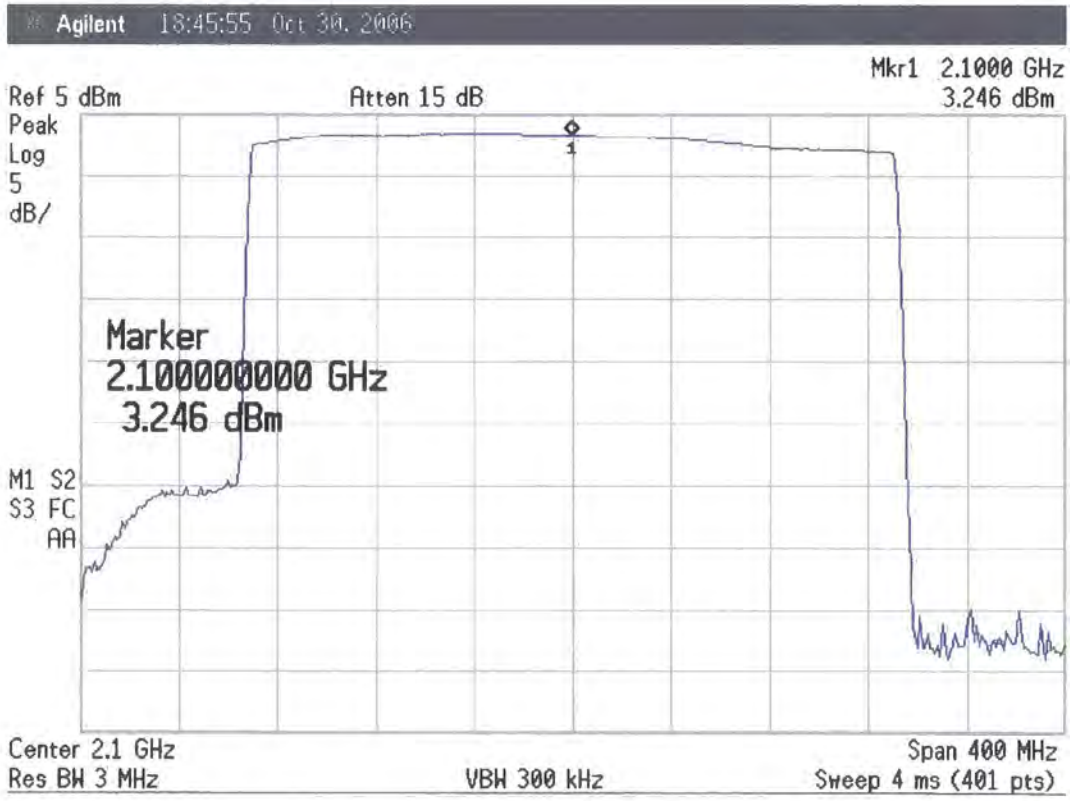

Figure 5.6 2.1 GHz IF flatness for 260 MHz sweep width

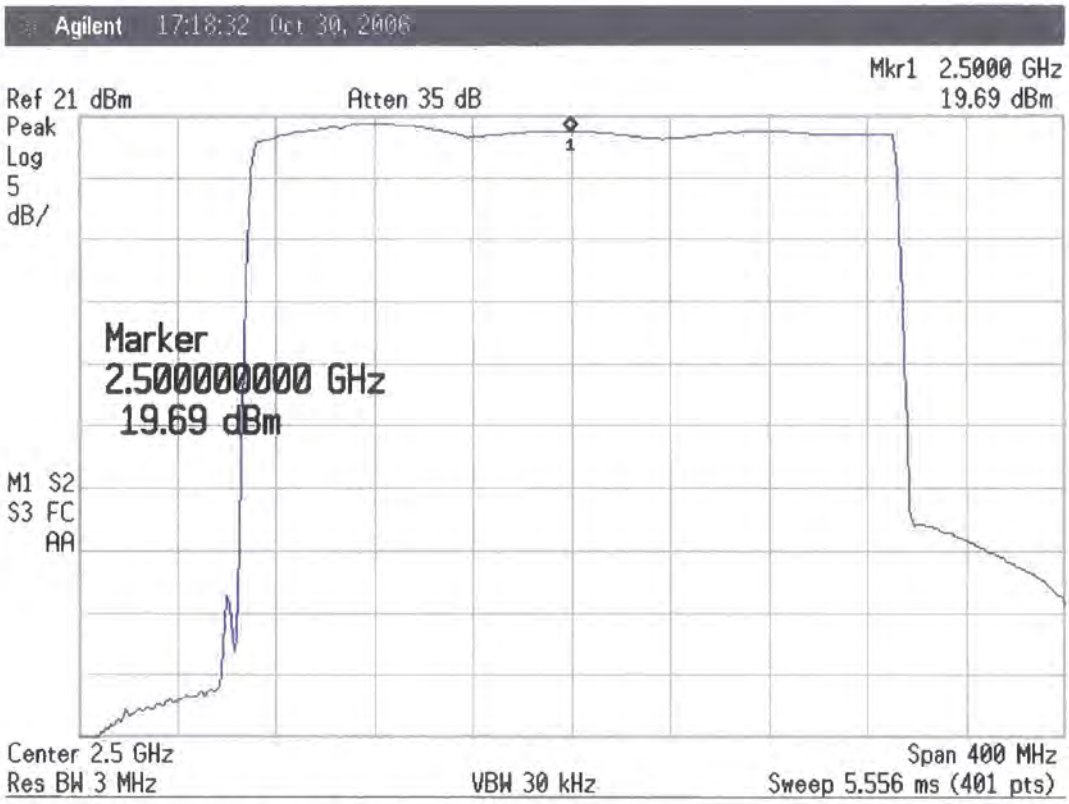

Figure 5.7 2.5 GHz TX Flatness for 260 MHz sweep width

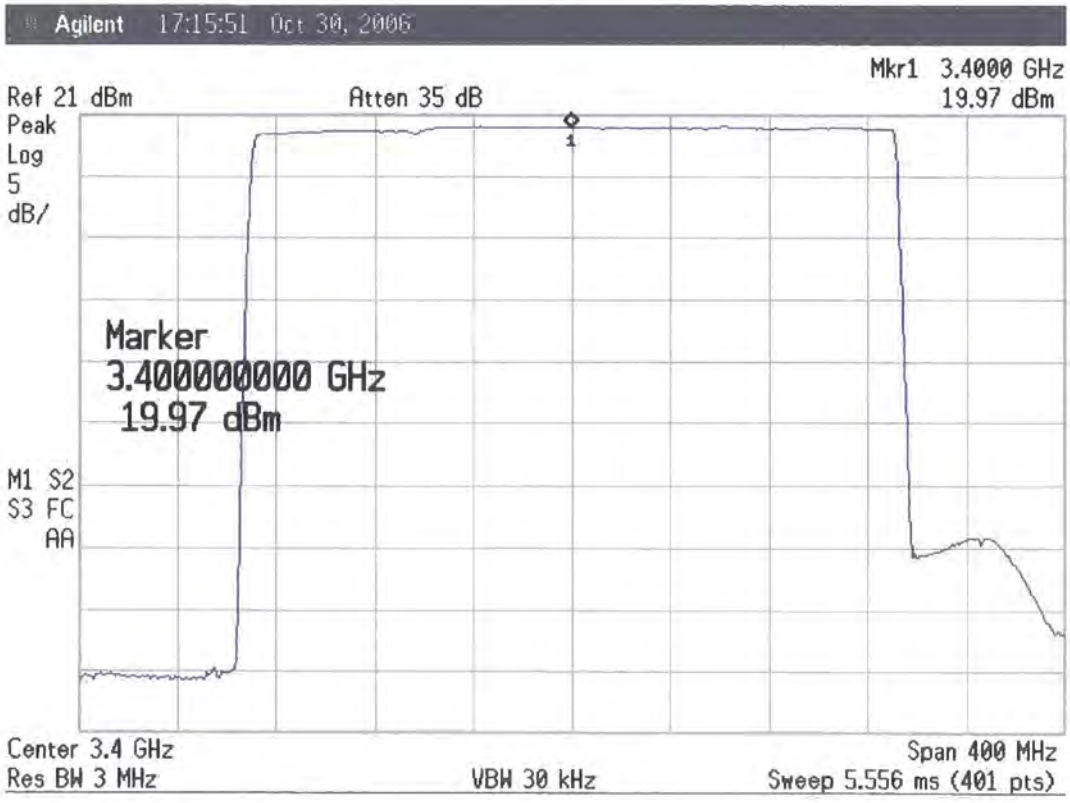

Figure 5.8 3.4 GHz TX flatness for 260 MHz sweep width

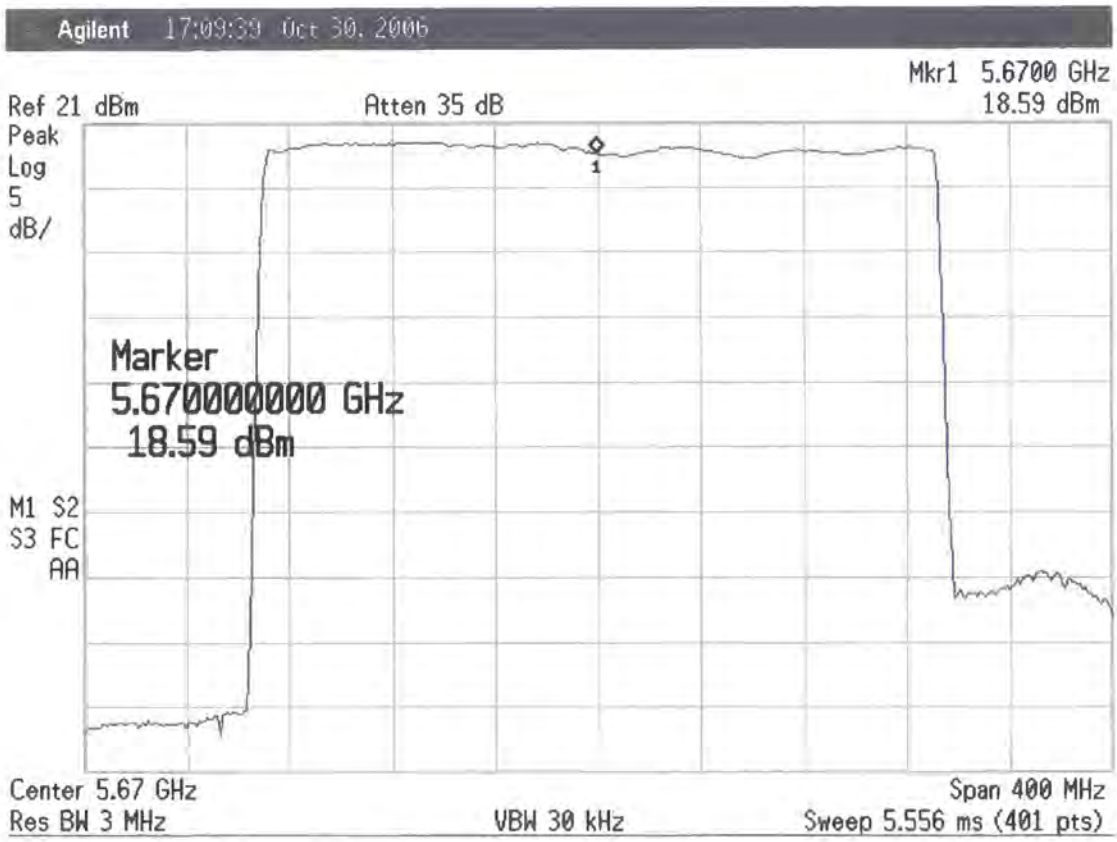

Figure 5.9 5.67 GHz TX flatness for 260 MHz wide sweep

The converters were originally designed to interface to an IF centred at 2 GHz with a maximum instantaneous width of 100 MHz. Due to limitations imposed on the base sounder to support the work of other students the actual sweep at IF is at present restricted to the range 1.97 GHz to 2.23 GHz. The sweep width has also been expanded to a maximum of 260 MHz. The filters utilised in the 3.5 GHz and 5.7 GHz converters are sufficiently wide to support operation with the shifted IF at the full sweep bandwidth of 260 MHz. However, the 2.5 GHz converter requires multiple narrow filters to provide discrimination between the IF at 1.8 GHz to 2.2 GHz and the RF at 2.3 GHz to 2.7 GHz. The up-converter includes two 5-pole 400 MHz wide filters centred at 2.5 GHz. The down-converter includes two 5-pole 400 MHz wide filters centred at 2.5 GHz plus an additional 5-pole filter centred at 2.0 GHz. To support 260 MHz sweep width at 2.5 GHz an IF of 1.87 GHz to 2.13 GHz would be required. As discussed, this is not supported by the base sounder at this time. To allow the sounder to be characterised for operation at 2.5 GHz a sweep width of 150 MHz has been used.

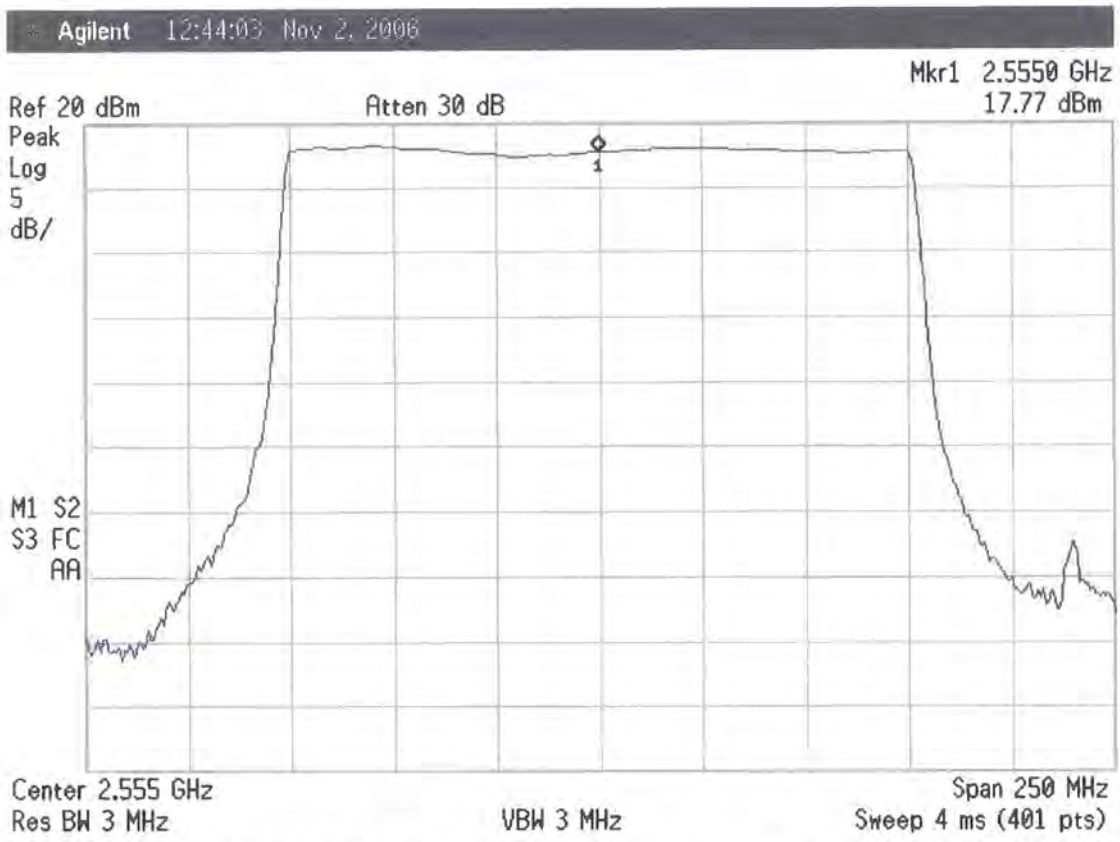

Figure 5.10 2.55 GHz TX flatness for 150 MHz sweep width

5.2 Receiver down-converter gain and noise figure measurement

The down converter gain was measured by providing a signal of known amplitude to the input of the converter and then to measure the level at the output of the down converter. The conversion gain is the difference between these two values. During the course of the measurement the input level was reduced by 10 dB and the output level was confirmed to also reduce by 10 dB. This was to ensure that the converters were operating in a linear mode without apparent gain compression due to overloading.

The up-converter rack was used to provide the input signal via a calibrated step attenuator (refer to figure 5.11). The attenuation was adjusted to establish a level of 0 dBm into the power sensor at the coaxial cable port to be connected to the down-converter input. An additional 30 dB of attenuation was then switched in to reduce the input signal to -30 dBm. The power sensor was then used to measure the power at the output port of the down-converter.

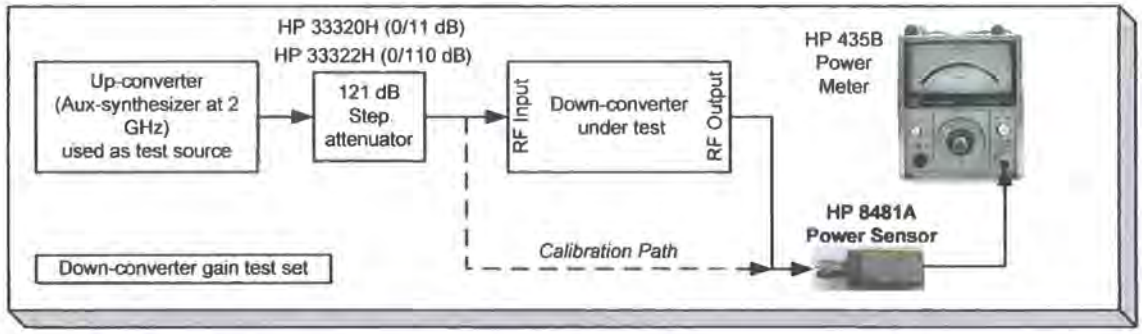

Figure 5.11 Equipment configuration to measure down-converter gain

The receiver noise figure was measured (refer to figure 5.12) using a moderate (15 dB) ENR noise source connected to the input connector of the down-converter. An additional amplifier (nominally 25 dB gain) was included between the output of the down-converter and the input to the spectrum analyser. This amplifier was required to raise the noise floor of the equipment under test to a level sufficiently far above the spectrum analyser that the measurement was not effected by the noise contribution of the spectrum analyser.

The measurement has been performed by firstly recording the noise floor of the spectrum analyser disconnected from the equipment to be tested (as shown as the green trace of figure 5.13). The noise density at the output of the equipment under evaluation was demonstrated to be more than 20 dB greater than the input noise density of the spectrum analyser, as shown as the red trace of figure 5.13. This contribution reduces the measured y-factor by <0.05 dB.

The "y-factor" is defined as the difference in the noise power output from the system under test with the noise source switched "on" or "off". In the "off" case the noise source provides a 50 Ω termination to the equipment under test. Under this condition the termination provides thermal noise only to the equipment. The output noise power is therefore the input noise multiplied by the gain of the equipment plus the noise generated within the equipment itself. In the "on" case the noise source provides additional noise. The output is therefore due to the gain multiplied by the thermal noise plus the "excess noise". This is shown as the blue trace in figure 5.13. The source is provided with a calibration table that states the value of the excess noise at a number of

spot frequencies, sufficient to allow interpolation to estimate intermediate values. The output noise in this case is now the thermal noise of the termination plus the excess noise multiplied by the equipment gain plus the noise generated from the equipment. If the "y-factor" and the "excess noise" are known then the noise figure of the equipment can be calculated {using equations (5.1) and (5.2)}.

The equipment noise figure can be calculated using:

$$F(dB) = ENR(dB) - 10Log10(Y - 1) \qquad (5.1)$$

Where: $$Y = 10\text{^}(y(dB)/10) \qquad (5.2)$$

Historically the output of the equipment under test was fitted with a variable attenuator and a signal level indicator. The system output noise level was measured with the attenuator set to zero and the noise source "off". The noise source was then operated and the attenuator adjusted until the indicated noise power was identical to the value noted with the noise source "off". The difference in the attenuator values was the classical "y-factor". This approach only requires the "excess noise" and the attenuator to be calibrated since the measurement bandwidth is common to both measurements and the indicator is operated at the same reading. With the development of modern calibrated spectrum analysers an equivalent "y-factor" can be read directly from the instrument. An additional advantage is that the measurement can be made across the entire bandwidth of the device under test.

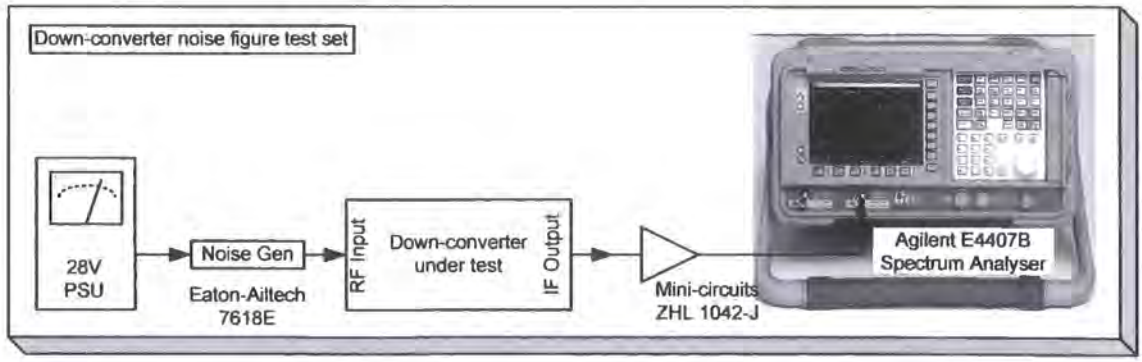

Figure 5.12 Equipment configuration to measure down-converter noise figure

The equipment under test was connected to the spectrum analyser and the noise source (refer to figure 5.12). The spectrum analyser was set to the IF output frequency range of the down-converter. The noise source (Eaton-Ailtech model 7618E) was specified for the range 10 MHz to 18.6 GHz. This equipment contains a semi-conductor avalanche break down device which produces a wide band noise output typically 35 dB above thermal noise. This is attenuated by an integral attenuator to provide an output ENR of nominally 15 dB. This 20 dB attenuator also ensures that the source termination presented to the equipment under test is very close to 50 Ω. The noise source provides a resistive termination with thermal noise when the active device is not biased. When provided with +28 V dc the noise source provides the calibrated noise to the device under test.

The response of the equipment under test is recorded using the spectrum analyser trace memory function with the noise source "on" and "off". The "y-factor" can be derived from the spectrum analyser using the marker function. Using the ENR information provided with the noise source, the effective noise figure of the equipment can be calculated from the observed "y-factor" [5.1].

The "y-factor" data recorded from the spectrum analyser are displayed in figures 5.13 to 5.20. Figure 5.13 demonstrates that the test set noise floor is sufficient to not materially effect the noise figure measurement. The gain and noise figure results for the down-converters are tabulated in table 5.2.

Down-converter	"y-factor" (dB)	Noise Figure (dB)	Gain (dB)
2.5 GHz	11.02	4.8	31
3.5 GHz	13.29	2.2	29
5.7 GHz	12.72	2.9	26
CH-1 5.7 GHz	13.10	2.5	25.4
CH-2 5.7 GHz	13.30	2.2	23.4
Ch-3 5.7 GHz	13.65	1.9	27.4
Ch-4 5.7 GHz	12.08	3.5	22.0

Table 5.2 Three-band down-converter gain and noise figure results

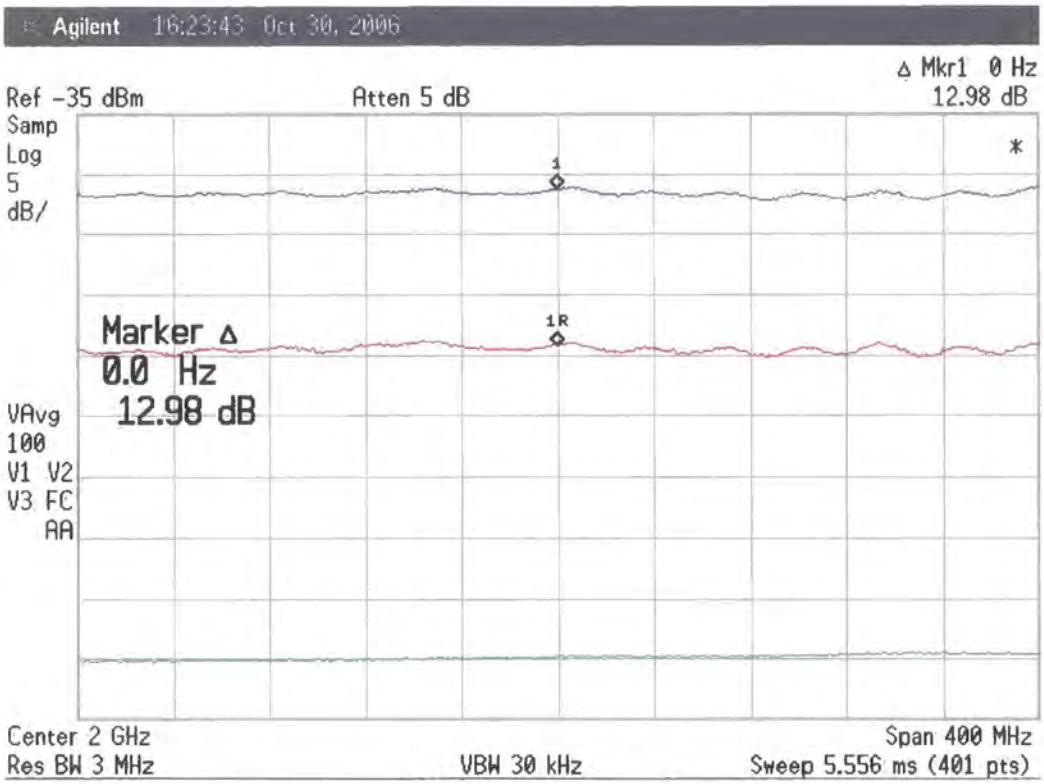

Figure 5.13 Comparison of spectrum analyser and equipment noise floor

Figure 5.14 "y-factor" measurement of the 2.5 GHz down-converter

Figure 5.15 "y-factor" measurement of the 3.5 GHz down-converter

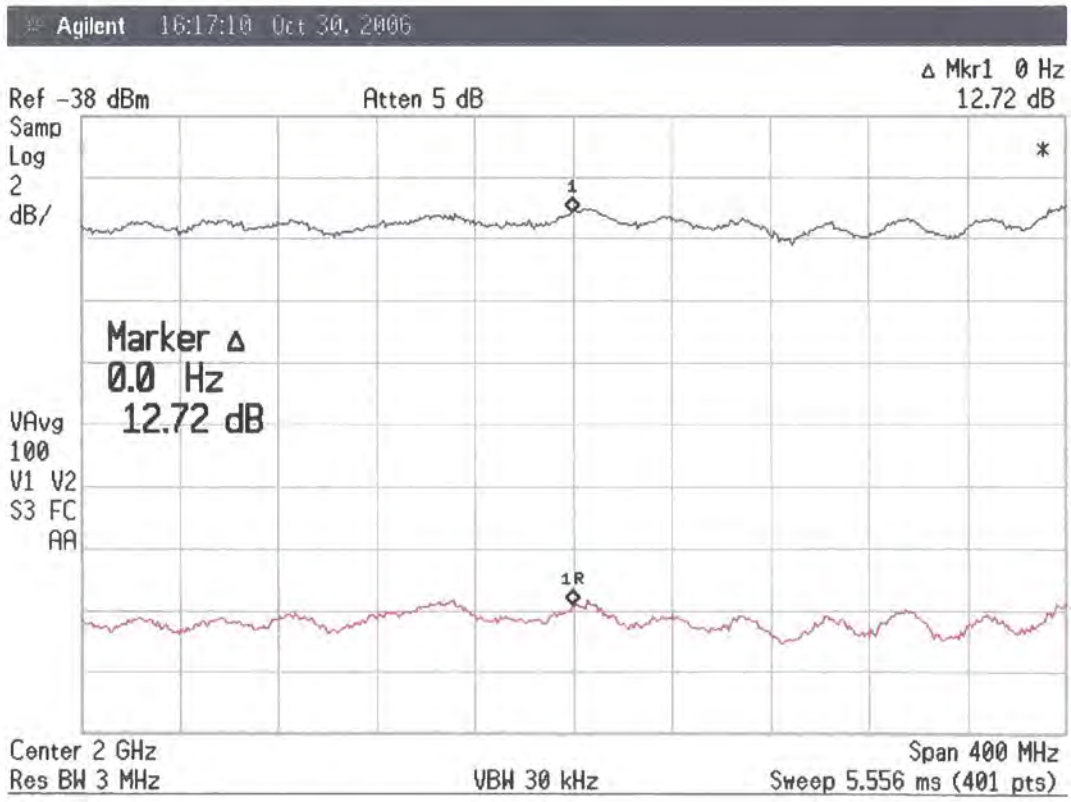

Figure 5.16 "y-factor" measurement of the 5.7 GHz down-converter

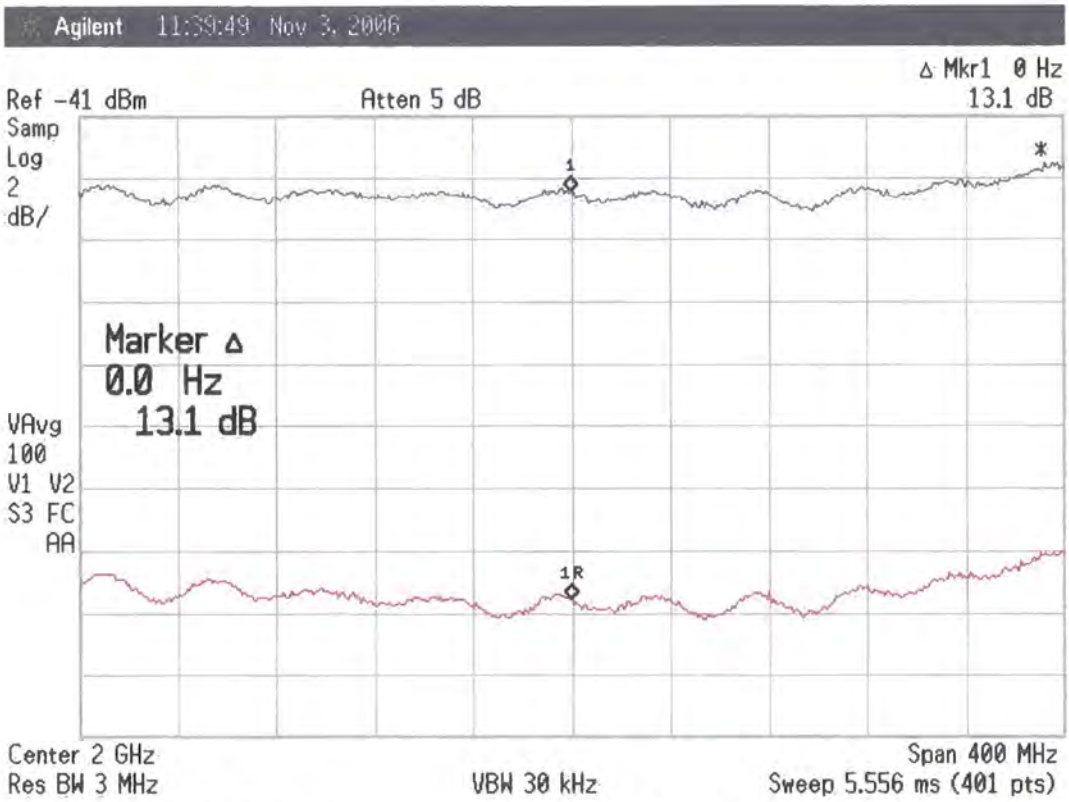

Figure 5.17 "y-factor" measurement of channel 1 of the four-channel converter

Figure 5.18 "y-factor" measurement of channel 2 of the four-channel converter

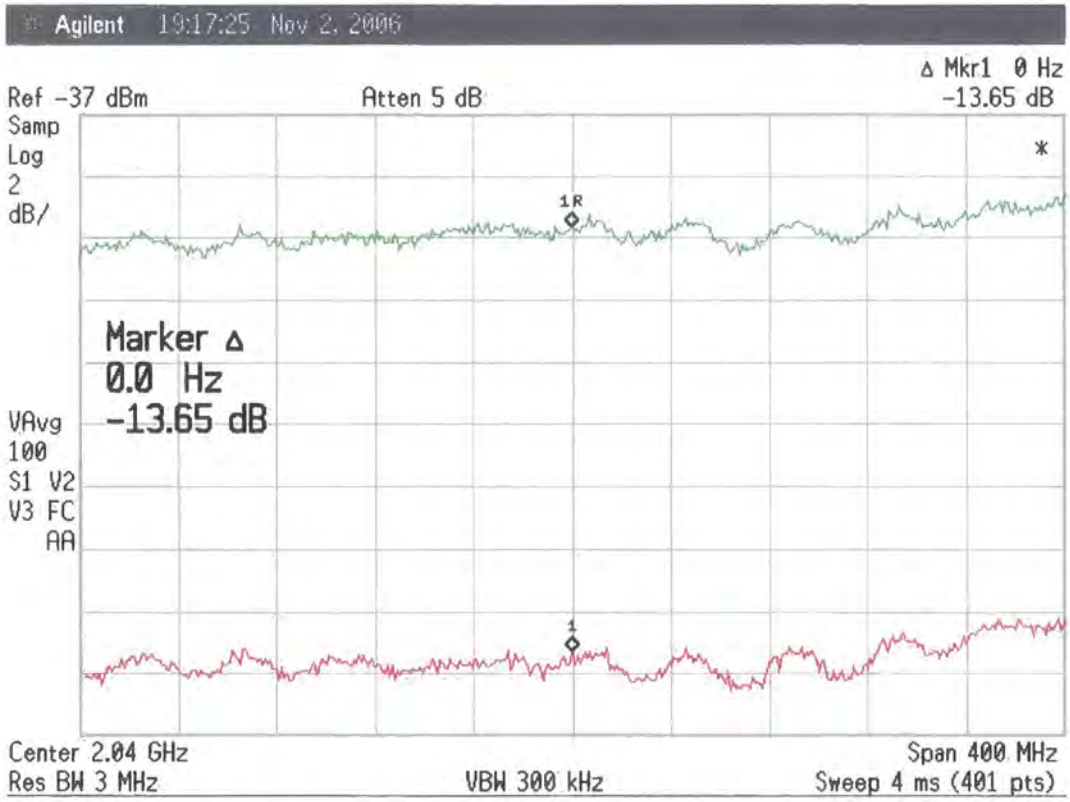

Figure 5.19 "y-factor" measurement of channel 3 of the four-channel converter

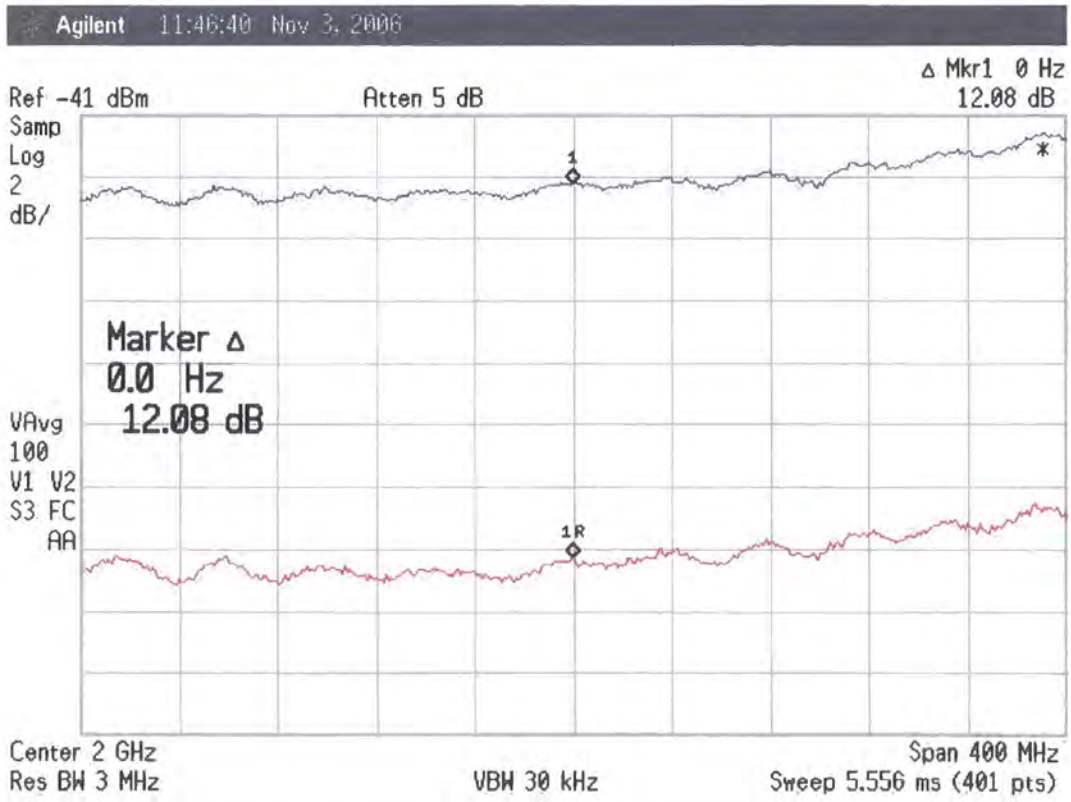

Figure 5.20 "y-factor" measurement of channel 4 of the four-channel converter

5.3 System level back to back evaluation

5.3.1 CW measurement

The CW measurement includes all significant phase noise sources within the system with the exception of the DDFS. This measurement investigates performance limits for the sounder due to close to carrier phase noise that is present in the synthesised sources which are used within the sounder and the up and down converters.

To determine the intrinsic performance of the signal conditioning and data acquisition system the outputs of the two synthesisers at nominally 260 MHz were mixed to produce a beat frequency of 50 kHz. This signal was provided to the input of the signal conditioning module within the base sounder receiver. This result is recorded in figures 5.21a and 5.21b. This measurement demonstrates a response in close agreement with the theoretical response for a Hamming window. [5.2]. The first side-lobe is -45 dB (-43 dB theoretically) with a 6 dB width quantised to 2 bins (1.81 bins theoretically). There appears to be some small asymmetry in the side lobes which may be due to some phase shift present across the signal conditioning channel. Since the side lobes are below the threshold considered for channel sounding measurements this has not been explored further here.

The DDFS were disconnected within the base channel sounder transmitter and receiver and were substituted by low phase noise synthesised signal sources. A Fluke 6071A was used at the transmitter and a Rhode and Schwartz SMS was used at the receiver. At the transmitter the synthesised source was set to 260 MHz which corresponds to the mid frequency of the DDFS under normal operation. At the receiver the synthesised source was offset slightly to produce a beat signal at 50 kHz. This beat signal was then processed by the signal conditioning and data acquisition in the normal way. The results of the base sounder for an RF signal of 2.1 GHz are presented in figures 5.22a and 5.22b.

The performance of the base sounder with the up-converter and down-converter were then evaluated for each of the bands. The 2.5 GHz converter results are presented in figures 5.23a and 5.23b, the 3.4 GHz converter in figures 5.24a and 5.24b and for the 5.7 GHz converter in figures 5.25a and 5.25b.

At 2.1 GHz IF and for the responses including the 2.4 GHz, 3.4 GHz and 5.7 GHz there is some degradation of the noise floor evident due to some additional noise introduced within the equipment.

The 60 GHz system demonstrates a more significant degradation in the noise floor due to the additional frequency translation and multiplication within the equipment (Refer to figures 5.26a and 5.26b). The broad-band noise floor is approximately 12 dB higher than the noise floor of the 5.7 GHz system. This is in accordance with the X 4 multiplication factor used in the final 60 GHz converters. The close to carrier noise (immediately adjacent to the main lobe is however only ~ 4dB worse than that of the 5.7 GHz system).

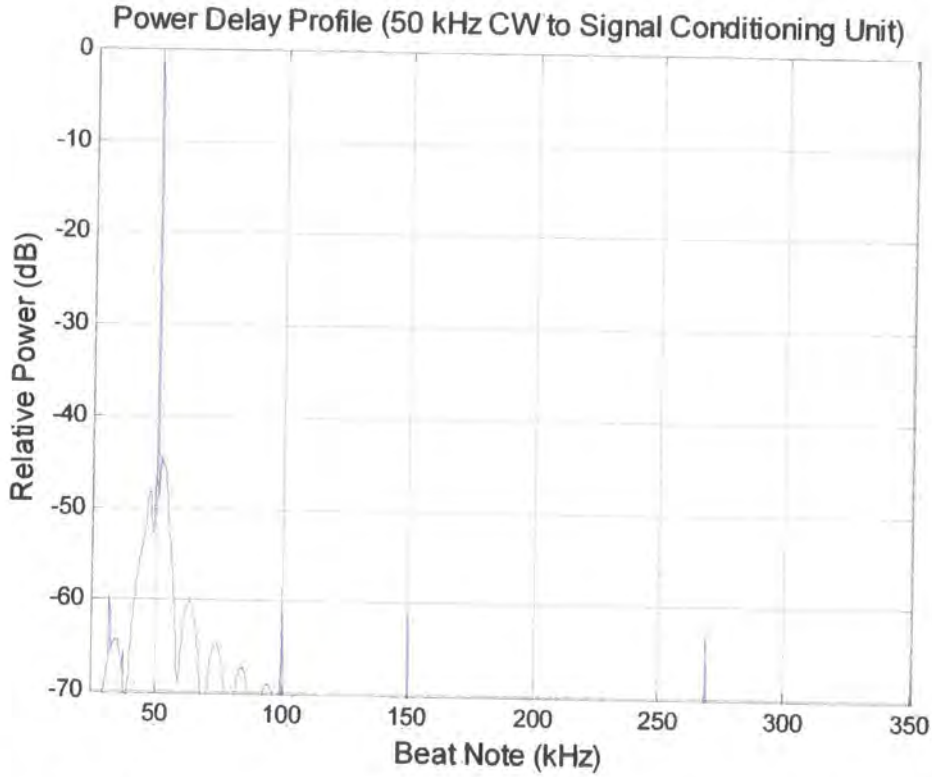

Figure 5.21a Data acquisition CW test (wide)

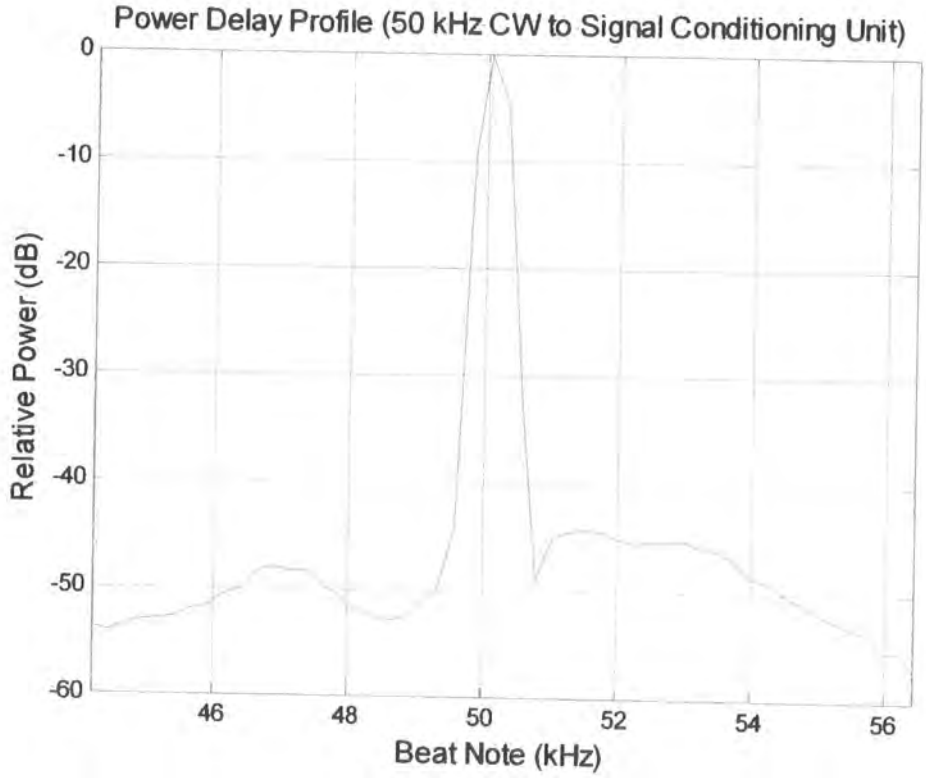

Figure 5.21b Data acquisition CW test (narrow)

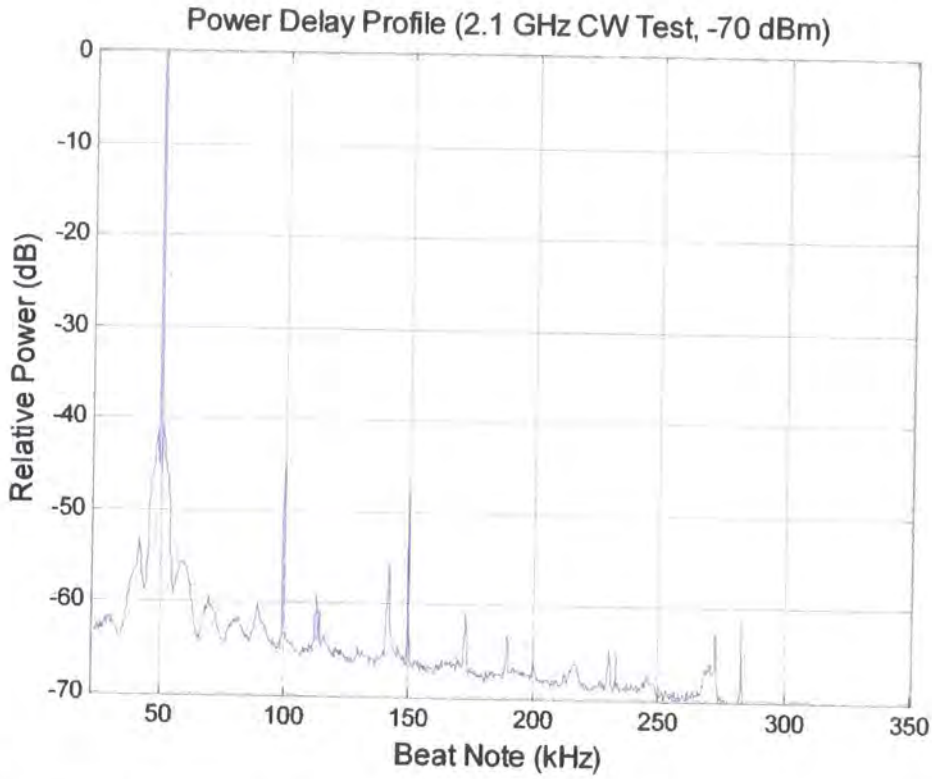

Figure 5.22a 2.1 GHz base sounder CW test (wide)

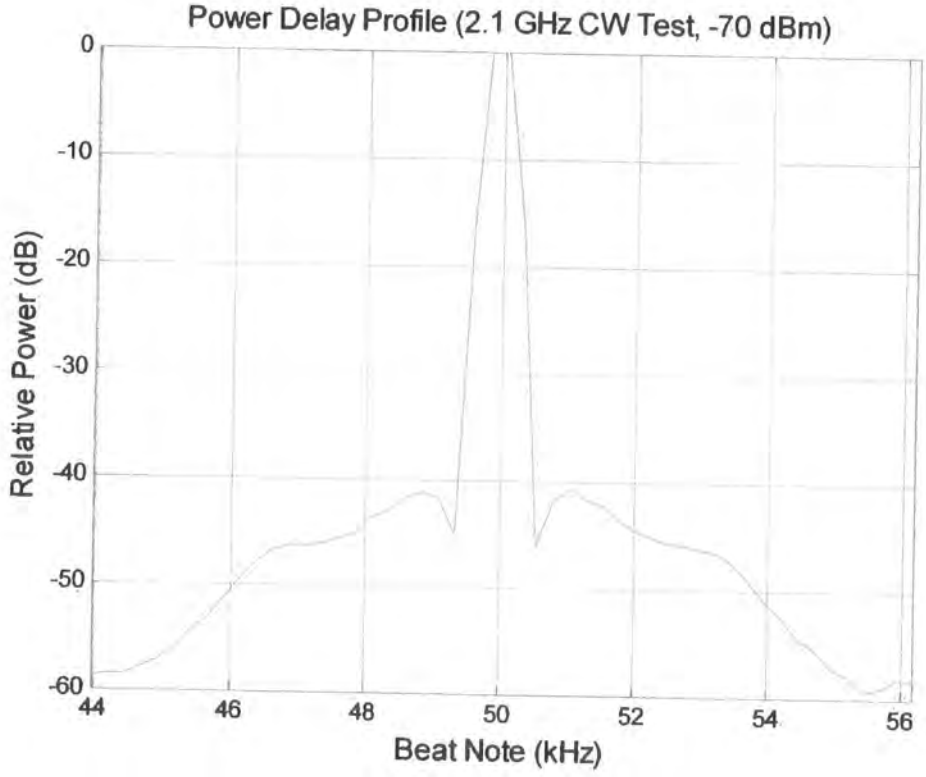

Figure 5.22b 2.1 GHz base sounder CW test (narrow)

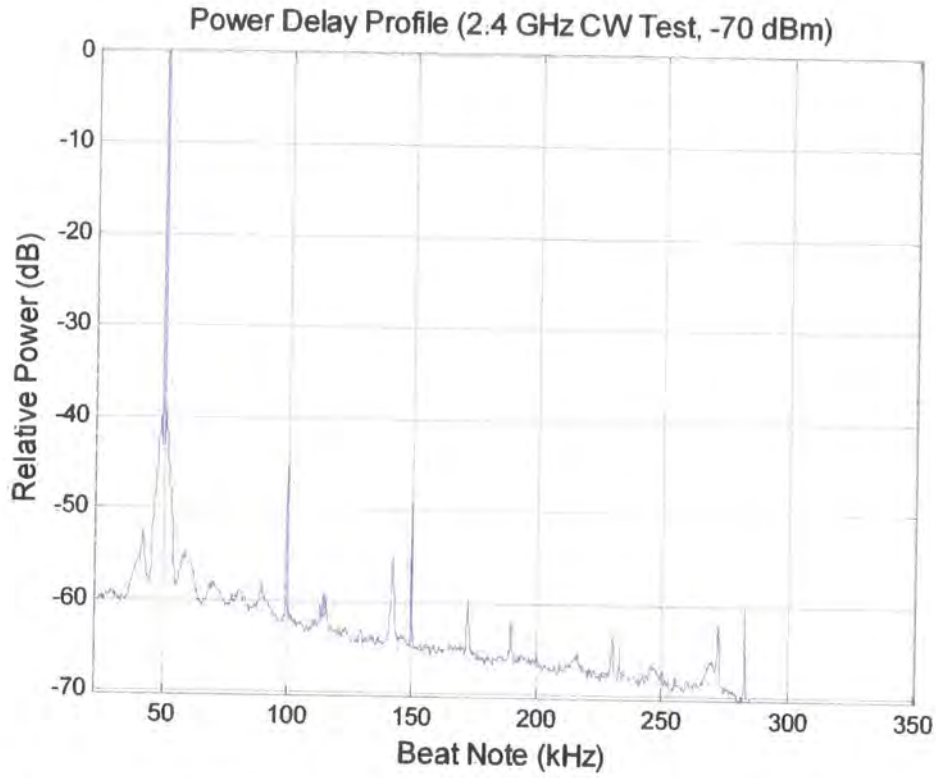

Figure 5.23a 2.5 GHz converter and sounder CW test (wide)

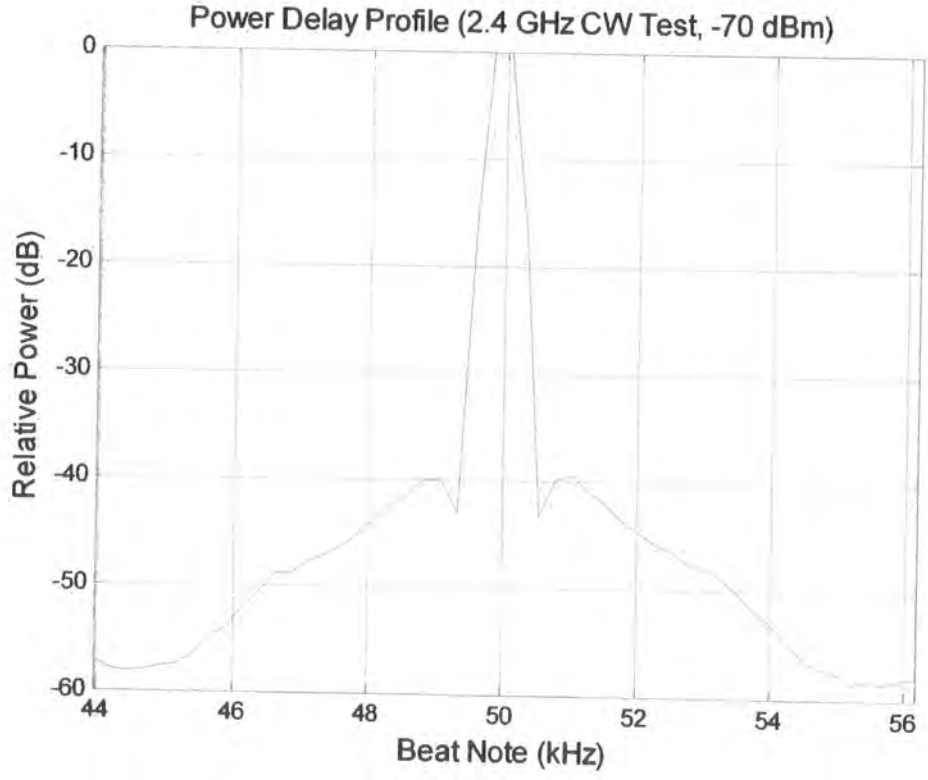

Figure 5.23b 2.5 GHz converter and sounder CW test (narrow)

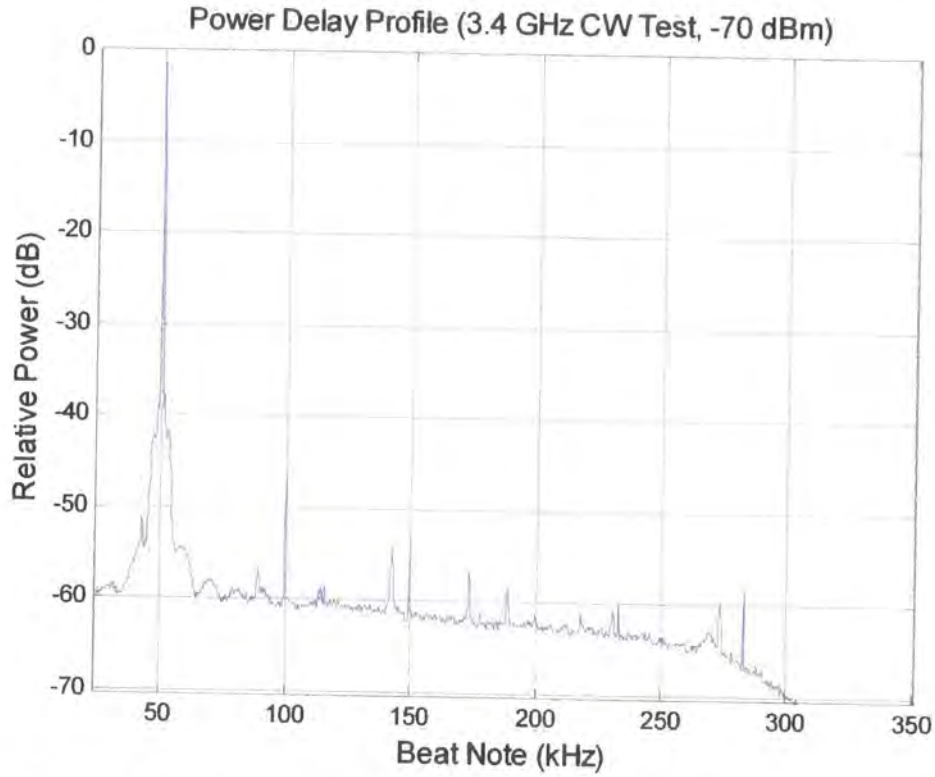

Figure 5.24a 3.4 GHz converter and sounder CW test (wide)

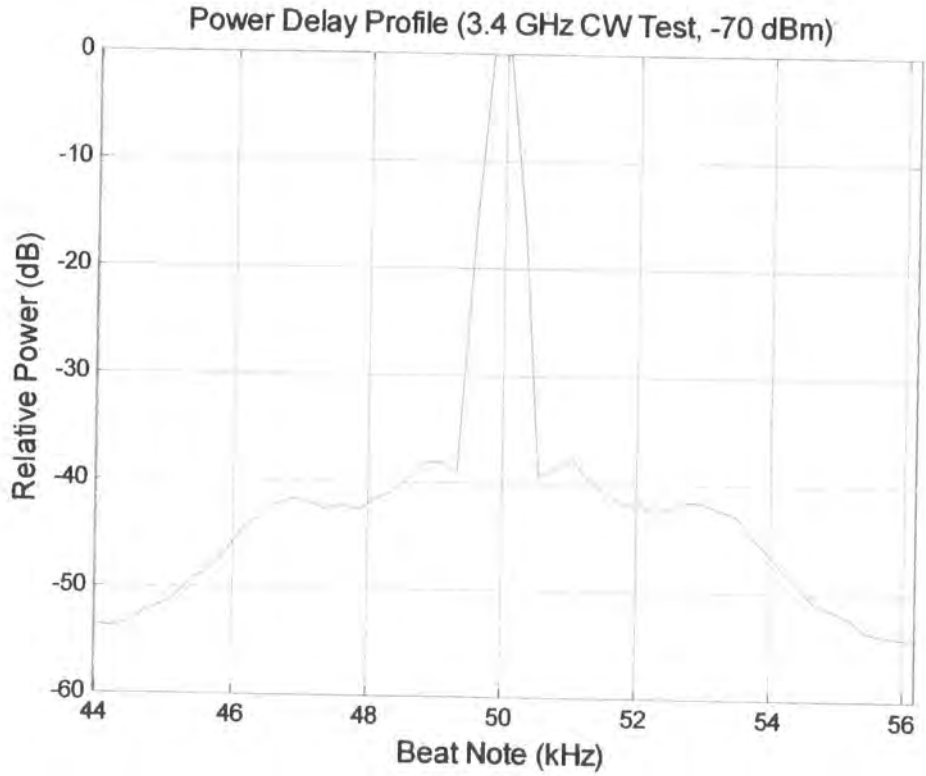

Figure 5.24b 3.4 GHz converter and sounder CW test (narrow)

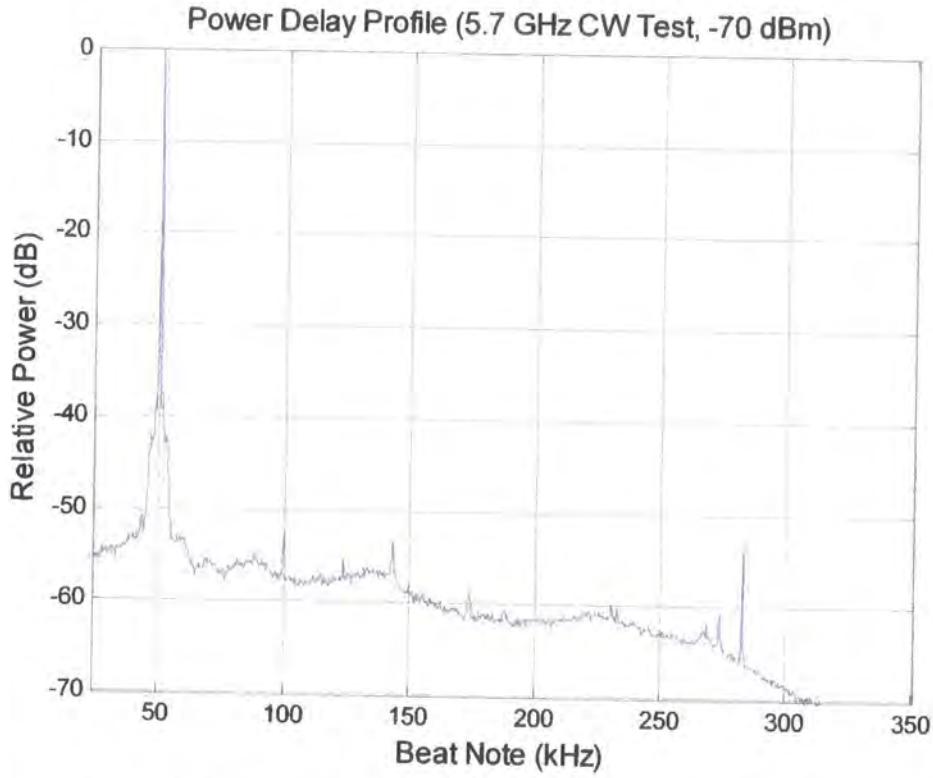

Figure 5.25a 5.7 GHz converter and sounder CW test (wide)

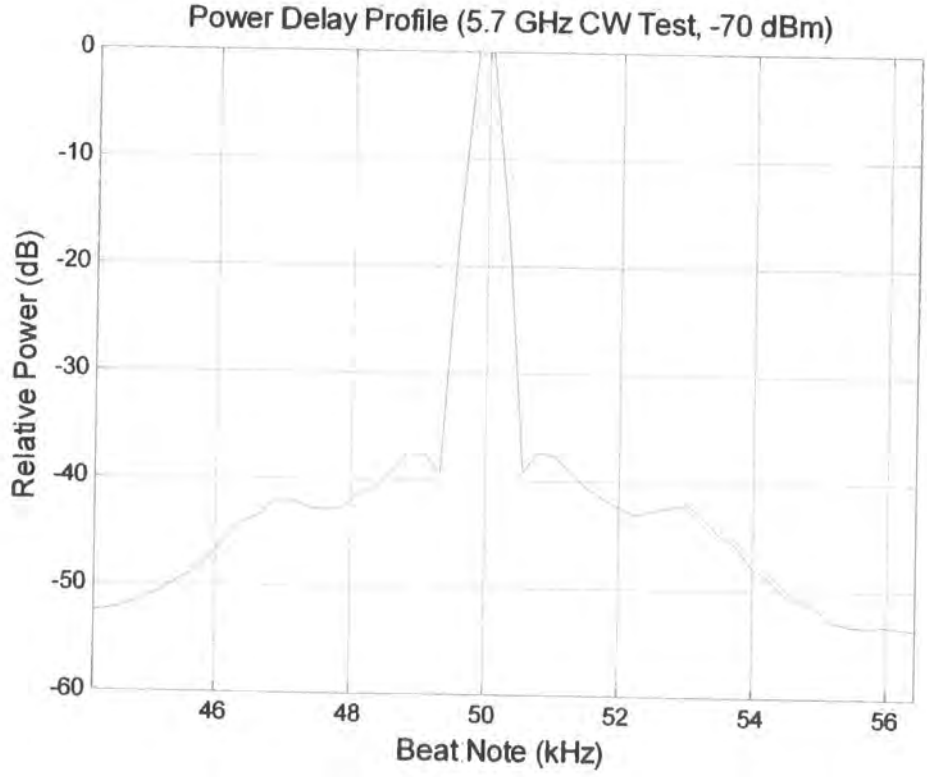

Figure 5.25b 5.7 GHz converter and sounder CW test (narrow)

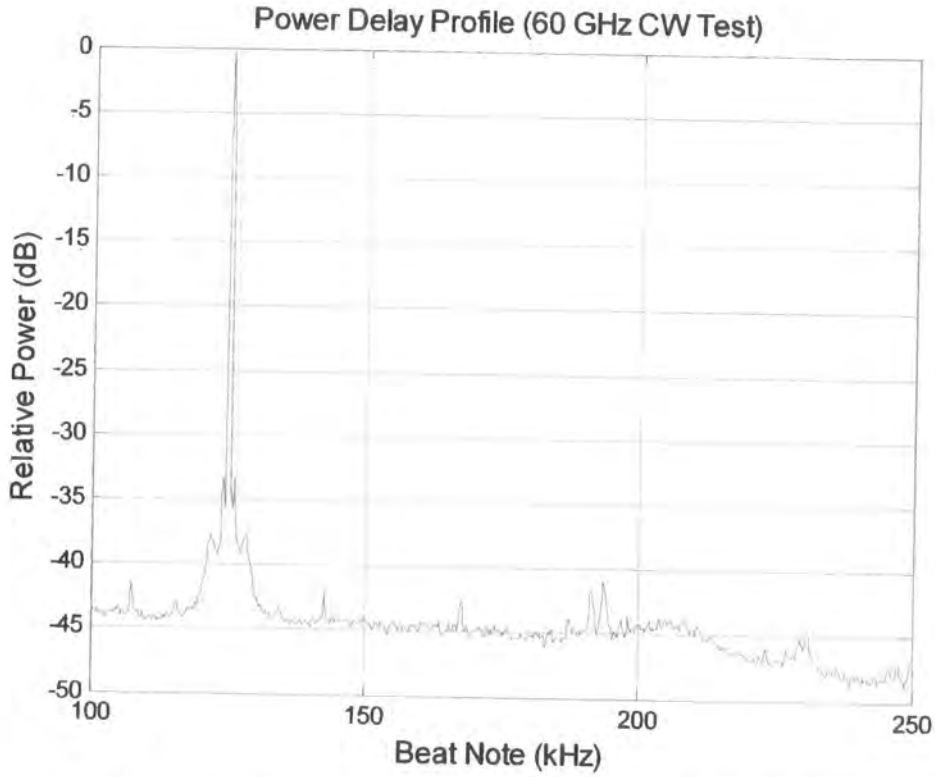

Figure 5.26a 60 GHz converter and sounder CW test (0 to 300 kHz)

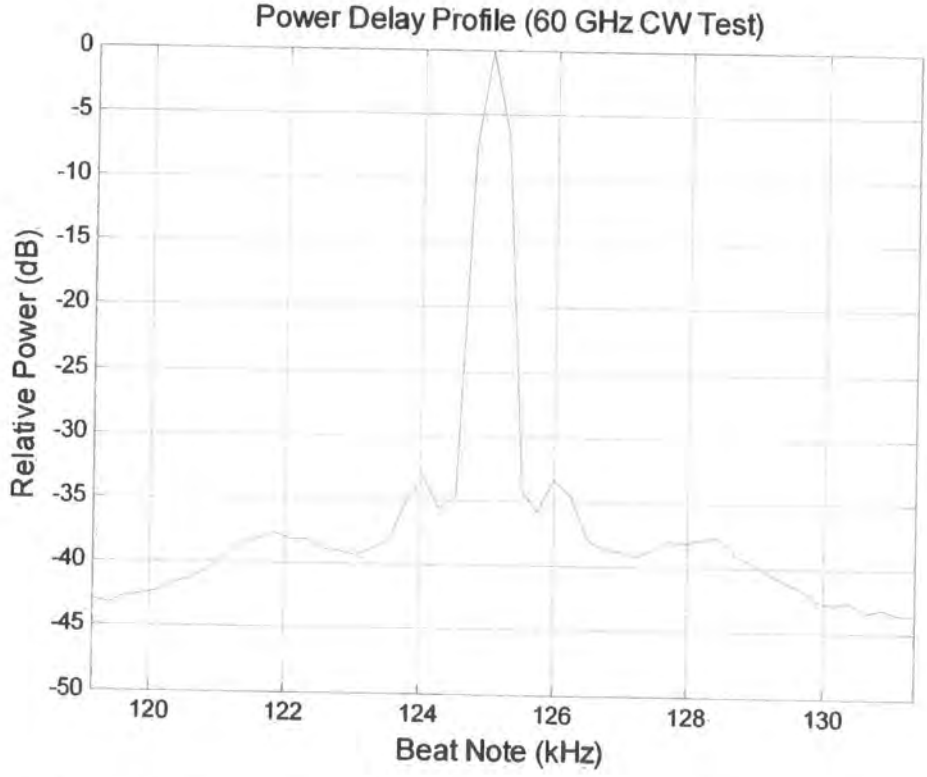

Figure 5.26b 60 GHz converter and sounder CW test (+/- 6.25 kHz)

5.3.2 Investigation of the noise contribution within the base sounder

The down-converters include an explicit filter between the low-noise amplifiers and the down-conversion mixer. This filter fulfils two functions. Firstly the filter provides a defined band of signal that the down-converter will process. Second, the filter provides attenuation of the "image" signal that the converter would otherwise exhibit responses to. For all the down-converters used here the LO is above the wanted signal. Thus the image band is above the LO spaced by the IF band.

The wanted response is defined by: IF = LO – Signal band

The image response is defined by: Image band = LO + IF

The amplifiers used here are anticipated to have noise output within the image band as well as within the signal band. Without a filter that rejects the noise from the image band between the amplifier and the mixer the IF will contain noise which has been converted from both the signal and image bands. If the noise contribution were equal from both bands, the total noise contribution would be doubled. This would cause a noise figure degradation of 3 dB. The filters included within the down-converters reduce this contribution to < 0.05 dB.

In the base sounder however, the down-conversion process is from the 2 GHz input band direct to base-band. The base-band response is 30 kHz to 250 kHz thus the image frequencies are only 60 kHz to 500 kHz away from the wanted band. Clearly this cannot be addressed by a filter function in the frequency domain at 2 GHz, particularly since the sounder is sweeping a band of frequencies that is much greater than the base-band width. (This issue could be addressed using phasing techniques to provide cancellation of the unwanted noise sideband, similar to that used in the SSB down-converter. However this is not what has been implemented here at present.)
On this basis it is presumed that the noise present from the image sideband will contribute equally and thus the operational noise floor of the base sounder will be degraded by 3 dB.

For a double sideband noise contribution, equal amounts of noise will be heterodyned to the output of the mixer from both the wanted and image signal bands. Under this condition the effective ENR of the noise source will be 3 dB higher and the noise figure will be incorrect and be under-reported by 3 dB.

This has been confirmed by measurement. The noise source and the chirp RF signal were connected to the input of the sounder via a 10 dB directional coupler. The chirp was connected via the -10 dB coupled path and the levels were adjusted to provide an input wanted signal level of -100 dBm. The noise source was connected to the "through" arm of the coupler. The loss of the test configuration for the noise source was measured to be 0.55 dB using a network analyser. The calibrated ENR for the source was 15.55 dB at 2 GHz. Hence, the ENR at the input to the sounder was 15 dB. The noise source was energised and the sounder levels were calibrated in the presence of noise and chirp. The resultant response is depicted in figure 5.27a. The noise source was then switched off and the system response was recorded (without adjusting the chirp signal level or equipment gain settings) as shown in figure 5.27b. The effective noise figure response can then be obtained by performing a "y-factor" calculation on the relative shift of the noise floor since this is only due to the change produced by the noise source as the other gain and signal levels have not been altered.

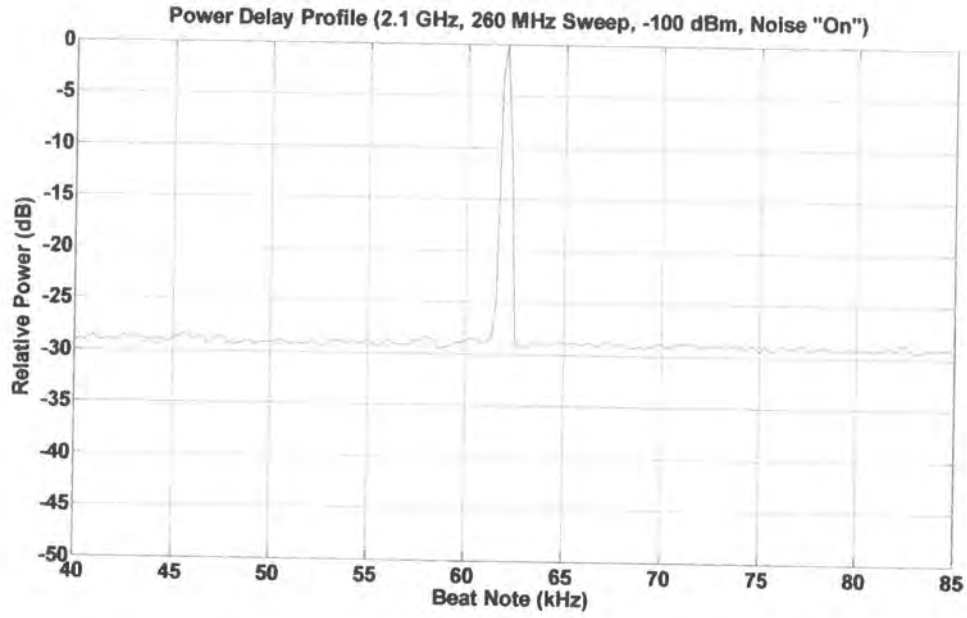

Figure 5.27a Sounder noise figure measurements (noise source operating)

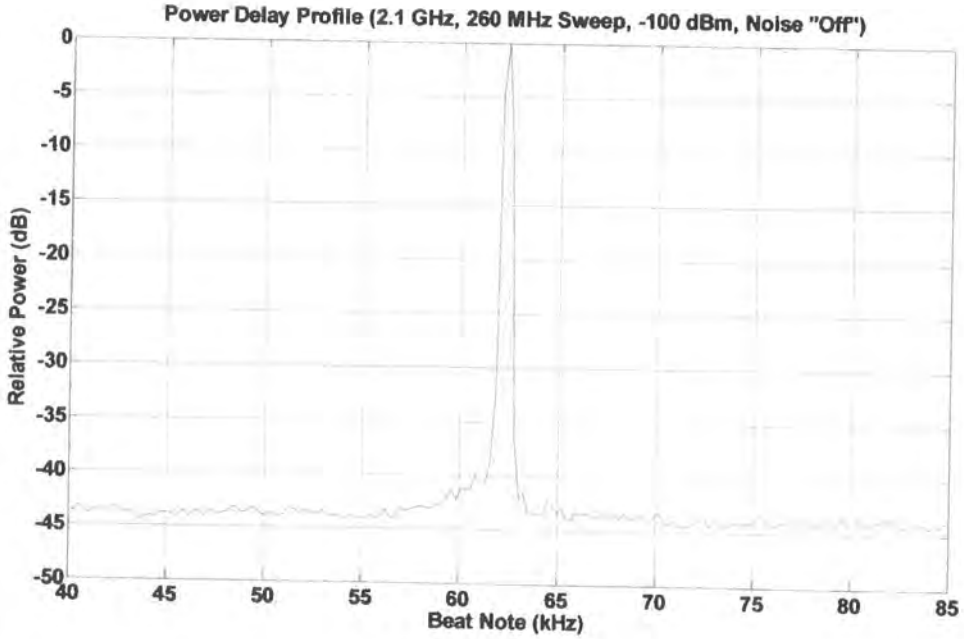

Figure 5.27b Sounder noise figure measurements (noise source off)

From the data in figures 5.27a and 5.27b, the shift in the noise floor is estimated to be:

Noise off – noise on = -144 dBm - -129 dBm = 15 dB

ENR = 15.55 dB – 0.55 dB = 15.0 dB

y = 15 dB, Y = 31.62

Using equation (5.1)

F(dB) = 15.0 – 14.86 = 0.14 dB

Since the input amplifier alone of the 2 GHz sounder itself has a specified maximum noise figure of 1.5 dB we are clearly observing a double-sideband noise conversion. Thus the actual noise figure is 3 dB above this since the effective ENR is 18 dB.

Measured system noise figure at 2.1 GHz is: 3.14 dB

On this basis the noise floor for the operational sounder can be estimated:

Thermal noise density:	-174 dBm / Hz
Plus noise figure:	3 dB
Plus DSB to SSB factor:	3 dB
Plus bandwidth:	25 dB *(10 Log (1.36*10^6/4096)*
Noise floor:	-143 dBm

This value is in close agreement with the observed value (above) of -144 dBm.

5.3.3 Single path power delay profile

The single path power delay provides an indication of the limits of measurement for the channel sounder when operating through an ideal flat fading channel with no discernable multi-paths present. This characterisation also indicates the resolution of the instrumentation for individually discernable multi-path components.

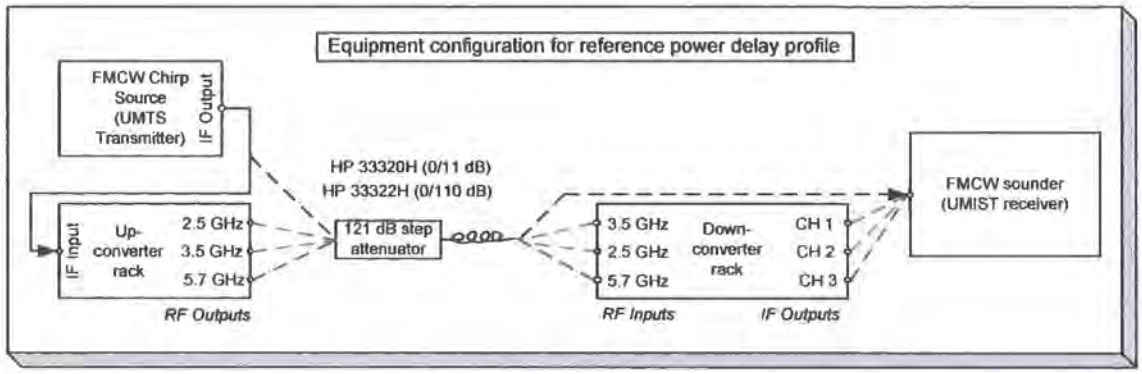

Figure 5.28 Sounder back to back calibration test configuration

Figure 5.28 illustrates the measurement configuration. The measurements were performed on an individual band basis with the output of the down-converter provided to the channel 1 input of the sounder receiver. This ensures a valid comparison between the various converters and the base UMTS channel sounder can be made.

Doppler ambiguity

The Doppler ambiguity provides an indication of the minimum Doppler and delay components that can be resolved.

Transfer function

The transfer function for the back to back measurement provides an indication of the residual channel flatness of the sounder.

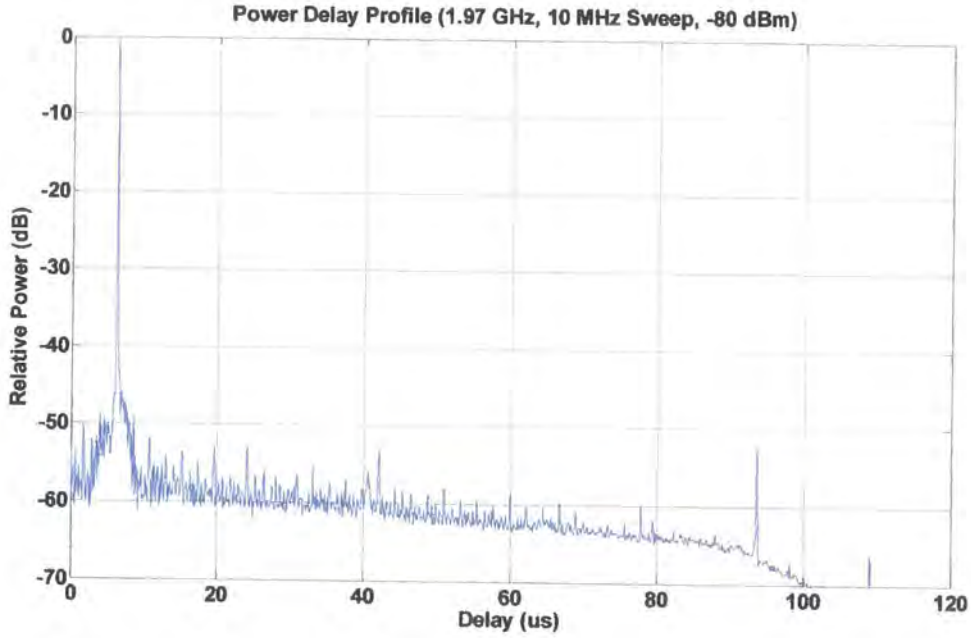

Figure 5.29a Base sounder power delay profile, -80 dBm input, 10 MHz

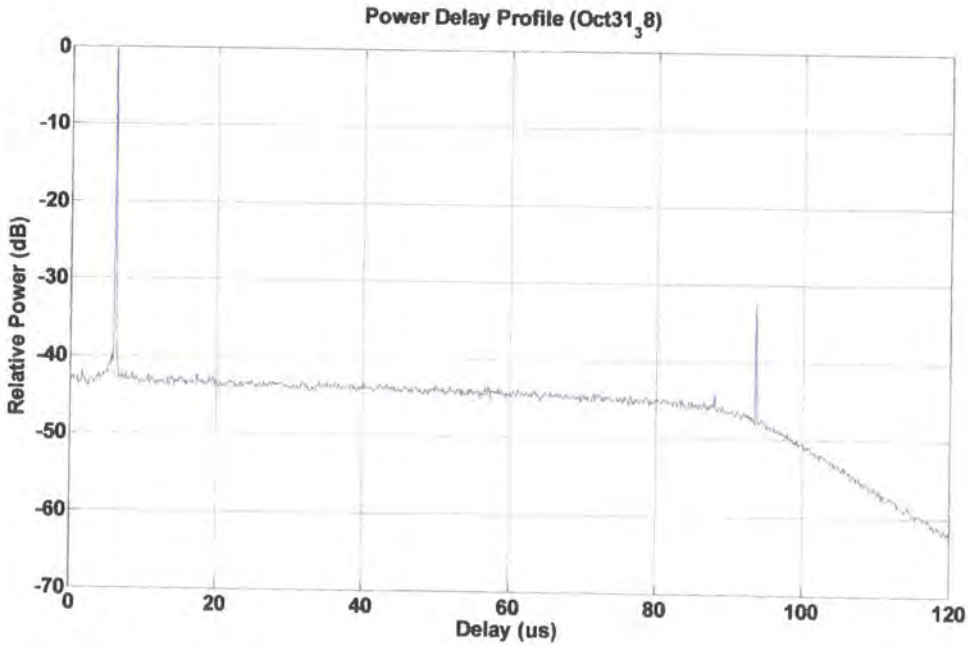

Figure 5.29b Base sounder power delay profile, -100 dBm input, 10 MHz

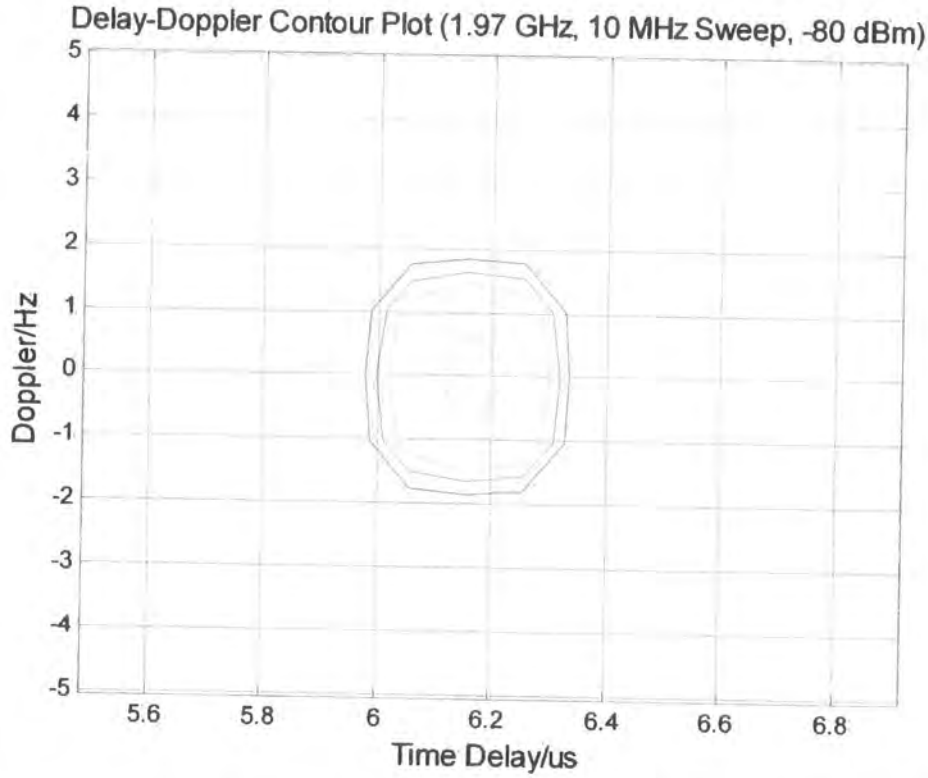

Figure 5.30a Base sounder Doppler ambiguity function, -80 dBm input, 10 MHz

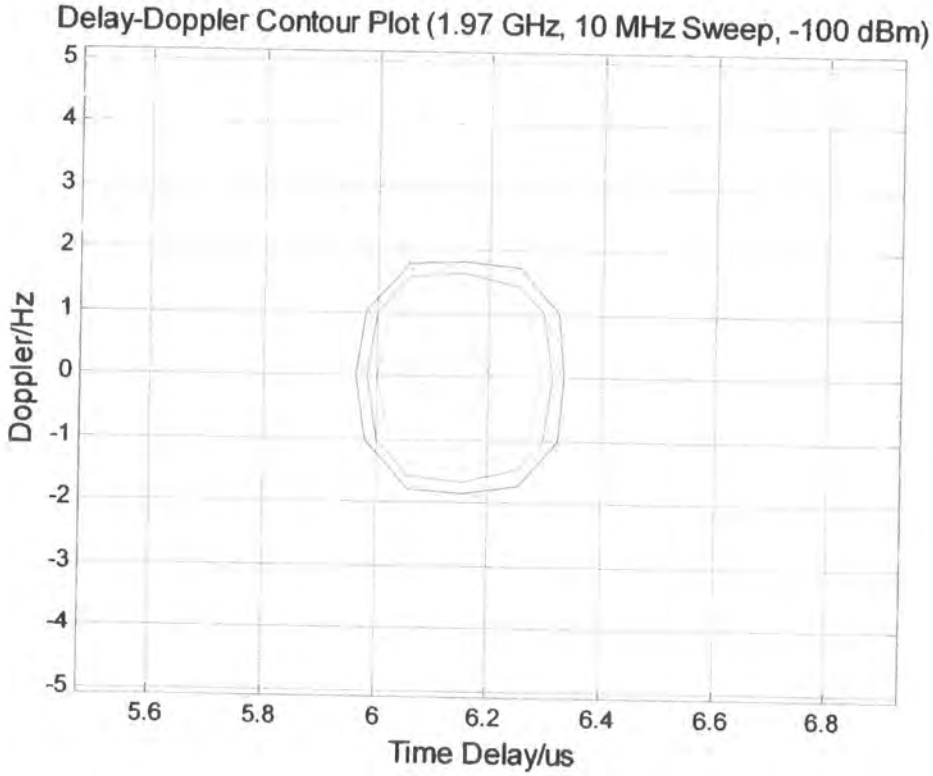

Figure 5.30b Base sounder Doppler ambiguity function, -100 dBm input, 10 MHz

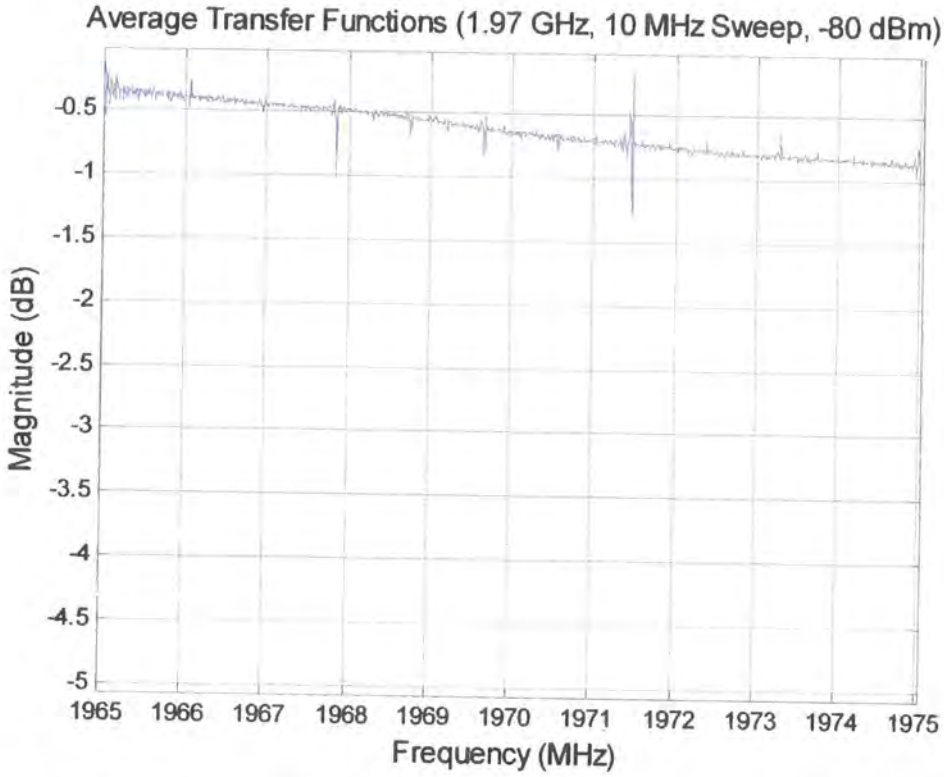

Figure 5.31a Base sounder frequency-transfer function, -80 dBm input, 10 MHz

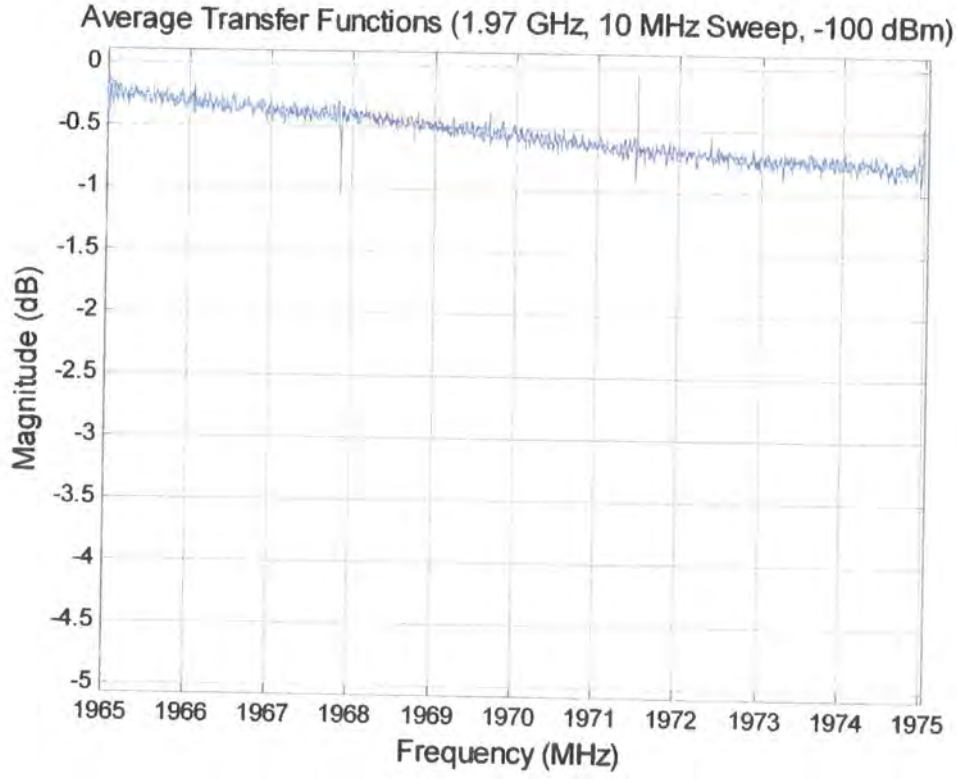

Figure 5.31b Base sounder frequency-transfer function, -100 dBm input, 10 MHz

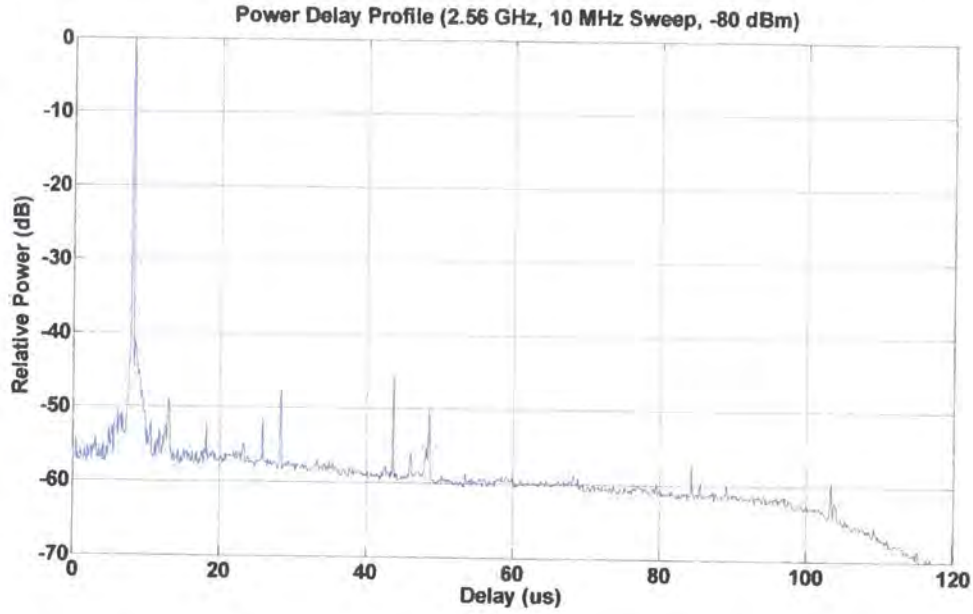

Figure 5.32a 2.5 GHz sounder power delay profile, -80 dBm input, 10 MHz

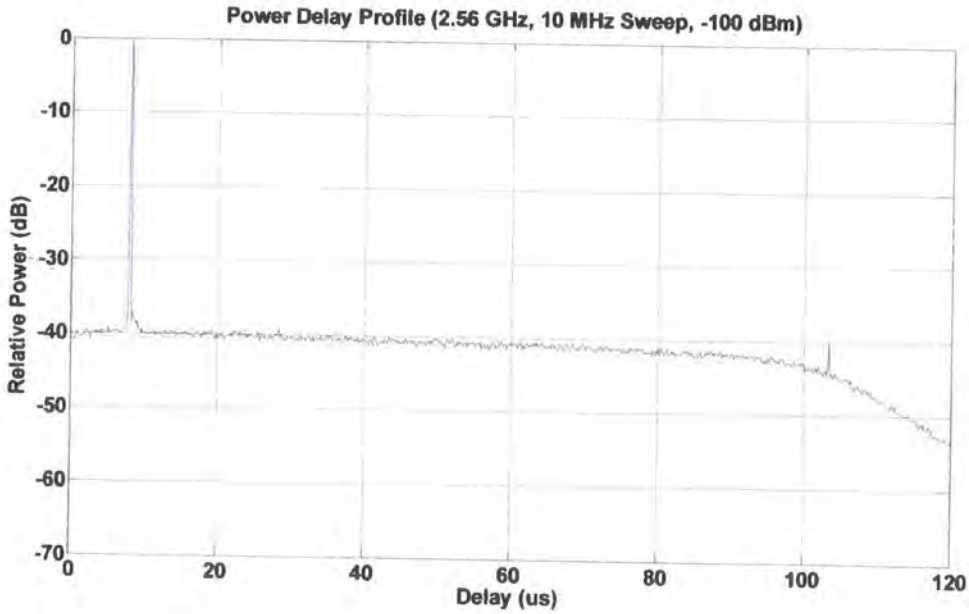

Figure 5.32b 2.5 GHz sounder power delay profile, -100 dBm input, 10 MHz

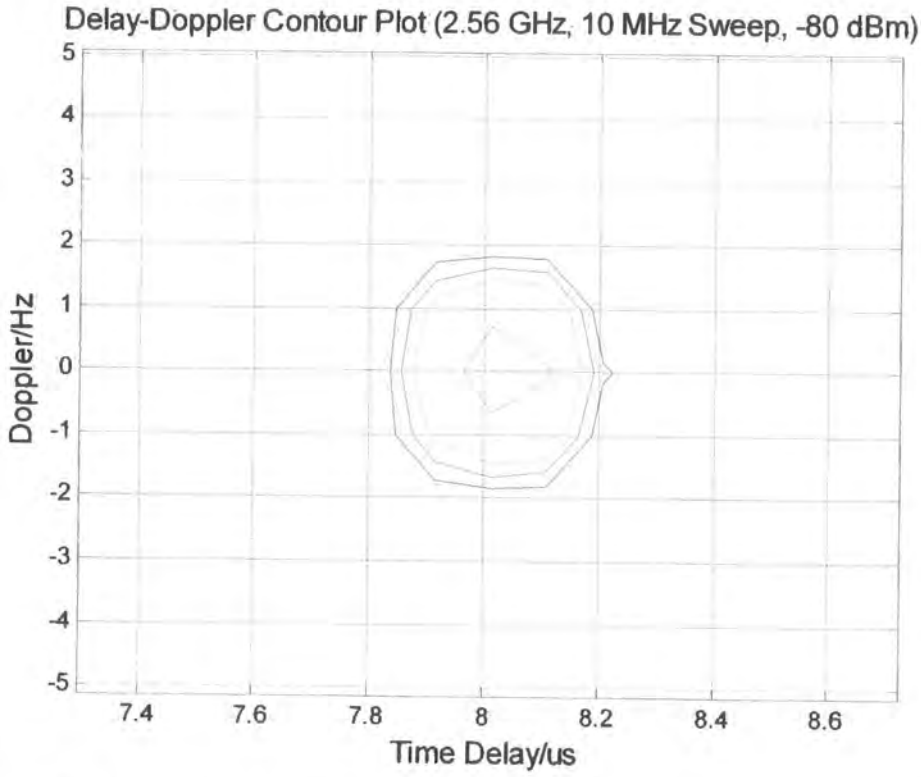

Figure 5.33a 2.5 GHz sounder Doppler ambiguity function, -80 dBm input, 10 MHz

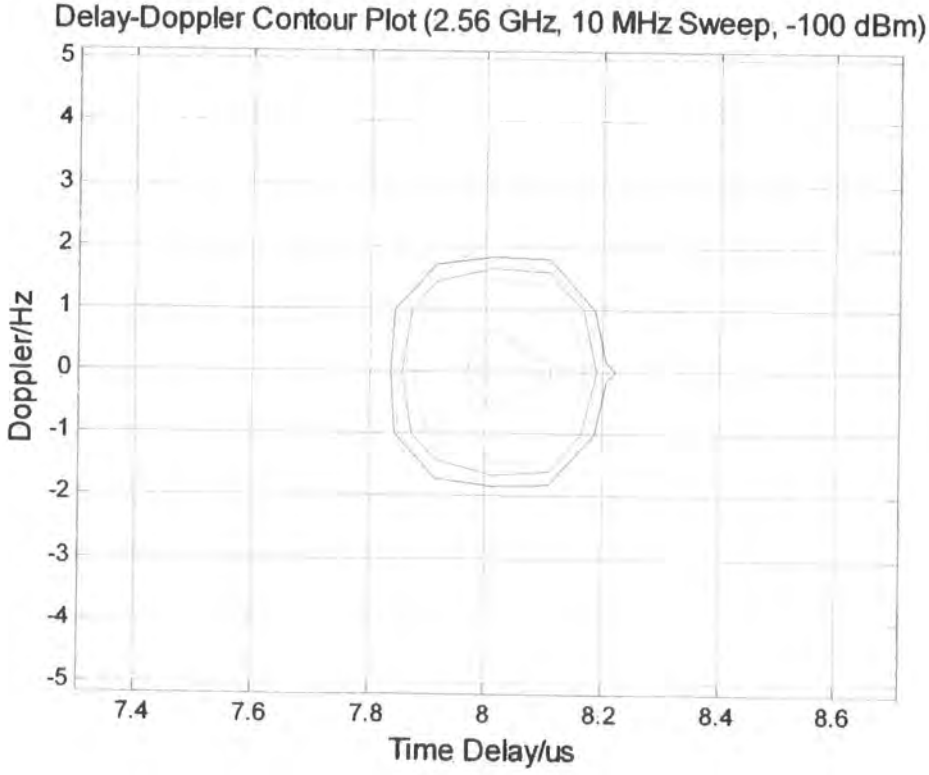

Figure 5.33b 2.5 GHz sounder Doppler ambiguity function, -100 dBm input, 10 MHz

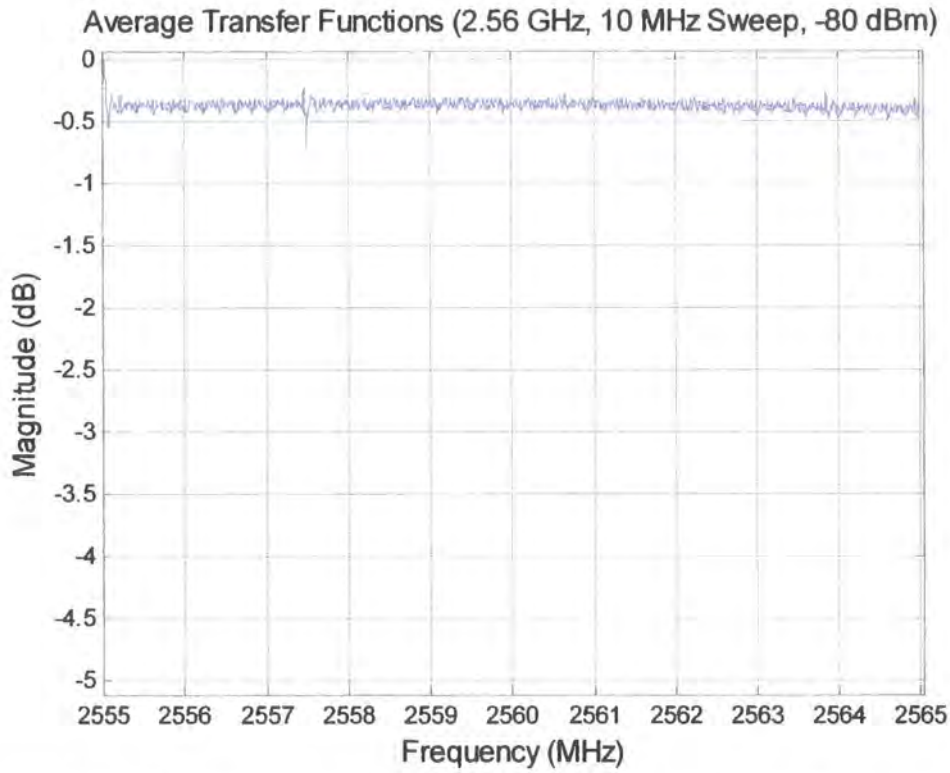

Figure 5.34a 2.5 GHz sounder frequency-transfer function, -80 dBm input, 10 MHz

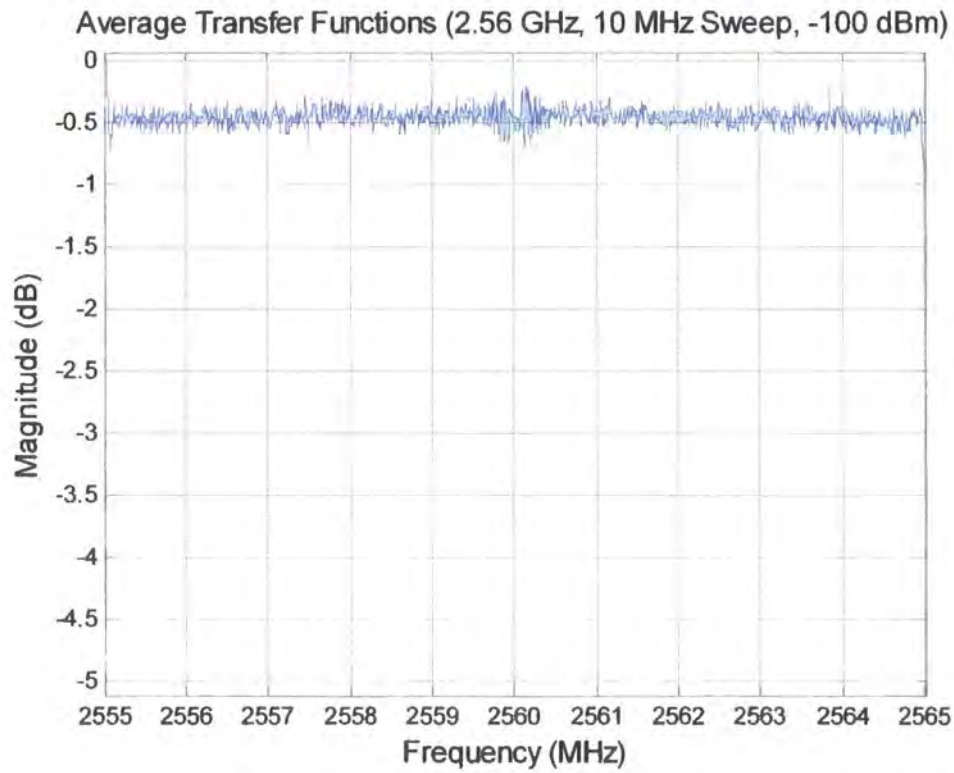

Figure 5.34b 2.5 GHz sounder frequency-transfer function, -100 dBm input, 10 MHz

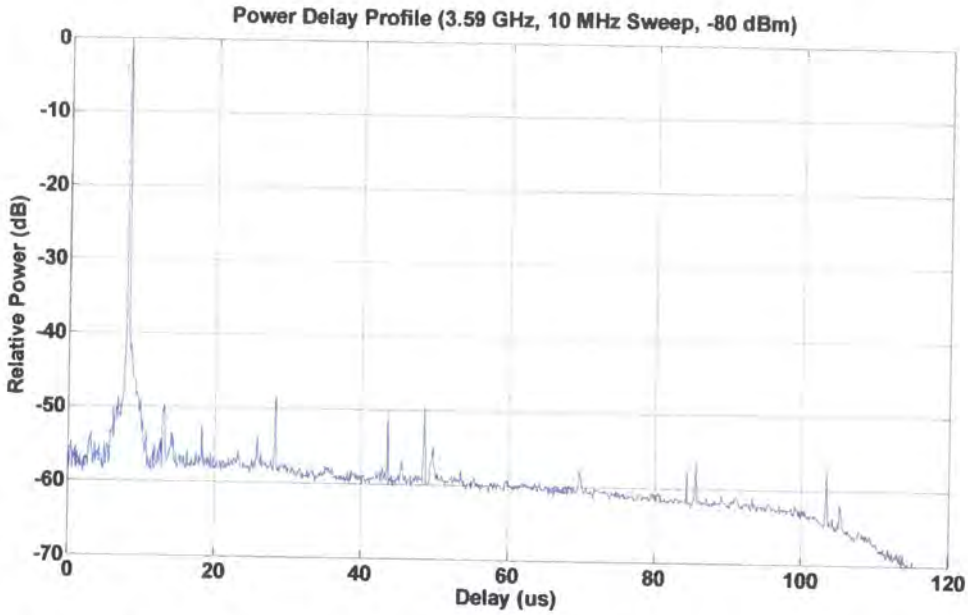

Figure 5.35a 3.5 GHz sounder power delay profile, -80 dBm input, 10 MHz

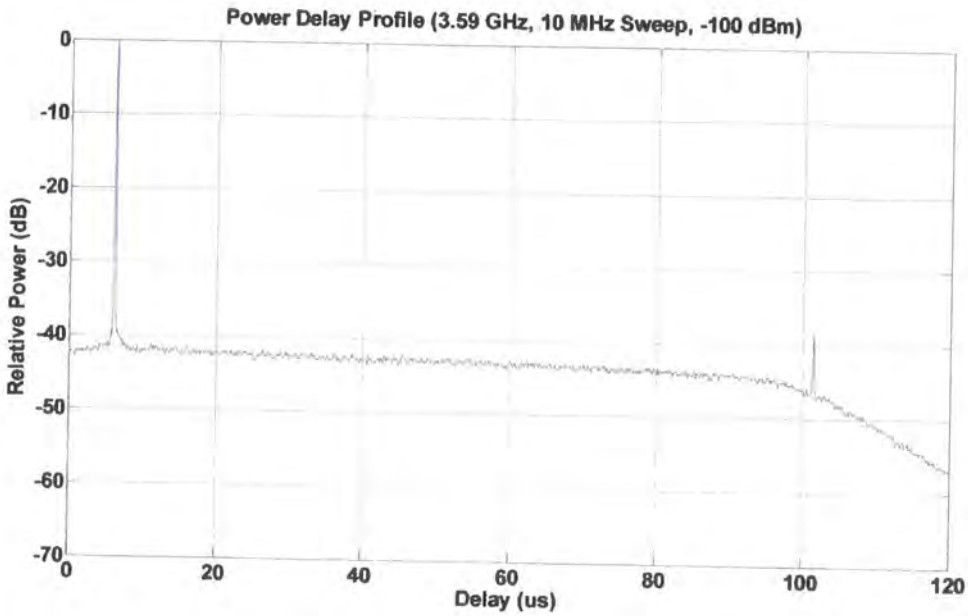

Figure 5.35b 3.5 GHz sounder power delay profile, -100 dBm input, 10 MHz

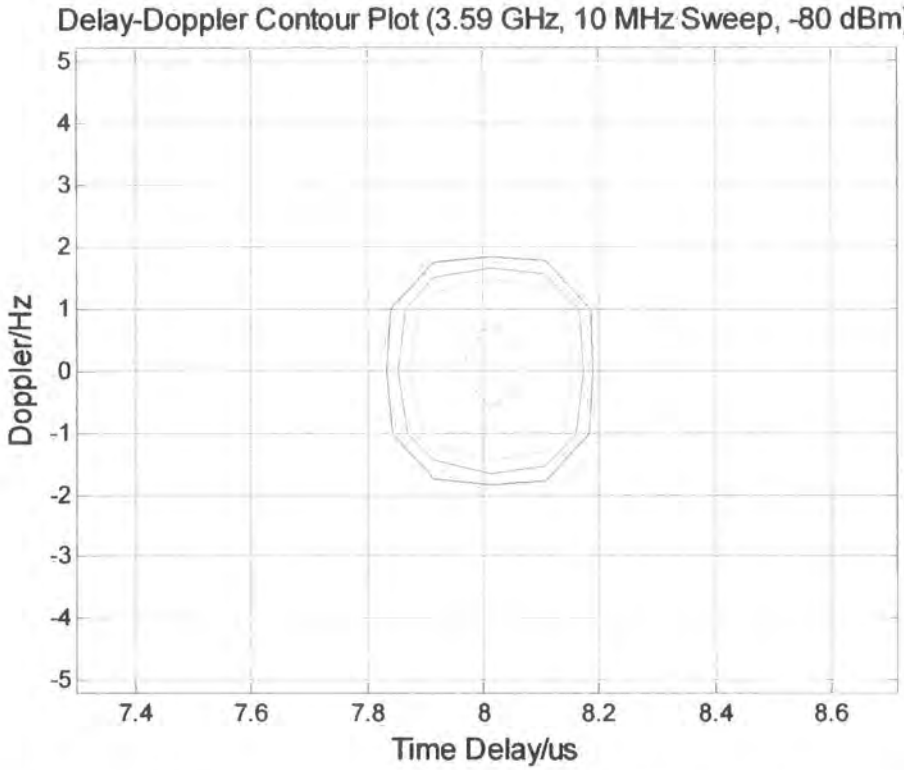

Figure 5.36a 3.5 GHz sounder Doppler ambiguity function, -80 dBm input, 10 MHz

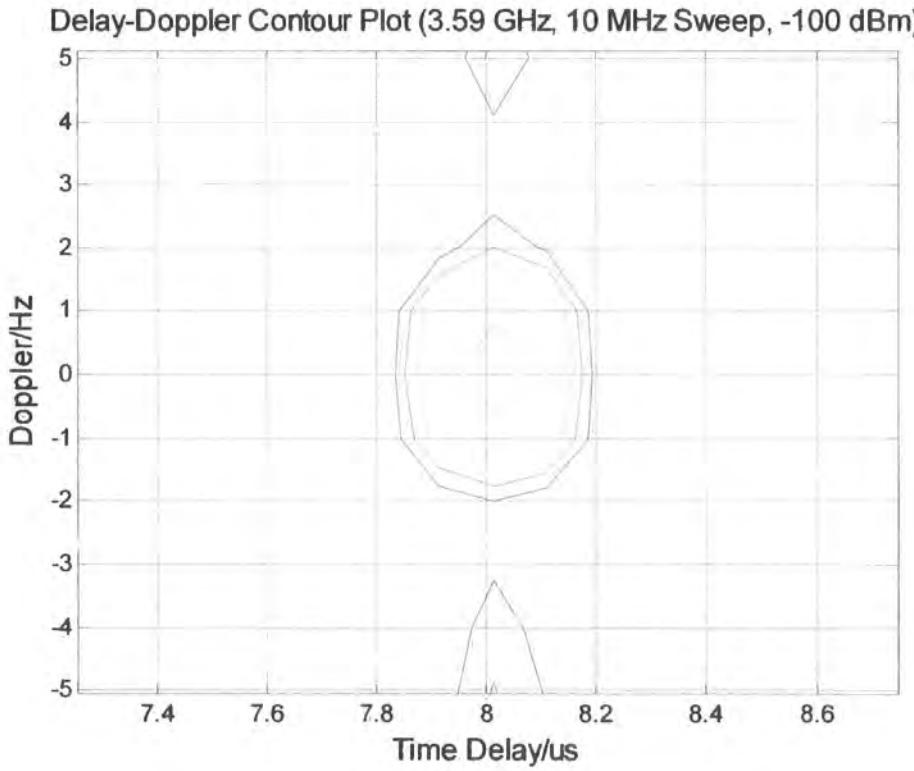

Figure 5.36b 3.5 GHz sounder Doppler ambiguity function, -100 dBm input, 10 MHz

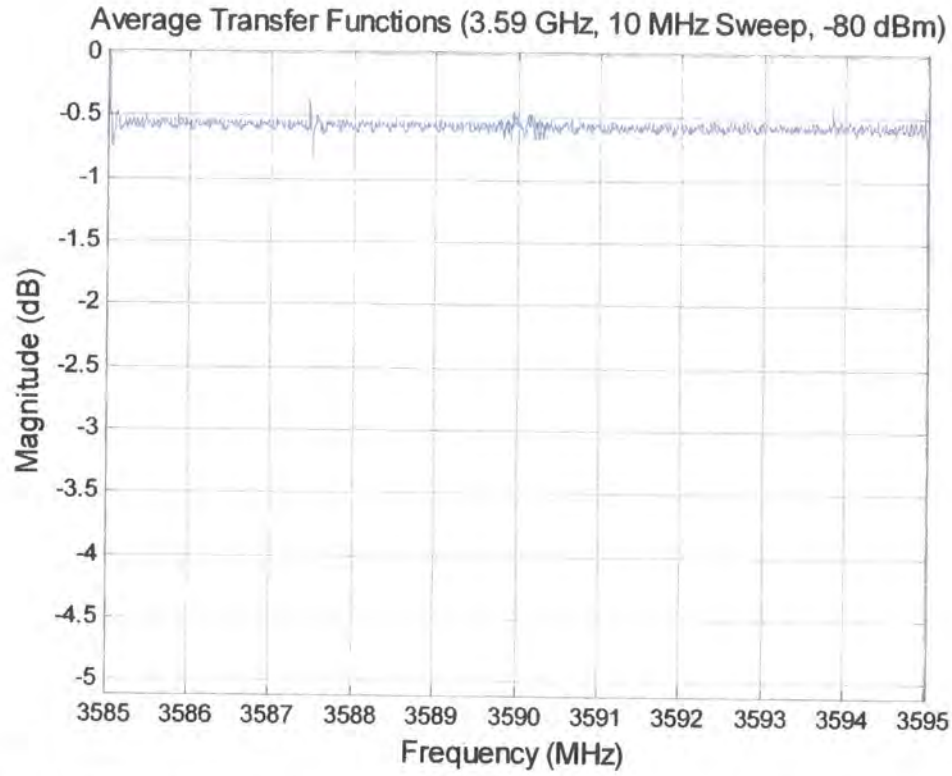

Figure 5.37a 3.5 GHz sounder frequency-transfer function, -80 dBm input, 10 MHz

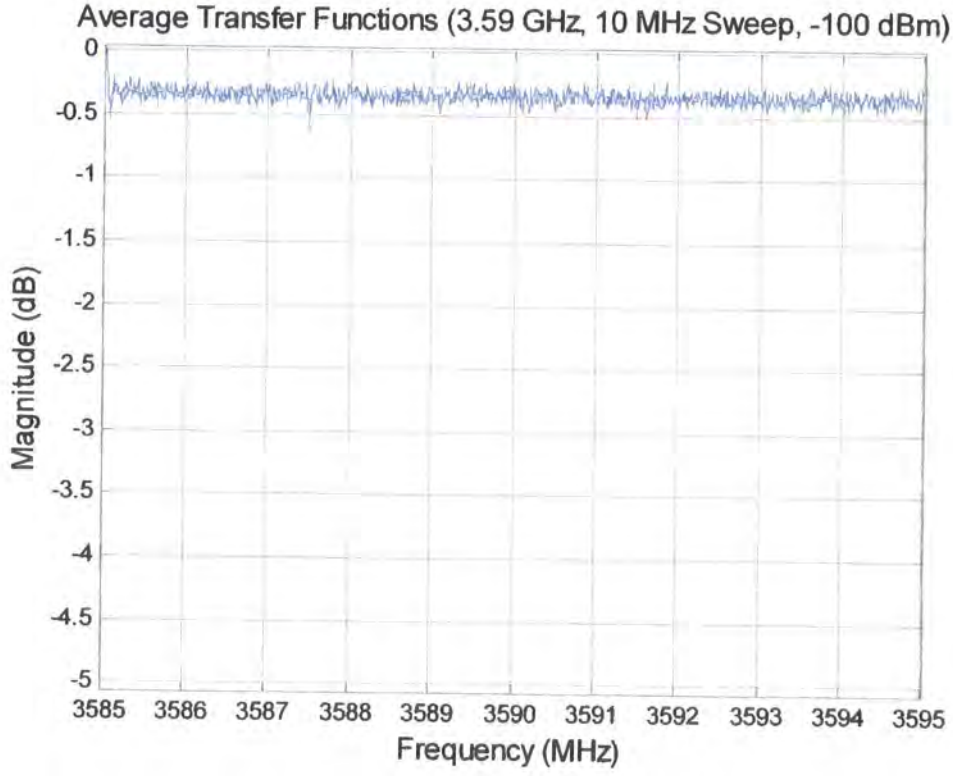

Figure 5.37b 3.5 GHz sounder frequency-transfer function, -100 dBm input, 10 MHz

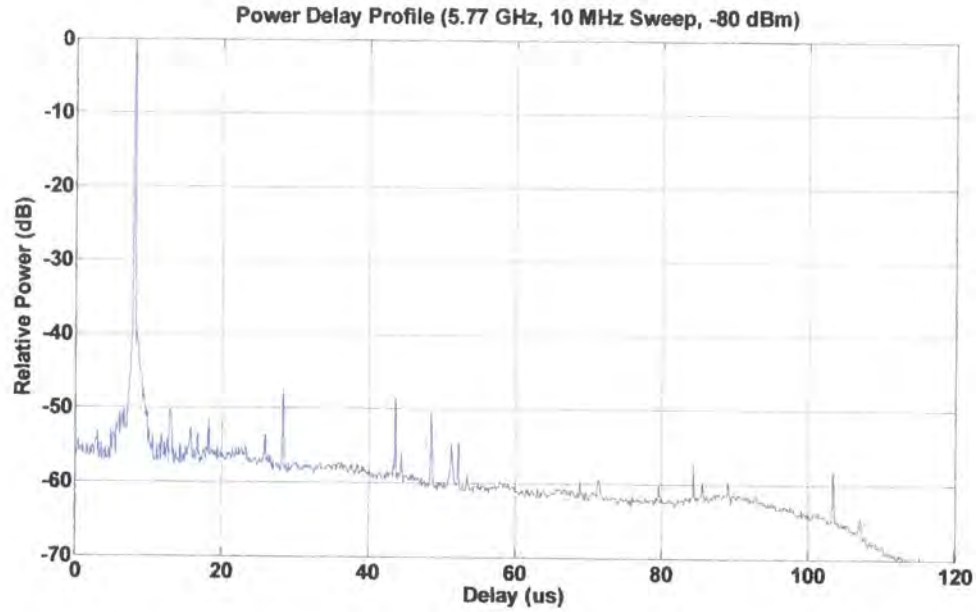

Figure 5.38a 5.7 GHz sounder power delay profile, -80 dBm input, 10 MHz

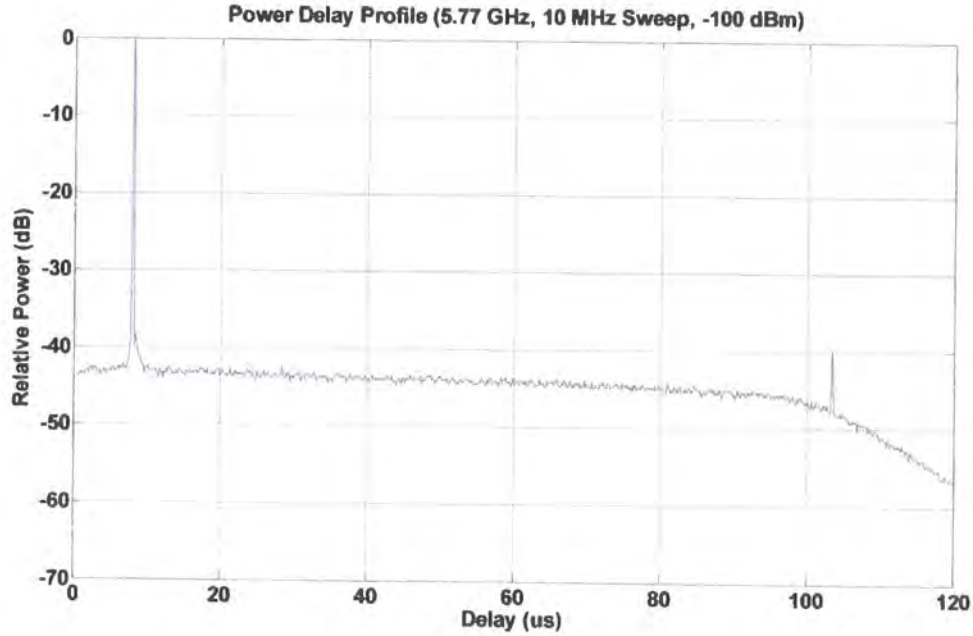

Figure 5.38b 5.7 GHz, sounder power delay profile, -100 dBm input, 10 MHz

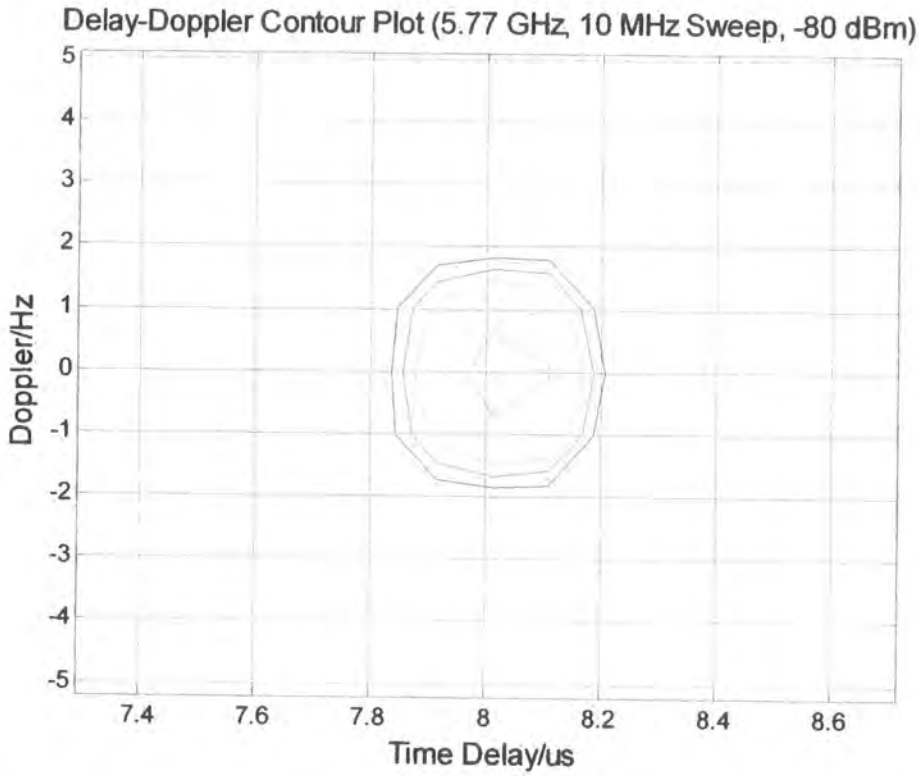

Figure 5.39a 5.7 GHz sounder Doppler ambiguity function, -80 dBm input, 10 MHz

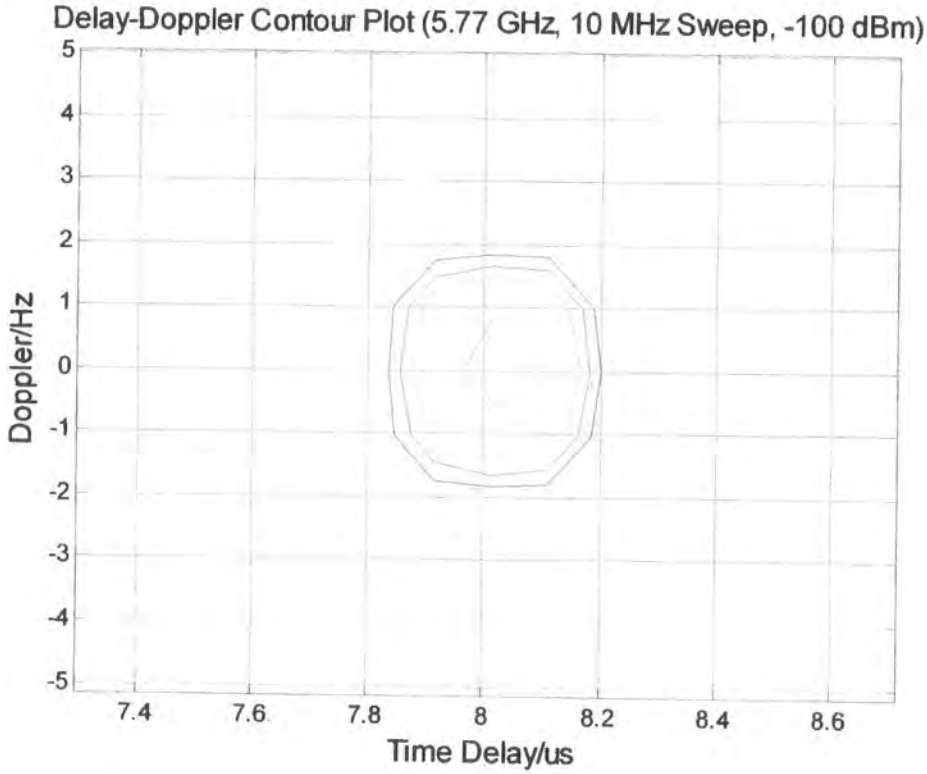

Figure 5.39b 5.7 GHz sounder Doppler ambiguity function, -100 dBm input, 10 MHz

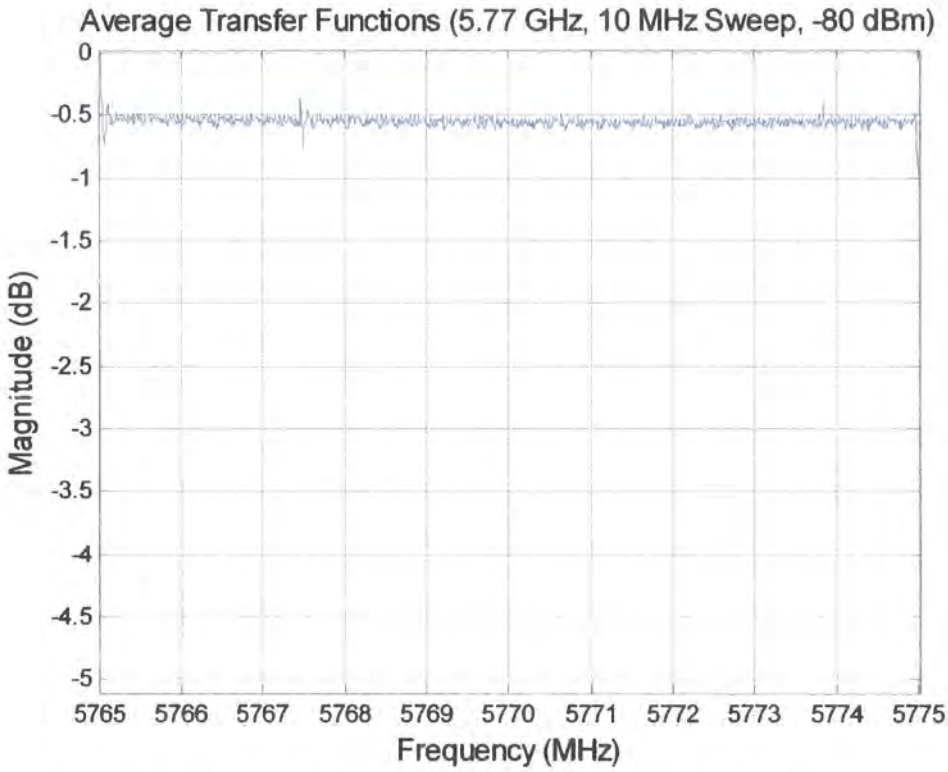

Figure 5.40a 5.7 GHz sounder frequency-transfer function, -80 dBm input, 10 MHz

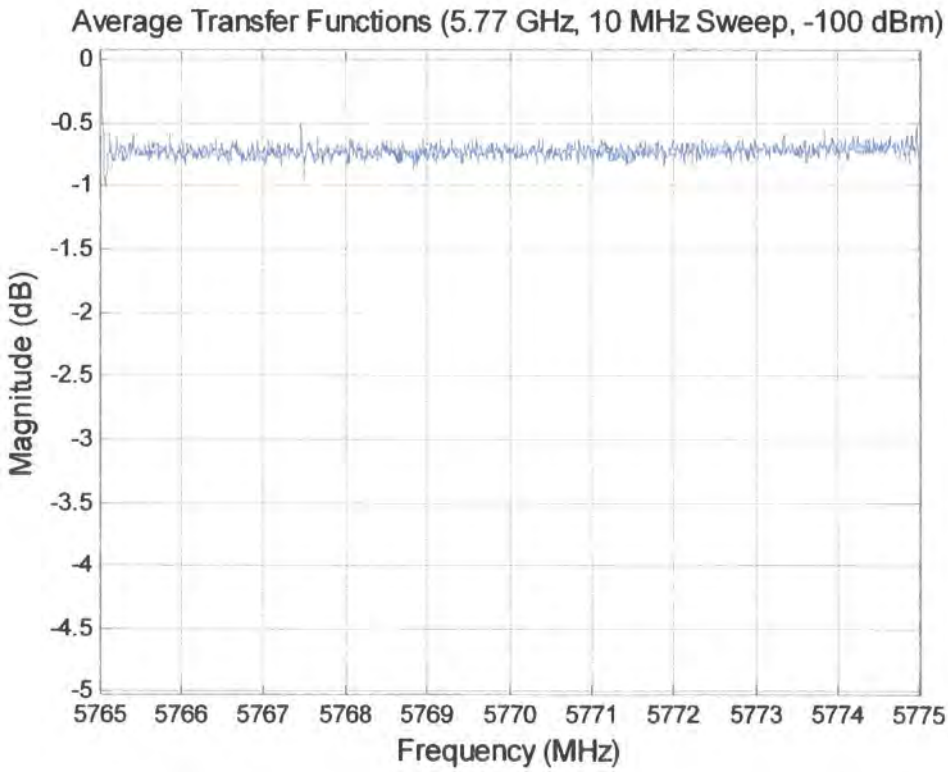

Figure 5.40b 5.7 GHz sounder frequency-transfer function, -100 dBm input, 10 MHz

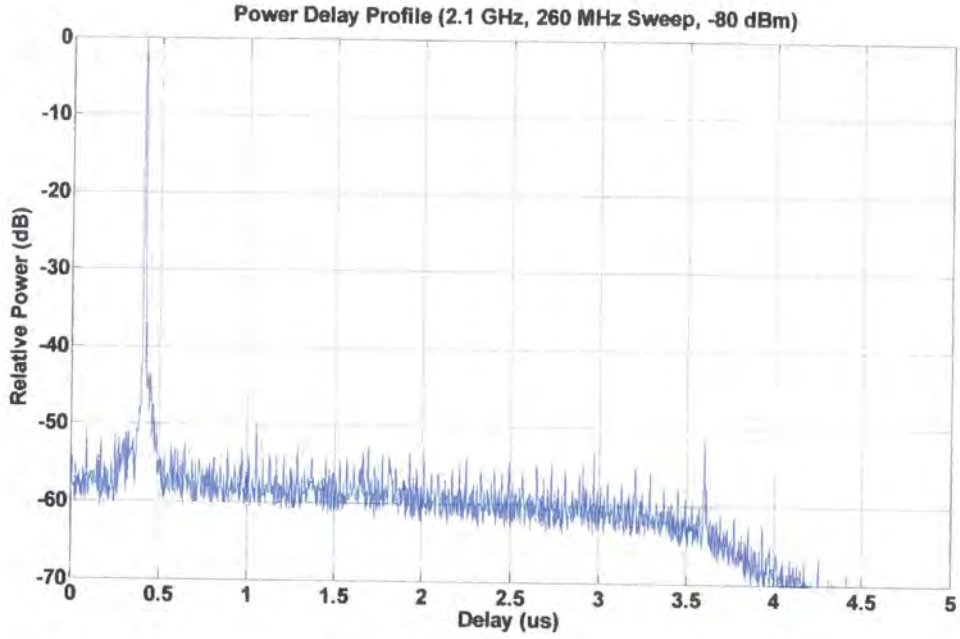

Figure 5.41a Base sounder power delay profile, -80 dBm input, 260 MHz

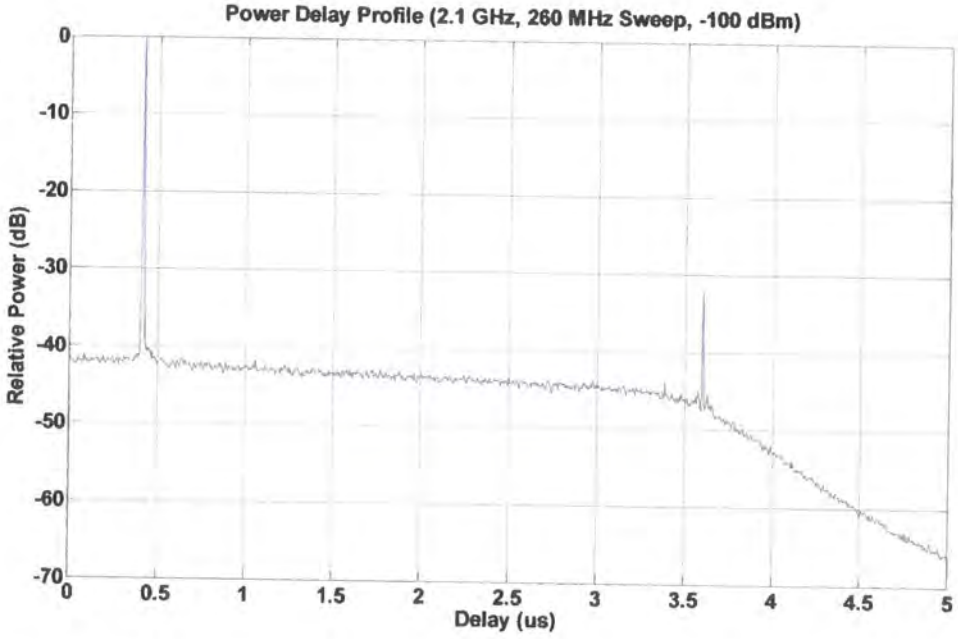

Figure 5.41b Base sounder power delay profile, -100 dBm input, 260 MHz

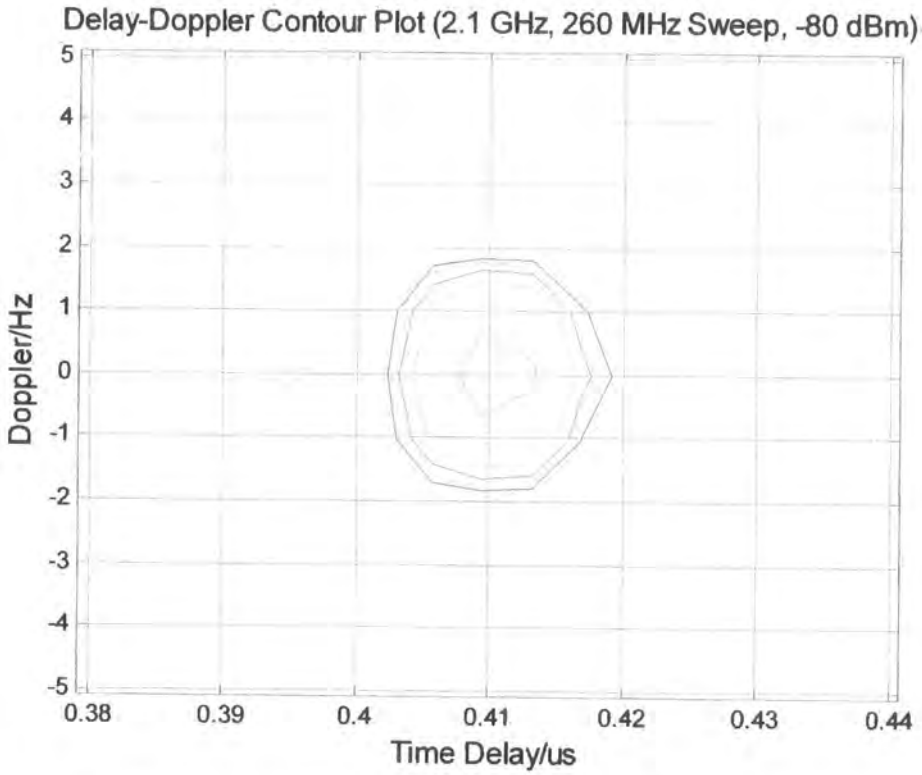

Figure 5.42a Base sounder Doppler ambiguity function, -80 dBm input, 260 MHz

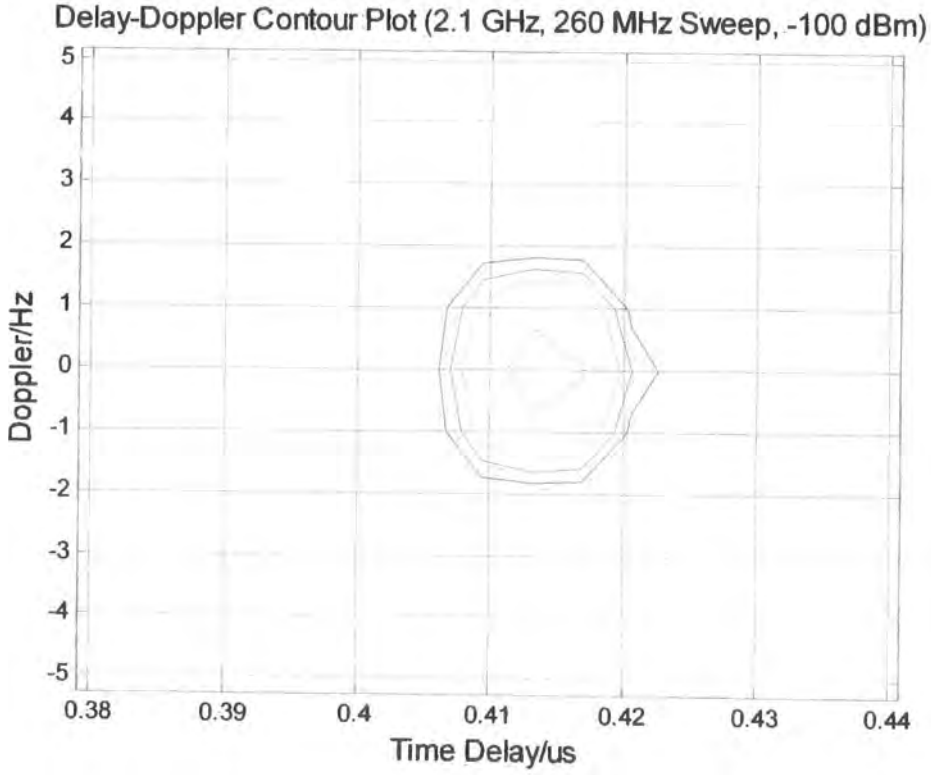

Figure 5.42b Base sounder Doppler ambiguity function, -100 dBm input, 260 MHz

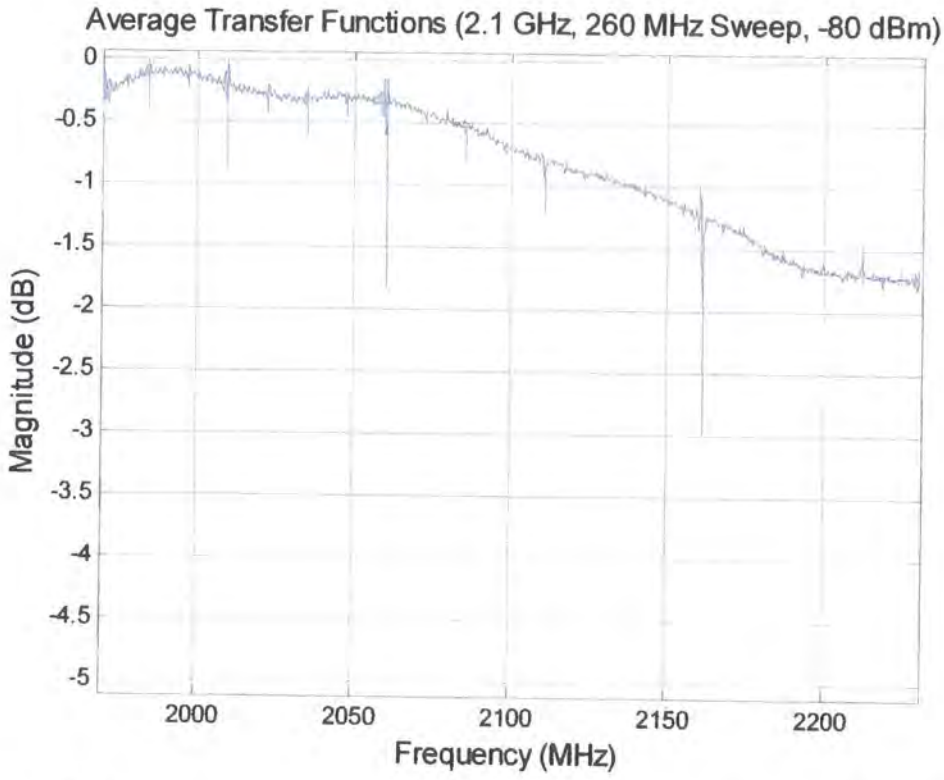

Figure 5.43a Base sounder frequency-transfer function, -80 dBm input, 260 MHz

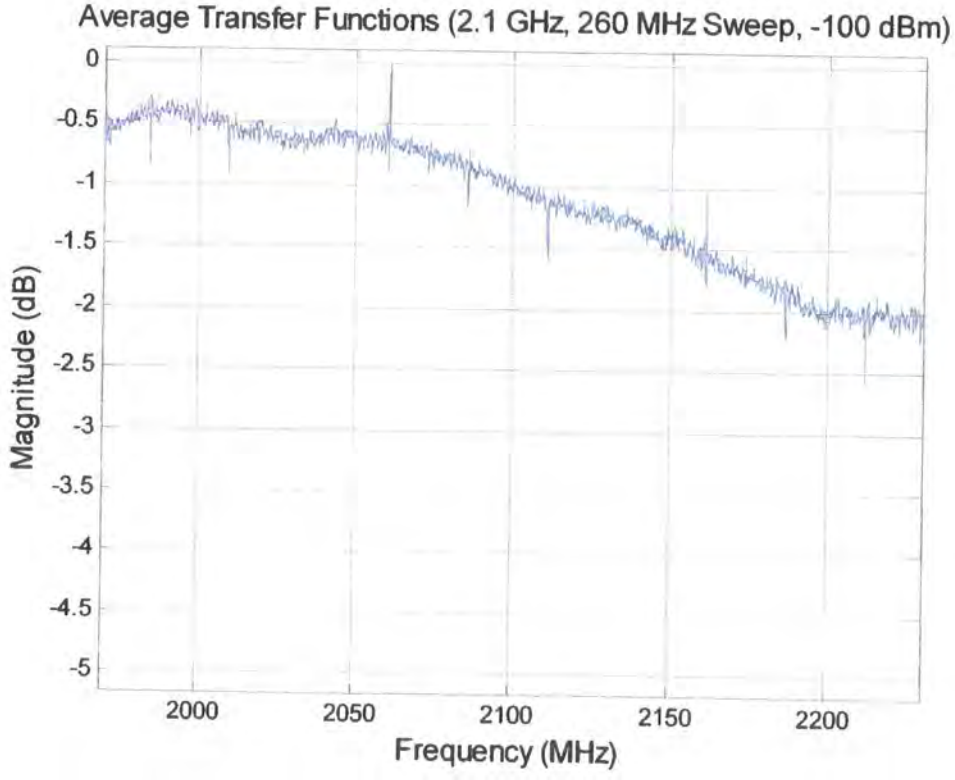

Figure 5.43b Base sounder frequency-transfer function, -100 dBm input, 260 MHz

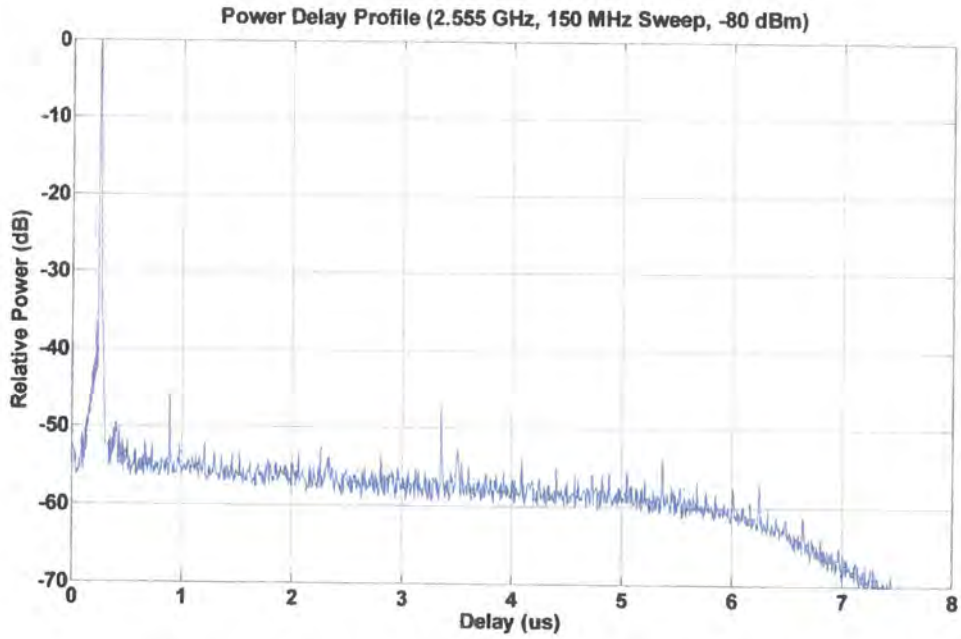

Figure 5.44a 2.5 GHz sounder power delay profile, -80 dBm input, 150 MHz

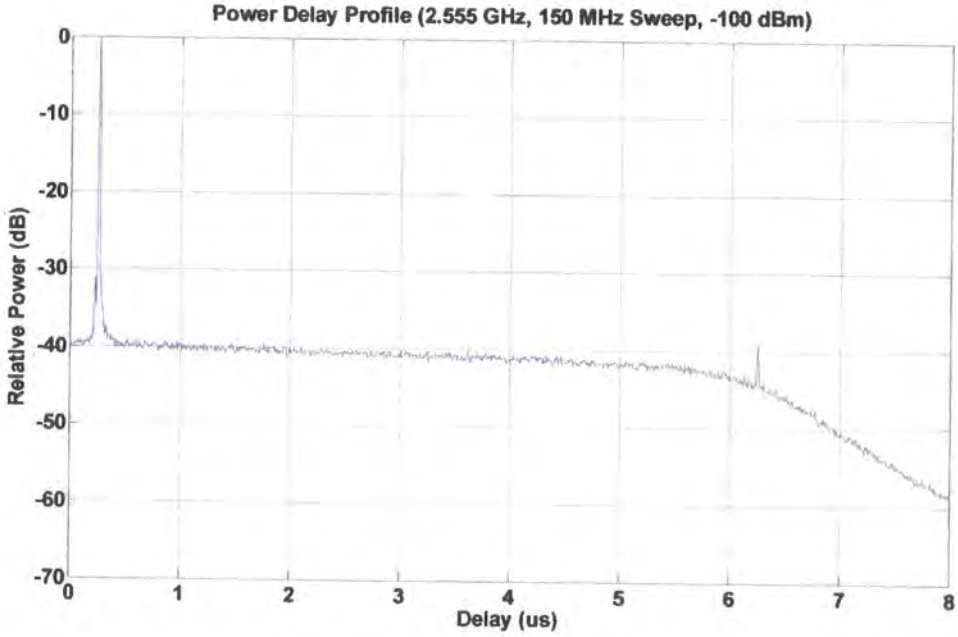

Figure 5.44b 2.5 GHz sounder power delay profile, -100 dBm input, 150 MHz

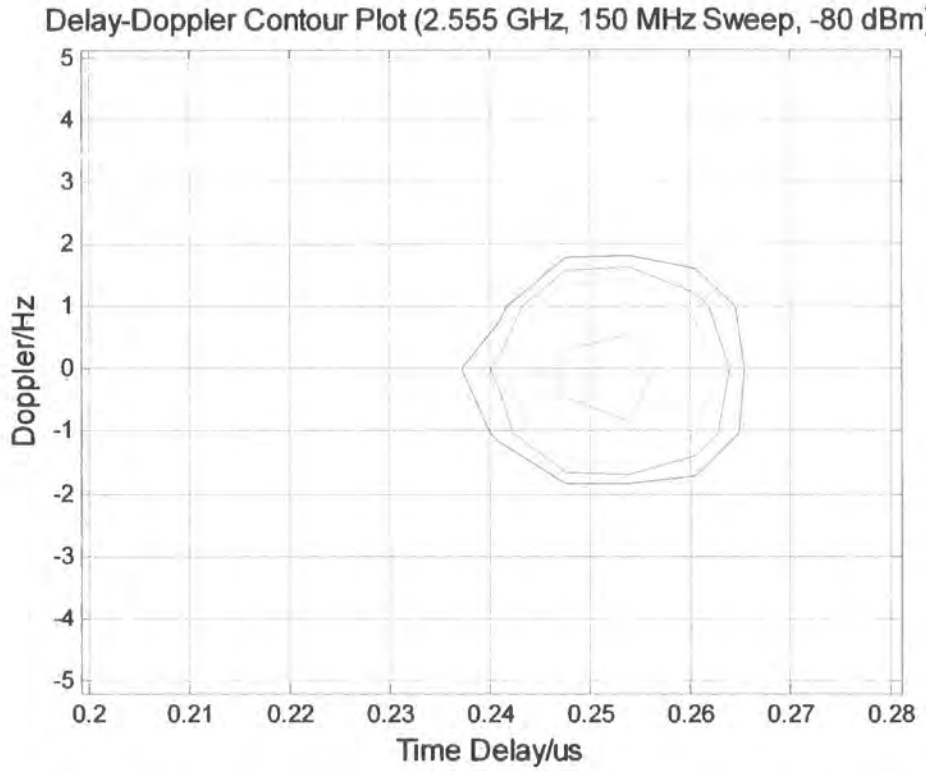

Figure 5.45a 2.5 GHz sounder Doppler ambiguity function, -80 dBm input, 150 MHz

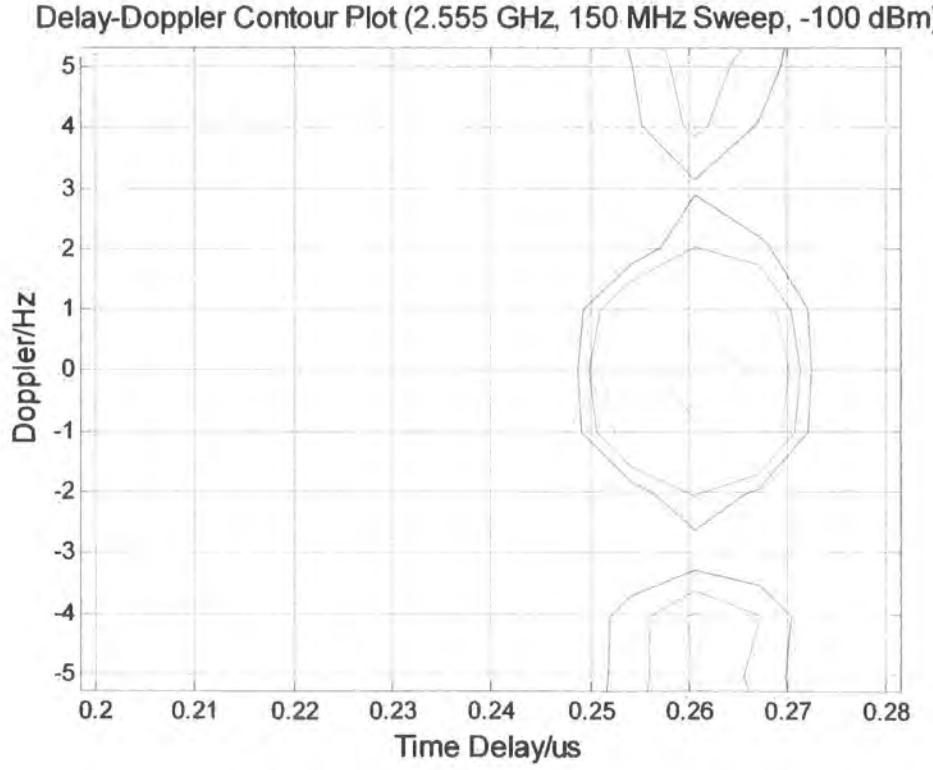

Figure 5.45b 2.5 GHz sounder Doppler ambiguity function, -100 dBm input, 150 MHz

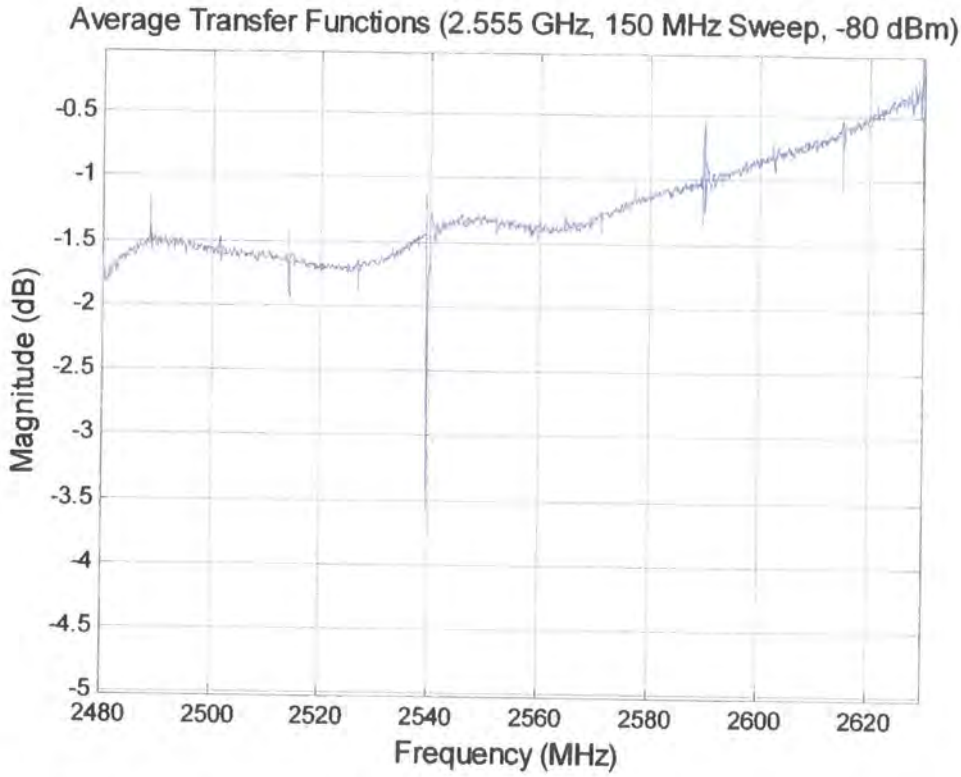

Figure 5.46a 2.5 GHz sounder frequency-transfer function, -80 dBm input, 150 MHz

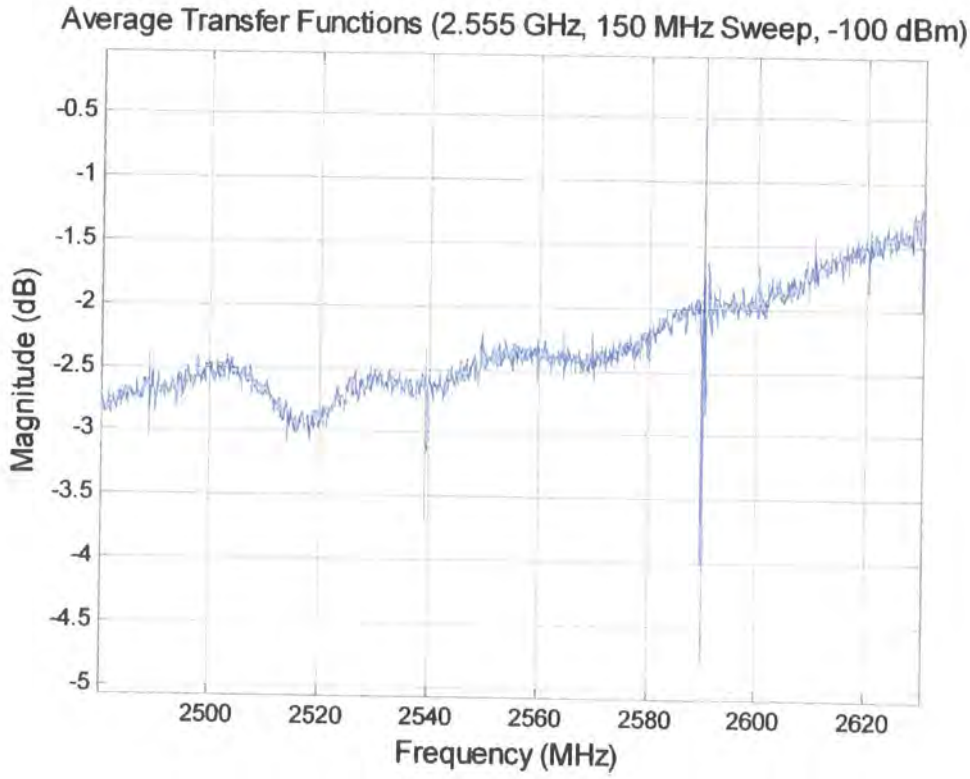

Figure 5.46b 2.5 GHz sounder frequency-transfer function, -100 dBm input, 150 MHz

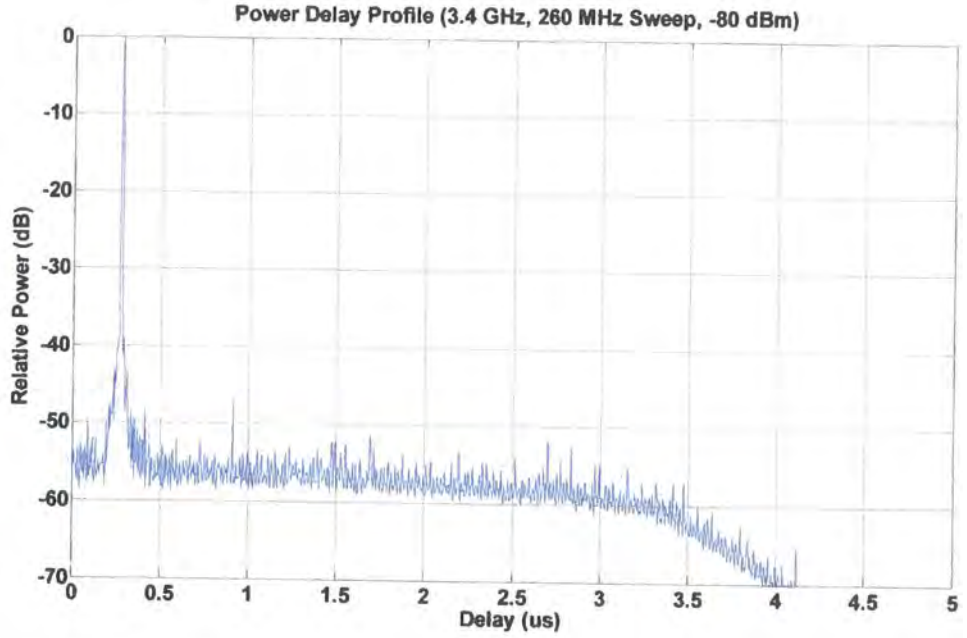

Figure 5.47a 3.5 GHz sounder power delay profile, -80 dBm input, 260 MHz

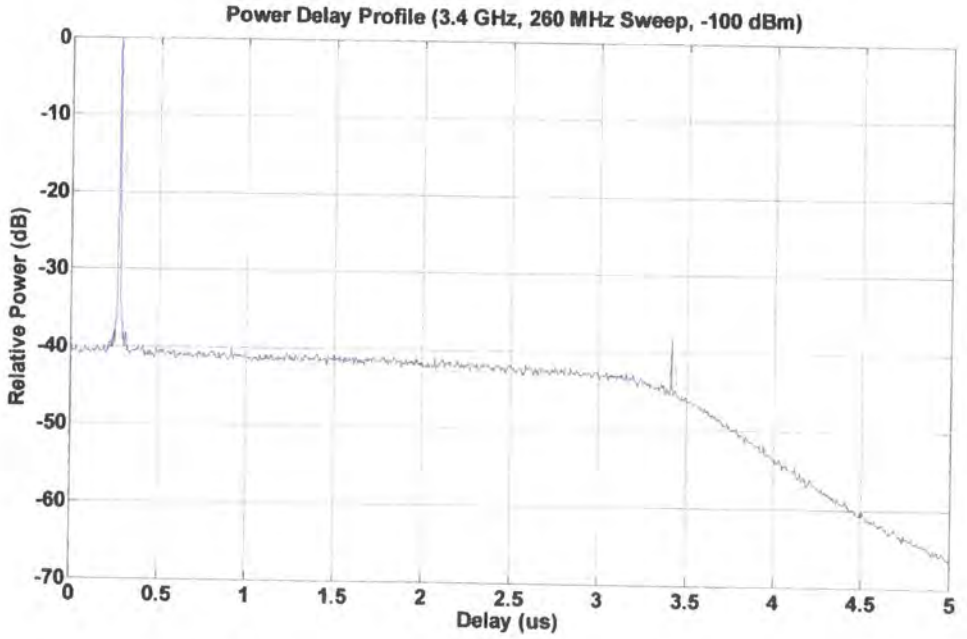

Figure 5.47b 3.5 GHz sounder power delay profile, -100 dBm input, 260 MHz

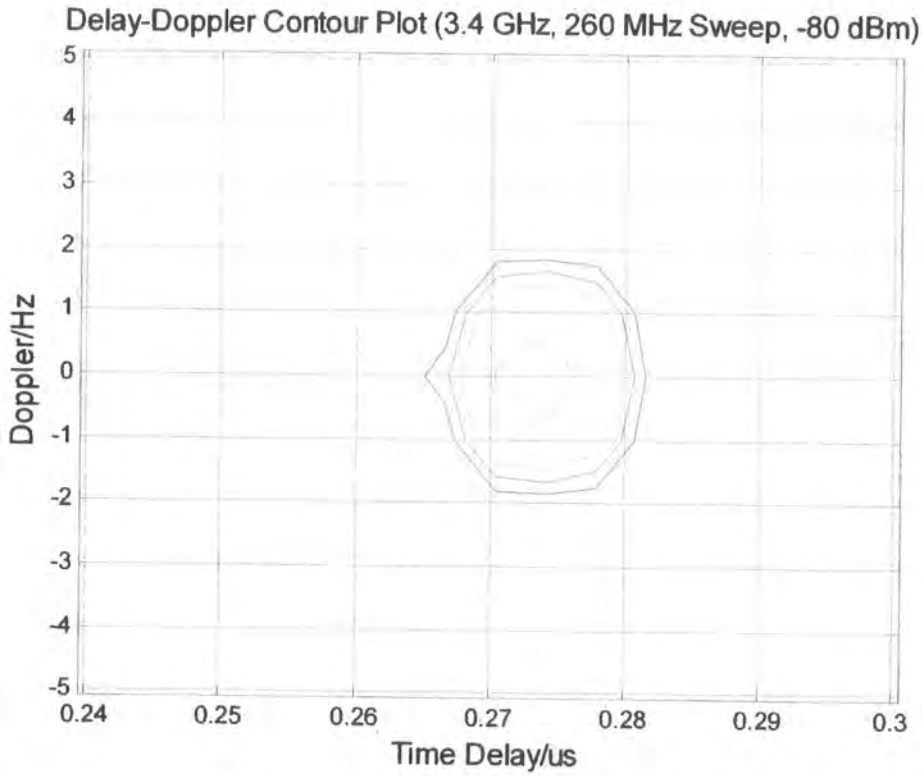

Figure 5.48a 3.5 GHz sounder Doppler ambiguity function, -80 dBm input, 260 MHz

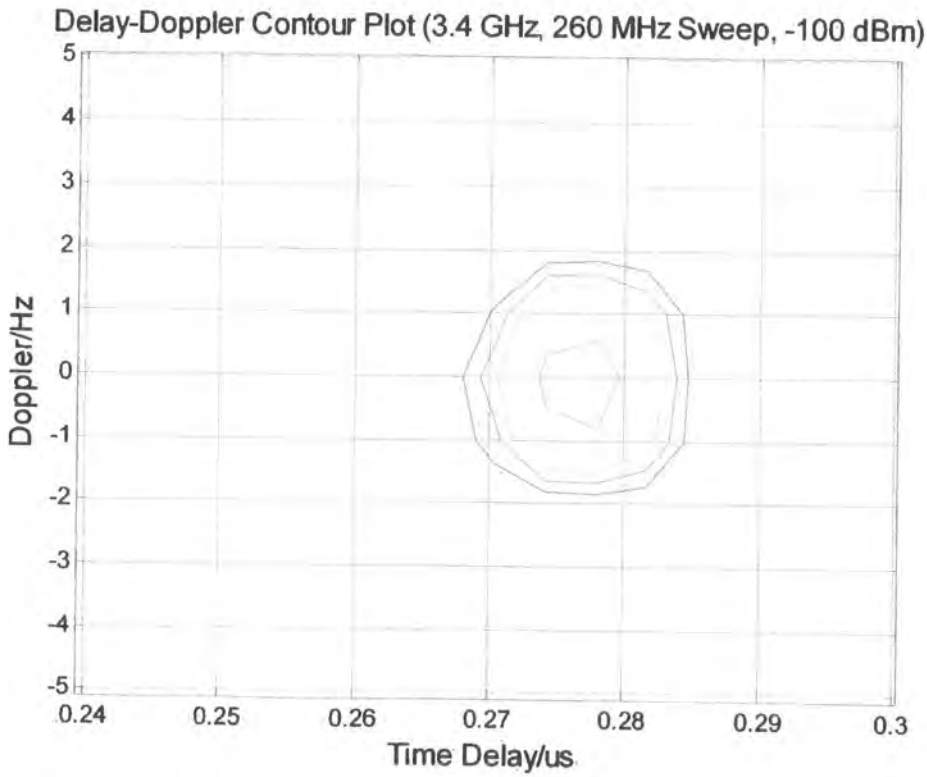

Figure 5.48b 3.5 GHz sounder Doppler ambiguity function, -100 dBm input, 260 MHz

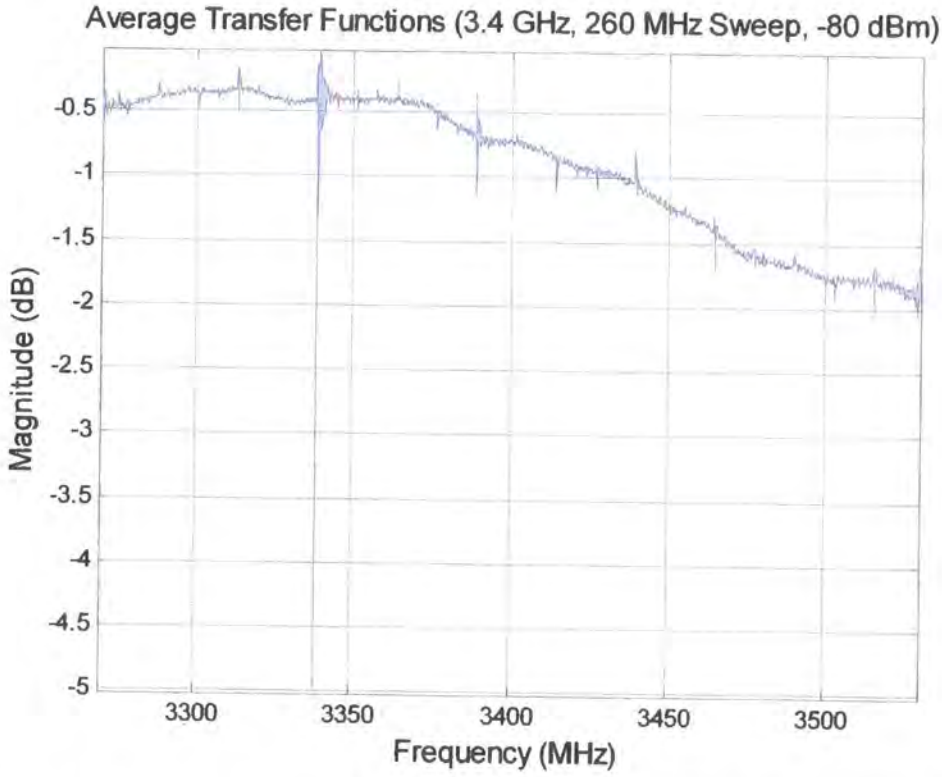

Figure 5.49a 3.5 GHz sounder frequency-transfer function, -80 dBm input, 260 MHz

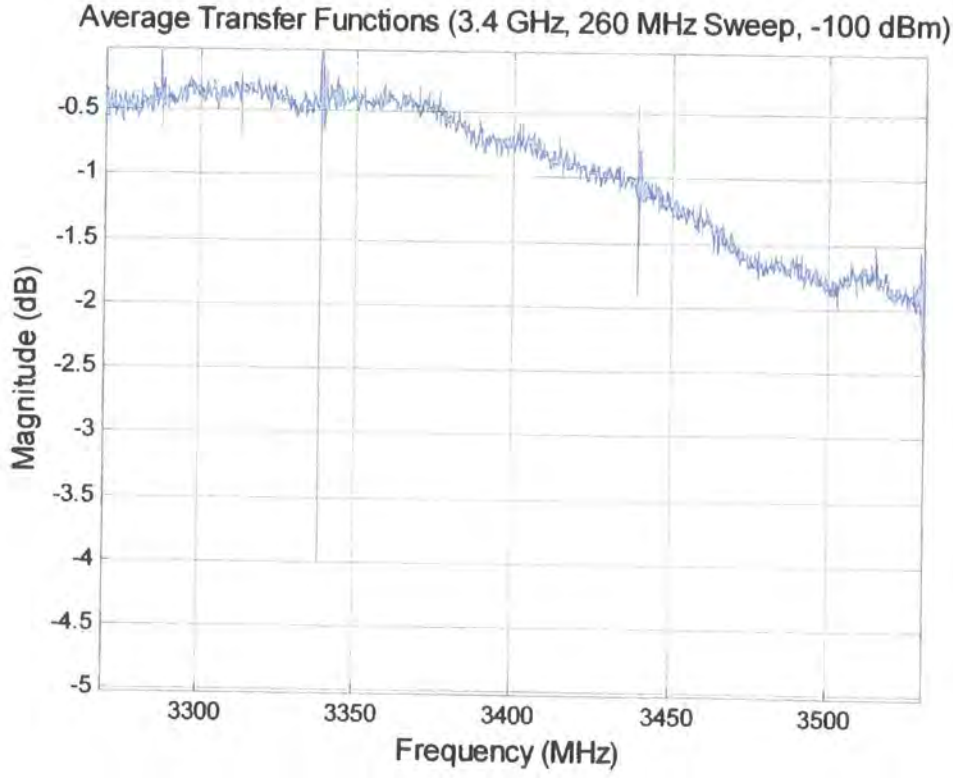

Figure 5.49b 3.5 GHz sounder frequency-transfer function, -100 dBm input, 260 MHz

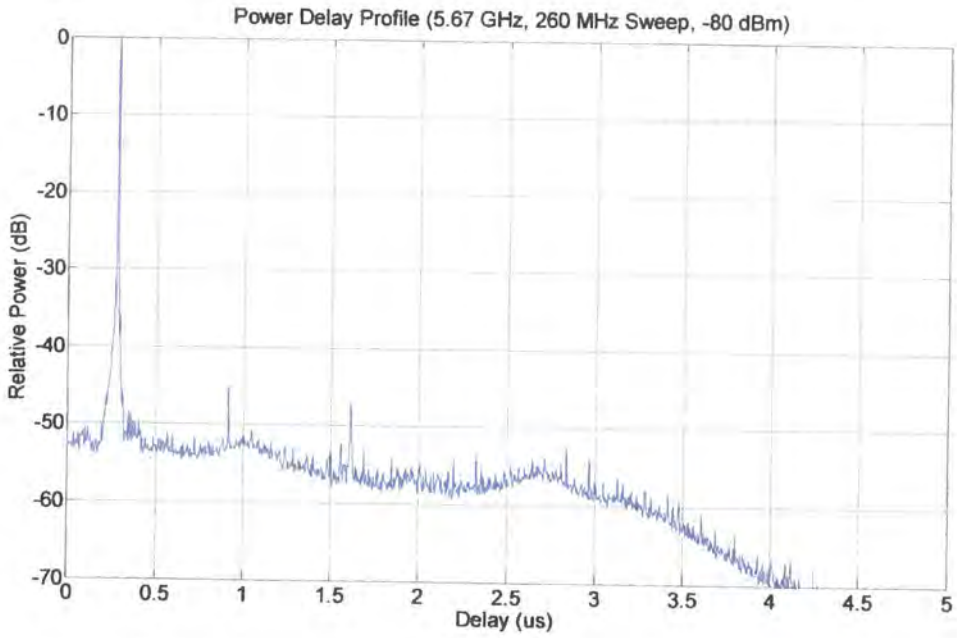

Figure 5.50a 5.7 GHz sounder power delay profile, -80 dBm input, 260 MHz

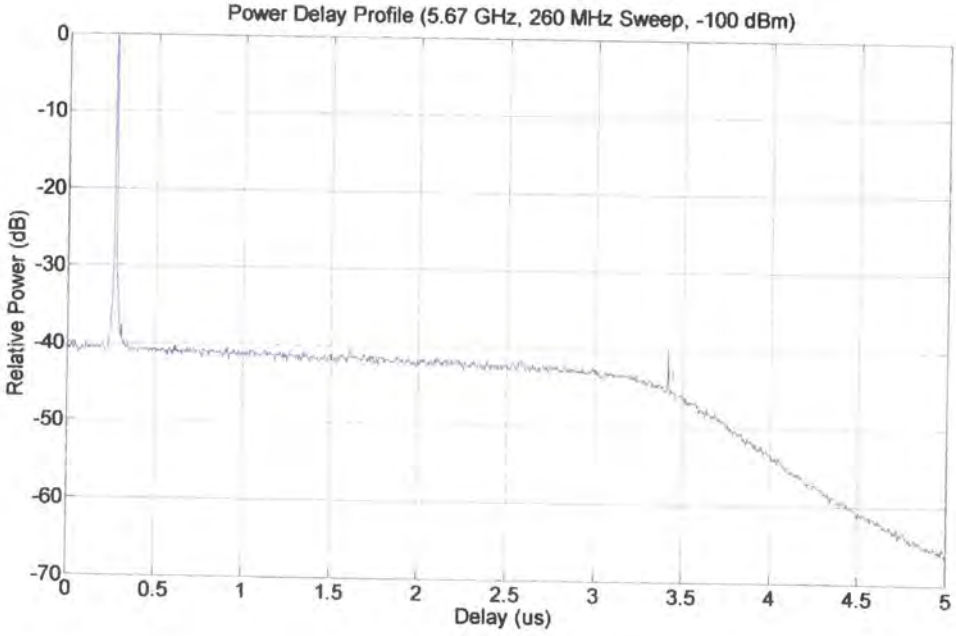

Figure 5.50b 5.7 GHz sounder power delay profile, -100 dBm input, 260 MHz

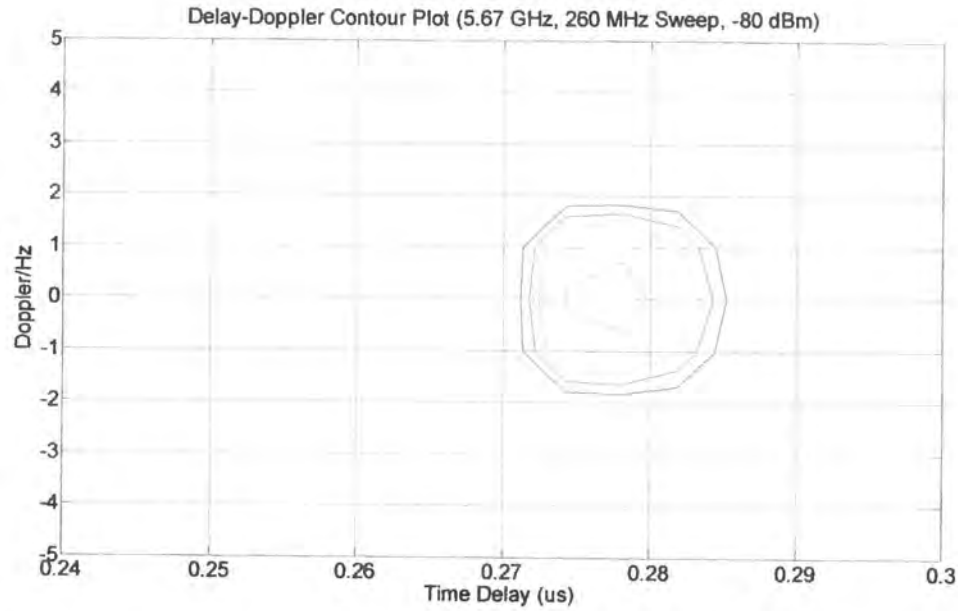

Figure 5.51a 5.7 GHz sounder Doppler ambiguity function, -80 dBm input, 260 MHz

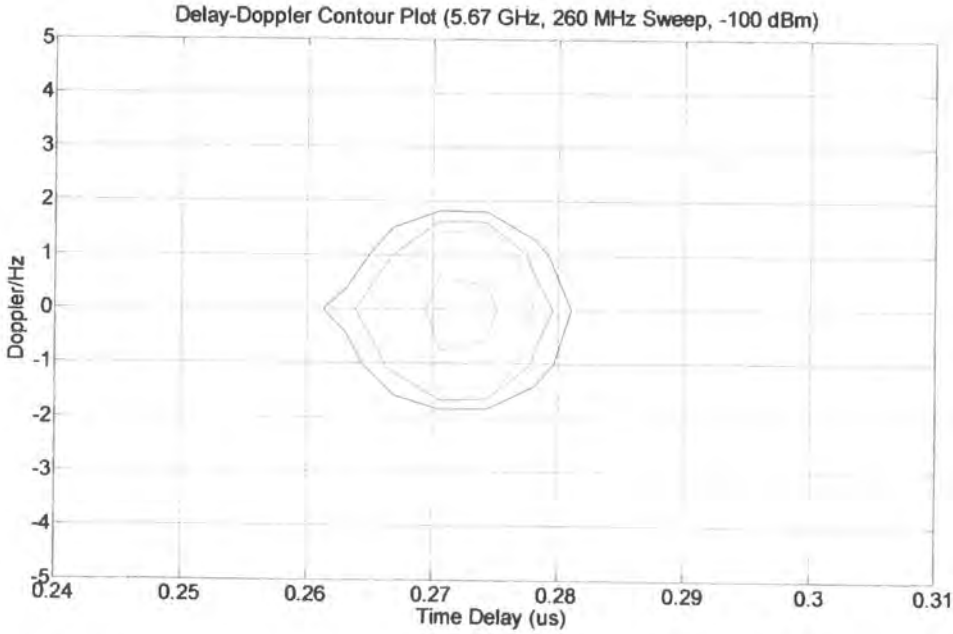

Figure 5.51b 5.7 GHz sounder Doppler ambiguity function, -100 dBm input, 260 MHz

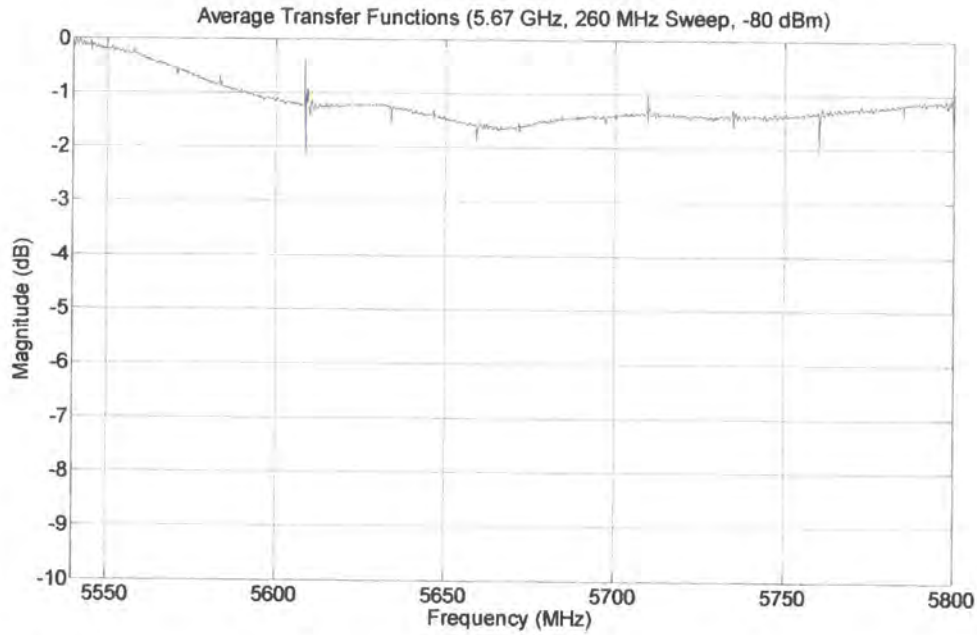

Figure 5.52a 5.7 GHz sounder frequency-transfer function, -80 dBm input, 260 MHz

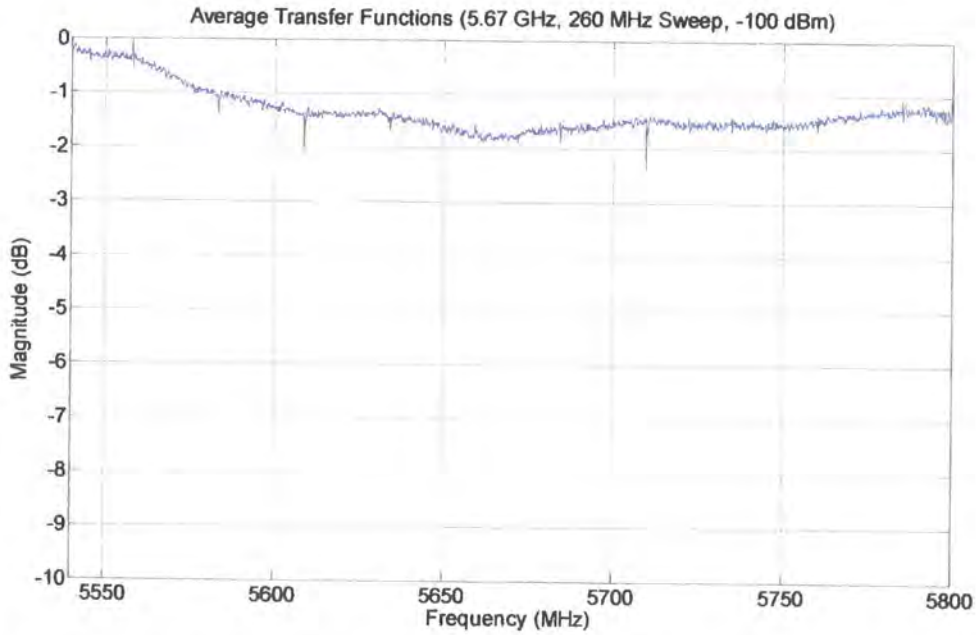

Figure 5.52b 5.7 GHz sounder frequency-transfer function, -100 dBm input, 260 MHz

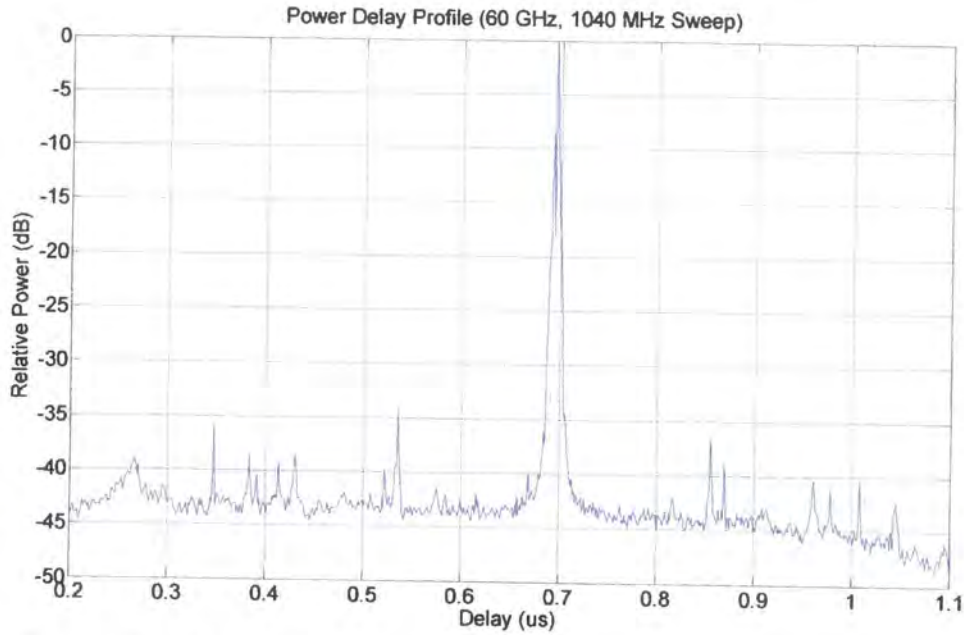

Figure 5.53 60 GHz sounder, 1040 MHz sweep width

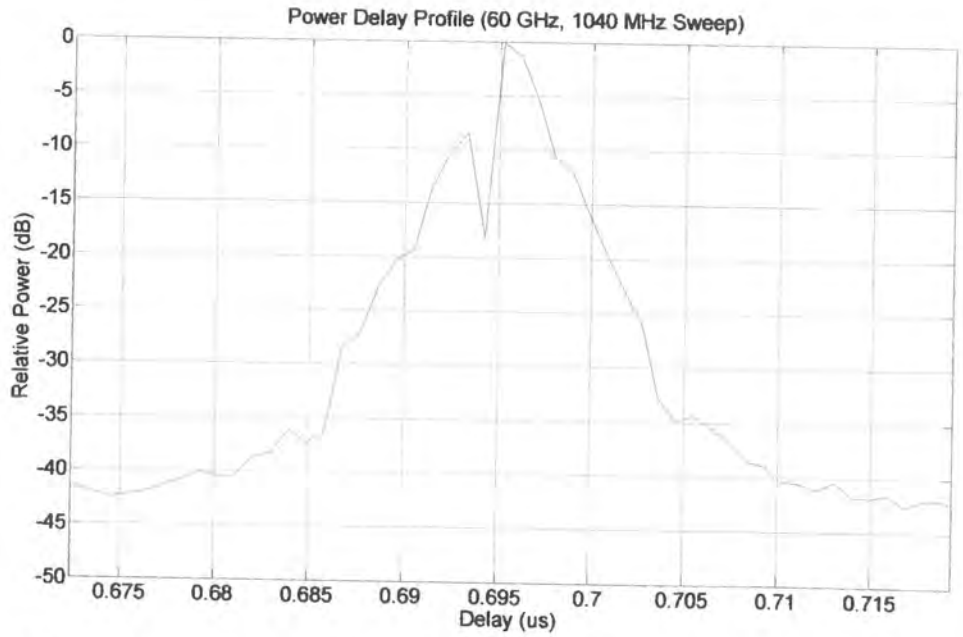

Figure 5.54 60 GHz sounder, 1040 MHz sweep width

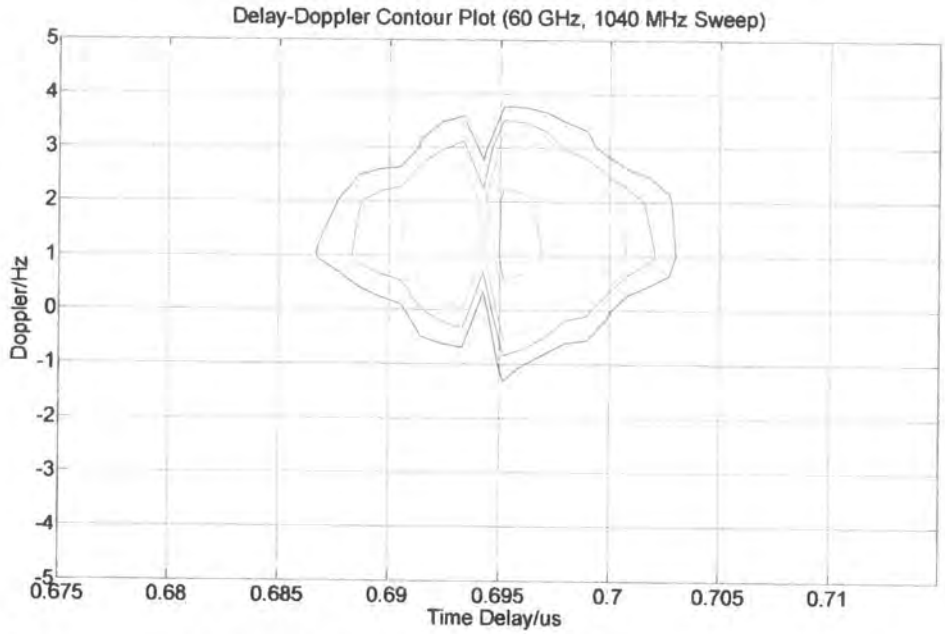

Figure 5.55 60 GHz sounder, 1040 MHz sweep width

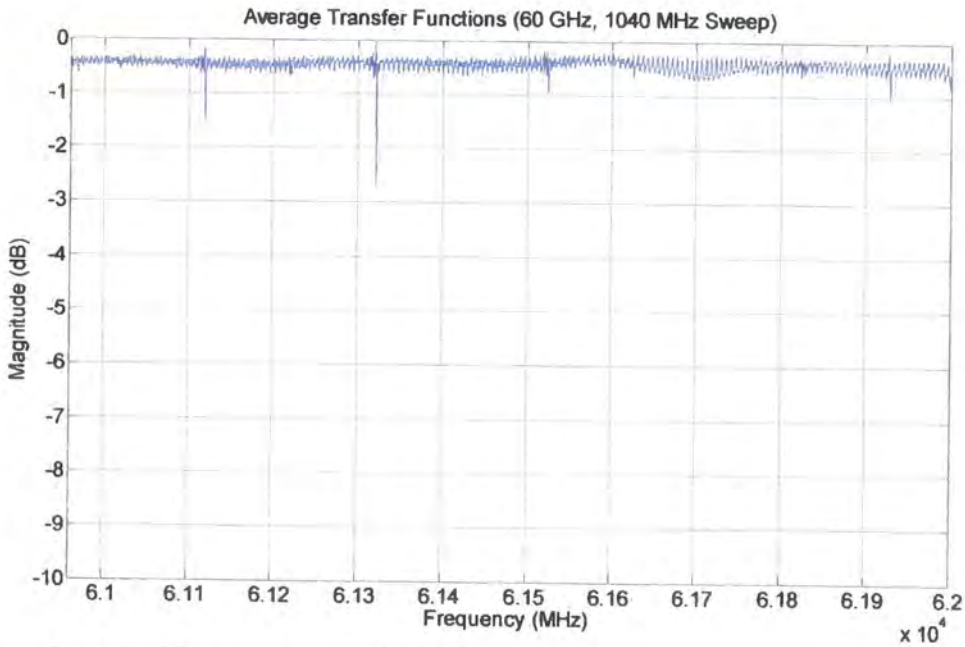

Figure 5.56 60 GHz sounder, 1040 MHz sweep width

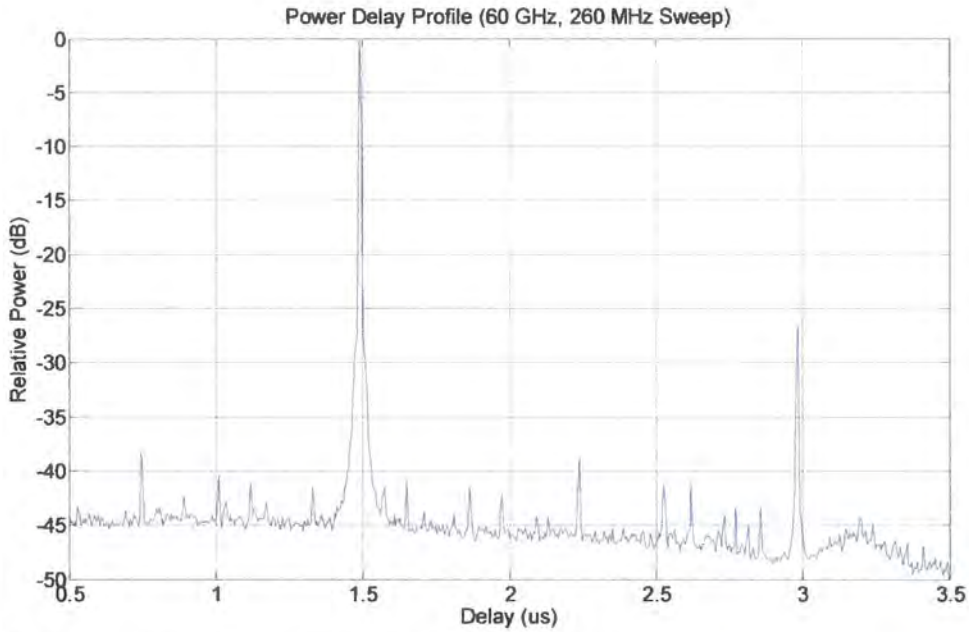

Figure 5.57 60 GHz sounder, 260 MHz sweep width

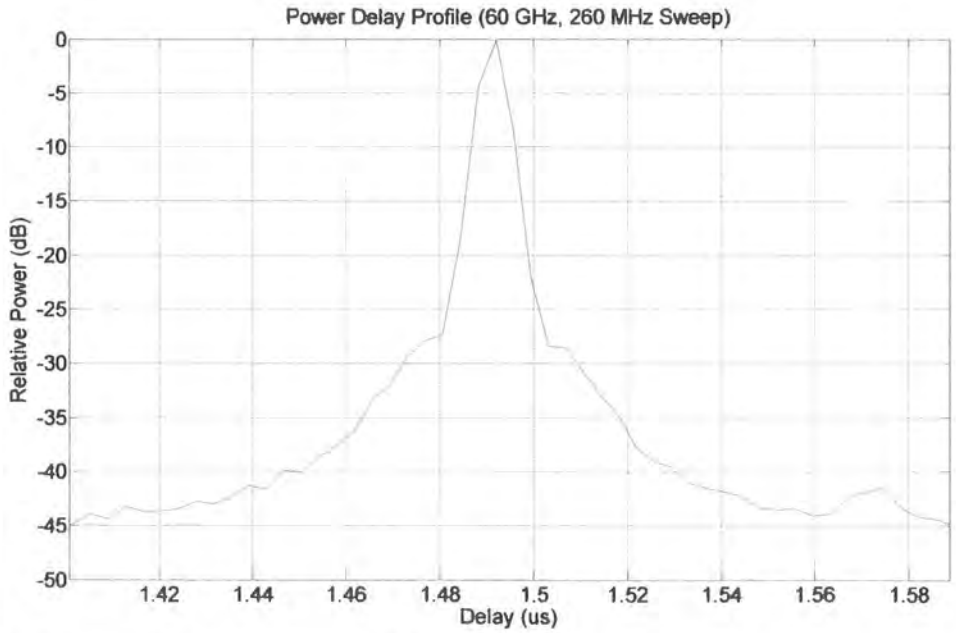

Figure 5.58 60 GHz sounder, 260 MHz sweep width

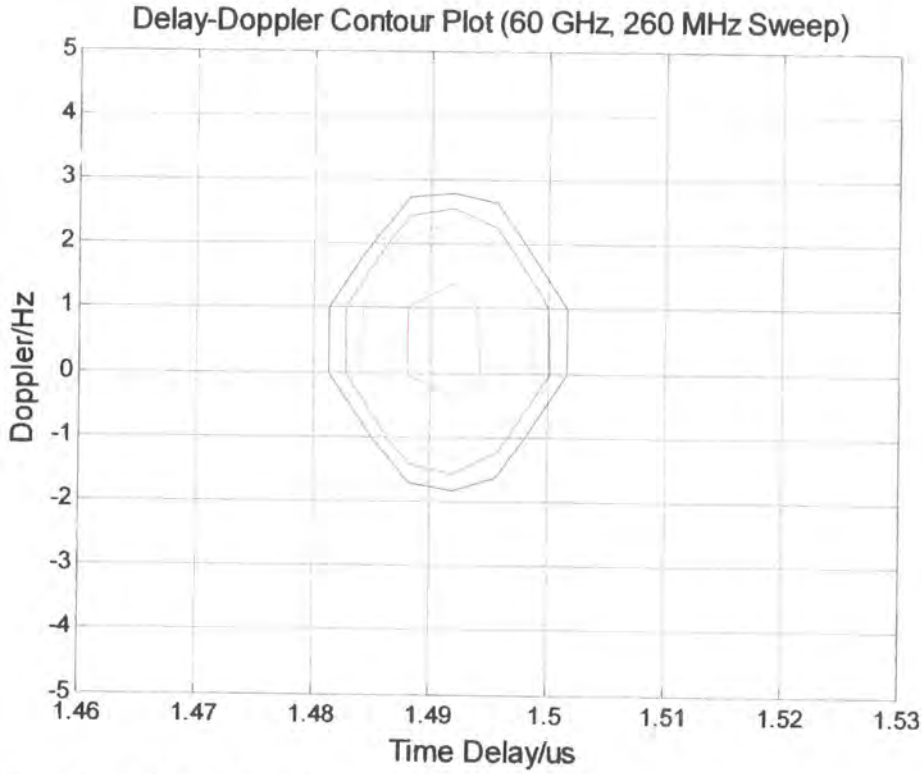

Figure 5.59 60 GHz sounder, 260 MHz sweep width

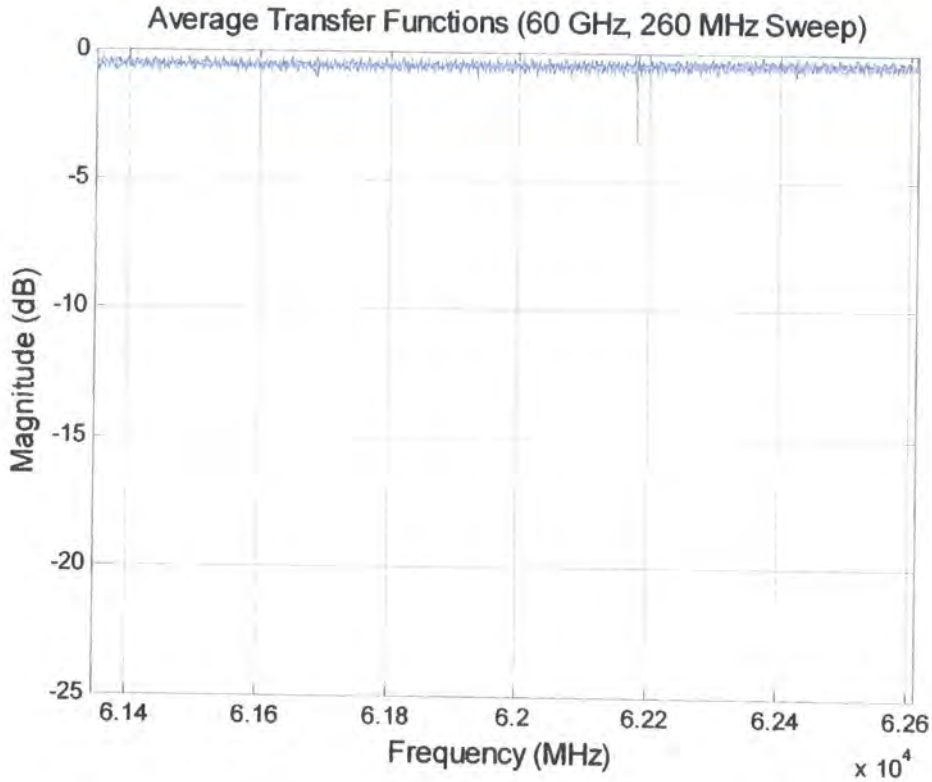

Figure 5.60 60 GHz sounder, 260 MHz sweep width

Comments to the single delay data (except 60 GHz)

The data presented in figures 5.29 to 5.52 provide the power delay profile, delay-Doppler and transfer functions for the 2 GHz IF, 2.5 GHz, 3.4 GHz and 5.7 GHz sounders for sweep widths in the range 10 MHz to 260 MHz. All functions have been demonstrated to be stable with signal level. The instantaneous spurious free dynamic range is 40 dB or greater for all configurations. The spurious level for all configurations degrades for input level above -80 dBm. This data demonstrate that this is a function of the base sounder. The Doppler-delay functions are maintained within +/- 2 Hz and +/- 2 delay bins (at the -30 dBc contour) for all configurations. Figures 5.36b and 5.45b show anomalous behaviour in the delay-Doppler function. This has at times been observed for all configurations and is believed to be an artefact of the base UMTS sounder. A minor shift in the delay shown in the delay-Doppler function can be observed for the wide sweeps. This is consistent with small frequency differences between the transmitter and receiver rubidium references. These differences are within the specification of the sources and are typically ~ $5*10^{-12}$. The transfer functions demonstrate a worst case ripple of <~ 1.5 dB. This is equal to or less than the ripple recorded for the base IF sounder. Note some of the frequency-transfer function plots (for example 5.49) include narrow spikes. These are due to un-modulated leakage signals which are "swept" through by the sounder receiver.

Comments on the 60 GHz single delay data

The data recorded for the 60 GHz system was taken including the upgraded DDFS to IF up-conversion synthesisers.

The data recorded here was obtained with the system configured in a homo-dyne configuration with the SSB down-converter bypassed. This was to avoid spurious components at ~ -20 dBc which are produced by the DDFS when operated with a delay offset to provide the appropriate 12.5 MHz offset for the 60 GHz system.

The 1040 MHz data demonstrates a discontinuity in the power-delay profile. This is also represented in the delay axis for the delay-Doppler function. It is possible that this is due to the 5 GHz IF signal being distorted by the lower edge of the RF filter in the up-converter. The -30 dBc contour represents 17 range bins. The Doppler is slightly degraded to ~ +/- 2.5 Hz at -30 dBc. The Doppler is shifted to ~ 0.5 to 1 Hz. This is consistent with a net difference frequency of ~ 0.5 to $1*10^{-12}$. The signal at ~ 800 range bins is the second harmonic of the wanted signal. This is consistent with an input of -13 dBm to the 60 GHz mixer as only a single 20 dB wave guide attenuator was available to attenuate the + 7dBm transmit source. A dynamic range of ~ 40 dB has been demonstrated to the spurious signals for this configuration. Since we are not usually concerned with components below -30 dBc this provides acceptable performance.

Calibration data was also recorded for a base sounder sweep of 65 MHz to produce a sweep of 260 MHz at 60 GHz. This was done to provide a comparison between systems operating over an RF sweep of 260 MHz. This demonstrates performance very similar to that achieved for the lower frequency sounders. The delay component for the delay-Doppler function is contained within 5 bins at the -30 dBc contour.

5.3.4 Two-path delay discrimination

The two path delay discrimination provides a confirmation of the multi-path time delay resolution that is achievable by the channel sounder. The test is performed by splitting the signal from the transmitter to the receiver into two paths of nominally equal attenuation. One path is delayed relative to the other using additional transmission distance [5.3]. The attenuator in the "short" path is adjusted to provide approximately equal signal levels from the direct and the delayed path. Coaxial cable was used to provide the delay for the low frequency systems (refer to figure 5.61). Waveguide was used for the 60 GHz system (refer to figure 5.62). The delay element is selected appropriate to the bandwidth of the system being evaluated.

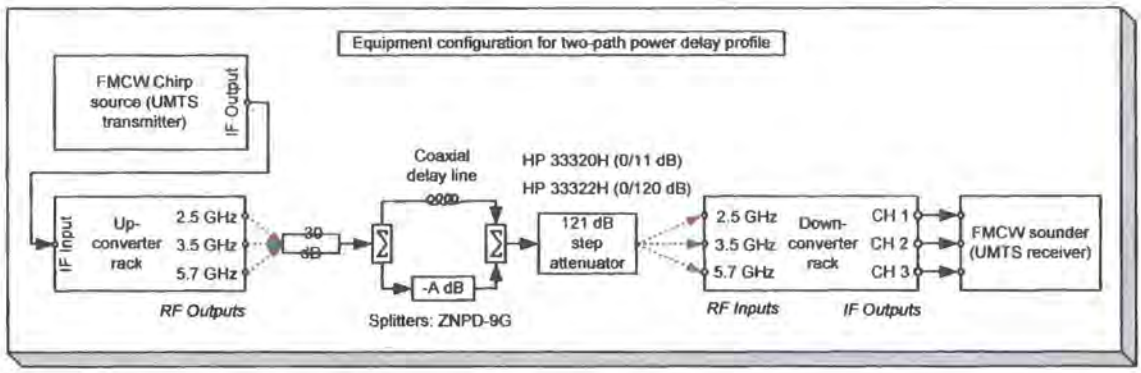

Figure 5.61 Two-path delay configuration (cable)

The coax delay was provided using Times LMR-240-UF cables. From the manufacturer's data for this cable, the velocity factor is 85% with attenuation of 0.27 dB/m (2.5 GHz), 0.32 dB/m (3.5 GHz) and 0.43 dB/m (5.8 GHz).

The delay in LMR-240-UF cable is described by:

$$\tau = l/(\upsilon \times c), \text{ in practice} \sim 3.9 \text{ ns/m}$$

The delay is frequency independent since the transmission medium is non-dispersive. A maximum of 103 m of cable provides a delay of ~ 400 ns. The loss including splitters and other fixed test set losses was 68 dB (before selecting additional attenuation to adjust the level) at 5.7 GHz.

The 103 m long delay cable has been used to characterise the 10 MHz sweep width channel sounder and 4 m for the 260 MHz sweep width sounder. An 8 m long cable was used to characterise the 2.5 GHz converter with 150 MHz sweep width.

Additional 9 dB attenuators were fitted to each end of the delay cable for the short 4 m and 8 m long cables to attenuate additional reflections that were observed to be introduced by the test configuration.

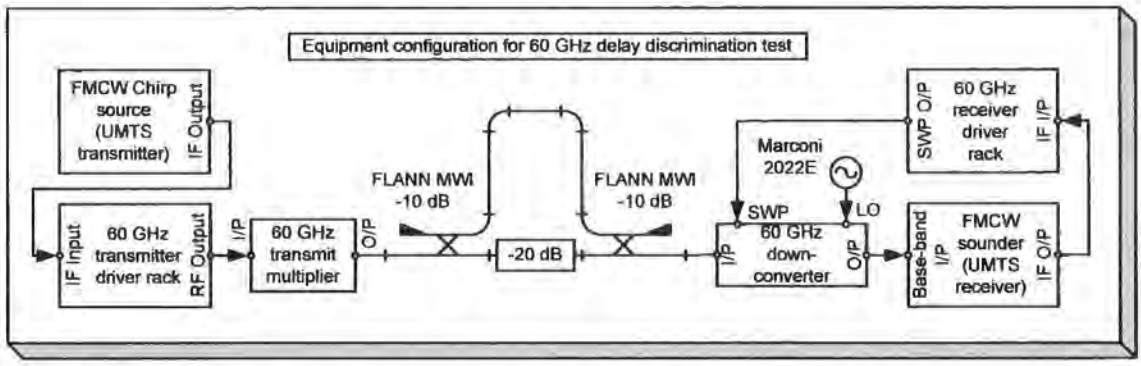

Figure 5.62 Two-path delay configuration (wave guide)

The delay in WG25 waveguide is described by:

$$\tau = l/c * \sqrt{1-(w/f)\wedge 2} \text{ in practice} \sim 4.4 \text{ ns/m}$$

The velocity of energy propagation through the waveguide however is frequency dependent. Thus the delay is also frequency dependent. Using the delay waveguide length of 2.07 m the dispersion is 0.1 ns with a sweep from 61 GHz to 62 GHz. This is in any case considerably within the minimum delay bin width of ~ 1.25 ns which is available from the maximum sweep width of 1040 MHz. Thus the waveguide based test configuration can be used to validate the delay discrimination of the 60 GHz wide band system without introducing significant delay dispersion.

A delay waveguide of 2.3 m has been used to evaluate the 60 GHz channel sounder.

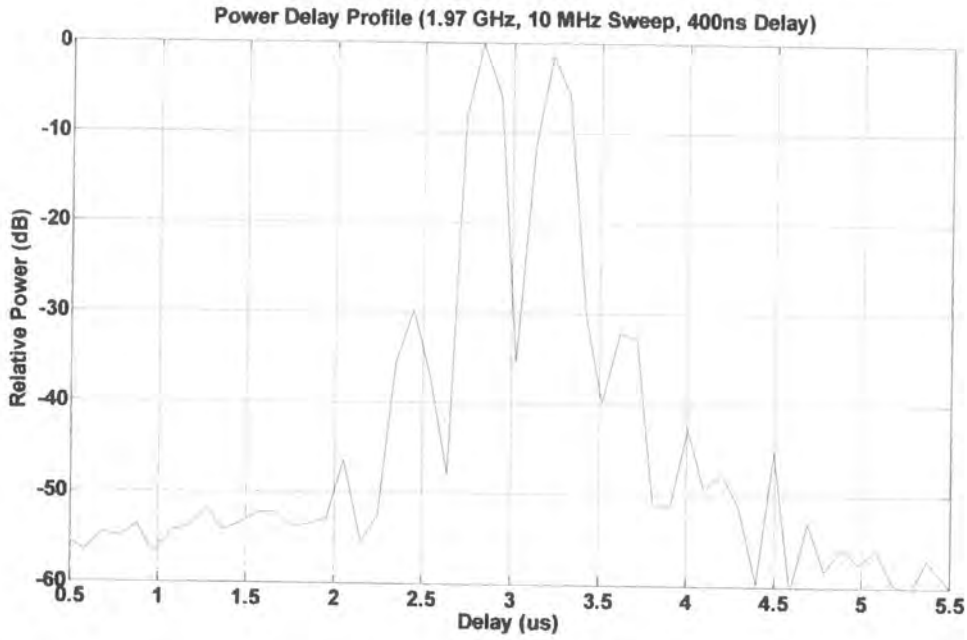

Figure 5.63a Two delay profile for base sounder, -90 dBm, 10 MHz

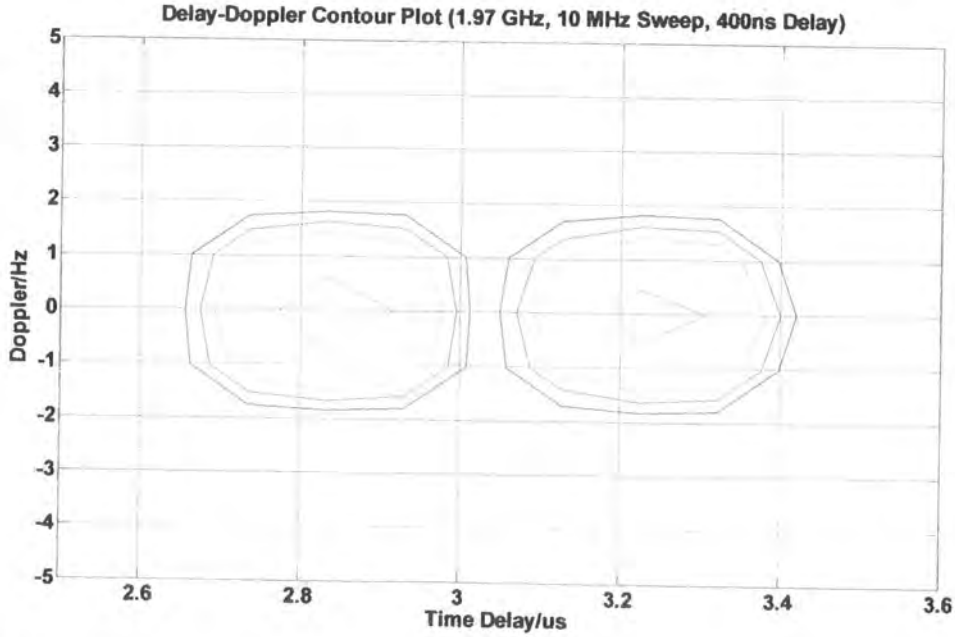

Figure 5.63b Two delay Doppler ambiguity for base sounder, -90 dBm, 10 MHz

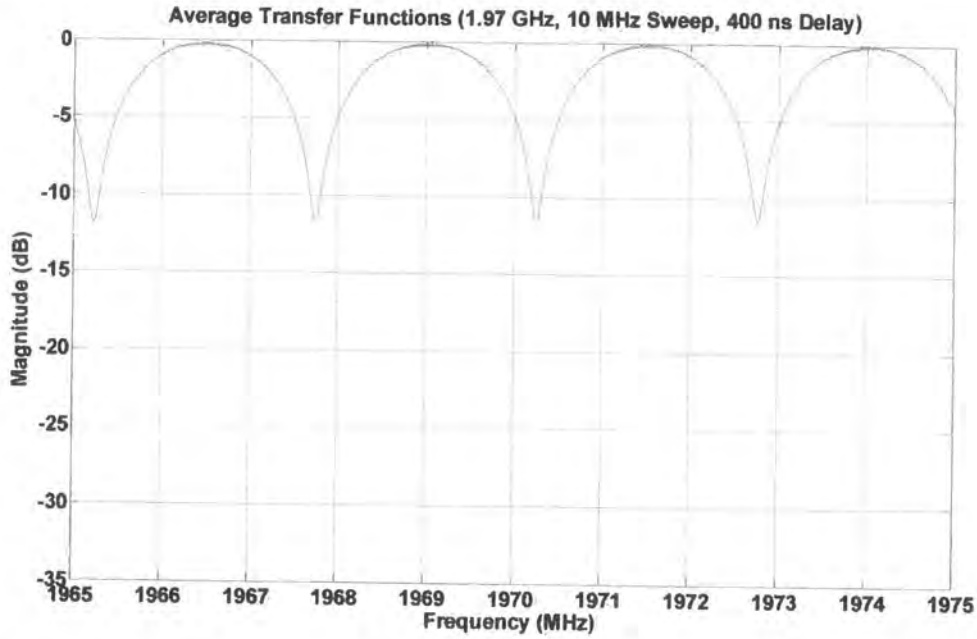

Figure 5.63c Two delay transfer function for base sounder, -90 dBm, 10 MHz

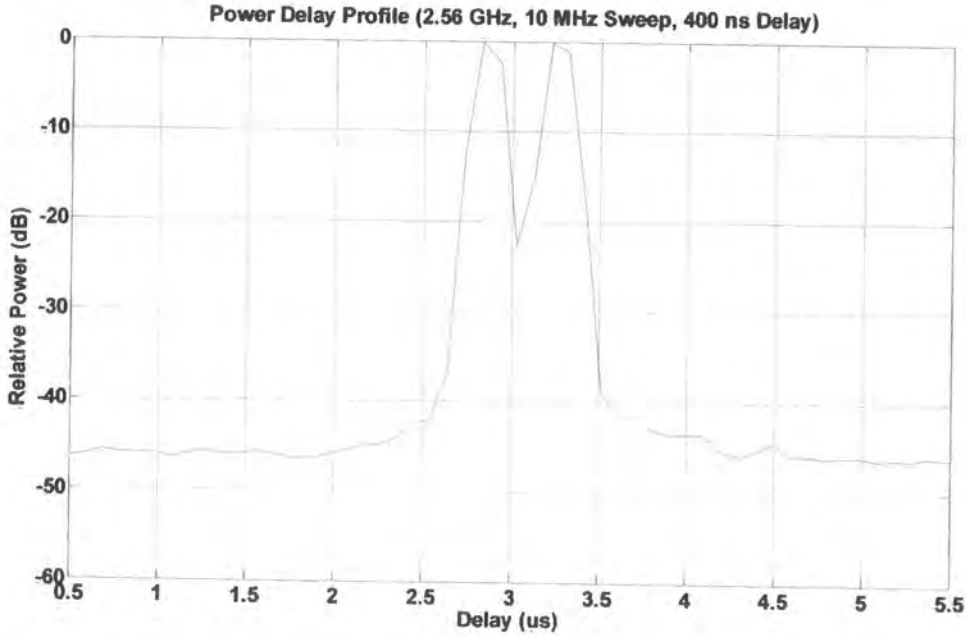

Figure 5.64a Two delay profile for 2.5 GHz sounder, -90 dBm, 10 MHz

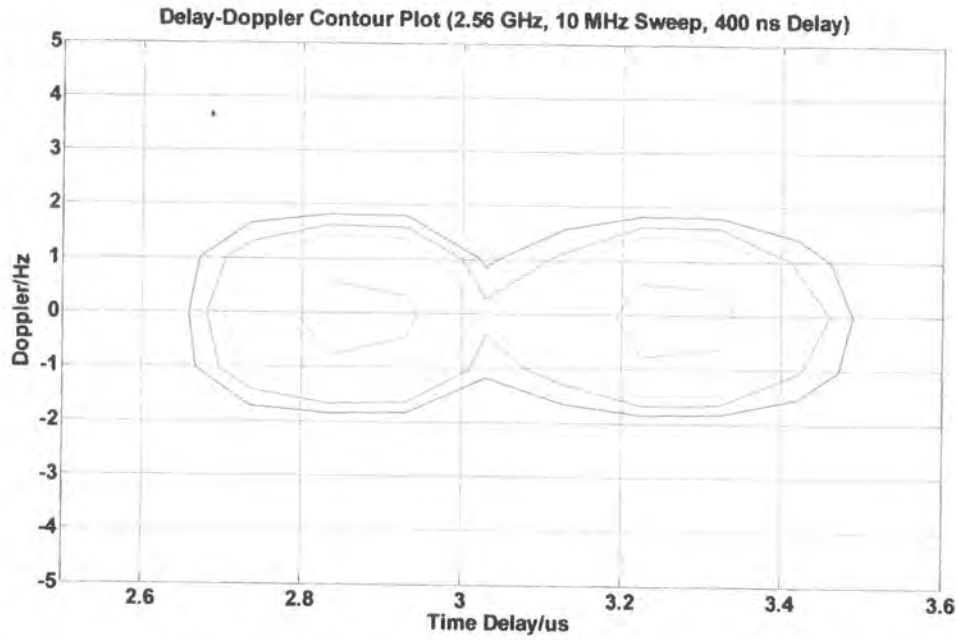

Figure 5.64b Two delay Doppler ambiguity for 2.5 GHz sounder, -90 dBm, 10 MHz

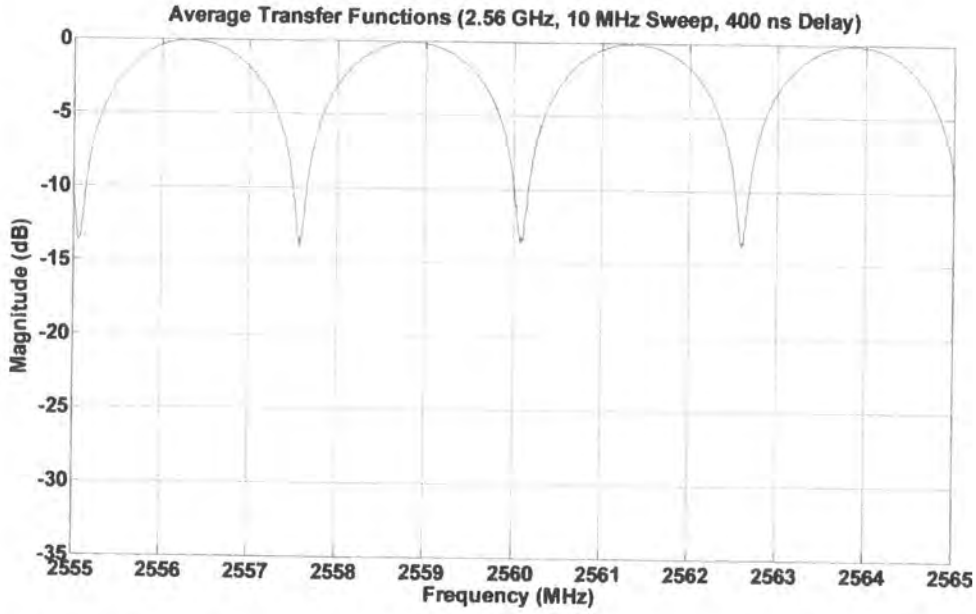

Figure 5.64c Two delay transfer function for 2.5 GHz sounder, -90 dBm, 10 MHz

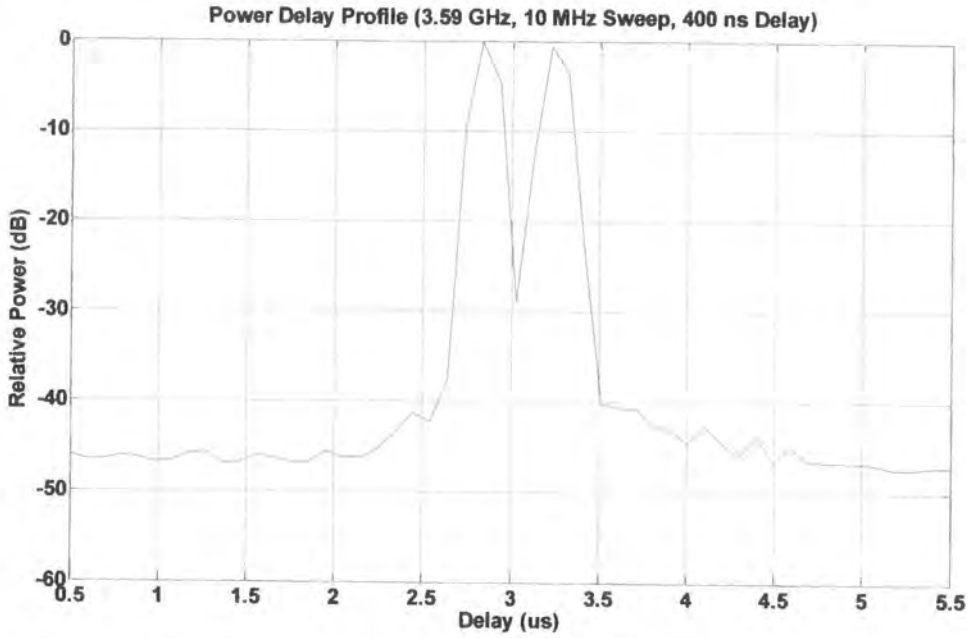

Figure 5.65a Two delay profile for 3.5 GHz sounder, -90 dBm, 10 MHz

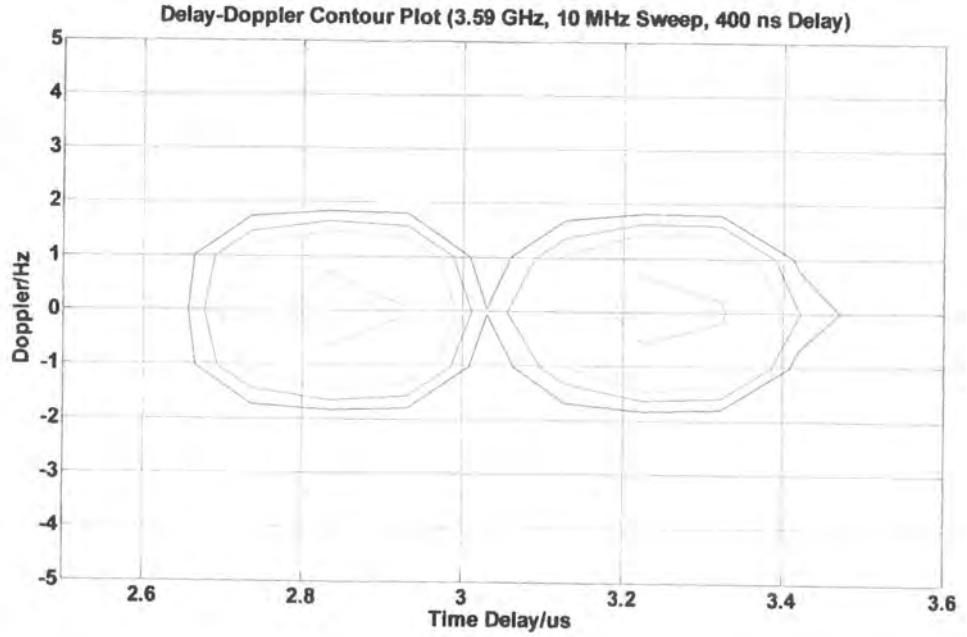

Figure 5.65b Two delay Doppler ambiguity for 3.5 GHz sounder, -90 dBm, 10 MHz

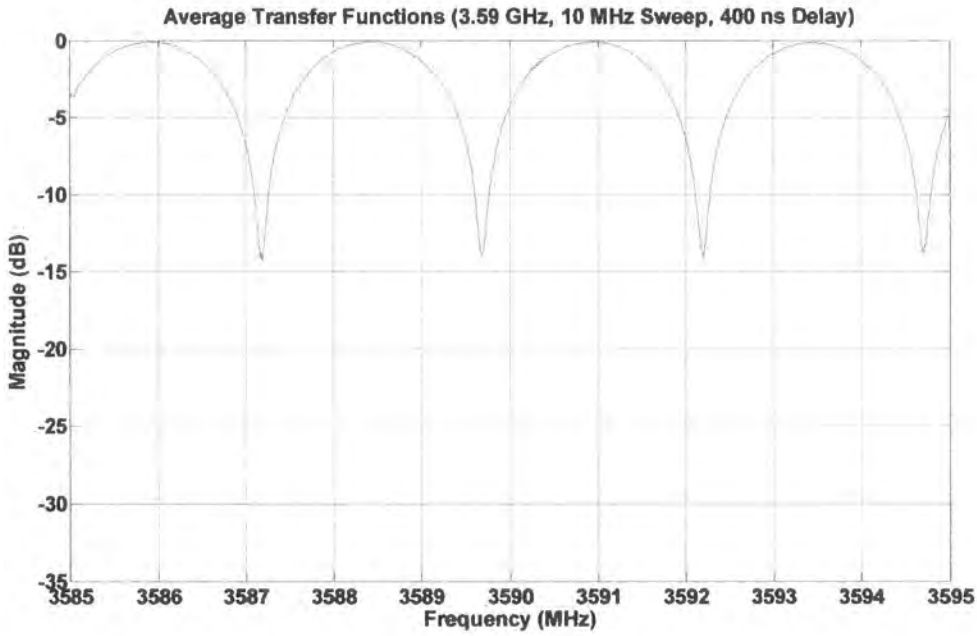

Figure 5.65c Two delay transfer function for 3.5 GHz sounder, -90 dBm, 10 MHz

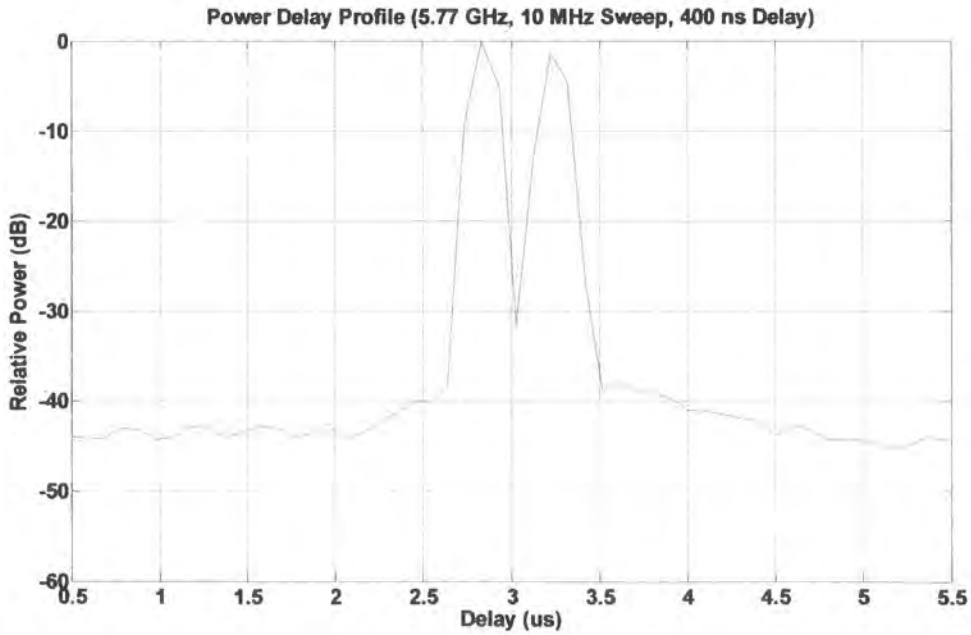

Figure 5.66a Two delay profile for 5.7 GHz sounder, -90 dBm, 10 MHz

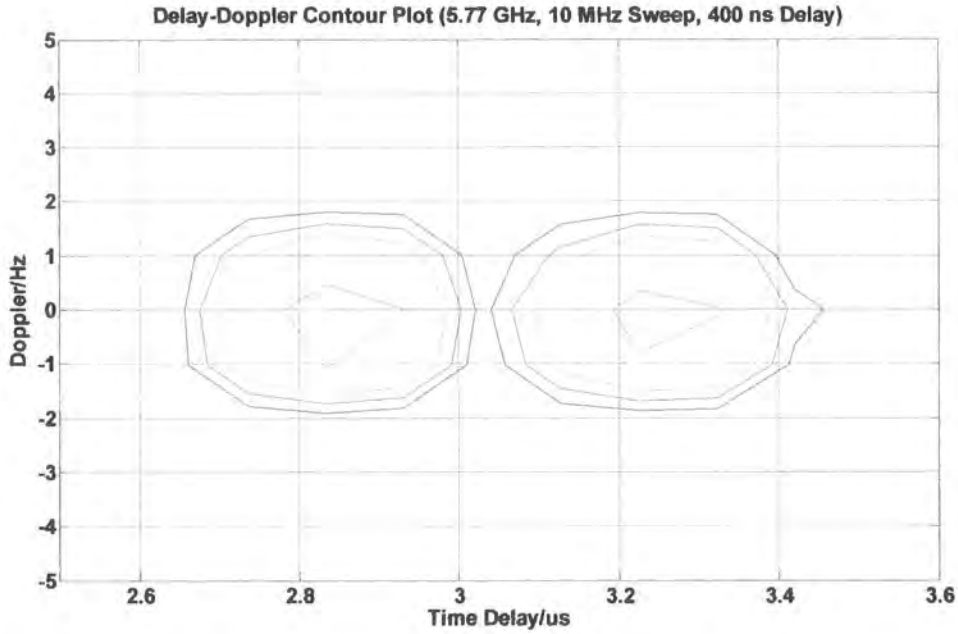

Figure 5.66b Two delay Doppler ambiguity for 5.7 GHz sounder, -90 dBm, 10 MHz

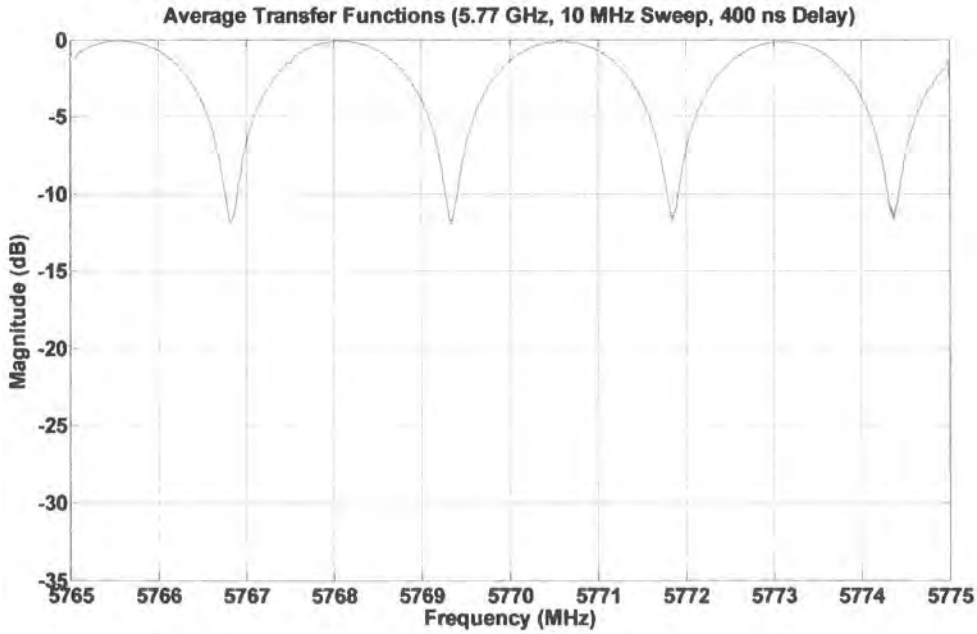

Figure 5.66c Two delay transfer function for 5.7 GHz sounder, -90 dBm, 10 MHz

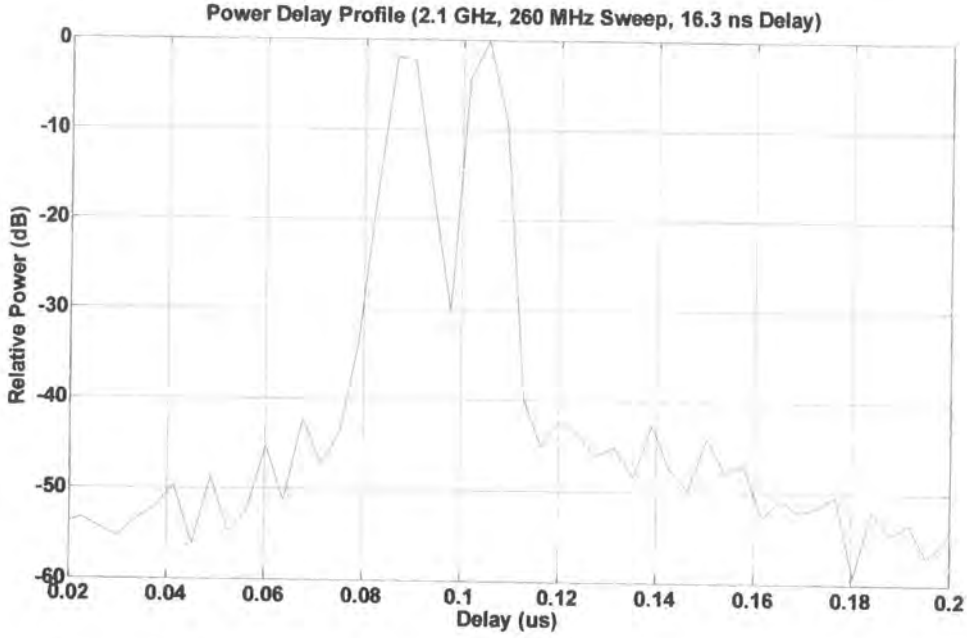

Figure 5.67a Two delay profile for base sounder, -90 dBm, 260 MHz

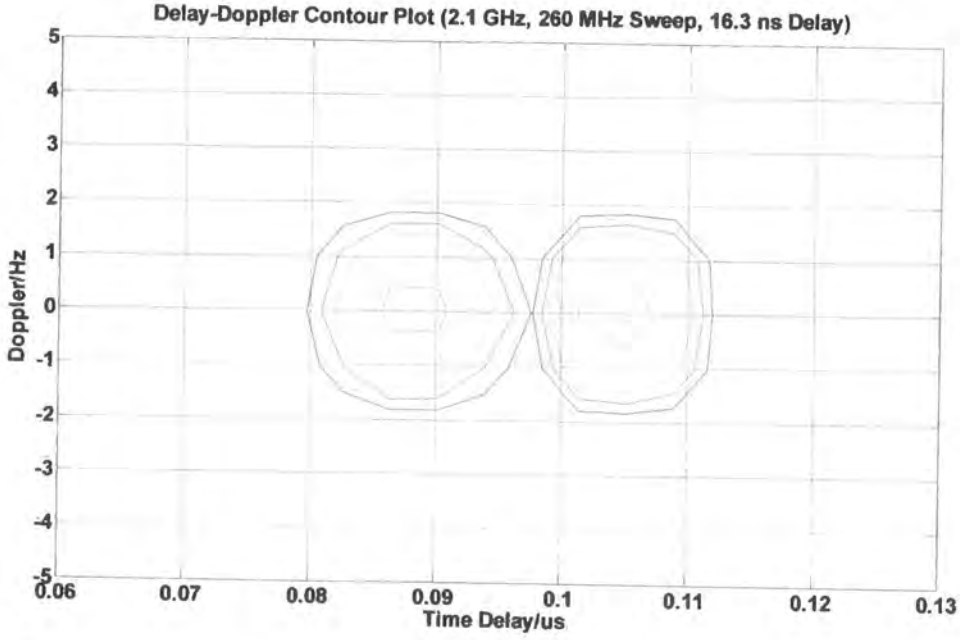

Figure 5.67b Two delay Doppler ambiguity for base sounder, -90 dBm, 260 MHz

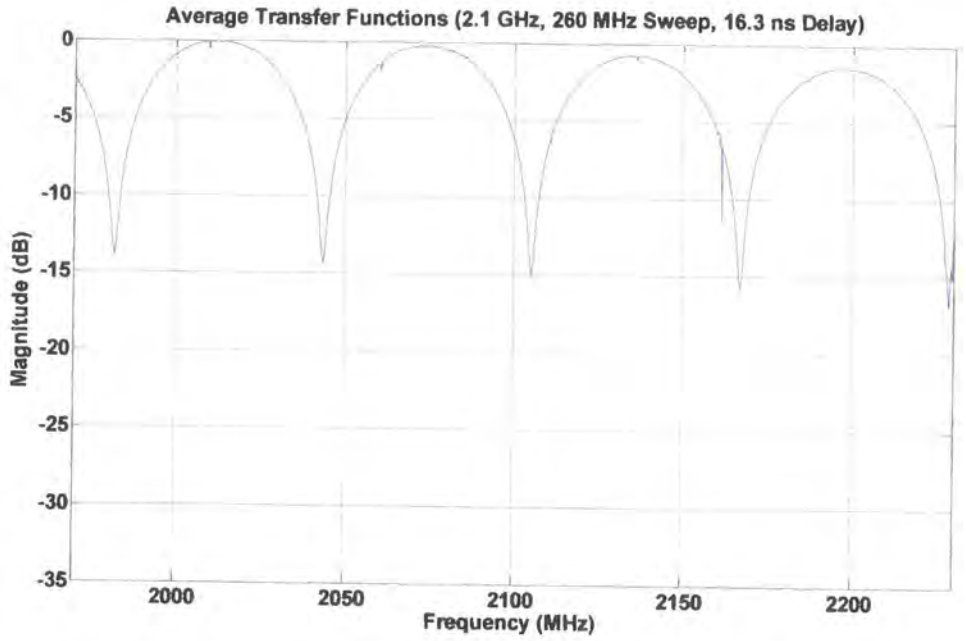

Figure 5.67c Two delay transfer function for base sounder, -90 dBm, 260 MHz

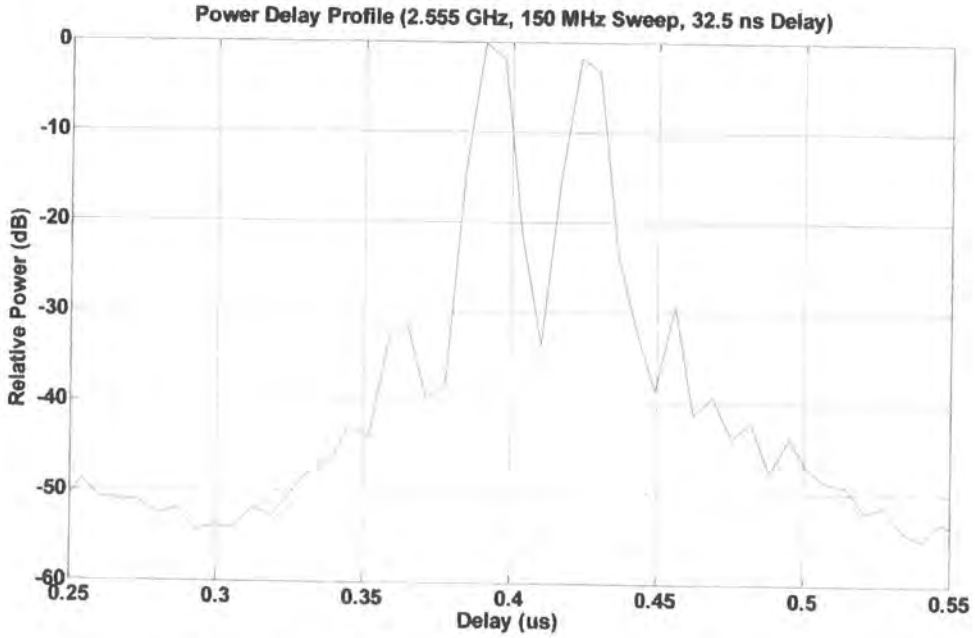

Figure 5.68a Two delay profile for 2.5 GHz sounder, -90 dBm, 150 MHz

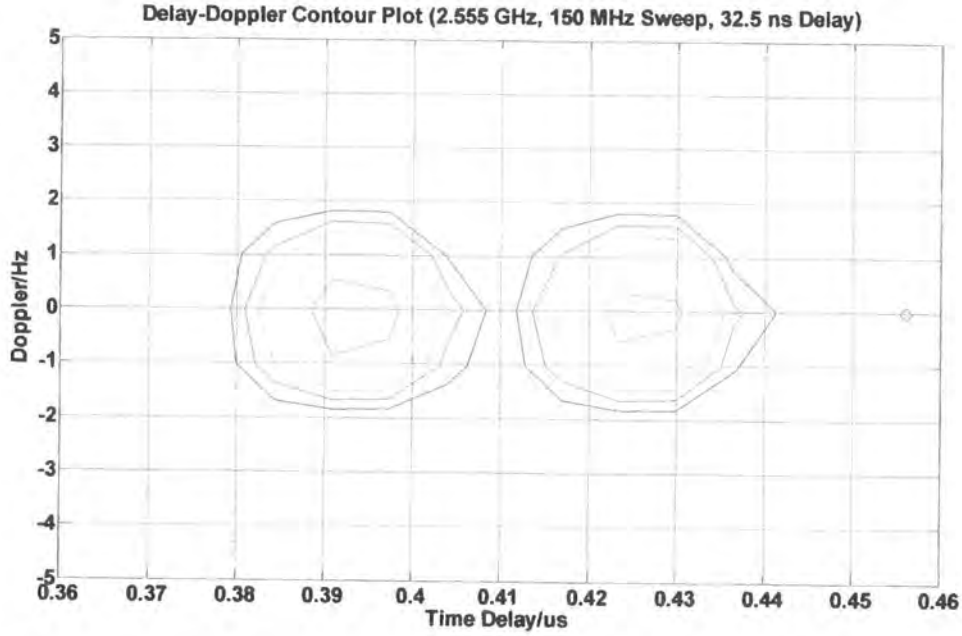

Figure 5.68b Two delay Doppler ambiguity for 2.5 GHz sounder, -90 dBm, 150 MHz

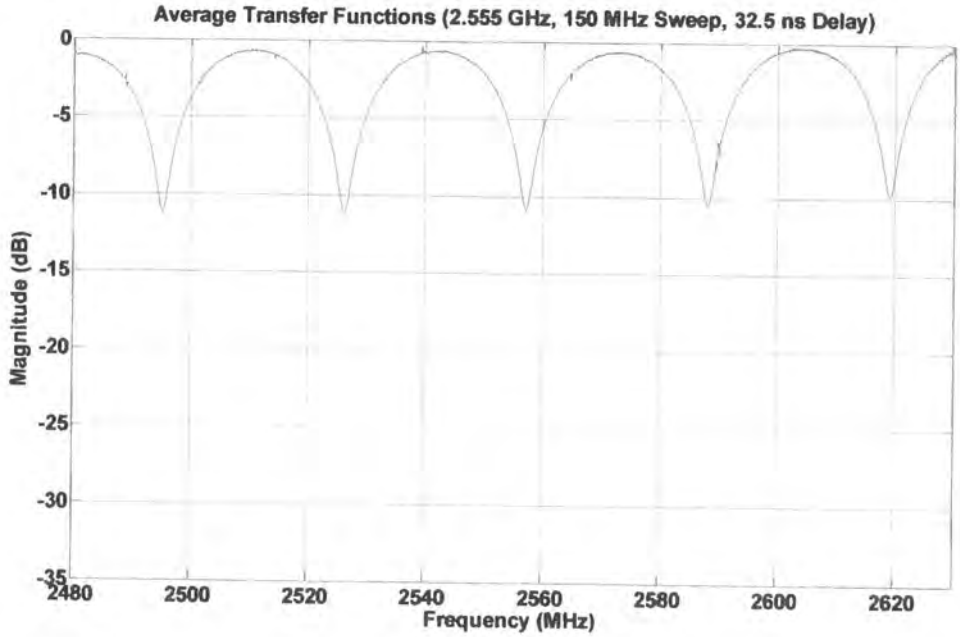

Figure 5.68c Two delay transfer function for 2.5 GHz sounder, -90 dBm, 150 MHz

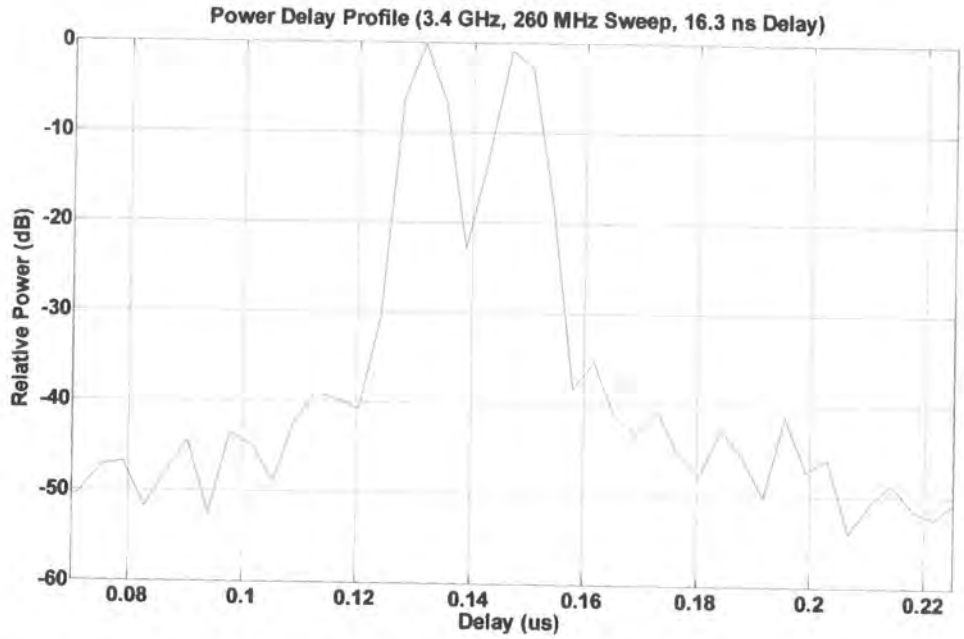

Figure 5.69a Two delay profile for 3.5 GHz sounder, -90 dBm, 260 MHz

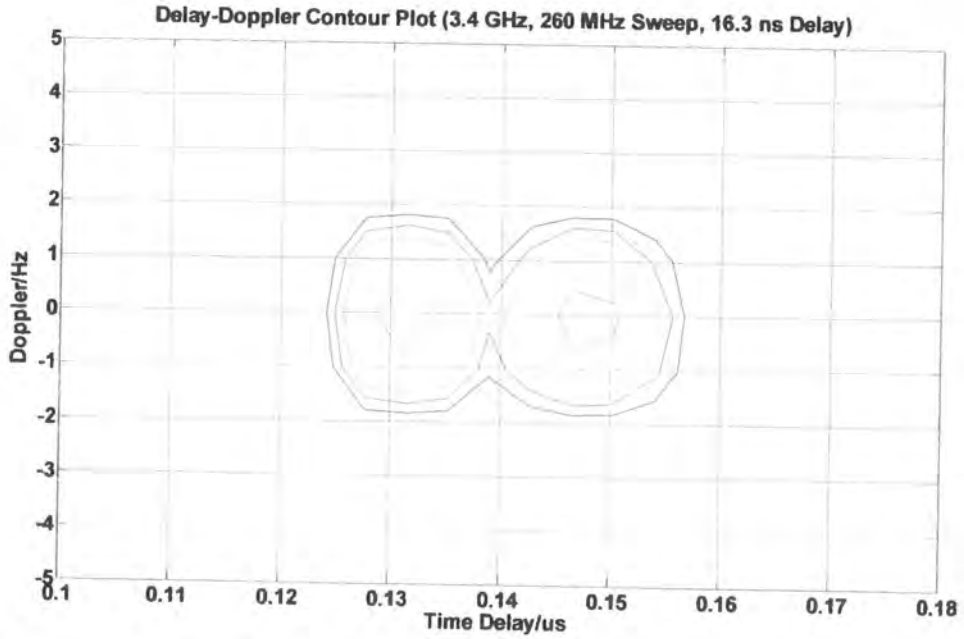

Figure 5.69b Two delay Doppler ambiguity for 3.5 GHz sounder, -90 dBm, 260 MHz

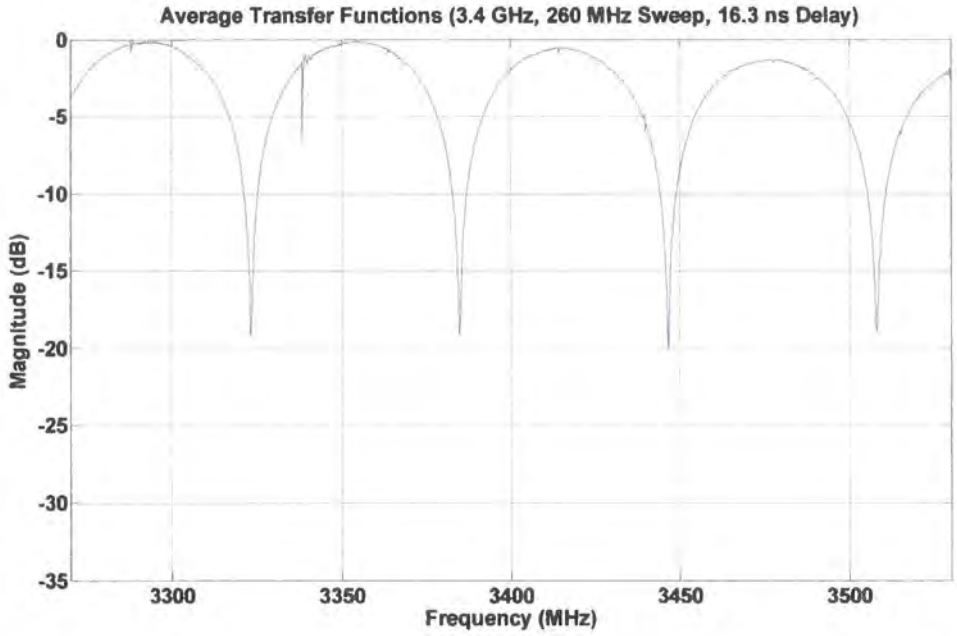

Figure 5.69c Two delay transfer function for 3.5 GHz sounder, -90 dBm, 260 MHz

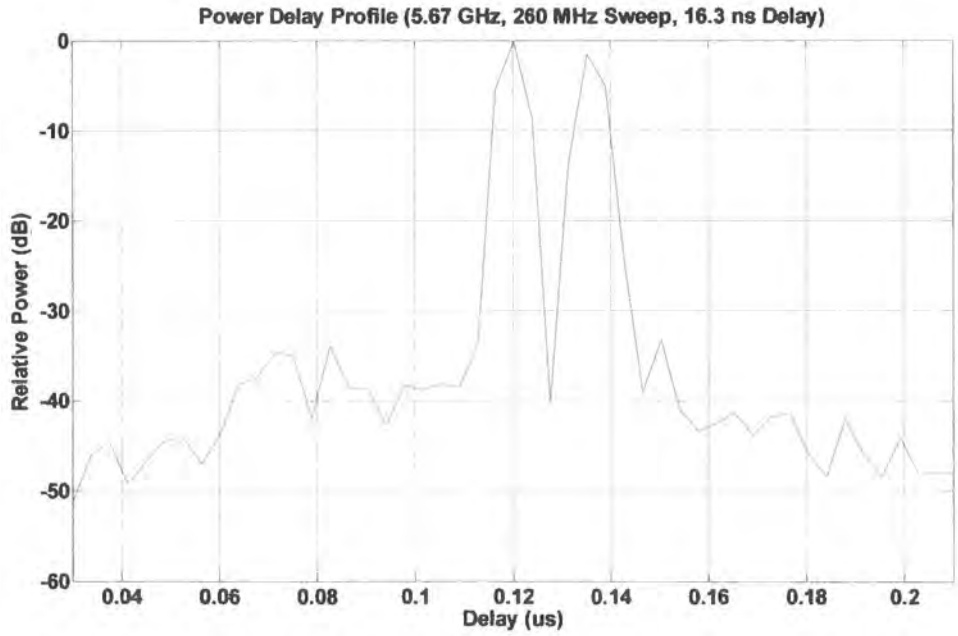

Figure 5.70a Two delay profile for 5.7 GHz sounder, -90 dBm, 260 MHz

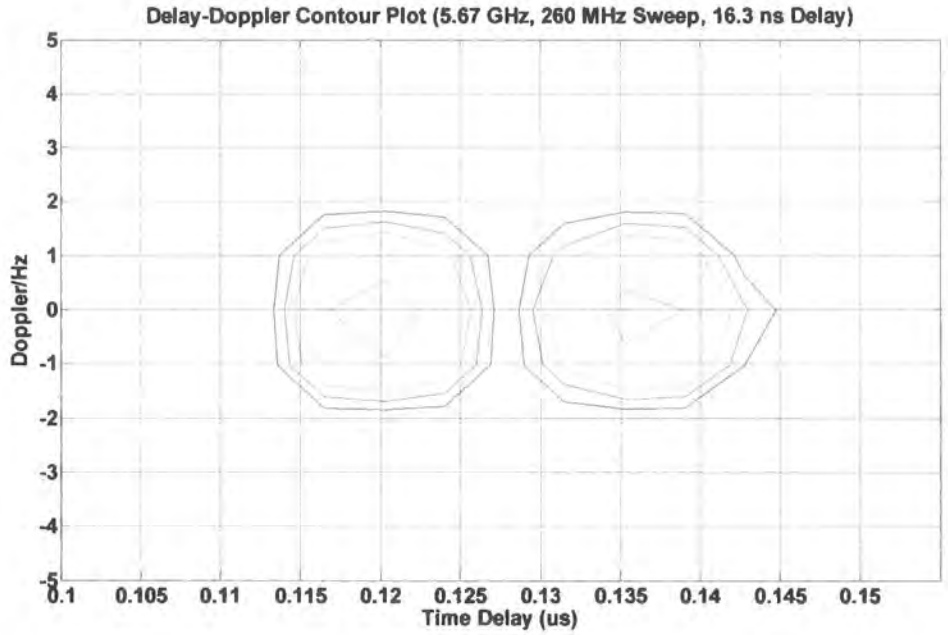

Figure 5.70b Two delay Doppler ambiguity for 5.7 GHz sounder, -90 dBm, 260 MHz

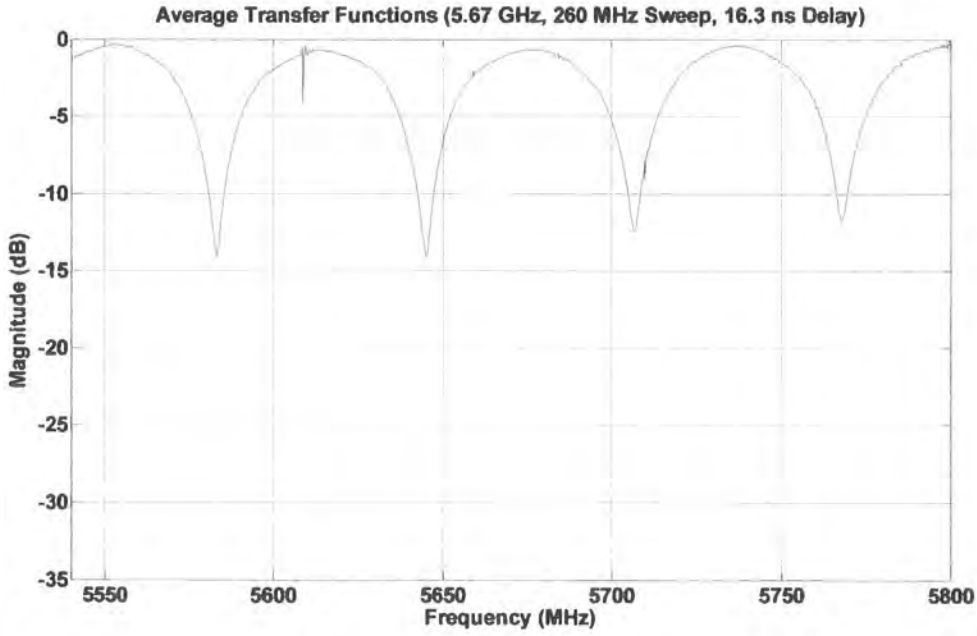

Figure 5.70c Two delay transfer function for 5.7 GHz sounder, -90 dBm, 260 MHz

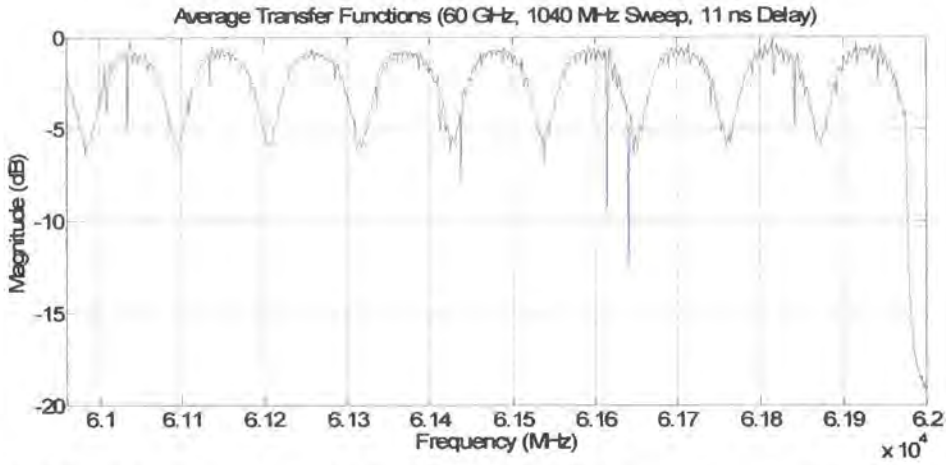

Figure 5.71 Two delay transfer function for 60 GHz sounder, -15 dBm, 1040 MHz

Comments on the two-path delay measurements

The results for the 2 GHz IF, 2.4 GHz, 3.4 GHz and 5.7 GHz sounders are recorded in figures 5.63 to 5.70 demonstrate useful discrimination for two components that are separated by 4.2 to 4.9 bins. The figures 5.63 and 5.68 demonstrate third-order inter-modulation distortion products. This is due to slight overloading of the data acquisition system..

The 60 GHz data were recorded with the IF synthesisers offset by 3.333 MHz providing an offset of 13.333 MHz at 60 GHz. It was noted that one of the sources (the DDFS in the sounder transmitter) was exhibiting some instability for this (final) measurement. While the delay response is visible within the transfer function response, the other data (power delay profile and Doppler ambiguity function) were not useable.

5.3.5 Channel matching (four channel down-converter)

The four channel down-converter is evaluated in the same manner as used to evaluate the single channel 5.7 GHz converter with the addition of a four way splitter (refer to figure 5.72). This allows four identical signals to be presented to each port of the down-converter which allows both the individual and the relative performance of the four channels of the converter to be assessed. The four channel converter has also been evaluated to determine the isolation between the channels. This test was performed by establishing the signal conditioning gains with the receive signal present across all four inputs from the splitter. The inputs to three of the four channels were then terminated with 50Ω loads. The signal was moved through the converter one channel at a time with the other inputs terminated. The four channel converter delay discrimination has been evaluated using a 6 m delay cable (refer to figure 5.73).

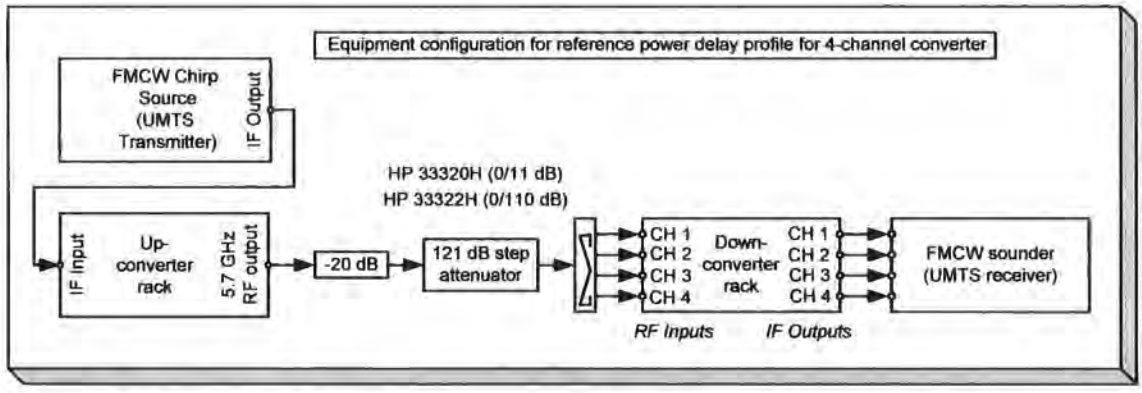

Figure 5.72 Back to back configuration for four channel down-converter

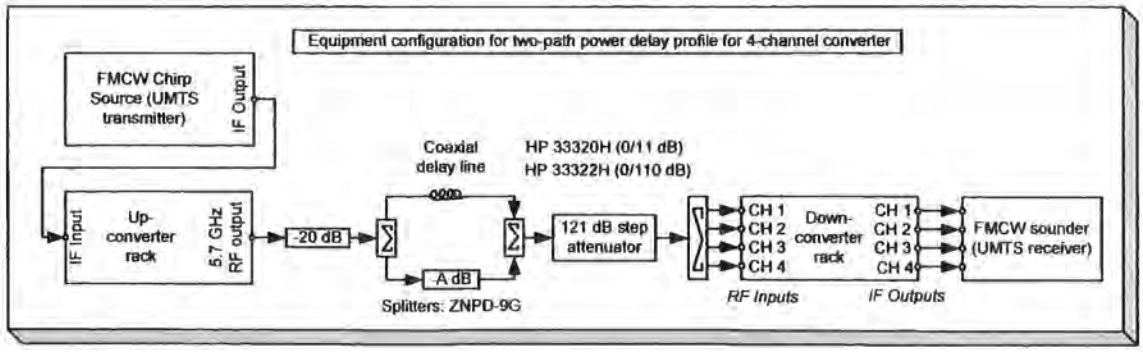

Figure 5.73 Two-path delay configuration for four channel converter

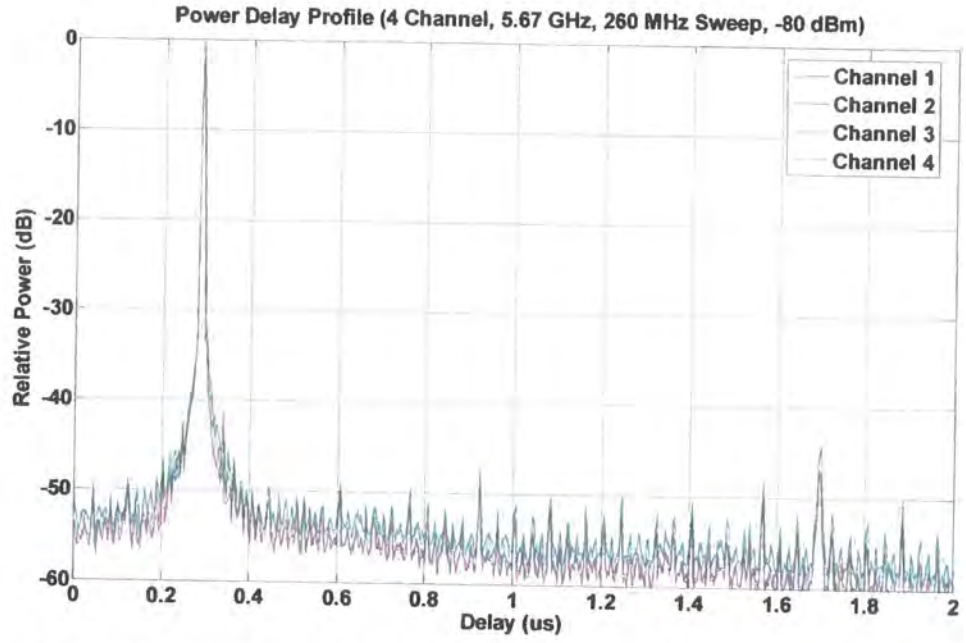

Figure 5.74a 5.7 GHz four channel power delay profile, -80 dBm, 260 MHz

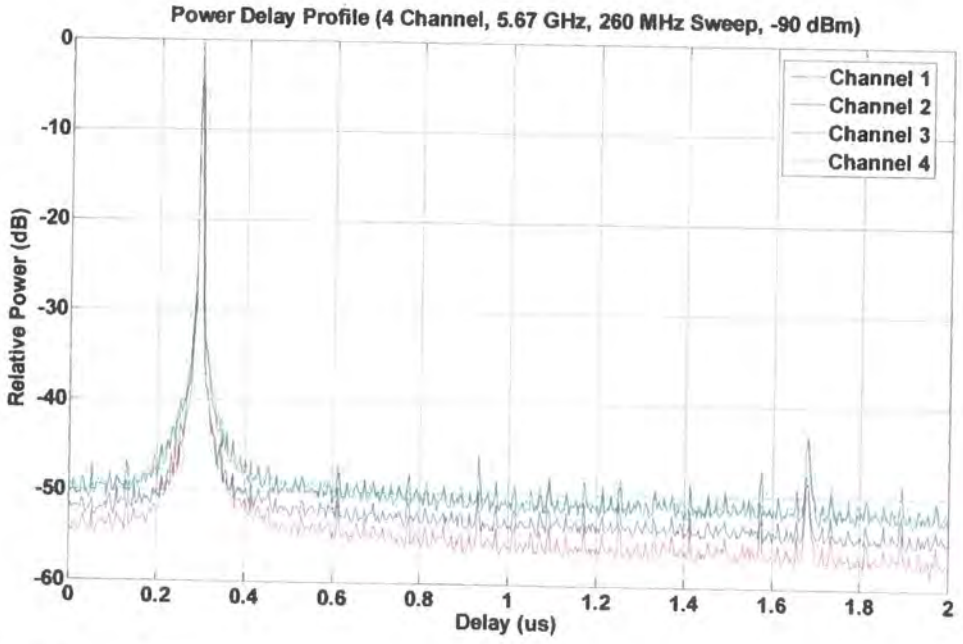

Figure 5.74b 5.7 GHz four channel power delay profile, -90 dBm, 260 MHz

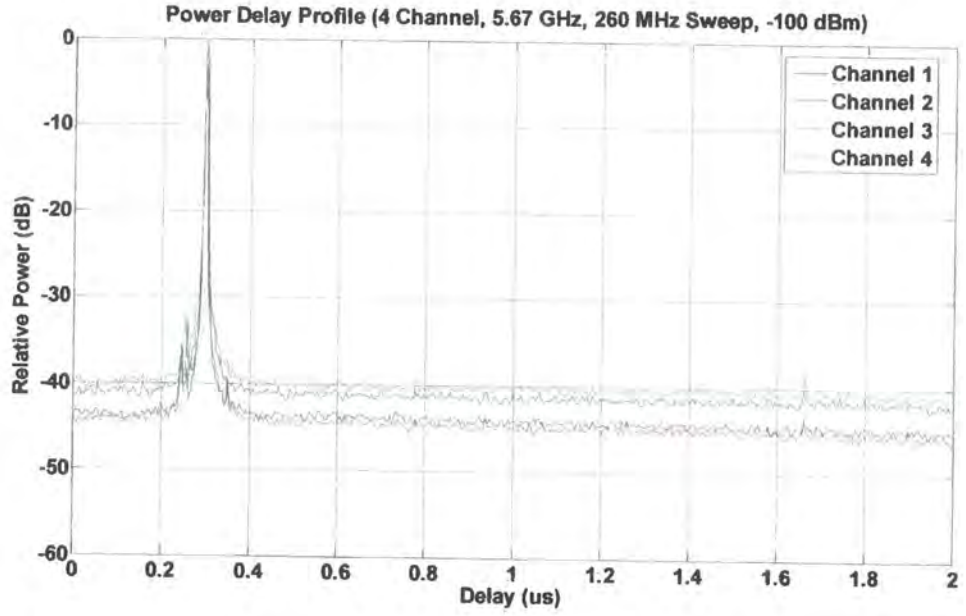

Figure 5.74c 5.7 GHz four channel power delay profile, -100 dBm, 260 MHz

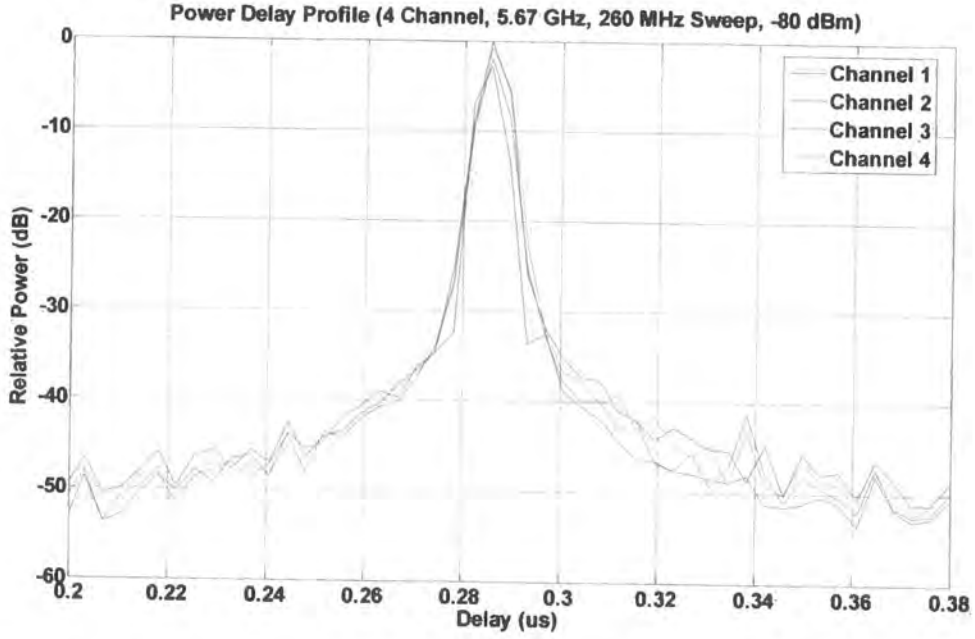

Figure 5.75 5.7 GHz four channel power delay profile, -80 dBm, 260 MHz, narrow

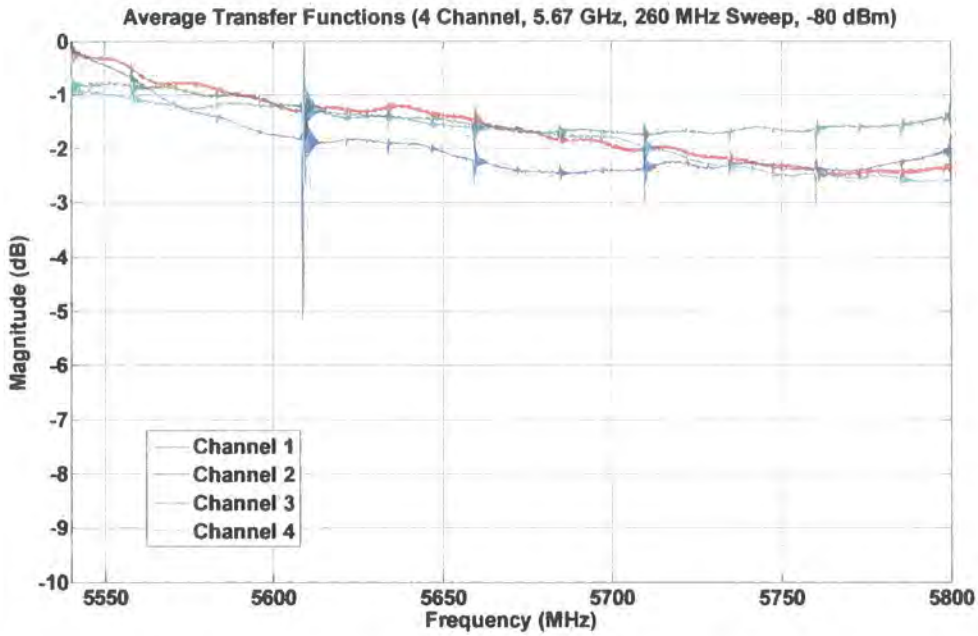

Figure 5.76 5.7 GHz four channel frequency transfer function, -80 dBm, 260 MHz

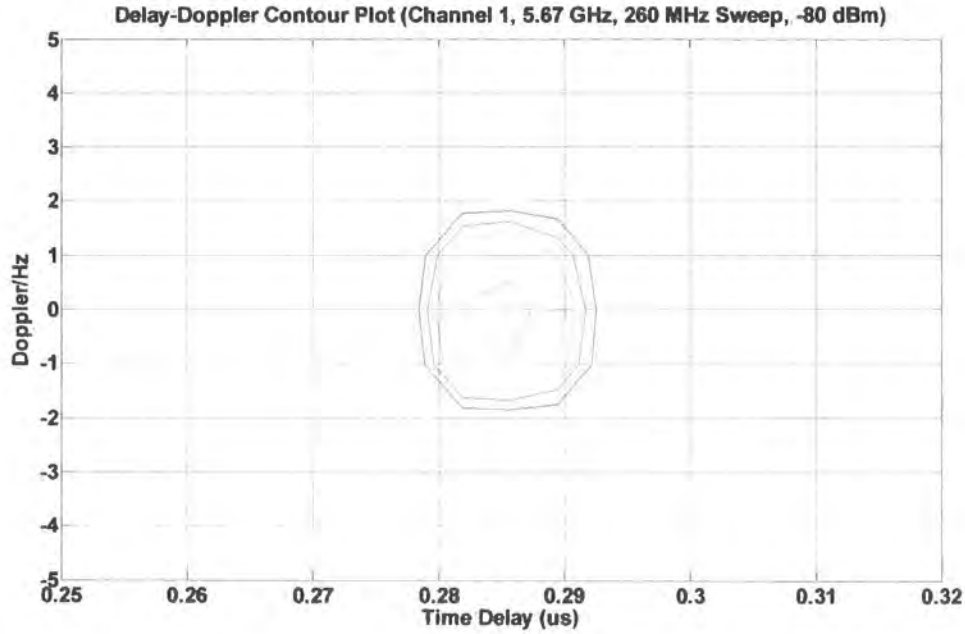

Figure 5.77a 5.7 GHz channel 1 of 4 Doppler ambiguity function, -80 dBm, 260 MHz

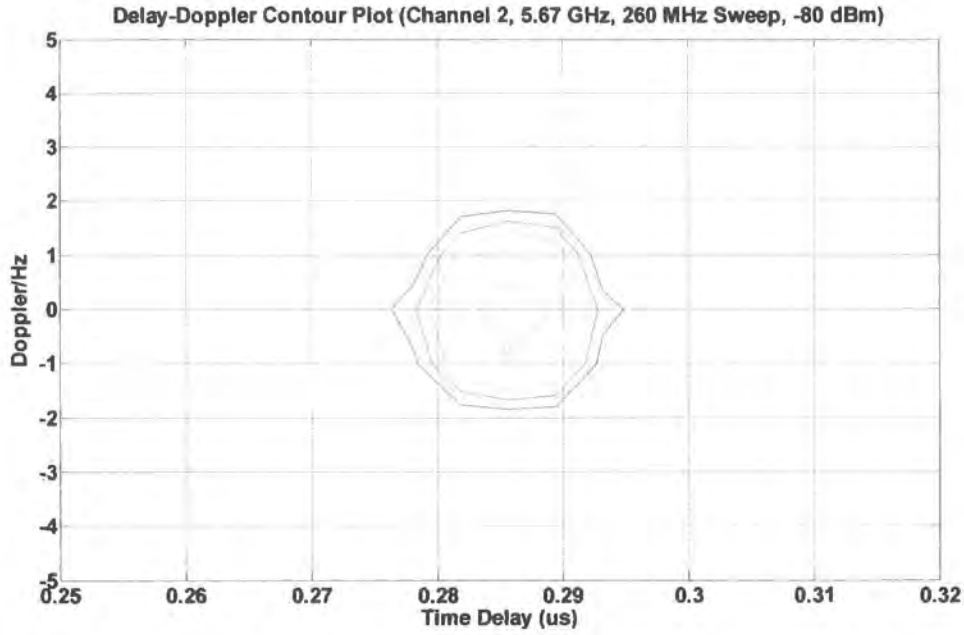

Figure 5.77b 5.7 GHz channel 2 of 4 Doppler ambiguity function, -80 dBm, 260 MHz

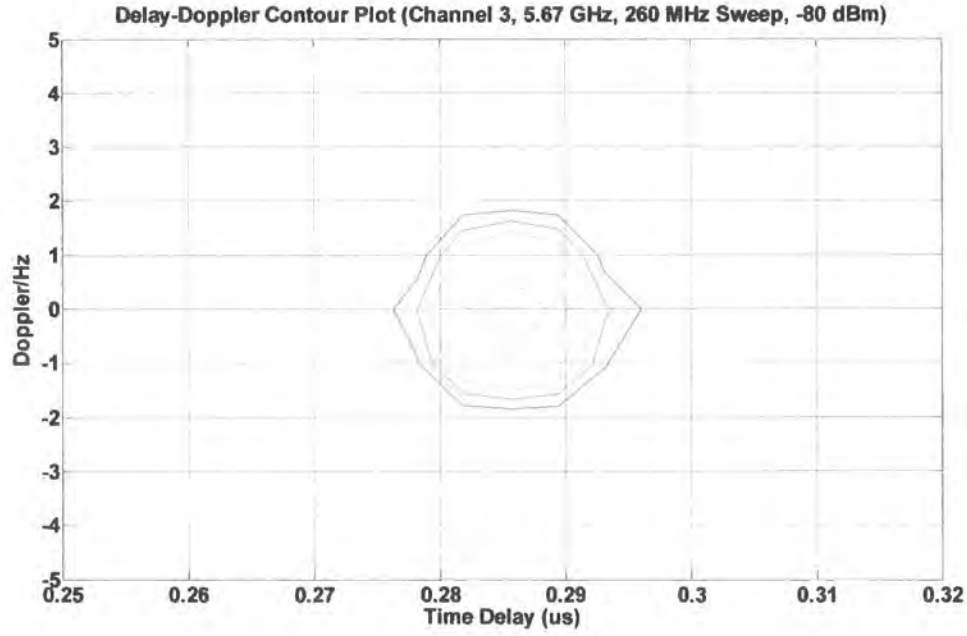

Figure 5.77c 5.7 GHz channel 3 of 4 Doppler ambiguity function, -80 dBm, 260 MHz

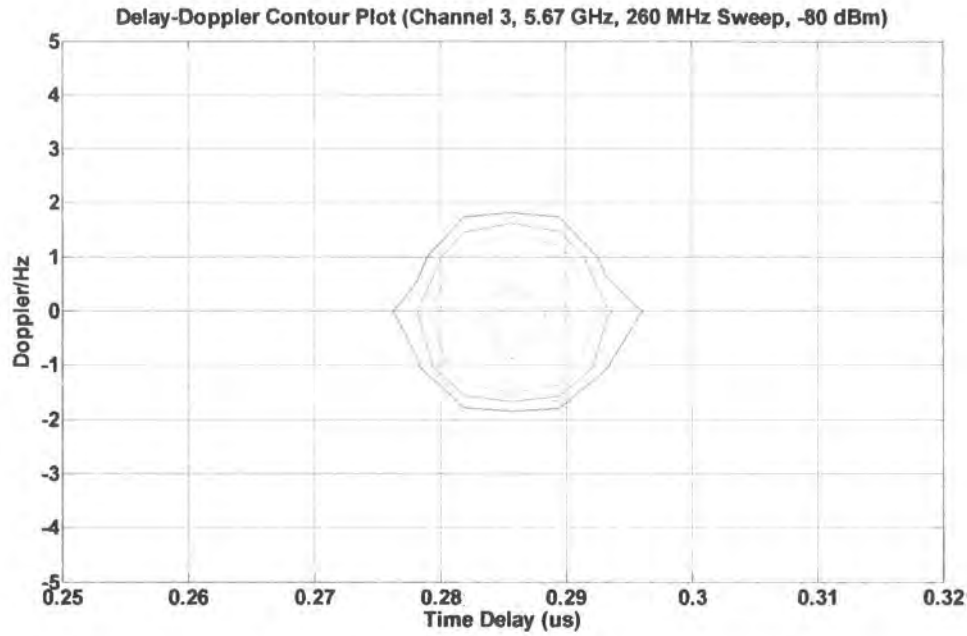

Figure 5.77d 5.7 GHz channel 4 of 4 Doppler ambiguity function, -80 dBm, 260 MHz

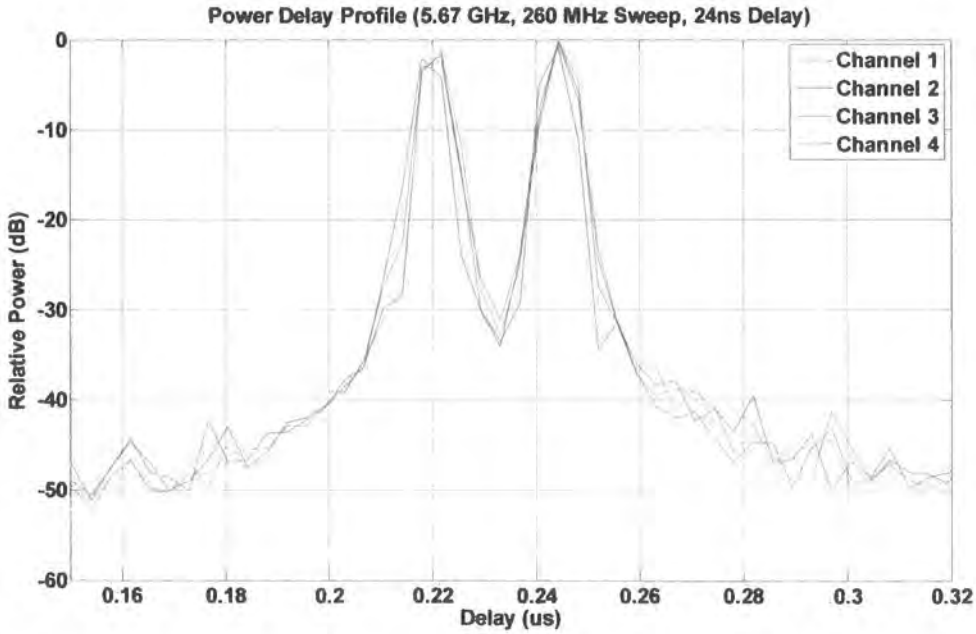

Figure 5.78a 5.7 GHz four channel dual delay profile, -80 dBm, 260 MHz

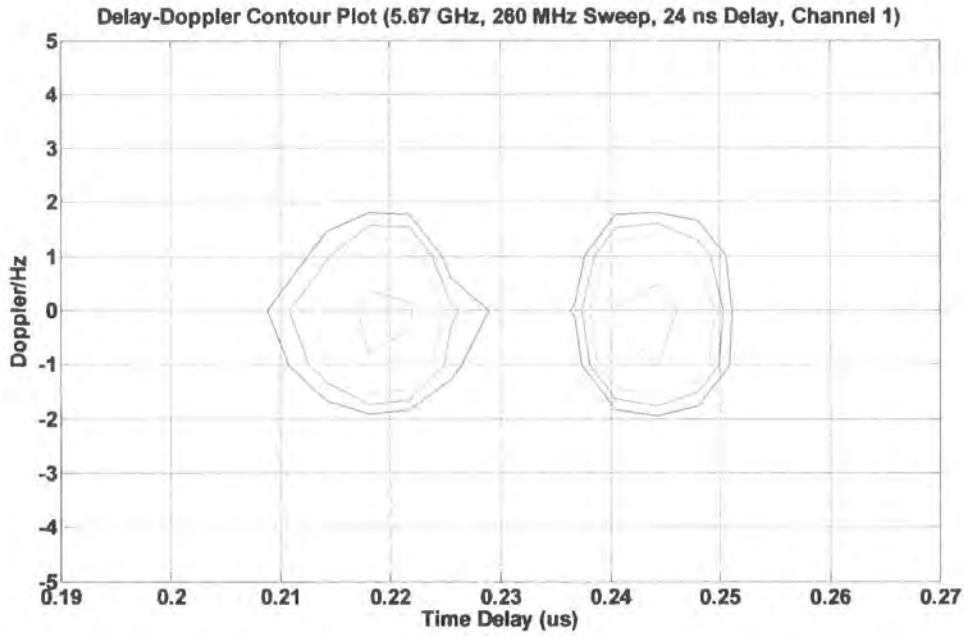

Figure 5.78b 5.7 GHz four channel Doppler ambiguity, -80 dBm, 260 MHz, Ch1

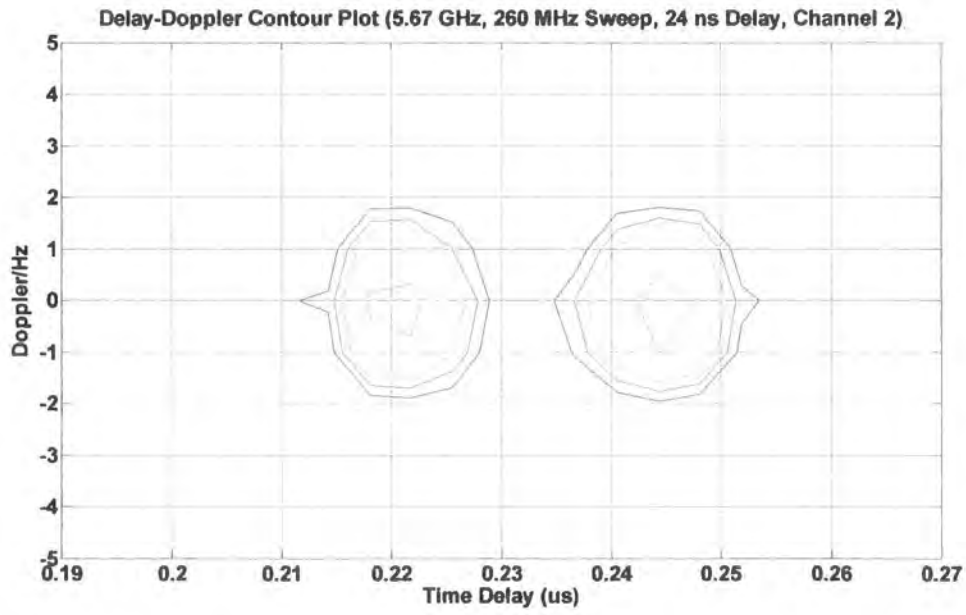

Figure 5.78c 5.7 GHz four channel Doppler ambiguity, -80 dBm, 260 MHz, Ch2

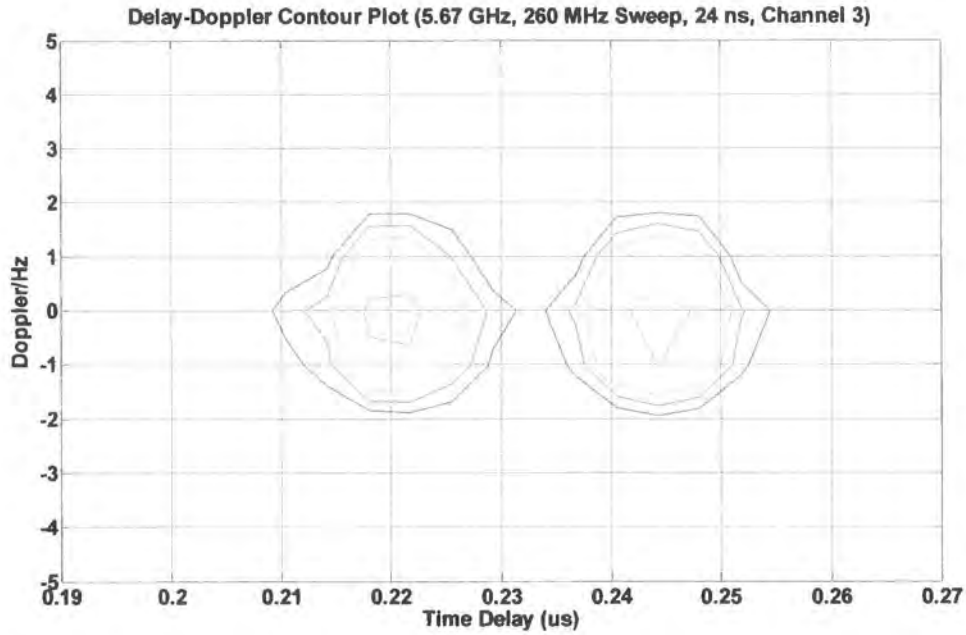

Figure 5.78d 5.7 GHz four channel Doppler ambiguity, -80 dBm, 260 MHz, Ch3

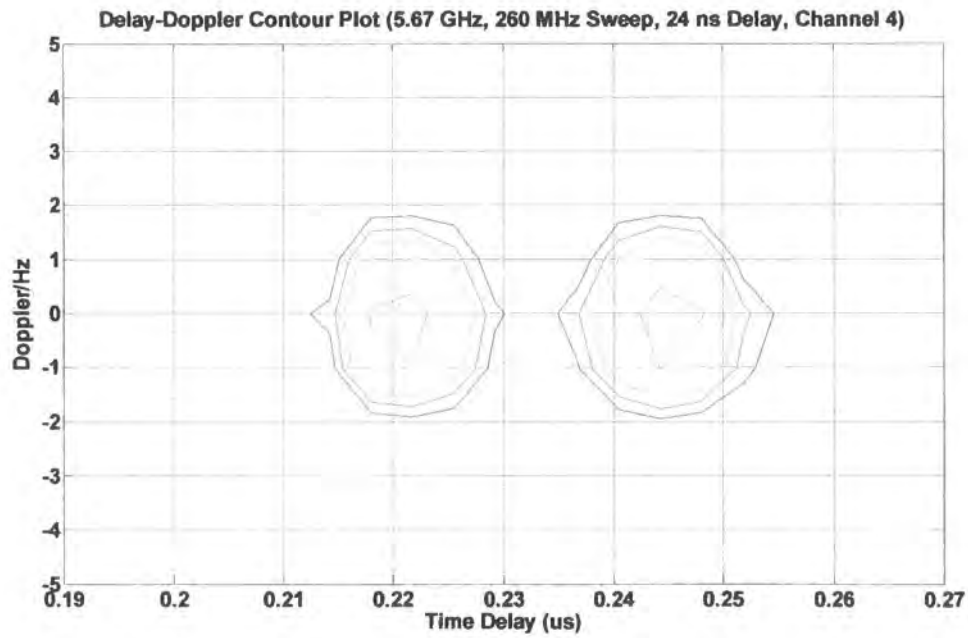

Figure 5.78e 5.7 GHz four channel Doppler ambiguity, -80 dBm, 260 MHz, Ch4

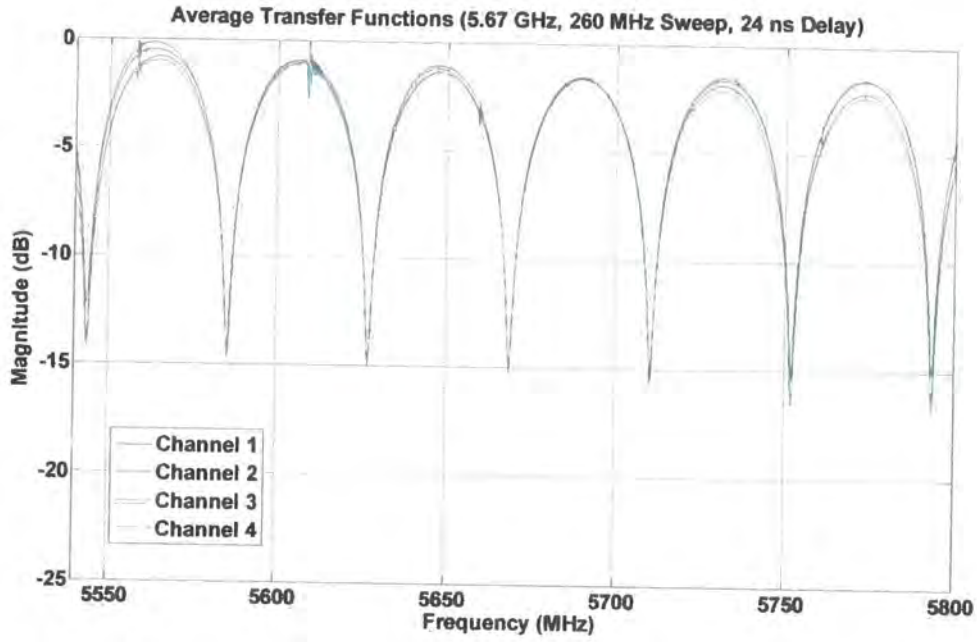

Figure 5.78f 5.7 GHz four channel dual delay transfer function, -80 dBm, 260 MHz

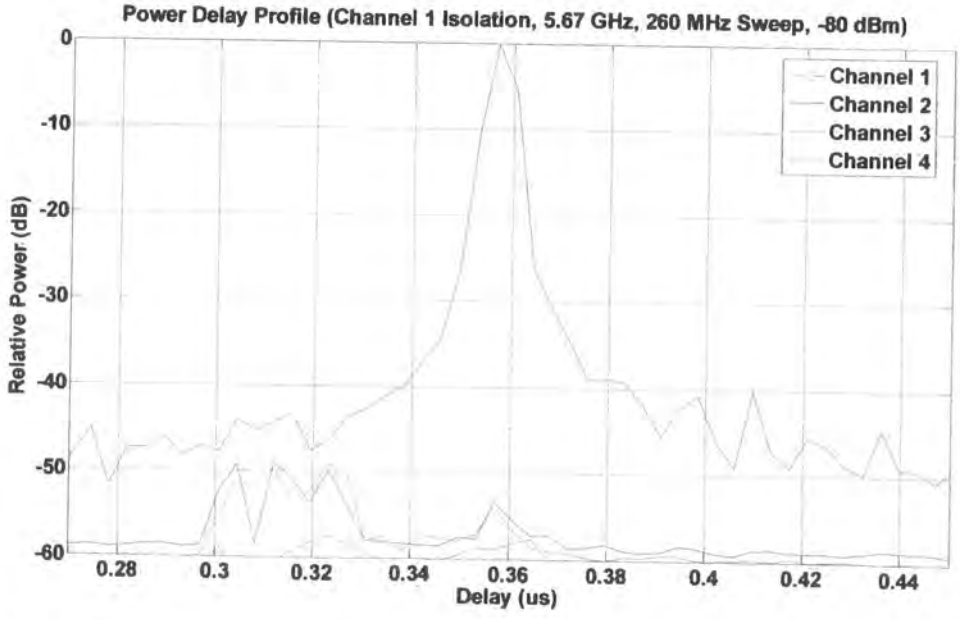

Figure 5.79a 5.7 GHz four channel isolation (Ch1), -80 dBm, 260 MHz

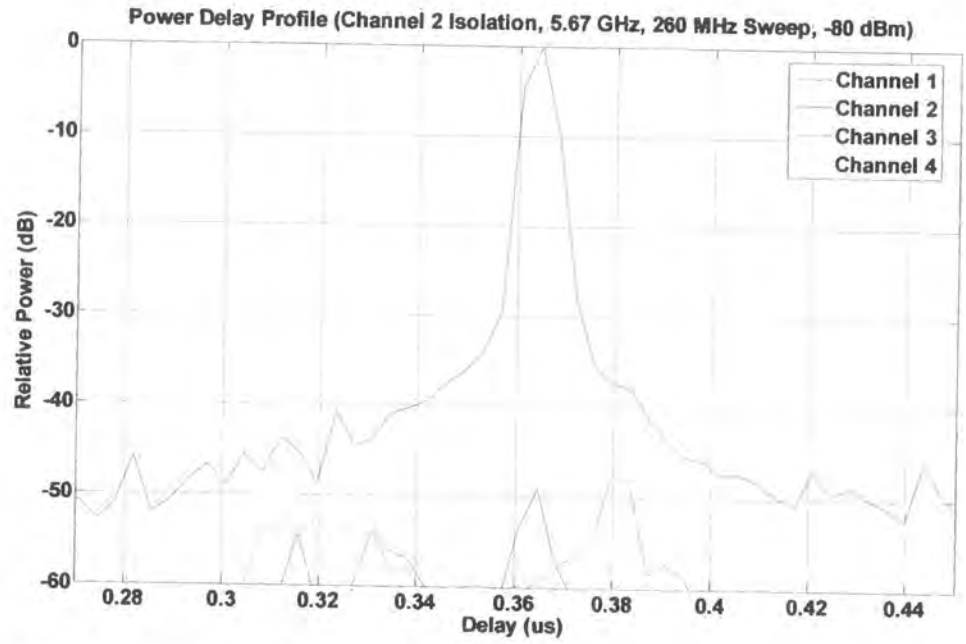

Figure 5.79b 5.7 GHz four channel isolation (Ch2), -80 dBm, 260 MHz

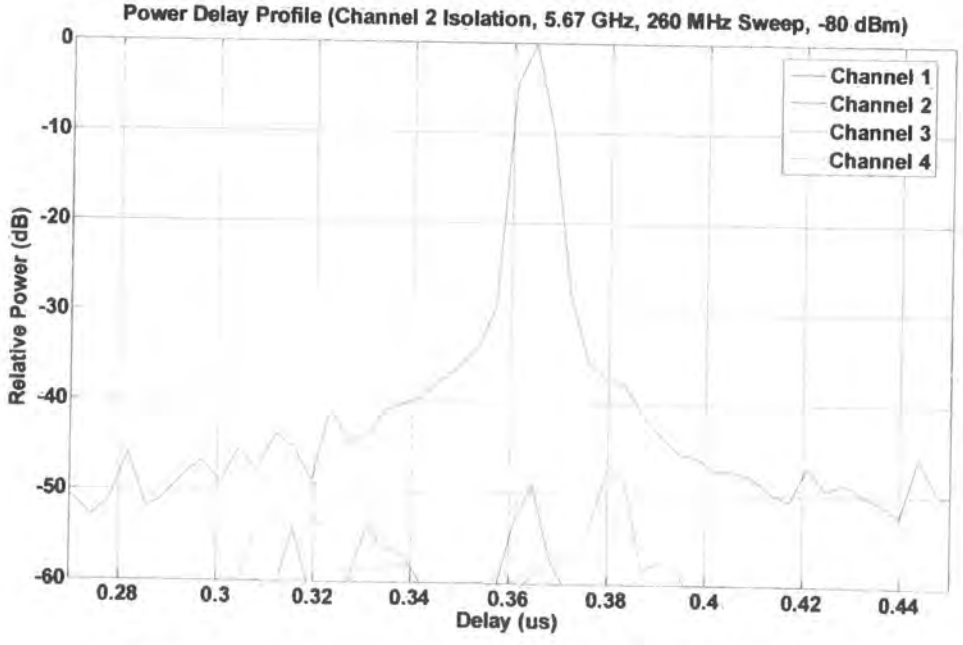

Figure 5.79c 5.7 GHz four channel isolation (Ch3), -80 dBm, 260 MHz

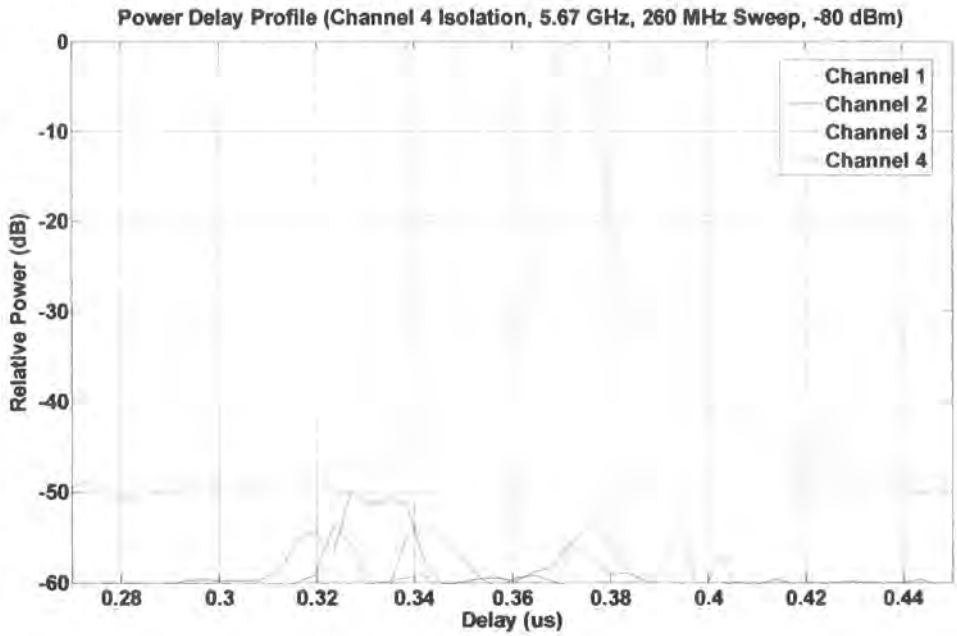

Figure 5.79d 5.7 GHz four channel isolation (Ch4), -80 dBm, 260 MHz

Comments on the 4-channel converter measurements

The single delay responses have been recorded as figures 5.74 to 5.77. These demonstrate behaviour very similar to the data recorded for the single channel 5.7 GHz down-converter with the exception of the transfer function which exhibits ~ 2.5 dB slope across the band. The delay-Doppler function data demonstrate that the peak of the delay profiles are all centred within one bin relative to each other.

The dual delay data are recorded in figure 5.78. This demonstrates virtually identical behaviour across all four channels. (This is also very similar to the single channel unit).

The isolation demonstrated (refer to figure 5.79) is in agreement with the results observed for the base channel sounder within the UMTS bands [5.4]. The measurements performed here demonstrate ~ 50 dB of isolation between the channels. Some leakage is evident from the sounder transmitter to receiver directly at 2.1 GHz. This is observable as components that are arriving before the principal response, since signals in the IF band have not been subject to the propagation delay present in the up and down-converters.

5.4 Antenna patterns for the 5.7 GHz array

The 5.7 GHz antenna array was measured using the test configuration described in section 4.6 with the up-converters, down-converters and four-channel quadrature down-converter configured as shown in figure 4.61. Pattern data were recorded for 5° angular rotations with a separation between the test source and the antenna under test of approximately 2 m. The measurements were performed within a general laboratory environment which was not anechoic. This provides a lower limit for the off-axis measurement level for this particular measurement. However the measurement does show that the antenna array provides approximately a useful gain response for each antenna across the respective 90° sector, with the adjacent sectors crossing at the point where the antenna gain response has reduced by 3 dB relative to the maximum. This is depicted in the Cartesian antenna response plot (refer to figure 5.80).

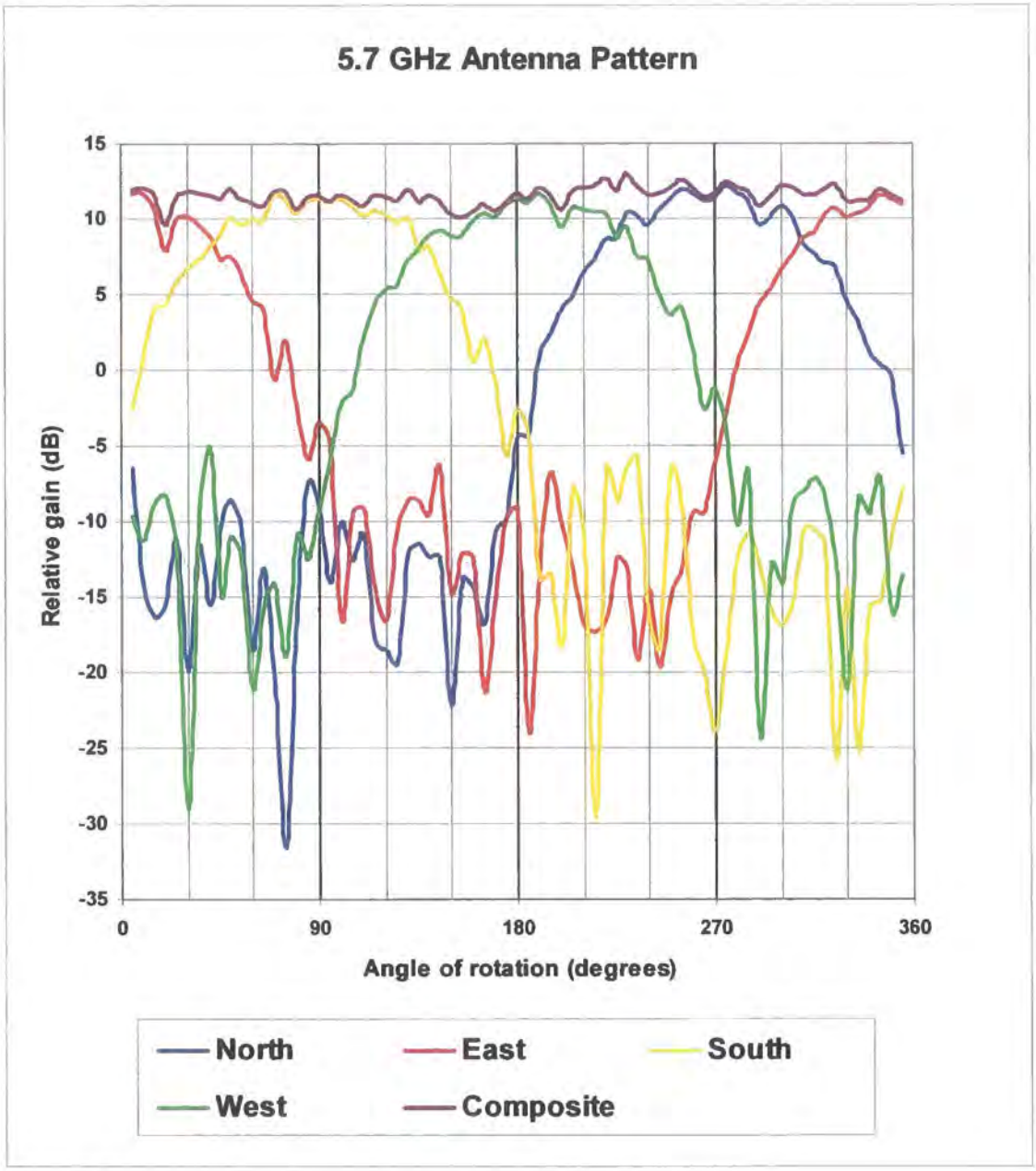

Figure 5.80 Polar response of the 5.7 GHz antenna array

The polar response of the antenna array is displayed in figure 5.81. The angular scale is 360° in 5° increments. The radial gain scale for this figure is -35 dB to +15 dB (with an arbitrary reference where 0 dB represents 1 V magnitude for the quadrature down-converter data). The composite response represents the sum of the individual antenna gain responses. This demonstrates that the antenna array provides 360° of coverage in azimuth with approximately 2 dB of ripple. Figure 5.82 displays the composite azimuth response with a radial gain scale of 2 dB per division.

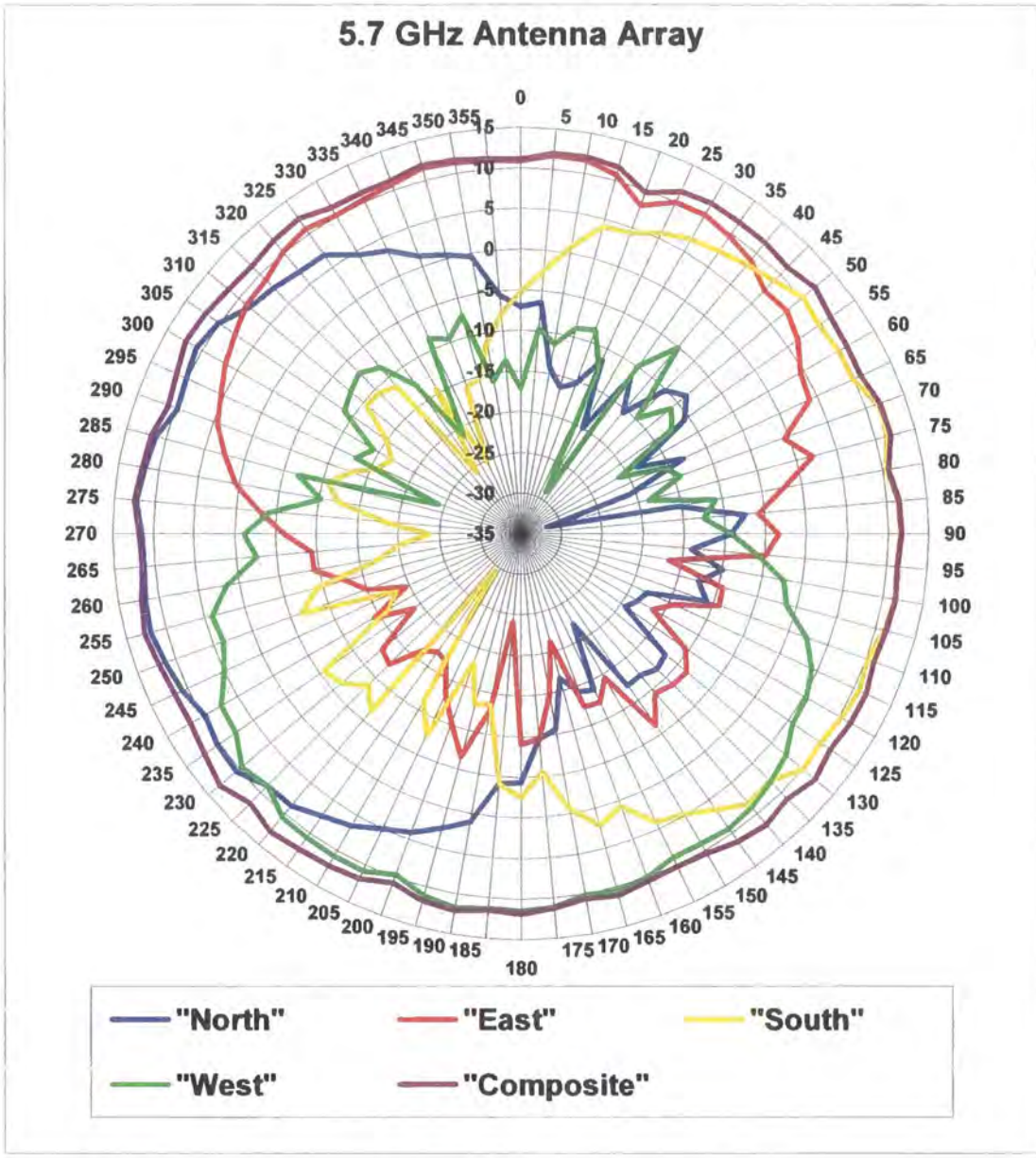

Figure 5.81 Polar response of the 5.7 GHz antenna array

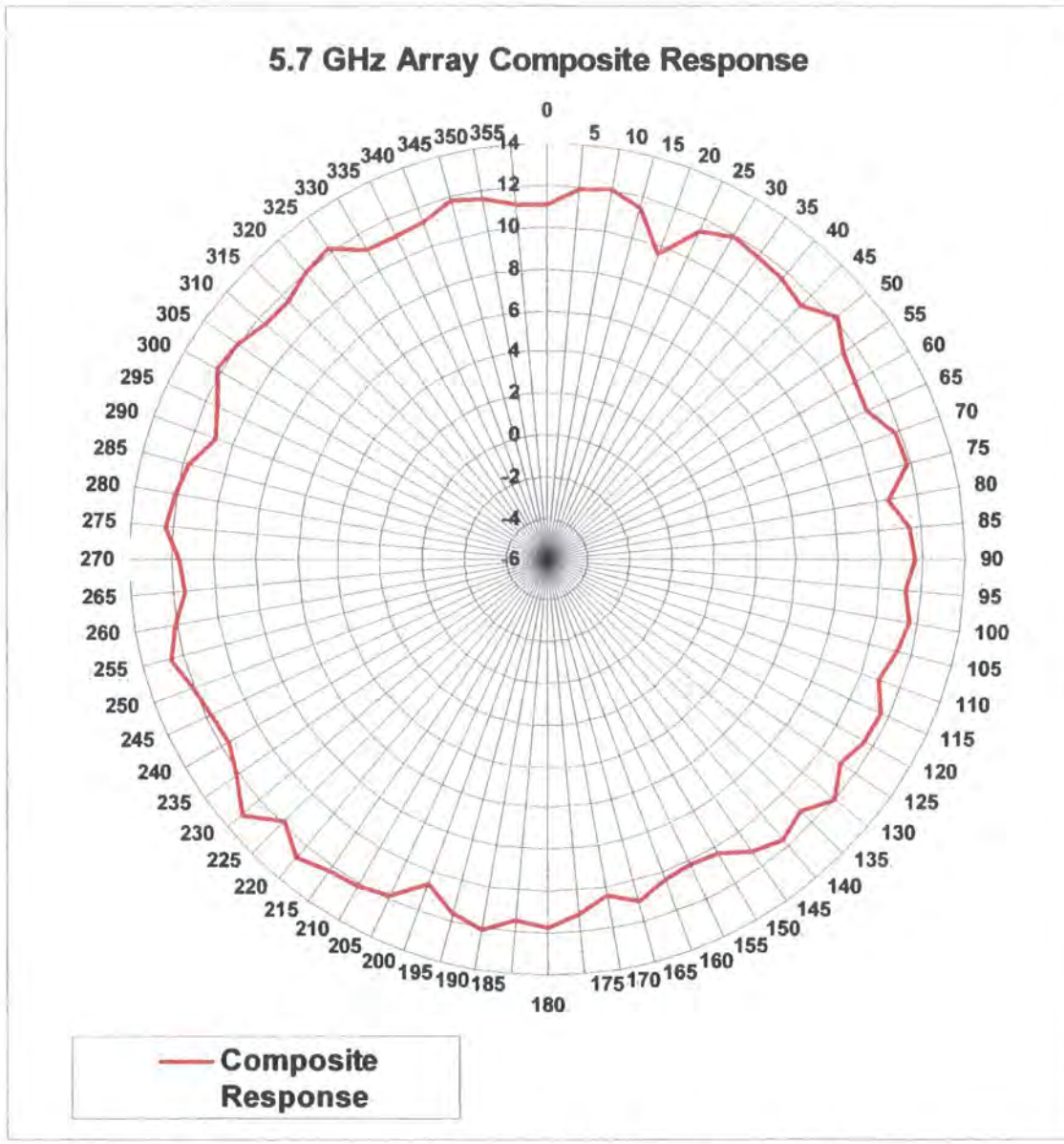

Figure 5.82 Composite response for the 5.7 GHz array (expanded scale)

5.5 Discussion and conclusion for sounder calibration and verification

1. Practical techniques have been developed and demonstrated to asses the primary functional parameters of the channel sounder, frequency converters and antennas. The sensitivity of the basic sounder has been explored and the double-sideband contribution to the noise floor has been confirmed.

2. The measurement limits of the sounder and the frequency converters have been investigated in detail. The performance of the sounder with the 2.5 GHz, 3.5 GHz and 5.7 GHz converters has been demonstrated to be virtually identical to the base 2 GHz sounder in all respects (transmit flatness, sensitivity, residual transfer function and delay resolution).

3. The four-channel converter demonstrates similar conformity of performance including close matching between channels for all parameters. The channel isolation has been demonstrated to be virtually identical to that previously demonstrated for the parallel channel receiver at 2 GHz.

4. The 60 GHz sounder has demonstrated basic levels of functionality. It has been possible to demonstrate that the equipment is capable of making power delay profile, Doppler ambiguity and frequency transfer function measurements. The close to carrier phase noise is sufficiently low that the width of the CW measurement is virtually identical to that of the lower frequency systems. The measured width of the CW response of the 60 GHz system is approximately 1 kHz wide (equivalent to four "range-bins") at the 30 dB threshold. The noise floor for the power delay profile is ~ 12 dB higher than the 5.7 GHz system. This is in reasonable agreement with the phase noise increase expected for X4 multiplication. This result also indicates that the dominant source of residual noise in the 60 GHz sounder at this signal level is phase noise. This is reasonable in view of the wide band phase locked loops that have been used in the frequency converters. A small shift (~ 1Hz) in the Doppler domain can be observed. This represents a short term stability of approximately $1*10^{-11}$ for the Rubidium references. This is in accordance with the specified performance.

5. The directional antenna assembly has been calibrated using the frequency converters in conjunction with the quadrature down-converter, antenna positioning and data acquisition system. The front to back isolation could not be measured fully due to the non-anechoic environment. However the measured

main-lobe performance demonstrated close agreement with the manufacturer's stated bandwidth of 90° at -3 dB.

5.6 References

[5.1] Vernon Morgan D., Howes M.J., and Pollard R.D. (editors); "Microwave and Solid-State Component and Subsystem Design proceedings of the 1983 Leeds IEE Microwave Summer School"; The University of Leeds, ISBN 0-85316-132-1.

[5.2] Harris F.J.; "On the Use of Windows for Harmonic Analysis with the Discrete Fourier Transform"; Proceedings of the IEEE, Vol. 66, No. 1, January 1978.

[5.3] Bailey R.J., and Summers G.R.; "Radio Channel Characterization for the Digital European Cordless Telecommunication System"; BT Telecom Technology Journal Vol.8, no 1, pp.25-30, January 1990.

[5.4] Filippidis P.; "Multi-Channel Sounder for Directional Measurements"; PhD Thesis, UMIST, 2002.

6.1 Introduction

The different channel sounder configurations have been used to perform measurements. The configurations that have been used are summarised below:

Three-band outdoor configuration

This data set uses the three-band configuration with simultaneous 10 MHz sweep width in all three bands. Separate band specific antennas were used for both the transmitter and the receiver. The transmitter antennas were directional with azimuth beam-widths of 30° at 2.5 GHz, 30° at 3.5 GHz and 120° at 5.7 GHz. The receiver antennas used were omni-directional in azimuth.

Three-band indoor configuration

This data set uses the three-band configuration with simultaneous 150 MHz sweep width in all three bands. The sweep outputs from each transmitter were combined using wideband (2 GHz to 9 GHz) couplers. A common wideband discone antenna was used for all three bands at the transmitter. An identical antenna and coupler configuration was used at the receiver. The antennas used were omni-directional in azimuth. The transmitter and the receiver were both located inside the building for most measurements. A sub-set of the measurements were made with the transmitter inside the building and the receiver outdoors. Some measurements were made with the receiver moving to deliberately generate Doppler shift.

Four-channel 5.7 GHz outdoor configuration

These measurements were made using a sweep width of 260 MHz in the 5.7 GHz band. An omni-directional antenna was used at the transmitter. Four directional antennas were used at the receiver in conjunction with the four-channel down-converter. An initial set of 15 measurements were made using +10 dBm input power to the transmitter antenna. Subsequently an additional set of 59 measurements were made using +28 dBm input

power to the transmitter antenna. The down-converter channel that demonstrated the highest peak signal level has been selected. The delay parameters have been processed for this channel of the down-converter. Examples of the power delay profiles recorded for all four antennas in the array have been provided to demonstrate spatial discrimination.

60 GHz

A limited set of data has been included to demonstrate the operation of the 60 GHz sounder. These measurements were made with a sweep width of 1,040 MHz using 20 dBi conical horn antennas at the transmitter and receiver.

6.2 Three-band sounding outdoors

The transmitter antennas were mounted on the roof of the Portman Road telephone exchange located on the western side of Ipswich town centre. The transmitter antenna orientation was approximately north-west at a height of approximately 15 m. The receiver antennas were mounted on the roof of the survey vehicle at a height of approximately 2 m.

A total of 178 files were recorded for the western side of Ipswich. Figure 6.1 describes the general area that was investigated using the channel sounder with twenty example locations depicted in the map. Each data file includes the sounder data for three channels corresponding to the 2.5 GHz, 3.5 GHz and 5.7 GHz bands. The power delay profiles for all three bands within a file were individually examined. The files were selected on the basis that the signal to noise ratio was sufficient to provide a power delay profile for all three bands down to a threshold level of 20 dB below the peak. Files that did not satisfy this requirement for all three frequencies were excluded from the results. This reduced the data set to 131 files. This data set has been used to compute the cumulative distributions for the average delay and the RMS delay spread at threshold levels of -10 dB, -15 dB and -20 dB below the peak of the power delay profile.

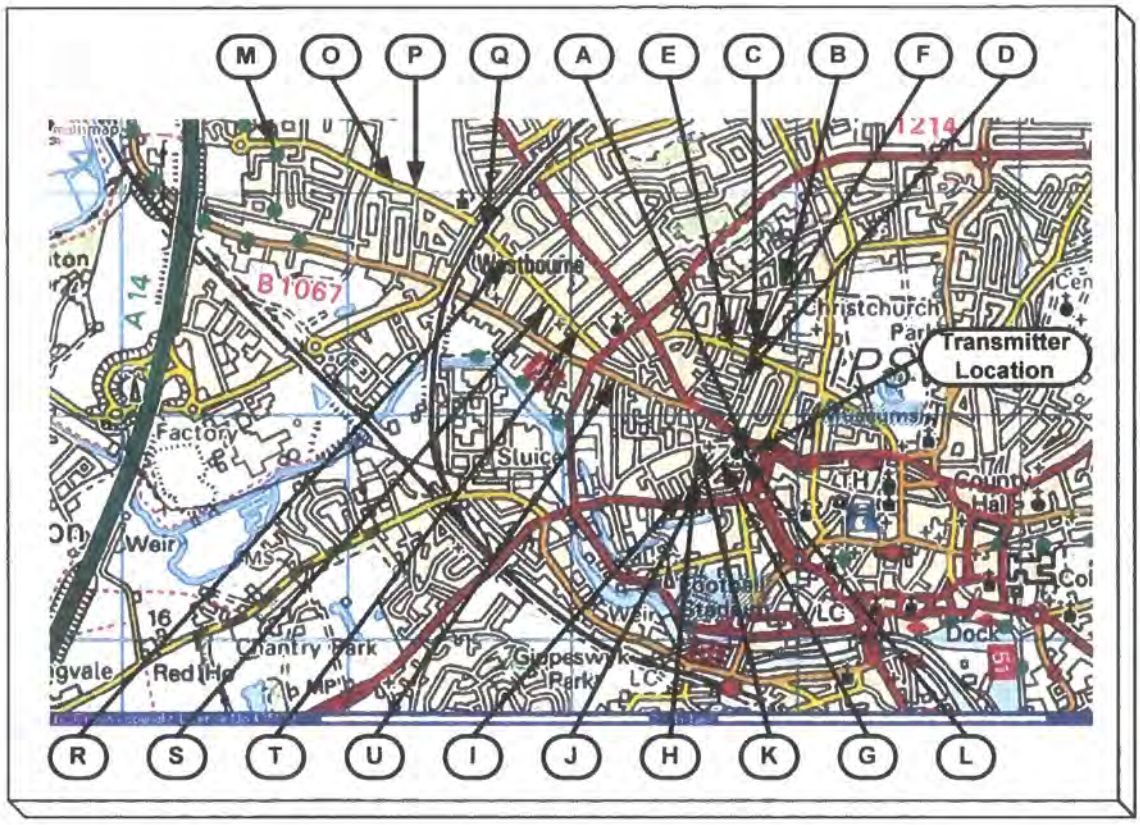

Figure 6.1: Locations used for three-band sounding in Ipswich

The distributions of the average delay as a function of frequency are shown in figures 6.2 to 6.4. The distributions of the average delay at different frequencies have been compared at the threshold values of -10 dB, -15 dB and -20 dB. These are shown in figures 6.5 to 6.7.

The observed values at the 50% and 90% intervals are shown in table 6.1.

Threshold value	Interval	Frequency			Delay
		2.5 GHz	3.5 GHz	5.7 GHz	
10 dB	50%	150	135	135	ns
	90%	450	420	400	ns
15 dB	50%	225	200	180	ns
	90%	520	500	500	ns
20 dB	50%	260	230	255	ns
	90%	660	580	650	ns

Table 6.1 Average delay measured in Ipswich

The distributions of the RMS delay spread as a function of frequency are shown in figures 6.8 to 6.10. The distributions of the RMS delay spread at different frequencies have been compared at the threshold values of -10 dB, -15 dB and -20 dB. These are shown in figures 6.11 to 6.13.

The observed values at the 50% and 90% intervals are shown in table 6.2.

Threshold value	Interval	Frequency			Delay
		2.5 GHz	3.5 GHz	5.7 GHz	
10 dB	50%	110	80	80	ns
	90%	325	320	300	ns
15 dB	50%	155	130	125	ns
	90%	370	390	330	ns
20 dB	50%	200	175	160	ns
	90%	445	455	420	ns

Table 6.2 RMS delay spreads measured in Ipswich

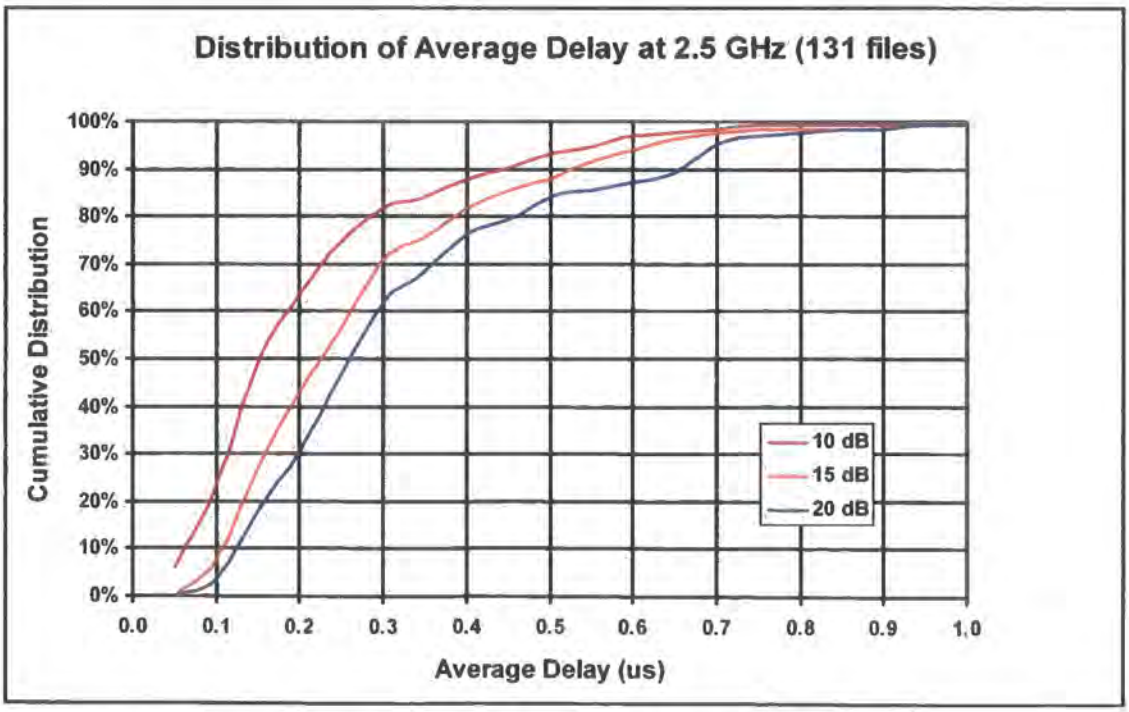

Figure 6.2 Distribution of average delay (Ipswich) at 2.5 GHz

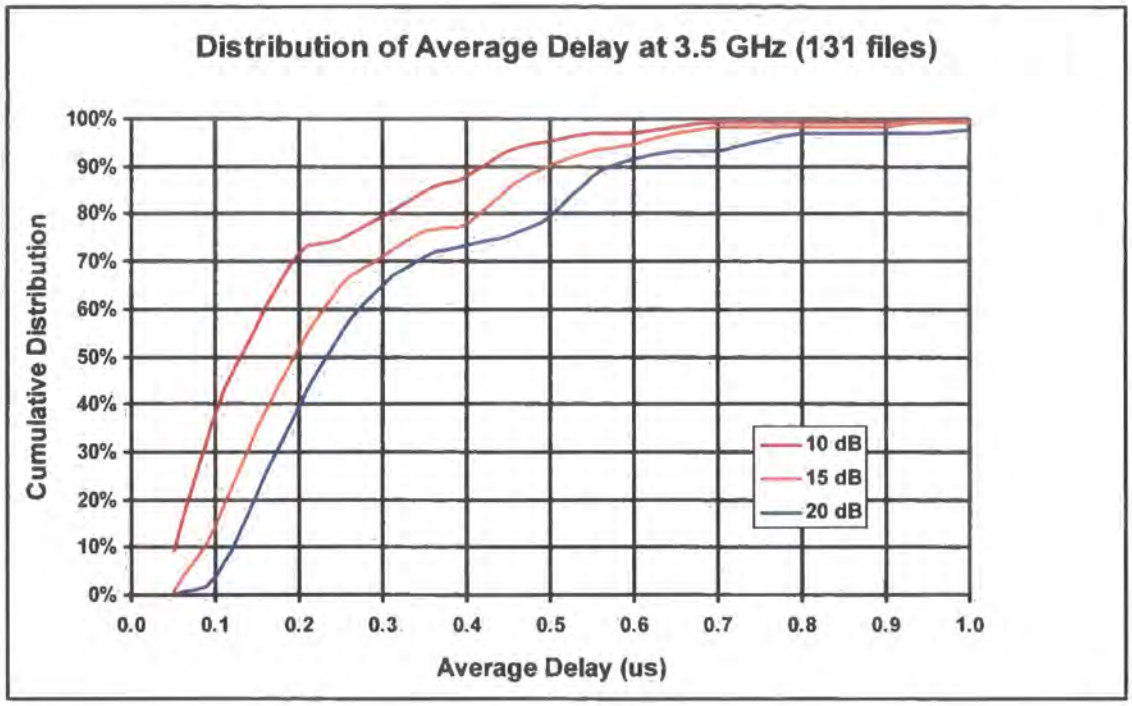

Figure 6.3 Distribution of average delay (Ipswich) at 3.5 GHz

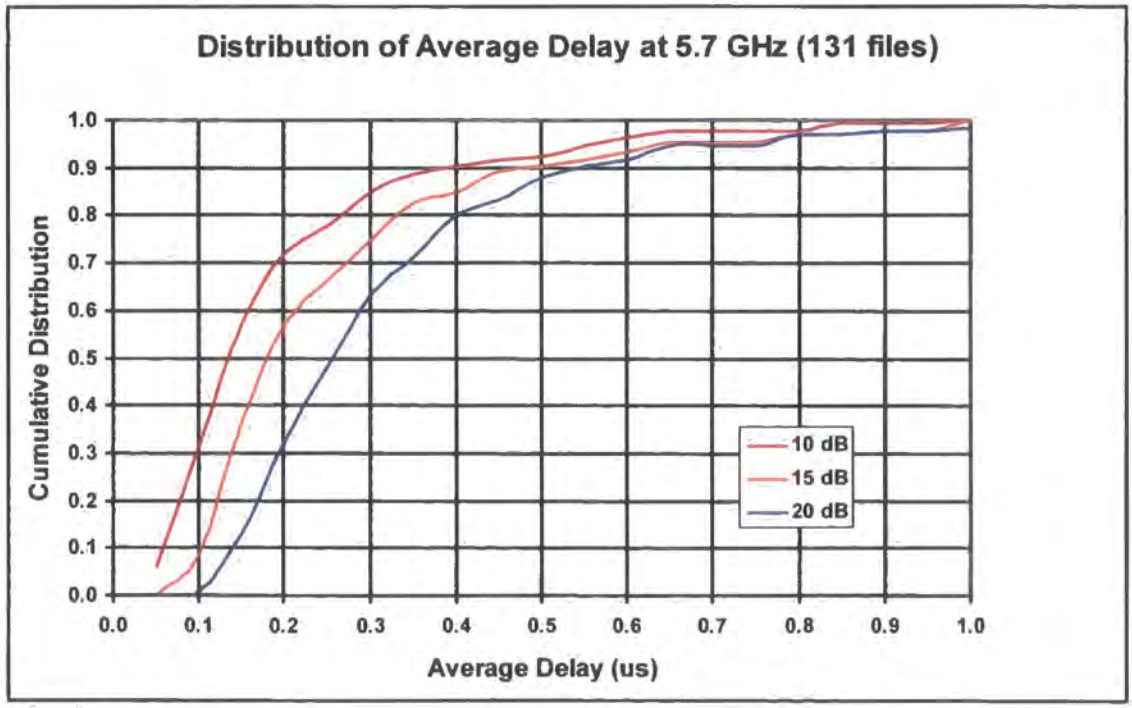

Figure 6.4 Distribution of average delay (Ipswich) at 5.7 GHz

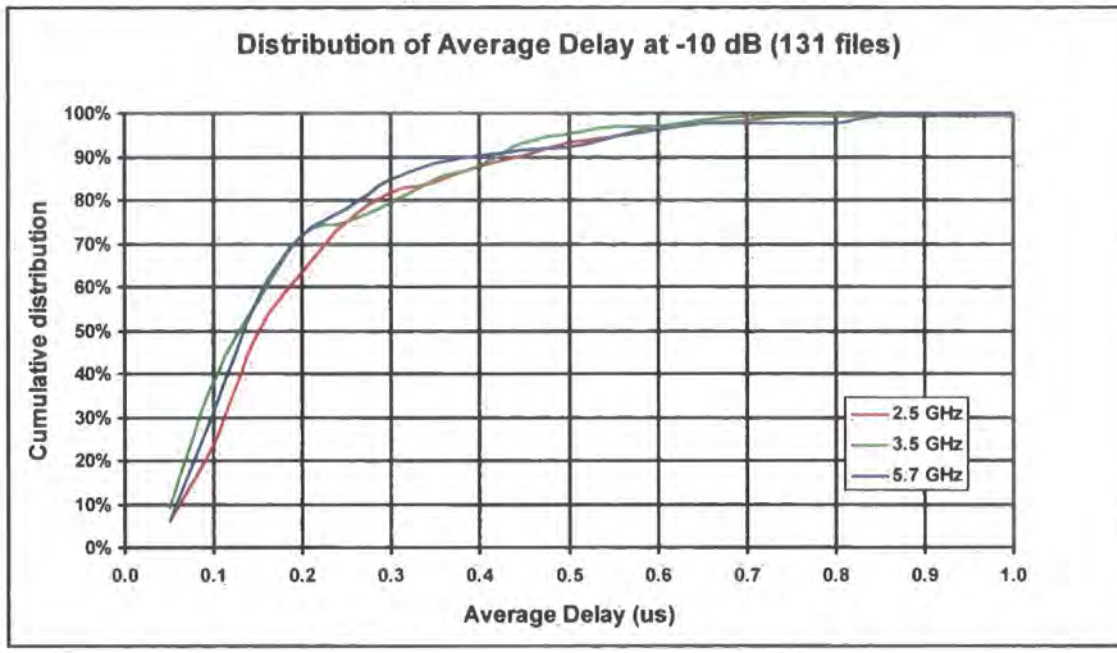

Figure 6.5 Comparison of average delay distributions (Ipswich) at -10 dB

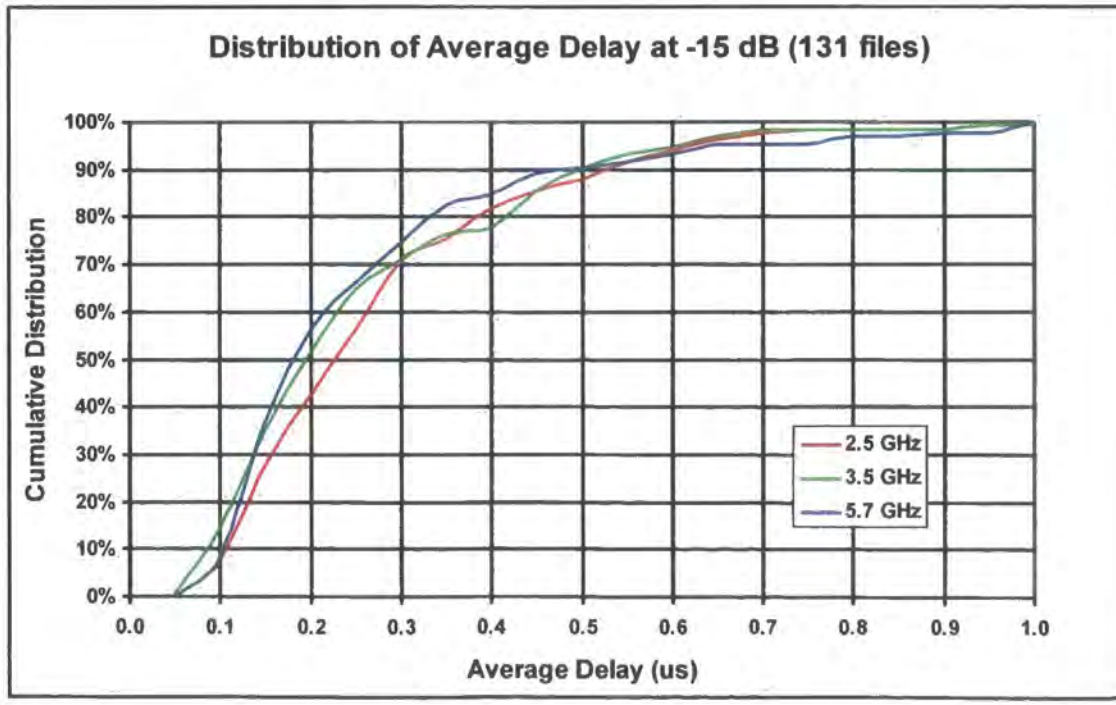

Figure 6.6 Comparison of average delay distributions (Ipswich) at -15 dB

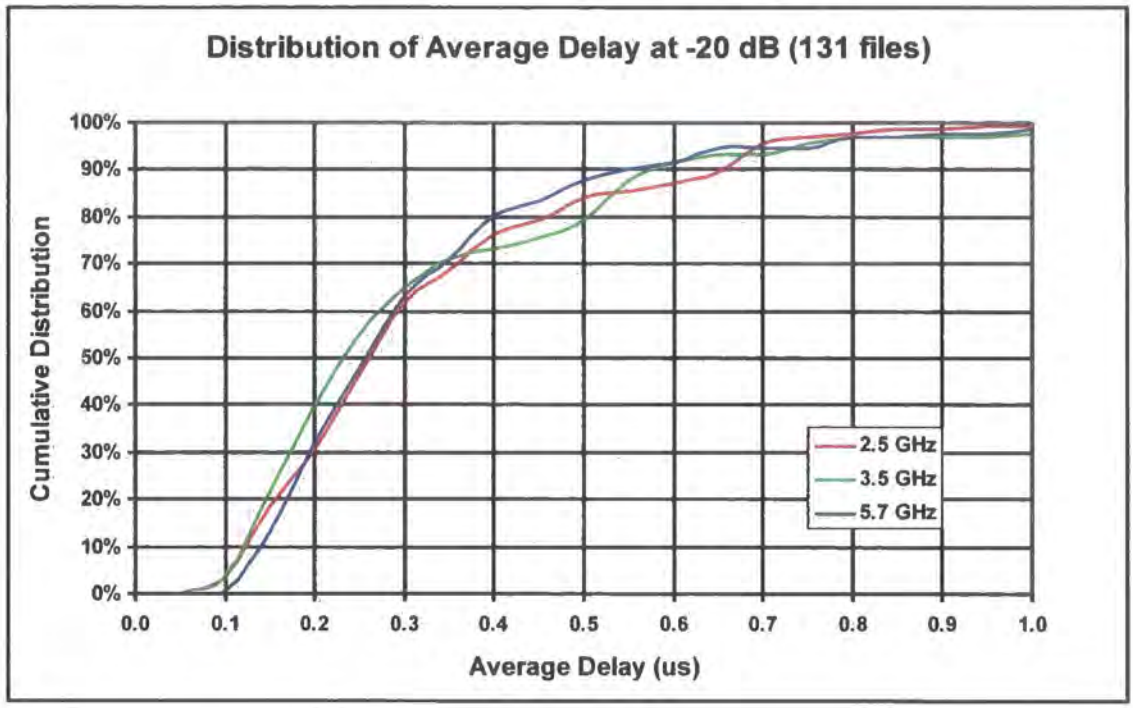

Figure 6.7 Comparison of average delay distributions (Ipswich) at -20 dB

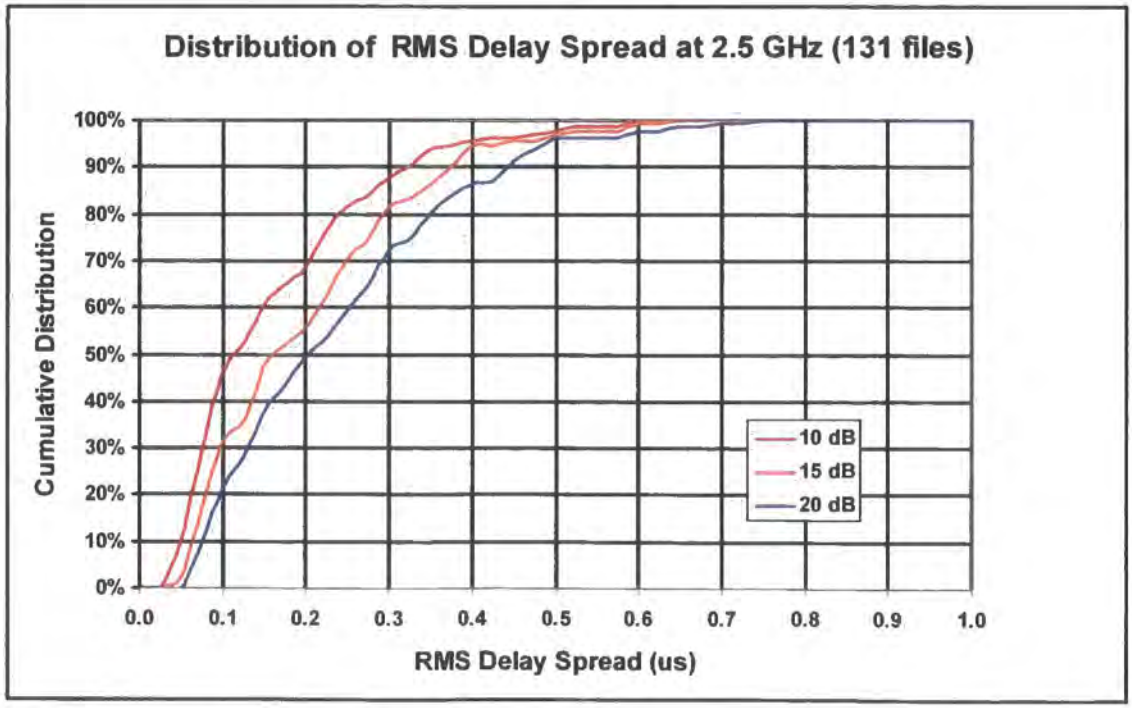

Figure 6.8 Distribution of RMS delay spread (Ipswich) at 2.5 GHz

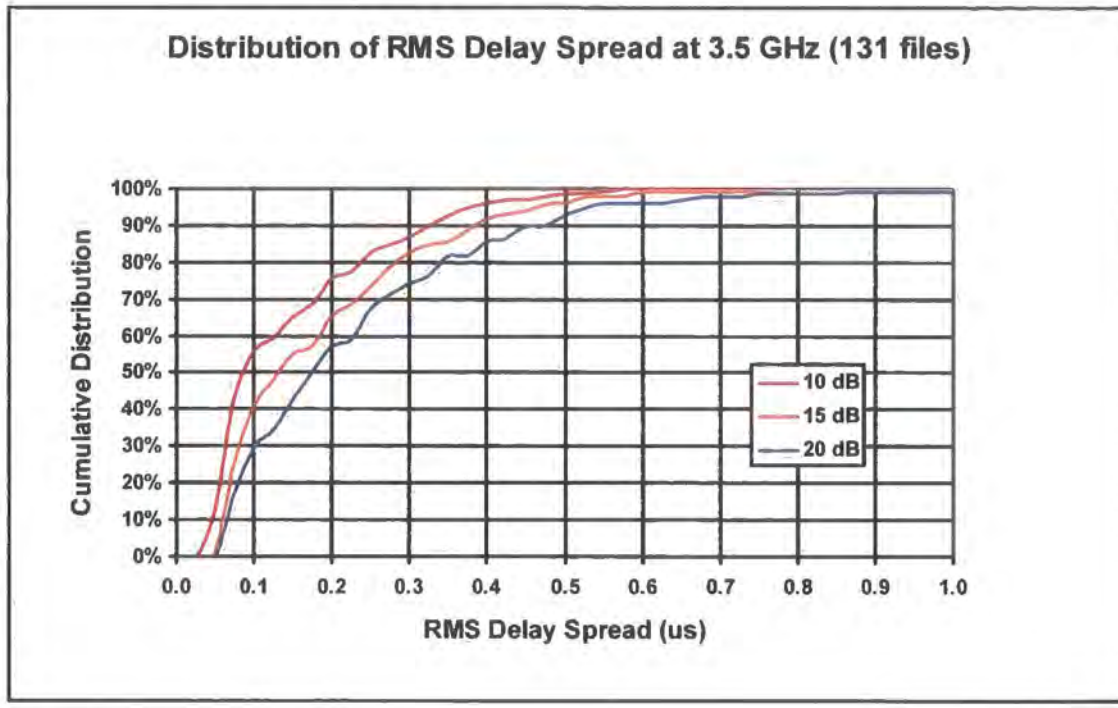

Figure 6.9 Distribution of RMS delay spread (Ipswich) at 3.5 GHz

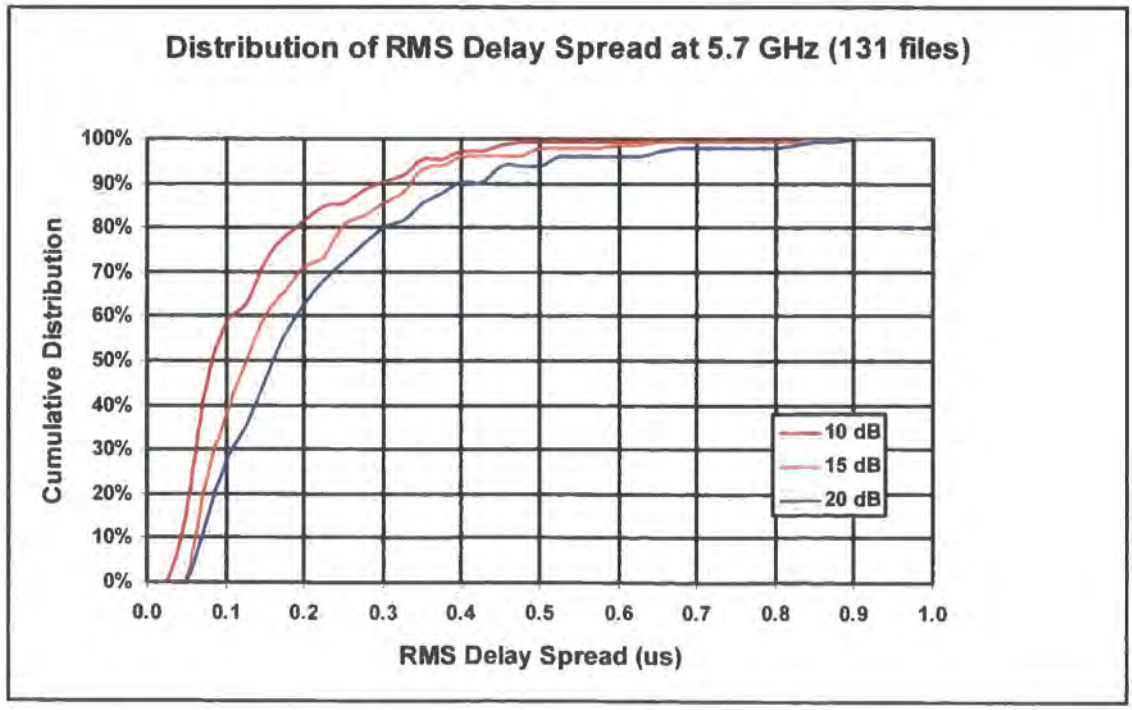

Figure 6.10 Distribution of RMS delay spread (Ipswich) at 5.7 GHz

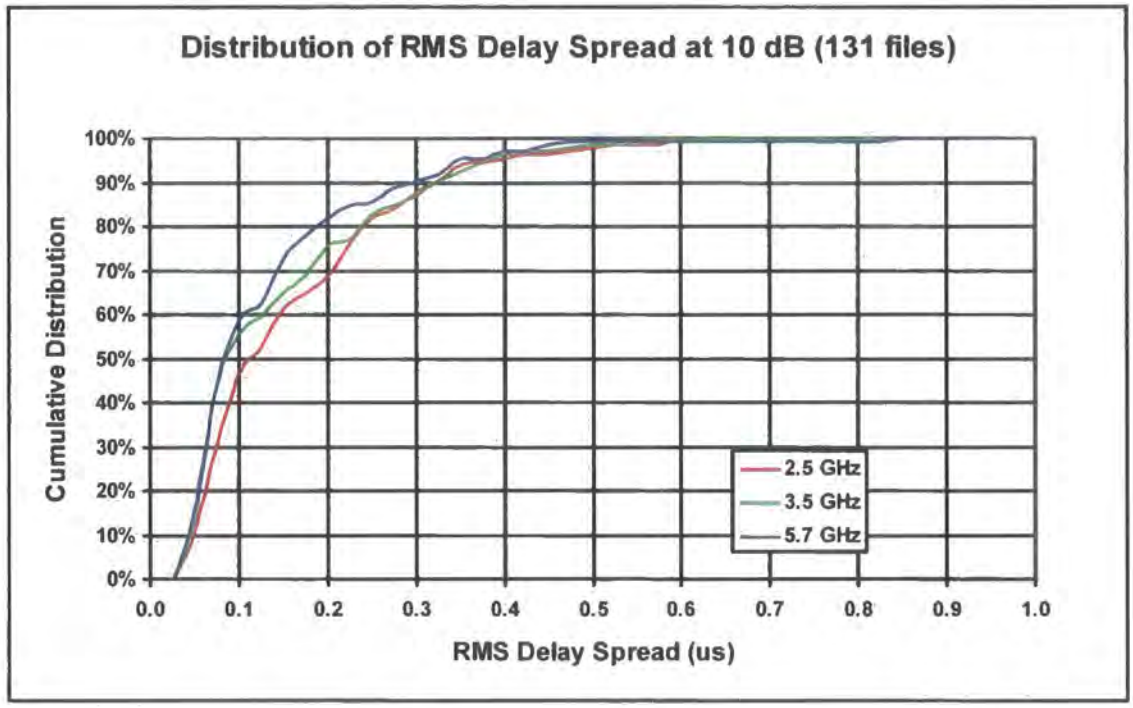

Figure 6.11 Comparison of RMS delay spread distributions (Ipswich) at -10 dB

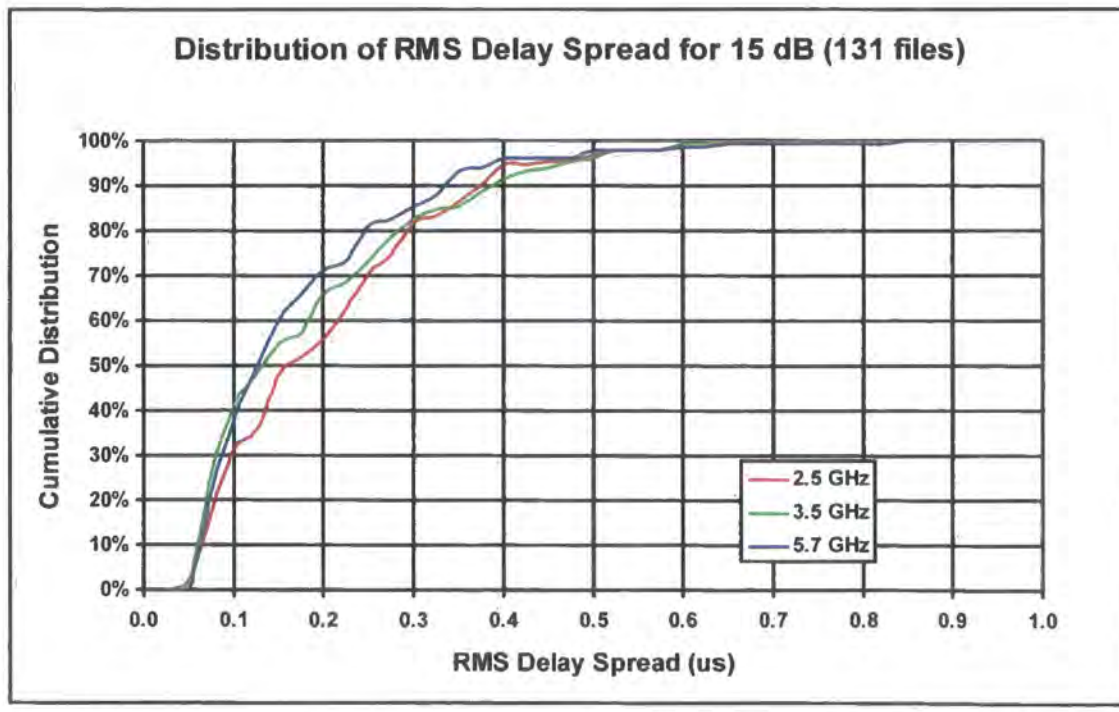

Figure 6.12 Comparison of RMS delay spread distributions (Ipswich) at -15 dB

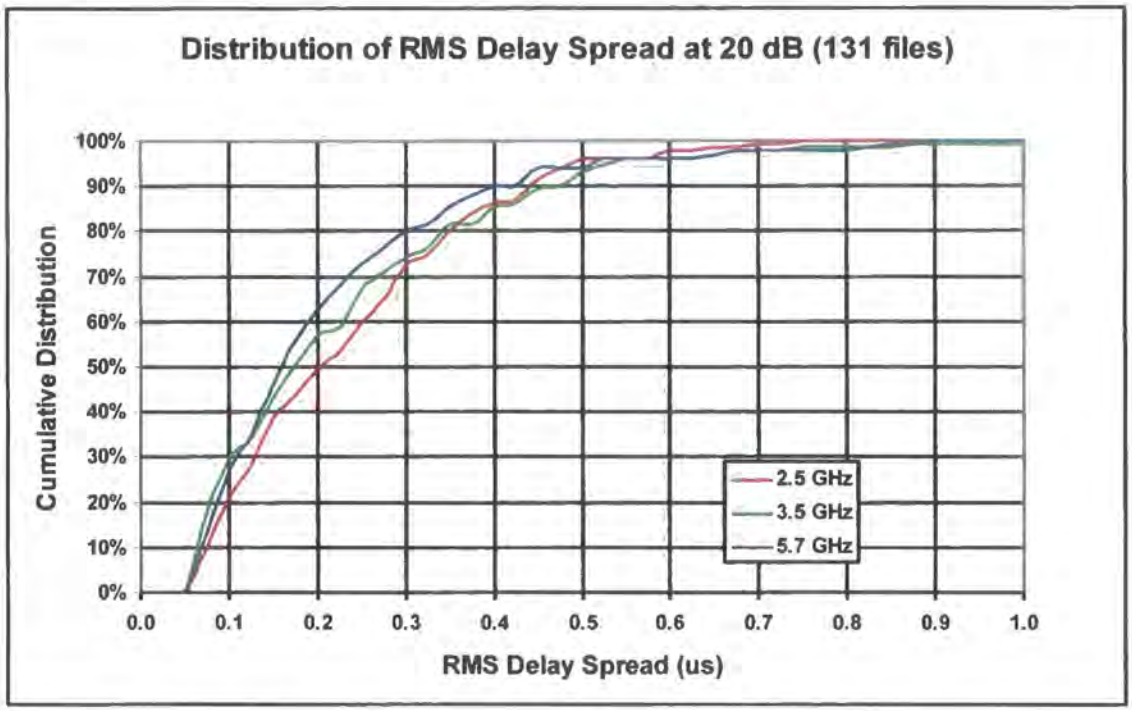

Figure 6.13 Comparison of RMS delay spread distributions (Ipswich) at -20 dB

A subset of the files demonstrate sufficient signal to noise ratio to allow the distributions to be extended for delays corresponding to the -25 dB and -30 dB threshold values. This reduces the sample size to 48 files.

The initial analysis included delay parameters at the -25 dB and -30 dB threshold levels where available. The right shift of the delay distributions as the threshold level is reduced (which is clearly apparent in the above results) was not clearly demonstrated for the -25 dB and -30 dB cases using this "hybrid" set of data.

Higher signal to noise ratios are required to allow observation of the power-delay profile down to -30 dB. It is anticipated that highly scattered paths tend to produce lower signal to noise ratio due to the signal being attenuated as it is scattered in the environment and then being spread across several bins in the power-delay profile. This would tend to skew the data in favour of the lower loss, more direct paths. Thus a valid comparison can only be performed for a population where all files are supported to -30 dB. This reduces the data set to 48 files only.

Results for this restricted set are presented in figures 6.14 to 6.16 (average delay) and figures 6.17 to 6.19 (RMS delay spread). These figures demonstrate that the trend for the distributions to shift to the right (larger delay parameter) as the threshold value of the power delay profile is reduced also applies for the -25 dB and -30 dB thresholds.

Example power delay profiles and channel transfer functions are presented in figures 6.20 through 6.25. (Disturbances on the 2.5 GHz transfer functions are due to self interference which was later corrected).

Figure 6.20 is a power delay profile that exhibits a generally low level of multi-path. Some delay is observable on the wider response for the 2.5 GHz band. Figure 6.21 is the corresponding frequency-transfer function. This shows a small amount of frequency selective behaviour (<2 dB) at 3.5 GHz and 5.7 GHz. The 2.5 GHz transfer function shows significant frequency selective behaviour (~8 dB ripple).

Figure 6.22 is the power delay profile for a channel with significant multi-path present for all three bands. The power delay profile shows the signal arrival followed be decaying echoes in the channel over a period of ~1.5 μs to the -30 dB threshold. This represents a diffused set of scattering events. Figure 6.23 is the corresponding frequency-transfer function which shows significant frequency selective behaviour across all three bands (~8 dB ripple).

Figure 6.24 is an interesting power delay profile that exhibits two distinct peaks in the power delay profile of near equal amplitude. The profile is also similar for all three bands. This represents two signal paths between the transmitter and receiver. This is probably a direct plus a reflection from a plain surface. Figure 6.25 is the corresponding frequency-transfer function for this path.

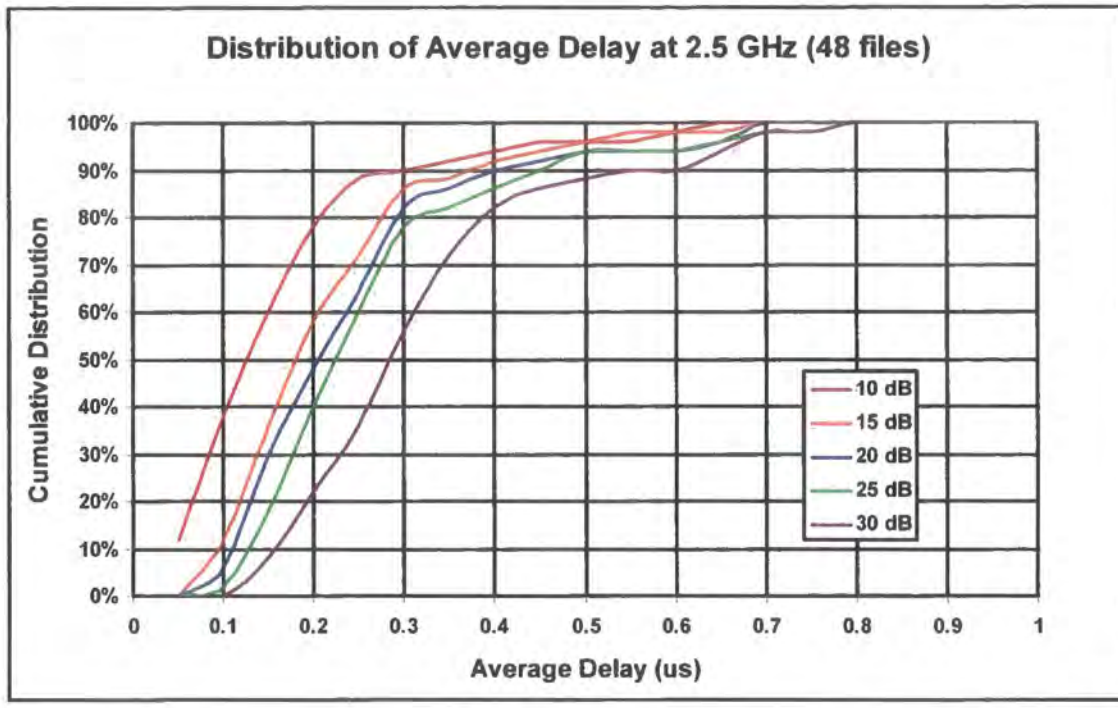

Figure 6.14 Extended distribution of average delay (Ipswich) at 2.5 GHz

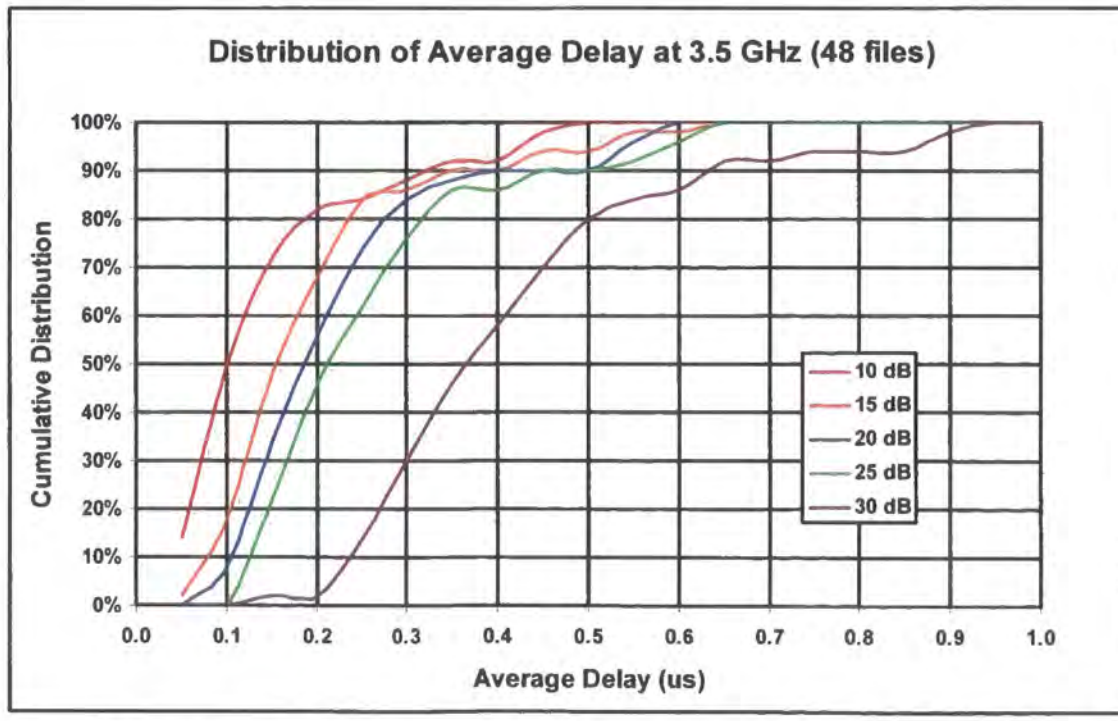

Figure 6.15 Extended distribution of average delay (Ipswich) at 3.5 GHz

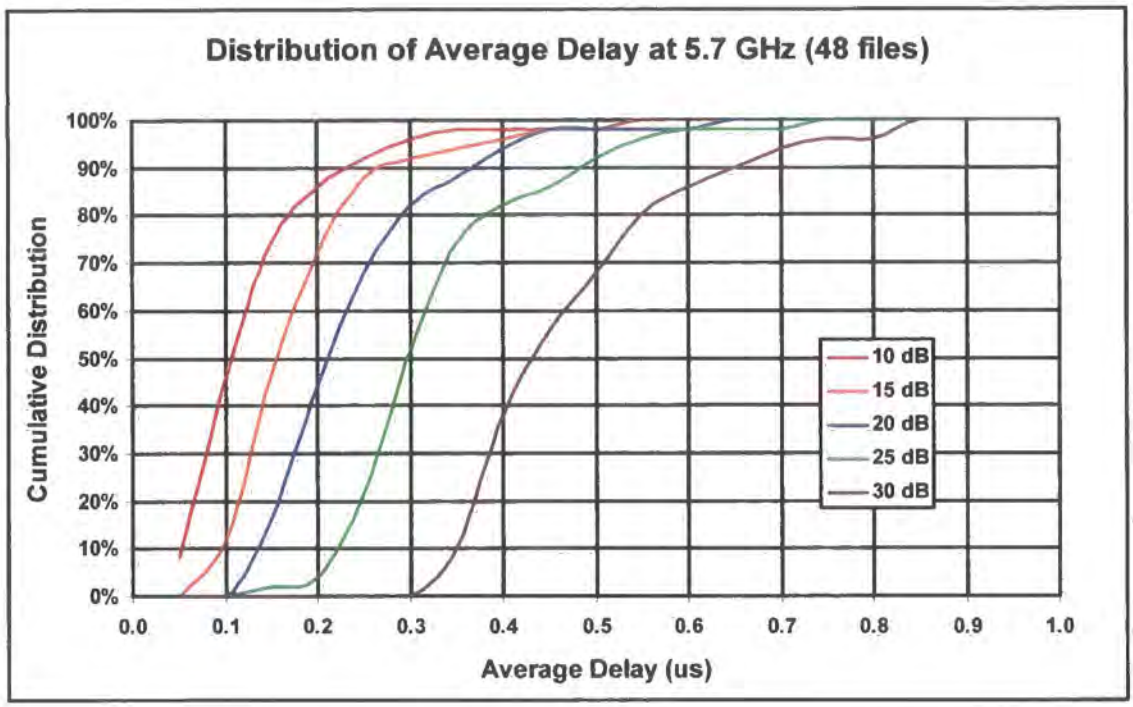

Figure 6.16 Extended distribution of average delay (Ipswich) at 5.7 GHz

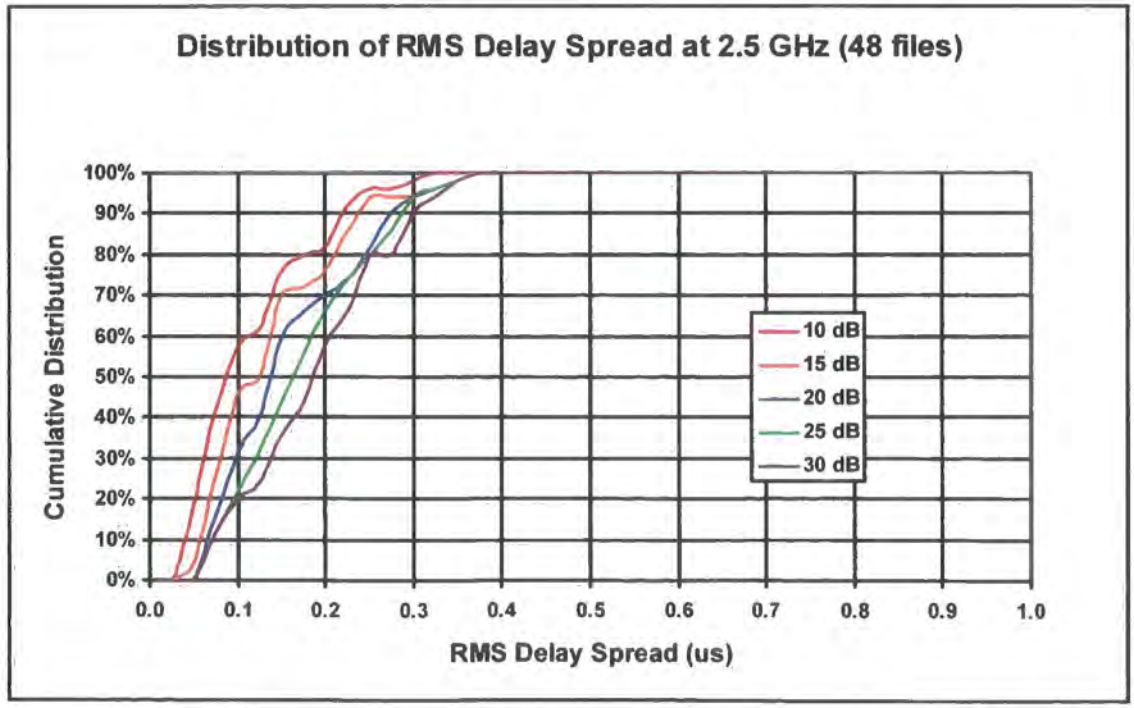

Figure 6.17 Extended distribution of RMS delay spread (Ipswich) at 2.5 GHz

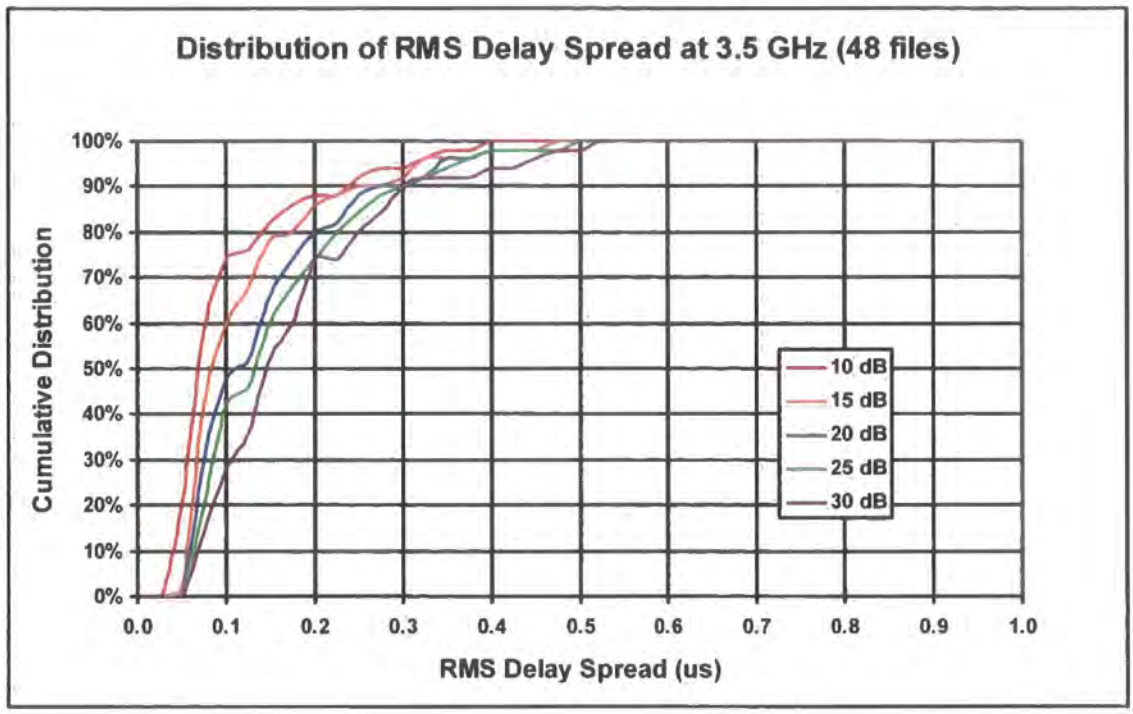

Figure 6.18 Extended distribution of RMS delay spread (Ipswich) at 3.5 GHz

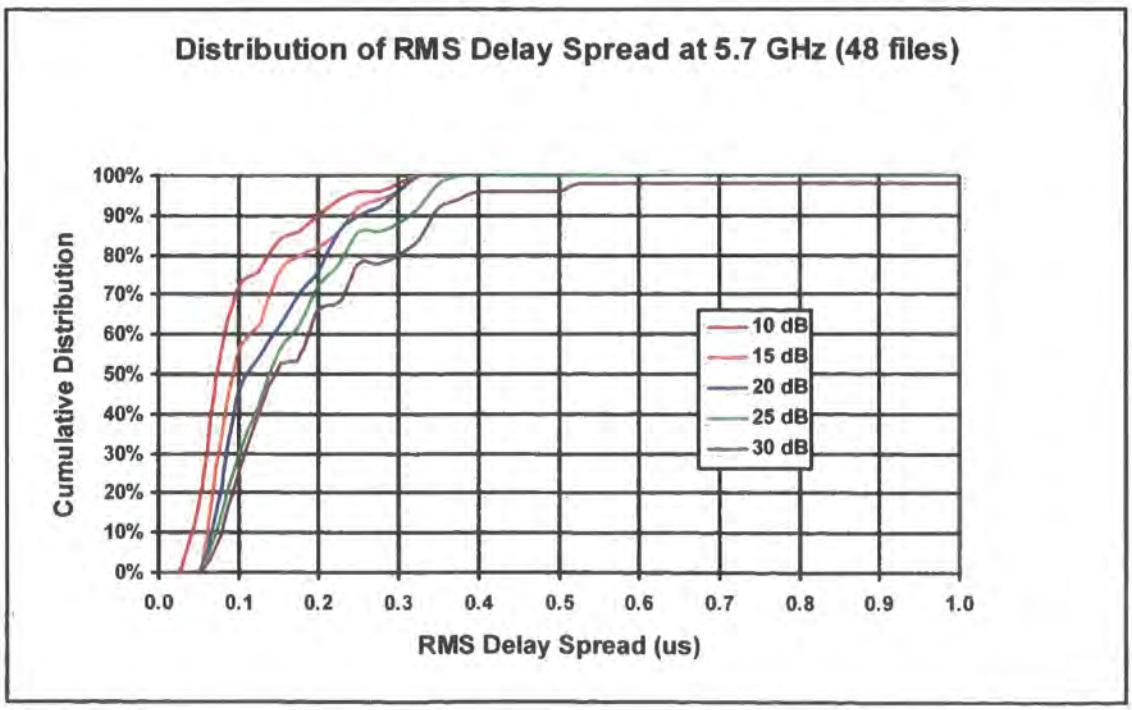

Figure 6.19 Extended distribution of RMS delay spread (Ipswich) at 5.7 GHz

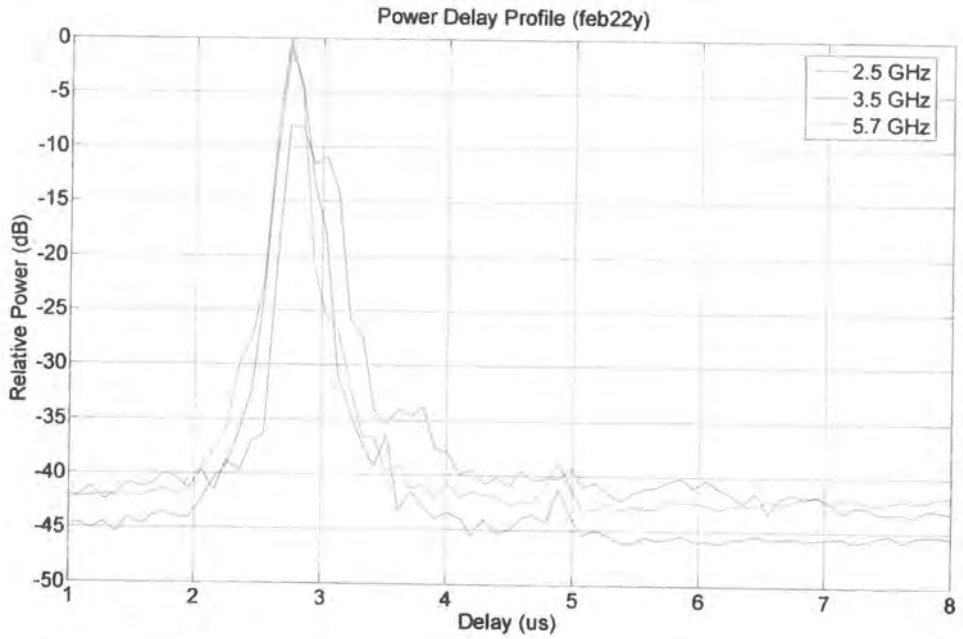

Figure 6.20 3-band 10 MHz sweep power delay profile with moderate multi-path

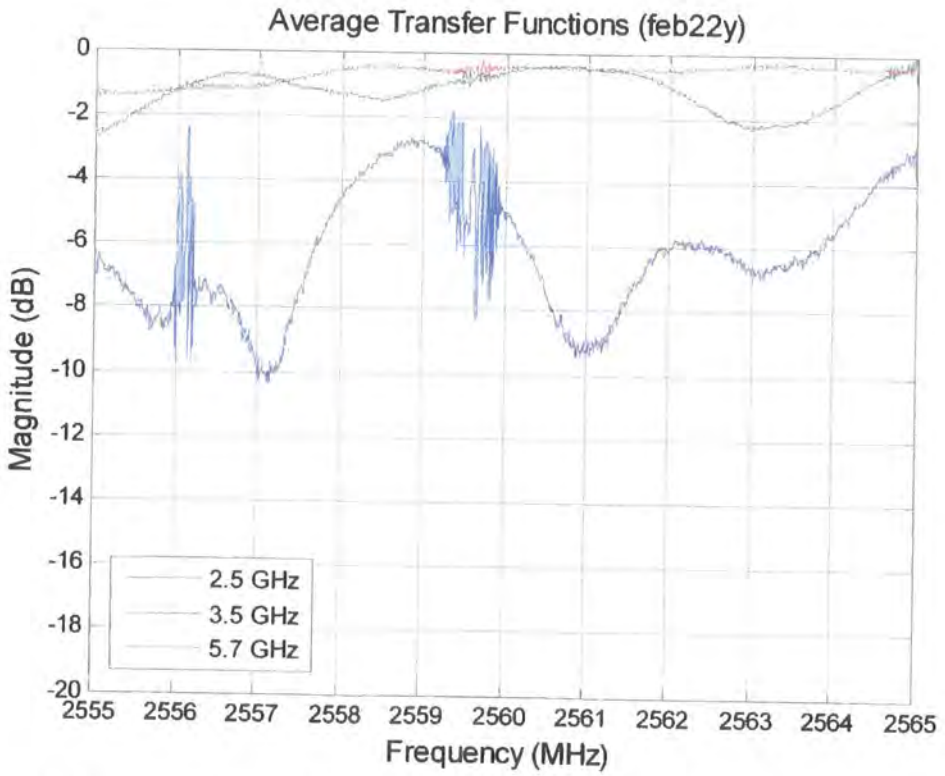

Figure 6.21 Example of channel transfer function with moderate multi-path

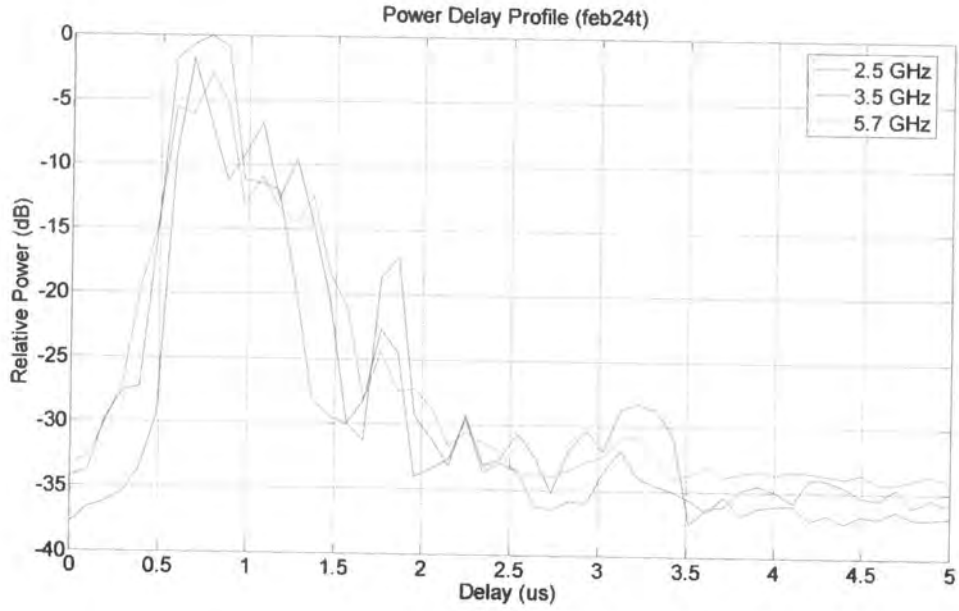

Figure 6.22 Example power delay profile with multi-path

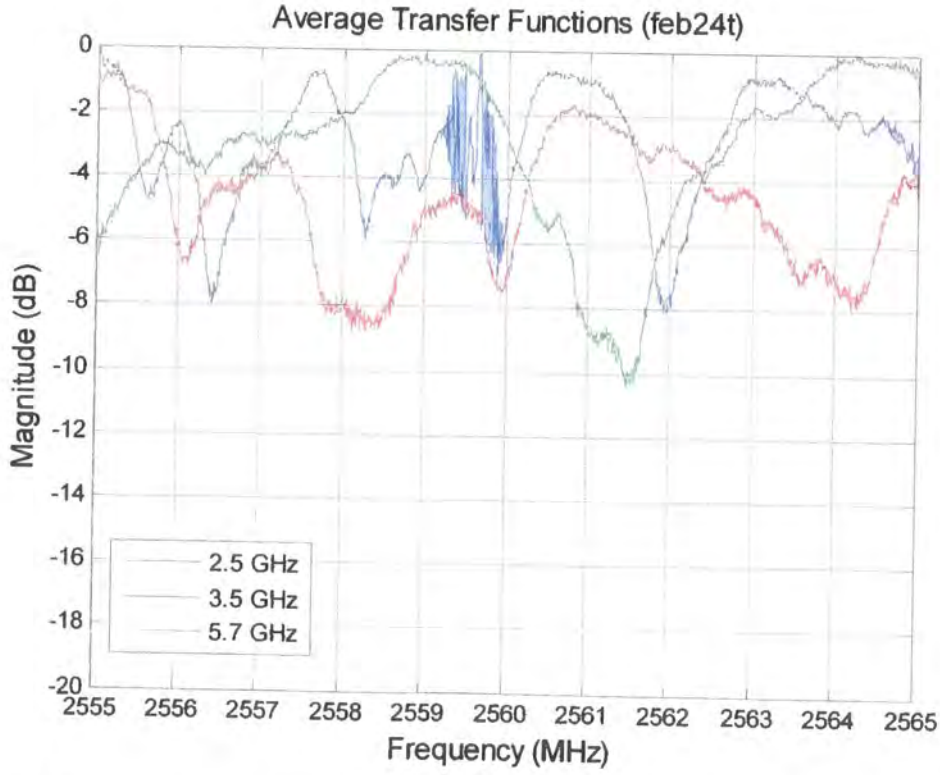

Figure 6.23 Example channel transfer function with multi-path

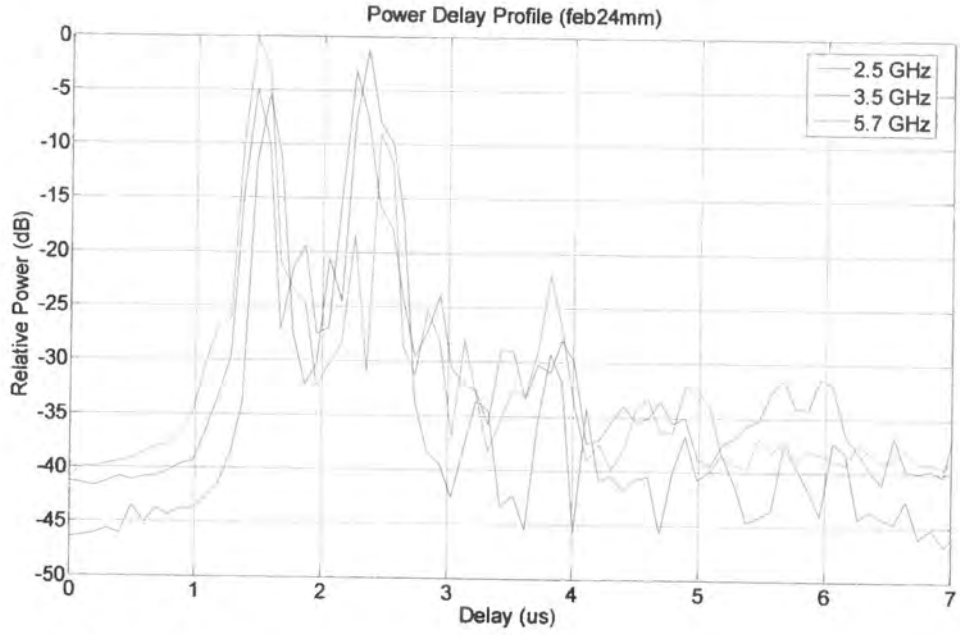

Figure 6.24 Example power delay profile with discrete multi-path

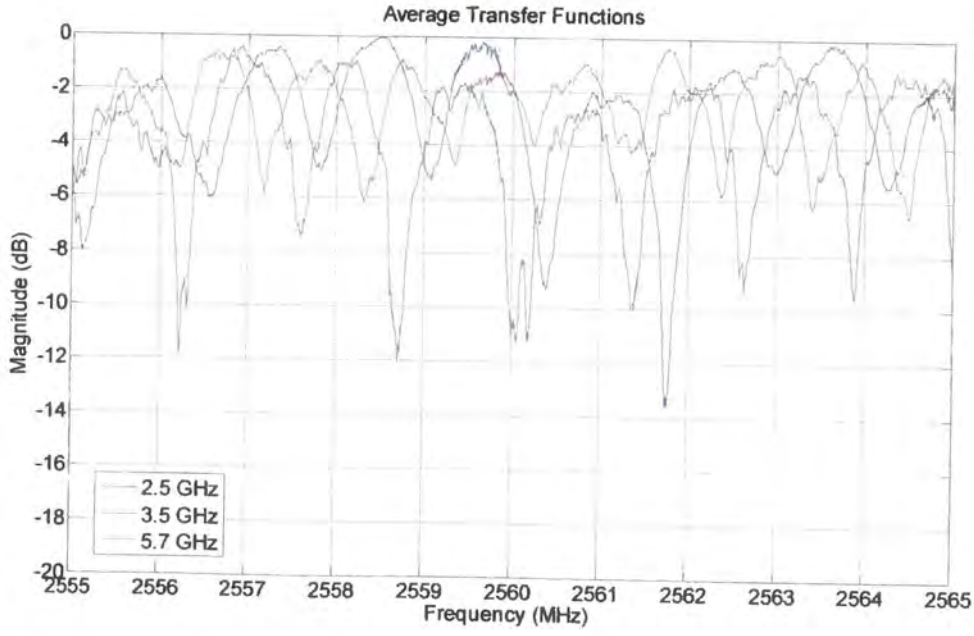

Figure 6.25 Example channel transfer function with discrete multi-path

6.3 Three-band sounding indoors

The channel sounder was operated in a three band configuration with a channel width of 150 MHz simultaneously in the 2.5 GHz, 3.5 GHz and 5.7 GHz bands. Three different transmitter locations were used in the Durham school of engineering. The receiver was then moved to different locations and the channel sounding was recorded. A total of 96 files were recorded with a power delay profile that could be used down to 30 dB below the peak. Of these, 8 files were recorded with the receiver outside the building.

The distribution of the average delay measurements are shown in figures 6.26 to 6.28 for each of the three bands. Figures 6.29 to 6.33 provide a comparison of the average delay distribution between the bands for the -10 dB, -15 dB, -20 dB, -25 dB and -30 dB thresholds. The 50% and 90% intervals of the distribution are recorded in table 6.3.

Threshold value	Interval	Frequency			Delay
		2.5 GHz	3.5 GHz	5.7 GHz	
10 dB	50%	22	19	22	ns
	90%	47	44	53	ns
15 dB	50%	27	24	30	ns
	90%	59	53	70	ns
20 dB	50%	32	30	38	ns
	90%	71	59	73	ns
25 dB	50%	35	32	40	ns
	90%	77	65	80	ns
30 dB	50%	40	37	44	ns
	90%	90	77	85	ns

Table 6.3 Average delay measured indoors

The distribution of the average delay measurements are shown in figures 6.34 to 6.36 for each of the three bands. Figures 6.37 to 6.41 provide a comparison of the RMS delay spread distribution between the bands for the -10 dB, -15 dB, -20 dB, -25 dB and -30 dB thresholds. The 50% and 90% intervals of the distribution are recorded in table 6.4.

Threshold value	Interval	Frequency			Delay
		2.5 GHz	3.5 GHz	5.7 GHz	
10 dB	50%	16	15	15	ns
	90%	33	30	37	ns
15 dB	50%	20	20	22	ns
	90%	42	37	37	ns
20 dB	50%	23	22	22	ns
	90%	45	42	42	ns
25 dB	50%	26	24	30	ns
	90%	48	43	54	ns
30 dB	50%	28	26	33	ns
	90%	49	43	46	ns

Table 6.4 RMS delay spread measured indoors

Figure 6.42 shows the power delay profile recorded while moving the receiver towards the transmitter. This demonstrates a very similar power delay profile for the three bands.

Figures 6.43 to 6.45 show the delay / Doppler plots for the three bands. All three demonstrate positive Doppler shifts that scale with frequency (red line is the contour at 5 dB below the peak).

Figure 6.46 shows the power delay profile recorded at nominally the same location as presented in figure 6.42. This time the movement of the receiver is away from the transmitter. This also shows very similar power delay profile for the three bands.

Figures 6.47 to 6.49 show the delay / Doppler plots for the three bands. All three demonstrate negative Doppler shifts that scale with frequency (red line is the contour at 5 dB below the peak).

Figure 6.50 shows a power delay profile that was measured across the indoor / outdoor boundary. This shows quite frequency selective behaviour. This is shown for the individual bands in figure 6.51 to 6.53.

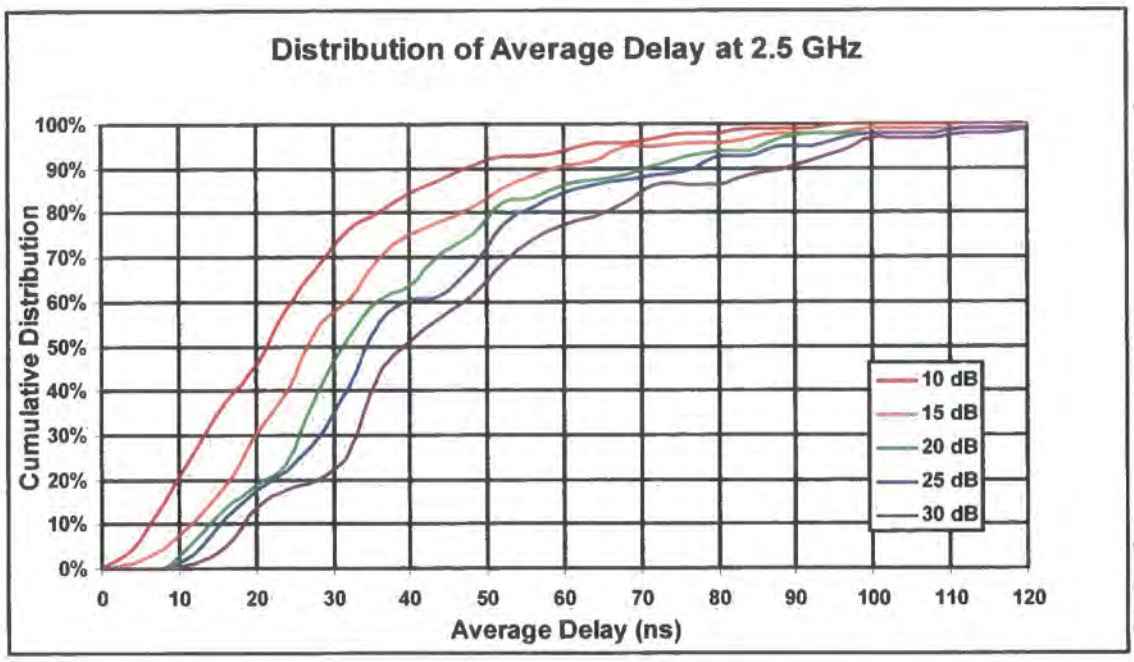

Figure 6.26 Distribution of average delay (indoors) at 2.5 GHz

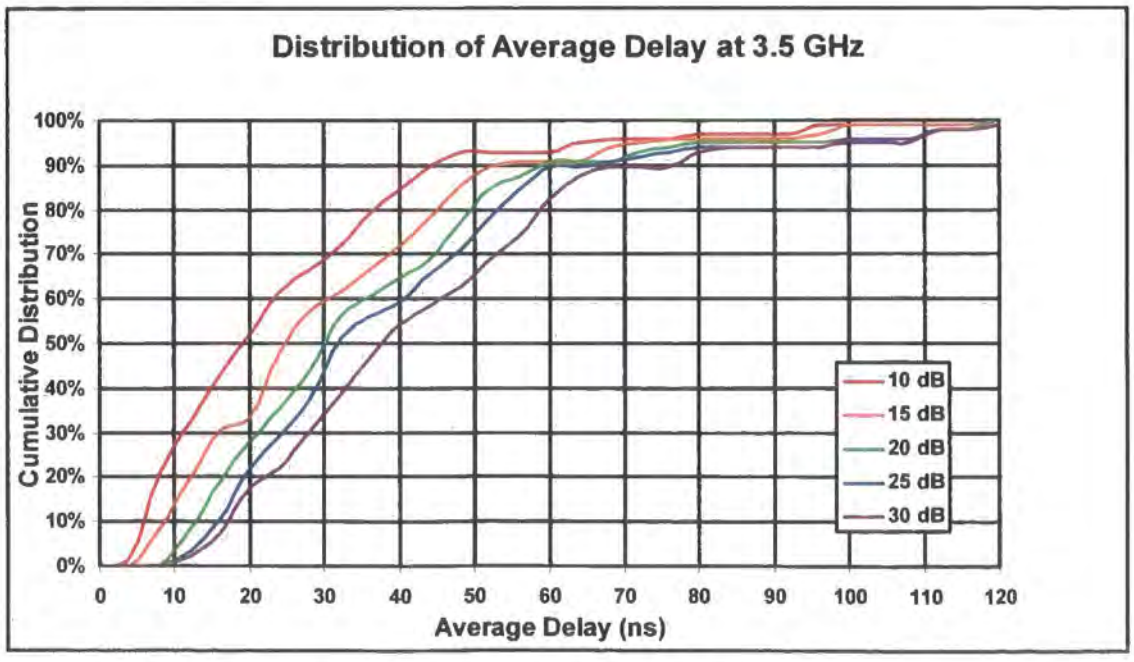

Figure 6.27 Distribution of average delay (indoors) at 3.5 GHz

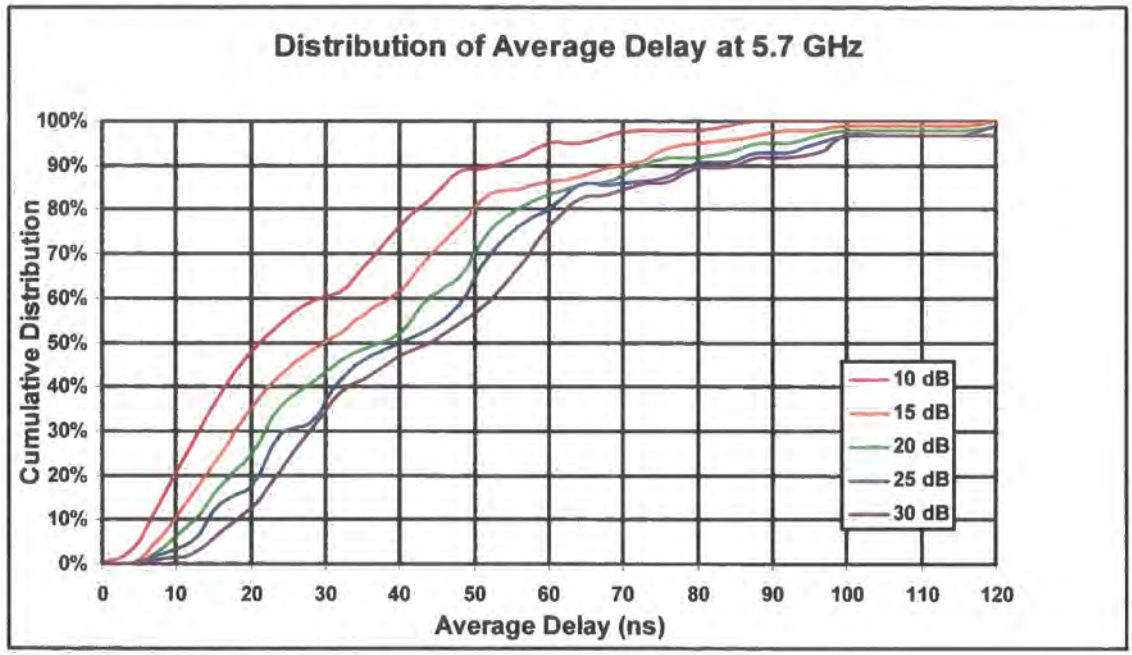

Figure 6.28 Distribution of average delay (indoors) at 5.7 GHz

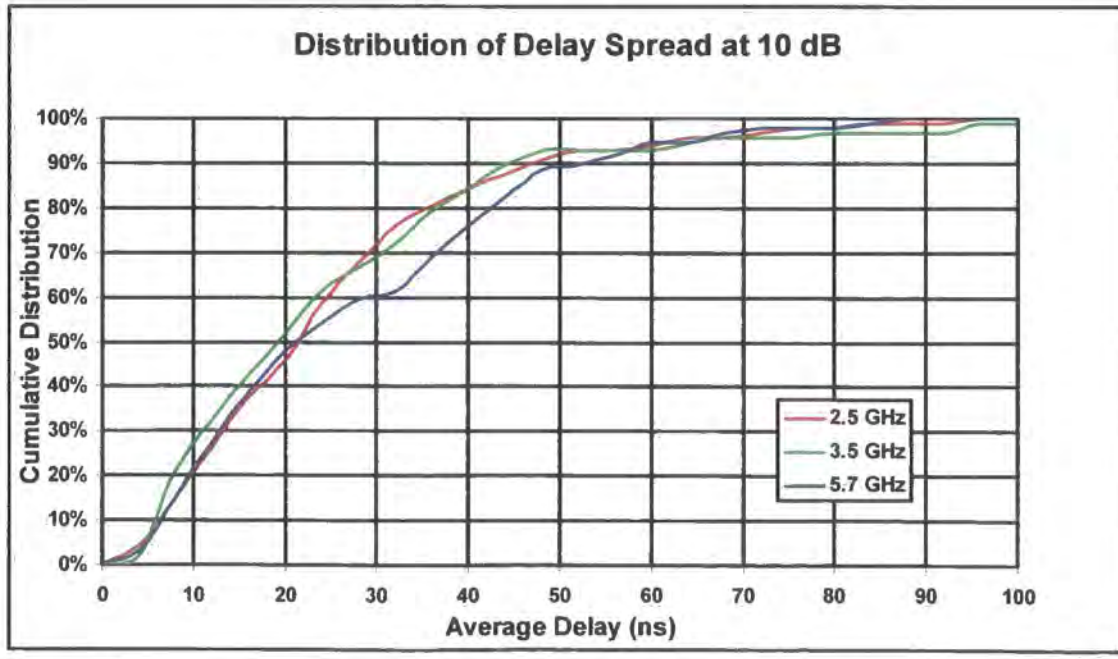

Figure 6.29 Comparison of average delay distributions (indoors) at -10 dB

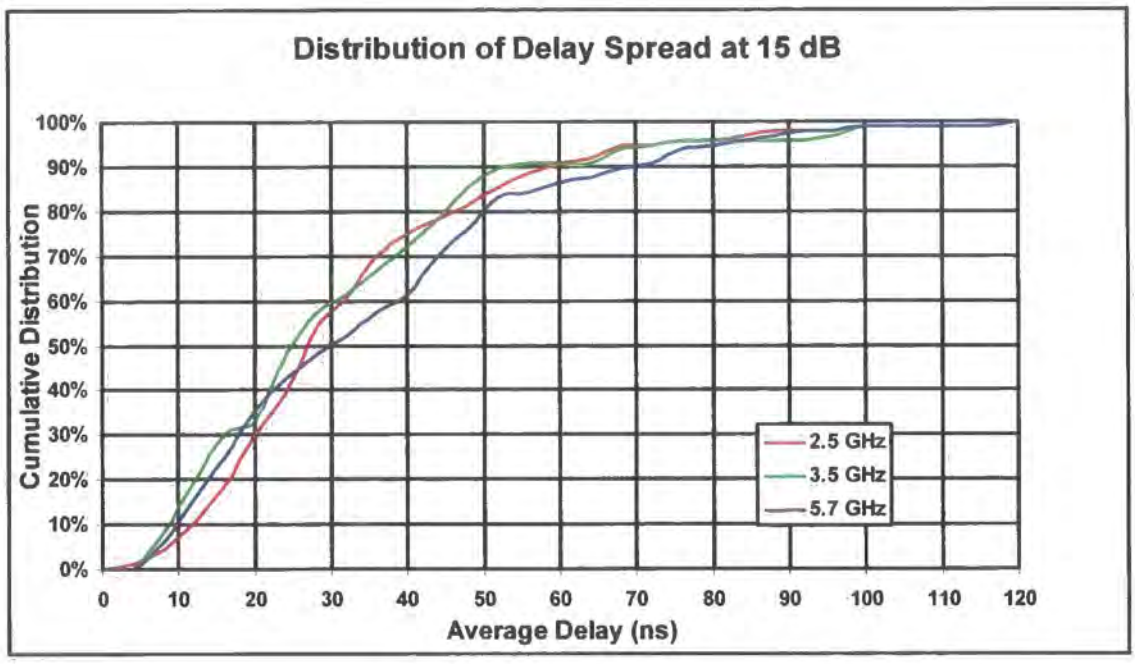

Figure 6.30 Comparison of average delay distributions (indoors) at -15 dB

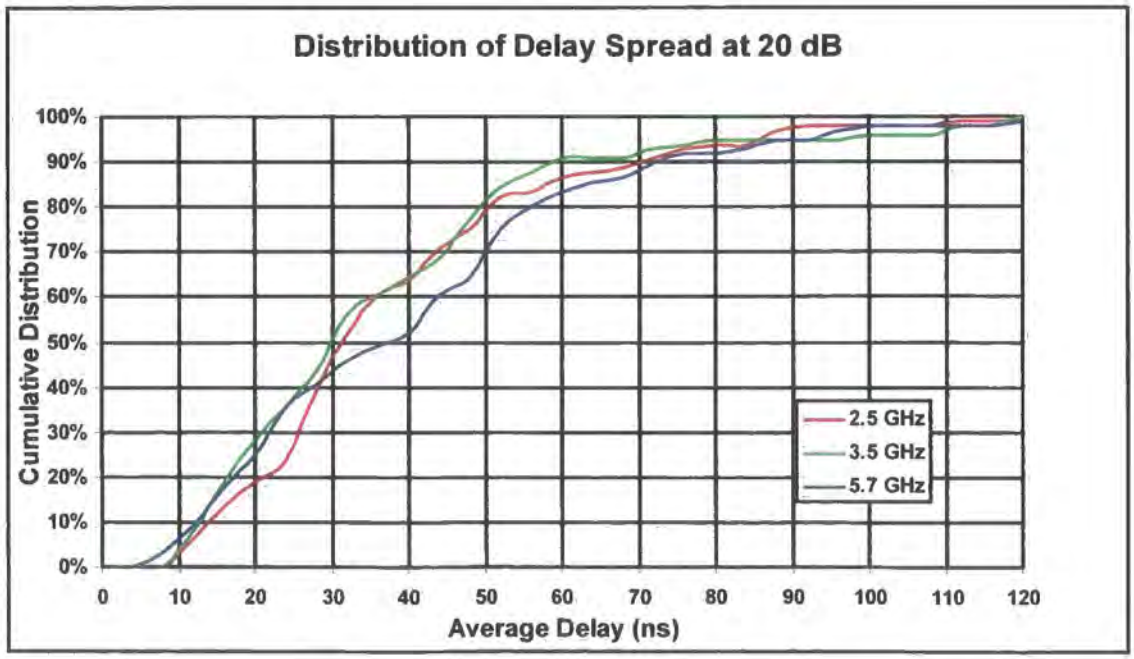

Figure 6.31 Comparison of average delay distributions (indoors) at -20 dB

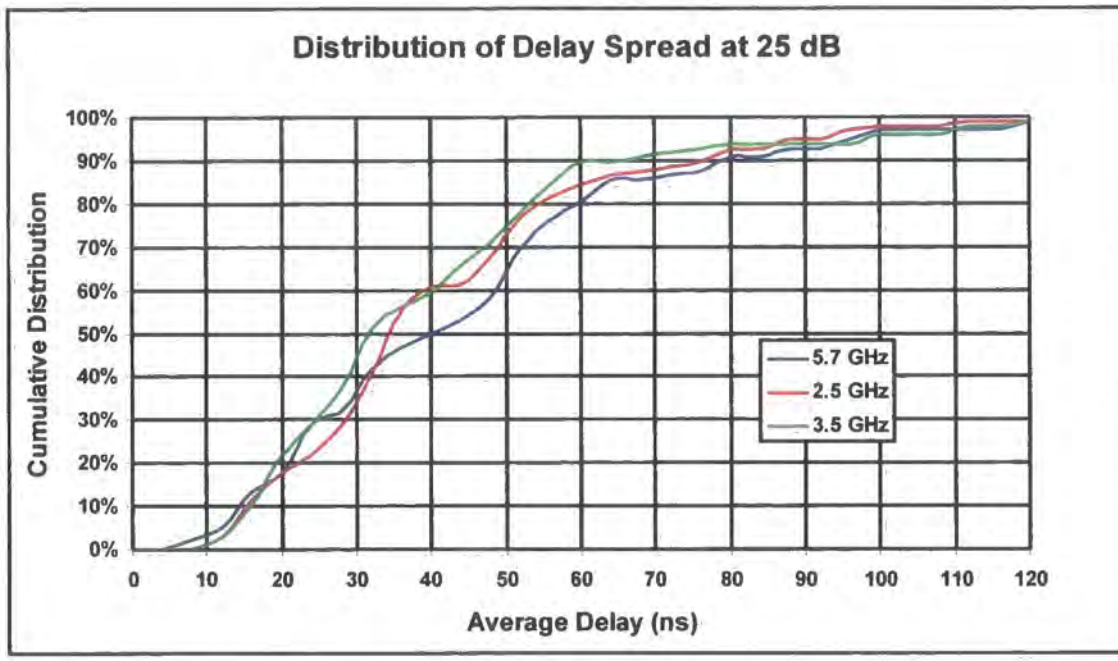

Figure 6.32 Comparison of average delay distributions (indoors) at -25 dB

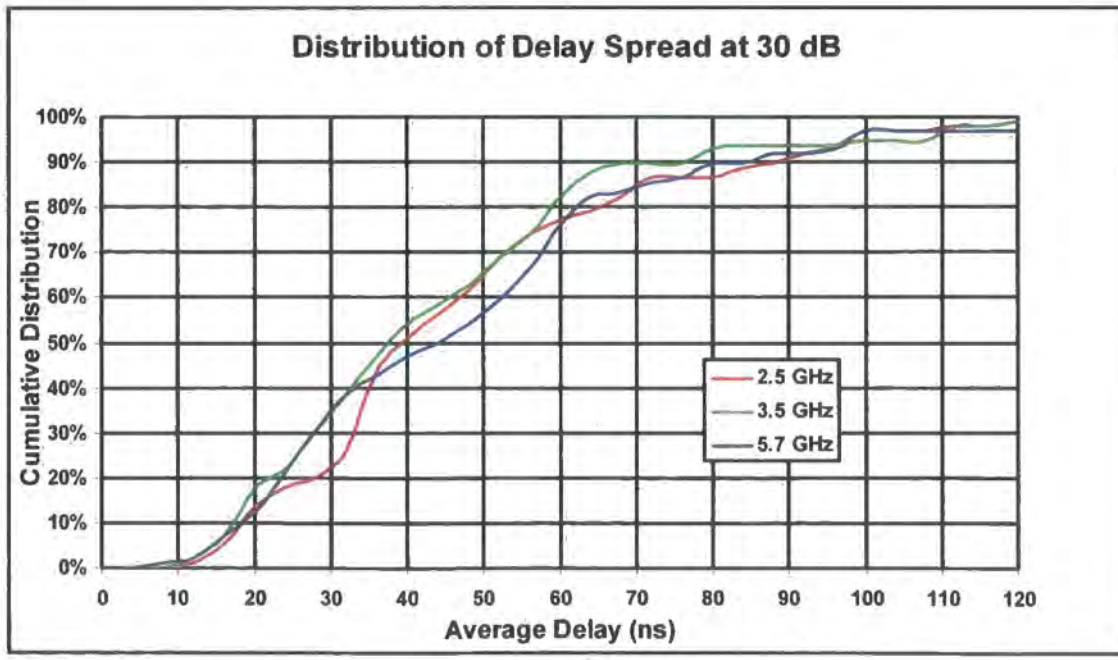

Figure 6.33 Comparison of average delay distributions (indoors) at -30 dB

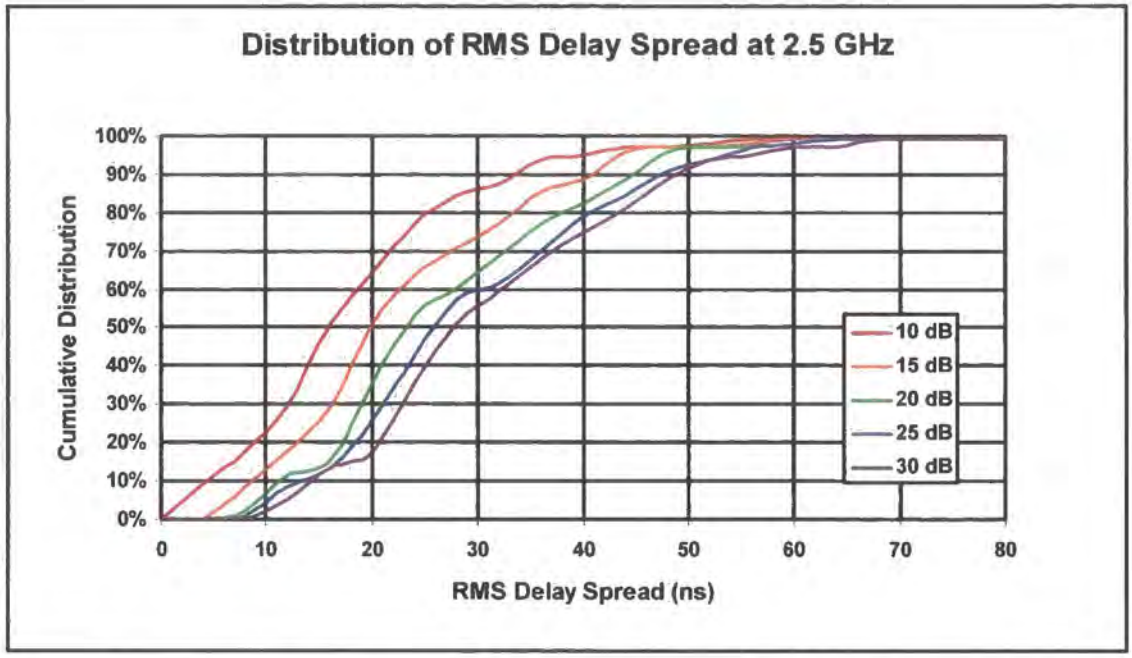

Figure 6.34 Distribution of RMS delay spread (indoors) at 2.5 GHz

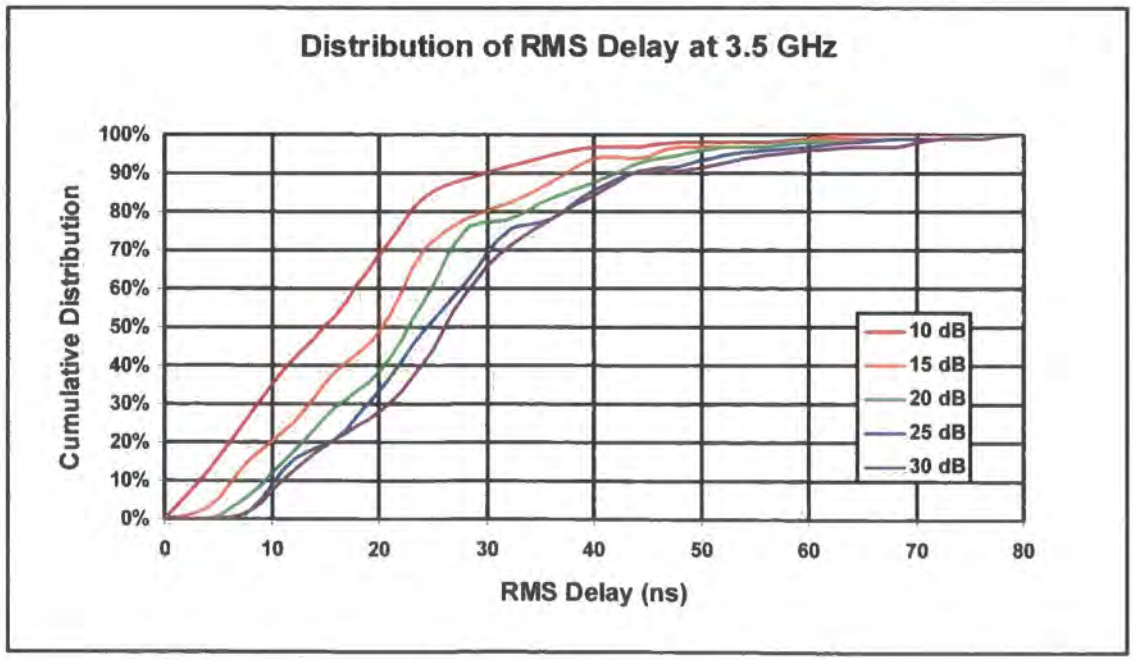

Figure 6.35 Distribution of RMS delay spread (indoors) at 3.5 GHz

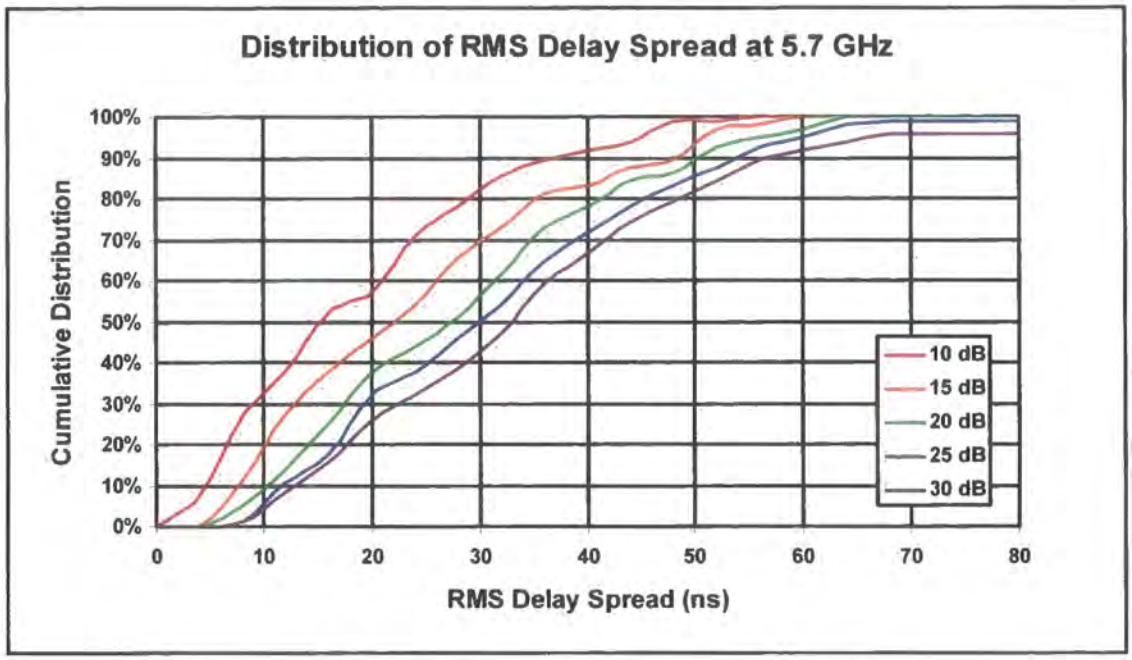

Figure 6.36 Distribution of RMS delay spread (indoors) at 5.7 GHz

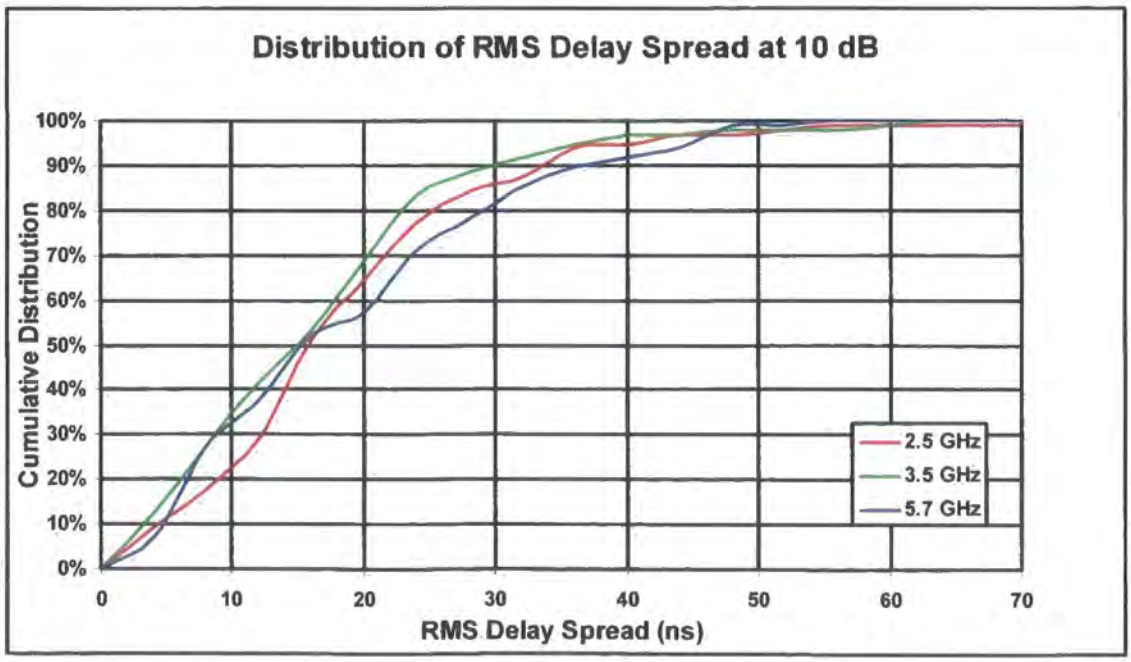

Figure 6.37 Comparison of RMS delay spread distributions (indoors) at -10 dB

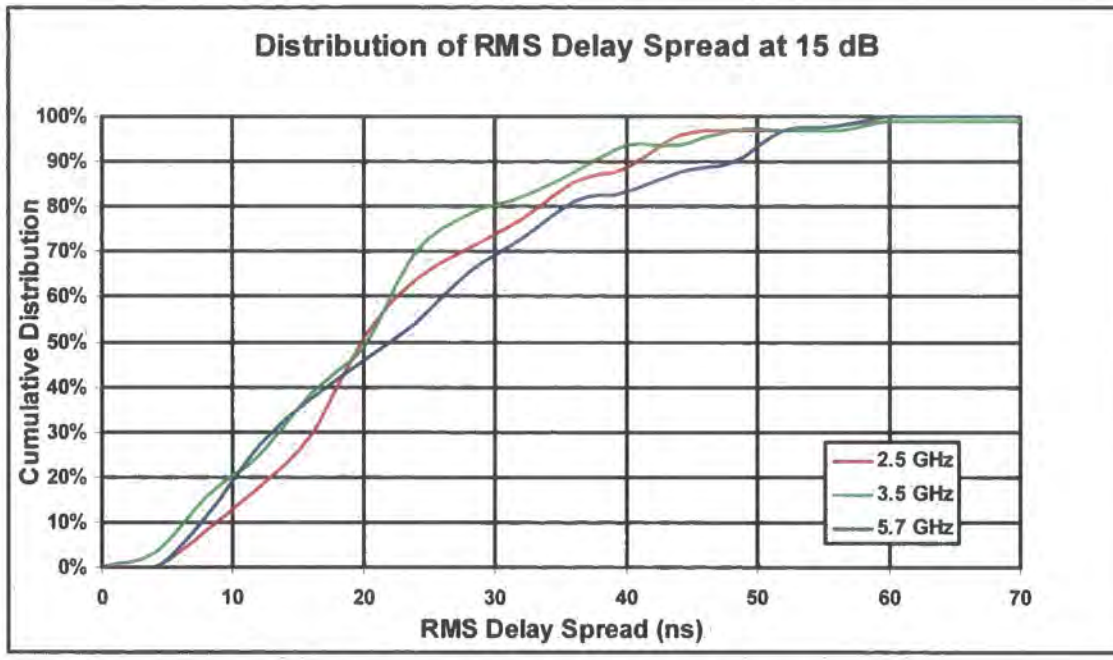

Figure 6.38 Comparison of RMS delay spread distributions (indoors) at -15 dB

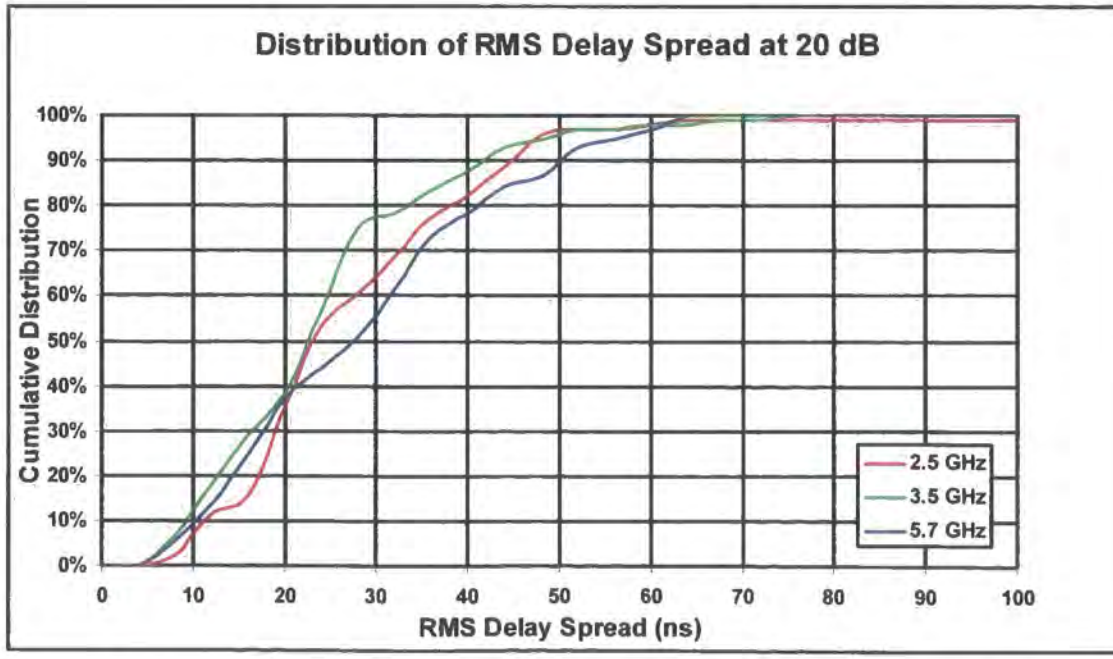

Figure 6.39 Comparison of RMS delay spread distributions (indoors) at -20 dB

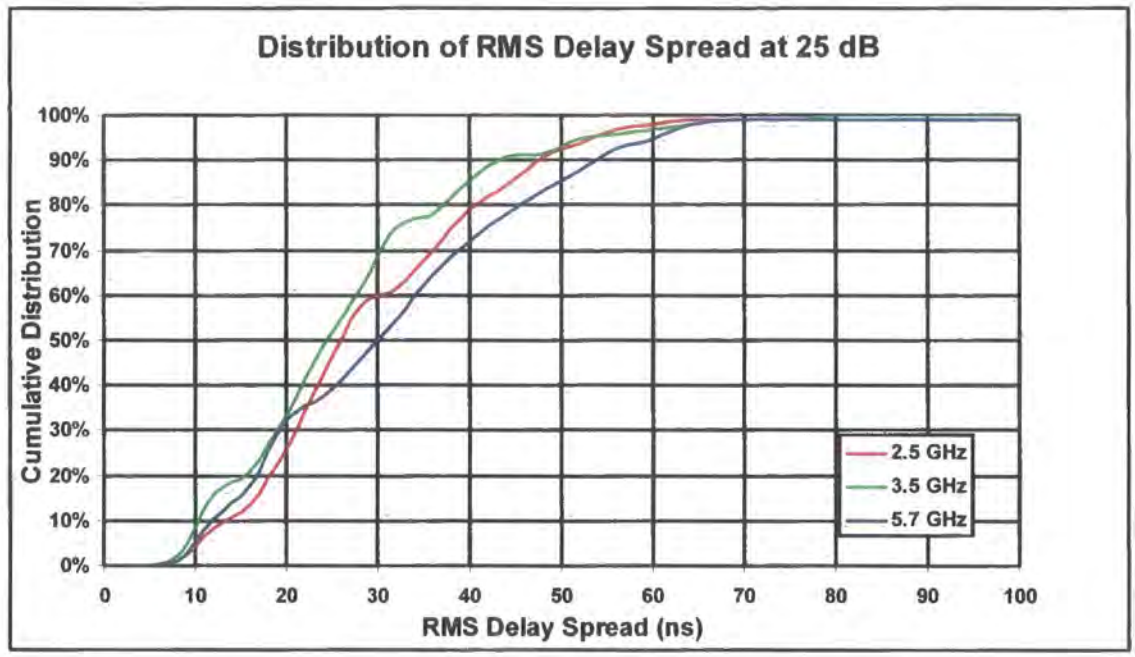

Figure 6.40 Comparison of RMS delay spread distributions (indoors) at -25 dB

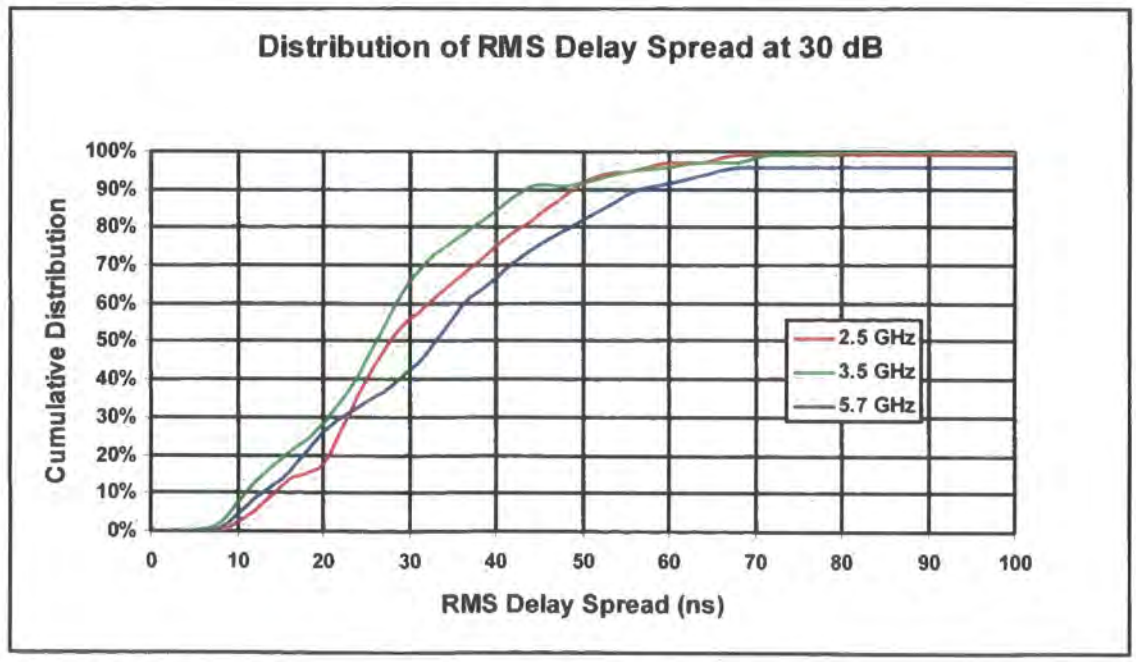

Figure 6.41 Comparison of RMS delay spread distributions (indoors) at -30 dB

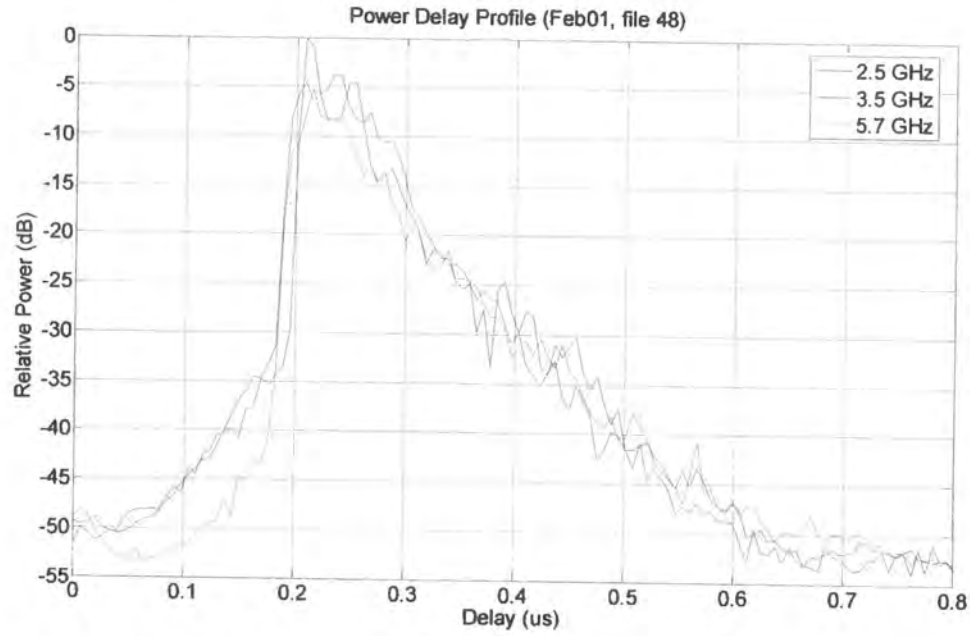

Figure 6.42 Power delay profile for receiver moving towards the transmitter

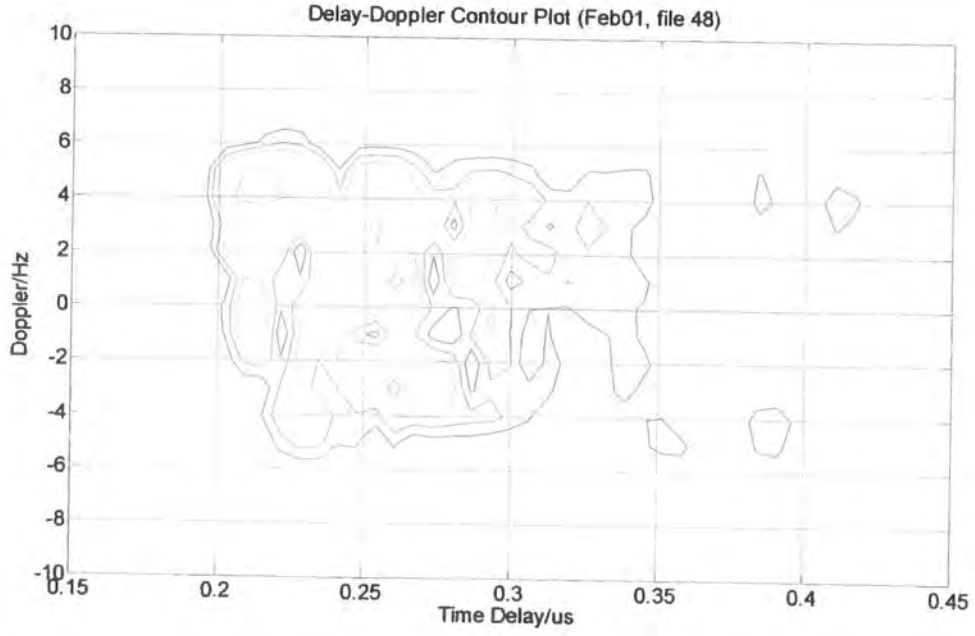

Figure 6.43 Delay - Doppler at 2.5 GHz for receiver moving towards transmitter

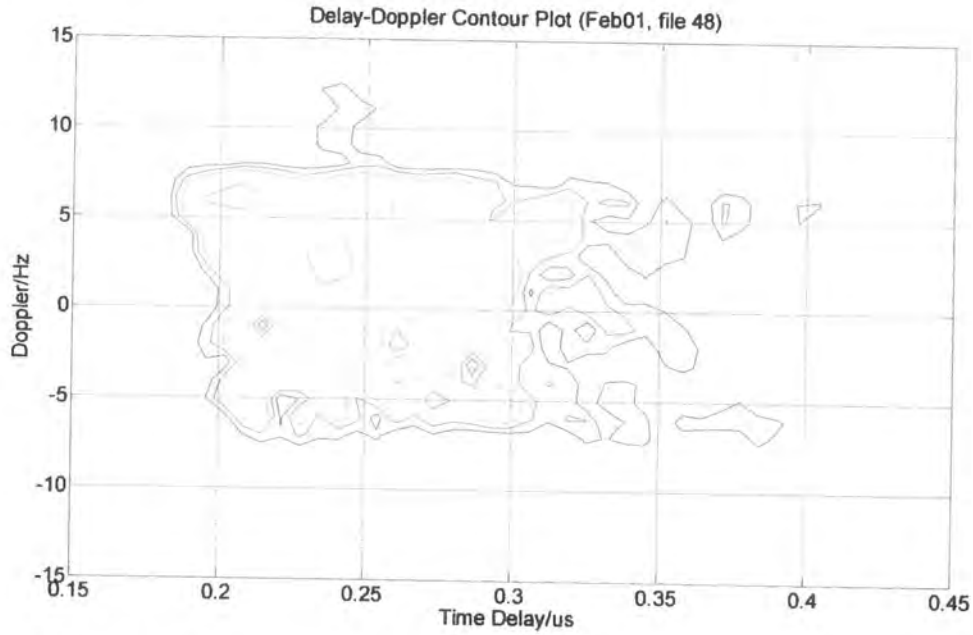

Figure 6.44 Delay - Doppler at 3.5 GHz for receiver moving towards transmitter

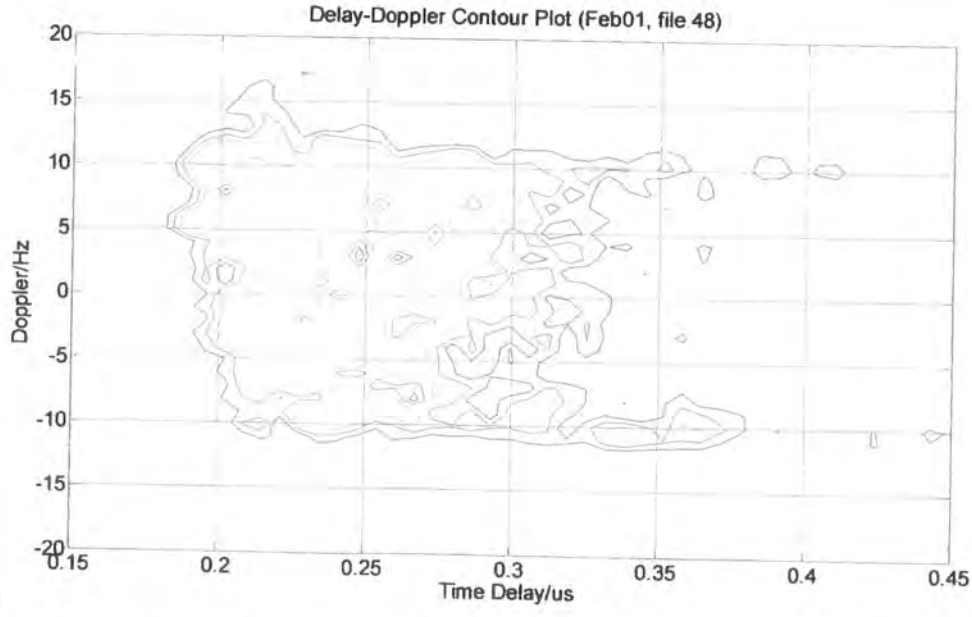

Figure 6.45 Delay - Doppler at 5.7 GHz for receiver moving towards transmitter

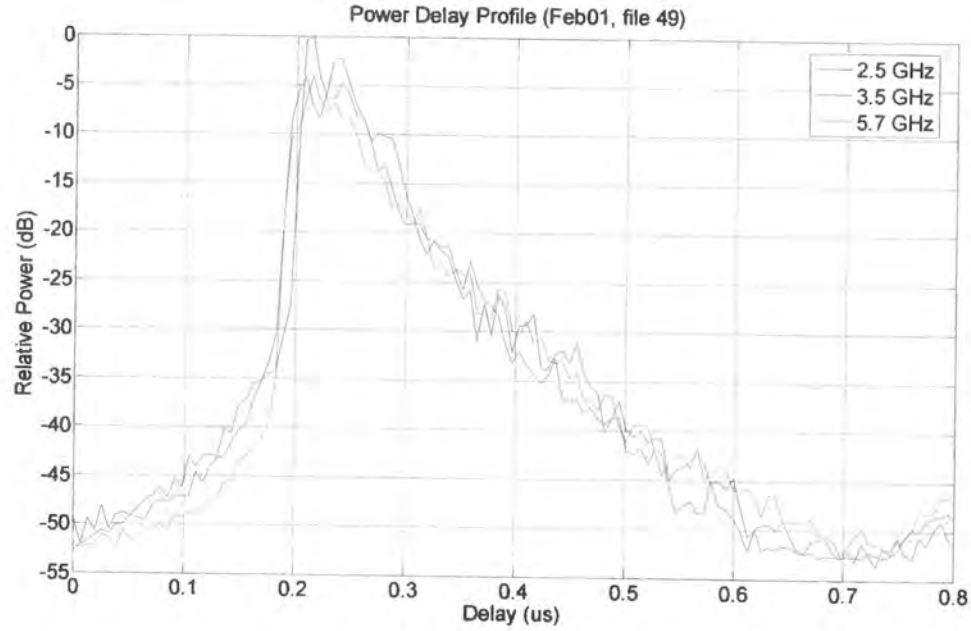

Figure 6.46 Power delay profile for receiver moving away from transmitter

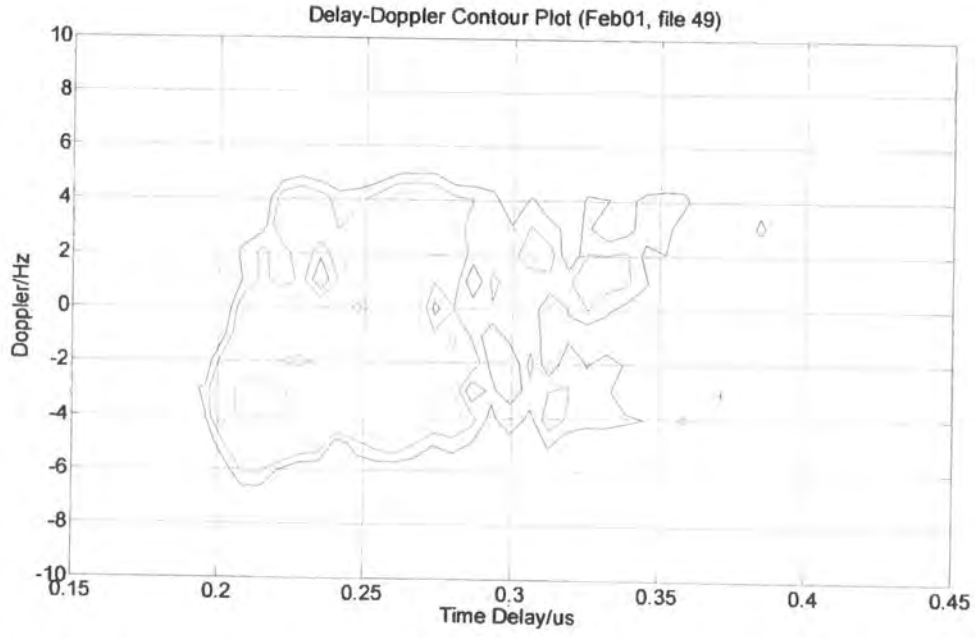

Figure 6.47 Delay - Doppler at 2.5 GHz for receiver away from transmitter

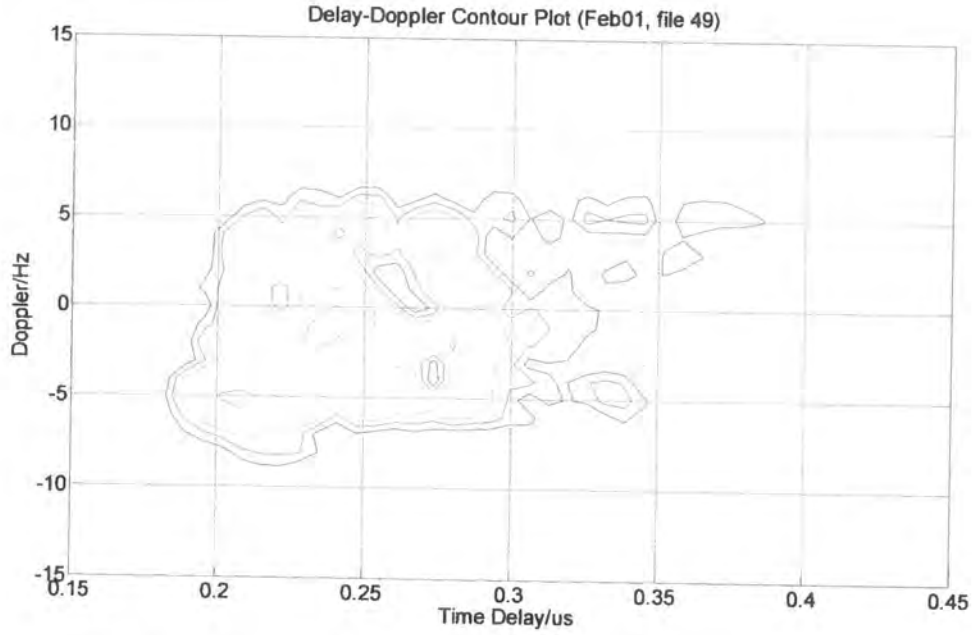

Figure 6.48 Delay - Doppler at 3.5 GHz for receiver away from transmitter

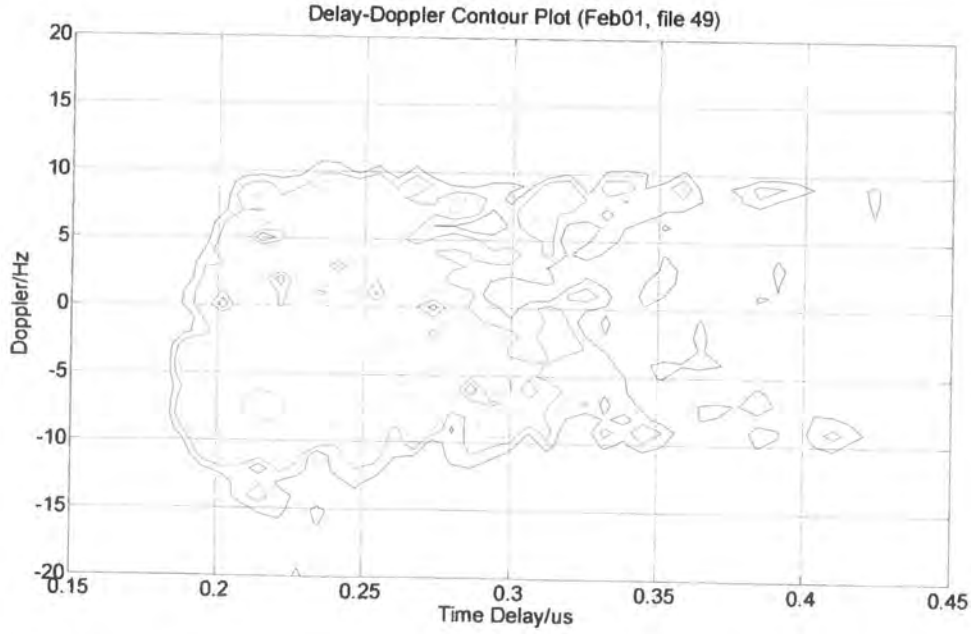

Figure 6.49 Delay - Doppler at 5.7 GHz for receiver away from transmitter

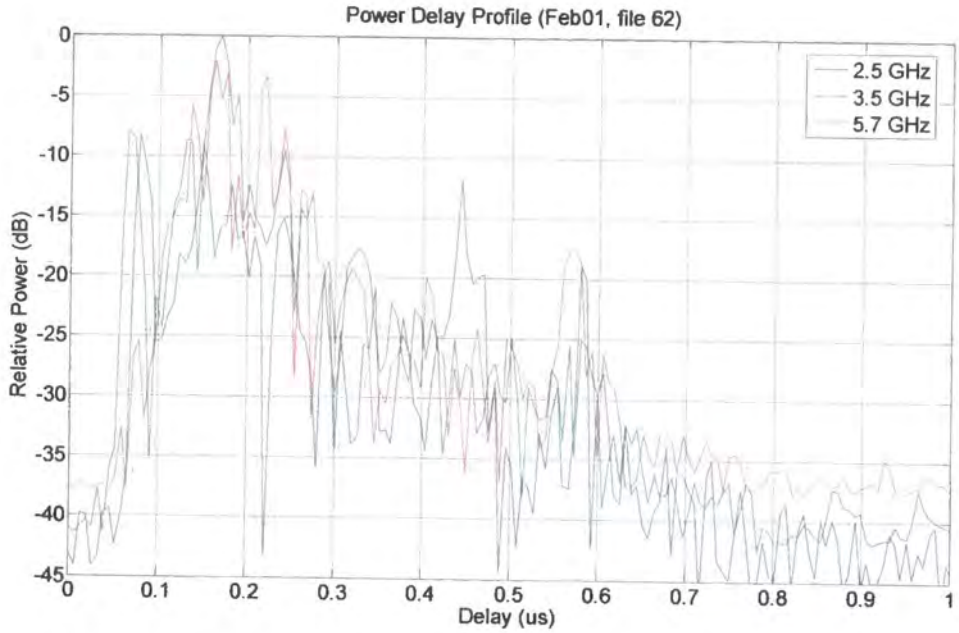

Figure 6.50 Composite indoor to outdoor power delay profile

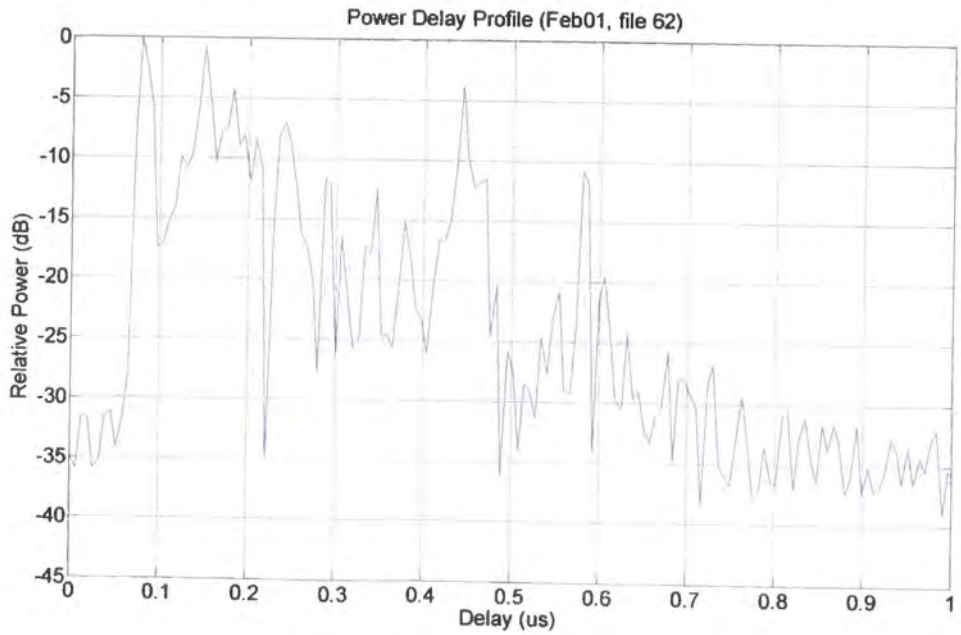

Figure 6.51 Indoor to outdoor power delay profile at 2.5 GHz

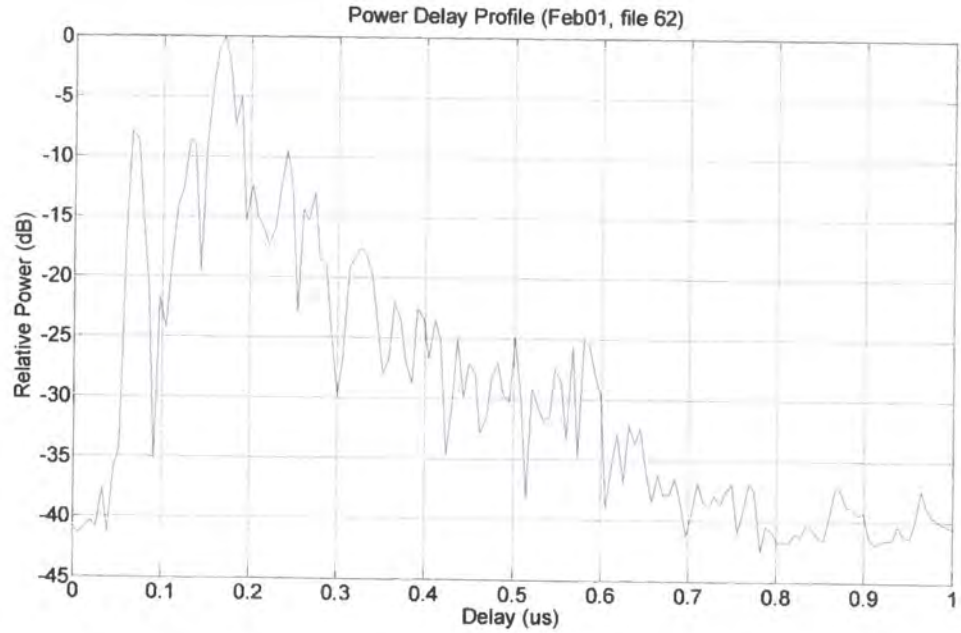

Figure 6.52 Indoor to outdoor power delay profile at 3.5 GHz

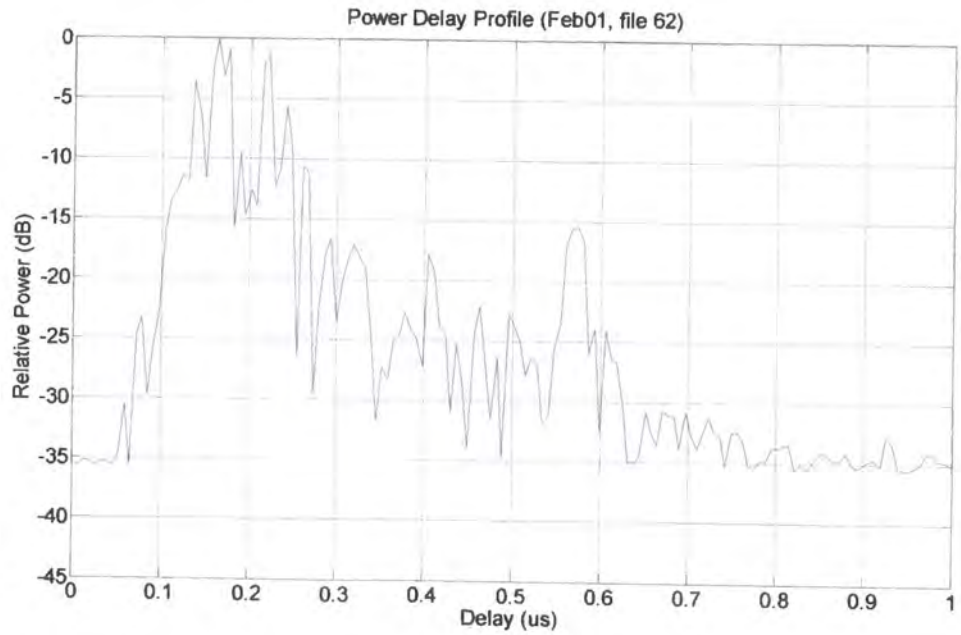

Figure 6.53 Indoor to outdoor power delay profile at 5.7 GHz

6.4 Four channel sounding at 5.7 GHz

Wideband channel sounding was performed outdoors using the 5.7 GHz four channel system.

The transmitter antenna used a 6 dBi omni-directional antenna. The antenna was raised to a height of 6 m using a tripod mounted mast located on the roof of the three storey section of the Durham school of engineering building. The channel was swept from 5.54 GHz to 5.80 GHz. The four channel antenna array was mounted on the pneumatic mast fitted to the landrover survey vehicle as shown in figure 4.66.

The survey vehicle was moved to the locations recorded on the map with the antennas orientated as shown on the map (figure 6.54). In a number of the locations data was taken with the mast extended as well as with the mast collapsed. The retracted antenna height is 2.5 m. The antenna height extended is 7.8 m.

An initial set of 20 files were recorded which were usable down to 20 dB below the power delay profile peak. These locations correspond to the numbered locations on figure 6.54. Fifteen of these files were usable to 30 dB below the peak. This data set was combined with a further 59 measurements that were performed in the same general locations. This provided a total set of 74 files usable to 30 dB below the power delay profile peak.

The cumulative distribution of the average delay as a function of threshold is recorded in figure 6.55. The cumulative distribution of the RMS delay spread as a function of threshold is recorded in figure 6.56.

The average delay and the RMS delay spread at the 50% and 90% interval of the distributions are detailed in table 6.5.

Threshold value	Interval	Average Delay	RMS Delay Spread	
10 dB	50%	14	14	ns
	90%	109	74	ns
15 dB	50%	28	30	ns
	90%	135	115	ns
20 dB	50%	42	42	ns
	90%	180	145	ns
25 dB	50%	52	56	ns
	90%	250	185	ns
30 dB	50%	66	78	ns
	90%	400	275	ns

Table 6.5 Average delay and RMS delay spread, 5.7 GHz, 260 MHz sweep

An example set of power delay profiles for the four channel system is shown in figures 6.57a to 6.57d. The antenna orientation and location is identified as location #14 in figure 6.54.

Channel 1 is connected to the antenna which is pointing away from the transmitter. It is also pointing towards building clutter further down the street. The power delay profile shows signals arriving at a time similar to the main signal observed for channel 3. This signal represents the finite front to back spatial discrimination for this antenna and also includes signals which are being reflected by close scattering sources. The main signal in the power delay profile can be seen to be due to the signal that has been reflected from the building clutter further down the street. This signal appears ~ 2 μs after the main signal has arrived. This represents a distance of ~ 300 m to the reflection.

Channel 2 is connected to an antenna which is pointing at a three story building block that is opposite the Durham student union and is higher than the Durham student union building. This antenna exhibits responses to both the direct and reflected signal.

Channel 3 is connected to the antenna pointing towards the transmitter. The signal is being propagated along a street with buildings of two to four stories height. The reflected signal that is present on channel 1 is evident just above the noise level.

Channel 4 is pointing towards the Durham student union building. This shows the lowest signal level. This antenna also exhibits response to both the direct and reflect signals.

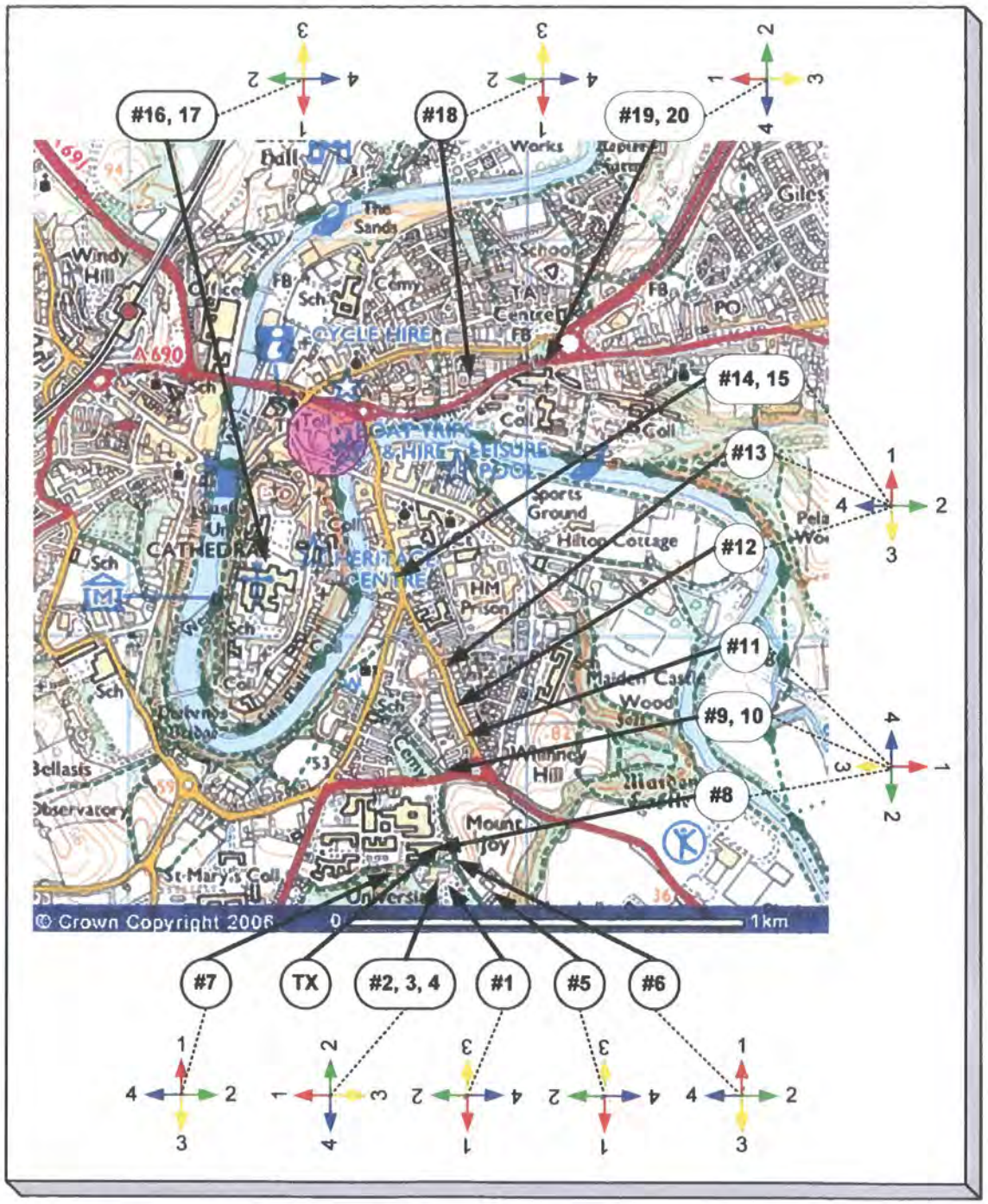

Figure 6.54 Channel sounding locations in Durham

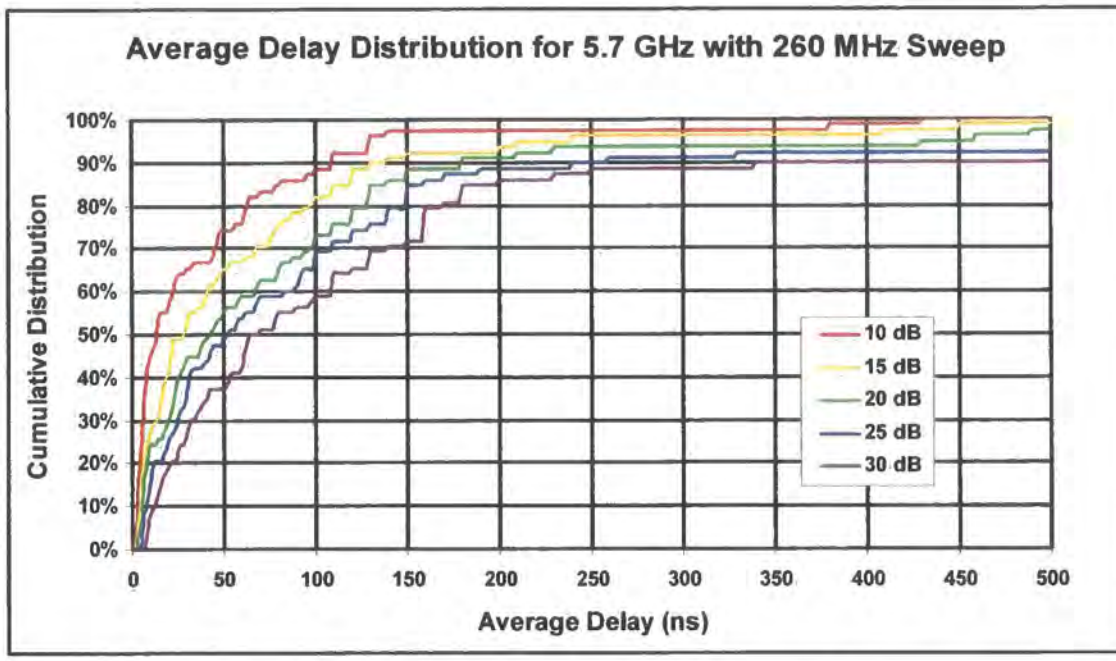

Figure 6.55 Distribution for the average delay, 5.7 GHz, 260 MHz sweep outdoors

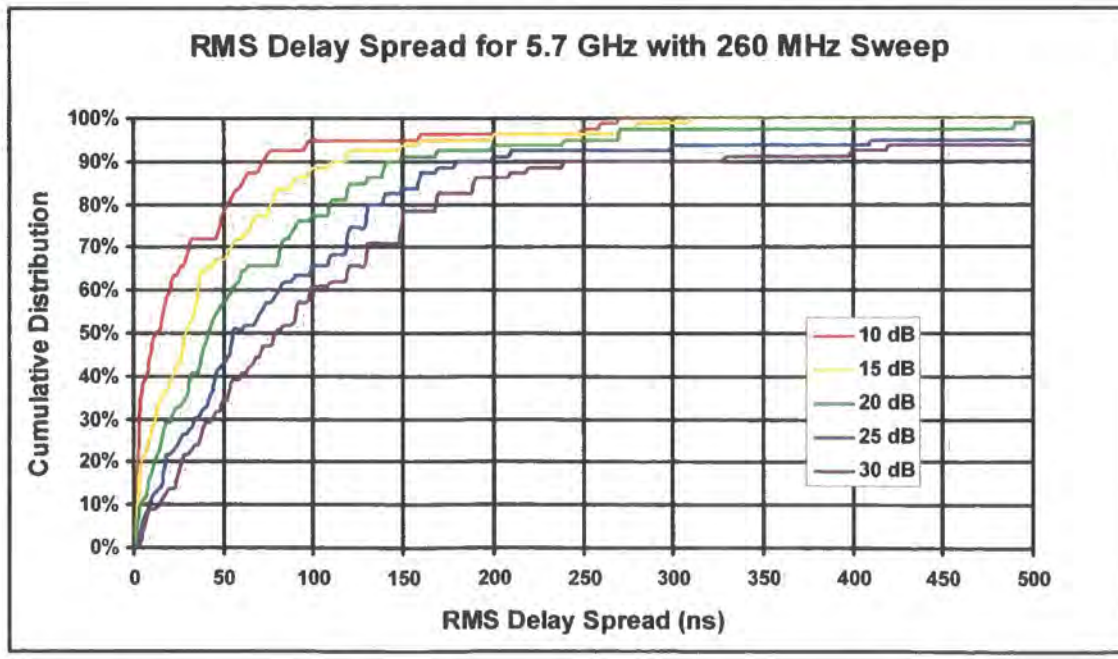

Figure 6.56 Distribution of RMS delay spread, 5.7 GHz, 260 MHz sweep outdoors

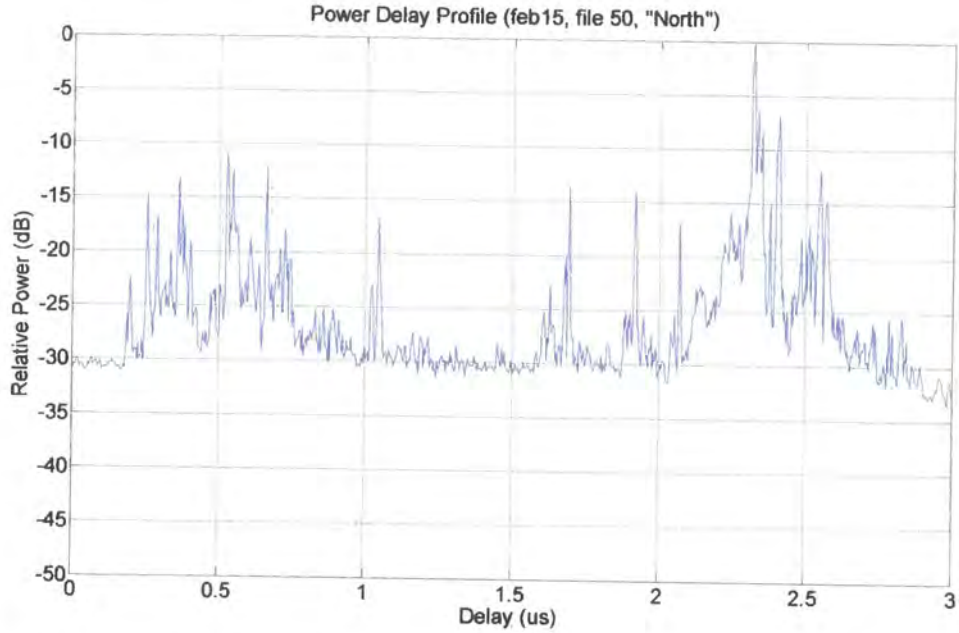

Figure 6.57a Signal into antenna pointing away from transmitter

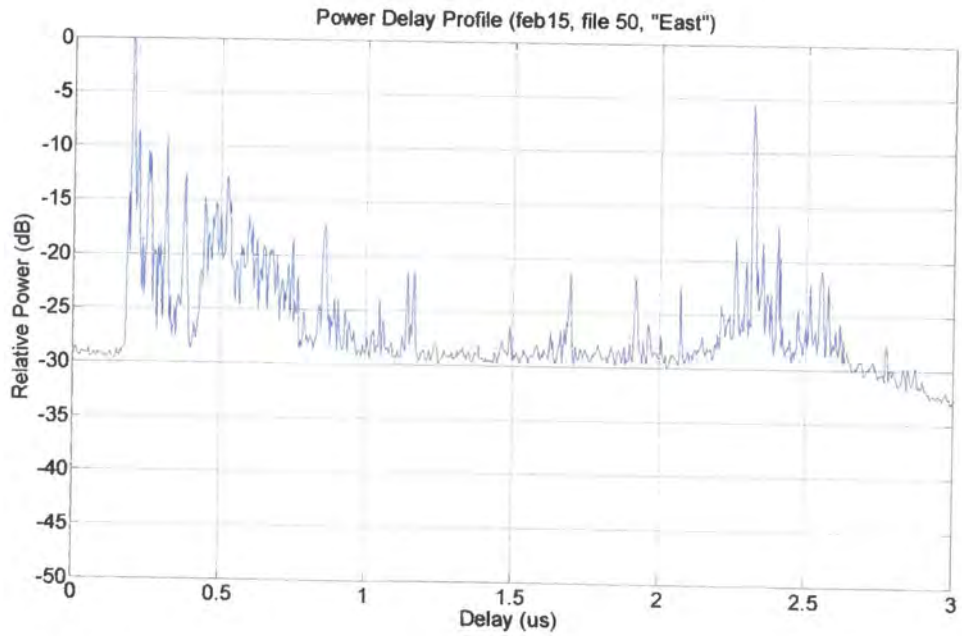

Figure 6.57b Signal into to antenna perpendicular to the incoming signal

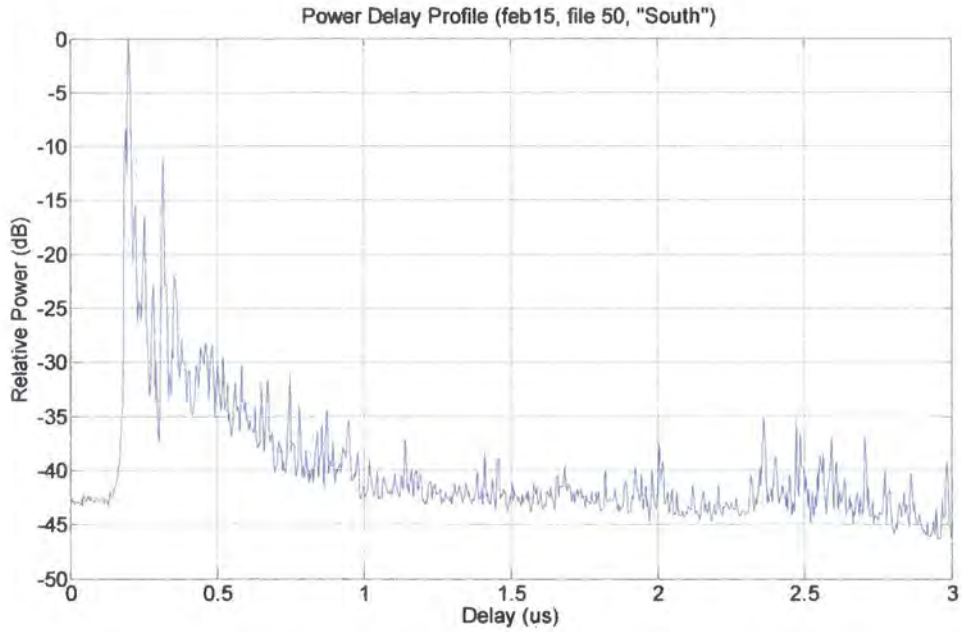

Figure 6.57c Signal into to antenna pointing towards the incoming signal

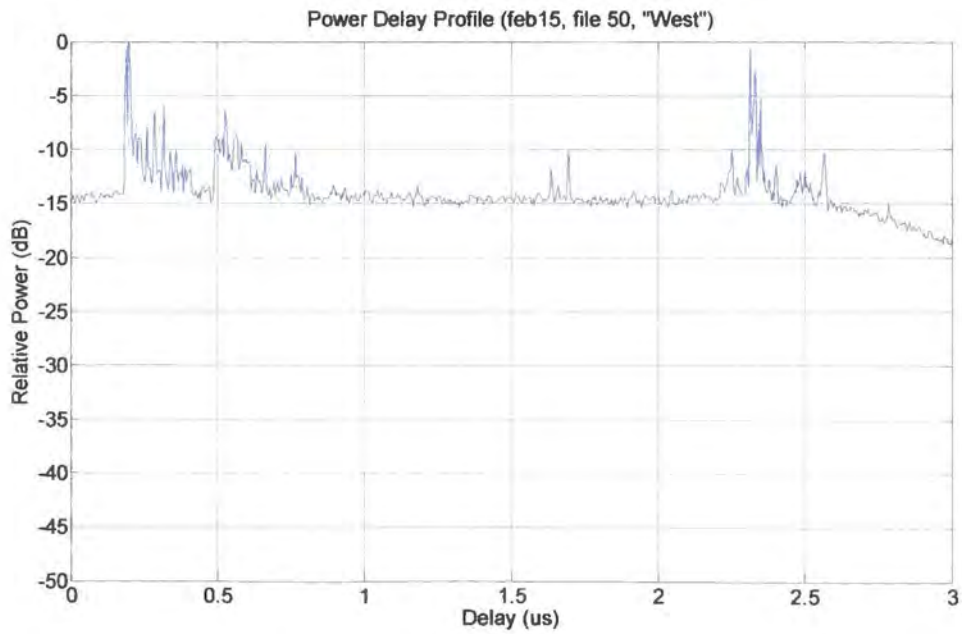

Figure 6.57d Signal into to antenna perpendicular to the incoming signal

6.5 Channel sounding in the 60 GHz band

Channel soundings were made in the locations shown in figure 6.58. This included operation through glass windows in the partition walls surrounding the computing lab.

Additional soundings were made with the receiver pointing outside from room E287 with the transmitter outside.

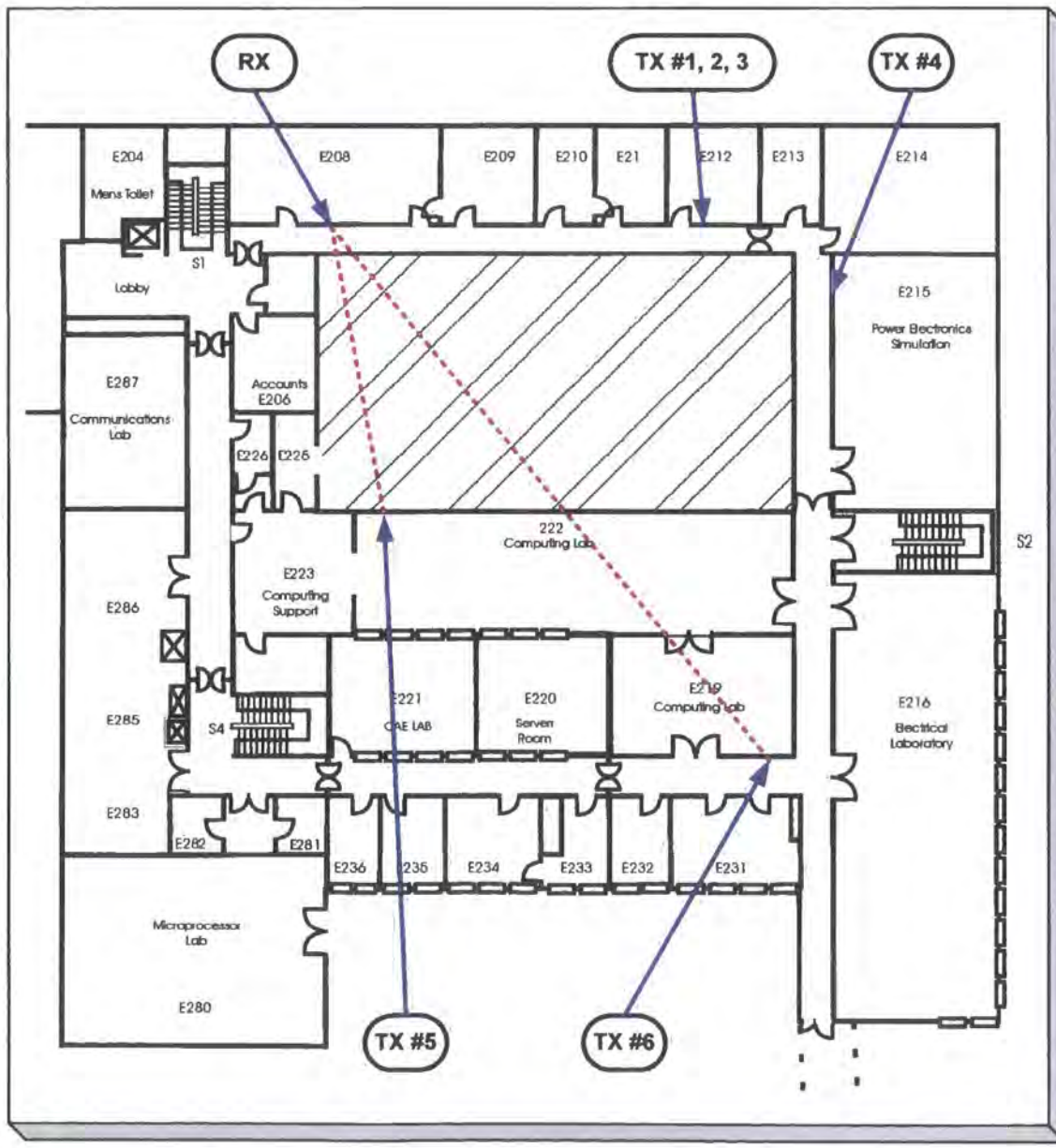

Figure 6.58 60 GHz soundings in the school of engineering

The results of this limited set of measurements are shown in figure 6.59 (average delay) and figure 6.60 (RMS delay spread).

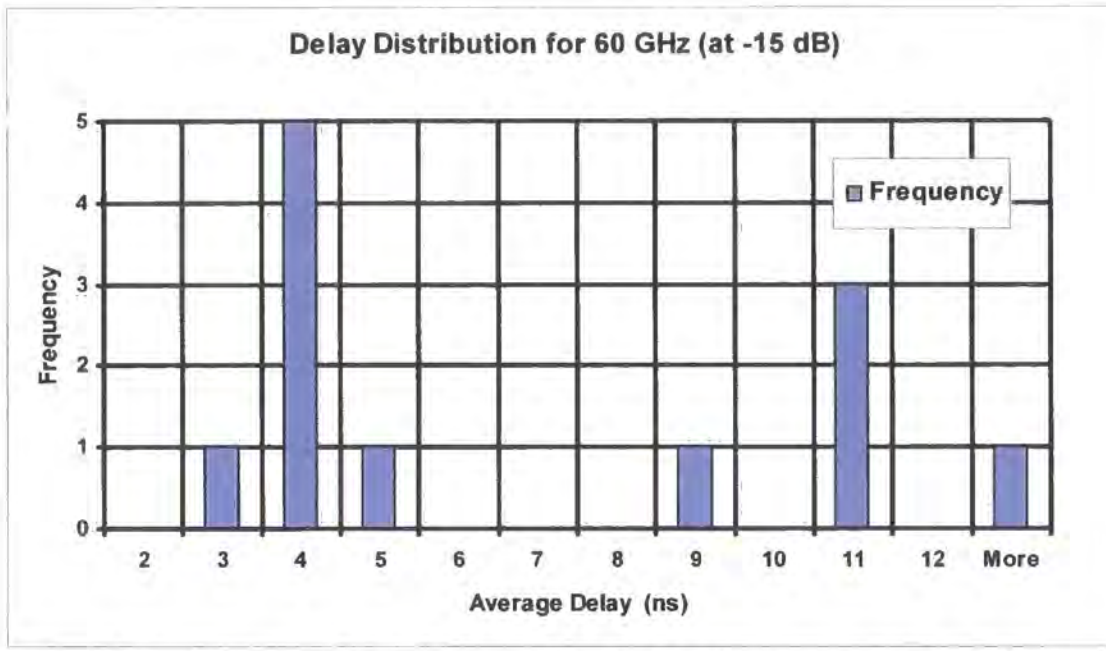

Figure 6.59 Histogram of the average delay for 60 GHz measurements (12 files)

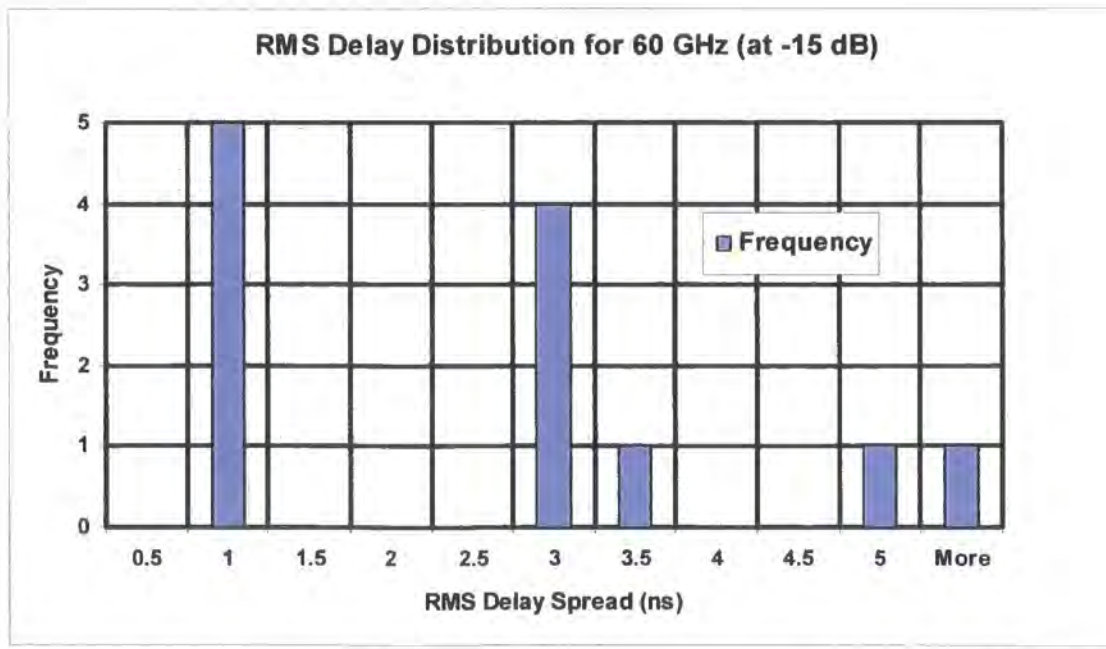

Figure 6.60 Histogram of the RMS delay spread for 60 GHz measurements (12 files)

6.6 Discussion of the channel sounding results

The delay measurements made in Ipswich do not appear to demonstrate any significant frequency dependency. The data does show a small reduction at 5.7 GHz relative to the results at 2.5 GHz and 3.5 GHz. The difference is however limited to a few percent.

The indoor delay measurements made at Durham using common antennas also do not appear to be significantly frequency dependent. There does appear to be a slight bias to the data. The average delay and delay spread results show slightly greater values at 5.7 GHz relative to those at 2.5 GHz. The results at 3.5 GHz show slightly lower values than those obtained at 2.5 GHz. The spread of results is within 10 % in any case.

These results are significantly different to the results obtained by Nobles et al [6.1] who observed that the delay spread decreased with increasing frequency. Specifically the RMS delay spread at 17 GHz was observed to be only 30 % of the value observed at 2.5 GHz. It is believed that this discrepancy may be explained by changes in the antenna characteristic and experimental bias in the observation of only the more favourable paths at high frequencies. The Nobles experiment used a bi-conical antenna. This will tend to exhibit an elevation beam-width which reduces as the wavelength decreases. The will attenuate the off-axis components as frequency rises. In addition, it was observed in the "Ipswich" measurements performed in this research that high frequencies were generally more attenuated than lower frequencies. Thus the data set becomes skewed in that only the high frequency paths which experience lower attenuation are recorded. These tend to be the more direct paths which have experienced less scattering and hence have lower delay spread. It has been observed here that when the data sets are compared on an equivalent basis, then this effect is eliminated. The data sets have been organised to only compare data from locations where viable paths were simultaneously available at the measurement threshold for all three frequencies. This eliminates the frequency selective bias. On this basis the correct interpretation is that the overall path loss in the environment is lower at lower frequencies. This allows lower frequencies to be propagated over less favourable paths. Hence delay spread for the population of viable paths appears to reduce with increasing frequency. However,

the delay spread for the population of paths where propagation is viable over the range of frequencies under investigation has been observed here to be frequency independent.

The Doppler results demonstrate scaling with frequency and directional discrimination. These results also demonstrate the ability of the sounder to discriminate between Doppler components from different multi-path components.

The four channel 5.7 GHz sounder and directional antenna array appears to demonstrate useful spatial discrimination.

The data collected at 60 GHz is limited at this time. A basic level of functionality has been demonstrated. However the data set is insufficient to provide any statistically relevant conclusions at this time.

6.7 Reference

[6.1] P. Nobles, D. Ashworth, and F. Halsall; "Indoor Radiowave Propagation Measurements at Frequencies up to 20 GHz"; In Proceedings 44th IEEE Vehicular Technology Conference, June 1994.

7.1 Summary and conclusions

a. The primary objectives for this work were to provide channel sounders capable of operating in the band between 2.5 GHz and 6 GHz and to use these to derive measured channel data.

b. Operational sounders have been demonstrated in the 2.5 GHz, 3.5 GHz and 5.7 GHz bands. In addition a four channel version has been produced to provide a parallel receiver operating in the 5.7 GHz band.

c. These sounders have been subjected to detailed assessment through an extensive verification process. This has demonstrated operational performance that is virtually identical to that obtained from the base sounder at 2 GHz.

d. The capability to make simultaneous soundings in all three bands (2.5 GHz, 3.5 GHz and 5.7 GHz) has been demonstrated.

e. This activity has been supported with a novel parallel channel phase-tracking quadrature down converter which has been demonstrated to provide relative amplitude and phase calibration of antennas. This has been extended to make relative antenna measurements for antenna arrays in the 5.7 GHz band.

f. Field measurements have been supported with a survey vehicle that has been specifically adapted to the channel sounders developed here.

g. Discone antennas that provide useable response from 2.2 GHz to 6 GHz have been produced.

h. Useful data has been collected in the 2.5 GHz, 3.5 GHz and 5.7 GHz bands which show that the average delay and RMS delay spread are essentially

independent of frequency for the antenna configurations and environments assessed.

i. The four channel parallel sounder used at 5.7 GHz with a directional antenna array demonstrates the capability of providing differentiation between the signals arriving at each antenna.

j. Non-linear frequency conversion of the FMCW chirp signal has been successfully demonstrated. This has supported the development of a 60 GHz sounder with > 1 GHz of channel width.

k. This has also been supported with the development of a SSB IF down-converter which has demonstrated > 50 dB of sideband rejection across the full data acquisition bandwidth.

l. The frequency converters have required the design and development of a wide range of application specific circuit functions including signal sources (synthesisers) amplifiers, multipliers and filters.

m. A novel impedance-matched broad-band frequency selective attenuator has been implemented to provide amplifier gain equalisation.

n. A novel broad-band balanced X3 multiplier structure has been realised with useful performance from 2 GHz to 3 GHz input to provide 6 GHz to 9 GHz output.

7.2 Suggested further work

1. It would be useful to fully characterise the antennas used for the three band measurements in Ipswich. This will become practical when the Durham anechoic chamber and antenna positioning system are available.

2. Similarly it would be useful to perform a full assessment of the discone antenna within an anechoic test environment.

3. Similarly it would be useful to calibrate the directional 5.7 GHz antenna array within an anechoic environment.

4. The 60 GHz sounder work needs to be completed. It is proposed to use the IF translation synthesisers to provide the sweep offset. This requires minor adjustments to the centre frequency of the SSB down-converter from 12.65 MHz to 13.48 MHz. This requires re-tuning of the 12.5 MHz to 13 MHz input filter and the intermediate 2.5 MHz to 3.0 MHz filters.

5. A measurement campaign at 60 GHz should be performed to provide statistically relevant results.

Annex 1: Circuit Schematics

a. Low noise 10 MHz OCXO reference support card

b. 10 MHz reference distribution card

c. Main power supply card

d. Auxiliary (-12 V) power supply card

e. Micro-controller

f. 10 MHz to 40 MHz X4 multiplier

g. Synthesiser

h. Radio frequency X2

i. Radio frequency X3

j. 2.5 GHz frequency converter

k. 3.3 GHz to 6.0 GHz up-converter

l. 3.3 GHz to 6.0 GHz down-converter

m. 2.3 GHz to 6.0 GHz power amplifier

n. 2.5 GHz low noise amplifier

o. 5.3 GHz to 8 GHz local oscillator buffer amplifier

p. Base-band pre-amplifier

q. Single-sideband down converter

REVISION RECORD			
LTR	ECO NO:	APPROVED:	DATE:

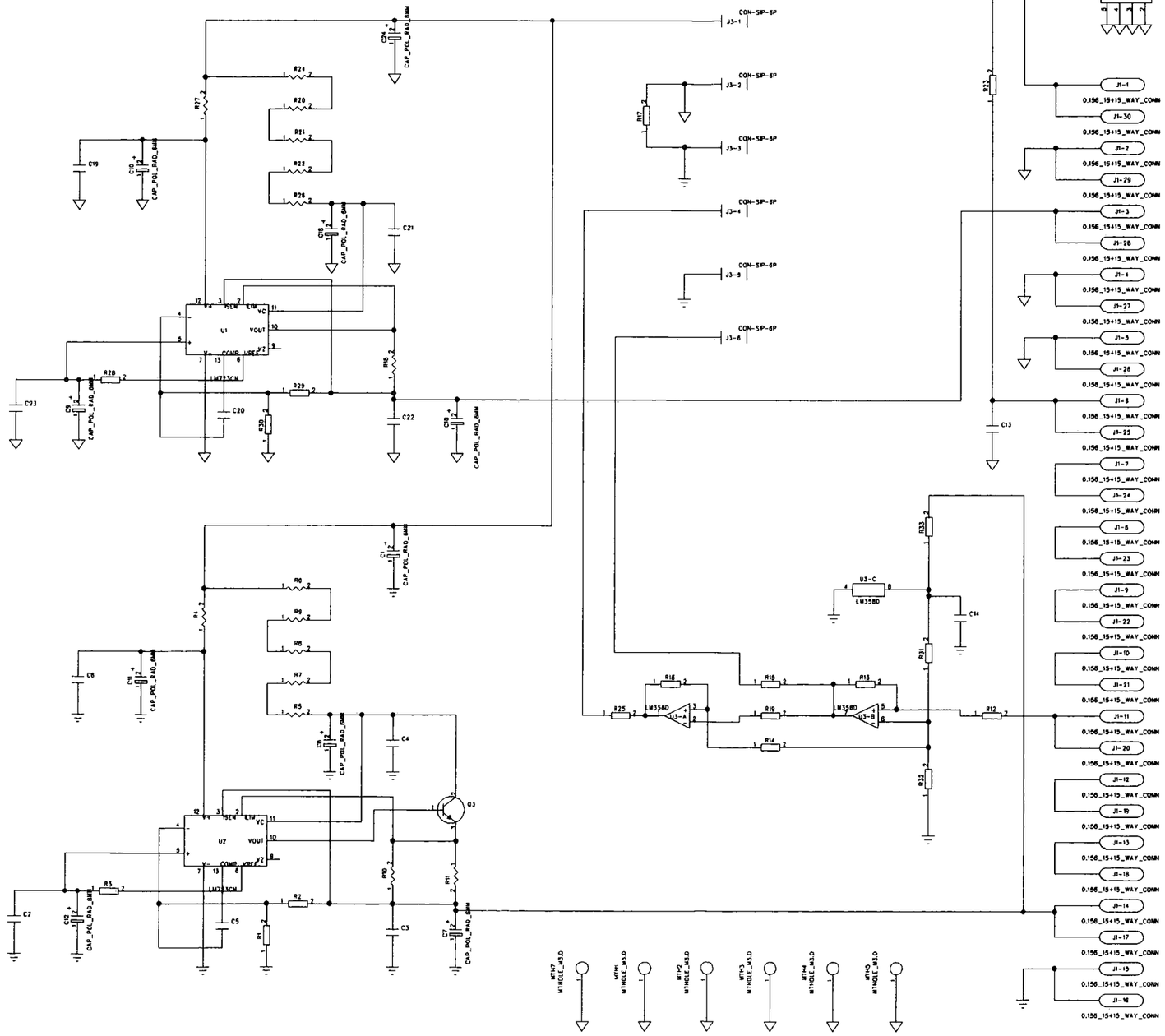

COMPANY:	PhD RF		
TITLE:	10MHz OCXO Reference Assy		
DRAWN: SMF	DATED: 05-Apr-18	CODE:	SIZE: DRAWING NO: REV:
CHECKED: SMF	DATED: 05-Apr-18		
QUALITY CONTROL:	DATED:		
RELEASED:	DATED:	SCALE:	SHEET: 1 OF 1

REVISION RECORD			
LTR	ECO NO.	APPROVED:	DATE:

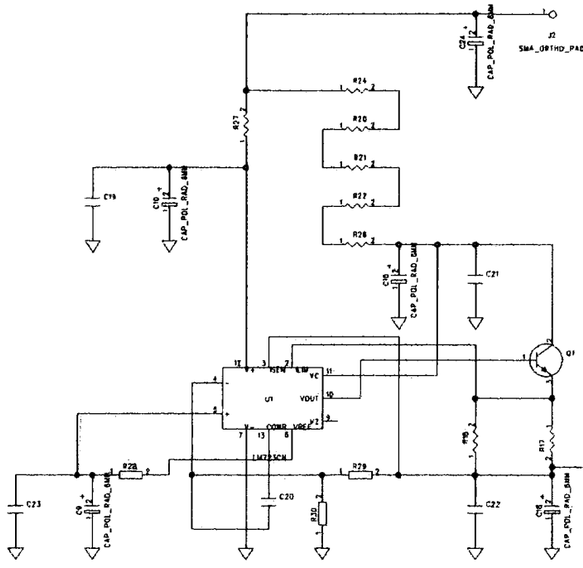

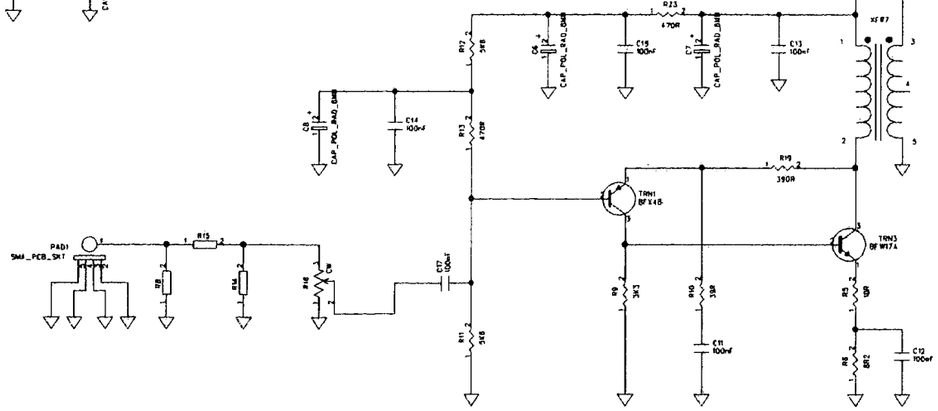

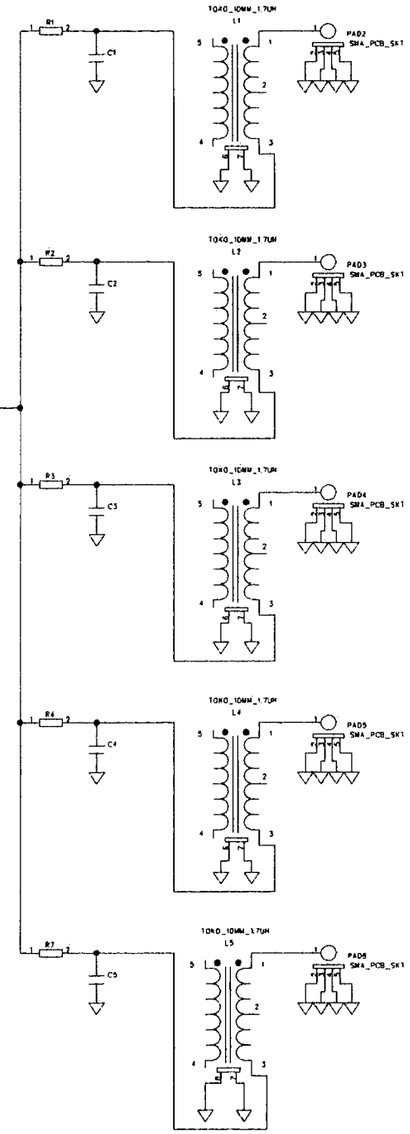

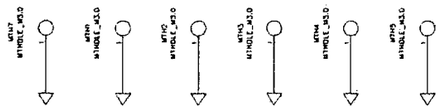

DRAWN: SMF	DATED: 05-Apr-18	COMPANY: PhD RF	
CHECKED: SMF	DATED: 05-Apr-18	TITLE: 10MHz Reference Distribution	
QUALITY CONTROL:	DATED:	CODE:	SIZE: DRAWING NO: REV:
RELEASED:	DATED:	SCALE:	SHEET: 1 OF 1

REVISION RECORD			
LTR	ECO NO:	APPROVED:	DATE:

DRAWN: SMF	DATED:	COMPANY:	
CHECKED: SMF	DATED:	TITLE: Power Supply Module	
QUALITY CONTROL:	DATED:	CODE:	SIZE: DRAWING NO: REV:
RELEASED:	DATED:	SCALE:	SHEET: OF

REVISION RECORD			
LTR	ECO NO:	APPROVED	DATE:

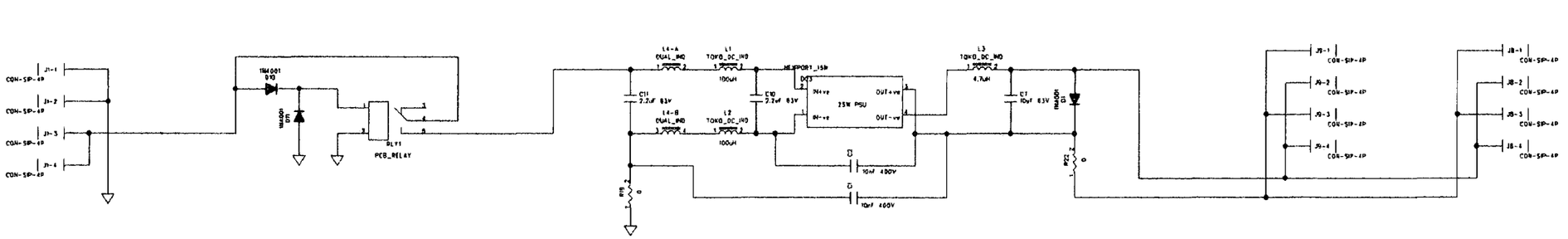

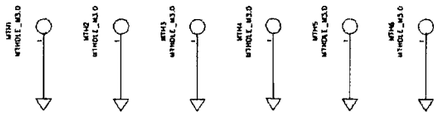

DRAWN: SMF	DATED:	COMPANY:	
CHECKED: SMF	DATED:	TITLE: AUX Power Supply Module	
QUALITY CONTROL:	DATED:	CODE:	SIZE: / DRAWING NO: / REV:
RELEASED:	DATED:	SCALE:	SHEET: OF

REVISION RECORD			
LTR	ECO NO:	APPROVED:	DATE:

Indicator LEDs

Power Input

10/100BaseT NEC Programmer Input

Rotary Encoder Input

RS 232 Interface

4*4 Key matrix #1

4*4 Key matrix #2

LCD Contrast

Interface to 16*2 LCD

PLL #1

PLL #2

PLL #3

PLL #4

PLL #5

PLL #6

PLL #7

COMPANY:	Stuart Feeney		
TITLE:	PhD_Microcontroller		
DRAWN: SMF	DATED:	CODE:	SIZE: DRAWING NO: Check 0.1 REV:
CHECKED:	DATED:		
QUALITY CONTROL:	DATED:		
RELEASED:	DATED:	SCALE:	SHEET: OF

REVISION RECORD			
LTR	ECO NO:	APPROVED:	DATE:

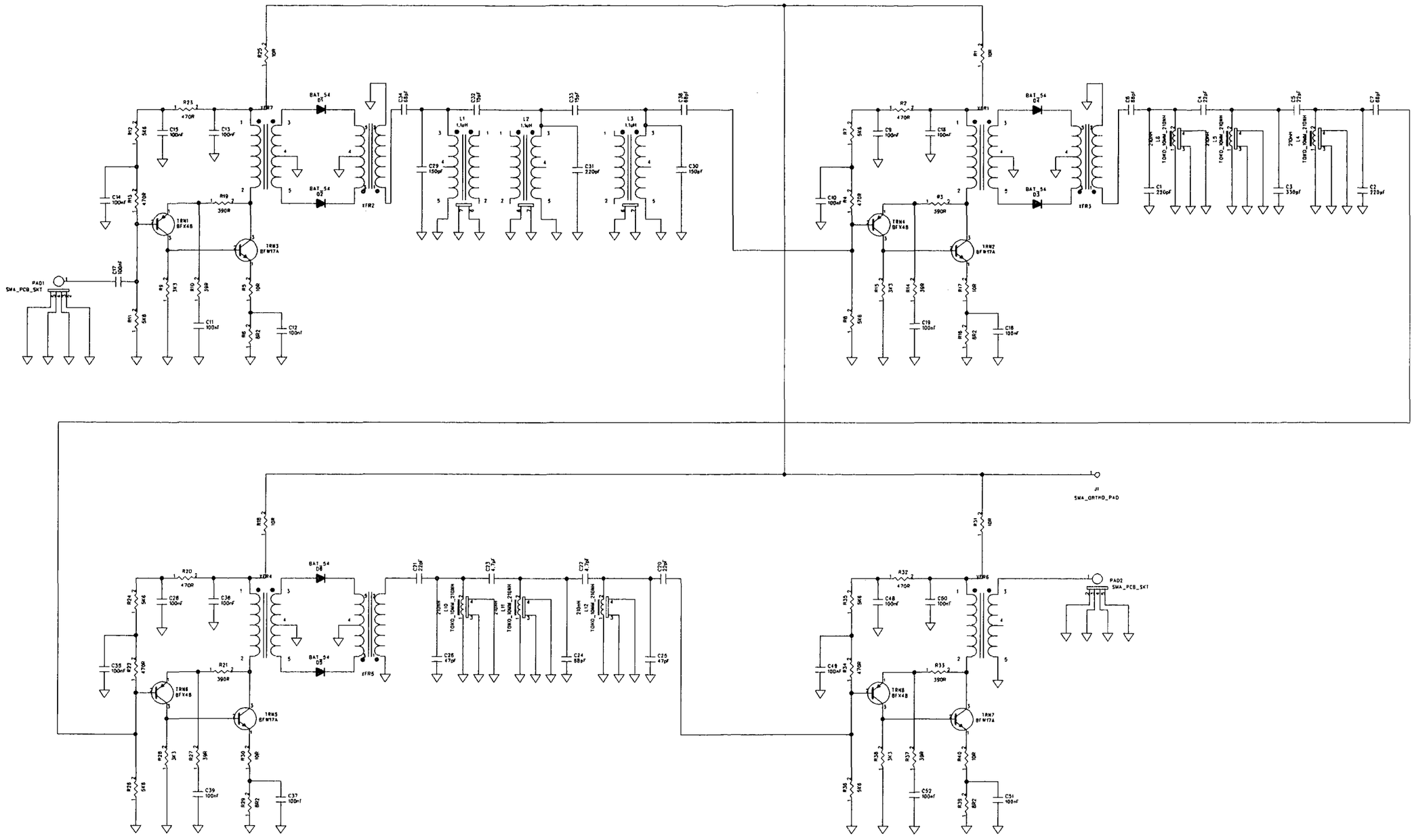

DRAWN:	SMF	DATED:	05-Apr-18
CHECKED:	SMF	DATED:	05-Apr-18
QUALITY CONTROL:		DATED:	
RELEASED:		DATED:	

COMPANY:	PhD RF		
TITLE:	Reference Multiplier		
CODE:	SIZE:	DRAWING NO:	REV:
SCALE:		SHEET: 1 OF 1	

REVISION RECORD			
LTR	ECO NO:	APPROVED:	DATE:

GROUND
LOCK_OUT
CLOCK_IN
DATA_IN
LATCH_IN
P24V_65mA
N12V_5mA
GROUND
P12V_65mA

COMPANY:	PhD RF		
TITLE:	Synthesiser		
	MCL_ROS_3000V 2.4GHz to 3.0GHz		
DRAWN: SMF	DATED: 04-May-31	CODE:	SIZE: DRAWING NO: REV:
CHECKED: SMF	DATED: 04-May-31		
QUALITY CONTROL:	DATED:		
RELEASED:	DATED:	SCALE:	SHEET: 1 OF 1

REVISION RECORD			
LTR	ECO NO:	APPROVED:	DATE:

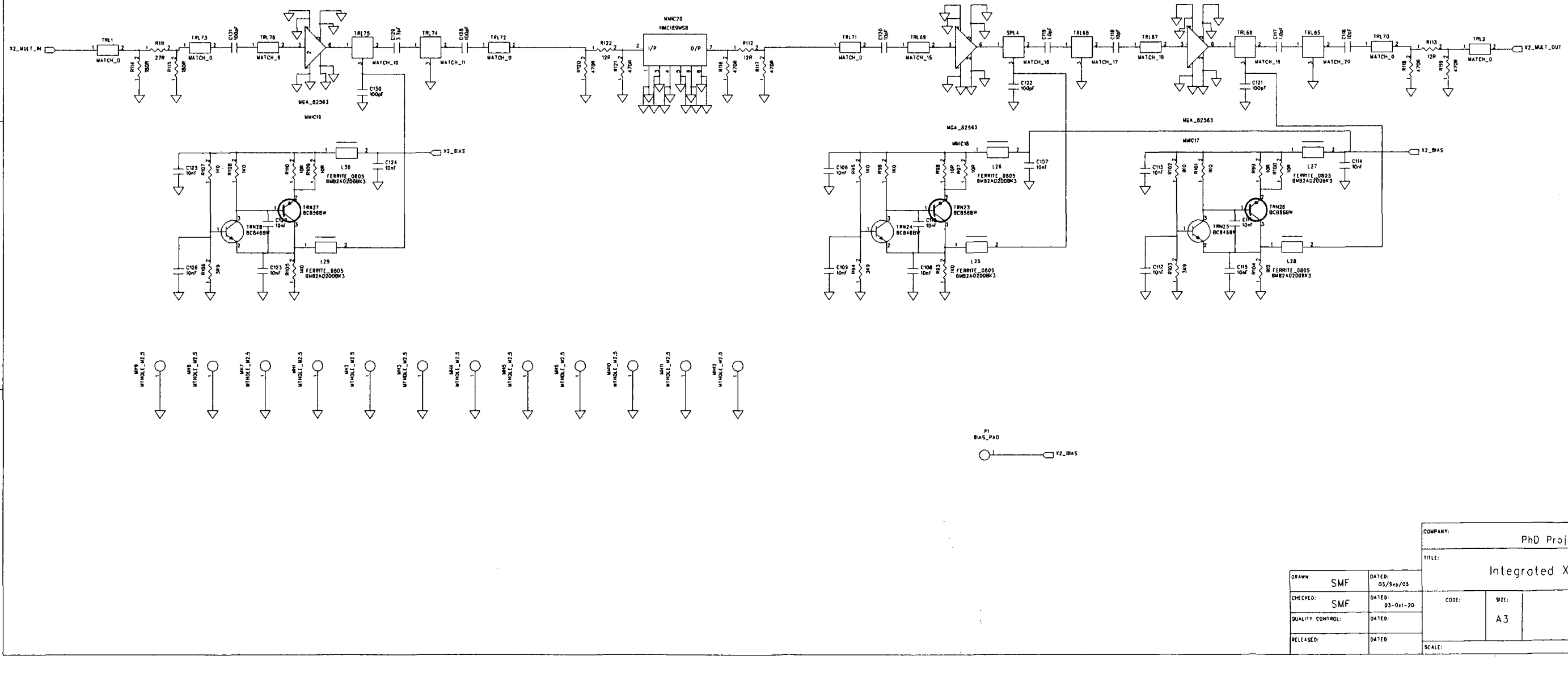

DRAWN:	SMF	DATED:	03/Sep/05	COMPANY:	PhD Project
CHECKED:	SMF	DATED:	03-Oct-20	TITLE:	Integrated X2 Multiplier
QUALITY CONTROL:		DATED:		CODE:	SIZE: A3
RELEASED:		DATED:		DRAWING NO:	REV: 1
				SCALE:	SHEET: 1 OF 1

REVISION RECORD			
LTR	ECO NO:	APPROVED:	DATE:

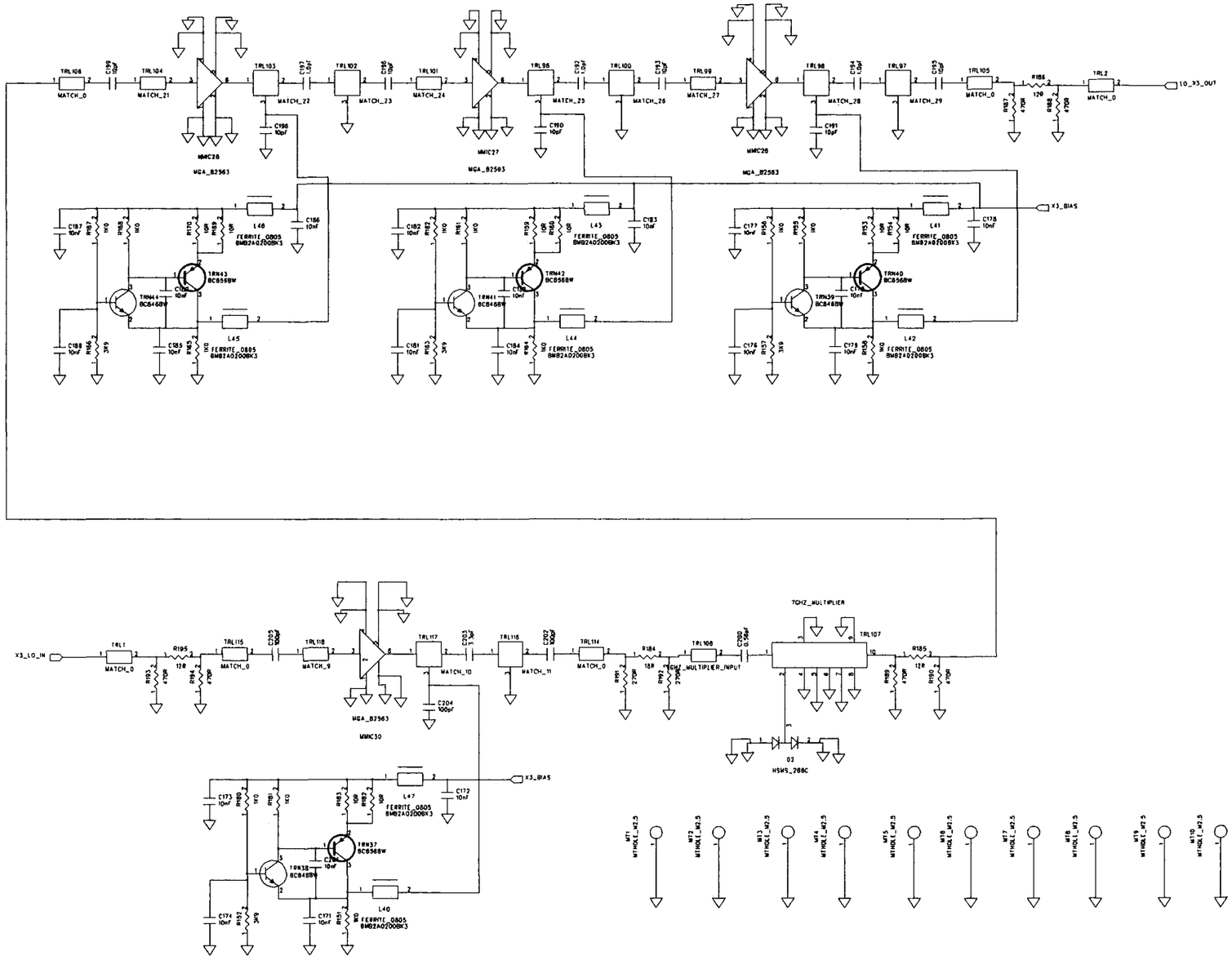

DRAWN:	SMF	DATED:	03-Oct-20
CHECKED:	SMF	DATED:	03-Oct-20
QUALITY CONTROL:		DATED:	
RELEASED:		DATED:	

COMPANY:	PhD Project		
TITLE:	Integrated X3 Multiplier		
CODE:	SIZE: A3	DRAWING NO:	REV: 1
SCALE:		SHEET: OF	

REVISION RECORD			
LTR	ECO NO:	APPROVED:	DATE:

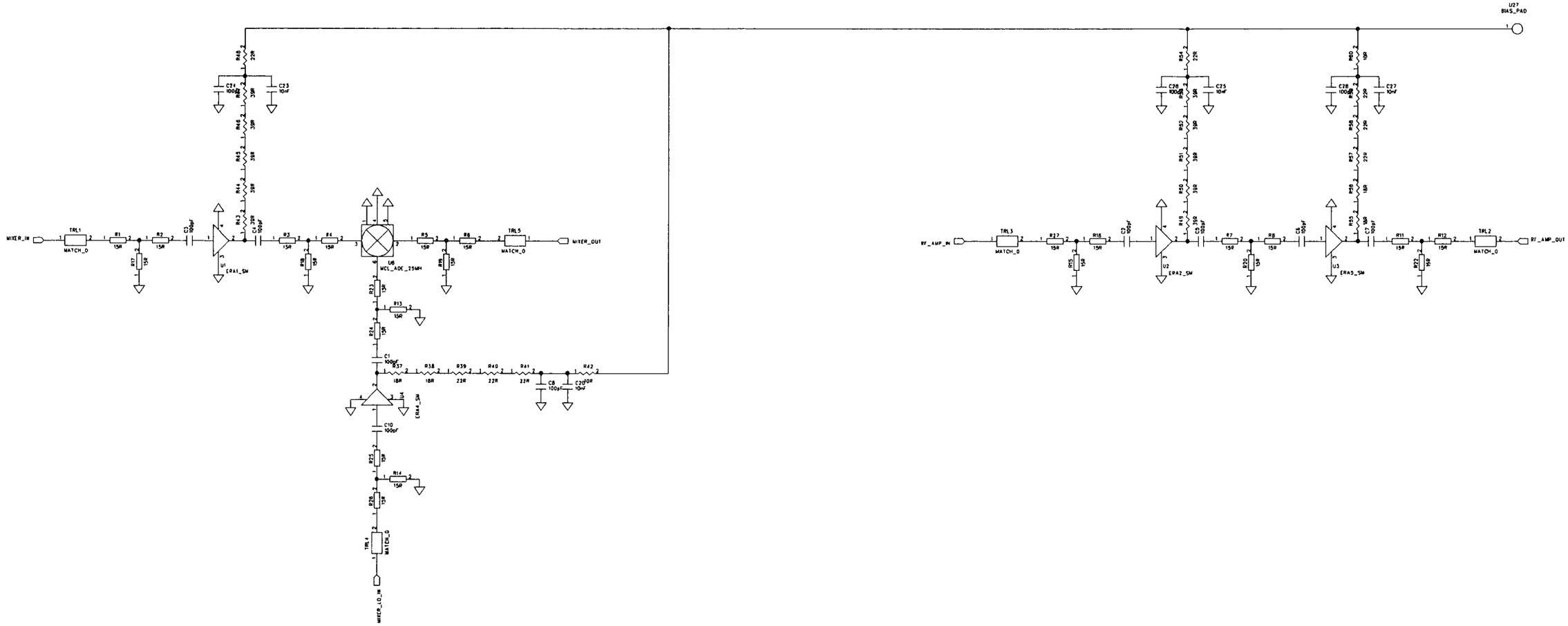

DRAWN: SMF	DATED:	COMPANY:	
CHECKED: SMF	DATED:	TITLE: 2GHz / 2.5GHz Converter	
QUALITY CONTROL:	DATED:	CODE:	SIZE: DRAWING NO: REV:
RELEASED:	DATED:	SCALE:	SHEET: OF

REVISION RECORD			
LTR	ECO NO:	APPROVED:	DATE:

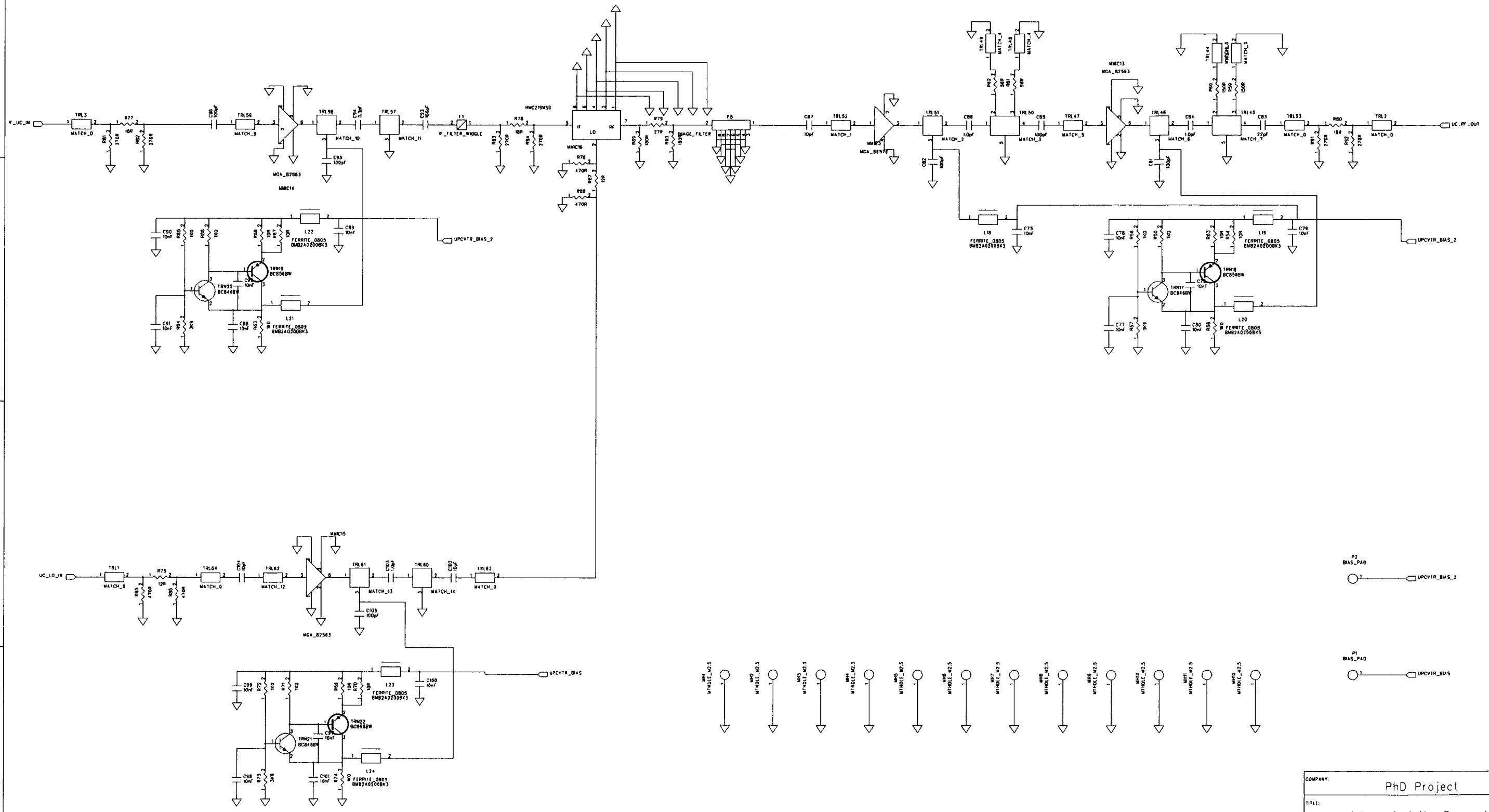

DRAWN: SMF	DATED: 03-Oct-16	COMPANY: PhD Project	
CHECKED: SMF	DATED: 03-Oct-16	TITLE: Integrated Up-Converter	
QUALITY CONTROL:	DATED:	CODE:	SIZE: A3 / DRAWING NO: / REV: 1
RELEASED:	DATED:	SCALE:	SHEET: OF

REVISION RECORD			
LTR	ECO NO:	APPROVED:	DATE:

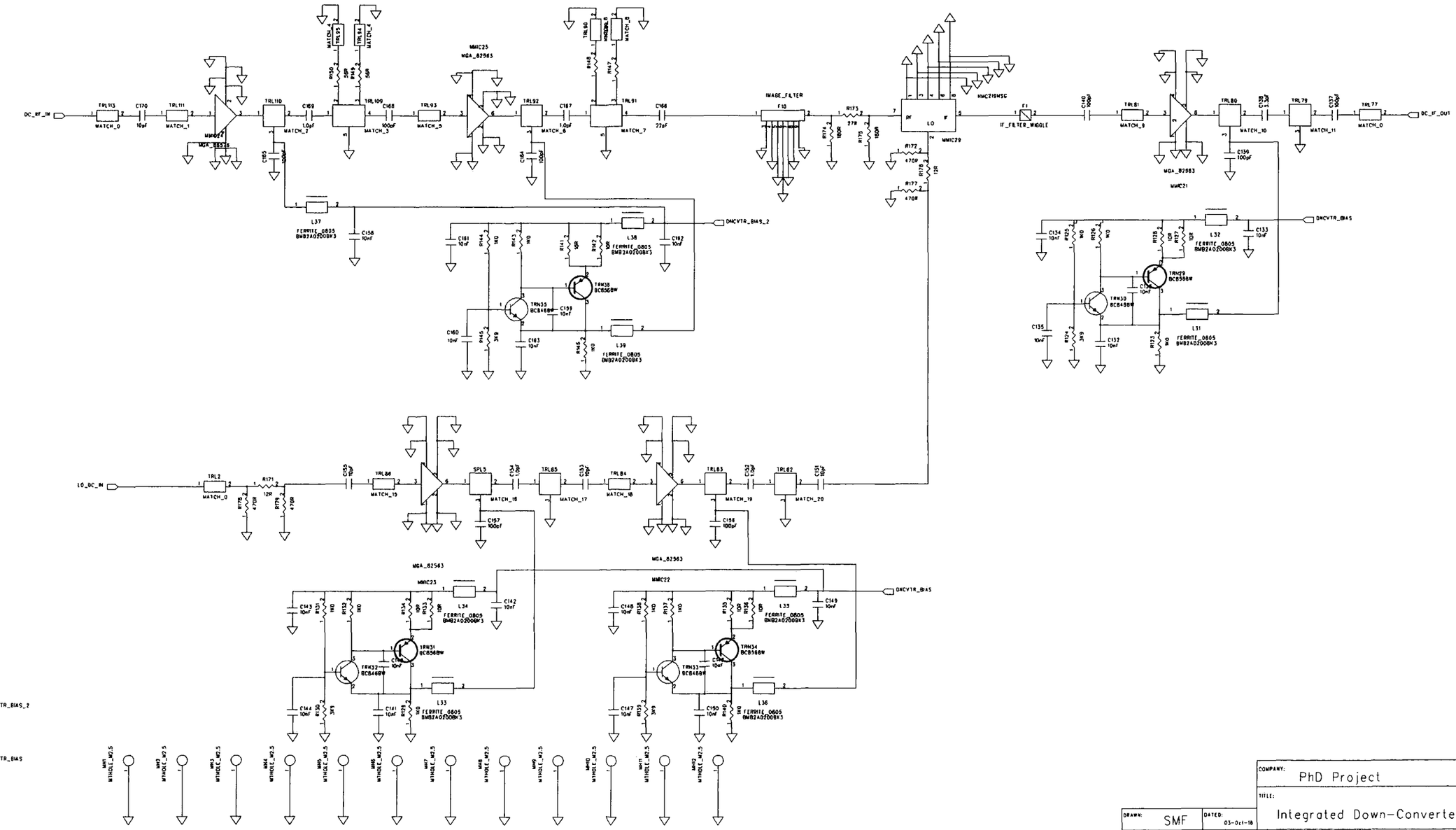

DRAWN: SMF	DATED: 03-Oct-18	COMPANY: PhD Project	
CHECKED: SMF	DATED: 03-Oct-18	TITLE: Integrated Down-Converter	
QUALITY CONTROL:	DATED:	CODE:	SIZE: A3 / DRAWING NO: / REV: 1
RELEASED:	DATED:	SCALE:	SHEET: of

REVISION RECORD			
LTR	ECO NO:	APPROVED:	DATE:

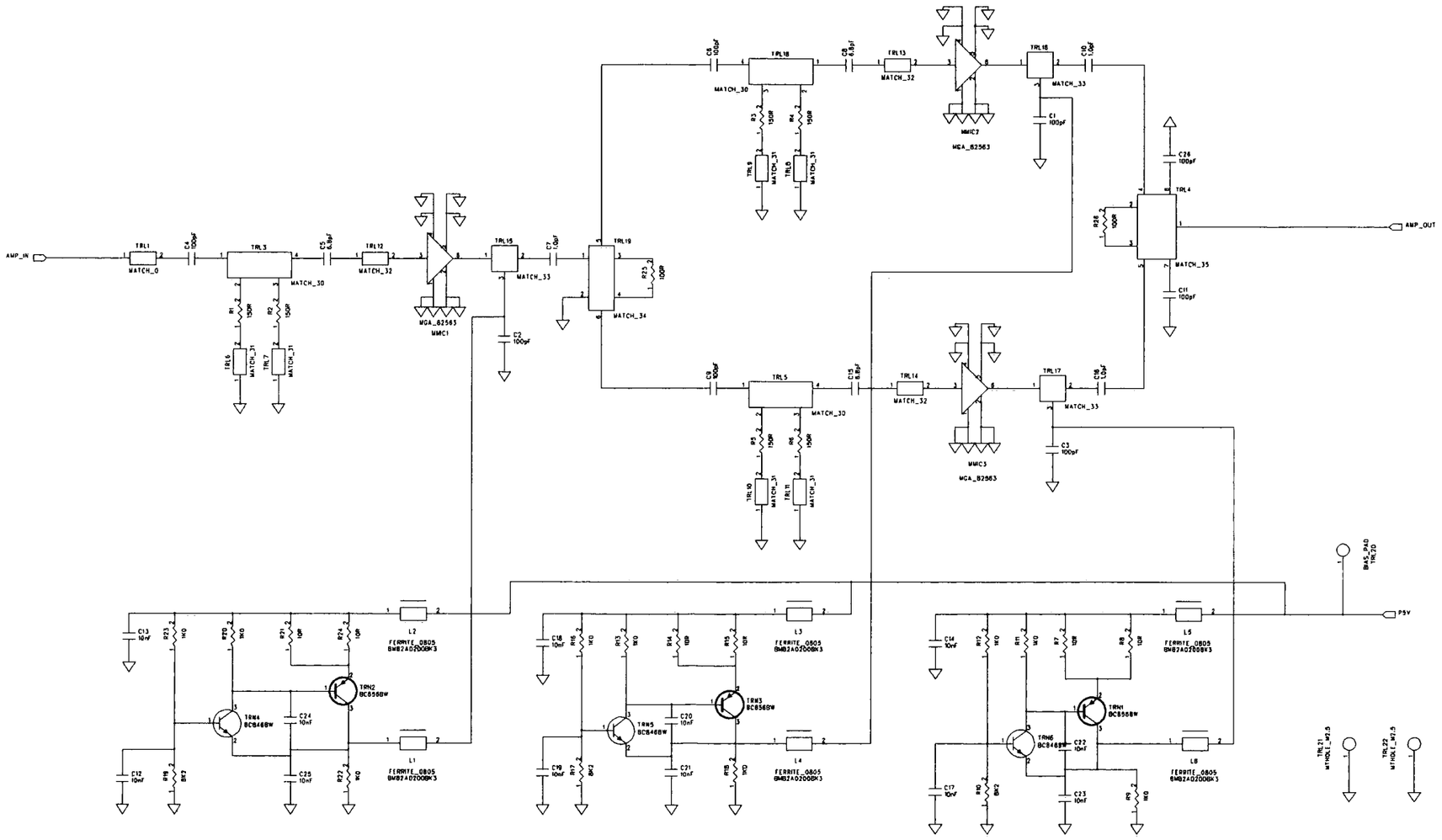

DRAWN: SMF	DATED:	COMPANY: PhD Project	
CHECKED: SMF	DATED:	TITLE: 2_Stage_Lab_Amp	
QUALITY CONTROL:	DATED:	CODE:	SIZE: A3 / DRAWING NO: / REV: 1
RELEASED:	DATED:	SCALE:	SHEET: OF

REVISION RECORD			
LTR	ECO NO:	APPROVED:	DATE:

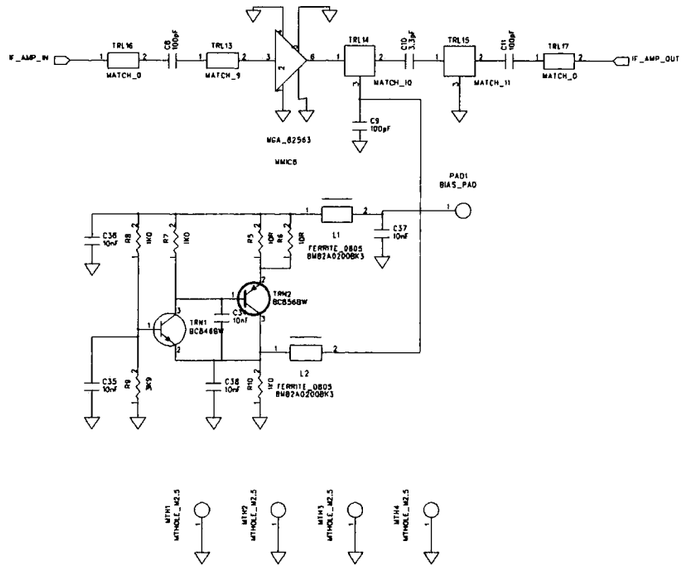

DRAWN: SMF	DATED: 03-Jul_16	COMPANY: PhD Project			
CHECKED: SMF	DATED: 03-Oct-20	TITLE: IF_AMPLIFIER			
QUALITY CONTROL:	DATED:	CODE:	SIZE: A3	DRAWING NO:	REV: 1
RELEASED:	DATED:	SCALE:		SHEET: 1 OF 1	

REVISION RECORD			
LTR	ECO NO:	APPROVED:	DATE:

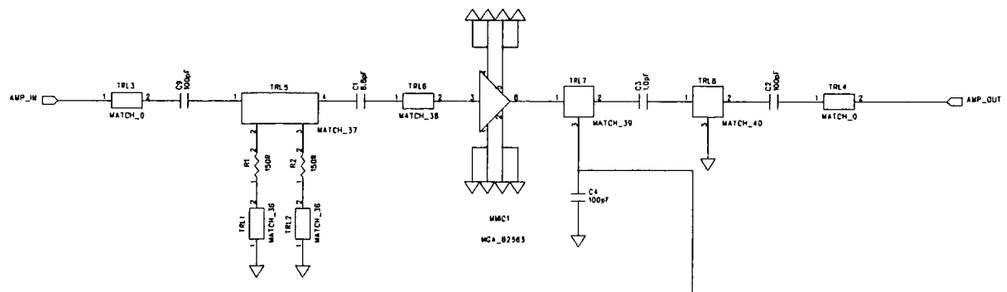

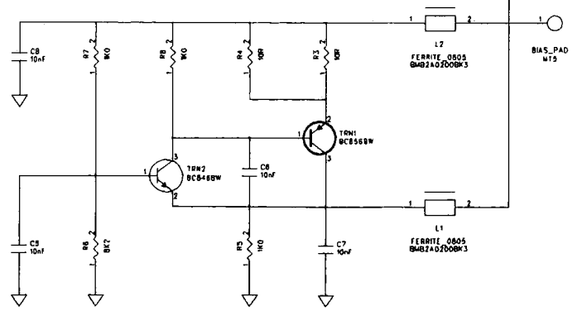

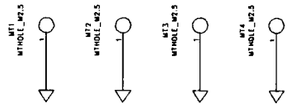

COMPANY: PhD Project			
TITLE: Single Stage Lab Amplifier			
DRAWN: SMF	DATED: 03-Oct-20		
CHECKED: SMF	DATED: 03-Oct-20		
QUALITY CONTROL:	DATED:		
RELEASED:	DATED:		
CODE:	SIZE: A3	DRAWING NO:	REV: 1
SCALE:		SHEET: OF	

REVISION RECORD			
LTR	ECO NO:	APPROVED:	DATE:

COMPANY:	PhD RF		
TITLE:	Baseband IF Amplifier		
DRAWN: SMF	DATED: 05-Apr-18		
CHECKED: SMF	DATED: 05-Apr-18		
QUALITY CONTROL:	DATED:		
RELEASED:	DATED:		
CODE:	SIZE:	DRAWING NO:	REV:
SCALE:	SHEET: 1 OF 1		

REVISION RECORD			
LTR	ECO NO:	APPROVED:	DATE:

COMPANY:			
TITLE:	SSB Down Converter		
DRAWN: S.M. Feeney	DATED: Sep_05	CODE:	SIZE:
CHECKED:	DATED:	DRAWING NO:	REV:
QUALITY CONTROL:	DATED:		
RELEASED:	DATED:	SCALE:	SHEET: 01

Annex 2: Publications

1. Abdalla M., Feeney S.M., and Salous S.; "Antenna Array and Quadrature Calibration for Angle of Arrival Estimation"; SCI2003, Florida, July 2003.
2. Feeney S., Filippidis P., Lewenze R., and Salous S.; "Multi-band Channel Sounder in the 2-6 GHz band"; BWA 2004, invited paper, presented at the BWA conference at Hinxton Hall (Cambridge)
3. Salous S., Feeney S.M., Razavi-Ghods N. and Lewenz R.; "Measurements in the 2-6 GHz Band"; presented at the URSI general assembly in New Delhi, October 23rd to 29th 2005.
4. Salous S., Feeney S., Razavi-Ghods N., Abdalla M.; "Sounders for MIMO Channel Measurements"; Eusipco 2005.
5. Feeney S., and Salous S.; "Wideband Sounder and Measurements in the 60 GHz Band"; Proceedings of The European Conference on Antennas and Propagation; EuCAP 2006 (ESA SP-626); 6-10 November 2006; Nice, France.

Antenna Array and Quadrature Calibration for Angle of Arrival Estimation

M. ABDALLA, S.M. FEENEY, and S. SALOUS
Department of Electrical Engineering and Electronics
UMIST, P.O. BOX 88, Manchester M 60 1QD UK

ABSTRACT

This paper reports on an active method that accurately measures the magnitude and phase information of multiple antenna arrays. The proposed method allows the estimation of amplitude and phase responses simultaneously. The analysis, architecture and implementation of the I/Q down-converter are described and the experimental results for single and multiple antennas are presented. Theoretical aspects supported by design, implementation and experimental results for the extraction of the antenna characteristics (amplitude & phase) will be presented. We have measured the phase and amplitude distributions of multiple antenna arrays at 2 GHz. The experimental results are in close agreement with the theoretical expectations. The measured amplitude and phase error is less than +/-1 dB and 2 degrees respectively and the system exhibits a dynamic range of 55 dB. The proposed measurement system is part of the channel sounder developed at UMIST and will be used for the estimation of angle of arrival in mobile communications.

Keywords: Antennas Array, Angle of Arrival, MIMO,

1. INTRODUCTION

Multiple antennas have drawn a great deal of interest recently as an essential component for channel characterisation systems. Measurements using multiple antennas provide angle of arrival information, and data necessary for the design of smart antennas and spectrally efficient systems such as multiple input multiple output (MIMO) systems. Assessment of frequency division duplex channels requires an optimal knowledge of both amplitude and relative phase characteristics of the antenna system.

With the introduction of the intelligent base station employing smart or adaptive antennas it is expected that the capacity and data rate of future cellular systems will be increased, thus producing high transfer rates and better quality services. Smart antennas employed at both base station and mobile station will be able to steer the antenna beam to minimize the effects of the interference and the multipath propagation, between the co-channel base stations and out stations therefore improving the overall system performance.

For several years UMIST has been undertaking a program of research into the characterization of the mobile channel within the 2 GHz frequency band. Several measurements have been taken within different environments and locations. A chirp sounder has been designed and implemented to take these measurements. Recently, a dual frequency chirp sounder has been up-graded to eight parallel channels at the receiver. By connecting an eight-element array of antennae to the channel, it is possible to extract the direction of arrival of each multipath component. Several types of antenna arrays have been designed and constructed to facilitate these measurements.

This paper describes a practical implementation of a quadrature down-converter that has been demonstrated to characterize amplitude and relative phase responses for an antenna array to support double directional estimation. The paper is organized as follows. Section 2 contains a brief description of the UMIST multiple channel sounder. Section 3 addresses the antenna array arrangement for angle of arrival estimation. In section 4 we describe the antenna array to be characterized. Section 5 presents the direct conversion approach as a method for extracting the amplitude and phase responses. Section 6 provides a full description for the I/Q down-converter technique. Section 7 details the measurement set-up. The experimental results illustrating the performance of the system are given in section 8. Section 9 concludes the paper.

2. UMIST MULTIPLE RECEIVER CHIRP SOUNDER

To meet the new requirement of MIMO channel characterization, the dual frequency sounder that had been designed and implemented at UMIST has been enhanced to support eight simultaneous channels at the receiver side [1, 2]. The chirp sounder transmits a signal that is characterized by a linear frequency increase or decrease over B Hz in T s. At the receiver, the signal is compressed in bandwidth using the heterodyne detector whose output over T seconds consists of the sum of the attenuated beat notes. These beat notes correspond to the different

multipath components present in the channel during that sweep. The frequency of each beat note is proportional to the product of the time delay of the echo and the sweep rate (B/T). Hence, the beat notes may therefore be spectrally analyzed (via FFT for example) to show the different multipath components arriving at the receiver. By observing the variation over a number of sweeps, the time variation and arrival times of the various multipath components can be resolved. Positional information was derived from GPS and a wheel sensor to log the measurement positions of the channel impulse response soundings.

3. ANTENNA ARRAY ARRANGEMENT AND THE DIRECTION OF ARRIVAL

Optimal direction of arrival measurements requires knowledge of both the amplitude and phase characteristics of the antenna system. To estimate the angle of arrival of multipath components resulting from rich scattering and reflection off buildings, the sounder must have the capability of angle estimation in the spatial domain. For a multi-channel sounder this is achieved by employing an array of antennas, each connected to a separate receiver channel. The channel measurement is processed to resolve the time delay of the multipath components received at the associated antenna.

A number of antenna array configurations such as, linear, circular, rectangular, zigzag, "L" shaped, and "X" or "Y" crossed elements have been considered and simulated to predict their effects and characteristics in an array geometry [3]. Each of these arrangements has advantages and drawbacks. Since the angle of arrival with 360 degrees coverage is desired a uniform circular array arrangement has been selected to support this requirement. To enhance the angular resolution capability of the sounder, it is possible to steer the antenna beam to one of three positions using electronic phase shifters. Thus providing a total of 24 beams for an array of eight antennas. By employing a super-resolution algorithm, the measurements of the angle of arrival as well as the direction of departure can be deduced.

4. ANTENNA ARRAY DESIGN

Briefly stated, the principle of operation and design for the antenna array is reported in [5], the full antenna description and design is a separate issue from the array characterisation. The antenna is a double-sided strip dipole etched on thin dielectric substrate with relative permittivity $\varepsilon_r = 2.2$ and a thickness of 1.57 mm. It consists of two series-fed printed strip dipoles. Two printed strip dipole of different lengths, with the arms printed on opposite side of an electrically thin substrate connected through a parallel strip line. The antenna is fed from a conventional 50-Ω connector through a micro-strip to parallel strip-line multi-section quarter-wavelength transformer. A shaped ground-plane reflector supports the antenna array. This provides support and restricts the radiation pattern to the end-fire direction. The primary features of the antenna are low cost, low weight and that it is easy to construct with high repeatability. The antenna provides a bandwidth of greater than 30 % for VSWR <1.5. To optimise the antenna beam to provide 45-degrees of interval resolution in the azimuth plane and to increase the antenna gain the elements of the antenna array are combined using a Wilkinson power combiner.

These antennas are fixed to a frame such that each antenna provides coverage of 45-degrees per sector giving in total 360 degrees coverage. The spacing between the antennas was kept to the minimum compatible with the mechanical arrangement. Since we are dealing with array geometry rather than a single antenna, it was anticipated that there would be coupling between the antenna elements. Thus calibration of the array must be performed with all antennas in the array present and active.

5. DIRECT CONVERSION TECHNIQUE

Initial measurements were attempted using quadrature down conversion from the measurement frequency directly.

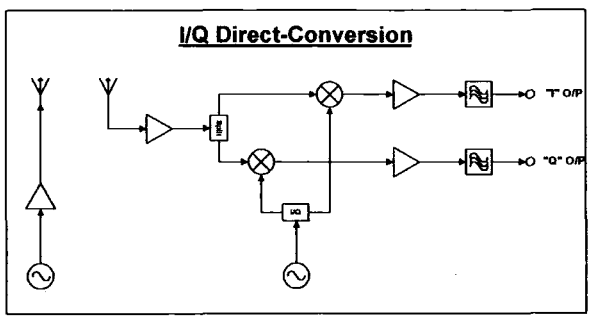

Figure 1. Block diagram of direct conversion architecture

In such a system, the signal under characterization (in this case from the antenna under test) is split into two equal level samples. Each of these signals is then down-converted to base-band (dc plus low frequency components) using a mixer. Each of these mixers is operated with local oscillator drive signals that are maintained in phase quadrature (90 degrees phase difference).

Two output signals are then available for processing, with each signal having a magnitude component only.

The total signal magnitude is then defined as the magnitude of the vector described in the I/Q plane.

That is: $Magnitude = \sqrt{I^2 + Q^2}$

The phase angle between the signals is defined by the angle of the vector in the I/Q plane referred to the real "I" axis.

That is: $\Phi = \tan^{-1}\left(\frac{Q}{I}\right)$

In principle it is possible to perform the quadrature down-conversion directly at the frequency of operation of the antenna.

The principal problems when performing direct down conversion were observed to be:

1. The presence of an offset voltage at the output of the down-converting mixers.
2. Quadrature errors in the mixer local oscillator drive signals.
3. Phase noise due to the summation of the phase noise present in both the transmit source and the receiver local oscillator.

It was observed that this approach was severely limited. This was due to the difficulty in controlling the quadrature components, the limited output swing from the radio frequency mixer, the relatively high (and variable) offset voltage and the sensitivity to phase-noise within the RF sources. Consequently this approach was abandoned and an approach using a fixed frequency measurement subsystem in conjunction with a primary down-converter has been developed as an alternative method to extract the amplitude and phase response.

6. FOUR CHANNEL I/Q DOWN-CONVERTER

The quadrature down-converter consisted of a reference channel and four identical measurement channels.

All channels included a band-pass filter operating at 10 MHz with a bandwidth of ± 1 MHz that reduced the influence of out-of-band signals on the measurements.

The reference channel provided quadrature local oscillator signals at 10 MHz that were phase locked to the 10 MHz reference signal. An automatic level control loop was included to ensure that the loop gain and therefore tracking bandwidth was independent of input signal level. The phase locked loop also included automatic in-lock detection and automatic sweep to acquire initial phase lock.

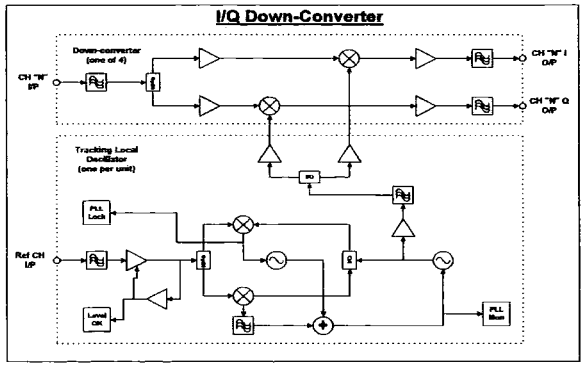

Figure 2. Block diagram of I/Q down-converter module

The four measurement channels were identical. The input signal was split into two, each of these was down-converted to dc using the appropriate quadrature local oscillator signals. Each measurement channel provided two outputs. The first of these corresponded to multiplying the input signal with the in-phase local signal from the reference channel-tracking oscillator. The second channel corresponded to the quadrature phase local signal from the reference-tracking oscillator. These formed the "I" and "Q" outputs which were then digitized using an eight input data acquisition card with 12-bit accuracy.

The quadrature down-converter was evaluated to determine the available precision of measurement and to confirm the carrier tracking operation.

The attenuation of close to carrier disturbances was evaluated by providing a stimulus to both the reference channel and one of the measurement channels simultaneously. This stimulus was a high index frequency modulation applied to the 10 MHz signal. A peak-to-peak deviation of 50 kHz was applied with a modulation frequency of 10 Hz. This corresponded to a peak-to-peak phase deviation of 31000 radians. The output of the down-converter was observed to indicate a resultant phase deviation of 0.056 radians. Thus the overall attenuation plus residual frequency to phase distortions due to filter delay, I/Q precision, etc was observed to be 115 dB.

The down-converter was characterized for the following:

- Residual offset voltages (Offset "I" and Offset "Q")
- Residual phase errors (Phase reference)
- Amplitude differences (Amplitude reference)
- Quadrature errors (Quadrature I:Q)
- Cross talk between channels
- Amplitude dynamic range
- Phase measurement dynamic range

Channel	Ch 1	Ch 2	Ch 3	Ch 4
Offset "I"	-1.0 (mV)	-1.0 (mV)	+0.1 (mV)	-0.5 (mV)
Offset "Q"	-0.8 (mV)	-1.0 (mV)	-0.6 (mV)	-0.6 (mV)
Phase Reference	90.0°	89.9°	90.0°	90.0°
Amplitude Reference	-0.18 (dB)	-0.16 (dB)	+0.33 (dB)	0dB (ref)
Quadrature I:Q	90.0°	91.6°	90.9°	90.6°

Cross talk (Channels 3 to 4) <2mV peak, equivalent to <-66dB.

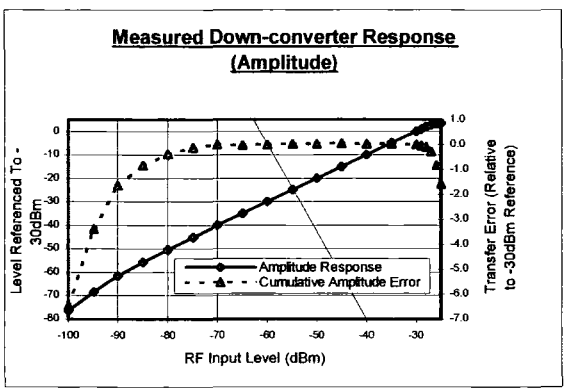

(a)

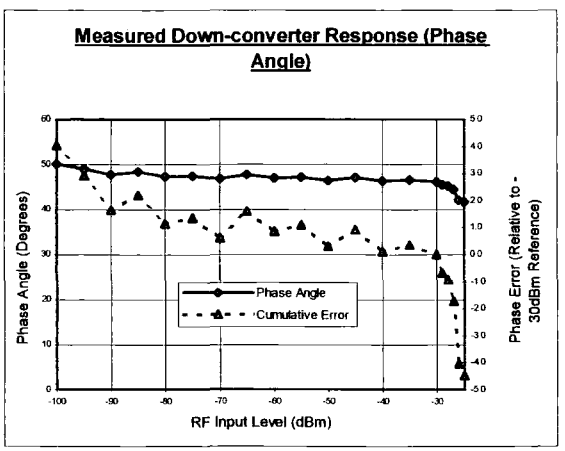

(b)

Figure 3. (a) The measured amplitude, (b) phase response of the quadrature down-converter.

The above graphs show that the quadrature down-converter demonstrated measured amplitude accuracy within 1dB and a measured phase angle within +/-1 degree for an input level range of –85 dBm to –30 dBm.

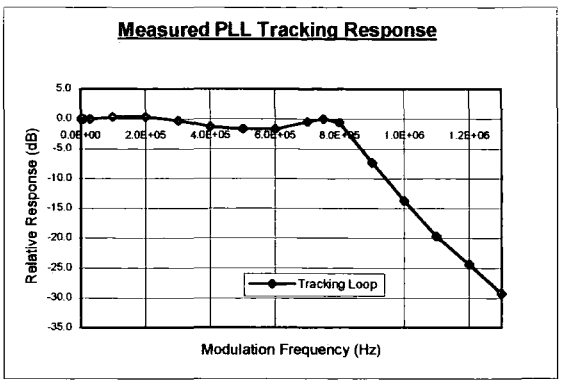

Figure 4. The measured frequency response of the tracking loop.

The above figure describes the measured frequency response of the tracking loop. This is a second order loop with a corner frequency of approximately 800 kHz.

7. MEASUREMENT SET-UP

To accurately characterise the antenna array it is necessary to perform the measurement of the magnitude and phase response in an anechoic environment. The antenna calibration rig was comprised of a turntable on which the antenna array under test is mounted and a separate test transmitter. The antenna was characterized at 2 GHz. The corresponding wavelength was 0.15 m. The antennas under test had an effective aperture of approximately 0.2 m. A separation of 5m was used to ensure that the measurements were performed in the far field for the transmitter antenna and the receiver antenna under test.

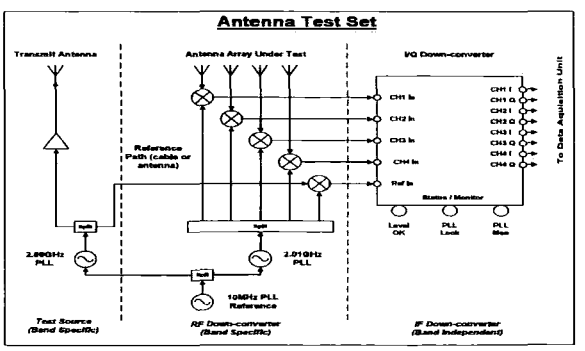

Figure 5. Block diagram of the antenna test set

The system consisted of a test RF source, a multi-channel RF down-converter, a multi-channel quadrature demodulator and a data acquisition unit. The RF test source and the RF down-converter are specific to the frequency range under measurement. The multi-channel quadrature down-converter is independent of the frequency range under measurement.

The test RF source consisted of a 2 GHz voltage controlled oscillator (VCO) that was phase locked to a 10 MHz reference. A sample of the output of the VCO was used to provide a reference signal for the receiver. An amplifier was included to provide sufficient output from the test RF source transmit antenna to enable peak signals of –30 dBm at the input of the quadrature down-converter.

The multi-channel RF down-converter was implemented using a VCO phase locked to the same 10 MHz reference used for the transmitter. An offset of 10 MHz was set between the sources used by the RF test source and the RF down-converter. Thus the outputs from the multi-channel down-converter were at 10 MHz.

One channel of the multi-channel down-converter was used to mix-down the sample signal from the RF test source and was used to provide a reference signal input to the multi-channel quadrature down-converter. The other four channels of the RF down-converter were used to perform down-conversion of the 2 GHz signals from the outputs of the antenna array under test to an intermediate frequency of 10 MHz. The 10 MHz intermediate frequency signals were then down-converted to extract quadrature dc outputs using the four-channel quadrature down-converter.

The quadrature down-converter used a local oscillator which was phase locked to the reference input. The phase locked local loop ensures that the multi-channel quadrature demodulator processes the measurement channels with a source that was phase coherent to the effective carrier of the 10 MHz intermediate frequency signals. This effective carrier contained phase noise terms that were due to both 2 GHz RF sources. The phase locked loop therefore also provided a means to attenuate close to carrier noise that would otherwise cause the output voltages to be smeared in phase.

The output of the quadrature down-converter consisted of eight voltage outputs with an "I" and "Q" value assigned to each of the four input channels. These voltages were then logged into a computer via an eight-channel data acquisition card with 12-bit accuracy. The computer also provided the stimulus to a rotator unit such that the antenna array could be characterized over 360 degrees of rotation.

8. RESULTS

Two sets of measurement have been performed. The first set of measurements a logarithmic amplifier to derive magnitude only. The second series of measurements used used the I/Q down-converter to derive magnitude and phase.

Figures 6a and 6b depict the measured performance of an antenna that has been characterized using both the I/Q down-conversion technique and direct amplitude measurement using a successive detection logarithmic amplifier (also operated at 10 MHz).

Close agreement can be observed with both methods over the relevant measurement range.

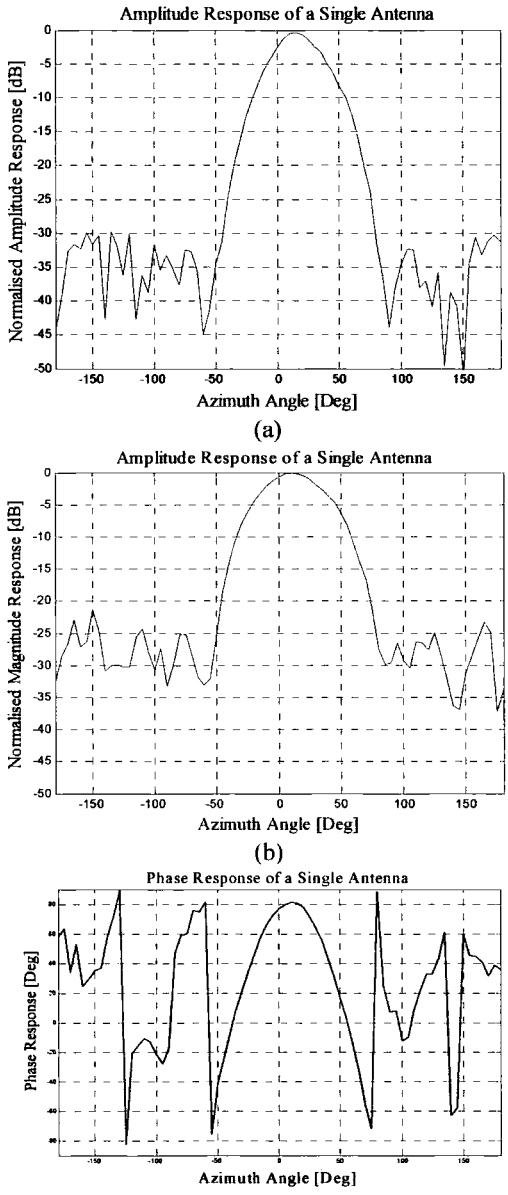

Figure 6. Experimental results for a single antenna (a) amplitude with log-amplifier, (b) amplitude with I/Q down-converter, (c) phase with I/Q down-converter

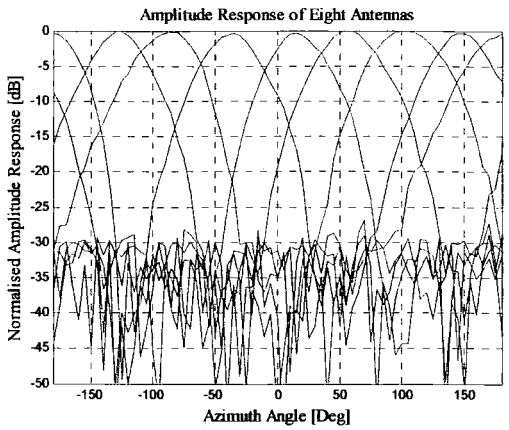

(a)

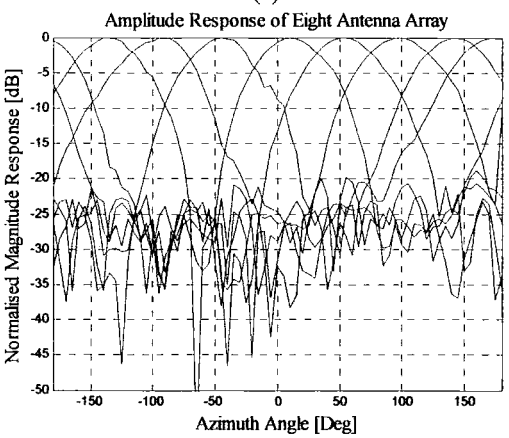

(b)

Figure 7. Experimental results for the amplitude of the realized eight-element antenna array (a) with log-amplifier, (b) with I/Q down-converter.

Figures 7a and 7b display the responses of eight antennas as a function of azimuth angle. It can be observed from the figure that the 3dB points of consecutive antennas cross to provide full coverage in azimuth over 360 degrees.

9. CONCLUSIONS

We have presented an efficient method to measure the amplitude and phase response for multiple antenna arrays simultaneously. Measurements carried out using the method described show the successful application of the technique. The measurements obtained are in good agreement (in terms of amplitude) between the results from logarithmic amplifier and the quadrature down-converter. The measured amplitude and phase error derived from the system are $\pm$1dB and 2 degrees respectively. The proposed system will form part of multiple antenna channel sounder for the estimation of direction of arrival and direction of departure for multipath components.

10. ACKNOWLEDGEMENTS

The authors would like to thank Mr. Roger Lewenz for building the mechanical part of the calibration rig, and Mr. Derek Vale for producing the PCB used in the system.

11. REFERENCES

[1] S. Salous, P. Fillipidis, and I. Hawkins, "Multiple antenna channel sounder using a parallel receiver architecture", **SCI2002**, Orlando Florida, July 2002.

[2] S. Salous, "Chirp waveforms for multiple antenna channel sounders", **URSI 27th General Assembly**, Maastricht, August 17-24.

[3] R. Lewenz, P. Fillipidis, M. Abdalla and S. Salous, "Antenna arrays for channel sounding with direction of arrival estimation and calibration", **SCI2002**, Orlando Florida, July 2002.

[4] RG. Lewenz , P. Fillipidis, and S. Salous, "Antenna array calibration for a multi-channel direction of arrival sounder", **HFPG Colloquium**, Cardiff, 2001

[5] Faton Tefku, and Caiag A. Grimes, "Design of broad-band and dual-band antennas comprised of series-fed printed-strip dipole pairs", **IEEE Transaction on antennas and propagation**, Vol.48, No.6, June 2000.

Multi-band Channel Sounder in the 2-6 GHz band

S. M. Feeney, P. Filippidis, R. Lewenz, S. Salous

Centre for Communication Systems, School of Engineering,
University of Durham, Durham DH1 3LE, UK
stuartfeeney@aol.com, Fax: +44 191 334 2407

Keywords: Radio Sounding, Chirp.

Abstract

This paper presents a multi-band frequency extender for use with the Durham FMCW parallel receiver channel sounder. This frequency extender provides the facility to make simultaneous measurements in the 2.5 GHz, 3.5 GHz and 5.2/5.8 GHz bands. The new up-converters will also form part of a system to make measurements in the 60 GHz to 75 GHz band.

1. Introduction

A dual band channel sounder with eight parallel receive channels has been designed and implemented to perform measurements at the two frequency division duplex bands of UMTS [1]. New wireless communication systems are being deployed in the bands above 2 GHz. Some of these systems may be operating within several possible bands of unlicensed spectrum such as the 2.5 GHz, 3.5 GHz and 5.2/5.8 GHz bands. Successful deployment of commercial services in these bands will require an understanding of the propagation within cluttered environments.

Recently, parametric modelling has been proposed as a means of characterising the channel for different antennas and possibly using the derived channel parameters to determine the channel behaviour at different frequencies [2]. The derived channel parameters include, time delay and amplitude of the multipath components, their angles of arrival and angles of departure in both elevation and azimuth.

To carry out propagation measurements for the higher frequency bands and to verify the parametric model, the frequency of the FDD multiple receiver channel sounder is being upgraded.

The paper provides a short description of the multiple receiver channel sounder system and the architecture employed to upgrade its operating frequency. The effect of spurious components associated with the frequency references used within the system and the method used to reduce their effect is outlined. This is followed by a description of the transmit up-converters and down converters to the 2 GHz band. Initial measurement results for the 3.5 GHz and 5.8 GHz bands are presented.

2. System Description

2.1 UMTS FDD parallel receive sounder

The block diagram of the dual band UMTS parallel receive channel sounder is shown in figure 1. The transmitter consists of a programmable chirp generator, and an up-converter to the FDD bands of UMTS (1920-1980 MHz and 2110-2170 MHz). Each band is amplified separately and the two bands are then combined to feed a single antenna, which can be switched for multiple transmit antenna measurements.

The receiver consists of eight parallel RF receive channels and an identical chirp generator, which feeds an eight way splitter. The received signal from each RF channel is mixed with the local replica to produce a beat note for each multipath component. The signal is subsequently low pass filtered, amplified and logged into the eight-channel data acquisition card with 128 Mbyte RAM. This enables logging in of 15 seconds of continuous data on each of the eight channels. The sounder has been used successfully to perform both single input multiple output (SIMO) and multiple input multiple output (MIMO) measurements in both indoor and outdoor environments [3].

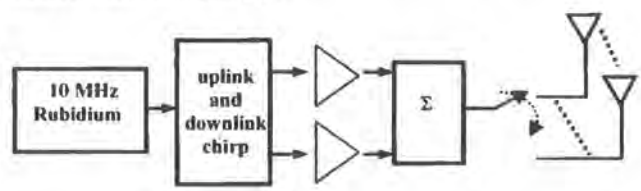

(a)

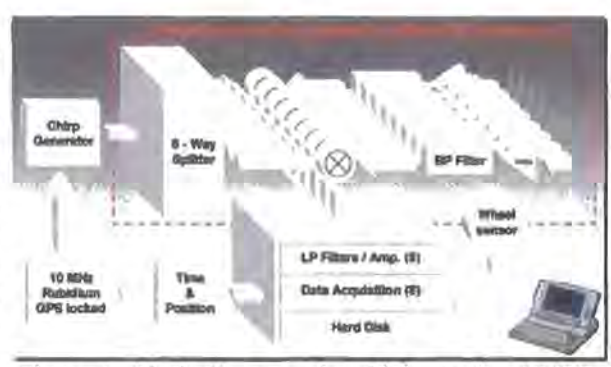

Figure 1. Block diagram of multiple receive UMTS FDD sounder (a) transmitter, (b) receiver.

2.2 Extension to higher frequency bands

Figure 2 displays the block diagram for the multiple frequency band extension. The chirp signal output of the UMTS sounder is split into three identical portions using a power divider. Each of these signals is then up-converted using separate up-converters to nominally 2.5 GHz (2.3-2.7 GHz), 3.5 GHz (3.3-4.5 GHz) and 5.8 GHz (4.5-6 GHz). The 2.5 GHz converter is implemented using a dual conversion scheme to simplify the separation of the IF (1.8 GHz to 2.2 GHz) and RF (2.3 GHz to 2.7 GHz) bands. The 3.5 GHz and 5.2/5.8 GHz converters use a single conversion scheme with the local oscillator above the IF and RF bands. The converter uses a common module capable of operating over the full band from 3.3 GHz to 6.0 GHz. The band has to be segmented to allow the local oscillator to be filtered since this falls in this band when operating in the lower region of the output band.

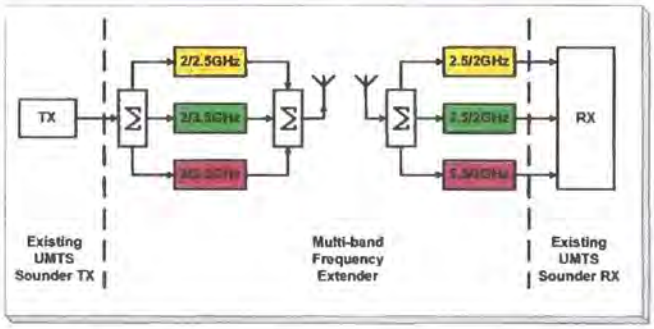

Figure 2. Block diagram for the multi-band sounder

The outputs of each of the converters can either be operated individually or simultaneously. The converter modules include amplifiers to provide a nominal output power of +22 dBm for each converter. For multiple frequency measurements the outputs of the three converters are combined using broadband Wilkinson combiners to provide a single output port with nominally +15 dBm per band. A discone antenna design has been selected to provide a broadband antenna to cover the 3-10 GHz band.

An identical discone antenna is used for the receiver. The signal from the receiver antenna is split to provide inputs to three down-converters, which provide down-conversion back to the UMTS band. These signals can be either then processed using three channels of the eight channel parallel sounder receiver as shown in figure 2 or each band can be duplicated for SIMO or MIMO measurements as required.

The 2.5 GHz down converter is implemented using a dual conversion with an intermediate frequency at 500 MHz to 900 MHz. The 3.3/4.5 GHz and 4.5/6.0 GHz down converters both use a high side local oscillator. The down-converter module provides coverage for the full band from 3.3 GHz to 6.0 GHz. The band is segmented by the input RF filter and the local oscillator multipliers (X2 and X3 respectively). The complete down-converter modules provide a net gain of 27 dB with an associated noise figure of 4 dB. Including the loss of the input splitters used in the multi-band configuration the net gain is 21 dB with a noise figure of 10 dB. The input compression point is > -15 dBm in this configuration.

The transmit up-converters and receive down-converters are constructed as individual modules that are contained in a transmit sub-rack and receive sub-rack. Each of these sub-racks includes a common support module. This module includes a microcontroller that is used to configure the individual converters, a power supply to derive the necessary voltages from the 24 V input supply and a low phase noise 10 MHz reference source that is locked to the transmitter and receiver Rubidium clocks in the UMTS channel sounder.

Figure 3 displays the UMTS sounder transmitter, which is contained in the lower two sub-racks and the transmitter frequency extender, which is contained in the upper rack. Figure 4 displays the receiver with the bottom 3U rack and middle 6U rack containing the eight-channel UMTS sounder. The top 3U rack contains the receiver frequency extender containing the controller / power supply / reference and the 2.5 GHz, 3.3/4.5 GHz and 4.5/6.0 GHz down-converters.

Figure 3. Complete multi-band sounder transmitter

Figure 4. Complete multi-band channel sounder receiver

3. System Reference Sources

The channel sounder utilises Rubidium stabilised oscillators to provide reference sources that have high long term stability (low drift). The source utilises a Quartz crystal oscillator that is locked to the primary atomic standard resonance frequency of the Rubidium atom. The control loop within this source operates at a comparison frequency of 127 Hz. Spurious signals due to this process are present as sidebands on the 10 MHz output signal at a very low level. For operation at frequencies up to 2 GHz the spurious level has been acceptable.

However the frequency extender includes local oscillator sources at 7.8 GHz. At this higher frequency the spurious signals at the output of the Rubidium stabilised source become problematic. These converters also form part of a system under development to perform measurements in the 60 GHz to 75 GHz band. Operation at these higher frequencies increases the sensitivity to these spurious signals by a further 20 dB due to the effect of frequency multiplication.

This problem has been solved by implementing a tracking phase locked loop operating on the Rubidium source. This phase locked loop locks a low phase noise oven stabilised Quartz resonator oscillator to the Rubidium source with a tracking bandwidth of 3 Hz. This provides a theoretical suppression of >70 dB to the sidebands at 127 Hz.

To illustrate the operation of the reference filter a low phase noise 2 GHz source was phase locked to the transmit system reference and used to provide an input to the up-converter. The up-converter was locked to the transmit system reference and the output of the up-converter at 5.8 GHz used as the input to the down-converter. The down-converter was locked to the receive system reference and provided an output at 2 GHz. This 2 GHz output was observed using a spectrum analyser. This output provides an indication of the total phase noise due to the test source, the up-converter and the down-converter.

The transmitter and receive system references were then operated in three different modes. In mode 1 the Rubidium stabilised source was used directly. In mode 2 the oven stabilised source was used in a free running mode. In mode 3 the oven stabilised oscillator was locked to the Rubidium stabilised to provide attenuation of the spurious signals. The behaviour is presented in figure 5.

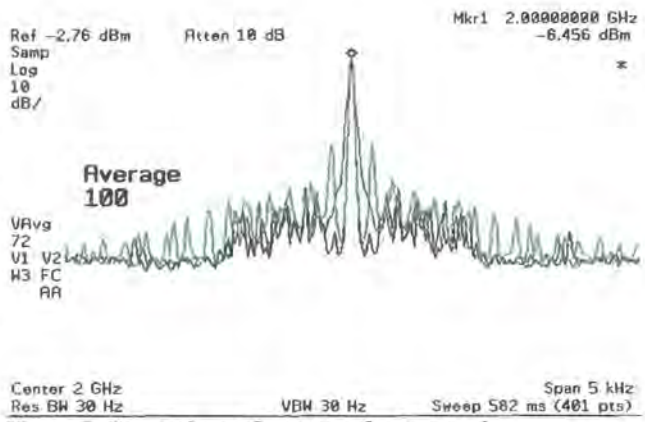

Figure 5. Comparison of system reference modes
Green: Mode 1 Rubidium source direct.
Red: Mode 2 Oven stabilised source direct.
Blue: Mode 3 Oven source locked to Rubidium.

4. Performance and measurements

The spectra of the generated signals at two of the frequency bands (3.53 GHz and 5.25 GHz) are shown in figures 6 and 7. Similar performance was observed on the other two frequency bands.

A measure of the performance of a channel sounder is its resolution in the time delay, which is determined from back to back tests. Figure 8 displays the back to back results for the 3.5 GHz and 5.8 GHz bands. The figure shows that the unwanted components level is less than 35 dB from the wanted component, which is adequate for radio channel measurements.

A preliminary measurement is displayed in figure 9 at the same two bands and shows the differences between the two bands and the extent of multipath spread. The measurement was taken on the Science Park of Durham University.

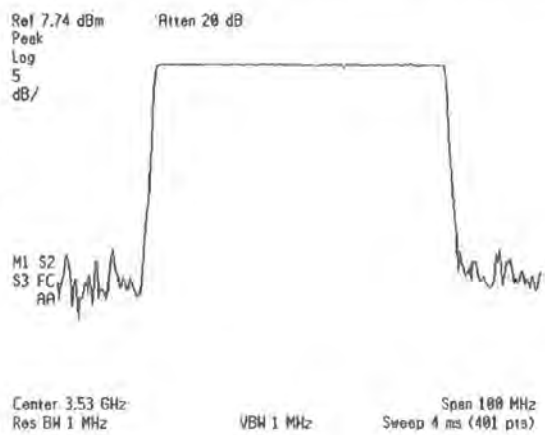

Figure 6. Output at 3.53GHz from the 3.3/4.5GHz converter

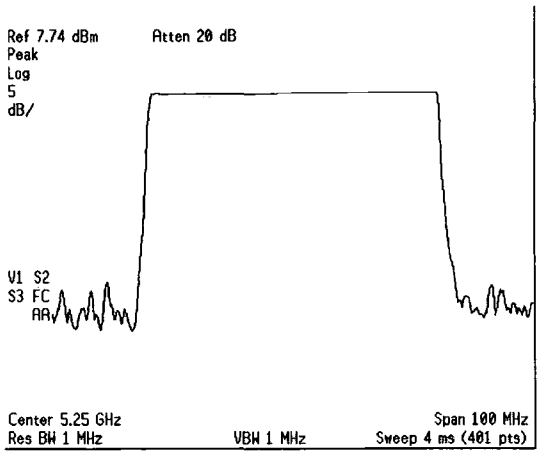

Figure 7. Output at 5.25GHz from the 4.5/6.0GHz converter

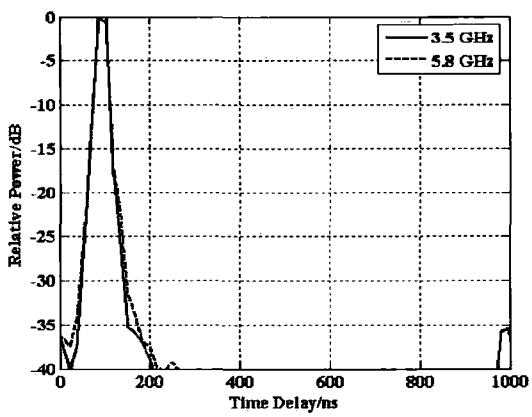

Figure 8. Back to back performance at two frequency bands.

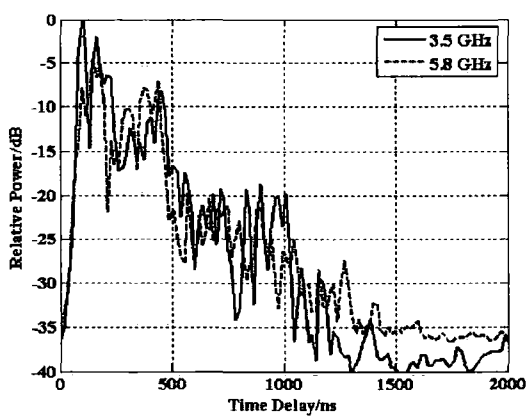

Figure 9. Power delay profile obtained at 3.5 GHz and 5.8 GHz.

5. Discussion and Conclusions

Basic channel sounding behaviour has been demonstrated simultaneously at 3.5 GHz and 5.8 GHz.

Future work will be concerned with further simultaneous measurements and with the upgrading of the sounder for SIMO and MIMO measurements at the extended frequency bands.

6. References

[1] S. Salous, P. Fillipidis and I. Hawkins, "Multiple Antenna Channel Sounder Using a Parallel Receiver Architecture", SCI2002, Orlando Florida, July 2002.

[2] A. F. Molisch, M. Steinbauer, M. Toeltsch, E. Bonek, and R. S. Thomä, "Capacity of MIMO Systems Based on Measured Wireless Channels", IEEE Journal on Selected Areas in Communications, Vol. 20, No. 3, April 2002, pp 561-569.

[3] S. Salous and N. Razavi-Ghods, 'Semi-sequential MIMO channel measurements in indoor environments', COST 273, TD (04) 79, Gothenburg, June 2004.

Acknowledgements

The authors would like to thank Applied Wave Research for providing "Microwave Office 2002" software used in the design of the RF circuits and John Feeney for the use of his machine tool workshop to produce the mechanical components (housings, filters and antennas).

MEASUREMENTS IN THE 2-6 GHZ BAND

S. Salous, S. Feeney, N. Razavi-Ghods, and R. Lewenz

Centre for Communication Systems, School of Engineering
University of Durham, Durham, DH1 3LE, UK
sana.salous@dur.ac.uk

ABSTRACT

Single input single output (SISO) and multiple input multiple output (MIMO) measurements at frequencies between 2-6 GHz have been performed using a specially designed and implemented multiple receive channel sounder. These include simultaneous SISO measurements at three frequency bands in rural environments and wideband MIMO measurements at two frequencies in a TV studio environment. The paper briefly discusses the architecture of the sounder and the results of the various measurements are presented.

INTRODUCTION

A dual band channel sounder with eight parallel receive channels has been designed and implemented to perform various single input multiple output SIMO and MIMO measurements at the two frequency division duplex bands of UMTS [1]. New wireless communication systems are being deployed in the bands above 2 GHz. Some of these systems may be operating within several possible bands in the unlicensed spectrum such as the 2.5 GHz, 3.5 GHz and 5.2/5.8 GHz bands. Successful deployment of commercial services in these bands will require an understanding of the propagation within various indoor and outdoor environments. To characterise these frequency bands, up-converters and down-converters with either a single channel or multiple receive channels have been designed and implemented. The upgraded channel sounder was then used to perform simultaneous frequency measurements at 2.5 GHz, 3.5 GHz and 5.8 GHz in rural areas for the characterization of WMAN channels with SISO configuration. These were performed with 10 MHz bandwidth, and subsequently processed with 5.7 MHz bandwidth for the 2.5 GHz and 3.5 GHz bands or with 10 MHz bandwidth for the 5.8 GHz band. The data were processed to determine various channel functions, which include the time variant frequency function, and the power delay profile. While the transfer function is preferred for the simulation of OFDM modulation as proposed for WMAN systems, the power delay profile can be used to determine the number of significant multipath components to use in a tapped delay line simulator.

MIMO measurements were performed either at a single frequency using up to eight receive channels or simultaneously at two frequencies using four receive channels at each frequency band. The single frequency measurements were carried out at the uplink frequency of UMTS using 60 MHz bandwidth [2], while the dual frequency measurements were conducted with 100 MHz bandwidth at 2.2 GHz and 5.8 GHz. These were mainly indoor measurements with the latter being performed in a typical TV studio. Results of the dual frequency measurements are presented here in terms of MIMO channel capacity for different antenna numbers.

MULTIBAND CHANNEL SOUNDER

The multi-band channel sounder designed and implemented for the purposes of the measurements, is based on the chirp sounder with eight parallel receive channels at the UMTS frequency division duplex bands (1920-1980 MHz and 2110-2170 MHz) with programmable bandwidth, waveform repetition frequency (WRF) and centre frequency [1]. For higher frequency bands, two separate units were designed and implemented which consist of up-converters and down converters, with either single channels or multiple channels. Fig. 1.a displays the block diagram for the single channel converter units whose output/input can be combined to feed a single antenna at both ends of the link or separate antennas as required. Fig. 1.b-c shows the realised transmitter and receiver with the converter units. The sounder can also be used in a number of other configurations which can be either single frequency band measurements with eight receive channels or four receive channels on two different frequencies as shown in Fig. 2 for the MIMO measurements performed in a TV studio.

The receiver of the sounder employs the heterodyne detector, which mixes the received chirp signal with a delayed replica. This results in a beat note for each multipath component, which can then be identified using spectral analysis. The technique compresses the signal in bandwidth and not in time, and since the frequency of a chirp signal is linearly related to time, the digitised signal can be processed for different frequencies and bandwidths by taking the relevant

section. Using the fast Fourier transform (FFT) different channel functions such as the power delay profile, the scattering function, the Doppler spectrum, and the time variant transfer function can be obtained.

MULTIBAND SISO AND MIMO MEASUREMENTS

Field trials were performed in both indoor and outdoor environments at different frequency bands. Simultaneous SISO measurements at three different frequencies (2.5 GHz, 3.5 GHz and 5.8 GHz) with 10 MHz bandwidth, 250 Hz WRF and 1 s duration per location, were performed in a typical rural residential environment. Three separate transmit antennas were mounted on top of a tower and three separate omni-directional dipoles were used for reception. Simultaneous 4 by 4 MIMO measurements using the configuration of Fig. 3 were performed in a studio environment with 100 MHz bandwidth, 250 Hz overall WRF and 1 s per run. Due to the switching at the transmitter, the effective WRF per antenna is 50 Hz giving an unambiguous Doppler coverage of $\pm$ 25 Hz. The antenna arrays employed for these measurements were 4-element discone antennas, which covered the two measured frequency bands of 2.2 GHz and 5.8 GHz. The antennas were mounted around a circle with a radius of 6.5 cm resulting in 9.5 cm spacing between antennas. The measurement environments for both sets of measurements and the discone array used at the transmitter are shown in Fig. 2.

MEASUREMENT RESULTS

The multiple SISO measurements were processed for the computation of the power delay profiles and for the estimation of the time variant transfer function. The 2.5 GHz and 3.5 GHz measurements were processed with 5.7 MHz bandwidth, and the 5.8 GHz were processed with 10 MHz. An example of power delay profiles measured at the three frequencies is shown in Fig. 4 with the corresponding number of multipath components for a 20 dB threshold. The differences in the number of multipath components and their relative level is evident from the figure.; however, all three frequencies show a small delay spread on the order of 2 μs. Since the 5.8 GHz band was processed with 10 MHz the number of detected multipath components is generally higher than the other two bands.

The stationary and dynamic MIMO measurements were processed to compute the channel capacity for 2 by 2 and 4 by 4 antenna arrays. The capacity was computed from the time variant channel transfer function using the following equation

$$C_{WB} = \frac{1}{N}\sum_{i=1}^{N}\log_2\left[\det\left(\mathbf{I}_{n_R} + \frac{\rho}{n_T}\mathbf{H}_i\mathbf{H}_i^H\right)\right] \tag{1}$$

where the transfer function for each frequency was normalised with respect to the overall sample norm (N snapshots) i.e. $\mathbf{H}^{(f_n)} = \beta\hat{\mathbf{H}}^{(f_n)}$. Here f_n represents the frequency sample index and β represents the normalisation constant for each snapshot, given by

$$\beta = 1\Big/\sqrt{\left(\frac{1}{N\cdot n_R n_T}\sum_{f_n=1}^{N}\sum_{i=1}^{n_R}\sum_{j=1}^{n_T}\left|\hat{H}_{ij}^{(f_n)}\right|^2\right)} \tag{2}$$

An example of a time variant MIMO channel for the two frequency bands is shown in Fig. 5, which displays the scattering function. The measurements were divided into line of sight and non line of sight and Fig. 6 displays the capacity results for the 2.2 GHz band for 30 dB signal to noise ratio. The results indicate an increase in the median capacity of about 5-13 b/s/Hz for the 2 by 2 and 4 by 4 antenna arrays for the NLOS case over the LOS locations.

CONCLUSIONS

The architecture of a multi-band multi-channel chirp sounder was briefly presented. The sounder was used in both multiple frequency SISO measurements and dual frequency MIMO measurements. The SISO measurements were performed in a rural environment where WMAN are likely to be used. The data were processed with 5.7 MHz and 10 MHz bandwidth, depending on the allocated spectrum for the relevant frequency band. The number of multipath components was subsequently computed for 20 dB threshold to determine the number of taps to be used in a tapped delay line simulator. Generally, the delay spread in most locations was limited to within 2 μs and the number of multipath components was between 3-4. The MIMO measurements were conducted with 100 MHz bandwidth in LOS and NLOS locations in a studio environment with both static and dynamic channels. The channel capacity was subsequently computed for 2 by 2 and 4 by 4 antenna combinations and the capacity of the LOS (correlated channels) showing a significant reduction in capacity.

REFERENCES

[1] S. Salous, P. Filippidis, R. Lewenz, I. Hawkins, N. Razavi-Ghods, and M. Abdallah, Parallel receiver channel sounder for spatial and MIMO characterisation of the mobile radio channel, *to be published in IEE Proc. Communications.*

[2] N. Razavi-Ghods, M. Abdalla, S. Salous, Characterisation of MIMO propagation channels using directional antenna arrays, presented at 3G2004 conference, London, UK, October 2004.

(a) (b) (c)

Fig. 1. (a) block diagram of converter units, (b) transmitter, (c) receiver

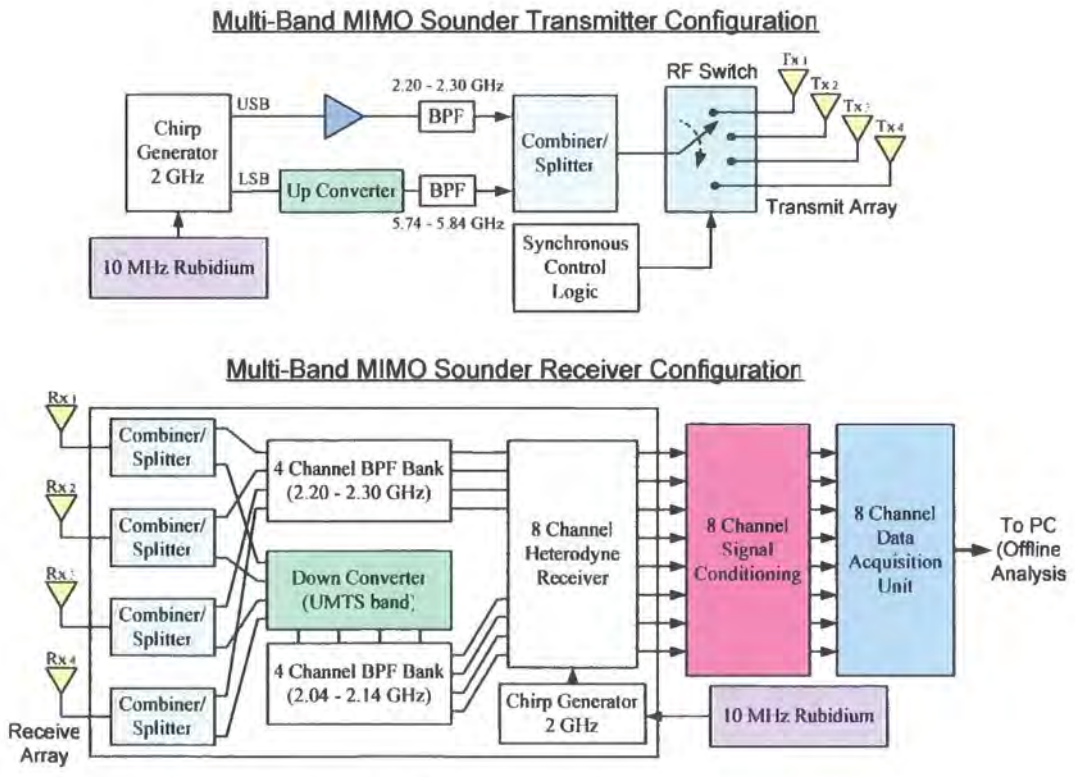

Fig. 2. Block diagram of sounder used for 4 by 4 dual band MIMO measurements

(a) (b) (c)

Fig. 3. (a) Rural environment for SISO measurements, (b) TV studio for MIMO measurements, (c) 4 by 4 array

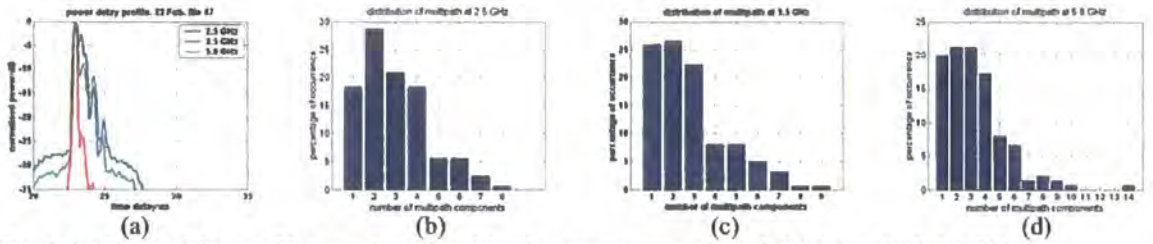

(a) (b) (c) (d)

Fig. 4. (a) Power delay profiles, number of multipath components at (b) 2.5, (c) 3.5 and (d) 5.8 GHz

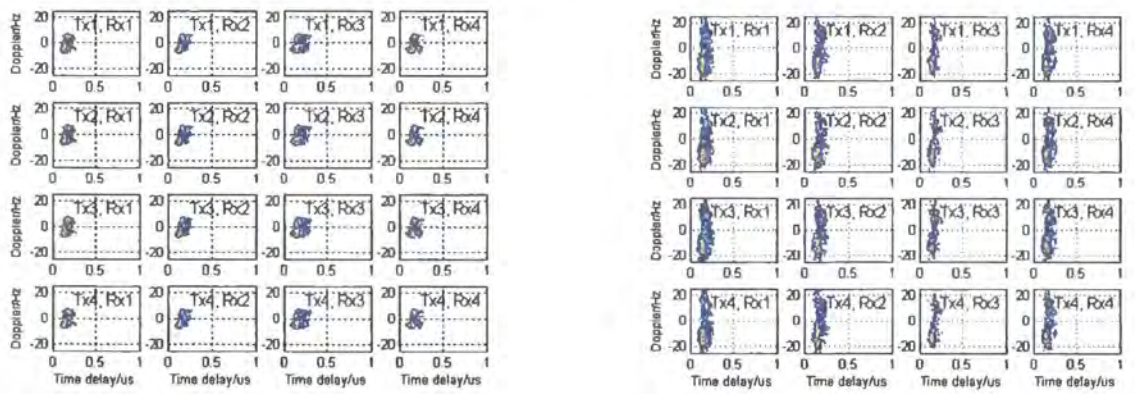

(a) (b)

Fig. 5. Dynamic scattering MIMO functions (a) 2.2 GHz, (b) 5.8 GHz

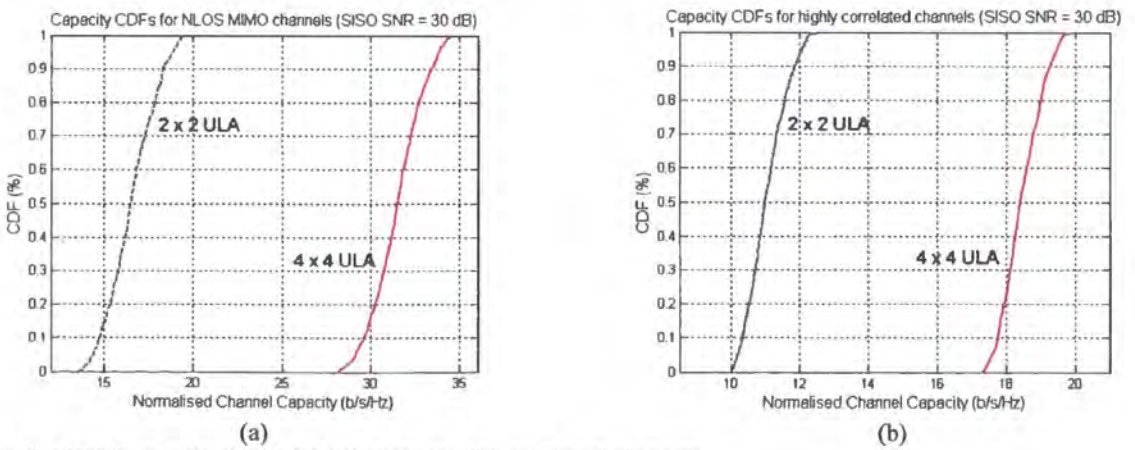

(a) (b)

Fig. 6. MIMO capacity for (a) NLOS channels, (b) correlated channels

SOUNDERS FOR MIMO CHANNEL MEASUREMENTS

S. Salous, S. Feeney, N. Razavi-Ghods, and M. Abdalla

Centre for Communication Systems, School of Engineering
University of Durham, Durham, DH1 3LE, England.
phone: + (44) 0191 334 2532, fax: + (44) 0191 334 2407, email: sana.salous@dur.ac.uk
web: www.durham.ac.uk/comms.systems

ABSTRACT

The paper discusses the architecture of MIMO channel sounders. The semi-sequential design is contrasted with the sequential and the parallel architectures. Measurements with an eight parallel receiver semi-sequential sounder performed in both indoor and outdoor environments at 2 GHz using different antenna arrays will be presented. The parallel receiver architecture is also shown to provide simultaneous multiple frequency measurements in the 2-6 GHz frequency bands.

1. INTRODUCTION

Multiple antenna array technologies can significantly enhance the performance of radio systems. MIMO (multiple-input multiple-output) signalling techniques in particular offer diversity/multiplexing gains to provide considerably higher channel throughputs as compared to conventional single antenna systems [1]. MIMO communication has been a topic of great interest by the international research community in the past few years. Whilst space-time coding and signal processing are essential to the implementation of MIMO technologies, it is often the radio propagation channel along with the antenna array type and geometry that proves to be the major restriction in utilising this technology. Thus the experimental characterisation of such propagation channels is vital to the future development of MIMO technologies, which are intended for ad-hoc as well as for cellular systems.

In this paper we present an overview of MIMO channel sounding techniques with emphasis on the high resolution semi-sequential MIMO sounder [2] which employs parallel RF channels at the receiver and has recently been upgraded for multiple frequency band measurements for the 2-6 GHz bands [3]. The architecture of the basic channel sounder which operates in the FDD, UMTS bands is discussed and the frequency converter units to and from 2.5 GHz, 3.5 GHz and 5.8 GHz are described. MIMO capacity results of 60 MHz bandwidth measurements at the uplink UMTS frequency band (1.95 GHz) are presented for different antenna arrays. Preliminary results of simultaneous frequency measurements at the three frequencies between the 2.5-5.8 GHz bands are presented for semi-urban to rural environments. These measurements were conducted with 10-MHz bandwidth and processed with 5.7 MHz or 10 MHz for OFDM applications of wireless metropolitan area network, WMAN standards.

2. MIMO RADIO CHANNEL SOUNDING

2.1 General consideration

In general, wideband channel sounding can employ different waveforms and techniques. These vary from the simple narrow pulse, to pulse compression techniques, which provide processing gain depending on the time bandwidth product of the waveform. These sounders use either specialised equipment or readily available instrumentation such as a network analyser. The choice of the particular waveform or equipment depends on the channel sounding requirements such as indoor versus outdoor, or single antenna measurements versus multiple antenna measurements.

The main channel sounding requirements are determined by the time delay resolution, which sets the transmitted bandwidth and the maximum expected Doppler shift which determines the waveform repetition frequency (WRF). The bandwidth of the measurements is usually 300 MHz for indoor measurements or a few tens of MHz for outdoor environments (60 MHz for third generation systems). The WRF depends on the carrier frequency and the environment, with a usual sampling distance every $\lambda/3$. At 2 GHz operating frequency and for measurements in urban environments, the maximum expected Doppler shift can be accommodated within 100 Hz for pedestrian users and 250 Hz for vehicular users (maximum vehicular speeds of 42 miles/hr). The WRF also determines the maximum time delay window that can be detected without ambiguity. For indoor environments this is only on the order of a few hundred ns while in outdoor measurements this can extend up to 40 μs in city centres with high-rise buildings or suburban areas with hilly terrain [4]. Since the effective time delay window decreases as the receiver moves away from the transmitter, the waveform duration should contain a guard time, which depends on the maximum range covered in the measurements to avoid ambiguity.

Dynamic operation where the transmitter and or receiver are capable of moving during the measurements gives flexibility for mobile measurements in outdoor environments and between floors for indoor

environments. An indirect requirement for wideband measurements is bandwidth compression, which enables the acquisition of the data at suitable rates. Table 1 compares the different types of sounders employed for channel measurements.

	Sliding correlator	CRDS	Digital chirp	Network analyser
Bandwidth/ Doppler range	Low BW/ high Doppler	Low BW/ high Doppler	High BW/ low Doppler	High BW/ low Doppler
Dynamic operation	Yes	Yes	Yes	No
Compression	Yes	Yes	Yes	Not necessary
Processing gain	Yes	Yes	Yes	Yes
complexity	Relatively complex	Relatively complex	Relatively complex	Relatively simple

Table 1. Channel sounding techniques

For MIMO measurements these requirements are essentially the same with the added requirement of multiple transmission and multiple reception. This can be achieved in one of two possible architectures. The first uses the same single transmit (input) single receive (output) (SISO) sounder architecture with switching between antennas at the transmitter and at the receiver. To enable Doppler measurement the scanning of all antennas should be completed within the coherent time of the channel. For the 2 GHz band and an 8 by 8 MIMO system, the required WRF is 64 times that for a SISO sounder. This number is usually doubled to 128 to permit for switching transients to die out. For 100-250 Hz Doppler coverage this corresponds to waveform duration between 78- 31 μs, respectively. While the 78 μs limit provides adequate time delay window, the 31 μs limit does not enable the detection of long delayed echoes.

Switching can be avoided using parallel transmitters and parallel receivers. Reported fully parallel sounders use either narrowband multiple frequency transmissions to distinguish the different transmit antennas and FFT processing at the receiver [5] or transmit different codes [6]. The highest bandwidth reported for such measurements is 25 MHz.

An alternative to these two techniques is the semi-sequential technique, which uses parallel receivers and an RF switch at the transmitter. Switching at the receiver can be avoided with an architecture, which employs parallel channels at the receiver. For eight parallel channels SIMO measurements can still be carried out with the same WRF as for SISO systems. For MIMO measurements the WRF is increased by the number of transmit antennas. For the example of eight antennas this corresponds to 800-2000 Hz, which still gives adequate range coverage.

2.2 Semi-sequential chirp channel sounder

To avoid the limitations of the SISO architecture when applied to SIMO/MIMO measurements, the dual frequency band chirp channel sounder, [7] has been upgraded to eight parallel channels at the receiver (see Fig.1). The receiver is based on the heterodyne detector, which uses a replica of the transmitted chirp signal to compress the RF wide bandwidth. The output of each mixer is filtered with a lowpass filter whose cut-off frequency depends on the chirp parameters (bandwidth and duration) and the maximum expected time delay window, amplified, digitised and stored first on a 128 Mbytes RAM whose contents are then transferred to the hard disk. For example for SIMO measurements with 60 MHz bandwidth, 100-250 Hz WRF, and 40 μs time delay window, the bandwidth is compressed to 240-600 kHz which requires a total data acquisition rate of 1.92-4.8 MHz sampling rate. For MIMO measurements this rate needs to be multiplied by the number of transmit antennas, which is still a much lower rate than the 320 Msps or the 1 Gsps required by the RUSK sounder or the AMERRIC sounder, respectively [8-9].

To continue measurements at the two UMTS frequency division duplex (FDD) bands, the transmitter and receiver generate both bands simultaneously. At the receiver, the two bands are switched every sweep where each band can be received on all the eight channels.

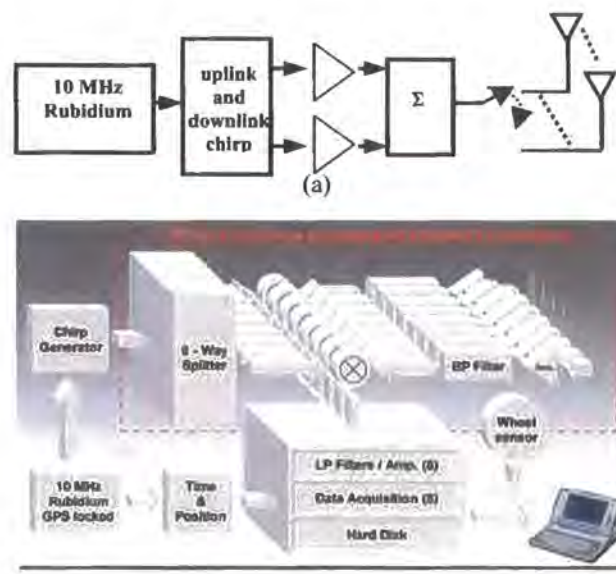

Figure 1. Block diagram of multiple receive UMTS FDD sounder (a) transmitter, (b) receiver.

Other three frequency bands (2.5 GHz, 3.5 GHz and 5.2/5.8 GHz) have been recently added to the sounder. These use the 2 GHz band as an IF for up-converters and

down converters (figure 2). This enables the sounder to be used either in a MIMO configuration at a single frequency or two frequencies for 4 antenna configurations or in a SISO configuration for several frequencies. Directional antenna arrays with 45° mounted around a circle to provide 360° coverage were designed and implemented for the MIMO measurements at the UMTS bands in addition to omni-directional antennas. The receiver and the antenna arrays are shown in figure 3.

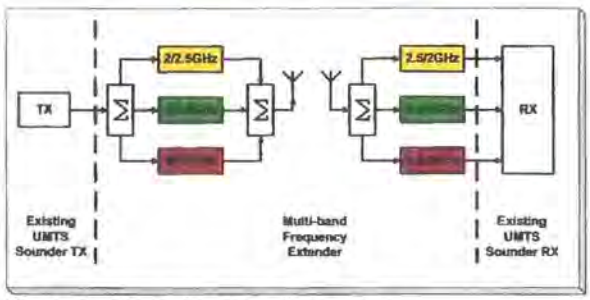

Figure 2. Block diagram of converters

(a) (b)

Figure 3. (a) Receiver of the sounder (b) antenna arrays

3. MULTIPLE ANTENNA /MULTIPLE FREQUENCY MEASUREMENTS

Measurements were performed both indoor and outdoor in various environments for both MIMO applications in the UMTS band and for WMAN in the 2.5 GHz, 3.5 GHz and 5.8 GHz bands.

The WMAN measurements were performed over 10 MHz bandwidth, where the three frequencies were transmitted simultaneously and received simultaneously using different channels of the receiver. The data were processed to determine the impulse response over bandwidths of 5.7 MHz for the 2.5 GHz and for the 3.5 GHz bands and with 10 MHz for the 5.8 GHz bands. These were used to obtain the parameters of the multipath components above 20 dB threshold for a tapped delay line model simulations and to estimate the time variant transfer function for OFDM simulations. Since the output of the receiver is the signal compressed in bandwidth and not in time, the time axis can be mapped into frequency thereby the required frequency range can be selected simply by taking the corresponding number of samples from the digitised data. The exact number of carriers can then be obtained by resampling the data if required. For the present study 512 carriers corresponding to 5.7 MHz were obtained for the lower two frequency bands and 9.8 MHz for the 5.8 GHz band. Examples of the power delay profiles are shown in figure 4. The figure displays the differences between the bands for different locations. The number of multipath components for the three frequency bands was computed for a 20 dB threshold and figure 5 gives the CDF for the three frequency bands. The figure shows that for the 2.5 GHz and 3.5 GHz bands the number of multipath components is similar whereas more components were detected in the 5.8 GHz band. This is due to the finer resolution used in the processing of the 5.8 GHz band, which corresponded to 10 MHz resolution rather than 5.7 MHz resolution for the other two bands (resolution of a chirp sounder is inversely proportional to the bandwidth).

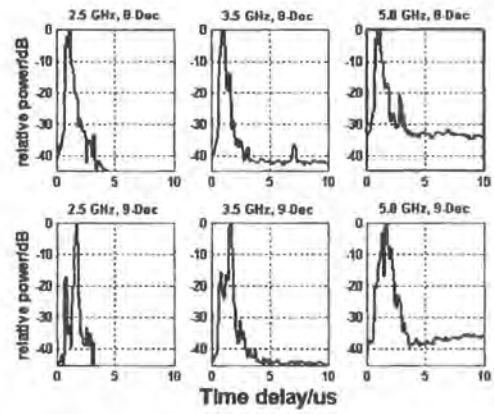

Figure 4. Power delay profiles at two different locations at the three frequency bands.

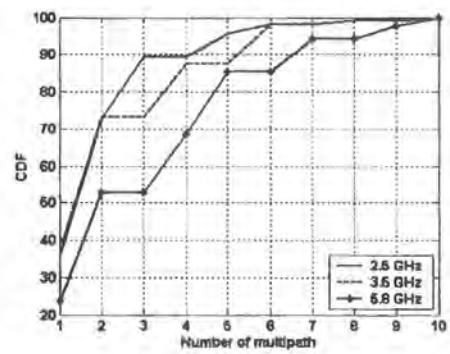

Figure 5. Cumulative distribution function for the number of multipath components.

The UMTS measurements were conducted with 60 MHz bandwidth at the uplink frequency of 1.95 GHz with 250 Hz WRF, with both arrays shown in figure 3.b. Figure 6 displays the impulse response for a 4 by 4 MIMO measurement channel using $\lambda/2$ spaced omnidirectional dipoles at both ends of the channel. The PDPs show considerable differences in the channel response from antenna to antenna at both ends of the radio link.

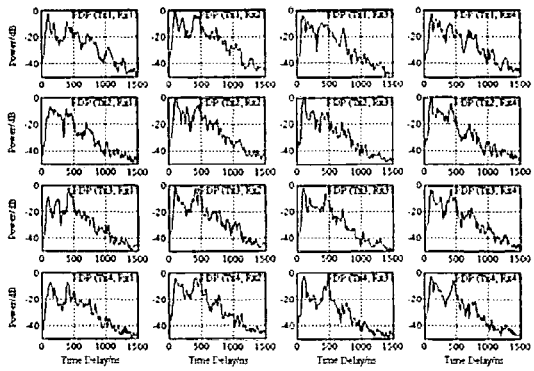

Figure 6. Multipath structure for a 4 by 4 antenna array.

The measurements were processed to determine the complex transfer function, which was subsequently used to estimate MIMO channel capacity. An example of channel capacity measurements obtained with 2 by 8 arrays where the receiver array was either vertically polarised directional circular patch array (VPDCPA) or vertically polarised uniform linear dipole array (VPULDA) is shown in figure 7 for an indoor non line of sight NLOS environment. The transmit array was a two element dipole. The transfer function was sampled at 2000 frequencies and the wideband capacity was computed as the average of the narrowband capacity using the following equation

$$C_{WB} = \frac{1}{N}\sum_{i=1}^{N}\log_2\left[\det\left(\mathbf{I}_{n_R} + \frac{\rho}{n_T}\mathbf{H}_i\mathbf{H}_i^H\right)\right]$$

where the transfer function for each frequency was normalised with respect to the sample norm i.e. $\mathbf{H} = \beta\hat{\mathbf{H}}$, where $\beta = \left(\frac{1}{n_R n_T}\sum_{i=1}^{n_R}\sum_{j=1}^{n_T}\left|\hat{H}_{ij}\right|^2\right)^{-1/2}$

The figure shows a slight increase in capacity for the circular patch array, which could be attributed to the reduced correlation between the elements.

4. CONCLUSIONS

The architecture of a semi-sequential MIMO channel sounder was presented and contrasted to the fully parallel and fully sequential sounders. The sounder is shown to also provide simultaneous measurements at different frequencies due to the parallel architecture employed at the receiver. MIMO measurements in the UMTS band were conducted and capacity results were presented for indoor NLOS with 60 MHz bandwidth. The results of measurements in suburban/rural environment at three different frequencies were also presented. The results are relevant to OFDM WMAN. The number of multipath components for these links was found to be between 1-8 components with 4 components being detected in more than 80% of the locations.

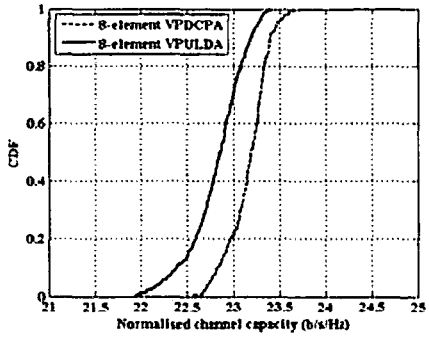

Figure 7. Capacity results for 2 by 8 arrays in indoor environments.

REFERENCES

[1] G. F. Foschini, "Layered space-time architecture for wireless communication in a fading environment using multiple antennas," *Bell Labs. Tech. Journal,* vol. 1, No. 2, 1996, pp 41-59.

[2] S. Salous, P. Filippidis, R. Lewenz, I. Hawkins, N. Razavi-Ghods, and M. Abdallah, "Parallel receiver channel sounder for spatial and MIMO characterisation of the mobile radio channel", to be published in the IEE Proc. on Communications.

[3] S. M. Feeney, P. Filippidis, R. Lewenz, and S. Salous, "Multi-band Channel Sounder in the 2-6 GHz band," *in Proc. of BWA,* Cambridge, 2004, pp 1-4.

[4] S. Salous, "W-CDMA measurements for 3G systems," *in Proc 'Fourth Journees d'etudes on Propgation Electromagnetique dans L'atmosphere du Decametrique a L'angstrom',* Rennes University, France, March 2002, pp 1-8.

[5] D. Chizhik, J. Ling, P. Wolniansky, R. Valenzuela, N. Costa and K. Huber, "Multiple input multiple output measurements and modeling in Manhattan," *IEEE Journal on Selected Areas in Communications,* April 2003, Volume 21, Number 3 MIMO systems and applications: part I.

[6] C.C. Martin, J.H. Winters, N.R. Sollenberger, "Multiple input multiple output (MIMO) radio channel measurements," *in Proc. VTC2000,* pp 774-779.

[7] S. Salous, and H. Gokalp, "Dual frequency sounder for UMTS frequency division duplex channels," *IEE Proceedings Communications,* vol. 149, No. 2, April 2002, pp 117-122.

[8] W. Wirnitzer, D. Bruckner, R. S. Thoma, G. Sommerkorn, and D. Hampicke, "Broadband vector channel sounder for MIMO channel measurement," *IEE seminar on MIMO: Communication systems from concept to implementation,* 12 Dec. 2001.

[9] J-M. Conrat, J-Y Thiriet, and P. Pajusco, "AMERICC, l'outile de mesure du canal large bande radioelectrique developpe par France Telecom R&D," *Fourth Journees d'etudes on Propgation Electromagnetique dans L'atmosphere du Decametrique a L'angstrom,* Rennes, France, March 2002.

WIDEBAND SOUNDER AND MEASUREMENTS IN THE 60 GHZ BAND

S. Feeney and S. Salous

University of Durham, Durham, UK
sana.salous@durham.ac.uk

ABSTRACT

The radio channel in the 60 GHz band offers wide bandwidths suitable for high-speed Ethernet radio transmissions on the order of 1 Gbit/s. To characterise the channel for such applications, a frequency up converter coupled with a frequency multiplier were designed and implemented to generate a 1 GHz chirp waveform at 60 GHz. The sounder architecture with preliminary indoor measurements are presented in the paper with the estimated rms delay spread.

INTRODUCTION

The 60 GHz band has recently attracted a great deal of attention due to the available wide bandwidth and the limited propagation range, which enables frequency reuse. This makes it particularly attractive for home and office environment for high data rates on the order of 1 Gbit/s such as those investigated in the WIGWAM project (Wireless Gigabit with Advanced Multimedia) [1].

The performance of a radio system is limited by the ability of the receiver to reconstruct the signal that was transmitted. Limitations to this reconstruction are having sufficient energy per bit of information with respect to noise and that the signal is not too dispersed in time.

The signal available at the receiver is due to energy arriving via both direct and scattered routes from the transmitter. The effect of dispersion (frequency selective fading) across the radio channel becomes more significant as the channel becomes wider. To support Gigabit Ethernet via a radio channel using low order modulation requires channel bandwidths in the region of 1 GHz.

For a Gigabit Ethernet radio using 4QAM (QPSK) modulation, the channel data rate including overhead will be approximately 700 M symbols / second. Energy dispersed between / across symbols will provide self-interference causing the link to fail. This can be mitigated through the use of adaptive time delay equalisers. Practical equalisers are able to span approximately 10 symbols. Thus channel echoes with delays of up to approximately 13n sec can be accommodated.

Without equalisation, 4QAM operation with self-interference levels in the range of 10 dB to 15 dB below the primary signal can be supported with forward error correction. More spectrally efficient modulation schemes (for example 8PSK or 16QAM) require further reductions in self-interference to 15 dB to 25 dB below the primary signal.

The channel soundings used here are able to investigate the distribution of the echoes and to present this as a power-delay profile for the path.

To provoke multi-path behaviour for short paths moderate directivity antennae have been used. The antennae used here were conical horns with a nominal gain of 20 dBi. Typical links within the 60 GHz band are using antennas with typically 40 dBi. These therefore exhibit an angular directivity ten times greater in both elevation and azimuth.

Whilst there are numerous techniques that can be used to measure the channel the use of an FMCW (frequency modulated continuous wave, also known as chirp) signal has advantages in particular for wideband channels. These advantages include the optimum use of the available transmit power, the high processing gain at the receiver, and bandwidth compression.

In this paper the architecture of the chirp sounder is presented with indoor measurements. The spurious free dynamic range of the power delay profiles obtained over 1 s was on the order of 20 dB. Therefore, rms delay spreads for a 15 dB threshold level were estimated. These range from 0.77 ns for a single detected component to 13.7 ns for the worst case.

CHANNEL SOUNDER ARCHITECTURE

Channel sounders in the 60 GHz band tend to mainly use network analysers due to the ease of the generation of the waveform and the wide bandwidth that can be achieved [2]. A swept CW source in conjunction with a spectrum analyser has also been used for such studies to obtain the frequency response of the channel [3]. These techniques generally require a long duration to determine the channel response and hence the time variability of the channel cannot be observed. This limitation can be avoided by using short PRBS sequences with high-speed analogue to digital converters [4-5]. These however share the same limitation with the network analyser in that they use a cable from the transmitter to provide a reference at the receiver.

The sounder reported here is based on the principle of heterodyne detection where both the transmitter and receiver have local chirp generators, each locked to its own Rubidium reference. This enables the dynamic operation of the sounder and bandwidth compression for low data acquisition cards. These advantages

permit measurements in different scenarios such as between buildings and between floors and also permit the acquisition of long records of data using a very low sampling rate on the order of 1 MHz. This is in contrast to the 400 MHz PRBS sounder reported in [4] or the 7 GHz UWB sounder reported in [5] where cables were needed to connect the 70 MHz IF signal [4] or the 14 GHz signal [5] between the transmitter and receiver to synchronise and phase lock the oscillators.

The basic architecture of the sounder reported here is described in [6]. The 2 GHz sounder's frequency was later extended to several frequency bands including 5.8 GHz [7]. For the 60 GHz band operation the 5.8 GHz band was used as an IF with frequency up converters to 15 GHz and subsequently to 60 GHz using a time four frequency multiplier. The latter stage increased the bandwidth to 1024 MHz, which provides a 1 ns time delay resolution. The architecture of the transmitter and the receiver of the sounder are shown in figures 1a. and 1.b. The local chirp generators at both ends consist of a 2 GHz input with a programmable sweep with bandwidths from 1-260 MHz. The 2 GHz sweep goes to a first stage up-converter in the 5 GHz band. The second up converter stage has a frequency doubler for the local oscillator module output to generate a fixed 10.24 GHz local oscillator. This is subsequently mixed with the sweep in the range 5.00 GHz to 5.26 GHz to up-convert the chirp to the range 15.24 GHz to 15.50 GHz. This signal is filtered and amplified to provide an input level of +12 dBm to the final multiplier.

The third stage has a multiplier, which is contained in a small aluminium enclosure with a waveguide interface to provide direct connection to the antenna. A 2m long flexible cable connects to the up-converter. With an input of 15.24 GHz to 15.50 GHz the module provides an output of nominally 5 mW (+7 dBm) at 60.96 GHz to 62.00 GHz.

The receiver consists of an up-converter similar to that at the transmitter, which is used to mix with the received signal. To acquire the data with the existing data acquisition unit it was necessary to down convert the output of the mixer to the frequency range 30 kHz to 300 kHz. This is achieved in the following stages. By off-setting the start point between the transmit and receive sweeps to generate an IF signal at 12.5 MHz. This signal is band pass filtered and amplified using a two-stage amplifier that includes a 5 bit switched attenuator to provide gain adjustment over a 31 dB range. This is followed by a 10 MHz mixer which down converts the signal to ~2.5 MHz (2.53 MHz to 2.8 MHz). The signal at 2.53 MHz to 2.8 MHz is then converted to base-band (30 kHz to 300 kHz) using a local signal at 2.5 MHz and a single-sideband conversion. A sideband rejection of 50 dB was achieved. Figure 2 shows the 60 GHz transmitter and receiver front ends.

SOUNDER REPSONSE

The performance of the designed units was verified by injecting 2 GHz CW signals from local oscillators with low phase noise at both the transmitter and the receiver instead of the 2 GHz sweep. This excludes the spurii of the direct digital synthesiser (DDFS) in the chirp generator and provides a measure of the performance of the 60 GHz up converter and down converter. Figure 3 shows that a 30 dB spurious free dynamic range is achieved.

Due to the high frequency range, it was not possible to perform the usual back-to-back test using a direct connection between the transmitter and receiver. Instead the transmit and the receive antennas were positioned to obtain a direct line of sight propagation geometry and the resulting output is displayed in figure 4 which shows a 20 dB dynamic range of wanted signal to spurii with a noise floor in excess of 30 dB. The deterioration of spurii performance from that at 2 GHz is due to the multiplication by 4, which degrades the performance by 12 dB.

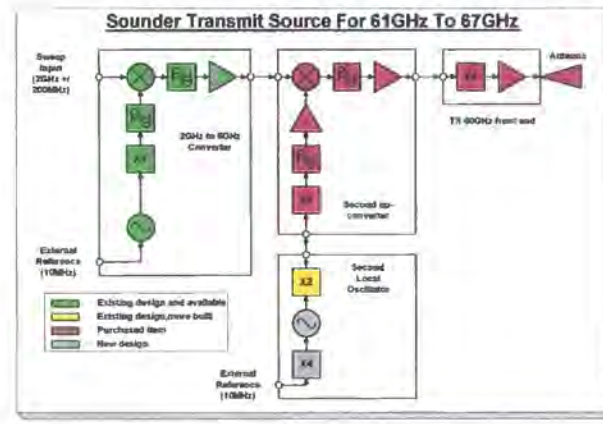

(a)

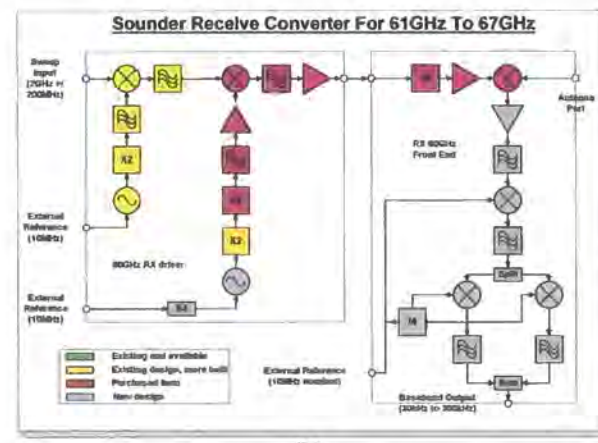

(b)

Figure 1. Block diagram of (a) the transmitter (b) the receiver.

(a)

(b)

Figure 2. RF Front ends of (a) transmitter, (b) receiver

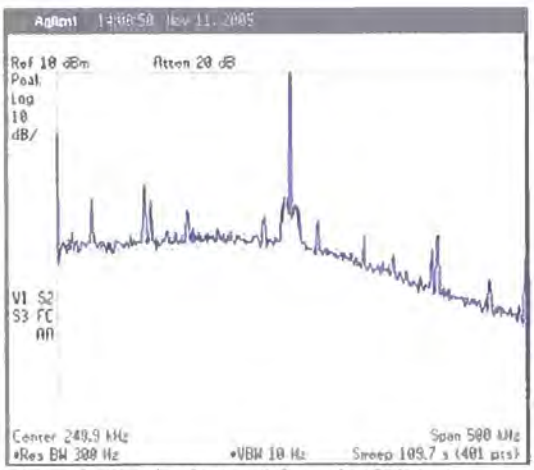

Figure 3. Received output from the CW test

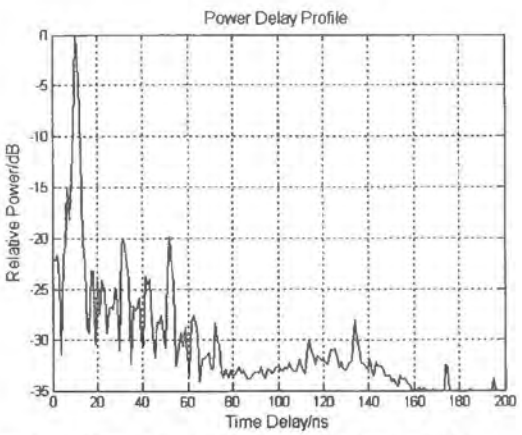

Figure 4. The output of the sounder from a LOS measurement.

MEASUREMENTS AND RESULTS

The sounder was used in measurements at different locations in an indoor environment with both line of sight and non line of sight arrangements. The measurements were performed using a 1024 MHz sweep every 4 ms with horn antennas shown in figure 5.

Figure 5. Horn antennas (20 dBi on left, 10 dBi on right).

Some of the measurement locations are identified in figure 6 where the receiver was fixed and the transmitter moved. As can be seen some of these locations are LOS and some are NLOS and can be considered as indoor to outdoor as location 5 and between buildings as location 6.

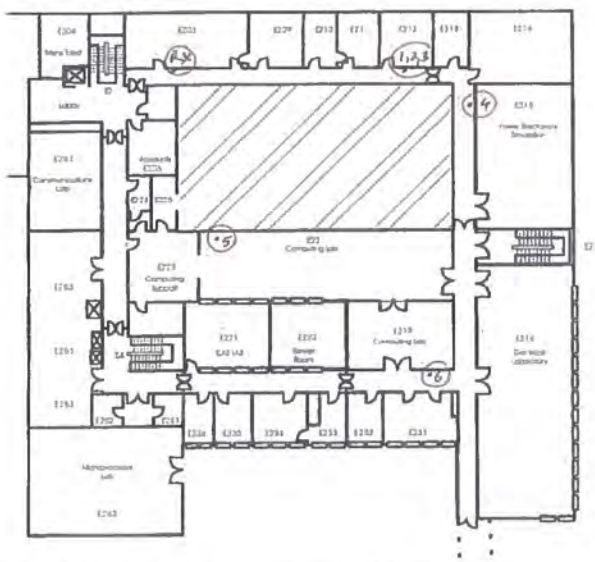

Figure 6. Layout of measurement environment

A NLOS power delay profile is shown in figure 7, where delay spread in excess of 45 ns is observed. To avoid the inclusion of any spurrii in the estimation of the rms delay spread, a 15 dB threshold was applied. The distribution of the values of rms delay spread is displayed in figure 8 where it is seen that in more than 35% of the locations the delay spread was that of a single component where no multipath was detected. The high value of 13.7 corresponds to that of figure 7 where the antennas were deliberately pointed upwards towards the ceiling. Therefore this value was only

observed in one location. The remainder of the locations showed a delay spread on the order of 2.7-5.6 ns, which appears to be more representative of the measured environment. However, further measurements would be required in a variety of indoor and indoor to outdoor locations to study the statistics of the channel in the 60 GHz band.

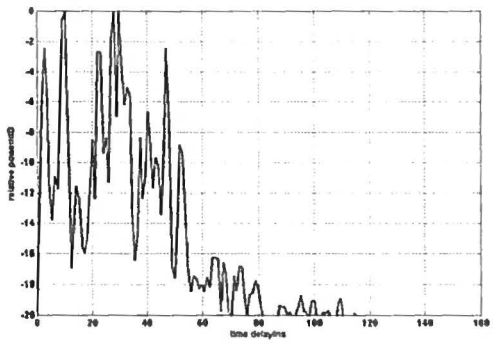

Figure 7. Power delay profile in NLOS situation

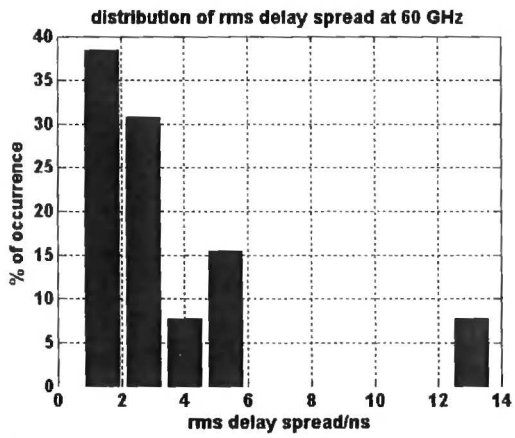

Figure 8. Distribution of rms delay spread for measurements in figure 6.

CONSLUSIONS

The architecture of a 60 GHz channel sounder with a bandwidth of 1024MHz was presented. The sounder was shown to have a 20 dB spurious free dynamic range, which is adequate for such applications. Measurements every 4 ms over a 1 s interval in an indoor environment were performed and rms delay spread values were estimated in both LOS and NLOS situations. The results show that the worst-case rms delay spread of 13.7 ns was measured when the antennas were turned around by 90° degrees from the LOS scenario. However, further measurements in different scenarios need to be measured both indoor and outdoor to obtain full characterisation of the channel.

REFERNCES

[1] G. Fettweis and R. Irmer, WIGWAM: system concept development for 1 Gbit/s air interface, Wirless World Research Forum, pp 1-7.

[2] H. Yang, P. Smulders and M. Herben, Indoor channel measurements and analysis in the frequency bands 2 GHz and 60 GHz, Proc. PIMRC 2005, Sept. 2005

[3] D. Matic, H. Harada and R. Prasad, Indoor and outdoor frequency measurements for mm-waves in the range of 60 GHz, Proceedings of IEEE Vehicular Technology Conference, volume 1, pages 567-571, 1998.

[4] Guillouard, S.,"Conception et realisation d'un sondeur de canal tres large bande a 60 GHz-mesures de propagation a l'interieur des batiments" 1999, PhD Thesis, L'Institut National Des Science Appliquees de Rennes.

[5] S. Ranvier, M. Kmee, R. Herrmann, J. Kivinen, J. Koivunen, R.S. Thoma and P. Vainikainen, URSI General Assembly, Delhi, 2005.

[6] S. Salous and V. Hinostroza, Wideband indoor frequency agile channel sounder and measurements, IEE Proceedings Antennas and Propagation, Dec. 2005, pp 573-580.

[7] S. Salous, S. Feeney, N. Razavi-Ghods, and R. Lewenz measurements in the 2-6 GHz band, URSI, General Assembly, Delhi, October 2005, pp 1-4.